

**Palaeoenvironmental and palaeogeographic
reconstruction of the Tequixquiac Basin, Central
Eastern Mexico: Mid to late Pleistocene
environments**

Emma Victoria Toole

A thesis is submitted in partial fulfilment of the requirements of
Liverpool John Moores University for the degree of Doctor of
Philosophy

This research was carried out in collaboration with NERC,
Nottinghamshire and SUERC, Glasgow

June 2019

Abstract

This PhD research utilises, for the first time, sedimentary evidence for mid to late Quaternary environmental change in the Tequiquiac region of Central-eastern Mexico. This project has logged over 50 stratigraphic sections and geochemically analysed a 55 m lithostratigraphic sequence for multi-proxy palaeoenvironmental information. The main research objective was to develop a spatial and temporal Palaeogeographic and Palaeoenvironmental model for the study area the covered the late Pleistocene to early Holocene. The findings of the study, based on the analysis of sedimentology, micromorphology, stable isotopes $\delta^{18}\text{O}_{\text{carbonate}}$ and $\delta^{13}\text{C}_{\text{DIC}}$ as well as ICP-OES sediment and tephra geochemistry, LOI, AMS radiocarbon, $^{40}\text{Ar}/^{39}\text{Ar}$ and Uranium-series dating has allowed a chronologically constrained paleoenvironmental and palaeogeographic reconstruction of the study area. The results of the study suggest that the Tequiquiac Basin has undergone a significant hydrological change from perennial lacustrine to ephemeral fluvial conditions between MIS15 – MIS 1 controlled by a combination of; climatic fluctuations, expressed as depositional cyclicity driven by precessional fluctuations to insolation levels. On shorter time-scales, changes in the mean position of the ITCZ related to SST, latitudinal gradients, atmospheric surface pressure gradients, the extent of Northern Hemisphere land and sea ice cover, and oceanic circulation patterns. Fluctuations in the TOC content of sediments are thought to be related to El Niño-like (dry) and La Niña-like (wet) events. While climate is thought to have been critical to the development the Quaternary localised uplift, deformation and normal faulting have also influenced paleohydrology and water-table elevation during the recorded depositional period (Figs 8.15 d & 8.16 d).

Acknowledgements

Firstly, I would like to thank NERC for their funding and SUERC, without whom I would not have had the support to conduct the isotope, geochemical and Ar-Ar work. Appreciation and thanks are given to my project supervisors Prof. Silvia Gonzalez, Prof. David Huddart and my unofficial supervisor Prof. Christopher Hunt, whom I am indebted to. Special thanks are given to Dr Gilbert Price for help and assistance with U-Series dating and Prof Darren Mark for support and guidance with Ar-Ar dating; and to Dave Williams and Hazel Clark who have helped me numerous times throughout my studies, providing informal discussions about the best way to adapt methods to suit the sediment type. Also, to Dr Isabel Israde and Dr Gabriela Dominguez from the de la Universidad Michoacana de San Nicolas, Mexico for help and support with diatom and pollen analysis, and to Dr Elizabeth Whitfield, who helped me from a distance and pushed me past the finish line. Remembrance and thanks are given to Prof. Alan Turner (1947 – 2012) for his advice, support, belief, wit and endless humour that still motivates and makes me smile today. Acknowledgement and gratitude are heaped onto my family (actual and adopted), partner Anthony and friends Laura and Sarah for their endless support, patience and for keeping me grounded. Lastly, endless thanks are given to my three amazing children Ethan, Callum and Jack who have equally sacrificed to get me to this point.

Statement of originality

All fieldwork, sample collection, laboratory work, data analysis, data interpretation and discussion, tables, images and figures were conducted and/or produced by Emma Toole unless otherwise stated. Below is a statement of co-workers and their contributions towards the research.

Carbonate stable isotope analysis of the first batch of carbonate sediment samples was carried out at SUERC by the author under the guidance and supervision of Dr Alex Brasier. The second batch of carbonate sediment samples was prepared at Liverpool John Moores University and sent to Dr Alex Brasier at SUERC for analysis.

For ICP- OES data analysis one week was spent at SUERC preparing sediment samples for analysis, and analysis methods were set out by Professor Rob Ellam. Preparation of blanks and reference materials along with sample mass spectrometric analysis was carried out by Anne Kelly at SUERC. All data were then forwarded to the author for interpretation.

Five bulk tephra samples were sent to the litho-geochemistry lab, Activation Laboratories, Ancaster, Ontario, Canada. Package 4B, (Lithium Metaborate /Tetraborate Fusion – ICP/OES) was used to obtain the bulk major oxide content of the samples.

Samples were sent to BETA Analytic, Miami, USA to obtain ¹⁴C AMS radiocarbon dates for five bulk organic sediment samples, two gastropods, and two bivalve shells.

The author prepared two tephra samples for Ar/Ar dating that were sent for irradiation and returned to the Scottish Universities Environmental Research Centre (SUERC) where all mass spectrometric analysis was carried out by Dr Darren Mark which was then forwarded to the author for interpretation.

The U – series dating three limestone samples were sent to Dr Gilbert Price, University of Queensland, Australia, for U-series dating. No preparation was carried out by the author (see Section 6.6).

| Content | Page |
|---|-------------|
| Abstract | I |
| Acknowledgements | II |
| Statement of originality | III |
| Content | IV |
| List of figures | XV |
| List of tables | XXVi |
| | |
| Chapter One: Introduction | |
| 1.1: Introduction | 1 |
| 1.2: Aims and objectives | 1 |
| 1.3: Research justification | 3 |
| 1.3.1: Quaternary sedimentology | 3 |
| 1.3.2: Mexican Quaternary Environments. | 6 |
| 1.4: PhD Thesis structure | 7 |
| | |
| Chapter Two: Background to the Research | |
| 2.1: Introduction | 9 |
| 2.1.1: The impact of Quaternary climate records from low latitude regions | 9 |
| 2.1.2: Quaternary environmental records from Central | 9 |
| 2.1.3: Forcing mechanisms of depositional change | 11 |
| 2.2: Physiography of Central Mexico | 11 |
| 2.3: Quaternary Climate forcing across Mexico | 12 |
| 2.4: Modern Climate of Central Mexico | 17 |
| 2.5: Quaternary lacustrine records from the Basin of Mexico | 18 |
| 2.5.1: Introduction | 18 |
| 2.5.2: Review of Quaternary records from the Basin of Mexico | 18 |
| 2.5.2.1: The early-mid Glacial: MIS 5 – MIS 4, 85,000 – 29,000 cal. BP | 19 |

| | |
|--|-----------|
| 2.5.2.2: The Northern Hemisphere LGM: MIS 2, ca. 29,000 – 19,000 cal. BP | 20 |
| 2.5.2.3: The Northern Hemisphere Deglaciation ca. 19,000 – 15,000 cal. BP | 22 |
| 2.5.2.4: Pleistocene – Holocene transition ca. 15,000 – 11,000 cal. BP | 22 |
| 2.5.2.5: Holocene | 25 |
| 2.6: A broad overview of Mexico’s Quaternary history | 25 |
| 2.6.1: Northern Mexico | 25 |
| 2.6.2: Central Mexico | 27 |
| 2.6.3: Southern Mexico | 32 |
| 2.7: Summary | 32 |
| 2.8: Gaps and Questions about Central Mexican Quaternary Environments | 33 |
| 2.8.1: Problems | 33 |
| 2.8.2: Gaps and open questions | 34 |
| 2.9: Further justification of research aims and objectives | 35 |
| 2.10: Conclusion | 36 |
| Chapter Three: Study area | |
| 3.1: Introduction | 37 |
| 3.2: Location | 37 |
| 3.3: The Tequixquiac Basin | 37 |
| 3.4: Topography | 39 |
| 3.5: Vegetation | 39 |
| 3.6: Drainage | 39 |
| 3.6.1: Barrancas and catchment drainage | 40 |
| 3.6.2: Natural springs | 40 |
| 3.6.3: Artificial drainage | 41 |
| 3.7: Geological Setting | 41 |
| 3.8: Surface geology in the study area | 42 |

| | |
|--|----|
| 3.8.1: Introduction | 42 |
| 3.8.2: Cretaceous limestone system | 43 |
| 3.8.2.1: El Doctor Limestone | 43 |
| 3.8.2.2: Cuautla Formation | 43 |
| 3.8.3: Cenozoic volcanic system | 43 |
| 3.8.3.1: El Morro Formation (fanglomerate) | 43 |
| 3.8.3.2: The Pachuca Group (Segerstrom, 1963) also known as the El Peñon Formation (Ledesma-Goerrror, 1987) | 44 |
| 3.8.3.3: San Juan Group | 44 |
| 3.8.4: Late Pliocene – early Pleistocene system | 46 |
| 3.8.4.1: The Trango and Atotonilco El Grande Formations | 46 |
| 3.8.5: The Quaternary system | 47 |
| 3.8.5.1: Basalt | 47 |
| 3.8.5.2: Tacubaya Formation | 48 |
| 3.8.5.3: Older Becerra Formation | 48 |
| 3.8.5.4: Younger Becerra Formation | 48 |
| 3.8.5.4: Totolzingo Formation | 48 |
| 3.9: Central eastern Mexico fault systems | 49 |
| 3.9.4: Faulting associated with the Basin of Mexico | 49 |
| 3.9.5: Faulting associated with the Mezquital Valley | 49 |
| 3.10: Faults influencing the Tequixquiac Basin | 50 |
| 3.11: Summary and conclusion | 50 |
| Chapter four: Methods used | |
| 4.1: Introduction | 52 |
| 4.2: Fieldwork | 52 |
| 4.2.1: Mapping | 52 |

| | |
|--|-----------|
| 4.2.2: Detailed sedimentological investigation | 52 |
| 4.2.3: Sediment sampling | 53 |
| 4.3: Petrographic analysis of hand specimens and sediment samples | 53 |
| 4.4: Framework for the identification of depositional environments | 54 |
| 4.4.1: Methodology used to describe the sediments | 54 |
| 4.4.2: Fluvial facies and depositional model | 55 |
| 4.4.3: Lacustrine carbonate facies and depositional model | 56 |
| 4.4.4: Palustrine carbonate facies and depositional model | 60 |
| 4.4.5: Spring carbonate facies and depositional model | 60 |
| 4.4.6: Pedogenic calcrete | 61 |
| 4.4.7: Groundwater calcrete formation | 62 |
| 4.5: Geochemical analysis of sediment samples | 64 |
| 4.5.1: ICP – OES $\delta^{18}\text{O}$ and $\delta^{13}\text{C}$ stable isotope carbonate geochemistry | 65 |
| 4.5.1.1: Isotope terminology | 65 |
| 4.5.1.2: Oxygen isotopes in lacustrine and marsh limestone carbonate deposits | 66 |
| 4.5.1.3: Carbon isotopes in lacustrine and marsh limestone carbonate deposits | 71 |
| 4.5.1.4: Composition of source waters | 72 |
| 4.5.1.5: Sample preparation for ICP – OES $\delta^{18}\text{O}$ and $\delta^{13}\text{C}$ analysis | 73 |
| 4.5.1.6: Sample analysis for ICP – OES $\delta^{18}\text{O}$ and $\delta^{13}\text{C}$ | 73 |
| 4.5.2: Terrestrial carbonate ICP – OES geochemistry | 74 |
| 4.5.2.1: Methodology | 74 |
| 4.5.3: Tephra geochemistry | 75 |
| 4.5.3.1: Methodology | 75 |
| 4.5.4: Loss on ignition (LOI) | 76 |
| 4.5.4.1: Methodology | 76 |
| 4.6: Dating of the Quaternary sequence | 76 |
| 4.6.1: AMS radiocarbon dating | 76 |
| 4.6.1.1: Sample preparation | 77 |

| | |
|---|-----------|
| 4.6.1.2: Gastropod and bivalve samples | 77 |
| 4.6.1.3: Bulk organic sediment | 78 |
| 4.6.1.4: Reporting Radiocarbon results | 79 |
| 4.6.2: ⁴⁰ Ar/ ³⁹ Ar dating | 79 |
| 4.6.2.1: Sample preparation and measurement | 80 |
| 4.6.3: Uranium-series (U - series) dating | 82 |
| 4.7: Conclusion | 83 |
| Chapter 5: Chapter Five: Tequixquiac Facies Descriptions | |
| 5.1: Introduction | 84 |
| 5.1.1.: Facies analysis | 84 |
| 5.2: Tequixquiac Basin sediment types and facies | 84 |
| 5.3: Terrestrial limestone facies | 86 |
| 5.3.1.: Facies 1, Framestone limestone | 86 |
| 5.3.1.1: Description | 86 |
| 5.3.1.2: Defining characteristics | 88 |
| 5.3.1.3: Tequixquiac Framestone deposits | 89 |
| 5.3.2: Facies 2 a & b, Stromatolitic limestone | 90 |
| 5.3.2.1: Description | 90 |
| 5.3.2.2: Defining characteristics | 91 |
| 5.3.2.3: Tequixquiac Stromatolitic limestone | 91 |
| 5.3.3: Facies 3, Calc-mudstone | 92 |
| 5.3.3.1: Description | 92 |
| 5.3.3.2: Defining characteristic | 93 |
| 5.3.3.3: Tequixquiac calc-mudstone deposits | 93 |
| 5.3.4: Facies 4, Peloidal limestones | 94 |
| 5.3.4.1: Description | 94 |
| 5.3.4.2: Defining characteristics | 97 |

| | |
|--|------------|
| 5.3.4.3: Tequixquiac peloidal limestone | 97 |
| 5.3.5: Facies 5, Pisolitic limestone | 99 |
| 5.3.5.1: Description | 99 |
| 5.3.5.2: Defining characteristics | 99 |
| 5.3.5.3: Tequixquiac pisolitic limestone | 99 |
| 5.3.6: Facies 6, Intraclastic limestone | 99 |
| 5.3.6.1: Description | 99 |
| 5.3.6.2: Defining characteristics | 101 |
| 5.3.6.3: Tequixquiac intraclastic limestone | 102 |
| 5.3.7: Facies 7, Laminated and bedded limestone deposits | 102 |
| 5.3.7.1: Description | 102 |
| 5.3.7.2: Defining characteristics | 102 |
| 5.3.7.3: Tequixquiac laminated limestone | 102 |
| 5.4: Mixed clastic and carbonate deposits | 107 |
| 5.4.1: Tequixquiac mixed clastic and carbonate deposits | 107 |
| 5.5: Clastic sedimentary facies | 110 |
| 5.5.1: Facies 11(a-c), Clay | 111 |
| 5.5.1.1: Description | 111 |
| 5.5.1.2: Defining characteristic | 112 |
| 5.5.1.3: Tequixquiac clay deposits | 112 |
| 5.5.2: Facies 12 (a-c), Mud | 113 |
| 5.5.2.1: Description | 113 |
| 5.5.2.2: Defining characteristic | 113 |
| 5.5.2.3: Tequixquiac mud deposits | 113 |
| 5.5.3: Facies 13 (a & b), Silt | 113 |
| 5.5.3.1: Description | 113 |
| 5.5.3.2: Defining characteristics | 113 |
| 5.5.3.3: Tequixquiac silt deposits | 115 |

| | |
|---|-----|
| 5.5.4: Facies 14(a-d), Sand | 115 |
| 5.5.4.1: Description | 115 |
| 5.5.4.2: Defining characteristics | 116 |
| 5.5.4.3: Tequixquiac sand deposits | 117 |
| 5.5.5: Gravels Facies 15 – Facies 17 | 119 |
| 5.5.5.1: Description | 120 |
| 5.5.5.2: Tequixquiac gravel deposits | 120 |
| 5.6: Facies 18 a - d, Volcanic tephra deposits | 121 |
| 5.6.1 Tequixquiac volcanic tephra deposits | 121 |
| 5.7: Facies 19, Calcrete | 121 |
| 5.7.1: Pedogenic calcrete facies found in the Tequixquiac Basin | 121 |
| 5.7.2: Groundwater calcrete facies found in the Tequixquiac Basin | 127 |
| 5.7.3: Calcite cements | 127 |
| 5.7.3.1: Sparry calcite cements | 132 |
| 5.7.3.2: Drusy calcite cement | 132 |
| 5.7.4: Non-carbonate evaporitic deposits | 132 |
| 5.8: Conclusion | 132 |
| Chapter 6: Tequixquiac Basin Stratigraphy | |
| 6.1: Introduction. | 133 |
| 6.2: Barranca el Pocito, Site TB14 | 133 |
| 6.2.1: Geomorphology, Site TB14 | 133 |
| 6.2.2: Sedimentological description, Log 1, Site TB14 | 133 |
| 6.2.3: Interpretation, Log 1, Site TB14 | 137 |
| 6.3: San Mateo Hill, Site TB17 | 137 |
| 6.3.1: Geomorphology, Site TB17 | 137 |
| 6.3.2: Sedimentological description, Site TB17 | 142 |
| 6.3.2.1: Logs 1 and 2, Site TB17 | 142 |

| | |
|--|------------|
| 6.3.2.2: Log 3, Site TB17 | 142 |
| 6.3.3: $^{40}\text{Ar}/^{39}\text{Ar}$ age, tephra Facies 18d, Site TB17 | 143 |
| 6.3.4: Interpretation, Logs 1 - 2, Site TB17 | 144 |
| 6.3.4.1: Logs 1 & 2, Site TB17 | 144 |
| 6.3.4.2: Interpretation, Log 3, Site TB17 | 147 |
| 6.4: San Jose Hill | 148 |
| 6.5: Barranca del Muerto, Site TB10 | 148 |
| 6.5.1: Geomorphology, Site TB10 | 150 |
| 6.5.2: Sedimentological description, Site TB10 | 150 |
| 6.5.2.1: Log 1, Site TB10 | 150 |
| 6.5.2.2: Log 2, Site TB10 | 156 |
| 6.5.2.3: Logs 3 and 4, Site TB10 | 157 |
| 6.5.4: Radiocarbon dating, Site TB10 | 157 |
| 6.5.5: Interpretation, Site TB10 | 158 |
| 6.5.5.1: Log 1, Site TB10 | 158 |
| 6.5.5.2: Log 2, Site TB10 | 160 |
| 6.5.5.3: Logs 3 and 4, Site TB10 | 162 |
| 6.6: Barranca de Colores, Site TB9 | 163 |
| 6.6.1: Geomorphology, Site TB9 | 165 |
| 6.6.2: Sedimentological descriptions, Site TB9 | 166 |
| 6.6.2.1: Log 1, Site TB9 | 166 |
| 6.6.2.2: Log 2, Site TB9 | 166 |
| 6.6.2.3: Log 3, Site TB9 | 177 |
| 6.6.2.4: Log 4, Site TB9 | 179 |
| 6.6.2.5: Log 5, Site TB9 | 179 |
| 6.6.3: Soft-sediment deformation features, Site TB9 | 179 |
| 6.6.4: Sediment geochemistry, Logs 1 & 2, Site TB9 | 180 |
| 6.6.4.1: Log 1, Combined geochemical results, Site TB9 | 180 |

| | |
|--|------------|
| 6.6.4.2: Log 2, Combined geochemical results, Site TB9 | 180 |
| 6.6.5: Dating of the logged sections, Site TB9 | 183 |
| 6.6.5.1: Radiocarbon ages | 183 |
| 6.6.5.2: $^{40}\text{Ar}/^{39}\text{Ar}$ ages | 183 |
| 6.6.5.3: U -Series ages | 185 |
| 6.6.6: Combined seismological and geochemical Interpretation, Log 1, Site TB9 | 186 |
| 6.6.6.1: Green mud and mixed carbonate-clastic beds Zones 1 – 5 | 186 |
| 6.6.6.2: Red mud, silt, sand and mixed carbonate-clastic Zones 1 – 5 | 187 |
| 6.6.6.3: Calc-mudstone and muddy micrite beds: Zones 1 – 6 | 187 |
| 6.6.8.4: Mud, silt, sand and carbonate and mixed carbonate-clastic: Zones 7 – 10 | 188 |
| 6.6.7: Combined sedimentological and geochemical Interpretation, Log 2, Site TB9 | 189 |
| 6.6.7.1: Massive to faintly laminated calc-mudstone sediments (Facies 3a & 3b) | 190 |
| 6.6.7.2: Pisolitic limestones (Facies 5) | 190 |
| 6.6.7.3: Peloidal limestones (Facies 4) | 191 |
| 6.6.7.4: Framestone deposits (Facies 1) | 191 |
| 6.6.7.5: Stromatolitic deposits (Facies 2) | 191 |
| 6.6.7.6: Mixed carbonate-clastic (Facies 8 – 10) | 192 |
| 6.6.7.7: Intraclastic beds (Facies 6 - 15) | 192 |
| 6.6.7.8: Paleosol deposits | 193 |
| 6.6.7.9: Tephra deposits | 193 |
| 6.6.8: Equilibrium $\delta^{18}\text{O}$ carbonate precipitation, Logs 1 & 2, Site TB9 | 193 |
| 6.6.9: Interpretation, Logs 4 and 5, Site TB9 | 194 |
| 6.6.9.1: Log 4, Site TB9 | 194 |
| 6.6.9.2: Log 5, Site TB9 | 194 |
| 6.6.10; Summary and conclusion | 194 |

Chapter Seven: Tephra geochemistry

| | |
|--------------------------|------------|
| 7.1: Introduction | 195 |
|--------------------------|------------|

| | |
|---|------------|
| 7.2: Regional Volcanic setting | 195 |
| 7.3: Previous work on tephra deposits associated with north-eastern Central Mexico | 197 |
| 7.3.1: Mafic tephtras | 197 |
| 7.3.2: Felsic tephtras | 197 |
| 7.4: Results and interpretation | 198 |
| 7.4.1: Basaltic-andesite (TEQ 4) | 198 |
| 7.4.2: Andesitic tephra layer (TEQ1) | 203 |
| 7.4.3: Dacitic tephra Layers | 204 |
| 7.5: Summary | 206 |
| Chapter Eight: Discussion | |
| 7.4: Introduction | 207 |
| 8.2: Tequixquiac Basin Quaternary stratigraphy | 207 |
| 8.2.1: The Lower Colores Formation, > MIS 12c, Interval 1, Facies group 1 | 207 |
| 8.2.1.1: Lacustrine to wetland environments, Facies Group 1:1 | 207 |
| 8.2.1.2: Lacustrine to playa environments, Facies Groups 1:2 | 208 |
| 8.2.1.3: Lacustrine limestone interbeds, Facies Group 1:3 | 208 |
| 8.2.1.4: Geographical distribution, Facies Group 1 | 209 |
| 8.2.1.5: Age, Facies Group 1 | 209 |
| 8.2.2: Mid Colores Formation, > MIS 12c, Interval 2, Facies group 2 | 209 |
| 8.2.2.1: Shallow lacustrine marsh, mud-flat and playa environments, Facies Group 2:1 | 210 |
| 8.2.2.2: Tephra, Facies Group 2:2 | 210 |
| 8.2.2.3: Geographical distribution, Facies Group 2 | 211 |
| 8.2.2.4: Age, Facies Group 2 | 211 |
| 8.2.3 San Mateo Formation, MIS 14d, Interval 3, Facies Group 3 | 211 |
| 8.2.3.1: Fluvial and alluvial environments, Facies Group 3:1 | 211 |
| 8.2.3.2: Tephra, Facies Group 3:2 | 212 |

| | |
|---|------------|
| 8.2.3.3: Geographical distribution, Facies Group 3 | 212 |
| 8.2.3.4: Age, Facies Group 3 | 213 |
| 8.2.4: Upper Colores Formation, MIS 12c – MIS 11, Interval 4, Facies Group 4 | 213 |
| 8.2.4.1: Fluvial-lacustrine to marsh environments, Facies Group 4:1 | 213 |
| 8.2.4.2: Tephra layers, Facies Group 4:2 and 4:3 | 214 |
| 8.2.4.3: Geographic distribution, Facies Group 4 | 214 |
| 8.2.4.4: Age, Facies Group 4 | 215 |
| 8.2.5: Quaternary fluvial and alluvial deposits, <MIS 3, Interval 5, Facies Group 5 | 215 |
| 8.2.5.1: Fluvial and alluvial depositional environments, Facies Group 5 | 215 |
| 8.2.5.2: Geographic distribution, Facies Group 5 | 216 |
| 8.2.5.3: Fossils, Facies Group 5 | 216 |
| 8.2.5.4: Age, Facies Group 5 | 216 |
| 8.3: Paleogeographic and palaeoenvironmental evolution of the study area | 231 |
| 8.3.1: Basin formation and subsidence | 231 |
| 8.3.2: Interval 1, > MIS 12c, Perennial lacustrine environments, Facies Group 1 | 235 |
| 8.3.3: Interval 2, > MIS 12c, Playa to mud-flat/marsh environments, Facies Group 2 | 237 |
| 8.3.4: Interval 3, MIS 14 d, Alluvial - fluvial environments, Facies Group 3 | 238 |
| 8.3.5: Interval 4, < MIS 12c, Fluvio-lacustrine environments, Facies Group 4 | 238 |
| 8.3.6: Interval 5, < MIS 3 Alluvial – fluvial environments, Facies Group 5 | 239 |
| 8.6: Conclusion | 240 |
| Chapter Nine: Conclusions | |
| 9.1: Original thesis aims and outcomes of research | 241 |
| 9.2: Limitations | 243 |
| 9.3: Future work | 243 |
| 9.4: Conclusions | 244 |
| References | 245 |

Appendix 1: Calibrated chronology for Mexico

Appendix 2: Mansell Colour chart

Appendix 3: San Mateo Hill (Site TB17) logs

Appendix 4: Barranca de Colores (Site TB9), Arroyo Salado de Hueyoptla (Site TB12), Tlapanaloya (Site TB13), Barranca la Gloria (Site TB7)

Appendix 5: Cattle Shed (Site TB15)

Appendix 6: The mound and Presa Xocoyotl (Sites TB6 & TB3)

Appendix 7: Loma Bonita (Site TB11), Apaxco Football field (Site TB8) and Apaxco Quarry (Site TB18)

Appendix 8: Barranca Acatlan (Sites TB1), Tajo de Tequixquiac (Site TB2), Barranca El Salto (TB4), Barranca la Macura (Site TB5), Barranca la Botica (Site TB6)

Appendix 9: Chronology for the study area

Appendix 10: Modern ground and surface water geochemistry

Appendix 11: Sediment geochemistry (Sites TB9 & TB12)

List figures

Page

- | | | |
|-----|--|----|
| 1.1 | A: Central eastern Mexico (Ypsilon, 2015). B: The location of the studied area (red box) in Central-eastern Mexico (blue box) and the TMVB (Volcanic Belt) (after Gómez-Tuena et al. 2007). C: Detail of the Basin of Mexico(after Cross et al. 2012). Study area, Tequixuac Basin, within the red square. | 2 |
| 1.2 | The Basin of Mexico and Tequixquiac Basin hydrology and drainage (modified after Fox, 1965). For the location of Figure 1.2 within Central Mexico, see Figure 1.1. Also see Fig 1.4a, c & d for Gran Canal Desagüa Figure 1.4b. | 3 |
| 1.3 | Average annual rainfall values (mm) from Tequixquiac in the North to Mexico City in the Southern Basin of Mexico (rainfall data are taken from Lamb et al. 2006; Parsons et al., 2008). For the location, see Figure 1.1. | 6 |
| 1.4 | Gran del Canal Desagüe Tunnel exit (Tajo de Tequixquiac) in Barranca Acatlan (www.es.wikipedia.org/tequixquiac). B: El Sacro on display at the: National Museum of Anthropology, Mexico City, 2012. C: Megafaunal bones in the Barrera family museum at San Jose, Tequixquiac D: The second published illustration of El Sacro published (Bárcena, 1882). | 8 |
| 2.1 | Climatology of the North American tropics and sub-tropics regions located within the North American Monsoon region today a) summer b) winter. (from Metcalfe et al. 2015). | 10 |

- 2.2 **Figure 2.2: a:** Simplified map of the fault-controlled sedimentary basins, lake systems, neotectonic fault systems and active (in some cases inactive) volcanoes that transect E-W and NNW-SSE across Central Mexico (from: Johnson & Harrison, 1990; Ferrari et al, 2000; Alaniz & Nieto, 2007; Ferrari et al, 2012). TLPFS – Tenango – La Pera fault system; TCFS – Tepic Chapala fault system; COFS – Chapala Oaxaca fault system; CTFS – Chapala Tula fault system; TQFS – Taxco Queretaro fault system; MAFS – Morelia Acambay fault system; MAFS – Morelia Acambay fault system; C1 - Donguinyó-Huichapan; C2 - Aocolulco caldera. TEQ – Tequixquiac. **b:** Basin of Mexico, Including the pre-1700's lake shoreline and the positioning and extent of the lakes, (Chalco, Xochimilco, Texcoco, Xaltocan and Zumpango), before the major artificial drainage began. ✱ - Study area. 13
- 2.3 Simplified expression of the present volcanic arch, the Trans Mexican Volcanic Belt (TMVB) and Sierra Madre Occidental (SMO) which was the Mexican volcanic arch before the transition during the mid-Miocene. The TMVB represents the most recent episode of magmatic activity that has occurred in stages since the Jurassic Period (Ferrari et al. 2012). Also, see Figure 2.4. 14
- 2.4 Contemporary climatology of Mexico (NAM region) (from Metcalfe et al. 2015). The movement of low-level moisture flows (LLF) moving north from the Gulf of Mexico and the Gulf of California which is blocked to the west and east by the Sierra Madre Occidental (see Fig 2.4) and Sierra Madre Oriental mountain ranges respectively. The movements of the mid-latitude Flow or mid-latitude Westerly depression (MLF). The northward movement of the ITCZ (NH Summer) drives tropical moisture. Tropical moisture is limited by the North Pacific (NP) and the Bermuda High (BH) high-pressure systems. Mid-level moisture from the Gulf of Mexico supplies much of the summer precipitation in Mexico and across the NAM region. The loop current is the primary surface-ocean current in the Gulf of Mexico that transports warm waters from the Caribbean Sea through the Yucatan Strait into the Gulf of Mexico (From Metcalfe et al. 2015). 15
- 2.5 Sedimentary basins and topographic change east-west along the TMVB. Approximate altitude to illustrate change. 17
- 2.6 Synthesis of Quaternary records from the Basin of Mexico. (Bradbury, 1971; Gonzalez & Fuenteo, 1980; Heine, 1984; Bradbury, 1989; White, 1986; Lozano 1986; Lozano et al. 1993; Lozano & Ortega, 1994; Lozano, 1996; Bradbury, 1997, 1998; Caballero, 1997; Caballero & Ortega, 1998; Ortega & Newton, 1998; Lozano & Ortega, 1998; Caballero et al. 1999; Ortega, 2000; Gonzalez et al. 2001; Sedov et al. 2001; Nordt et al. 2002; Vázquez & Heine, 2004; Solleiro et al. 2006; Marcías, 2007; Lamb et al. 2009; Roy et al. 2009; Caballero et al. 2010; Sedov et al. 2010; Vázquez & Heine, 2011; In Ehlers et al. 2011; Roy et al. 2012; Cantarero, 2013; Lozano et al. 2015; Torres-Rodríguez et al. 2015; Siebe et al. 2017. * H: Hueyatlaco glaciation. M: Milpulco glaciation. Number s 1 – 9 correspond to the figure key above. * The numbers at the top and bottom of the columns correspond to the number in the key below. Roman numerals indicate interval numbers related to each lake system. 23
- 2.7 Mexican Quaternary environmental records from the NAM region (from Metcalfe et al. 2015). The figure highlights the uneven distribution of terrestrial records that predominantly come from the central and northern regions. Site 50: Babicora as referenced to in the text. For site names and references, see Metcalfe et al. (2015) and Appendix 1, Table 6. The red cross indicates the approximate location of the studies area. 26

| | | |
|-----|--|----|
| 2.8 | 2.8 Summary of Mexico's recorded Quaternary Environmental History. Northern Mexico (Metcalfe et al, 2002; Metcalfe et al. 2000, 2015; Metcalfe, 2006; Felstead, 2012): Western Central Mexico , predominantly Lakes Cuitzeo (Israde et al. 2002) and Pátzcuaro (Metcalfe et al. 2002, 2015; Metcalfe, 2006): Eastern Central Mexico records mainly from the south and central Basin of Mexico (Bradbury, 1971; Gonzalez & Fuenteo, 1980; Heine, 1984; Bradbury, 1989; White, 1986; Lozano 1986; Lozano et al. 1993; Lozano & Ortega, 1994; Lozano, 1996; Bradbury, 1997, 1998; Caballero, 1997; Caballero & Ortega, 1998; Ortega & Newton, 1998; Lozano & Ortega, 1998; Caballero et al. 1999; Ortega, 2000; Gonzalez et al. 2001; Sedov et al. 2001; Nordt et al. 2002; Vázquez & Heine, 2004; Solleríro et al. 2006; Marcías, 2007; Lamb et al. 2009; Roy et al. 2009; Caballero et al. 2010; Sedov et al. 2010; Vázquez & Heine, 2011; In Ehlers et al. 2011; Roy et al. 2012; Cantarero, 2013; Lozano et al. 2015; Torres-Rodríguez et al. 2015; Siebe et al. 2017). General trends across Central Mexico (Metcalfe et al. 2002, 2015; Metcalfe, 2006). Pre-57,000 ca. BP Lake Chalco (Lozano et al. 2015; Torres-Rodríguez et al. 2015); Southern Mexico, Yucatán (Metcalfe et al. 2002, 2015; Metcalfe, 2006). Numbers at the top of columns correspond to the key numbers below. SL: sea level, H: Hueyatenco glaciation. M: Milpulco glaciation, N1: Nexcoalango glaciation. | 28 |
| 3.1 | Google image of the study area, The Tequiquiac Basin, the dashed blue line indicates the limits of the basin | 38 |
| 3.2 | Simplified expression of the key crustal blocks and terranes that make-up Mexico (modified from Dickinson & Lawton, 2009). The Trans Mexican Volcanic Belt represents the most recent episode of long-running and continual magmatic activity occurring in stages since the Jurassic Period (Ferrari et al. 2012). SMO: Sierra Madre Occidental. SMOR: Sierra Madre Oriental. | 42 |
| 3.3 | Geological map of the study area (Sub-section of the geological map taken from Segerstrom, 1952, 1956, 1962) | 45 |
| 3.4 | The Tarango Formation, over 150 m of exposed lacustrine muds, tephra and limestones that were exposed when the drainage channel was cut through San Mateo Hill (Site TB17) for the Nochistongo in the southwestern study area (see Chapter 6) (image is taken from Segerstrom, 1962). | 46 |
| 4.1 | Conceptual model of the degree of a continuum between different terrestrial carbonate depositional environments (modified after Brasier, 2011). See section 4.4.8 | 58 |
| 4.2 | Bench and ramp lake margin facies models for partially and dominantly carbonate lakes that are surface fed (from Platt & Wright, 1992. In: Gierlowski-Kordesch, 2010). See Table 4.11 for full facies description. | 63 |
| 4.3 | Transitional pedogenic – palustrine – lacustrine facies associations. Calcrete (1 – 3); palustrine carbonates (4 – 8), from the less developed (4) to more mature deposits (8); and none pedogenically altered lacustrine carbonates (9) (from Alonzo-Zarza, 2003; Alonzo-Zarza & Wright, 2010b). Facies in 1 – 3 are described in Figure 4.4 and Table 4.16. 5 – 8 facies codes are defined in Tables 4.12 and 4.13. Facies 9 is described in Table 4.10. | 66 |
| 4.4 | Idealised pedogenic calcrete profile development based on Manchette, (1985) after Esteban & Klappa, (1983) and Alonso-Zarza & Wright, (2010b). | 67 |
| 4.5 | The hydrological cycle, including fluxes for meteoric water between the oceans, atmosphere, terrestrial land surface and the ice caps expressed in m ³ /yr (modified after Sharp, 2007). The behaviour of the stable isotopes of deuterium and oxygen within the water cycle, during the | 69 |

| | | |
|------|---|----|
| | flux of meteoric waters between phase changes and different water stores and, the effects of temperature, altitude and continentality are also shown (adapted after, Brasier, pers comm, 2011). | |
| 4.6 | Main regional-scale environmental factors which affect the $\delta^{18}\text{O}$ and $\delta^{13}\text{C}$ of microbial carbonates (from Andrews et al. 1997). | 70 |
| 4.7 | Carbon isotope values of carbon sources into lakes resulting in $\delta^{13}\text{C}$ TDIC (Total dissolved inorganic carbon) from Leng and Marsahll (2004). | 70 |
| 4.8 | AMS Radiocarbon dated sample images, the image number, is related to sample numbers see Appendix 9, Table 2 and Chapters 6 & 8. Samples 6 (Site TB1) and 9 (Site TB3) are aquatic species, and samples 7 (Site TB10, Log 4) and 8 (Site TB9, Log 5) are land species. | 78 |
| 4.9 | Modern analogue conditions for fluvial and marsh environments and organic carbon sources in clastic sediments. Barranca La Macura (Site TB5). | 79 |
| 4.10 | A: Facies 18d (Table 5.23) medium light grey coarse ash to lapilli from San Mateo Hill (SMH, Site TB17). B: Facies 18c (Table 5.23) white fine dacitic sandy ash, from Barranca de Colores (BC, Site TB9). | 80 |
| 5.1 | Grain size classification used by this research for carbonate and clastic rocks (from Miall, 2016). | 85 |
| 5.2 | Example of framestone facies form Site TB9 a) Bed 19, Barranca de Colores (BDC) sample BDC T2 (see Chapter 6, Fig 6.33, and Appendix 4, Table). See Table 5.6 for bed descriptions. | 88 |
| 5.3 | Examples of a) Microdetrital limestone (Bed 2), Framestone limestone (bed 1) (Bed 5, sample ASH T7) b) Framestone limestone (sample ASH T7). c) The upper surface of sample ASH T7 (bed 2 a & b) in-situ before collection (see Table 5.7 for bed descriptions). d) section above sample ASH T7, Log 2 (samples ASH T8 to T10). Sample and images are from site TB12, Log 2 (Appendix 4, Table 6). | 90 |
| 5.4 | Example of stromatolitic limestone from the study area. Site TB12, Log 2, Bed 5, corresponding to sample ASH T11 (Appendix 4, Table 6). See Table 5.8 for bed descriptions. | 92 |
| 5.5 | Field examples of stromatolitic limestone from the study area a: Facies 2a, Greyish pink (5R 8/2) stromatolitic limestone with peloidal beds Site TB12, Log 2, Bed 5 (see Appendix A4, Table 6). Hand sample collected from the bed is shown in Figure 5.4 and bed descriptions are given in Table 5.8. b: Facies 2b, Greyish yellow green (5GY 7/2) agglutinated (?) stromatolitic limestone. Site TB9, Log 2, Bed 1, BDC T32 (see Appendix 4, Table 2 and Chapter 6, Fig 6.33). c & d: Barranca la Botica (Figs 8.1 & 8.9) fluvial tufa? (see Table 4.8) lining the bottom of the barranca (Site TB6). | 94 |
| 5.6 | Example of calc-mudstone from the study area, site TB9, Log 2, Bed 16, BDC T5 (see Appendix 4, Table 2, and Chapter 6). For bed descriptions, see Table 5.10. | 96 |
| 5.7 | Example of calc-mudstone from the study area, sparse biogenic calc-mudstone, with shell (enlarged). Sample from site TB12, Log 2, Bed 4, sample ASH T7 (Appendix 4, Table 6). See Figure 5.3 also which shows the other half of this cut hand sample and Table 5.7 for bed descriptions. | 96 |

| | | |
|------|---|-----|
| 5.8 | Example of calc-mudstone from the study area. White (N9) to very light grey (N8) biogenic calc-mudstone. Calc-mudstone with scattered bioturbation burrows (<1 mm in diameter), and organic detritus that are represented as void spaces with sparry calcite fill. The upper bed (5 mm) is medium grey (N5) and has desiccation features and manganese clusters. The upper right-hand side of the sample has a large (6 mm in diameter) root trace filled with drusy cement. Sample from Site TB13, Log 1, Bed 8 TLAP (Tlapanaloya) T31 (see Appendix 4, Table 7). | 97 |
| 5.9 | Example of pisolitic (brecciated) limestone from the study area. Sample from site TB9, Log 2, Bed 19, BDC T3 (Appendix 4, Table 2 and Fig 6.33). See Table 5.12 for bed descriptions. | 98 |
| 5.10 | Example of pisolitic (brecciated) limestone from the study area. Sample from site TB9, Log 2, Bed 19, BDC T3 (Appendix 4, Table 2 and Fig 6.33). See Table 5.12 for bed descriptions. | 100 |
| 5.11 | Example of intraclastic limestone from the study area. Sample is from site TB13 Log 2, Bed 15, TLAP T16 (Appendix 4, Table 7). See Table 5.13 for bed descriptions. | 101 |
| 5.12 | Example of laminated limestone despoths and associated facies from the study area. Site TB12, Log 2, Bed 5, ASH T8 (see Appendix 4, Table 6). See Table 5.14 for bed descriptions. | 103 |
| 5.13 | Barranca de Colores site showing a field example of interbedded and laminated (1) Greyish yellow green (5GY 7/2) and moderate pink (5R 7/4) mud; Pale, greenish yellow (10Y 8/2) fine sand; Yellowish, grey (5Y 8/1) and white (N9) calc-mud; (2) Greyish yellow green (5GY 7/2) and moderate pink (5R 7/4) micritic mud; White (N9), yellowish grey (5Y 8/1) and moderate pink (5R 7/4) muddy micrite. All the above can be poorly lithified, massive or vertically jointed. Site TB9, Logs 1 and 2 (see Appendix 4, Tables 1 & 2 and Chapter 6 Figs 6.26 – 6.34). | 104 |
| 5.14 | Example of laminated limestone deposits from the study area. Greyish pink (5R 8/2), laminated muddy micrite. Site TB12, Log 2, Bed 3, sample ASH T3 (see Appendix 4, Tables 5 & 6). | 104 |
| 5.15 | Mixed carbonate and siliciclastic sediment deposit classification used by this PhD research (after Mount, 1985). | 107 |
| 5.16 | Example of muddy micrite from the study area and associated facies. Bed descriptions are given in Table 5.16. Sample from site TB12, Log 2, Bed 3, ASH T4. (See Appendix 4, Table 6). | 108 |
| 5.17 | Example of intraclastic muddy micritic and associated, Sample from site TB12, Log 3, ASH T5, Bed 3 (See Appendix 4, Table 6). Bed description is given in Table 5.17. | 109 |
| 5.18 | Example of intraclastic fine sandy micritic and associated facies, site TB13, Log 2, Bed 6, TLAP L2 (Appendix 4, Table 7). Bed description is given in Table 5.18. | 110 |
| 5.19 | Example of micritic mud deposits and associated facies from the study area. Site TB9, Log 2, Bed13, BDC T10 (see Appendix 4, Table 2 and Chapter 6, Fig 6.33). | 111 |
| 5.20 | Field examples of laterally discontinuous, mixed carbonate and clastic sediments. 1: Moderate red (5R 5/4) muddy micrite (L28) . Laterally continuous, blocky in appearance and the bed, before desiccation, had horizontal to wavy, very fine lamination. Along brecciated jointing fractures secondary white (N9) silt (micrite) in-fill has occurred. Bed 2: Yellowish grey (5Y 8/1) clay (L27) . Very blocky in appearance and the bed, before desiccation, had horizontal to wavy, very fine lamination and trough-cross bedding. Bed 3: Moderate red (5R 5/4) muddy gravel (L24-L27) . Bed contains sub-angular to sub-rounded mud and muddy micrite | 112 |

| | | |
|------|---|-----|
| | lithoclasts < 5 mm – 0.40 m in diameter. Limestone gravel with sub-angular to sub-rounded clayey silt balls and rip-up clasts < 0.20 m in diameter. Bed 2: Yellowish grey (5Y 8/1) clay (L27) . Very blocky in appearance and the bed, before desiccation, had horizontal to wavy, very fine lamination. Bed 4: Moderate red (5R 5/4) gravel . Gravel contains a relatively high proportion of volcanoclastics (10%) and angular, greyish pink (5R 8/2) rip-up clasts (<5 mm in diameter). Site TB10, Barranca del Muerto, the upper contact of Log 1 overlain by Log 3 (Figs 6.15, 6.16a & b, 6.18, 6.19). | |
| 5.21 | Field example of mixed clastic and carbonate deposits from Site TB9. 1, Log 1. 2: Gravels , Log 5 cutting Log 1. (see Appendix 4, Tables 1, & 4 and Chapter 6). | 115 |
| 5.22 | Field examples of clay, silt and sand beds from the study area. Site TB2, Log 3, Beds 1, 2, 3 and 4 (see Appendix 8, Table 15). | 116 |
| 5.23 | Field examples of silt and angular-rounded gravels (Facies 17). Massive organic silt, Bed 9. Massive silt with erosional scours, Bed 8. Weakly bedded pebble to cobble angular to rounded gravel (Facies 17), Bed 6. Site TB1, Log 7 (see Appendix 8, Table 12). | 117 |
| 5.24 | Field examples of silt, sand and gravel deposits from the study area. Extraformational, massive, fine to medium sand fine pebble, polymictic gravel (Bed 1 base of section). Composite bed sets of tabular cross-bedded coarse sand and upper wave-rippled to plane cross-bedded and trough cross-bedded medium sand (Bed 2 of log). Example from site TB1, Log 1 (see Appendix 8, Table 6). | 118 |
| 5.25 | Field example of Facies 15, massive gravel. Site TB1, Logs 5 & 6 (see Appendix 8, Tables 10 & 11). | 119 |
| 5.26 | Field examples of Facies 16, massive matrix supported gravel (Facies 16). Site TB10, Log 3. | 120 |
| 5.27 | Field example of poorly sorted, matrix-supported angular-rounded gravel (Facies 17). Site TB5, Log 7. | 121 |
| 5.28 | Field example of Fine light grey (N7) ash interbedded with coarse sand sheets (CGwsh?). Site TB15 (see Chapter 6 and Appendix 5, Table 1) | 126 |
| 5.29 | Field example of pedogenic root-nodules. Site TB16, Log 1, bed 1 (see Appendix 6, Table 1 and Chapter 6). | 128 |
| 5.30 | Field example of soft nodular groundwater calcrete horizon that join to form thin (<5 mm) lamina in places. Site TB9, Log 1, bed 19 1 (see Appendix 4, Table 1 and Chapter 6). Arrows indicate examples. | 128 |
| 5.31 | Field example of coarse sand sheets containing sandy calcified horizons that transect stratigraphic boundaries (CGwsh?) (<15 mm). Site TB17, Log 1, bed 4 (see Appendix 3, Table 1 and Chapter 6). Arrows indicate examples. | 129 |
| 6.1 | TB14, Barranca el Pocito and Site TB17, San Mateo Hill. a) The green dashed line indicates the general location of the studied sites. b) Location of stratigraphic logs. L = Log. See also Figures 8.1 & 8.6. | 134 |
| 6.2 | Location map for Site TB14 and Site TB17. Source, Google Earth. Popo: Popocatepetl volcano. B. Acatlan = Barranca Acatlan. | 135 |

| | | |
|------|--|-----|
| 6.3 | Site TB14, Log 1. See Figure 6.4 for stratigraphic log (see Figs 6.1, 6.2, 6.3, 8.1 and 8.9). | 135 |
| 6.4 | Site TB14, Log 1. See Figure 6.3 for a photograph of the logged site. See also Figures 8.1, 8.3, 8.11 & 8.12. | 136 |
| 6.5 | Site TB17. a) Log 1 (see Figs 6.1, 6.2, 6.8, 8.1 and Appendix 3, Table 1). b) Nodule. Bed 2 (Fig 6.8). c) Carbonate nodules in-situ Bed 2 (Fig 6.8). d) Sandy carbonate layer (Facies 19d). Upper bed 4 (Fig 6.8). | 138 |
| 6.6 | Site TB1, Log 2 (see Figs 6.1, 6.2, 8.1). a): Upper section of a composite sequence. b): Lower section of composite log. Log locations indicated by grey arrows. See Figure 6.4. For the stratigraphic log. c): 19 b & c: Pedogenic calcrete horizon. See Figure 6.9 for the stratigraphic log. | 139 |
| 6.7 | Site TB17 a): Log 3, Barranca (see Figs 6.1 & 6.2). White lines indicate Log 1 location, is a composite section, see Figure 6.11 for the stratigraphic log. b): Southern wall of the barranca were interbedding of Facies 3a can be seen. | 140 |
| 6.8 | TB17, Log 1, see Figure 6.5 for a photograph of log site. For a sedimentological description of this sequence, see Appendix 3, Table 1. See Figure 6.5 a, b & c for Bed 2 and Figure 6.5 d for Bed 4. See also Figures 8.1, 8.5, 8.10. The blue triangle indicates the area highlighted in Figure 6.5 b & c. | 141 |
| 6.9 | TB17, Log 2, composite log. See Figure 6.6 for photographs of logged sections. The sedimentological description is given in Appendix 3, Table 2. See Figure 6.6a for Beds 6, 7 & 8 and 6.6 b & c for Beds 1 – 6. See also Figures 8.1 & 8.5. | 143 |
| 6.10 | Fence diagram, Site TB17, Logs 2 & 1. See also Figures 8.1, 8.5, 8.9 & 8.10 | 144 |
| 6.11 | TB17, Log 3, San Mate, composite log. Lower and upper and lower portions shown in Figure 6.7. Sedimentological descriptions are given in Appendix 3, Table 3. See also Figs 8.1, 8.3, 8.9, 8.11 & 8.12 | 145 |
| 6.12 | Ar/Ar dating of volcanic ash at San Mateo Hill: Inverse Isochron for Facies 18d (tephra sample SMH). The x-axis plots the $^{39}\text{Ar}/^{40}\text{Ar}$ ratios and $^{36}\text{Ar}/^{40}\text{Ar}$ ratios of the individual heating steps. The best line fit through the data set gives the trapped $^{40}\text{Ar}/^{36}\text{Ar}$ values from the y-intercept and the $^{40}\text{Ar} / ^{39}\text{Ar}$ age value from the x-intercept (McIntosh et al. 2015). Left graph: Age probability spectrum for Facies 18d (tephra sample SMH). Data at 1 – sigma and results at 1 – sigma. | 146 |
| 6.13 | Location map for Sites TB1 Agua Negra, TB3 The Mound, TB4 El Salto, TB7 Barranca la Gloria, TB9 Barranca de Colores, TB10 Barranca del Muerto, TB12 Arroyo Salado de Hueypoxtla, TB13 Tlapanaloya. a) The green dashed line indicates the general location of the studied sites. b) Indicates the location of the studies sites. L = Log. See Figure 8.1 & 8.9 for the location of all logged sites and study area. | 149 |
| 6.14 | Location map, Sites TB9 and TB10. Log sites indicated. Source, Google Earth. See also Figure 8.1. | 150 |
| 6.15 | Site TB10. a) Log 4, b) Logs 1 & 2. Photograph was taken looking west, close to the head of the barranca. Also see Figure 6.13, 6.16 b & c & 8.1. | 151 |
| 6.16 | Site TB10. a) Logs 1 & 2 b) Log 2, see also Figure 6.17b c) Log 3. | 152 |

| | | |
|------|---|-----|
| 6.17 | a) The base of Log 4, terrace one, see Figures 6.15a and 6.22. b) Horse molar found in-situ. The black arrow in the image (a) c) Facies 18b, andesitic tephra. | 153 |
| 6.18 | Log 1, Site TB10. See Figure 6.16 a & b for photographs of logged sequence and Figure 6.19 for the upper section of the sequence (also see Figs 6.13, 8.1 & 8.9). | 154 |
| 6.19 | Log 2, Site TB10. See Figure 6.16 a & b for photographs of logged sequence and Figure 6.18 for the lower section of the sequence (also see Figs 6.13, 8.1 & 8.9). | 155 |
| 6.20 | Log 3, Site TB10. For a photograph of log, see Figure 6.16c. T1: Terrace 1. For the location, see Figures 6.13, 8.1 & 8.9. | 156 |
| 6.21 | Log 4, Site TB10. For images of the log see Figures 6.15a, 6.17 a & b. | 158 |
| 6.22 | Fence diagram for site TB10, Logs 1, 3 and 4. For log site locations, see Figures 6.13, 8.1 and 8.9. | 159 |
| 6.23 | Examples of fossil fauna bones associated with gravels (Figs 6.20 – 6.22), Site TB10. See Table 6.3 for descriptions | 161 |
| 6.24 | Location map for Site TB9, Barranca de Colores and Barranca la Bola. Google Earth image. | 163 |
| 6.25 | Site TB9. a) Log locations at the head of the barranca. b) Log 5 (Fig 6.35) incising the sequence described in Logs 1 & 2 and the position of the dacitic tephra layer below log 5. | 164 |
| 6.26 | a): Site TB9, Logs 1 & 2, see Figure 6.30. c & d): Bed 18, Log 1, Fig 6.30 | 165 |
| 6.27 | View of Site TB9 from the western end of the barranca. Locations of photographs indicated on Fig 6.24. T1 = gravel terrace 1, see Log 5, Figure 6.35. b) Thick beds of unconsolidated clastic material located at the junction between Barrancas de Colores and la Bola | 167 |
| 6.28 | Log 1 lower; Site TB9 Log 1 (Fig 6.29). a) In-situ calc-mudstone interbedded within the unconsolidated clastic and mixed carbonate-clastic beds (for the location of photograph see Fig 6.24, for the stratigraphic sequence see Log 1, Fig 6.29). b) Calc-mudstone sample collected for U-series dating, sample C1 (see Section 6.6.7.3), the photographed bed is equivalent to bed 8, Log 1 (Fig 6.29). | 168 |
| 6.29 | Site TB9, Log 1, lower section (Figs 6.24, 6.25a, 6.26, 6.27a, 6.28, Table 6.4). For a photograph of the logged section, see Figure 6.25a. For U-Series age data see Section 6.6.7.3. ▲ Micromorphological analysis of sample BDC 56 (see Fig 6.36, Bed 6 and Appendix 4, Table 1, Bed 6) | 169 |
| 6.30 | Site TB9, Log 1, upper section (Figs 6.24, 6.25a, & 6.36, Table 6.4). For a photograph of the logged section, see Figure 6.26. | 170 |
| 6.31 | Site TB9, Log 2, logged and sampled limestone section at the head of the barranca (Fig 6.24, 6.25a & 6.36). see Figure 6.33 | 171 |
| 6.32 | Site TB9, field example of the freshly exposed section recorded from the northern end of the limestone sequence logged at the head of the barranca (Fig 6.24). Beds that are indicated in Log 2 (Fig 6.33) can be traced along from the central section (Fig 6.33) to the lateral limits of the sequence where they thin and lens out. Basaltic-andesite (Facies 18a). See Appendix 4, Table 1. | 172 |

| | | |
|------|---|-----|
| 6.33 | Site TB9, Log 2, limestone sequence, (Figs 6.24, 6.25a, 6.27a & 6.31, Table 6.4, Appendix 4, Table 3 and section 6.6.6 onwards. For a photograph of the logged section, see Figure 6.31. | 173 |
| 6.34 | Site TB9, Log 3 (Figs 6.24 & Table 6.4). See Figure 6.39 for an image of the logged section. | 174 |
| 6.35 | Site TB9, Log 4, (Figs 6.24, 6.25b, 6.36, Table 6.4). T1 = Terrace 1. For a photograph of the logged section, see Figure 6.25b. See Section 6.6.6 the details of the ¹⁴ C age. | 175 |
| 6.36 | Barranca de Colores, Site TB9, Fence diagram Logs 1, 2, 3, 4 and 5. See Section 6.6.6 for details of the chronology. | 176 |
| 6.37 | Images of TX89 Mammoth molar collected from gravel, sand and silt deposits like those recorded Logs 5 (Fig 6.35) at Site TB9. See Table 6.5 for descriptions of specimens | 177 |
| 6.38 | a - c) Displaced beds in Barranca de Colores (Site TB9) of beds that correspond to the upper portion of Log 1 located at the southern end of the sequence at the head of the Barranca, the position of Log 3 is also indicated (see Fig 6.24 for location. b) Slumping sediments, basal contacts indicated by the black arrows. These sediments correspond to the top of the lower portion of Log 1. Location of photo indicated on Fig 6.24. | 178 |
| 6.39 | Geochemistry and stratigraphy, Log 1, Site TB9, composite section, 55 m. Beds 1 - 14 lower log (Fig 6.29). Beds 15 – 24 upper log (Fig 6.30). Mineral concentrations, ppm, TOC and TIC % (g), Mg/Ca and Sr/Ca molar concentrations (Appendix 11, Table 1). Facies key, Figs 5.25, 6.29 & 6.30. Z = Zones. Bed numbers on the left-hand side of log. ▲ = Bed 5, Sample BDC L58; Micromorphological analysis (Appendix 4, Table 2) and U-Series age of >500 ka BP, which is beyond the capabilities of the dating method. | 181 |
| 6.40 | Geochemistry and stratigraphy Log 2, Site TB9, 8.5 m. Mineral concentrations, ppm. TOC and TIC % (g). Mg/Ca and Sr/Ca molar concentrations. Facies key Figs 5.25 & 6.33. Z = Zones. Bed numbers on the left-hand side of log.▲= Bed 5, Sample BDC L58; Micromorphological analysis (Appendix 4, Table 2). | 182 |
| 6.41 | Age probability spectrum for the basaltic-andesite tephra layer, Barranca de Colores, Site TB9, Logs 2 & 4 (Figs 6.33, 6.34 & 6.36) Data at 1 – sigma and results at 1 – sigma. | 184 |
| 6.42 | Inverse Isochron for the basaltic-andesite tephra layer barranca de Colores, Site TB9 Logs 2 & 4 (Figs 6.33, 6.34 & 6.36). The x-axis plots the ³⁹ Ar / ⁴⁰ Ar ratios and ³⁶ Ar / ⁴⁰ Ar ratios of the individual heating steps. The best line fit through the data set gives the trapped ⁴⁰ Ar / ³⁶ Ar values from the y-intercept and the ⁴⁰ Ar / ³⁹ Ar age value from the x-intercept (McIntosh et al. 2015). | 185 |
| 7.1 | a) The Trans Mexican Volcanic Belt with the dashed black box: study area from Roy et al. (2012 (see b). b) Roy et al. (2012) study area (see a) and the volcanic structures that lie within that area. The Black arrow represents the location of Roy et al.'s core site. (image was taken Roy et al. 2012 and annotated for this study). | 196 |
| 7.2 | TEQ 4, Barranca de Colores basaltic-andesite tephra layer. Site TB 9, Logs 2 & 4, Figs 6.33 & 6.34. Scale 1:10. See Table 7.3 for beds descriptions. Blue triangle Ar/AR date 405.3 ± 5.1/5.8 ka bp (see Chapter 6) | 200 |
| 7.3 | Average K ₂ O+Na ₂ O vs SiO ₂ (TSA) geochemical data for samples TEQ 1 – 5 and ASH 1 (see Tables 7.4). See Table 7.2 for sedimentological descriptions and sample site details and see | 201 |

Figs 6.13 and 8.1 for a location map of sample sites (Chapter 6). TEQ1; Andesite. TEQ 2, TEQ 3, TEQ 5, ASH 1; Dacite. TEQ 4; Basaltic-andesite.

| | | |
|------|--|-----|
| 7.4 | a & b) Chemical classification diagram of Silica vs total alkalis. c - f) Bivariate plots of silica vs aluminium oxide (c), calcium oxide (d), magnesium oxide (e), and titanium oxide (f). Plotted samples include the tephra layers sampled from the study area (Table 7.2), the bulk chemistry of the surrounding volcanic structures, and the tephra layers sampled from the Pachuca sub-basin (Table 7.1) by Roy et al. (2012). (Data were taken from Roy et al. (2012) and combined with sampled tephra layers from the study area; see Key and Table 7.4 & 7.5) | 202 |
| 7.5 | Example of andesitic coarse to fine ash (TEQ 1, Andesite) collected from Barranca del Muerto, Site TB10, Log 2. Ungulate imprint can be seen on the righthand side photograph. | 203 |
| 7.6 | Total alkali vs Silica (TAS) diagram based on the classification from Le Bas et al. (1986) (In Aguirre-Díaz & López-Martínez, 2009). Main products of the Donguinyó-Huichapan caldera complex and the surrounding volcanic structures see (Fig 7.1). ◊ TEQ 4, Basaltic-Andesite: ◆ TEQ 1, Andesite. | 204 |
| 7.7 | Donguinyó-Huichapan Caldera complex volcanic products. Bivariate plots of silica vs calcium oxide (a), titanium oxide (b) magnesium oxide (e), aluminium oxide (f). Plotted samples include the tephra layers sampled from the study area, the bulk chemistry of the Jiltopec volcanic field (Hu 54 & 50, Hux 28 & 29), Taxbathá andesite (Hue 31), Donguinyó Tuff (Hue 34 & 20-5), and the Nopala andesite (Hux 8 & (jil 42) from Aguirre-Díaz & López-Martínez, (2009), combined with sampled tephra layers from the study area; see Key) | 205 |
| 8.1 | Geological map of the study area and location sites of logged sequences. Modified after Mooser (1975) and Segerstrom, (1956, 1962) to include the results of this PhD Research. Position of SE – NW in Fence diagrams shown in Figures 8.3 – 8.7. | 217 |
| 8.2 | Fence diagram sedimentological/geological key for all the logged sections (Figs 8.3 – 8.7). MIS (Marine isotope stages), odd numbers represent warm interglacial stages, and even numbers represent cold glacial stages (Chapters 5 – 7 and Appendix 3 & 4). | 219 |
| 8.3 | Cross Section 1: A – B, SE – NW | 220 |
| 8.4 | Cross Section 2: C – D, SE – NW | 221 |
| 8.5 | Cross Section 3: E – F, SE – NW | 222 |
| 8.6 | Cross Section 4: G – H, SE – NW | 223 |
| 8.7 | Cross Section 5: I – J, SE – NW | 224 |
| 8.8 | Cross Section 1: K – L, SE – NW | 225 |
| 8.9 | Geological map of the study area and location sites of logged sequences. Modified after Mooser (1975) and Segerstrom, (1956, 1962) to include the results of this PhD Research. Figure also shows SW – NE cross sections. Fence diagrams shown in Figures 8.10 – 8.13). | 226 |
| 8.10 | Cross Section 1: M – N, SW – NE | 227 |
| 8.11 | Cross Section 1: O – P, SW – NE | 228 |
| 8.12 | Cross Section 1: Q – R, SW – NE | 229 |

| | | |
|-------|---|-----|
| 8.13 | Cross Section 1: S – T, SW – NE | 230 |
| 8.14 | A conceptual model for the geological formation of the study area related to extensional deformation and subsidence in the Basin of Mexico. These are 16 NE – SW normal and/or strike-slip faults that form horst and graben structures. Figure adapted from Marín-Córdova et al. (2004) and based on geological studies of the Basin of Mexico by Mooser (1975); Marín-Córdova et al. (1986); De Cserna et al. (1988) and the Mezquital Basin by Suter et al. (2001); Medel & Armienta (2004). All the graben basins orientated NE – SW. Black arrows represent distensive axis and extensional faulting that, to the west of the figure, join Popocatepetl Volcano, the Tequixquiac - Huehuetoca zone, the lowest portion of the Basin of Mexico (central lakes) including Lake Texcoco and the Penón de los Baños zones. To the east, extensional faulting (orientation is NW –SE) joins the Ixmiquilpan (Hidalgo) valley, the Apizaco region of Tlaxcala and the La Malinche Volcano. The blue dashed line represents the watershed of the Basin of Mexico. The proposed half graben indicated for the study area is based on this PhD research and is the proposed working hypothesis of basin formation and evolution for the study area. Not to scale. | 231 |
| 8.15 | Geological key | 232 |
| 8.15a | Interval 1: Facies Group 1, MIS 15 lacustrine environments. An aggregational lacustrine system, climate warm and humid, initial active subsidence followed by sediment loading and reduced accommodation space (Fig 8.16a) | 233 |
| 8.15b | Interval 2: Facies Group 2, MIS 15 - 14 shallow marsh to playa lacustrine environments. Reduced available moisture, likely related to the onset of MIS 13, intermittent subsidence followed by sediment loading (Fig 8.16b). End of interval water body dried. Possible uplift along the southern margin (Fig 8.16b). | 233 |
| 8.15c | Interval 3, Facies Group 3, MIS 14d Fluvial-alluvial environments, possibly with sub-basinal lacustrine environments (Fig 8.16c). End of lacustrine aggregational phase (sediment loading exceeded capacity) and the onset of alluvial-fluvial aggradation, incision and erosion. Localised deformation may have allowed standing water bodies to develop during periods of uplift along the southern margin (Fig 8.16c). | 234 |
| 8.15d | Interval 4, Facies Group 4, MIS 12 & 11, fluvial-lacustrine pool – marsh environments possibly with sub-basinal lacustrine environments. Dry conditions and hydrological change in the study related the MIS 11 interglacial climates, reduced accommodation space and localised deformation and faulting. Alluvial-fluvial aggradation, incision and erosion continue. Potential for 30 m + of incision, deformation and/or uplift to have occurred between interval 3 and interval 4. | 234 |
| 8.15e | Interval 5, Facies Group 5, MIS 3 – 1. Fluvial-Alluvial depositional environments: Changeable late glacial climates related to ITCZ, DO and HE climate anomalies. Alluvial-fluvial aggradation, incision and erosion continue. Potential for 60 m + of incision, deformation and/or uplift to have occurred between interval 4 and interval 5. | 235 |
| 8.16 | Potential tectonic and incisional evolution along of the study area between the Basin of Mexico and the southern hills in the Tequixquiac Basin. Up-lift and/or deformation related to NE – SW oriented normal fault associated with the Cuautitlan horst in the Basin of Mexico (Figs 8.14) likely influenced the study area along its southern margin due to its position immediately north | 236 |

of this end of the horst graben system in the Basin of Mexico. See Fig 8.15 for descriptions of intervals a – e. BA = Barranca Acatlan. RS = Rio Salado. TB = Tequixquiac Basin

| List of tables | Page |
|--|-------------|
| 1.1 Proposed late Quaternary formations that have been identified for the Tequixquiac Basin (Fig 1.2) (Furlong, 1925; Maldonado & Aveleyra, 1949; De Terra, 1949; Hibbard, 1955; Aveleyra, 1965). The older sediments identified in these studies (1 – 4, below) have also been grouped under the heading of the Tarango Formation and number 6 under the heading of Quaternary alluvial deposits (see Chapter 3). | 5 |
| 4.1 Hydrodynamic erosional structures. The description, defined by Boggs, 2006; Nichols, 2009 and Miall, 2016, outlines the criteria used for the identification of similar deposits in the study area. | 53 |
| 4.2 Hydrodynamic depositional structures. The description, defined by Boggs, 2006; Nichols, 2009 and Miall, 2016, outlines the criteria used for the identification of similar deposits in the study area. | 54 |
| 4.3 Syndepositional deformation structures. The description, defined by Boggs, 2006; Nichols, 2009 and Miall, 2016, outlines the criteria used for the identification of similar deposits in the study area. | 55 |
| 4.4 Carbonate grain (allogenic) classification. The description, defined by Flügel (2010) and combined with Tucker & Wright, 1990; Nichols, 2009; Brasier, 2011 outlines the criteria used for the identification of similar deposits in the study area. Also, see Table 4.9. | 56 |
| 4.5 Carbonate grain classification and definitions. Adapted from Flügel (2010) and combined with Tucker & Wright, 1990; Nichols, 2009; Brasier, 2011 for this study. | 57 |
| 4.6 Visual petrographic characteristics of spring, stream and lacustrine (SSL) carbonates and calcretes used for identification (from Brasier, 2011). Alpha refers to the micromorphological features of calcrete discussed in Section 4.4.8. | 57 |
| 4.7 The defining characteristic of tufa and travertine, from Capezzuoli et al. (2014) (main numerical data is taken from Pentecost, 2005; Gandin & Capezzuoli, 2008 and the references within these papers. | 58 |
| 4.8 Fluvial facies model. The description, defined by Miall, 1977; 1996; 2016 and combined with Pedley (2009) and Arenas-Abad et al. 2010, outlines the criteria used for the identification of similar depositional environments in the study area. See also Tables 4.1, 4.2 & 4.3. | 59 |
| 4.9 Architectural elements in fluvial deposits. The description, defined by Miall, (1985), outlines the criteria used for the identification of similar depositional environments in the study area. See Table 4.8. | 61 |
| 4.10 Common carbonate and clastic lacustrine facies, The description defined by Gierlowski-Kordesch, 2010 (and references therein), outlines the criteria used for the identification of similar depositional environments in the study area. | 62 |
| 4.11 Lake margin facies model for partially and dominantly carbonate lakes that develop with a surface input of carbonate. The description, defined by Gierlowski-Kordesch, (2010), outlines | 63 |

| | | |
|------|---|----|
| | the criteria used for the identification of similar deposits in the study area. See also Table 4.10). | |
| 4.12 | Palustrine facies, defined by Alonso-Zarza, 2003 & Alonso-Zarza & Wright, (2010a) and references therein), outlines the criteria used for the identification of similar depositional environments in the study area. | 64 |
| 4.13 | Interchangeable lacustrine, palustrine and fluvial facies defined by Alonso-Zarza, (2003) & Alonso-Zarza & Wright, (2010a) and reference therein, outlines the criteria used for the identification of similar depositional environments in the study area. | 65 |
| 4.14 | Classification of autogenic, freshwater carbonate that displays an organic in-situ framework. Defined by Cipriani et al. (1977), Pedley, (1990 & 1992) and Ford & Pedley, (1996), outlines the criteria used for the identification of similar depositional environments in the study area. | 67 |
| 4.15 | Carbonate depositional models defined by Capezzuoli et al. (2014), outlines the criteria used for the identification of similar marsh depositional environments in the study area. Also, see Tables 4.8 & 4.10. | 67 |
| 4.16 | The six main types of Groundwater calcrete facies (adapted from Alonso-Zarza & Wright, 2010b and references therein). | 68 |
| 5.1 | Codes used for the description of facies | 85 |
| 5.2 | Prefix codes used for the description of grain size | 85 |
| 5.3 | Suffixes used for sedimentary structure description (Tables 4.1, 4.2 & 4.3) | 86 |
| 5.4 | Carbonate and mixed clastic-carbonate bed codes used for description (Tables 4.5 & 4.14, Fig 4.1) | 86 |
| 5.5 | Suffixes used for carbonate and mixed carbonate and clastic sedimentary structures and grains (see Table 4.4 & 4.6) | 87 |
| 5.6 | Example of framestone facies from the study area. Bed descriptions from site TB9, Log 2, sample BDC T2, (see Fig 5.2, Fig 6.33 and Appendix 4, Table 2). | 89 |
| 5.7 | Examples of bed descriptions from site TB12, Log 2, sample ASH T7, (Appendix 4, Table 6). See Figure 5.3 a, b & c images of the beds. | 90 |
| 5.8 | Example of stromatolitic limestone bed descriptions from the study area, site TB12, Log 2, Bed 5, corresponding to sample ASH T11, stromatolitic limestone, (Appendix 4, Table 6). For images of beds, see Figure 5.4. | 93 |
| 5.9 | Summary of the recorded Tequiquiac bio-mediated limestone and carbonate facies formed in-situ | 95 |
| 5.10 | Bed descriptions, calc-mudstone, site TB9, Log 2, Bed 16, BDC T5 (see Appendix 4, Table 2, Chapter 6). For images of beds, see Figure 5.6. | 96 |
| 5.11 | Example of peloidal limestone bed descriptions and associated facies from site TB9, Log 2, Bed 11, BDC T13 (Appendix 4, Table 2 and Chapter 6). See Figure 5.9 for images of the beds. | 98 |

| | | |
|------|--|-----|
| 5.12 | Example of pisolitic limestone bed descriptions from the study area, site TB9, Log 3, Bed 19, BDC T3 (Appendix 4, Table 2 and Fig 6.33). See Figure 5.10 for images of the beds. | 100 |
| 5.13 | Example of bed description of Intraclastic limestone, a sample from site TB13 Log 2, Bed 15, TLAP T13 (see Appendix 4, Table 7). See Figure 5.11 for images of the bed. | 101 |
| 5.14 | Examples of bed descriptions for laminated limestone and associated facies from the study area. Site TB12, Log 2, Bed 5, sample ASH T8 (see Appendix 4, Table 6). See Figure 5.12 for sample images. | 103 |
| 5.15 | Summary of the recorded carbonate grain (allogenic) limestone and carbonate facies | 105 |
| 5.16 | Examples of muddy micrite bed descriptions and associated facies. Site TB12, Log 2, Bed 3, ASH T4, (see Appendix 4, Table 6). See Figure 5.16 (a - e) for images of the beds. | 108 |
| 5.17 | Example of muddy micrite from the study area. Site TB12, Log 2, Bed 3, ASH T5 (See Appendix 4, Table 6). See Figure 5.17 for images of beds. | 109 |
| 5.18 | Example of an intraclastic sandy micrite bed description. Site TB13, Log 2, Bed 6, Sample TLAP L2 (see Appendix 4, Table 7). See Figure 5.18 for the image of beds. | 110 |
| 5.19 | Example of a micritic mud bed description Site TB9, Log 2, Bed 13, Sample BDC T10 (see Appendix 2, Table 4 and Chapter 6, Fig 6.33). See Figure 5.19 for sample image. | 111 |
| 5.20 | Summary of the recorded, mixed carbonates and clastic facies recorded in the study area. | 114 |
| 5.21 | Summary of the recorded clastics in the study area | 122 |
| 5.22 | Grain-size classification for tephra fragments used in the study area (Mullineaux, 1996). | 126 |
| 5.23 | Summary of recorded volcanoclastic facies recorded from the study area (also Chapter 7 and Table 7.2) | 127 |
| 5.24 | Summary of recorded calcrete facies recorded from the study area. See Figure 4.4 & Table 4.16. | 129 |
| 5.25 | Sedimentological symbol key for stratigraphic logs | 130 |
| 6.1 | Site information. Altitude recorded from the base of logged sequences. See Figures 6.1, 6.2, 8.1 & 8.9. | 135 |
| 6.2 | Site TB10, Log site location. Altitude recorded from the base of the logged sequence. Also, see Figure 8.1 & 8.9. | 150 |
| 6.3 | Examples of fossil fauna collected from gravels (Logs 3 and 4 Figs 6.20 – 6.22) at Site TB10. Mammalian Fauna collections housed at the Museum del Pueblo, Temoatzin totals. See Figure 6.23 for Photographs of some of the samples. | 160 |
| 6.4 | Site TB9, Barranca de Colores, altitude recorded at the base of logged sequence (see Figs 6.13, 6.24, 8.1 & 8.9) | 163 |
| 6.5 | TX89 Mammoth molar collected from T1 type deposits, Log 5 (Figs 6.24, 6.25a, 6.35 6.36), Site TB9. See Figure 6.37. | 177 |

| | | |
|-----|--|-----|
| 7.1 | Tephra samples from Roy et al. 2012. Samples were collected from a 30 m thick tephra sediment sequence exposed in different parts of a mine exposure in the Pachuca sub-basin (see Fig 7.1). | 197 |
| 7.2 | Tephra samples geochemically analysed from the study area. For the location of the sampled tephra layers, see Chapters 6 & 8. | 199 |
| 7.3 | The lithology of TEQ 4, Basaltic-andesite, Barranca de Colores. Site TB 9, Logs 2 & 4. See Section 6.6 | 199 |
| 7.4 | Major main oxide concentrations (%) of the Tequixquiac tephra layers (see Table 7.2) | 201 |
| 7.5 | Trace element concentrations (ppm) of the Tequixquiac tephra layers (Table 7.2). | 201 |

Chapter One: Introduction

1.1: Introduction

Aspects of the late Quaternary history of Central-eastern Mexico are still poorly known and the subject of discussion. This PhD research addresses, for the first time, sedimentary evidence for mid to late Quaternary environmental change in the Tequixquiac region of Central-eastern Mexico (Figs 1.1 - 1.3). The research focuses on the identification, description, geochemical characterisation and interpretation of aspects of the Quaternary sediment sequence and geology for palaeoenvironmental reconstruction. Palaeoenvironmental information is obtained from the lithology of sediment sequences and tephra layers, and their stratigraphic relationship with the geological and geomorphic catchment. The focus of the research is an interpretation of mid to late Quaternary geographical and environmental change. The research also considers, for the first time, the significance of a record of Quaternary environmental change from the study area in the context of the broader Quaternary History of Mexico (Figs 1.1a & 1.2).

1.2: Aims and objectives

The research aims to establish a Quaternary depositional history for the Tequixquiac Basin in eastern Central Mexico (Figs 1.1 – 1.3). From the depositional history, the intention is to interpret a palaeogeographic and palaeoenvironmental history for the study reconstructing the evolution of the basin throughout the Quaternary. A further aim is to examine if the Tequixquiac Quaternary sedimentary succession has the potential to extend the Central Mexican environmental record beyond the last 90,000 years to produce the oldest palaeoenvironmental record from Mexico from a previously unstudied area. The following objectives were developed to achieve the thesis aims:

- 1:** To carry out basin-wide stratigraphic logging, focused on the Quaternary succession to establish a mid to late Pleistocene to early Holocene sequence of deposition for the study area to generate a lithostratigraphic and depositional framework.
- 2:** To select key, representative stratigraphic sections of the logged sequence to build a detailed sedimentological, isotopic ($\delta^{18}\text{O}$ & $\delta^{13}\text{C}$) and geochemical record for depositional episodes.
- 3:** To establish a geochronological framework for the study area to allow the identification of the timing of depositional events.

4: To combine objectives one to three to develop a spatial and temporal Palaeogeographic and Palaeoenvironmental model for the study area.

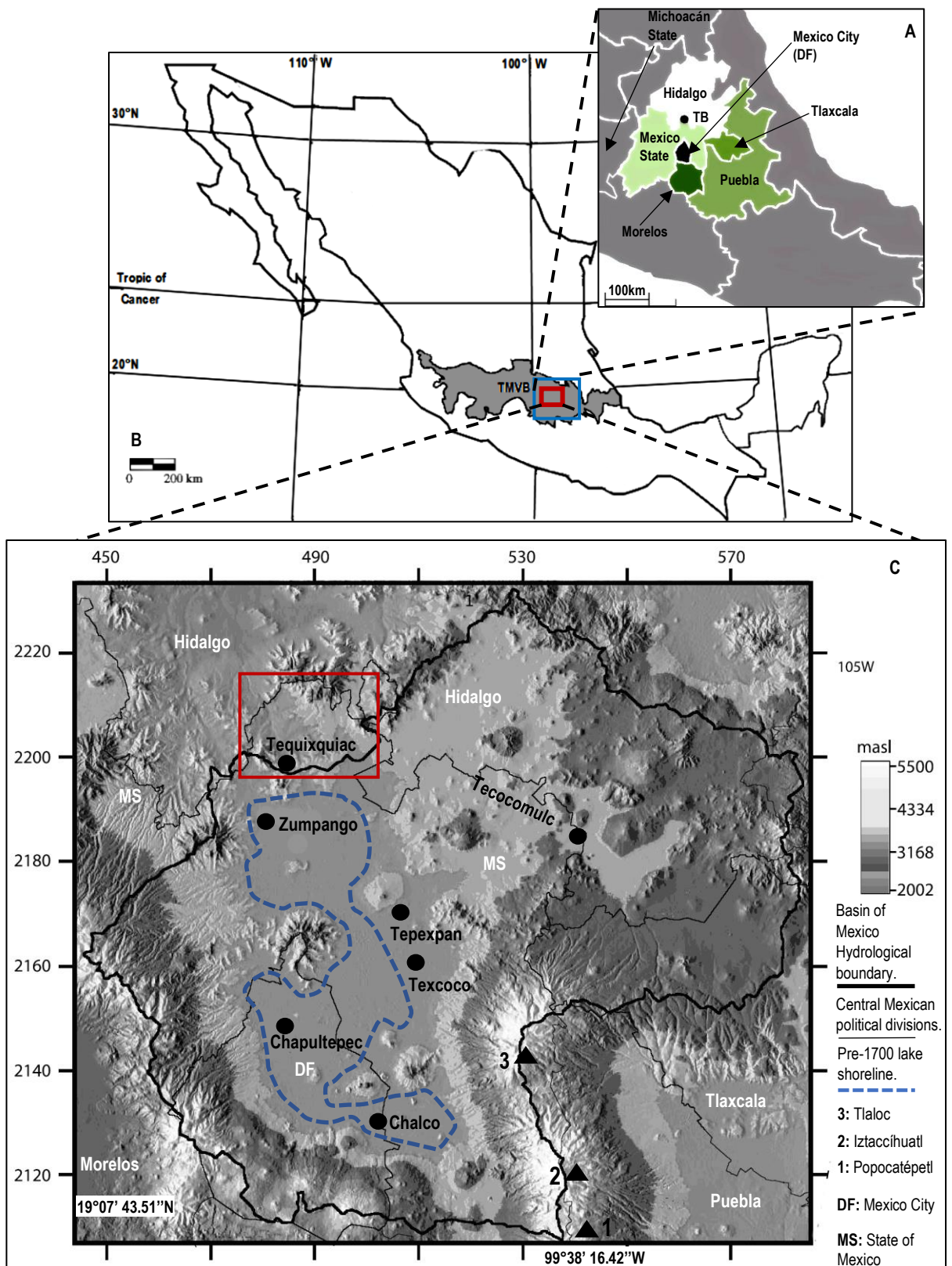


Figure 1.1: A: Central eastern Mexico (Ypsilon, 2015). B: The location of the studied area (red box) in Central eastern Mexico (blue box) and the TMVB (Volcanic Belt) (after Gómez-Tuena et al. 2007). C: Detail of the Basin of Mexico (after Cross et al. 2012). Study area, Tequixuac Basin, within red square.

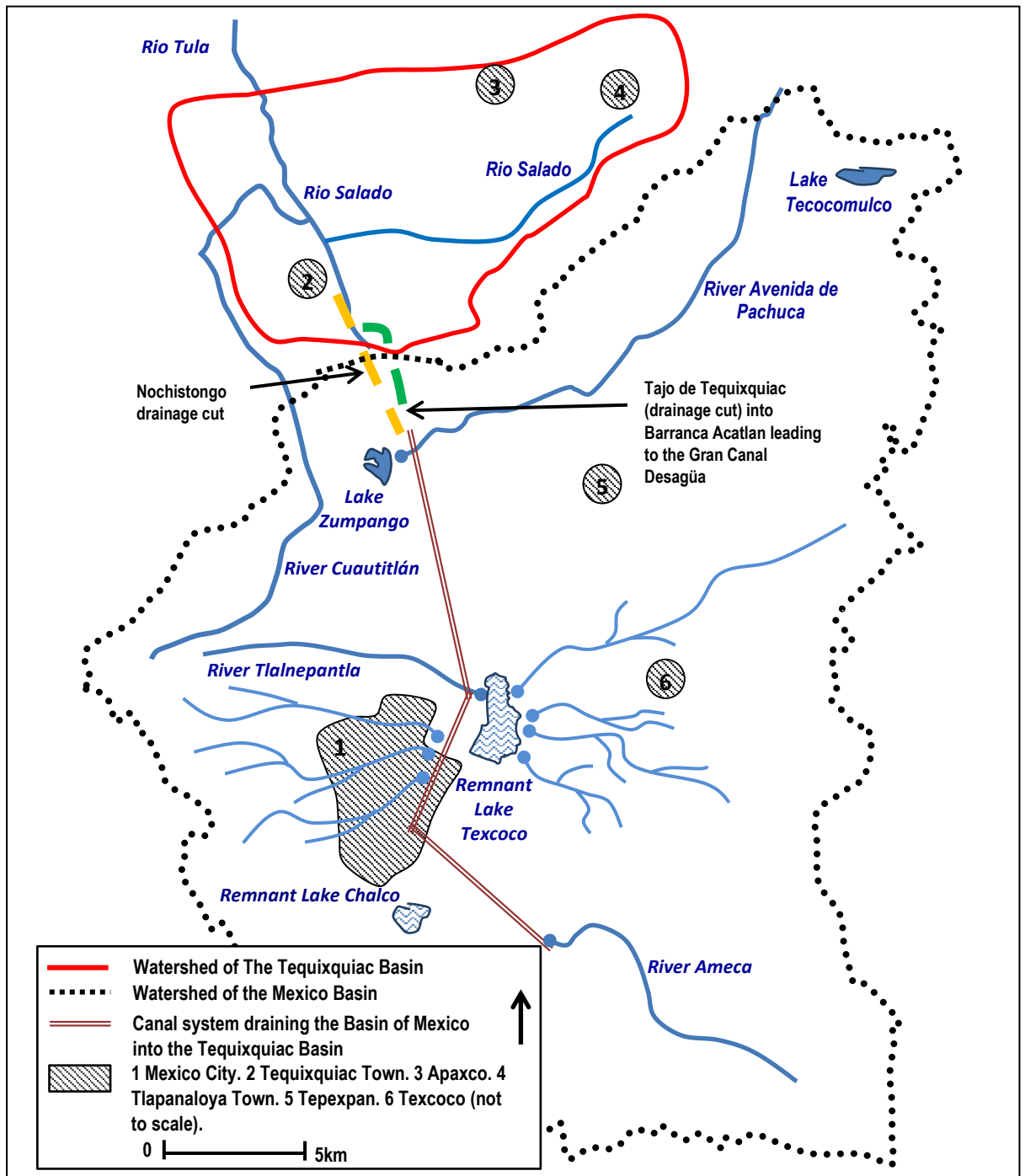


Figure 1.2: The Basin of Mexico and Tequixquiac Basin hydrology and drainage (modified after Fox, 1965). For the location of Figure 1.2 within Central Mexico see Figure 1.1. Also see Fig 1.4a, c & d for Gran Canal Desagüa Figure 1.4b

1.3: Research justification

1.3.1: Quaternary sedimentology

The motivation for early sedimentological work around the Town of Tequixquiac between 1925 and 1965 was to understand the stratigraphic position of artefacts and fossil megafaunal bones associated with Barranca

Acatlan and the Gran Canal Desagüa (see Furlong, 1925; Bárcena, 1882; Aveleyra, 1964; Lorenzo, 1964) which are still the focus of on-going discussions today (Alberd et al. 2014; Ramírez-Cruz & Montellano-Ballesteros, 2014; Yuen et al. 2014; Corona, 2015; Bravo-Cuevas et al. 2016; Campos-Martínez & Pérez-Roldán, 2016; Griffin, 2017; Perez-Crespro et al., 2016; Griffin, 2017; Jasso, 2017; Stinnesbeck et al., 2017; Universalis, 2017).

Early work that was interested in understanding the stratigraphic context of the fossil bones and artefacts (Furlong, 1925; Maldonado & Aveleyra, 1949; De Terra, 1949; Hibbard, 1955; Aveleyra, 1965) reported, for the first time, a description of the Quaternary basin-fill sequence from the study area. Several Quaternary facies were identified from the study area and grouped into associations that were linked to formations identified for the Basin of Mexico (the Tacubaya Formation, Old Becerra Formation, Young Becerra Formation, Totolzingo Intraformational caliche (I, II & III); see Table 1.1, Chapter 3 and Maldonado & Aveleyra, 1949; De Terra, 1949, Hibbard, 1955, Aveleyra, 1965). These formations were used in early work to describe and link Central Mexican Quaternary stratigraphy across a large geographic area (e.g. De Terra, 1949), and to similar deposits in North America (e.g. Furlong, 1925).

Later work described the formation names, when classifying Central Mexican stratigraphy, as antiquated (see Miller & Carranza-Castaneda, 1984) and redundant because depositional systems and the resulting basin-fill stratigraphy is individual to that basin. Across the Trans Mexican Volcanic Belt volcanic activity and volcanogenic deposition, tectonics, topography, regionally variable climates and complex drainage and hydrological systems mean that the stratigraphy of sedimentary basins that transect Central Mexico is variable and governed locally by these factors (see Chapters 2, 3 & 8). If these factors are understood, and a chronology is established for a succession, regional links between chronologically controlled depositional episodes can be made (see Lozano 1986; Lozano et al. 1993; Lozano & Ortega, 1994; Lozano, 1996; Bradbury, 1997, 1998; Caballero, 1997; Caballero & Ortega, 1998; Ortega & Newton, 1998; Lozano & Ortega, 1998; Caballero et al. 1999; Ortega, 2000; Gonzalez et al. 2001; Sedov et al. 2001; Nordt et al. 2002; Vázquez & Heine, 2004; ; Metcalfe, 2006; Solleiro et al. 2006; Marcías, 2007; Lamb et al. 2009; Roy et al. 2009; Caballero et al. 2010; Sedov et al. 2010; Vázquez & Heine, 2011; In Ehlers et al. 2011; Roy et al. 2012; Cantarero, 2013; Lozano et al. 2015; ; Metcalfe, 2015; Torres-Rodríguez et al. 2015; Siebe et al. 2017).

Despite lithofacies and biofacies being proposed for Quaternary sediments in the Tequixquiac Basin between 1949 and 1965 (see Table 1.1 and Maldonado & Aveleyra, 1949; De Terra, 1949; Hibbard, 1955, Aveleyra, 1965) the Quaternary sediments have no chronological framework or basin specific characterisation, classification

or palaeogeographic model. Further sedimentological, geochemical and chronological work, which is absent from the earlier work (Table 1.1), would allow for these sediments to be correctly classified, interpreted and compared to other regional sequences deposited within the same time frame.

Table 1.1: Proposed late Quaternary formations that have been identified for the Tequiquiac Basin (Fig 1.2) (Furlong, 1925; Maldonado & Aveleyra, 1949; De Terra, 1949; Hibbard, 1955; Aveleyra, 1965). The older sediments identified in these studies (1 – 4, below) have also been grouped under the heading of the Tarango Formation and number 6 under the heading of Quaternary alluvial deposits (see Chapter 3).

| Facies associations | Formation |
|---|--|
| 8: Dark silt and sand (top of sequence) | Totalzingo Formation |
| 7: Caliche | III Intraformational caliche |
| 6: Fossil rich gravel units with well-rounded pebbles (Fig 1.4c). Can be overlain by grey cross-bedded sand and gravel layers that grade into yellow to cream silts (8 – 10m). Units sit disconformably over (4). | Young Becerra Formation (associated with the Sacro in the Tequiquiac Basin; Quaternary alluvial deposits) |
| 5: Caliche | II Informational caliche |
| 4a: Bentonite topped by pink clays that end in gravelly sands that grade into yellow and grey silts (4b). | Older Becerra Formation |
| 3: Caliche | I Intraformational |
| 2: Hard brown/ochre, hard, gritty clay coated in carbonate | Tacubaya Formation |
| 1: Basal basalt (base of sequence) | ? |

This thesis aims to focus on developing the Quaternary palaeogeography from the sediment sequences identified by the early research carried out in the Tequiquiac Basin. The objectives are to establish a chronologically controlled stratigraphic framework for the mid to late Quaternary Tequiquiac Basin sedimentary succession to reconstruct depositional environments. Because the megafaunal fossil remains are found in gravel units, the taphonomy, provenance and age of the bones are not considered or discussed in this thesis. However, because the gravel deposits containing fossil bones in the study area are found in the same stratigraphic position, with some units having chronological control, the fossils serve as visual biostratigraphic markers that help to identify similar units found within the stratigraphy across the study area (see Chapters 6 & 8), and they are utilised in this capacity here. Placing the gravel units into a chronological and stratigraphic context within the Quaternary basin-fill sequence also has the potential to aid and further new research that wishes to focus on the fossil faunal remains (e.g. Alberd et al. 2014; Ramirez-Cruz & Montellano-Ballesteros, 2014; Yuen et al. 2014; Corona, 2015; Bravo – Cuevas et al. 2016; Perez-Crespro et al. 2016; Jasso, 2017; Stinnesbeck et al. 2017).

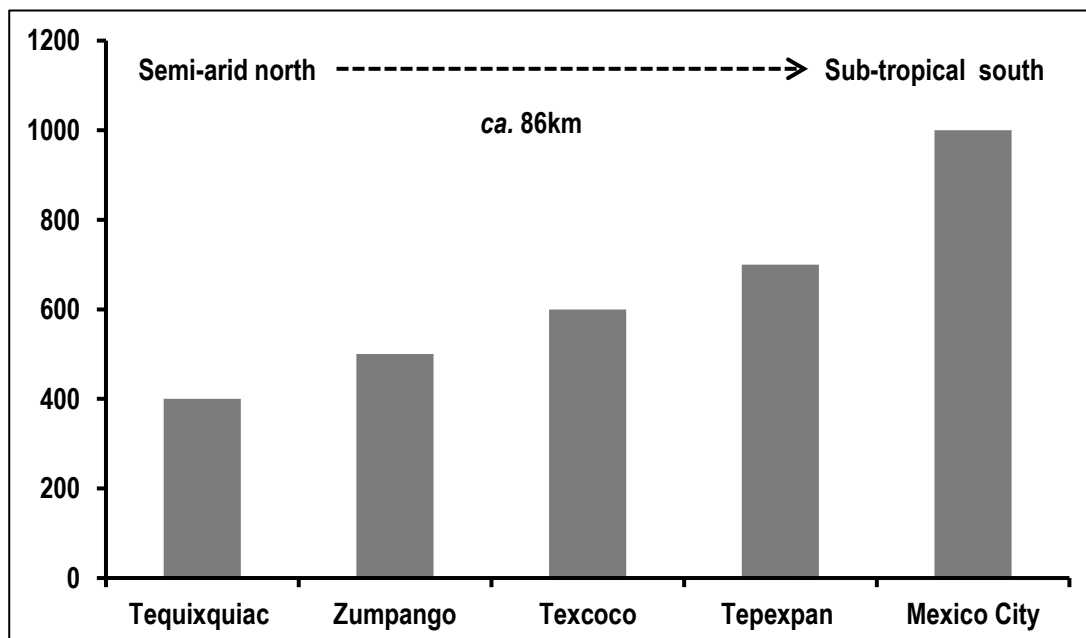


Figure 1.3: Average annual rainfall values (mm) from Tequixquiac in the North to Mexico City in the Southern Basin of Mexico (rainfall data taken from Lamb et al 2006; Parsons et al, 2008). For location see Figure 1.1.

1.3.2: Mexican Quaternary Environments

A distinct environmental gradient exists between the northern and southern regions of central-eastern Mexico today (Fig1.3), with the north being relatively unexplored compared to the south. In the far North, climatic conditions are semiarid (Parsons et al. 2008), the central Basin of Mexico is effectively a transition zone between the semi-arid north and tropical-temperate south (Ovando-Shelly & Ossa. 2007; Lamb et al. 2009; Parsons et al. 2008; Roy et al. 2009; see Fig 1.3). Consequently, understanding how northeastern Central Mexico responded to Quaternary environmental change is important in helping understand and predict future change (see Caballero et al. 1999).

The history of Quaternary environmental change in the Northern Basin of Mexico and the Hidalgo region of Central Mexico (Fig 1.1 a & c) is unexplored. Currently, there is little (published) environmental or climate-related Quaternary data available (see Chapter, Figs 2.6 & 2.8) to compare with other regions of Central-eastern Mexico. The majority of Central-eastern Mexican (Fig 1.1 a) Quaternary environmental data covers the later Pleistocene and comes from Lakes Chalco and Texcoco in the Basin of Mexico (see Figs 1.1c, 1.2, 2.6 and Chapter 2). Sedimentological Lake core records have reconstructed the last ca.90,000 years BP (see Chapter 2, Figs 2.6 & 2.8) with no records covering the mid Pleistocene (see Chapter 2, Figs 2.6 & 2.8).

In addition, Quaternary environmental data also exists for western Mexico State (Fig 1.1 a), which has produced the longest (195 ka BP, Fig 2.8) Central Mexican lacustrine record (see Chapter 2 and Metcalfe et al.

1991; Caballero et al. 2002; Lozano-García et al. 2005; Lozano-García et al. 2013), Puebla (Fig 1.1 a & b) (see Chapter 2 and Heine, 2003; Stevens et al. 2012; Tovar et al. 2014; Metcalfe et al. 2016), Tlaxcala (Fig 1.1 a & b) (see Chapter 2 and Heine. 2003; Sedov et al. 2009; Salinas et al. 2016), and to a lesser extent Morelos (Fig 1.1 a & b) (see Chapter 2 and Solleriro-Rebolledo et al. 2003). A new lake core (300m+) (no published data yet) from Lake Chalco is expected to produce a 500,000-year-old lacustrine record of Quaternary paleoenvironments (see Brown et al. 2012).

From the available research it remains unclear at what point modern summer monsoonal rainfall regime became established (see Chapter 2, Figs 2.6 & 2.8), and when the environmental, temperature and precipitation gradient developed north to south across Mexico (See Lozano & Ortega, 1997; Lozano & Xelhuanzi, 1997; Metcalfe et al, 2000; Metcalfe, 2006; Lamb et al, 2009; Metcalfe et al.2015 and Chapter 2). The cause and timing of moisture changes, particularly during the LGM and Late Pleistocene – Holocene transition, are unclear for Central Mexico (see Chapter 2 and Figs 2.6 & 2.8)

The Younger Dryas (YD) climatic event is thought to have had little influence on the Gulf of Mexico and subsequently little impact on Mexican glaciers (meltwater was released into the North Atlantic and not the Gulf of Mexico during the YD (see Heine, 1994). However, evidence of the YD is said to be present in northern and Central Mexican stratigraphy (Caballero, 1995; Metcalfe et al. 1997; Metcalfe et al. 2000). Higher resolution, interdecadal sedimentary records are needed from multiple sites to help resolve this.

This thesis aims to use facies associations identified in the study area combined with sediment geochemistry and tephrochronology to reconstruct aspects of the study areas depositional history and produce a record of past depositional change for the Tequixquiac Basin. This record can then be compared with the Quaternary history that is now known as the Basin of Mexico (see Tables 2.5 and 2.8. for summaries), and will also test the potential for the Quaternary sequence to extend the record beyond the last ca 80 ka bp (see Chapter 2). The PhD research also aims to establish a new tephrochronology for the study area that can be used as a local and possibly regional, chronological marker.

1.4: PhD Thesis structure

The remainder of this thesis has the following structure to satisfy the aims set out in this chapter. In Chapter 2, the background to the research is described to establish a framework for the current research, and further justification for the PhD research is given. Chapter 3 describes the physiographic characteristics of the research

area. The methodologies utilised by this thesis are detailed and justified in Chapter 4. Sedimentary facies identified from the Tequixuiac sedimentary sequences are described and interpreted in Chapter 5. The sedimentology and stratigraphy of the mid to late Pleistocene stratigraphic succession is described in Chapter 6. Chapter 7 details the tephra geochemistry and provenance. The information generated from the sedimentology and stratigraphy reported in Chapters 5 – 7 is synthesised in Chapter 8 to interpret and reconstruct the palaeoenvironmental history of the study area. Finally, this thesis concludes in Chapter 9.

- Adamson, K., Candy, I. and Whitfield, L., 2015. Coupled micromorphological and stable isotope analysis of Quaternary calcrete development. *Quaternary Research*, 84(2), pp.272-286.
- Aguirre-Díaz, G.D.J., ZÚÑIGA DÁVILA, F.R., Pacheco Alvarado, F.J., Guzmán Speziale, M. and Y NIETO OBREGÓN, J., 2000. El graben de Querétaro, Mexico, observaciones de fallamiento activo. *Unión Geofísica Mexicana, Geos*, 20(1), pp.2-7.
- Alaniz-Álvarez, S.A., Nieto-Samaniego, Á.F. and Mexicana, S.G. eds., 2007. *Geology of México: Celebrating the centenary of the Geological Society of México (Vol. 422)*. Geological Society of America.
- Alaniz-Álvarez, S.A., Nieto-Samaniego, Á.F., 2007. The Taxco-San Miguel de Allende fault system and the Trans-Mexican Volcanic Belt: two tectonic boundaries in central Mexico active during the Cenozoic., In: Alaniz-Álvarez, S.A., Nieto-Samaniego, Á.F., (Eds.), *Geology of Mexico: Celebrating the Centenary of the Geological Society of México: Geological Society of America Special Paper*, 422: 301 - 316.
- Alberdi, M.T., Arroyo-Cabrales, J., Marín-Leyva, A.H. and Polaco, O.J., 2014. Study of Cedral Horses and their place in the Mexican Quaternary. *Revista Mexicana de Ciencias Geológicas*, 31(2).
- Allen, J.R.L., 1986. Pedogenic calcretes in the Old Red Sandstone facies (late Silurian-early Carboniferous) of the Anglo-Welsh area, southern Britain. *Paleosols. Their recognition and interpretation*, pp.58-86.
- Alonso-Zarza, A.M. and Tanner, L.H., 2010. *Carbonates in continental settings: facies, environments, and processes (Vol. 61)*. Elsevier.
- Alonso-Zarza, A.M. and Wright, V.P., 2010a. Palustrine Carbonates. *Developments in Sedimentology*, 61, pp.103-131.
- Alonso-Zarza, A.M. and Wright, V.P., 2010b. Calcretes. *Developments in Sedimentology*, 61, pp.225-267.
- Alonso-Zarza, A.M., 1999. Initial stages of laminar calcrete formation by roots: examples from the Neogene of central Spain. *Sedimentary Geology*, 126(1), pp.177-191.
- Alonso-Zarza, A.M., 2003. Palaeoenvironmental significance of palustrine carbonates and calcretes in the geological record. *Earth-Science Reviews*, 60(3), pp.261-298.
- Alonso-Zarza, A.M., Sanz, M.E., Calvo, J.P. and Estévez, P., 1998. Calcified root cells in Miocene pedogenic carbonates of the Madrid Basin: evidence for the origin of *Microcodium* b. *Sedimentary Geology*, 116(1-2), pp.81-97.
- Alonso-Zarza, A.A., Calvo, J.P. and Del Cura, M.G., 1992. Palustrine sedimentation and associated features-grainification and pseudo-microkarst-in the Middle Miocene (Intermediate Unit) of the Madrid Basin, Spain. *Sedimentary Geology*, 76(1-2), pp.43-61.
- Anadón, P., Cabrera, L. and Kelts, K. eds., 1991. *Lacustrine Facies Analysis*. Blackwell.
- Anderson, N.J. and Leng, M.J., 2004. Increased aridity during the early Holocene in West Greenland inferred from stable isotopes in laminated-lake sediments. *Quaternary Science Reviews*, 23(7), pp.841-849.
- Anderson, R.S., Jiménez-Moreno, G., Ager, T. and Porinchu, D.F., 2014. High-elevation paleoenvironmental change during MIS 6-4 in the central Rockies of Colorado as determined from pollen analysis. *Quaternary Research*, 82(3), pp.542-552.
- Anderton, R., 1985. *Clastic facies models and facies analysis*. Geological Society, London, Special Publications, 18(1), pp.31-47.
- Andrews, J.E. 2006. Palaeoclimatic records from stable isotopes in riverine tufas: Synthesis and review. *Earth-Science Reviews Isotopes in Palaeoenvironmental reconstruction (ISOPAL)*, 75: 85-104.
- Andrews, J.E. and Brasier, A.T., 2005. Seasonal records of climatic change in annually laminated tufas: short review and future prospects. *Journal of Quaternary Science*, 20(5), pp.411-421.
- Andrews, J.E., 2006. Palaeoclimatic records from stable isotopes in riverine tufas: synthesis and review. *Earth-Science Reviews*, 75(1-4), pp.85-104.

- Andrews, J.E., Riding, R. and Dennis, P.F., 1997. The stable isotope record of environmental and climatic signals in modern terrestrial microbial carbonates from Europe. *Palaeogeography, Palaeoclimatology, Palaeoecology*, 129(1-2), pp.171-189.
- Andrews, J.T. and Barber, D.C., 2002. Dansgaard-Oeschger events: is there a signal off the Hudson Strait Ice Stream?. *Quaternary Science Reviews*, 21(1), pp.443-454.
- Arakel, A.V., 1982. Genesis of calcrete in Quaternary soil profiles, Hutt and Leeman lagoons, Western Australia. *Journal of Sedimentary Research*, 52(1).
- Arce, J.L., Cervantes, K.E., Macías, J.L. and Mora, J.C., 2005. The 12.1 ka Middle Toluca Pumice: A dacitic Plinian-subplinian eruption of Nevado de Toluca in central Mexico. *Journal of Volcanology and Geothermal Research*, 147(1), pp.125-143.
- Arce, J.L., Layer, P.W., Morales-Casique, E., Benowitz, J.A., Rangel, E. and Escolero, O., 2013. New constraints on the subsurface geology of the Mexico City Basin: The San Lorenzo Tezonco deep well, on the basis of $^{40}\text{Ar}/^{39}\text{Ar}$ geochronology and whole-rock chemistry. *Journal of Volcanology and Geothermal Research*, 266, pp.34-49.
- Arce, J.L., Macías, J.L. and Vázquez-Selem, L., 2003. The 10.5 ka Plinian eruption of Nevado de Toluca volcano, Mexico: Stratigraphy and hazard implications. *Geological Society of America Bulletin*, 115(2), pp.230-248.
- Arenas, C., Cabrera, L. and Ramos, E., 2007. Sedimentology of tufa facies and continental microbialites from the Palaeogene of Mallorca Island (Spain). *Sedimentary Geology*, 197(1), pp.1-27.
- Arenas-Abad, C., Vázquez-Urbez, M., Pardo-Tirapu, G. and Sancho-Marcén, C., 2010. Fluvial and associated carbonate deposits. *Developments in Sedimentology*, 61, pp.133-175.
- Armenteros, I., Daley, B. and García, E., 1997. Lacustrine and palustrine facies in the Bembridge Limestone (late Eocene, Hampshire Basin) of the Isle of Wight, southern England. *Palaeogeography, Palaeoclimatology, Palaeoecology*, 128(1-4), pp.111-132.
- Arp, G., Reimer, A. and Reitner, J., 2001. Photosynthesis-induced biofilm calcification and calcium concentrations in Phanerozoic oceans. *Science*, 292(5522), pp.1701-1704.
- Arreygue-Rocha, E., 1999. Le condizioni di pericolosità idrogeologica nella città di Morelia, Michoacan (Messico). Tesi di dottora to XI Ciclo 1995-1998, Università degli studi di Perugia. 171pp.
- Arroyo-Cabrales, J. and Polaco, O.J., 2003. Caves and the Pleistocene vertebrate paleontology of Mexico. *Ice Age cave faunas of North America* (BW Schubert, JI Mead, and RW Graham, editors). Indiana University Press, Bloomington, pp.273-291.
- Arroyo-Cabrales, J., Polaco, O.J. and Johnson, E., 2006. A preliminary view of the coexistence of mammoth and early peoples in Mexico. *Quaternary International*, 142, pp.79-86.
- Assereto, R.L. and Kendall, C.G., 1977. Nature, origin and classification of peritidal tepee structures and related breccias. *Sedimentology*, 24(2), pp.153-210.
- Asta, M.P., Auqué, L.F., Sanz, F.J., Gimeno, M.J., Acero, P., Blasco, M., García-Alix, A., Gómez, J., Delgado-Huertas, A. and Mandado, J., 2017. Travertines associated with the Alhama-Jaraba thermal waters (NE, Spain): Genesis and geochemistry. *Sedimentary Geology*, 347, pp.100-116.
- Aveleyra Arroyo de Anda, L., 1950. Prehistoria de Mexico. Ediciones Mexicanas, SA Mexico City, Mexico, 167.
- Aveleyra de Anda, L.A.A., 1965. The Pleistocene Carved Bone from Tequixquiac, Mexico: A Reappraisal. *American Antiquity*, pp.261-277.
- Aveleyra, L., 1964. El sacro de Tequixquiac. *Cuadernos del Museo Nacional de Antropología*, 2, pp.9-52.
- Avilés, J. and Pérez-Rocha, L.E., 2010. Regional subsidence of Mexico City and its effects on seismic response. *Soil Dynamics and Earthquake Engineering*, 30(10), pp.981-989.
- Báez, A., Belmont, R., García, R., Padilla, H. and Torres, M.D.C., 2007. Chemical composition of rainwater collected at a southwest site of Mexico City, Mexico. *Atmospheric Research*, 86(1), pp.61-75.

- Bárcena, M., 1882. Antropología.-Descripción de un hueso labrado, de llama fósil, encontrado en los terrenos postterciarios de Tequixquiac, Estado de México.-Estudio. *Anales del Museo Nacional de México, primera época (1877-1903)*, 2, pp.439-444.
- Barker, P., Gasse, F., Roberts, N. and Taieb, M., 1990. Taphonomy and diagenesis in diatom assemblages; a Late Pleistocene palaeoecological study from Lake Magadi, Kenya. In *Environmental History and Palaeolimnology* (pp. 267-272). Springer Netherlands.
- Barker, P., Telford, R., Gasse, F. and Thevenon, F., 2002. Late Pleistocene and Holocene palaeohydrology of Lake Rukwa, Tanzania, inferred from diatom analysis. *Palaeogeography, Palaeoclimatology, Palaeoecology*, 187(3), pp.295-305.
- Bar-Matthews, M., Ayalon, A. and Kaufman, A., 1998. Middle to Late Holocene (6,500 yr. period) paleoclimate in the Eastern Mediterranean region from stable isotopic composition of speleothems from Soreq Cave, Israel. In *Water, environment and society in times of climatic change* (pp. 203-214). Springer Netherlands.
- Barnes CJ, Allison GB (1988) Tracing of water movement in the unsaturated zone using stable isotopes of hydrogen and oxygen. *J Hydrol* 100:143-176.
- Battarbee, R.W., Jones, V.J., Flower, R.J., Cameron, N.G., Bennion, H., Carvalho, L. and Juggins, S., 2002. *Diatoms* (pp. 155-202). Springer Netherlands.
- Behling, H., 2002. Carbon storage increases by major forest ecosystems in tropical South America since the Last Glacial Maximum and the early Holocene. *Global and Planetary Change*, 33(1), pp.107-116.
- Beier, J.A., 1987. Petrographic and geochemical analysis of caliche profiles in a Bahamian Pleistocene dune. *Sedimentology*, 34(6), pp.991-998.
- Benvenuti, M., 2003. Facies analysis and tectonic significance of lacustrine fan-deltaic successions in the Pliocene-Pleistocene Mugello Basin, Central Italy. *Sedimentary Geology*, 157(3), pp.197-234.
- Berglund, B.E. and Ralska-Jasiewiczowa, M., 1986. *Handbook of Holocene palaeoecology and palaeohydrology*. Handbook of Holocene palaeoecology and palaeohydrology.
- Bershaw, J., Penny, S.M. and Garzione, C.N., 2012. Stable isotopes of modern water across the Himalaya and eastern Tibetan Plateau: Implications for estimates of paleoelevation and paleoclimate. *Journal of Geophysical Research: Atmospheres*, 117(D2).
- Bertini, A., Minissale, A. and Ricci, M., 2014. Palynological approach in upper Quaternary terrestrial carbonates of central Italy: anything but a 'mission impossible'. *Sedimentology*, 61(1), pp.200-220.
- Bibliography**
- Bogard, D.D., 1995. Impact ages of meteorites: A synthesis. *Meteoritics & Planetary Science*, 30(3), pp.244-268.
- Boggs, S., 2006. *Principles of sedimentology and stratigraphy*, fourth edition. Pearson prentice Hall, Upper Saddle River, New Jersey, US.
- Bond, G., Heinrich, H., Broecker, W., Labeyrie, L., McManus, J., Andrews, J., Huon, S., Jantschik, R., Clasen, S., Simet, C. and Tedesco, K., 1992. Evidence for massive discharges of icebergs into the North Atlantic ocean during the last glacial period. *Nature*, 360(6401), pp.245-249.
- Borejsza, A. and Frederick, C.D., 2010. Fluvial response to Holocene climate change in low-order streams of central Mexico. *Journal of Quaternary Science*, 25(5), pp.762-781.
- Bourgeon, L., Burke, A. and Higham, T., 2017. Earliest Human Presence in North America Dated to the Last Glacial Maximum: New Radiocarbon Dates from Bluefish Caves, Canada. *PLoS one*, 12(1), p.e0169486.
- Bowman, S., 1990. *Radiocarbon dating (Vol. 1)*. Univ of California Press.
- Boyd, R., Dalrymple, R.W. and Zaitlin, B.A., 2006. Estuarine and incised-valley facies models. *SPECIAL PUBLICATION-SEPM*, 84, p.171.
- Bradbury, J.P., 1971. Paleolimnology of Lake Texcoco, Mexico. Evidence from diatoms. *Limnology and Oceanography*, 16(2), pp.180-200.

- Bradbury, J.P., 1989. Late Quaternary lacustrine paleoenvironments in the Cuenca de Mexico. *Quaternary Science Reviews*, 8(1), pp.75-100.
- Bradbury, J.P., 1997. Sources of glacial moisture in Mesoamerica. *Quaternary International*, 43, pp.97-110.
- Braithwaite, C.J.R., 1989. Displacive calcite and grain breakage in sandstones. *Journal of Sedimentary Research*, 59(2).
- Brasier, A.T., 2011. Searching for travertines, calcretes and speleothems in deep time: processes, appearances, predictions and the impact of plants. *Earth-Science Reviews*, 104(4), pp.213-239.
- Bravo-Cuevas, V.M., Priego-Vargas, J., Cabral-Perdomo, M.Á. and Pineda Maldonado, M.A., 2016. First occurrence of *Panthera atrox* (Felidae, Pantherinae) in the Mexican state of Hidalgo and a review of the record of felids from the Pleistocene of Mexico. *Fossil Record*, 19(2), pp.131-141.
- Brennan, R. and Quade, J., 1997. Reliable Late-Pleistocene Stratigraphic Ages and Shorter Groundwater Travel Times from ¹⁴C in Fossil Snails from the Southern Great Basin. *Quaternary Research*, 47(3), pp.329-336.
- Brett, M.J., Baldini, J.U. and Gröcke, D.R., 2014. Environmental controls on stable isotope ratios in New Zealand Podocarpaceae: Implications for palaeoclimate reconstruction. *Global and Planetary Change*, 120, pp.38-45.
- Broecker, W.S., 2003. Does the trigger for abrupt climate change reside in the ocean or in the atmosphere?. *Science*, 300(5625), pp.1519-1522.
- Bronk Ramsey, C., 2008. Radiocarbon dating: revolutions in understanding. *Archaeometry*, 50(2), pp.249-275.
- Brook, G.A., Ellwood, B.B., Railsback, L.B. and Cowart, J.B., 2006. A 164 ka record of environmental change in the American Southwest from a Carlsbad Cavern speleothem. *Palaeogeography, Palaeoclimatology, Palaeoecology*, 237(2-4), pp.483-507.
- Brown, E.T., Werne, J.P., Lozano-García, S., Caballero, M., Ortega-Guerrero, B., Cabral-Cano, E., Valero-Garces, B.L., Schwalb, A. and Arciniega-Ceballos, A., 2012. Scientific drilling in the basin of Mexico to evaluate climate history, hydrological resources, and seismic and volcanic hazards. *Scientific Drilling*, 14, pp.72-75.
- Brunner, C.A., 1982. Paleooceanography of surface waters in the Gulf of Mexico during the late Quaternary. *Quaternary Research*, 17(1), pp.105-119.
- Bull, W.B., 1997. Discontinuous ephemeral streams. *Geomorphology*, 19(3-4), pp.227-276.
- Burjachs, F. and Julià, R., 1994. Abrupt climatic changes during the last glaciation based on pollen analysis of the Abric Romani, Catalonia, Spain. *Quaternary Research*, 42(3), pp.308-315.
- Caballero, M. and Guerrero, B.O., 1998. Lake levels since about 40,000 years ago at Lake Chalco, near Mexico City. *Quaternary Research*, 50(1), pp.69-79.
- Caballero, M. and Ortega, G.B., 1998. Lake levels since about 40,000 years ago at Lake Chalco, near Mexico City. *Quaternary Research*, 50(1), pp.69-79.
- Caballero, M., 1997. The last glacial maximum in the basin of Mexico: the diatom record between 34,000 and 15,000 years BP from Lake Chalco. *Quaternary International*, 43, pp.125-136.
- Caballero, M., Lozano, S., Ortega, B., Urrutia, J. and Macias, J.L., 1999. Environmental characteristics of Lake Tecocomulco, northern basin of Mexico, for the last 50,000 years. *Journal of Paleolimnology*, 22(4), pp.399-411.
- Caballero, M., Lozano-García, S., Vázquez-Selem, L. and Ortega, B., 2010. Evidencias de cambio climático y ambiental en registros glaciales y en cuencas lacustres del centro de México durante el último máximo glacial. *Boletín de la Sociedad Geológica Mexicana*, 62(3), pp.359-377.
- Caballero, M., Ortega, B., Valadez, F., Metcalfe, S., Macias, J.L. and Sugiura, Y., 2002. Sta. Cruz Atizapán: a 22-ka lake level record and climatic implications for the late Holocene human occupation in the Upper Lerma Basin, Central Mexico. *Palaeogeography, Palaeoclimatology, Palaeoecology*, 186(3), pp.217-235.
- Caballero, M.C., 1997. The last glacial maximum in the basin of Mexico: the diatom record between 34,000 and 15,000 years BP from Lake Chalco. *Quaternary International*, 43, pp.125-136.
- Cameron, N.G., 1995. The representation of diatom communities by fossil assemblages in a small acid lake. *Journal of Paleolimnology*, 14(2), pp.185-223.

- Campos - Enríquez, J., Sánchez - Zamora, O., 2000. Crustal structure across Southern Mexico, inferred from gravity data. *Journal of South America Earth Sciences*, 13: 479 - 489.
- Campos-Martínez, M.S. and Pérez-Roldán, G., WORKED HUMAN BONE FROM TEOTIHUACAN, MEXICO (1ST-6TH CENTURIES AD). *Close to the bone: current studies in bone technologies*, p.98.
- Camuera, J., Alonso-Zarza, A.M., Rodríguez-Berriguete, Á. and Meléndez, A., 2015. Variations of fluvial tufa sub-environments in a tectonically active basin, Pleistocene Teruel Basin, NE Spain. *Sedimentary Geology*, 330, pp.47-58.
- Candy, I., Abrook, A., Elliot, F., Lincoln, P., Matthews, I.P. and Palmer, A., 2016. Oxygen isotopic evidence for high?magnitude, abrupt climatic events during the Lateglacial Interstadial in north?west Europe: analysis of a lacustrine sequence from the site of Tirinie, Scottish Highlands. *Journal of Quaternary Science*, 31(6), pp.607-621.
- Candy, I., Adamson, K., Gallant, C.E., Whitfield, E. and Pope, R., 2012. Oxygen and carbon isotopic composition of Quaternary meteoric carbonates from western and southern Europe: their role in palaeoenvironmental reconstruction. *Palaeogeography, Palaeoclimatology, Palaeoecology*, 326, pp.1-11.
- Candy, I., Farry, A., Darvill, C.M., Palmer, A., Blockley, S.P.E., Matthews, I.P., MacLeod, A., Deepprose, L., Farley, N., Kearney, R. and Conneller, C., 2015. The evolution of Palaeolake Flixton and the environmental context of Star Carr: an oxygen and carbon isotopic record of environmental change for the early Holocene. *Proceedings of the Geologists' Association*, 126(1), pp.60-71.
- Cant, D.J. and Walker, R.G., 1976. Development of a braided-fluvial facies model for the Devonian Battery Point Sandstone, Quebec. *Canadian Journal of Earth Sciences*, 13(1), pp.102-119.
- Cantagrel, J.M. and Robin, C., 1979. K-Ar dating on eastern Mexican volcanic rocks-relations between the andesitic and the alkaline provinces. *Journal of volcanology and geothermal research*, 5(1-2), pp.99-114.
- Cantarero, S., 2013. Multiproxy paleoclimatic record from geochemical analyses of Lake Chalco sediments, a closed basin lake in central Mexico. University of Minnesota.
- Capezzuoli, E., Gandin, A. and Pedley, M., 2014. Decoding tufa and travertine (fresh water carbonates) in the sedimentary record: The state of the art. *Sedimentology*, 61(1), pp.1-21.
- Capra, L., Bernal, J.P., Carrasco-Núñez, G. and Roverato, M., 2013. Climatic fluctuations as a significant contributing factor for volcanic collapses. Evidence from Mexico during the Late Pleistocene. *Global and Planetary Change*, 100, pp.194-203.
- Capra, L., Mac?as, J.L., Scott, K.M., Abrams, M. and Garduño-Monroy, V.H., 2002. Debris avalanches and debris flows transformed from collapses in the Trans-Mexican Volcanic Belt, Mexico-behavior, and implications for hazard assessment. *Journal of Volcanology and Geothermal Research*, 113(1-2), pp.81-110.
- Carroll, A.R. and Bohacs, K.M., 1999. Stratigraphic classification of ancient lakes: Balancing tectonic and climatic controls. *Geology*, 27(2), pp.99-102.
- Caso, J.M.R., 2010. El bulldog y el arzobispo: una discusión evolutiva.
- Castro, C.L., McKee, T.B. and Pielke Sr, R.A., 2001. The relationship of the North American monsoon to tropical and North Pacific sea surface temperatures as revealed by observational analyses. *Journal of Climate*, 14(24), pp.4449-4473.
- Catuneanu, O., 2006. *Principles of sequence stratigraphy*. Elsevier.
- Catuneanu, O., Galloway, W.E., Kendall, C.G.S.C., Miall, A.D., Posamentier, H.W., Strasser, A. and Tucker, M.E., 2011. Sequence stratigraphy: methodology and nomenclature. *Newsletters on stratigraphy*, 44(3), pp.173-245.
- Cervantes - Mendel, A., Armienta, M, A., 2004. Influence of faulting on groundwater quality in the Valle del Mezquita, Mexico. *Geofísica Internacional* 43: 3 477 - 493
- Chafetz, H., Rush, P.F. and Utech, N.M., 1991. Microenvironmental controls on mineralogy and habit of CaCO₃ precipitates: an example from an active travertine system. *Sedimentology*, 38(1), pp.107-126.
- Chafetz, H.S. and Folk, R.L., 1984. Travertines: depositional morphology and the bacterially constructed constituents. *Journal of Sedimentary Research*, 54(1).

- Chafetz, H.S., Utech, N.M. and Fitzmaurice, S.P., 1991b. Differences in the ^{18}O and ^{13}C signatures of seasonal laminae comprising travertine stromatolites. *Journal of Sedimentary Research*, 61(6).
- Chang, C., 2007. Impacts, Adaptation and Vulnerability. Contribution of Working Group II to the Fourth Assessment Report of the Intergovernmental Panel on Climate Change/ML Parry, OF Canziani, JP Palutikof et al., eds.
- Chang, P., Ji, L. and Li, H., 1997. A decadal climate variation in the tropical Atlantic Ocean from thermodynamic air-sea interactions. *Nature*, 385(6616), p.516.
- Chen, Y., 2013. Early Holocene vegetation dynamics of lake Barrine basin northeast Queensland Australia.
- Cheng, H., Adkins, J., Edwards, R.L. and Boyle, E.A., 2000. U-Th dating of deep-sea corals. *Geochimica et Cosmochimica Acta*, 64(14), pp.2401-2416.
- Cheng, W., Bitz, C.M. and Chiang, J.C., 2007. Adjustment of the global climate to an abrupt slowdown of the Atlantic meridional overturning circulation. *Ocean Circulation: Mechanisms and Impacts-Past and Future Changes of Meridional Overturning*, pp.295-313.
- Chiang, J.C. and Bitz, C.M., 2005. Influence of high latitude ice cover on the marine Intertropical Convergence Zone. *Climate Dynamics*, 25(5), pp.477-496.
- Chiang, J.C., Biasutti, M. and Battisti, D.S., 2003. Sensitivity of the Atlantic intertropical convergence zone to last glacial maximum boundary conditions. *Paleoceanography*, 18(4).
- Chiang, J.C., Kushnir, Y. and Giannini, A., 2002. Deconstructing Atlantic Intertropical Convergence Zone variability: Influence of the local cross-equatorial sea surface temperature gradient and remote forcing from the eastern equatorial Pacific. *Journal of Geophysical Research: Atmospheres*, 107(D1).
- Chivas, A.R., De Deckker, P., Cali, J.A., Chapman, A., Kiss, E., Shelley, G. and Michael, J., 1993. Coupled Stable Isotope and Trace Element Measurements of Lacustrine Carbonates as Paleoclimatic Indicators. *Climate change in continental isotopic records*, pp.113-121.
- Cipriani, N., Malesani, P., Vannucci, S., 1977. I travertine dell'Italia Centrale. *Boll. Serv. Geol. Ital.* 98: 58 - 115.
- Clark, I.D. and Fritz, P., 1997. *Environmental isotopes in hydrogeology*. CRC press.
- Clark, P.U., Dyke, A.S., Shakun, J.D., Carlson, A.E., Clark, J., Wohlfarth, B., Mitrovica, J.X., Hostetler, S.W. and McCabe, A.M., 2009. The last glacial maximum. *science*, 325(5941), pp.710-714.
- Clausing, A. and Boy, J.A., 2000. Lamination and primary production in fossil lakes: relationship to palaeoclimate in the Carboniferous-Permian transition. *Geological Society, London, Special Publications*, 181(1), pp.5-16.
- Clemens, S.C., Prell, W.L., Sun, Y., Liu, Z. and Chen, G., 2008. Southern Hemisphere forcing of Pliocene ^{18}O and the evolution of Indo-Asian monsoons. *Paleoceanography*, 23(4).
- Clement, A.C. and Peterson, L.C., 2008. Mechanisms of abrupt climate change of the last glacial period. *Reviews of Geophysics*, 46(4).
- CNA, B., LSHTM and UB, 1998. Effects of Wastewater Reuse on Groundwater in the Mezquital Valley, Hidalgo State, Mexico. Final Report-November 1998. BGS Technical Report WC/98/42.
- Cochran, U.A., 2002. Detection of large Holocene earthquakes in the sedimentary record of Wellington, New Zealand, using diatom analysis.
- Colman, S.M., Kaufman, D.S., Bright, J., Heil, C., King, J.W., Dean, W.E., Rosenbaum, J.G., Forester, R.M., Bischoff, J.L., Perkins, M. and McGeekin, J.P., 2006. Age model for a continuous, ca 250-ka Quaternary lacustrine record from Bear Lake, Utah-Idaho. *Quaternary Science Reviews*, 25(17), pp.2271-2282.
- Corona-M, E., 2008. The origin of archaeozoology in México: An overview. *Quaternary International*, 185(1), pp.75-81.
- Corona-M, E., 2015. An Overview of Late Pleistocene Faunal Research and the Early Peopling of Mexico. *WORLD HERITAGE HEADS* 5, p.75.
- Correa-Metrio, A., Lozano-García, S., Xelhuantzi-López, S., Sosa-Nájera, S. and Metcalfe, S.E., 2012. Vegetation in western Central Mexico during the last 50 000 years: modern analogs and climate in the Zacapu Basin. *Journal of Quaternary Science*, 27(5), pp.509-518.

- Cortes, A. and Farvolden, R.N., 1989. Isotope studied of precipitation and groundwater in the sierra de las Cruces, Mexico. *Journal of Hydrology*, 107(1), pp.147-153.
- Cortés, A., Durazo, J. and Farvolden, R.N., 1997. Studies of isotopic hydrology of the basin of Mexico and vicinity: annotated bibliography and interpretation. *Journal of Hydrology*, 198(1-4), pp.346-376.
- Craig, H., 1961. Isotopic variations in meteoric waters. *Science*, 133(3465), pp.1702-1703.
- Cross, J.K., Roberge, J. and Jerram, D.A., 2012. Constraining the degassing processes of Popocatepetl Volcano, Mexico: A vesicle size distribution and glass geochemistry study. *Journal of Volcanology and Geothermal Research*, 225, pp.81-95.
- Dalrymple, R.W. and James, N.P. eds., 2010. *Facies models 4*. Geological Association of Canada
- Damuth, J.E. and Fairbridge, R.W., 1970. Equatorial Atlantic deep-sea arkosic sands and ice-age aridity in tropical South America. *Geological Society of America Bulletin*, 81(1), pp.189-206.
- Dansgaard, W., Johnsen, S.J., Clausen, H.B., Dahl-Jensen, D., Gundestrup, N.S., Hammer, C.U., Hvidberg, C.S., Steffensen, J.P., Sveinbjörnsdóttir, A.E., Jouzel, J. and Bond, G., 1993. Evidence for general instability of past climate from a 250-kyr ice-core record. *Nature*, 364(6434), pp.218-220.
- Davis, O.K., 1999. Pollen analysis of Tulare Lake, California: Great Basin-like vegetation in Central California during the full-glacial and early Holocene. *Review of Palaeobotany and Palynology*, 107(3), pp.249-257.
- De Cserna, Z. M., De la Fuente - Duch, M., Palacios Nieto, L., Triay, L., Mitres Saazar., Mota Palomino, R., 1988. Estructurava geologica, gravimetría, sismicidad y relaciones neotectónions regionales de la Cuenca de Mexico. *Boletín 104*. Mexico, Instituto de Geología UNAM, 71.
- De Filippis, L., Faccenna, C., Billi, A., Anzalone, E., Brillì, M., Özkul, M., Soligo, M., Tuccimei, P. and Villa, I.M., 2012. Growth of fissure ridge travertines from geothermal springs of Denizli Basin, western Turkey. *Geological Society of America Bulletin*, 124(9-10), pp.1629-1645.
- De Terra, H., Romero, J., Stewart, T.D. and Linton, R., 1949. Tepexpan man (No. 11-12). Viking Fund.
- Dean Jr, W.E., 1974. Determination of carbonate and organic matter in calcareous sediments and sedimentary rocks by loss on ignition: comparison with other methods. *Journal of Sedimentary Research*, 44(1).
- Delcourt, H.R. and Delcourt, P., 1991. *Quaternary ecology: a paleoecological perspective*. Springer Science & Business Media.
- Delworth, T.L., Clark, P.U., Holland, M., Johns, T., Kuhlbrodt, T., Lynch-Stieglitz, C., Morrill, C., Seager, R., Weaver, A. and Zhang, R., 2008. The potential for abrupt change in the Atlantic meridional overturning circulation. *Abrupt climate change. A report by the US climate change science program and the subcommittee on global change research*, pp.258-359.
- DFID (1998) *Better Water Services in Developing Countries: Public-Private Partnership-The Way Ahead*. London: Department for International Development
- Dhir, R.P., Tandon, S.K., Sareen, B.K., Ramesh, R., Rao, T.K.G., Kailath, A.J. and Sharma, N., 2004. Calcretes in the Thar desert: genesis, chronology and palaeoenvironment. *Journal of Earth System Science*, 113(3), pp.473-515.
- Dickinson, W.R. and Lawton, T.F., 2001. Carboniferous to Cretaceous assembly and fragmentation of Mexico. *Geological Society of America Bulletin*, 113(9), pp.1142-1160.
- Dimbleby, G.W., 1957. Pollen analysis of terrestrial soils. *New Phytologist*, 56(1), pp.12-28.
- Douglas, M.W., Maddox, R.A., Howard, K. and Reyes, S., 1993. The mexican monsoon. *Journal of Climate*, 6(8), pp.1665-1677.
- Drake, N.A., Blench, R.M., Armitage, S.J., Bristow, C.S. and White, K.H., 2011. Ancient watercourses and biogeography of the Sahara explain the peopling of the desert. *Proceedings of the National Academy of Sciences*, 108(2), pp.458-462.

- Droxler, A.W., Alley, R.B., Howard, W.R., Poore, R.Z. and Burckle, L.H., 2003. Unique and exceptionally long interglacial Marine Isotope Stage 11: window into Earth warm future climate. *Earth's Climate and Orbital Eccentricity: The Marine Isotope Stage 11 Question*, pp.1-14.
- Durand, N., Gunnell, Y., Curmi, P. and Ahmad, S.M., 2007. Pedogenic carbonates on Precambrian silicate rocks in South India: Origin and paleoclimatic significance. *Quaternary International*, 162, pp.35-49.
- Durazo, J. and Farvolden, R.N., 1989. The groundwater regime of the Valley of Mexico from historic evidence and field observations. *Journal of Hydrology*, 112(1-2), pp.171-190.
- Dutton, A.R., 1995. Groundwater isotopic evidence for paleorecharge in US High Plains aquifers. *Quaternary Research*, 43(2), pp.221-231.
- Edmunds, M., Carrillo-Rivera, J. J., Cardona, A., 2002. Geochemical evolution of groundwater beneath Mexico City. *Journal of Hydrology*, 258: 1 - 24.
- Edwards, R.L., Gallup, C.D., Ludwig, K.R., Simmons, K.R., Winograd, I.J., Szabo, B.J. and Riggs, A.C., 1993. Dating of the Devils Hole calcite vein. *Science*, 259(5101), pp.1626-1628.
- Ehlers, J., Ehlers, J., Gibbard, P.L. and Hughes, P.D. eds., 2011. *Quaternary glaciations-extent and chronology: a closer look*. Elsevier.
- Elliot, T., Andrews, J.N. and Edmunds, W.M., 1999. Hydrochemical trends, palaeorecharge and groundwater ages in the fissured Chalk aquifer of the London and Berkshire Basins, UK. *Applied Geochemistry*, 14(3), pp.333-363.
- Elliott, J. G., Gellis, A. C., Aby, J. C., 1999. *Incised River Channels*.
- Enzel, Y., Ely, L.L., Mishra, S., Ramesh, R., Amit, R., Lazar, B., Rajaguru, S.N., Baker, V.R. and Sandler, A., 1999. High-resolution Holocene environmental changes in the Thar Desert, northwestern India. *Science*, 284(5411), pp.125-128.
- Ersoy, O., Chinga, G., Aydar, E., Gourgaud, A., Cubukcu, H.E. and Ulusoy, I., 2006. Texture discrimination of volcanic ashes from different fragmentation mechanisms: A case study, Mount Nemrut stratovolcano, eastern Turkey. *Computers & geosciences*, 32(7), pp.936-946.
- Esteban, M. and Klappa, C.F., 1983. Subaerial exposure environment. *Carbonate Depositional Environments: American Association of Petroleum Geologists, Memoir*, 33, pp.1-54.
- Farrell, J.W. and Prell, W.L., 1989. Climatic change and CaCO₃ preservation: an 800,000 year bathymetric reconstruction from the central equatorial Pacific Ocean. *Paleoceanography*, 4(4), pp.447-466.
- Felstead, N.J., 2012. *Palaeoenvironmental Reconstruction and Geoarchaeology of the Cuatro Ciénegas Basin, NE Mexico, from the Late Pleistocene to the present (Doctoral dissertation, Ph. D. thesis) Liverpool John Moores University, UK*.
- Ferrari, L., 2009. Geological origins of the lacustrine basins of the Trans Mexican Volcanic Belt. Abstract taken from the Programme of Abstracts, International Palaeolimnology Symposium, IPA, Guadalajara, Mexico, December 2009., pres.com, unpublished.
- Ferrari, L., Conticelli, S., Vaggelli, G., Petrone, C.M. and Manetti, P., 2000. Late Miocene volcanism and intra-arc tectonics during the early development of the Trans-Mexican Volcanic Belt. *Tectonophysics*, 318(1), pp.161-185.
- Ferrari, L., Morán - Zenteno, D., González-Torres, E.A., 2007. *Actualización de la Carta Geológica de México, escala 1:4,000,000: Universidad Nacional Autónoma de México, Instituto de Geografía, Nuevo Atlas Nacional de México*
- Ferrari, L., Orozco-Esquivel, T., Manea, V. and Manea, M., 2012. The dynamic history of the Trans-Mexican Volcanic Belt and the Mexico subduction zone. *Tectonophysics*, 522, pp.122-149.
- Ferreira, M.G. and Absy, M.L., 2017. Pollen analysis of honeys of *Melipona (Michmelia) seminigra merrillae* and *Melipona (Melikerria) interrupta* (Hymenoptera: Apidae) bred in Central Amazon, Brazil. *Grana*, pp.1-14.
- Fielding, C.R., Allen, J.P., Alexander, J. and Gibling, M.R., 2009. Facies model for fluvial systems in the seasonal tropics and subtropics. *Geology*, 37(7), pp.623-626.
- Flenley, J.R., 1979. *A geological history of tropical rainforest*.

- Flores-Márquez, E.L., Jiménez-Suárez, G., Martínez-Serrano, R.G., Chávez, R.E. and Pérez, D.S., 2006. Study of geothermal water intrusion due to groundwater exploitation in the Puebla Valley aquifer system, Mexico. *Hydrogeology Journal*, 14(7), pp.1216-1230.
- Flügel, E., 2004. *Microfacies Data: Fabrics*. In *Microfacies of Carbonate Rocks* (pp. 177-242). Springer Berlin Heidelberg.
- Fogg, G.E., 1989, March. Emergence of geologic and stochastic approaches for characterization of heterogeneous aquifers. In *Proceedings of the Robert S. Kerr Research Laboratory of the USEPA Conference on: New Field Techniques for Quantifying the Physical and Chemical Properties of Heterogeneous Aquifers*, Dallas, TX.
- Forbes, E.B., 2010. Holocene paleoclimate variation from major and trace elements and stable isotopes in a Wisconsin tufa deposit.
- Ford, T. D., Pedley, H. M., 1996. A review of tufa and travertine deposits of the world. *Earth-Science Reviews*, 41: 117 - 175.
- Ford, T.D. and Pedley, H.M., 1992. Tufa deposits of the world. *Journal of the Speleological Society of Japan*, 17, pp.46-63.
- Fox, D.J., 1965. Man-water relationships in metropolitan Mexico. *Geographical review*, 55(4), pp.523-545.
- Frank, N., Turpin, L., Cabioch, G., Blamart, D., Tressens-Fedou, M., Colin, C. and Jean-Baptiste, P., 2006. Open system U-series ages of corals from a subsiding reef in New Caledonia: implications for sea level changes, and subsidence rate. *Earth and Planetary Science Letters*, 249(3), pp.274-289.
- Freytet, P. and Plaziat, J.C., 1982. Continental carbonate sedimentation and pedogenesis-Late Cretaceous and Early Tertiary of southern France.
- Freytet, P. and Verrecchia, E.P., 1998. Freshwater organisms that build stromatolites: a synopsis of biocrystallization by prokaryotic and eukaryotic algae. *Sedimentology*, 45(3), pp.535-563.
- Freytet, P. and Verrecchia, E.P., 2002. Lacustrine and palustrine carbonate petrography: an overview. *Journal of Paleolimnology*, 27(2), pp.221-237.
- Fronval, T., Bo Jensen, N. and Buchardt, B., 1995. Oxygen isotope disequilibrium precipitation of calcite in Lake Arresø, Denmark. *Geology*, 23(5), pp.463-466.
- G?slason, S. and Eugster, H.P., 1987. Meteoric water-basalt interactions. II: a field study in NE Iceland. *Geochim. Cosmochim. Acta*, 51, pp.2841-2855.
- Gandin, A. and Capezzuoli, E., 2008. Travertine versus calcareous tufa: distinctive petrologic features and stable isotopes signatures. *Italian Journal of Quaternary Sciences*, 21(1B).
- Gandin, A. and Capezzuoli, E., 2014. Travertine: Distinctive depositional fabrics of carbonates from thermal spring systems. *Sedimentology*, 61(1), pp.264-290.
- Gani, M.R. and Alam, M.M., 2004. Fluvial facies architecture in small-scale river systems in the Upper Dupi Tila Formation, northeast Bengal Basin, Bangladesh. *Journal of Asian Earth Sciences*, 24(2), pp.225-236.
- García-Palomo, A., Macías, J.L. and Garduño, V.H., 2000. Miocene to Recent structural evolution of the Nevado de Toluca volcano region, central Mexico. *Tectonophysics*, 318(1-4), pp.281-302.
- Garcés, B.L.V. and Aguilar, J.G., 1992. Shallow carbonate lacustrine facies models in the Permian of the Aragon-Bearn basin (Western Spanish-French Pyrenees). *Carbonates and Evaporites*, 7(2), p.94.
- Garcés, B.V., Moreno, A., Navas, A., Mata, P., Machín, J., Huertas, A.D., Sampériz, P.G., Schwalb, A., Morellón, M., Cheng, H. and Edwards, R.L., 2008. The Taravilla lake and tufa deposits (Central Iberian Range, Spain) as palaeohydrological and palaeoclimatic indicators. *Palaeogeography, Palaeoclimatology, Palaeoecology*, 259(2), pp.136-156.
- García-Castellanos, D., Vergés, J., Gaspar-Escribano, J. and Cloetingh, S., 2003. Interplay between tectonics, climate, and fluvial transport during the Cenozoic evolution of the Ebro Basin (NE Iberia). *Journal of Geophysical Research: Solid Earth*, 108(B7).

- García-Palomo, A., Macías, J.L., Arce, J.L., Capra, L., Garduño, V.H. and Espíndola, J.M., 2002. Geology of the Nevado de Toluca volcano and surrounding areas, Central Mexico.
- Gargaud, M., Amils, R. and Cleaves, H.J. eds., 2011. Encyclopedia of astrobiology (Vol. 1). Springer Science & Business Media.
- Garnett, E.R., Andrews, J.E., Preece, R.C. and Dennis, P.F., 2004. Climatic change recorded by stable isotopes and trace elements in a British Holocene tufa. *Journal of Quaternary Science*, 19(3), pp.251-262.
- Garnett, J., 2006. Analytic capacity and measure (Vol. 297). Springer.
- Garrison, J.M., Davidson, J.P., Hall, M. and Mothes, P., 2011. Geochemistry and petrology of the most recent deposits from Cotopaxi Volcano, Northern Volcanic Zone, Ecuador. *Journal of Petrology*, p.egr023.
- Garziona, C.N., Dettman, D.L., Quade, J., DeCelles, P.G. and Butler, R.F., 2000. High times on the Tibetan Plateau: Paleoelevation of the Thakkhola graben, Nepal. *Geology*, 28(4), pp.339-342.
- Gasse, F., 2000. Hydrological changes in the African tropics since the Last Glacial Maximum. *Quaternary Science Reviews*, 19(1), pp.189-211.
- Genise, J.F., Melchor, R.N., Belloso, E.S. and Verde, M., 2010. Invertebrate and vertebrate trace fossils from continental carbonates. *Developments in Sedimentology*, 61, pp.319-369.
- Ghannem, N., Tlili, F., Riahi, C. and Regaya, K., 2016. Sedimentologic study of palustrine continental carbonate deposits of the Tajerouine area, NW Tunisia. *CARNETS DE GEOLOGIE*, 16(4).
- Ghinassi, M. and Ielpi, A., 2015. Stratal architecture and morphodynamics of downstream-migrating fluvial point bars (Jurassic Scalby Formation, UK). *Journal of Sedimentary Research*, 85(9), pp.1123-1137.
- Ghosh, S. and Guchhait, S.K., 2014. Palaeoenvironmental significance of fluvial facies and archives of Late Quaternary deposits in the floodplain of Damodar River, India. *Arabian Journal of Geosciences*, 7(10), pp.4145-4161.
- Gierlowski-Kordesch, E. and Rust, B.R., 1994. The Jurassic East Berlin Formation, Hartford Basin, Newark Supergroup (Connecticut and Massachusetts): A Saline Lake Playa Alluvial Plain System.
- Gierlowski-Kordesch, E.H., 2010. Lacustrine carbonates. *Developments in Sedimentology*, 61, pp.1-101.
- Gile, L.H., Hawley, J.W. and Grossman, R.B., 1981. Soils and geomorphology in the Basin and Range area of southern New Mexico: Guidebook to the Desert Project (Vol. 39). New Mexico Bureau of Mines & Mineral Resources.
- Gillespie, R., 1997. Burnt and unburnt carbon: dating charcoal and burnt bone from the Willandra Lakes, Australia. *Radiocarbon*, 39(03), pp.239-250.
- Glenn, C.R. and Kelts, K., 1991. Sedimentary rhythms in lake deposits. *Cycles and events in stratigraphy*, pp.188-221.
- Glover, C. and Robertson, A.H., 2003. Origin of tufa (cool?water carbonate) and related terraces in the Antalya area, SW Turkey. *Geological journal*, 38(3?4), pp.329-358.
- Godwin, H., 1962. Half-life of radiocarbon. *Nature*, 195, p.984.
- Golubic, S., Violante, C., Ferreri, V., D'Argenio, B. and Barattolo, F., 1993. Algal control and early diagenesis in Quaternary travertine formation (Rocchetta a Volturno, Central Apennines). *Studies on fossil benthic algae. Boll Soc Paleont Ital, Spec*, 1, pp.231-247.
- Gómez-Tuena, A., Orozco-Esquivel, M.T. and Ferrari, L., 2007. Igneous petrogenesis of the Trans-Mexican volcanic belt. *Geological Society of America Special Papers*, 422, pp.129-181.
- Gonzalez, S. and Huddart, D., 2008. The late pleistocene human occupation of Mexico. In *Memoria de Simposio Internacional de FUMDHAM*.
- Gonzalez, S., Huddart, D., Israde-Alcántara, I., Domínguez-Vázquez, G., Bischoff, J. and Felstead, N., 2015. Paleoinian sites from the Basin of Mexico: Evidence from stratigraphy, tephrochronology and dating. *Quaternary International*, 363, pp.4-19.

- Gonzalez, S., Jimenez-Lopez, J. C., Hedges, R., Huddart, D., Ohman, J. C., Turner, A., Pompa y Padilla, J. A., 2003. Earliest Humans in the Americas, New Evidence from Mexico, *Journal of Human Evolution* 44: 379-387.
- Gonzalez, S., Pastrana, A., Siebe, C. and Duller, G., 2000. Timing of the prehistoric eruption of Xitle Volcano and the abandonment of Cuicuilco Pyramid, Southern Basin of Mexico. Geological Society, London, Special Publications, 171(1), pp.205-224.
- González-Quintero, L. and Fuentes Mata, M., 1980. El Holoceno de la porción central de la Cuenca de México. *Mem Inst N Antrop Hist III Coloquio sobre Paleobotanica y PalinologmHa* (Mexico City, 1977), 86, pp.133-158.
- Goodfriend, G.A. and Stipp, J.J., 1983. Limestone and the problem of radiocarbon dating of land-snail shell carbonate. *Geology*, 11(10), pp.575-577.
- Goudie, A., 1975. Petrographic Characteristics of Calcrete (caliches): Modern Analogues of Ancient Concretions.
- Goudie, A.S., 1996. Organic agency in calcrete development. *Journal of Arid Environments*, 32(2), pp.103-110.
- Gradziński, M., 2010. Factors controlling growth of modern tufa: results of a field experiment. Geological Society, London, Special Publications, 336(1), pp.143-191.
- Griffin, D.G., 2017. Ancient Artifact or New Age Totem: Analysis of a Carved Sacrum from the Oregon Coast. *Journal of Northwest Anthropology*, 51(1).
- Grimm, E.C., 1991. 2004. TILIA, TILIA.GRAPH, and TGView. Illinois State Museum, Research and Collections Center, Springfield, USA.
- Grove, A.T. and Goudie, A.S., 1971. Late quaternary lake levels in the rift valley of southern Ethiopia and elsewhere in tropical Africa. *Nature*, 234(5329), pp.403-405.
- Gruszka, B. and van Loon, A.T., 2007. Pleistocene glaciolacustrine breccias of seismic origin in an active graben (central Poland). *Sedimentary Geology*, 193(1), pp.93-104.
- Gruszka, B., 2007. The Pleistocene glaciolacustrine sediments in the Be?chatów mine (central Poland): Endogenic and exogenic controls. *Sedimentary Geology*, 193(1), pp.149-166.
- Guerreiro, P., Cunha, L. and Ribeiro, C., 2011. Geomorphological settings and tufa models in Algre flexure (Algarve, Portugal).
- Guerrero, B.O., Thompson, R. and Fucugauchi, J.U., 2000. Magnetic properties of lake sediments from Lake Chalco, central Mexico, and their palaeoenvironmental implications. *Journal of Quaternary Science*, 15(2), pp.127-140.
- Gulbranson, E.L., 2004, November. Calcretes and Plaustrine Carbonates as indicators of Climate Shift, Late Triassic and Early Cretaceous of the Southwestern. In 2004 Denver Annual Meeting.
- Guo, L. and Riding, R., 1992. Aragonite laminae in hot water travertine crusts, Rapolano Terme, Italy. *Sedimentology*, 39(6), pp.1067-1079.
- Guo, L. and Riding, R., 1998. Hot?spring travertine facies and sequences, Late Pleistocene, Rapolano Terme, Italy. *Sedimentology*, 45(1), pp.163-180.
- Guo, X. and Chafetz, H.S., 2012. Large tufa mounds, Searles Lake, California. *Sedimentology*, 59(5), pp.1509-1535.
- Harvey, A.M., Whitfield, E., Stokes, M. and Mather, A., 2014. The late Neogene to Quaternary drainage evolution of the uplifted neogene sedimentary basins of Almería, Betic chain. In *Landscapes and Landforms of Spain* (pp. 37-61). Springer, Dordrecht.
- Heath, R.C., 1989. Basic Ground-Water Hydrology. U.S. Geological Survey Water-Supply Paper 2220, 84p
- Hedges, J.I., 1992. Global biogeochemical cycles: progress and problems. *Marine chemistry*, 39(1-3), pp.67-93.
- Heiken, G. and Wohletz, K., 1985. Volcanic ash. University Presses of California, Chicago, Harvard & MIT.
- Heine, K. and Schönhals, E., 1973. Entstehung und Alter der" toba"-Sedimente in Mexiko. *Eiszeitalter und Gegenwart= E & G*, 23, pp.201-215.

- Heine, K., 1984. The classical Late Weichselian climatic fluctuations in Mexico. In *Climatic changes on a yearly to millennial basis* (pp. 95-115). Springer Netherlands.
- Heine, K., 2003. Paleopedological evidence of human-induced environmental change in the Puebla-Tlaxcala area (Mexico) during the last 3,500 years. *Revista Mexicana de Ciencias Geológicas*, 20(3), pp.235-244.
- Hemming, S.R., 2004. Heinrich events: Massive late Pleistocene detritus layers of the North Atlantic and their global climate imprint. *Reviews of Geophysics*, 42(1).
- Henchiri, M., 2014a. Quaternary paludal tufas from the Ben Younes spring system, Gafsa, southwestern Tunisia: Interactions between tectonics and climate. *Quaternary International*, 338, pp.71-87.
- Henchiri, M., 2014b. Sedimentology of Quaternary calcareous tufas from Gafsa, southwestern Tunisia. *Arabian Journal of Geosciences*, 7(5), pp.2081-2091.
- Hendy, I.L., Minckley, T.A. and Whitlock, C., 2016. Eastern tropical Pacific vegetation response to rapid climate change and sea level rise: A new pollen record from the Gulf of Tehuantepec, southern Mexico. *Quaternary Science Reviews*, 145, pp.152-160.
- Hernández-Cerda, M.E. and Carrasco-Anaya, G., 2007. Rasgos climáticos más importantes. *Biodiversidad de la Faja Volcánica Transmexicana*, Universidad Nacional Autónoma de México, pp.57-72.
- Hibbard, C.W., 1955. Pleistocene vertebrates from the Upper Becerra (Becerra Superior) formation, Valley of Tequiquiac, Mexico, with notes on other Pleistocene forms.
- Higgins, R.W., Mo, K.C. and Yao, Y., 1998. Interannual variability of the US summer precipitation regime with emphasis on the southwestern monsoon. *Journal of Climate*, 11(10), pp.2582-2606.
- Hjulstrom, F., 1939. Transportation of detritus by moving water: Part 1. Transportation.
- Hodell, D.A., Anselmetti, F.S., Ariztegui, D., Brenner, M., Curtis, J.H., Gilli, A., Grzesik, D.A., Guilderson, T.J., Müller, A.D., Bush, M.B. and Correa-Metrio, A., 2008. An 85-ka record of climate change in lowland Central America. *Quaternary Science Reviews*, 27(11), pp.1152-1165.
- Holz, M., Troccoli, E. and Vieira, M., 2014. Sequence Stratigraphy of Continental Rift Basins II: An Example from the Brazilian Cretaceous Recôncavo Basin. In *STRATI 2013* (pp. 15-18). Springer International Publishing.
- Horbury, A.D. and Adams, A.E., 1996. Microfacies associations in Asbian carbonates: an example from the Urswick Limestone Formation of the southern Lake District, northern England. *Geological Society, London, Special Publications*, 107(1), pp.221-237.
- HSÜ, K., 1979. Non-annual cycles of varve-like sedimentation in Walensee, Switzerland. *Sedimentology*, 26(3), pp.453-461.
- <https://www.usgs.gov/>
- Huang, Y. and Fairchild, I.J., 2001. Partitioning of Sr²⁺ and Mg²⁺ into calcite under karst-analogue experimental conditions. *Geochimica et Cosmochimica Acta*, 65(1), pp.47-62.
- Hughes, P.D., Gibbard, P.L. and Ehlers, J., 2013. Timing of glaciation during the last glacial cycle: evaluating the concept of a global 'Last Glacial Maximum'(LGM). *Earth-Science Reviews*, 125, pp.171-198.
- Ihlenfeld, C., Norman, M.D., Gagan, M.K., Drysdale, R.N., Maas, R. and Webb, J., 2003. Climatic significance of seasonal trace element and stable isotope variations in a modern freshwater tufa. *Geochimica et Cosmochimica Acta*, 67(13), pp.2341-2357.
- Imbrie, J., 1979. Imbrie.
- INEGI., 1997. Carta Topografica, 1: 50,000, Zumpango de Ocampo, E14A19, Mexico, Hidalgo.
- Irion, G. and Müller, G., 1968. Mineralogy, petrology and chemical composition of some calcareous tufa from the Schwäbische Alb, Germany. In *Recent developments in carbonate sedimentology in Central Europe* (pp. 157-171). Springer Berlin Heidelberg.
- Israde Alcántara, I., Garduño-Monroy, V.H. and Ortega Murillo, R., 2002. Paleambiente lacustre del Cuaternario tardío en el centro del lago de Cuitzeo. *Hidrobiológica*, 12(1), pp.61-78.

- Israde-Alcántara, I., Garduño-Monroy, V.H., Fisher, C.T., Pollard, H.P. and Rodríguez-Pascua, M.A., 2005. Lake level change, climate, and the impact of natural events: the role of seismic and volcanic events in the formation of the Lake Patzcuaro Basin, Michoacan, Mexico. *Quaternary International*, 135(1), pp.35-46.
- Israde-Alcántara, I., Miller, W.E., Garduño-Monroy, V.H., Barron, J. and Rodríguez-Pascua, M.A., 2010. Palaeoenvironmental significance of diatom and vertebrate fossils from Late Cenozoic tectonic basins in west-central México: A review. *Quaternary International*, 219(1-2), pp.79-94.
- Issar, A., Quijano, J.L., Gat, J.R. and Castro, M., 1984. The isotope hydrology of the groundwaters of central Mexico. *Journal of Hydrology*, 71(3), pp.201-224.
- Jacobson, G. and Arakel, A.V., 1986. Calcrete aquifers in the Australian arid zone. In *Proceedings of the International Conference on Groundwater Systems Under Stress*, Brisbane, Australian Water Resources Council (pp. 515-523).
- James, N.P. and Dalrymple, R.W., 2010. *Facies Models 4: St. John's, Newfoundland*, Geological Association of Canada.
- Jasso, R.H., 2017. Dinámica de la estructura de comunidades del Cenozoico tardío de Norteamérica: Episodios de Recambio Rápido de Fauna (RTE) dentro del concepto de Cronofauna. *Estudios Geológicos*, 73(1), p.063.
- Jiménez, B. and Asano, T., 2008. Water reclamation and reuse around the world. *Water Reuse: an international survey of current practice, issues and needs*, 20, p.3.
- Jiménez, B. and Chávez, A., 2004. Quality assessment of an aquifer recharged with wastewater for its potential use as drinking source: "El Mezquital Valley" case. *Water Science and Technology*, 50(2), pp.269-276.
- Jimenez, B., Asano, T., 2008. *Water Reuse an international survey of current practices, issues and needs*. Scientific and Technical report, 20. IWA. London.
- Johnson, C.A. and Harrison, C.G.A., 1990. Neotectonics in central Mexico. *Physics of the Earth and Planetary Interiors*, 64(2-4), pp.187-210.
- Jones, B. and Renaut, R.W., 2010. Calcareous spring deposits in continental settings. *Developments in Sedimentology*, 61, pp.177-224.
- Jones, V.J. and Birks, H.J.B., 2004. Lake-sediment records of recent environmental change on Svalbard: results of diatom analysis. *Journal of Paleolimnology*, 31(4), pp.445-466.
- Jourdan, F., Mark, D.F. and Verati, C. eds., 2014, April. *Advances in ⁴⁰Ar/³⁹Ar Dating: From Archaeology to Planetary Sciences*. Geological Society of London.
- Jutras, P., Utting, J. and McLeod, J., 2007. Link between long-lasting evaporitic basins and the development of thick and massive phreatic calcrete hardpans in the Mississippian Windsor and Percé groups of eastern Canada. *Sedimentary Geology*, 201(1), pp.75-92.
- Kabanov, P., Anadón, P. and Krumbein, W.E., 2008. Microcodium: an extensive review and a proposed non-rhizogenic biologically induced origin for its formation. *Sedimentary geology*, 205(3), pp.79-99.
- Kadir, S. and Akbulut, A., 2011. Palygorskite-dominated clayey sedimentary beds of the Çameli formation in the Neogene Sapaca lacustrine basin, Honaz, Denizli Province, SW Turkey. *Neues Jahrbuch für Mineralogie-Abhandlungen: Journal of Mineralogy and Geochemistry*, 188(2), pp.151-167.
- Kämpf, L., Plessen, B., Lauterbach, S., Nantke, C., Meyer, H., Chaplignin, B., Höllerer, H. and Brauer, A., 2016, April. Impact of flood events on lacustrine carbonate isotope records. In *EGU General Assembly Conference Abstracts* (Vol. 18, p. 7814).
- Kendall, A.C. and Broughton, P.L., 1978. Origin of fabrics in speleothems composed of columnar calcite crystals. *Journal of Sedimentary Research*, 48(2).
- Kendall, C. and Caldwell, E.A., 1998. *Fundamentals of isotope geochemistry. Isotope tracers in catchment hydrology*, pp.51-86.
- Kendall, C. and McDonnell, J.J. eds., 2012. *Isotope tracers in catchment hydrology*. Elsevier.

- Kendall, C., Burns, D.A., Silva, S.R., Chang, C.C.Y. and McMahon, P.B., 1995. Sources of variation in the oxygen and nitrogen isotopic composition of nitrate in soils. *AGU Trans*, 76, p.210.
- Kerr, R.A., 2001. The tropics return to the climate system.
- Khadkikar, A.S., Merh, S.S., Malik, J.N. and Chamyal, L.S., 1998. Calcretes in semi-arid alluvial systems: formative pathways and sinks. *Sedimentary Geology*, 116(3-4), pp.251-260.
- Khalaf, F.I. and Gaber, A.S., 2008. Occurrence of cyclic palustrine and calcrete deposits within the lower Pliocene Hagul formation, East Cairo district, Egypt. *Journal of African Earth Sciences*, 51(5), pp.298-312.
- Klappa, C.F., 1978. Biolithogenesis of *Microcodium*: elucidation. *Sedimentology*, 25(4), pp.489-522.
- Klappa, C.F., 1979. Lichen stromatolites: criterion for subaerial exposure and a mechanism for the formation of laminar calcretes (caliche). *Journal of Sedimentary Research*, 49(2).
- Klappa, C.F., 1980. Rhizoliths in terrestrial carbonates: classification, recognition, genesis and significance. *Sedimentology*, 27(6), pp.613-629.
- Klein, J., Lerman, J.C., Damon, P.E. and Ralph, E.K., 1982. Calibration of radiocarbon dates: tables based on the consensus data of the Workshop on Calibrating the Radiocarbon Time Scale. *Radiocarbon*, 24(02), pp.103-150.
- Knox, G.J., 1977. Caliche profile formation, Saldanha Bay (South Africa). *Sedimentology*, 24(5), pp.657-674.
- Knudsen, M.F., Seidenkrantz, M.S., Jacobsen, B.H. and Kuijpers, A., 2011. Tracking the Atlantic Multidecadal Oscillation through the last 8,000 years. *Nature communications*, 2, p.178.
- Koçun, E., 2012. Facies characteristics and depositional environments of Quaternary tufa deposits, Antalya, SW Turkey. *Carbonates and evaporites*, 27(3-4), pp.269-289.
- Košir, A., 2004. *Microcodium* revisited: root calcification products of terrestrial plants on carbonate-rich substrates. *Journal of Sedimentary Research*, 74(6), pp.845-857.
- Kowallis, B.J., Swisher, C.C., III, Carranza-Castaneda, O., Miller, W.E., and Tingey, D.G., 1998. Fission-track and single crystal $^{40}\text{Ar}/^{39}\text{Ar}$ laser-fusion ages from volcanic ash layers in fossil-bearing Pliocene sediments in central Mexico. *Revista Mexicana de Ciencias Geológicas*, 15: 157-160.
- Kraus, S., Kurbatov, A. and Yates, M., 2013. Geochemical signatures of tephras from Quaternary Antarctic Peninsula volcanoes. *Andean Geology*, 40(1), pp.1-40.
- Kutzbach, J.E. and Street-Perrott, F.A., 1985. Milankovitch forcing of fluctuations in the level of tropical lakes from 18 to 0 kyr BP. *Nature* 317, 130-34.
- Lamb, A.L., Gonzalez, S., Huddart, D., Metcalfe, S.E., Vane, C.H. and Pike, A.W., 2009. Tepexpan Palaeoindian site, Basin of Mexico: multi-proxy evidence for environmental change during the late Pleistocene-late Holocene. *Quaternary Science Reviews*, 28(19), pp.2000-2016.
- Larrasoaña, J.C., Roberts, A.P., Rohling, E.J., Winkhofer, M. and Wehausen, R., 2003. Three million years of monsoon variability over the northern Sahara. *Climate Dynamics*, 21(7-8), pp.689-698.
- Larsen, C.P.S., Pienitz, R., Smol, J.P., Moser, K.A., Cumming, B.F., Blais, J.M., MacDonald, G.M. and Hall, R.I., 1998. Relations between lake morphometry and the presence of laminated lake sediments: a re-examination of Larsen and MacDonald (1993). *Quaternary Science Reviews*, 17(8), pp.711-717.
- Ledesma-Guerrero, O., 1967. Resumen de la geología de la Hoja Parras, 13R-1 (6) escala 1: 100000: México, DF, Universidad Nacional Autónoma de México, Instituto de Geología. Carta Geológica de México Serie de, 1(100000), p.1.
- Ledru, M.P., Rousseau, D.D., Cruz, F.W., Riccomini, C., Karmann, I. and Martin, L., 2005. Paleoclimate changes during the last 100,000 yr from a record in the Brazilian Atlantic rainforest region and interhemispheric comparison. *Quaternary Research*, 64(3), pp.444-450.
- Lee, J.Y., Marti, K., Severinghaus, J.P., Kawamura, K., Yoo, H.S., Lee, J.B. and Kim, J.S., 2006. A redetermination of the isotopic abundances of atmospheric Ar. *Geochimica et Cosmochimica Acta*, 70(17), pp.4507-4512.

- Leite, Y.L., Costa, L.P., Loss, A.C., Rocha, R.G., Batalha-Filho, H., Bastos, A.C., Quaresma, V.S., Fagundes, V., Paresque, R., Passamani, M. and Pardini, R., 2016. Neotropical forest expansion during the last glacial period challenges refuge hypothesis. *Proceedings of the National Academy of Sciences*, 113(4), pp.1008-1013.
- Leng, M. J., Marshall, J. D., 2004. Palaeoclimate interpretation of stable isotope data from lake sediment archives, *Quaternary Science Reviews*, 23: 811-831.
- Leng, M.J. ed., 2006. *Isotopes in palaeoenvironmental research* (Vol. 10, p. 307). New York: Springer.
- Leng, M.J., Baneschi, I., Zanchetta, G., Jex, C.N., Wagner, H. and Vogel, H., 2010. Late Quaternary palaeoenvironmental reconstruction from Lakes Ohrid and Prespa (Macedonia/Albania border) using stable isotopes. *Biogeosciences discussion*.
- Leng, M.J., Lamb, A.L., Heaton, T.H., Marshall, J.D., Wolfe, B.B., Jones, M.D., Holmes, J.A. and Arrowsmith, C., 2006. *Isotopes in lake sediments* (pp. 147-184). Springer Netherlands.
- Leng, M.J., Roberts, N., Reed, J.M. and Sloane, H.J., 1999. Late Quaternary palaeohydrology of the Konya Basin, Turkey, based on isotope studies of modern hydrology and lacustrine carbonates. *Journal of Paleolimnology*, 22(2), pp.187-204.
- Levin, N.E., Quade, J., Simpson, S.W., Semaw, S. and Rogers, M., 2004. Isotopic evidence for Plio-Pleistocene environmental change at Gona, Ethiopia. *Earth and Planetary Science Letters*, 219(1), pp.93-110.
- Li, J., Pang, Z., Froehlich, K., Huang, T., Kong, Y., Song, W. and Yun, H., 2015. Paleo-environment from isotopes and hydrochemistry of groundwater in East Junggar Basin, Northwest China. *Journal of Hydrology*, 529, pp.650-661.
- Li, Z., Shi, X., Chen, M.T., Wang, H., Liu, S., Xu, J., Long, H., Troa, R.A., Zuraida, R. and Triarso, E., 2016. Late Quaternary fingerprints of precession and sea level variation over the past 35 kyr as revealed by sea surface temperature and upwelling records from the Indian Ocean near southernmost Sumatra. *Quaternary International*, 425, pp.282-291.
- Libby, W.F., Anderson, E.C. and Arnold, J.R., 1949. Age determination by radiocarbon content: world-wide assay of natural radiocarbon. *Science*, 109(2827), pp.227-228.
- Linares, R., Rosell, J., Roqué, C. and Gutiérrez, F., 2009. Origin and evolution of tufa mounds related to artesian karstic springs in Isona area (Pyrenees, NE Spain). *Geodinamica Acta*, 22(5-6/1-3), p.129.
- Lindqvist, J.K., 1994. Lacustrine stromatolites and oncoids: Manuherikia Group (Miocene), New Zealand. In *Phanerozoic stromatolites II* (pp. 227-254). Springer Netherlands.
- Liutkus, C.M., Wright, J.D., Ashley, G.M. and Sikes, N.E., 2005. Palaeoenvironmental interpretation of lake-margin deposits using $\delta^{13}\text{C}$ and $\delta^{18}\text{O}$ results from early Pleistocene carbonate rhizoliths, Olduvai Gorge, Tanzania. *Geology*, 33(5), pp.377-380.
- Lopez Pearce, J., 2010. Syntectonic deposition and paleohydrology of the spring-fed Hualapai Limestone and implications for 5-6 MA integration of the Colorado River system through Grand Canyon: evidence from sedimentology, geochemistry and detrital zircon analysis (Doctoral dissertation).
- Lopez-Hernandez, A. and Castillo-Hernandez, D., 1997. Exploratory drilling at Acoculco, Puebla, Mexico: a hydrothermal system with only nonthermal manifestations (No. CONF-971048-). Geothermal Resources Council, Davis, CA (United States).
- Lorenzo, J.L., 1969. *Piezas de arte mobiliario en la prehistoria de México* (Vol. 3). Instituto Poblano de Antropología e Historia.
- Lounejeva Baturina, E., Morales Puente, P., Cabadas Báez, H.V., Cienfuegos Alvarado, E., Sedov, S., Vallejo Gómez, E. and Solleiro Rebolledo, E., 2006. Late Pleistocene to Holocene environmental changes from $\delta^{13}\text{C}$ determinations in soils at Teotihuacan, Mexico. *Geofísica internacional*, 45(2), pp.85-98.
- Love, K.M. and Chafetz, H.S., 1988. Diagenesis of laminated travertine crusts, Arbuckle Mountains, Oklahoma. *Journal of Sedimentary Research*, 58(3).
- Lowe, J.J. and Walker, M.J., 2014. *Reconstructing quaternary environments*. Routledge.

- Lozano-García, M.S., Ortega-Guerrero, B., Caballero-Miranda, M. and Urrutia-Fucugauchi, J., 1993. Late Pleistocene and Holocene paleoenvironments of Chalco lake, central Mexico. *Quaternary Research*, 40(3), pp.332-342.
- Lozano-García, M. and Ortega-Guerrero, B., 1998. Late Quaternary environmental changes of the central part of the Basin of Mexico; correlation between Texcoco and Chalco basins. *Review of Palaeobotany and Palynology*, 99(2), pp.77-93.
- Lozano-García, S., 1996. La vegetación Cuaternaria en el Centro de México: Registros Palinológicos e Implicaciones Paleoclimáticas. *Boletín de la Sociedad Botánica de México* 57, 79-102.
- Lozano-García, S., Ortega, B., Roy, P.D., Beramendi-Orosco, L. and Caballero, M., 2015. Climatic variability in the northern sector of the American tropics since the latest MIS 3. *Quaternary Research*, 84(2), pp.262-271.
- Lozano-García, S., Sosa-Nájera, S., Sugiura, Y. and Caballero, M., 2005. 23,000 yr of vegetation history of the Upper Lerma, a tropical high-altitude basin in Central Mexico. *Quaternary Research*, 64(1), pp.70-82.
- Lozano-García, S., Torres-Rodríguez, E., Ortega, B., Vázquez, G. and Caballero, M., 2013. Ecosystem responses to climate and disturbances in western central Mexico during the late Pleistocene and Holocene. *Palaeogeography, Palaeoclimatology, Palaeoecology*, 370, pp.184-195.
- Machette, M.N., 1985. Calcic soils of the southwestern United States. *Geological Society of America Special Papers*, 203, pp.1-22.
- Macías, J.L., 2007. Geology and eruptive history of some active volcanoes of México. *Geological Society of America Special Papers*, 422, pp.183-232.
- Macías, J.L., Arce, J.L., García-Tenorio, F., Layer, P.W., Rueda, H., Reyes-Agustín, G., López-Pizaña, F. and Avellán, D., 2012. Geology and geochronology of Tlaloc, Telapón, Iztaccihuatl, and Popocatepetl volcanoes, Sierra Nevada, central Mexico. *Field Guides*, 25, pp.163-193.
- Macías, J.L., Capra, L., Arce, J.L., Espíndola, J.M., García-Palomo, A. and Sheridan, M.F., 2008. Hazard map of El Chichón volcano, Chiapas, México: Constraints posed by eruptive history and computer simulations. *Journal of Volcanology and Geothermal Research*, 175(4), pp.444-458.
- Macías, M.C. and Tagle, S.G., 1989. *El origen del hombre en América*. GV Editores.
- Mack, G.H., Cole, D.R. and Treviño, L., 2000. The distribution and discrimination of shallow, authigenic carbonate in the Pliocene-Pleistocene Palomas Basin, southern Rio Grande rift. *Geological Society of America Bulletin*, 112(5), pp.643-656.
- Macklin, M.G., Benito, G., Gregory, K.J., Johnstone, E., Lewin, J., Michczyńska, D.J., Soja, R., Starkel, L. and Thorndycraft, V.R., 2006. Past hydrological events reflected in the Holocene fluvial record of Europe. *Catena*, 66(1), pp.145-154.
- Magaña, V.O., Vázquez, J.L., Pérez, J.L. and Pérez, J.B., 2003. Impact of El Niño on precipitation in Mexico. *Geofísica internacional*, 42(3), pp.313-330.
- Magnani, G., Bartolomei, P., Cavulli, F., Esposito, M., Marino, E.C., Neri, M., Rizzo, A., Scaruffi, S. and Tosi, M., 2007. U-series and radiocarbon dates on mollusc shells from the uppermost layer of the archaeological site of KHB-1, Ra's al Khabbah, Oman. *Journal of Archaeological Science*, 34(5), pp.749-755.
- Maher, E. and Harvey, A.M., 2008. Fluvial system response to tectonically induced base-level change during the late-Quaternary: The Rio Alias southeast Spain. *Geomorphology*, 100(1-2), pp.180-192.
- Mahlknecht J, Schneider J, Merkel B, de Leon IN, Bernasconi S. 2004. Groundwater recharge in a sedimentary basin in semi-arid Mexico. *Hydrogeology Journal* 12: 511-530.
- "Mahlknecht, J., Garfias-Solis, J., Aravena, R., Tesch, R., 2006. Geochemical and isotopic investigations on groundwater residence time and flow in the Independence Basin, Mexico. *Journal of Hydrology* 324 (1-4), 283-300."
- Mahoney, J.B., 2005. Nd and Sr isotopic signatures of fine-grained clastic sediments: A case study of western Pacific marginal basins. *Sedimentary Geology*, 182(1), pp.183-199.

- Maldonado-Koerdell, M. and de Anda, L.A.A., 1949. Nota preliminar sobre dos artefactos del pleistoceno superior hallados en la región de Tequixquiak, México. na.
- Mann, A.W. and Horwitz, R.C., 1979. Groundwater calcrete deposits in Australia: some observations from Western Australia. *Journal of the Geological Society of Australia*, 26.
- Marín-Córdova, S., Aguayo, C.J.E. and Mandujano, V.J., 1986. Sistemas mayores de fallamiento en la Cuenca de México y su relación con la sismicidad.
- Marín-Córdova, S., Campos - Enríquez, O., Herrera - Moro - Castillo, M., 2004. Neotectonic related risk to dams in the Mexico Basin - Guadalupe dam. *Geofísica International* 43: 3. 435 - 443.
- Mark, D.F., Rice, C.M., Fallick, A.E., Trewin, N.H., Lee, M.R., Boyce, A. and Lee, J.K.W., 2011. 40 Ar/39 Ar dating of hydrothermal activity, biota and gold mineralization in the Rhynie hot-spring system, Aberdeenshire, Scotland. *Geochimica et Cosmochimica Acta*, 75(2), pp.555-569.
- Matsuoka, J., Kano, A., Oba, T., Watanabe, T., Sakai, S. and Seto, K., 2001. Seasonal variation of stable isotopic compositions recorded in a laminated tufa, SW Japan. *Earth and Planetary Science Letters*, 192(1), pp.31-44.
- Mattey, D., Lowry, D., Duffet, J., Fisher, R., Hodge, E. and Frisia, S., 2008. A 53 year seasonally resolved oxygen and carbon isotope record from a modern Gibraltar speleothem: reconstructed drip water and relationship to local precipitation. *Earth and Planetary Science Letters*, 269(1), pp.80-95.
- Mayte, G.B., García-Zepeda, M.L., López-García, R., Arroyo-Cabrales, J., Marín-Leyva, A.H., Meléndez-Herrera, E. and Fuentes-Farías, A.L., 2016. Diet and habitat of *Mammuthus columbi* (Falconer, 1857) from two Late Pleistocene localities in central western Mexico. *Quaternary International*, 406, pp.137-146.
- McDougall, I. and Harrison, T.M., 1999. *Geochronology and Thermochronology by the 40Ar/39Ar Method*. Oxford University Press on Demand.
- McGuire, W.J. ed., 2000. *The archaeology of geological catastrophes*. Geological Society.
- Metcalfe, S., Say, A., Black, S., McCulloch, R. and O'Hara, S., 2002. Wet conditions during the last glaciation in the Chihuahuan Desert, Alta Babicora Basin, Mexico. *Quaternary Research*, 57(1), pp.91-101.
- Metcalfe, S.E. and Nash, D.J. eds., 2012. *Quaternary environmental change in the tropics*. John Wiley & Sons.
- Metcalfe, S.E., 1997. Palaeolimnological records of climate change in México-Frustrating past, promising future?. *Quaternary International*, 43, pp.111-116.
- Metcalfe, S.E., 2006. Late Quaternary environments of the northern deserts and central transvolcanic belt of Mexico. *Annals of the Missouri Botanical Garden*, 93(2), pp.258-273.
- Metcalfe, S.E., Barron, J.A. and Davies, S.J., 2015. The Holocene history of the North American Monsoon: 'known knowns' and 'known unknowns' in understanding its spatial and temporal complexity. *Quaternary Science Reviews*, 120, pp.1-27.
- Metcalfe, S.E., Leng, M.J., Kirby, J.R., Huddart, D., Vane, C.H. and Gonzalez, S., 2016. Early-Mid Pleistocene environments in the Valsequillo Basin, Central Mexico: a reassessment. *Journal of Quaternary Science*.
- Metcalfe, S.E., O'Hara, S.L., Caballero, M. and Davies, S.J., 2000. Records of Late Pleistocene-Holocene climatic change in Mexico-a review. *Quaternary Science Reviews*, 19(7), pp.699-721.
- Metcalfe, S.E., Street-Perrott, F.A., Perrott, R.A. and Harkness, D.D., 1991. Palaeolimnology of the Upper Lerma Basin, Central Mexico: a record of climatic change and anthropogenic disturbance since 11 600 yr BP. *Journal of Paleolimnology*, 5(3), pp.197-218.
- Meurant, G., 1976. *Tectonics and Metamorphism: Indexes of* (Vol. 1). Elsevier.
- Meyers, P.A. and Lallier-Vergès, E., 1999. Lacustrine sedimentary organic matter records of Late Quaternary paleoclimates. *Journal of Paleolimnology*, 21(3), pp.345-372.
- Miall, A., 2013. *The geology of fluvial deposits: sedimentary facies, basin analysis, and petroleum geology*. Springer.
- Miall, A.D., 1977. *Fluvial sedimentology: an historical review*.

- Miall, A.D., 1980. Cyclicity and the facies model concept in fluvial deposits. *Bulletin of Canadian Petroleum Geology*, 28(1), pp.59-80.
- Miall, A.D., 1985. Architectural-element analysis: a new method of facies analysis applied to fluvial deposits. *Earth-Science Reviews*, 22(4), pp.261-308.
- Miall, A.D., 1997. The Four Basic Types of Stratigraphic Cycle. In *The Geology of Stratigraphic Sequences* (pp. 49-56). Springer Berlin Heidelberg.
- Miall, A.D., 2016. Facies Models. In *Stratigraphy: A Modern Synthesis* (pp. 161-214). Springer International Publishing.
- Miller, W.E. and Carranza-Castañeda, O., 1984. Late Cenozoic mammals from central Mexico. *Journal of Vertebrate Paleontology*, 4(2), pp.216-236.
- Miranda, M.C., 1997. The last glacial maximum in the basin of Mexico: the diatom record between 34,000 and 15,000 years BP from Lake Chalco. *Quaternary International*, 43, pp.125-136.
- Mohtadi, M., Hebbeln, D., Nuñez Ricardo, S. and Lange, C.B., 2006. El Niño-like pattern in the Pacific during marine isotope stages (MIS) 13 and 11?. *Paleoceanography*, 21(1).
- Moore, P.D., Webb, J.A. and Collison, M.E., 1991. *Pollen analysis*. Blackwell scientific publications.
- Mooser F., 1975. *Historia geológica de la Cuenca de México: Memorias sobre las Obras del*
- Mooser, F., 1975. *Historia geológica de la Cuenca de México. Memoria de las obras del sistema de drenaje profundo del Distrito Federal: México, DF, Departamento del Distrito Federal*, 1, pp.7-38.
- Moreno, P.I., Denton, G.H., Moreno, H., Lowell, T.V., Putnam, A.E. and Kaplan, M.R., 2015. Radiocarbon chronology of the last glacial maximum and its termination in northwestern Patagonia. *Quaternary Science Reviews*, 122, pp.233-249.
- Morett, A.L., González, S., Arroyo-Cabrales, J., Polaco, Ó.J., Sherwood, G.J. and Turner, A., 2003. The late Pleistocene paleoenvironment of the Basin of Mexico. *Deinsea*, 9(1), pp.267-272.
- Moretti, M. and Sabato, L., 2007. Recognition of trigger mechanisms for soft-sediment deformation in the Pleistocene lacustrine deposits of the Sant'Arcangelo Basin (Southern Italy): seismic shock vs. overloading. *Sedimentary Geology*, 196(1), pp.31-45.
- Mueller, R.G., Joyce, A.A. and Borejsza, A., 2012. Alluvial archives of the Nochixtlan valley, Oaxaca, Mexico: age and significance for reconstructions of environmental change. *Palaeogeography, Palaeoclimatology, Palaeoecology*, 321, pp.121-136.
- Mukhopadhyay, A., Mazumdar, P. and Van Loon, A.T., 2016. A new 'superassemblage' model explaining proximal-to-distal and lateral facies changes in fluvial environments, based on the Proterozoic Sanjauli Formation (Lesser Himalaya, India). *Journal of Palaeogeography*, 5(4), pp.391-408.
- Mullineaux, D.R., 1996. *Pre-1980 tephra-fall deposits erupted from Mount St. Helens, Washington*. US Government Printing Office.
- Myrow, P.M., 1990. A new graph for understanding colors of mudrocks and shales. *Journal of Geological Education*, 38(1), pp.16-20.
- Nanson, G.C. and Huang, H.Q., 2008. Least action principle, equilibrium states, iterative adjustment and the stability of alluvial channels. *Earth Surface Processes and Landforms*, 33(6), pp.923-942.
- Nash, D.J. and Smith, R.F., 1998. Multiple calcrete profiles in the Tabernas Basin, southeast Spain: their origins and geomorphic implications. *Earth Surface Processes and Landforms*, 23(11), pp.1009-1029.
- Nash, D.J. and Smith, R.F., 2003. Properties and development of channel calcretes in a mountain catchment, Tabernas Basin, southeast Spain. *Geomorphology*, 50(1), pp.227-250.
- Nelson, D., 2002. *Natural variations in the composition of groundwater. Drinking Water Program*. Oregon Department of Human Services, Springfield, Oregon, 3.
- Netterberg, F., 1969. The interpretation of some basic calcrete types. *The South African Archaeological Bulletin*, 24(95/96), pp.117-122.

- Neu, T.R., 2000. Confocal laser scanning microscopy (CLSM) of biofilms. *Biofilms-Investigative Methods and Applications*. Flemming, H.-C., U. Szewzyk, and T. Griebel (Eds.). Technomic Publishing Co. Inc., PA, USA, pp.211-224.
- Newton, A.J. and Metcalfe, S.E., 1999. Tephrochronology of the Toluca basin, central Mexico. *Quaternary Science Reviews*, 18(8-9), pp.1039-1059.
- Nichols, G., 2009. *Sedimentology and stratigraphy*. Wiley - Blackwell, Oxford.
- Nickel, E., 1983. Environmental significance of freshwater oncoids, Eocene guarga formation, Southern Pyrenees, Spain. In *Coated Grains* (pp. 308-329). Springer Berlin Heidelberg.
- Nowak, M. and Weiss, C., 2013, April. Facies, facies architecture and formation processes of a calcareous, self-build tufa channel (Steinerne Rinne) from Engelthal, Southern Germany. In *EGU General Assembly Conference Abstracts* (Vol. 15, p. 3348).
- Oguchi, T., Hori, K. and Oguchi, C.T., 2008. Paleohydrological implications of late Quaternary fluvial deposits in and around archaeological sites in Syria. *Geomorphology*, 101(1), pp.33-43.
- O'Hara, S.L. and Metcalfe, S.E., 1997. The climate of Mexico since the Aztec period. *Quaternary International*, 43, pp.25-31.
- Oliver, R.D., Nieva, F., Flores, H.F., Verma, S.P., Santoyo, E. and Portugal, E., 1987. Evaluación hidrogeológica en la cuenca de México y parte del Alto Lerma (Proceedings). *Geos-Boletín de la Unión Geofísica Mexicana*, 1: 27.
- Olsen, P.E., 1990. Tectonic, climatic, and biotic modulation of lacustrine ecosystems-examples from Newark Supergroup of eastern North America. *Lacustrine basin exploration: Case studies and modern analogs: AAPG Memoir*, 50, pp.209-224.
- Ortega, A. and Farvolden, R.N., 1989. Computer analysis of regional groundwater flow and boundary conditions in the Basin of Mexico. *Journal of Hydrology*, 110(3-4), pp.271-294.
- Ortega, B., Caballero, C., Lozano, S., Israde, I. and Vilaclara, G., 2002. 52 000 years of environmental history in Zacapú basin, Michoacán, Mexico: the magnetic record. *Earth and Planetary Science Letters*, 202(3), pp.663-675.
- Ortega-Guerrero, B. and Newton, A.J., 1998. Geochemical characterization of Late Pleistocene and Holocene tephra layers from the Basin of Mexico, Central Mexico. *Quaternary Research*, 50(1), pp.90-106.
- Ortega-Guerrero, B., 1992. *Paleomagnetismo, magnetoestratigrafía y paleoecología del Cuaternario tardío en el Lago de Chalco, Cuenca de México* (Doctoral dissertation, Dissertation, National University of México).
- Ortiz, J.E., Gallego, J.L.R., Torres, T., Díaz-Bautista, A. and Sierra, C., 2010. Palaeoenvironmental reconstruction of Northern Spain during the last 8000calyr BP based on the biomarker content of the Roñanzas peat bog (Asturias). *Organic Geochemistry*, 41(5), pp.454-466.
- Ovando-Shelley, E., Ossa, A. and Romo, M.P., 2007. The sinking of Mexico City: Its effects on soil properties and seismic response. *Soil Dynamics and Earthquake Engineering*, 27(4), pp.333-343.
- Padmakumari, V.M. and Ahmad, S.M., 2004. Ash layer at? 8 Ma in ODP Site 758 from the Bay of Bengal: evidence from Sr, Nd isotopic compositions and rare earth elements. *CURRENT SCIENCE-BANGALORE*, 86(9), pp.1323-1325.
- Parsons, J.R., Gorenflo, L.J., Parsons, M.H. and Wilson, D.J., 2008. Prehispanic settlement patterns in the northwestern Valley of Mexico: the Zumpango region (Vol. 45). University of Michigan Museum.
- Pastouret, L., Chamley, H., Delibrias, G., Duplessy, J.C. and Thiede, J., 1978. Late Quaternary climatic changes in western tropical Africa deduced from deep-sea sedimentation off the Niger delta. *Oceanologica Acta*, 1(2), pp.217-232.
- Payne, B.R., 1976. The interaction of irrigation water with groundwater and River Tula in the Mezquital Valley. Int. At. Energy Agency--Sect. Agric. Recur. Hidraul. (I.A.E.A. -- S.A.R.H.) Rep.(unpublished).
- Pedley, H. M. 2009. Tufas and travertines of the Mediterranean region: a testing ground for freshwater carbonate concepts and developments. *Sedimentology*, 56: 221 - 246

- Pedley, H. M., 1990. Classification and environmental models of cool freshwater tufas. *Sedimentary Geology*, 68: 143-154.
- Pedley, H. M., 1992. Freshwater (phytoherm) reefs: the role of biofilms and their bearing on marine reef cementation. *Sediment geology*, 79: 255 - 274
- Pedley, H. M., Rogerson, M., Middleton, R. 2009. Freshwater calcite precipitates from in vitro mesocosm flume experiments: a case for biomediation of tufas. *Sedimentology*, 56: 511 - 257
- Pedley, H.M. and Rogerson, M. eds., 2010. Tufas and speleothems: unravelling the microbial and physical controls. Geological Society of London.
- Pedley, H.M. and Rogerson, M., 2010. In vitro investigations of the impact of different temperature and flow velocity conditions on tufa microfabric. Geological Society, London, Special Publications, 336(1), pp.193-210.
- Pedley, H.M., Hill, I., Denton, P. and Brasington, J., 2000. Three-dimensional modelling of a Holocene tufa system in the Lathkill Valley, north Derbyshire, using ground-penetrating radar. *Sedimentology*, 47(3), pp.721-738.
- Pedley, M. and Hill, I., 2003. The recognition of barrage and paludal tufa systems by GPR: case studies in the geometry and correlation of Quaternary freshwater carbonates. Geological Society, London, Special Publications, 211(1), pp.207-223.
- Pedley, M., 1992. Freshwater (phytoherm) reefs: the role of biofilms and their bearing on marine reef cementation. *Sedimentary Geology*, 79(1-4), pp.255-274.
- Pedley, M., Andrews, J., Ordonez, S., del Cura, M.A.G., Martin, J.A.G. and Taylor, D., 1996. Does climate control the morphological fabric of freshwater carbonates? A comparative study of Holocene barrage tufas from Spain and Britain. *Palaeogeography, Palaeoclimatology, Palaeoecology*, 121(3-4), pp.239-257.
- Pedley, M., Martin, J. A. G., Delgado, S. O., Garcia Del Cura, M., 2003. Sedimentology of Quaternary perched springline and paludal tufas: criteria for recognition, with examples from Guadalajara Province, Spain *Sedimentology*, 50: 23-44.
- Pedley, M., Rogerson, M. and Middleton, R., 2009. Freshwater calcite precipitates from in vitro mesocosm flume experiments: a case for biomediation of tufas. *Sedimentology*, 56(2), pp.511-527.
- Pellicer, X.M., Corella, J.P., Gutiérrez, F., Roqué, C., Linares, R., Carbonel, D., Zarroca, M., Guerrero, J. and Comas, X., 2016. Sedimentological and palaeohydrological characterization of Late Pleistocene and Holocene tufa mound palaeolakes using trenching methods in the Spanish Pyrenees. *Sedimentology*, 63(6), pp.1786-1819.
- Pentecost, A. and Viles, H., 1994. A review and reassessment of travertine classification. *Géographie physique et Quaternaire*, 48(3), pp.305-314.
- Pentecost, A., 1990. The formation of travertine shrubs: Mammoth Hot springs, Wyoming. *Geological Magazine*, 127(2), pp.159-168.
- Pentecost, A., 2005. *Travertine*. Springer Science & Business Media.
- Pentecost, A., Riding, R., 1986. Calcification in cyanobacterial. In: *Biom mineralization in Lower Plants and Animals* (Eds B.S.C. Leadbeater and R. Riding), 73 - 86. Clarendon Press, Open University Oxford.
- Pérez-Crespo, V.A., Arroyo-Cabrales, J., Alva-Valdivia, L.M., Morales-Puente, P., Cienfuegos-Alvarado, E. and Otero, F.J., 2016. Inferences of feeding habits of Late Pleistocene *Equus* sp. from eight Mexican localities. *Neues Jahrbuch für Geologie und Paläontologie-Abhandlungen*, 279(1), pp.107-121.
- Peterson, L.C., Haug, G.H., Hughen, K.A. and Röhl, U., 2000. Rapid changes in the hydrologic cycle of the tropical Atlantic during the last glacial. *Science*, 290(5498), pp.1947-1951.
- Pietras, J.T. and Carroll, A.R., 2006. High-resolution stratigraphy of an underfilled lake basin: Wilkins Peak member, Eocene Green River Formation, Wyoming, USA. *Journal of Sedimentary Research*, 76(11), pp.1197-1214.
- Pigati, J.S., Rech, J.A. and Nekola, J.C., 2010. Radiocarbon dating of small terrestrial gastropod shells in North America. *Quaternary Geochronology*, 5(5), pp.519-532.
- Pilcher, J.R., 1991. Radiocarbon dating for the Quaternary scientist. In *Quaternary Proceedings* (pp. 27-33).

- Pla-Pueyo, S., Viseras, C., Candy, I., Soria, J.M., García-García, F. and Schreve, D., 2015. Climatic control on palaeohydrology and cyclical sediment distribution in the Plio-Quaternary deposits of the Guadix Basin (Betic Cordillera, Spain). *Quaternary International*, 389, pp.56-69.
- Platt, N.H. and Wright, V.P., 1992. Palustrine carbonates and the Florida everglades: towards an exposure index for the fresh-water environment?. *Journal of Sedimentary Research*, 62(6).
- Platt, N.H. and Wright, V.P., 2009. Lacustrine carbonates: facies models, facies distributions and hydrocarbon aspects. *Lacustrine facies analysis*, pp.57-74.
- Platt, N.H., 1989. Lacustrine carbonates and pedogenesis: sedimentology and origin of palustrine deposits from the Early Cretaceous Rupelo Formation, W Cameros Basin, N Spain. *Sedimentology*, 36(4), pp.665-684.
- Poage, M.A. and Chamberlain, C.P., 2001. Empirical relationships between elevation and the stable isotope composition of precipitation and surface waters: Considerations for studies of paleoelevation change. *American Journal of Science*, 301(1), pp.1-15.
- Polyak, V.J. and Asmerom, Y., 2005. Orbital control of long-term moisture in the southwestern USA. *Geophysical research letters*, 32(19).
- Porter, R.J. and Gallois, R.W., 2008. Identifying fluvio-lacustrine intervals in thick playa-lake successions: An integrated sedimentology and ichnology of arenaceous members in the mid-late Triassic Mercia Mudstone Group of south-west England, UK. *Palaeogeography, Palaeoclimatology, Palaeoecology*, 270(3-4), pp.381-398.
- Posamentier, H.W. and Walker, R.G., 2006. Facies models revisited.
- Potter, P.E., 1959. Facies model conference. *Science*, 129(3358), pp.1292-1294.
- Potter, P.E., Maynard, J.B. and Depetris, P.J., 2005. *Mud and mudstones: Introduction and overview*. Springer Science & Business Media.
- Price, G.J., Webb, G.E., Zhao, J.X., Feng, Y.X., Murray, A.S., Cooke, B.N., Hocknull, S.A. and Sobbe, I.H., 2011. Dating megafaunal extinction on the Pleistocene Darling Downs, eastern Australia: the promise and pitfalls of dating as a test of extinction hypotheses. *Quaternary Science Reviews*, 30(7), pp.899-914.
- Price, G.J., Zhao, J.X., Feng, Y.X. and Hocknull, S.A., 2009. New records of Plio-Pleistocene koalas from Australia: palaeoecological and taxonomic implications. *Records of the Australian Museum*, 61(1), pp.39-48.
- Prokopenko, A.A., Hinnov, L.A., Williams, D.F. and Kuzmin, M.I., 2006. Orbital forcing of continental climate during the Pleistocene: a complete astronomically tuned climatic record from Lake Baikal, SE Siberia. *Quaternary Science Reviews*, 25(23-24), pp.3431-3457.
- Quade, J., Miffin, M.D., Pratt, W.L., McCoy, W. and Burckle, L., 1995. Fossil spring deposits in the southern Great Basin and their implications for changes in water-table levels near Yucca Mountain, Nevada, during Quaternary time. *Geological Society of America Bulletin*, 107(2), pp.213-230.
- Quijano, L., 1978. Comentario sobre el muestreo isotópico de las aguas subterráneas de la zona de Texcoco. Int. At. Energy Agency -- Secr. Agric. Recur. Hidraul. (I.A.E.A. -- S.A.R.H.) Rep. (unpublished).
- Quijano, L., 1980. Isotope analysis done by Earth Science Department, University of Waterloo, Canada. Chemical analysis done by Secr. Agric. Recur. Hidraul. (S.A.R.H.), Mexico (unpublished).
- Quintanar, L., Rodríguez-González, M., Campos-Enríquez, O., 2004. A shallow crustal earthquake doublet from the Trans-Mexican Volcanic Belt (Central Mexico). *Bulletin of the Seismological Society of America*, 94: 845 - 855.
- Ramírez-Cruz, G.A. and Montellano-Ballesteros, M., 2014. Two new glyptodont records (Mammalia: Cingulata) from the late Pleistocene of Tamaulipas and Tlaxcala, Mexico: Implications for the taxonomy of the genus *Glyptotherium*. *The Southwestern Naturalist*, 59(4), pp.522-530.
- Ramsey, B. C. 2008. Radiocarbon dating: Revolutions in understanding. *Archaeometry*, 50 (2): 249 - 275.
- Ramsey, B. C. 2008. Radiocarbon dating: Revolutions in understanding. *Archaeometry*, 50 (2): 249 - 275.
- Remy, R.R. and Ferrell, R.E., 1989. Distribution and origin of analcime in marginal lacustrine mudstones of the Green River Formation, south-central Uinta Basin, Utah. *Clays and Clay minerals*, 37(5), pp.419-432.

- Renne, P.R., Balco, G., Ludwig, K.R., Mundil, R. and Min, K., 2011. Response to the comment by WH Schwarz et al. on "Joint determination of 40 K decay constants and 40 Ar³⁹/40 K for the Fish Canyon sanidine standard, and improved accuracy for 40 Ar/39 Ar geochronology" by PR Renne et al.(2010). *Geochimica et Cosmochimica Acta*, 75(17), pp.5097-5100.
- Renne, P.R., Sharp, W.D., Deino, A.L., Orsi, G. and Civetta, L., 1997. 40Ar/39Ar dating into the historical realm: calibration against Pliny the Younger. *Science*, 277(5330), pp.1279-1280.
- Renne, Paul R., Greg Balco, Kenneth R. Ludwig, Roland Mundil, and Kyoungwon Min. "Response to the comment by WH Schwarz et al. on "Joint determination of 40K decay constants and 40Ar³⁹/40K for the Fish Canyon sanidine standard, and improved accuracy for 40Ar/39Ar geochronology" by PR Renne et al.(2010)." *Geochimica et Cosmochimica Acta* 75, no. 17 (2011): 5097-5100.
- Rich, J., 2013. A 250,000-year record of lunette dune accumulation on the Southern High Plains, USA and implications for past climates. *Quaternary Science Reviews*, 62, pp.1-20.
- Riding, R. ed., 2012. *Calcareous algae and stromatolites*. Springer Science & Business Media.
- Rivas, H., Bostelmann, E., Le Roux, J. and Ugalde, R., 2015. Fluvial facies and architecture of the late middle Miocene, Mayoan, deposits of Chilean Patagonia. In XIV Congreso Geológico Chileno, Actas (Vol. 1, pp. 812-815).
- Rodríguez-Pascua, M., Becker, A., Calvo, J.P., Davenport, C.A. and Gómez-Gras, D., 2003. Sedimentary record of seismic events, with examples from recent and fossil lakes. *Limnogeology in Spain: a tribute to Kerry Kelts*. Consejo Superior de Investigaciones Científicas, pp.253-280.
- Rosenbaum, J. and Sheppard, S.M.F., 1986. An isotopic study of siderites, dolomites and ankerites at high temperatures. *Geochimica et Cosmochimica Acta*, 50(6), pp.1147-1150.
- Rosenmeier, M.F., Hodell, D.A., Brenner, M., Curtis, J.H. and Guilderson, T.P., 2002. A 4000-year lacustrine record of environmental change in the southern Maya lowlands, Peten, Guatemala. *Quaternary Research*, 57(2), pp.183-190.
- Rosenmeier, M.F., Hodell, D.A., Brenner, M., Curtis, J.H., Martin, J.B., Anselmetti, F.S., Ariztegui, D. and Guilderson, T.P., 2002. Influence of vegetation change on watershed hydrology: implications for paleoclimatic interpretation of lacustrine $\delta^{18}O$ records. *Journal of Paleolimnology*, 27(1), pp.117-131.
- Rowley, D.B., Pierrehumbert, R.T. and Currie, B.S., 2001. A new approach to stable isotope-based paleoaltimetry: implications for paleoaltimetry and paleohypsometry of the High Himalaya since the Late Miocene. *Earth and Planetary Science Letters*, 188(1-2), pp.253-268.
- Roy, P.D., Arce, J.L., Lozano, R., Jonathan, M.P., Centeno, E. and Lozano, S., 2012. Geochemistry of late Quaternary tephra-sediment sequence from north-eastern Basin of Mexico (Mexico): implications to tephrochronology, chemical weathering and provenance. *Revista Mexicana de Ciencias Geológicas*, 29(1).
- Roy, P.D., Caballero, M., Lozano, R. and Smykatz-Kloss, W., 2008. Geochemistry of late quaternary sediments from Tecocomulco lake, central Mexico: Implication to chemical weathering and provenance. *Chemie der erde-geochemistry*, 68(4), pp.383-393.
- Roy, P.D., Caballero, M., Lozano, R., Ortega, B., Lozano, S., Pi, T., Israde, I. and Morton, O., 2010. Geochemical record of Late Quaternary paleoclimate from lacustrine sediments of paleo-lake San Felipe, western Sonora Desert, Mexico. *Journal of South American Earth Sciences*, 29(3), pp.586-596.
- Roy, P.D., Caballero, M., Lozano, R., Pi, T. and Morton, O., 2009. Late Pleistocene-Holocene geochemical history inferred from Lake Tecocomulco sediments, Basin of Mexico, Mexico. *Geochemical Journal*, 43(1), pp.49-64.
- Roy, P.D., Quiroz-Jiménez, J.D., Chávez-Lara, C.M., Sánchez-Zavala, J.L., Pérez-Cruz, L.L. and Sankar, G.M., 2014. Humid Pleistocene-Holocene transition and early Holocene in subtropical northern Mexico and possible Gulf of California forcing. *Boreas*, 43(3), pp.577-587.
- Rozanski, K., 1985. Deuterium and oxygen-18 in European groundwaters-links to atmospheric circulation in the past. *Chemical Geology: Isotope Geoscience section*, 52(3-4), pp.349-363.
- Rueda, H., Arce, J., Macías, J. and García-Palomo, A., 2006, December. A ~ 31 ka Plinian-subplinian eruption at Tláloc volcano, Sierra Nevada, México. In AGU Fall Meeting Abstracts (Vol. 1, p. 0668).

- Rueda, H., Arce, J.L., Macías, J.L. and García-Palomo, A., 2007. Pyroclastic sequences at the N-NE slopes of Tlaloc volcano, Sierra Nevada, central Mexico, in a Commemorative Conference, El Chichón volcano: 25 years later,. San Cristóbal de las Casas. Chiapas, México, p.100.
- Rueda, H., Macías, J.L., Arce, J.L., Gardner, J.E. and Layer, P.W., 2013. The ~ 31 ka rhyolitic Plinian to sub-Plinian eruption of Tlaloc Volcano, Sierra Nevada, central Mexico. *Journal of Volcanology and Geothermal Research*, 252, pp.73-91.
- Rühlemann, C., Mulitza, S., Müller, P.J., Wefer, G. and Zahn, R., 1999. Warming of the tropical Atlantic Ocean and slowdown of thermohaline circulation during the last deglaciation. *Nature*, 402(6761), pp.511-514.
- Ryan, M.C., 1989. An investigation of nitrogen compounds in the groundwater in the Valley of Mexico. *Geof? s. Int.*, 28(2): 417-433.
- Salinas, M.S., Hidalgo, J. and Posadas, C., 2016. Mamíferos fósiles del Pleistoceno tardío (Rancholabreano) de San Mateo Huexoyucán, Tlaxcala, México. *Boletín de la Sociedad Geológica Mexicana*, p.497.
- Sato, Y., Matsuoka, H., Okamura, M. and Kashima, K., 2016. Late Holocene environmental changes of coastal lagoon inferred from a fossil diatom analysis of sediment core from Lake Hamana, central Japan. *Quaternary International*, 397, pp.317-329.
- Scherer, C.M., Goldberg, K. and Bardola, T., 2015. Facies architecture and sequence stratigraphy of an early post-rift fluvial succession, Aptian Barbalha Formation, Araripe Basin, northeastern Brazil. *Sedimentary Geology*, 322, pp.43-62.
- Schneider, J., Schröder, H.G. and Le Campion-Alsumard, T., 1983. Algal micro-reefs-coated grains from freshwater environments. In *Coated grains* (pp. 284-298). Springer Berlin Heidelberg.
- Schnellmann, M., Anselmetti, F.S., Giardini, D. and McKenzie, J.A., 2006. 15,000 Years of mass-movement history in Lake Lucerne: Implications for seismic and tsunami hazards. *Eclogae Geologicae Helveticae*, 99(3), pp.409-428.
- Schumm, S.A., 1977. *The Fluvial System* PDF.
- Schütt, B., 1998. Chemical and mineralogical characters of lacustrine sediments as paleoenvironmental indicators- An example from the Laguna Jabonera, Central Ebro Basin. *Terra Nostra*, 98(6), pp.115-120.
- Schütt, B., 2000. Holocene paleohydrology of playa lakes in northern and central Spain: a reconstruction based on the mineral composition of lacustrine sediments. *Quaternary International*, 73, pp.7-27.
- Schweger, C.E., 2013. Late Pleistocene vegetation of eastern Beringia: pollen analysis. *Paleoecology of Beringia*, p.95.
- Sedov, S., Lozano-García, S., Solleiro-Rebolledo, E., de Tapia, E.M., Ortega-Guerrero, B. and Sosa-Nájera, S., 2010. Tepexpan revisited: A multiple proxy of local environmental changes in relation to human occupation from a paleolake shore section in Central Mexico. *Geomorphology*, 122(3), pp.309-322.
- Sedov, S., Solleiro-Rebolledo, E., Gama-Castro, J.E., Vallejo-Gómez, E. and González-Velázquez, A., 2001. Buried palaeosols of the Nevado de Toluca: an alternative record of Late Quaternary environmental change in central Mexico. *Journal of Quaternary Science*, 16(4), pp.375-389.
- Sedov, S., Solleiro-Rebolledo, E., Terhorst, B., Solé, J., Flores-Delgadillo, M.D.L., Werner, G. and Poetsch, T., 2009. The Tlaxcala basin paleosol sequence: a multiscale proxy of middle to late Quaternary environmental change in central Mexico. *Revista Mexicana de Ciencias Geológicas*, 26(2), pp.448-465.
- Seegerstrom, K., 1962. *Geology of South-central Hidalgo and North-eastern México*, Mexico. US Government Printing Office.
- Seegerstrom, K., 1963. *Geology of South Central Hidalgo and Northeastern Mexico*, Mexico. Geological Survey Bulletin, pp.87-162.
- Seegerstrom, K., Williams, H., Wilcox, R.E., Foshag, W.P. and Gonzales, J.R., 1956. *Geologic investigations in the Parícutin area, Mexico* (No. 965). US Government Printing Office.
- Semeniuk, V. and Meagher, T.D., 1981. Calcrete in Quaternary coastal dunes in southwestern Australia: A capillary-rise phenomenon associated with plants. *Journal of Sedimentary Research*, 51(1).

- Sharp, Z., 2007. Principles of stable isotope geochemistry (p. 344). Upper Saddle River, NJ: Pearson education.
- Siebe, C., 2000. Age and archaeological implications of Xitle volcano, southwestern Basin of Mexico-City. *Journal of Volcanology and Geothermal Research*, 104(1), pp.45-64.
- Siebe, C., Salinas, S., Arana-Salinas, L., Macías, J.L., Gardner, J. and Bonasia, R., 2017. The ~ 23,500 y 14 C BP White Pumice Plinian eruption and associated debris avalanche and Tochimilco lava flow of Popocatepetl volcano, México. *Journal of Volcanology and Geothermal Research*, 333, pp.66-95.
- Siemens, J., Huschek, G., Siebe, C. and Kaupenjohann, M., 2008. Concentrations and mobility of human pharmaceuticals in the world's largest wastewater irrigation system, Mexico City-Mezquital Valley. *Water Research*, 42(8), pp.2124-2134.
- Sienkiewicz, E., 2013. Limnological record inferred from diatoms in sediments of Lake Skalska (north-eastern Poland). *Acta Palaeobotanica*, 53(1), pp.99-104.
- Sigleo, W.R. and Colhoun, E.A., 1982. Terrestrial dunes, man and the late Quaternary environment in southern Tasmania. *Palaeogeography, Palaeoclimatology, Palaeoecology*, 39(1-2), pp.87-121.
- Singh, A. and Bhardwaj, B.D., 1991. Fluvial facies model of the Ganga River sediments, India. *Sedimentary Geology*, 72(1-2), pp.135-146.
- Sinha, R., Smykatz-Kloss, W., Stüben, D., Harrison, S.P., Berner, Z. and Kramar, U., 2006. Late Quaternary palaeoclimatic reconstruction from the lacustrine sediments of the Sambhar playa core, Thar Desert margin, India. *Palaeogeography, Palaeoclimatology, Palaeoecology*, 233(3), pp.252-270.
- Smith, P., 2004. How long before a change in soil organic carbon can be detected?. *Global Change Biology*, 10(11), pp.1878-1883.
- Smol, J.P. and Stoermer, E.F. eds., 2010. The diatoms: applications for the environmental and earth sciences. Cambridge University Press.
- Smoot, J.P. and Olsen, P.E., 1988. Massive mudstones in basin analysis and paleoclimatic interpretation of the Newark Supergroup. In *Developments in Geotectonics* (Vol. 22, pp. 249-274). Elsevier.
- Soler-Arechalde, A.M. and Urrutia-Fucugauchi, J., 2000. Paleomagnetism of the Acambay Graben, central Trans-Mexican volcanic belt. *Tectonophysics*, 318(1), pp.235-248.
- Solleiro-Rebolledo, E., Sedov, S., de Tapia, E.M., Cabadas, H., Gama-Castro, J. and Vallejo-Gómez, E., 2006. Spatial variability of environment change in the Teotihuacan Valley during the Late Quaternary: Paleopedological inferences. *Quaternary International*, 156, pp.13-31.
- Solleiro-Rebolledo, E., Sedov, S., Gama-Castro, J., Roman, D.F. and Escamilla-Sarabia, G., 2003. Paleosol-sedimentary sequences of the Glacis de Buenavista, Central Mexico: interaction of Late Quaternary pedogenesis and volcanic sedimentation. *Quaternary International*, 106, pp.185-201.
- Steel, R.J., 1974. Cornstone (fossil caliche): its origin, stratigraphic, and sedimentological importance in the New Red Sandstone, Western Scotland. *The Journal of Geology*, 82(3), pp.351-369.
- Stevens, R.E., Metcalfe, S.E., Leng, M.J., Lamb, A.L., Sloane, H.J., Naranjo, E. and González, S., 2012. Reconstruction of late Pleistocene climate in the Valsequillo Basin (Central Mexico) through isotopic analysis of terrestrial and freshwater snails. *Palaeogeography, Palaeoclimatology, Palaeoecology*, 319, pp.16-27.
- Stinnesbeck, S.R., Frey, E., Stinnesbeck, W., Olguín, J.A., Zell, P., Mata, A.T., Sanvicente, M.B., González, A.G., Sandoval, C.R. and Nuñez, E.A., 2017. A new fossil peccary from the Pleistocene-Holocene boundary of the eastern Yucatán Peninsula, Mexico. *Journal of South American Earth Sciences*, 77, pp.341-349.
- Stojanowski, C.M. and Johnson, K.M., 2011. Labial canine talon cusp from the early Holocene site of Gobero, Central Sahara Desert, Niger. *International Journal of Osteoarchaeology*, 21(4), pp.391-406.
- Stow, D.A., 2005. *Sedimentary rocks in the field: a color guide*. Gulf Professional Publishing.
- Street, F.A. and Grove, A.T., 1976. Environmental and climatic implications of late Quaternary lake-level fluctuations in Africa. *Nature*, 261(5559), pp.385-390.
- Stuiver, M. and Polach, H.A., 1977. Discussion reporting of 14 C data. *Radiocarbon*, 19(03), pp.355-363.

- Sun, Y., Chen, J., Clemens, S.C., Liu, Q., Ji, J. and Tada, R., 2006. East Asian monsoon variability over the last seven glacial cycles recorded by a loess sequence from the northwestern Chinese Loess Plateau. *Geochemistry, Geophysics, Geosystems*, 7(12).
- Suter, M., Aguirre, G., Siebe, C., Quintero, O., Komorowski, J. C., 1991. Volcanism and active faulting in the central part of the Trans-Mexican volcanic belt, Mexico. In: Walawender, M.J., Hanan, B.B., eds., *Geological excursions in southern California and Mexico: San Diego, California, Department of Geological Sciences, San Diego State University, Guidebook, 1991 Annual Meeting, Geological Society of America, San Diego, California, October 21-24, 1991*, p. 224-243.
- Suter, M., Carrillo-Martínez, M., Quintero-Legorreta, O., 1996. Macroseismic study of shallow earthquakes in the central and eastern parts of the Trans-Mexican volcanic belt, Mexico. *Seismological Society of America Bulletin*, 86: p. 1952 - 1963.
- Suter, M., López-Martínez, M., Quintero-Legorreta, O., Carrillo-Martínez, M., 2001. Quaternary intra-arc extension in the central Trans-Mexican volcanic belt. *Geological Society of America Bulletin*, 113 (6): 693 - 703.
- Sutton, R.T. and Hodson, D.L., 2005. Atlantic Ocean forcing of North American and European summer climate. *science*, 309(5731), pp.115-118.
- Szynkaruk, E., Graduño-Monroy, V.H. and Bocco, G., 2004. Active fault systems and tectono-topographic configuration of the central Trans-Mexican Volcanic Belt. *Geomorphology*, 61(1-2), pp.111-126.
- Talbot, M.R., 1990. A review of the palaeohydrological interpretation of carbon and oxygen isotopic ratios in primary lacustrine carbonates. *Chemical Geology: Isotope Geoscience Section*, 80(4), pp.261-279.
- Talbot, M.R., Holm, K. and Williams, M.A.J., 1994. Sedimentation in low-gradient desert margin systems: A comparison of the Late Triassic of northwest Somerset. *Paleoclimate and basin evolution of playa systems*, 289, p.97.
- Talma, A.S. and Vogel, J.C., 1992. Late Quaternary paleotemperatures derived from a speleothem from Cango caves, Cape province, South Africa. *Quaternary Research*, 37(2), pp.203-213.
- Talma, A.S. and Vogel, J.C., 1993. A simplified approach to calibrating 14 C dates. *Radiocarbon*, 35(02), pp.317-322.
- Tandon, S.K. and Friend, P.F., 1989. Near-surface shrinkage and carbonate replacement processes, Arran Cornstone Formation, Scotland. *Sedimentology*, 36(6), pp.1113-1126.
- Tandon, S.K. and Gibling, M.R., 1997. Calcretes at sequence boundaries in Upper Carboniferous cyclothems of the Sydney Basin, Atlantic Canada. *Sedimentary Geology*, 112(1-2), pp.43-67.
- Tandon, S.K. and Narayan, D., 1981. Calcrete conglomerate, case-hardened conglomerate and cornstone—a comparative account of pedogenic and non-pedogenic carbonates from the continental Siwalik Group, Punjab, India. *Sedimentology*, 28(3), pp.353-367.
- Tanner, L.H., 2000. Palustrine-lacustrine and alluvial facies of the (Norian) Owl Rock Formation (Chinle Group), Four Corners region, southwestern uSa: implications for Late Triassic paleoclimate. *Journal of Sedimentary Research*, 70(6).
- Teller, J.T. and Last, W.M., 1990. Paleohydrological indicators in playas and salt lakes, with examples from Canada, Australia, and Africa. *Palaeogeography, Palaeoclimatology, Palaeoecology*, 76(3-4), pp.215-240.
- Theriault, P. and Desrochers, A., 1993. Carboniferous calcretes in the Canadian Arctic. *Sedimentology*, 40(3), pp.449-465.
- Timmermann, A., Okumura, Y., An, S.I., Clement, A., Dong, B., Guilyardi, E., Hu, A., Jungclaus, J.H., Renold, M., Stocker, T.F. and Stouffer, R.J., 2007. The influence of a weakening of the Atlantic meridional overturning circulation on ENSO. *Journal of climate*, 20(19), pp.4899-4919.
- Tófaló, O.R. and Pazos, P.J., 2010. Paleoclimatic implications (Late Cretaceous-Paleogene) from micromorphology of calcretes, palustrine limestones and silcretes, southern Paraná Basin, Uruguay. *Journal of South American Earth Sciences*, 29(3), pp.665-675.

- Toker, M.E., 2016. Quaternary fluvial tufas of Sar?kavak area, southwestern Turkey: Facies and depositional systems. *Quaternary International*.
- Tooth, S., 2009. Arid geomorphology: emerging research themes and new frontiers. *Progress in Physical Geography*, 33(2), pp.251-287.
- TORRES?RODRÍGUEZ, E., LOZANO?GARCÍA, S., Roy, P., Ortega, B., BERAMENDI?OROSCO, L., CORREA?METRIO, A. and Caballero, M., 2015. Last Glacial droughts and fire regimes in the central Mexican highlands. *Journal of Quaternary Science*, 30(1), pp.88-99.
- Tovar, R.E., Sedov, S., Montellano-Ballesteros, M., Solleiro, E. and Benammi, M., 2014. Paleosols, bones, phytoliths, and $\delta^{13}C$ signatures of humus and teeth in the alluvial sequence of Axamilpa, Puebla: Inferences for landscape evolution and megafauna paleoecology during MIS 3-2 in Southern Mexico. *Catena*, 112, pp.25-37.
- Tovar, R.E., Sedov, S., Solís, B. and Solleiro, E., 2013. Dark humic alluvial paleosols in Central and Southern Mexico: micromorphological indicators of Late Pleistocene megafauna habitats. *J Soil Sci*, 3, pp.217-223.
- Tucker, G.E. and Slingerland, R., 1996. Predicting sediment flux from fold and thrust belts. *Basin Research*, 8(3), pp.329-349.
- Tucker, M.E. and Wright, V.P., 1990. Carbonate mineralogy and chemistry. *Carbonate Sedimentology*, pp.284-313.
- Tucker, M.E. and Wright, V.P., 1990. Dolomites and dolomitization models. *Carbonate sedimentology*, pp.365-400.
- Tucker, M.E., 2003. Mixed clastic-carbonate cycles and sequences: Quaternary of Egypt and Carboniferous of England. *Geologia Croatica*, 56(1), pp.19-37.
- Tzedakis, P.C., 2010. The MIS 11-MIS 1 analogy, southern European vegetation, atmospheric methane and the "early anthropogenic hypothesis". *Climate of the Past*, 6(2), pp.131-144.
- UCL, 2017. <https://www.ucl.ac.uk/earth-sciences/impact/geology/london/ucl/materials/clay>
- Universalis, E., 2017. Méso-Amérique: Les Grands Articles d'Universalis. *Encyclopaedia Universalis*.
- Unkel, I., Kadereit, A., Mächtle, B., Eitel, B., Kromer, B., Wagner, G. and Wacker, L., 2007. Dating methods and geomorphic evidence of palaeoenvironmental changes at the eastern margin of the South Peruvian coastal desert (14° 30' S) before and during the Little Ice Age. *Quaternary International*, 175(1), pp.3-28.
- Valero, L., Huerta, P., Garcés, M., Armenteros, I., Beamud, E. and Gómez?Paccard, M., 2015. Linking sedimentation rates and large?scale architecture for facies prediction in nonmarine basins (Paleogene, Almazán Basin, Spain). *Basin Research*.
- Van Devender, T.R. and Burgess, T.L., 1985. Late Pleistocene woodlands in the Bolson de Mapimi: A refugium for the Chihuahuan Desert Biota?. *Quaternary Research*, 24(3), pp.346-353.
- Vandenbergh, J. and Maddy, D., 2001. The response of river systems to climate change.
- Vandenschrck, G., Van Wesemael, B., Frot, E., Pulido-Bosch, A., Molina, L., Stievenard, M. and Souchez, R., 2002. Using stable isotope analysis (δD - $\delta^{18}O$) to characterise the regional hydrology of the Sierra de Gador, south east Spain. *Journal of Hydrology*, 265(1), pp.43-55.
- Vázquez?Urbez, M.A.R.T.A., Arenas, C. and Pardo, G., 2012. A sedimentary facies model for stepped, fluvial tufa systems in the Iberian Range (Spain): the Quaternary Piedra and Mesa valleys. *Sedimentology*, 59(2), pp.502-526.
- Vázquez-Sánchez, E. and Jaimes-Palomera, R., 1989. Geología de la Cuenca de México. *Geofísica Internacional*, 28(2), pp.133-190.
- Vázquez-Selem, L. and Heine, K., 2004. Late quaternary glaciation of Mexico. *Developments in Quaternary Sciences*, 2, pp.233-242.
- Verati, C. and Jourdan, F., 2014. Modelling effect of sericitization of plagioclase on the $^{40}K/^{40}Ar$ and $^{40}Ar/^{39}Ar$ chronometers: implication for dating basaltic rocks and mineral deposits. *Geological Society, London, Special Publications*, 378(1), pp.155-174.

- Verrecchia, E.P., Dumont, J.L. and Verrecchia, K.E., 1993. Role of calcium oxalate biomineralization by fungi in the formation of calcretes: a case study from Nazareth, Israel. *Journal of Sedimentary Research*, 63(5).
- Verrecchia, E.P., Freytet, P., Verrecchia, K.E. and Dumont, J.L., 1995. Spherulites in calcrete laminar crusts: biogenic CaCO₃ precipitation as a major contributor to crust formation. *Journal of Sedimentary research*, 65(4).
- Verrecchia, E.P.V.K.E., 1994. Needle-fiber calcite: a critical review and a proposed classification. *Journal of Sedimentary Research*, 64(3).
- Viles, H. and Pentecost, A., 2007. Tufa and travertine. *Geochemical Sediments and Landscapes*, pp.173-199.
- Violante, C., Ferreri, V., D'Argenio, B. and Golubic, S., 1994. -Quaternary Travertines at Rocchetta a Volturno (Isernia, Central Italy). *Facies analysis and Sedimentary model of an Organogenic Carbonate System*.
- Walker, R.G. and James, N.P., 1992. *Facies models: Response to sea level change: St. John's, Newfoundland*, Geological Association of Canada.
- Walker, R.G., 1976. *Facies models 2. Turbidites and associated coarse clastic deposits*. *Geoscience Canada*, 3(1).
- Walker, R.G., 1990. *Facies modeling and sequence stratigraphy: perspective*. *Journal of Sedimentary Research*, 60(5).
- Walther, J., 1894. *Einleitung in die Geologie als historische Wissenschaft* Fischer Verlag. Léna, Allemagne (1893-1894)(3 vols.).
- Wang, L.C., Behling, H., Kao, S.J., Li, H.C., Selvaraj, K., Hsieh, M.L. and Chang, Y.P., 2015. Late Holocene environment of subalpine northeastern Taiwan from pollen and diatom analysis of lake sediments. *Journal of Asian Earth Sciences*, 114, pp.447-456.
- Wang, P., Tian, J., Cheng, X., Liu, C. and Xu, J., 2004. Major Pleistocene stages in a carbon perspective: The South China Sea record and its global comparison. *Paleoceanography*, 19(4).
- Waters, M. R., Haynes, C. V., 2001. Late Quaternary arroyo formation and climate change in the American Southwest. *Geology*, 29: 399 - 402.
- Waters, M.R., 2008. Alluvial chronologies and archaeology of the Gila River drainage basin, Arizona. *Geomorphology*, 101(1), pp.332-341.
- Watts, N.L., 1980. Quaternary pedogenic calcretes from the Kalahari (southern Africa): mineralogy, genesis and diagenesis. *Sedimentology*, 27(6), pp.661-686.
- Wayne Higgins, R., Douglas, A., Hahmann, A., Berbery, E.H., Gutzler, D., Shuttleworth, J., Stensrud, D., Amador, J., Carbone, R., Cortez, M. and Douglas, M., 2003. Progress in Pan American CLIVAR research: the North American monsoon system. *Atmósfera*, 16(1), pp.29-65.
- Webb, G.E., Price, G.J., Nothdurft, L.D., Deer, L. and Rintoul, L., 2007. Cryptic meteoric diagenesis in freshwater bivalves: implications for radiocarbon dating. *Geology*, 35(9), pp.803-806.
- Wei, K. and Gasse, F., 1999. Oxygen isotopes in lacustrine carbonates of West China revisited: implications for post glacial changes in summer monsoon circulation. *Quaternary Science Reviews*, 18(12), pp.1315-1334.
- Weissmann, G.S., Hartley, A.J., Nichols, G.J., Scuderi, L.A., Olson, M., Buehler, H. and Banteah, R., 2010. Fluvial form in modern continental sedimentary basins: Distributive fluvial systems. *Geology*, 38(1), pp.39-42.
- Wendt, K.A., Moseley, G.E., Dublyansky, Y.V., Spötl, C. and Edwards, R.L., 2016, April. 500,000 years of water table fluctuations recorded in Devils Hole 2 cave from southwestern Nevada, USA. In *EGU General Assembly Conference Abstracts* (Vol. 18, p. 11194).
- Weninger, B. and Jöris, O., 2008. A 14 C age calibration curve for the last 60 ka: the Greenland-Hulu U/Th timescale and its impact on understanding the Middle to Upper Paleolithic transition in Western Eurasia. *Journal of Human Evolution*, 55(5), pp.772-781.
- Westall, F., Steele, A., Toporski, J., Walsh, M., Allen, C., Guidry, S., McKay, D., Gibson, E. and Chafetz, H., 2000. Polymeric substances and biofilms as biomarkers in terrestrial materials: implications for extraterrestrial samples. *Journal of Geophysical Research: Planets*, 105(E10), pp.24511-24527.

- White, S.E., 1986. Quaternary glacial stratigraphy and chronology of Mexico. *Quaternary Science Reviews*, 5, pp.201-205.
- Wieder, M. and Yaalon, D.H., 1982. Micromorphological fabrics and developmental stages of carbonate nodular forms related to soil characteristics. *Geoderma*, 28(3-4), pp.203-220.
- Wilber, R.J. and Neumann, A.C., 1993. Effects of submarine cementation on microfibrils and physical properties of carbonate slope deposits, Northern Bahamas. In *Carbonate microfibrils* (pp. 79-94). Springer, New York, NY.
- Winograd, I., Coplen, T., Landwehr, J., Riggs, A., Ludwig, K., Szabo, B., Kolesar, P. and Revesz, K., 1992. Continuous 500, 000-year climate record from vein calcite in Devils Hole, Nevada. *Science*, 258(5080), pp.255-260.
- Woodbridge, J. and Roberts, N., 2011. Late Holocene climate of the Eastern Mediterranean inferred from diatom analysis of annually-laminated lake sediments. *Quaternary Science Reviews*, 30(23), pp.3381-3392.
- Wright, V., 1986. The role of fungal biomineralization in the formation of Early Carboniferous soil fabrics. *Sedimentology*, 33(6), pp.831-838.
- Wright, V.P. and Tucker, M.E. eds., 1991. *Calcretes*. Blackwell Scientific Publications.
- Wright, V.P., Beck, V.H. and Sanz-Montero, M.E., 1996. Spherulites in calcrete laminar crusts: Biogenic CaCO₃ precipitation as a major contributor to crust formation: discussion. *Journal of Sedimentary Research*, 66(5).
- Wright, V.P., Platt, N.H. and Wimbledon, W.A., 1988. Biogenic laminar calcretes: evidence of calcified root/mat horizons in paleosols. *Sedimentology*, 35(4), pp.603-620.
- www.es.wikipedia.org/tequiquiac
- Yang, X., Scuderi, L., Paillou, P., Liu, Z., Li, H. and Ren, X., 2011. Quaternary environmental changes in the drylands of China—a critical review. *Quaternary Science Reviews*, 30(23), pp.3219-3233.
- Yokoo, Y., Nakano, T., Nishikawa, M. and Quan, H., 2004. Mineralogical variation of Sr-Nd isotopic and elemental compositions in loess and desert sand from the central Loess Plateau in China as a provenance tracer of wet and dry deposition in the northwestern Pacific. *Chemical Geology*, 204(1), pp.45-62.
- Ypsilon., 2015. en.wikivoyage.org/wiki/Central_Mexico
- Yu, P.S. and Chen, M.T., 2011. A prolonged warm and humid interval during marine isotope stage 13-15 as revealed by hydrographic reconstructions from the South China Sea (IMAGES MD972142). *Journal of Asian Earth Sciences*, 40(6), pp.1230-1237.
- YUEN, S.G., 2014, October. PLEISTOCENE MAMMALS FROM EL TAJO QUARRY, STATE OF MEXICO, MEXICO. In 2014 GSA Annual Meeting in Vancouver, British Columbia.
- Zanchetta, G., Borghini, A., Fallick, A.E., Bonadonna, F.P. and Leone, G., 2007. Late Quaternary palaeohydrology of Lake Pergusa (Sicily, southern Italy) as inferred by stable isotopes of lacustrine carbonates. *Journal of Paleolimnology*, 38(2), pp.227-239.
- Zhang, R. and Delworth, T.L., 2006. Impact of Atlantic multidecadal oscillations on India/Sahel rainfall and Atlantic hurricanes. *Geophysical Research Letters*, 33(17).
- Zhang, S., Cui, K., Zhang, C. and Jin, M.Y., 2011. Controlling factors and distribution patterns of lithologic pools in the fluvial facies of the 3rd and 4th members of the Quantou Formation in the Songliao Basin. *Oil & gas geology*, 32(3), pp.411-419.

Chapter Two: Background to the Research

2.1: Introduction

Explained in this chapter is the background of the PhD research. The purpose of the overview is to provide context to the palaeoenvironmental reconstructions reviewed and synthesised here, and the palaeoenvironmental data presented Chapters 5 – 9.

2.1.1: The impact of Quaternary climate records from low latitude regions

Knowledge of environmental system responses to specific climatic forcing mechanisms is valuable, particularly for those that cause global temperature change on a similar magnitude to predicted global warming. Although naturally forced palaeoclimatic variations are not direct analogues for predicted “anthropogenically induced” climate change, a better understanding can be developed by reconstructing how regions responded to global environmental shifts in the past. These data can be used to help inform about how the same geographic area may react in the future, and on what magnitude (Price, 2009; Metcalfe et al. 2015). Unlike the mid-latitude regions of Europe and North America, the continental tropics have the least amount of Quaternary environmental records, especially the western Northern Hemisphere tropics (Figs 2.1 & 2.4) (Metcalfe et al. 2000; Metcalfe & Nash, 2012) which frustrates, and limits attempts to further knowledge of, and model, global system responses to past climate change.

Despite the above, since the 1970s, detailed analysis of low latitude lake (Grove & Goudie, 1971; Street & Grove, 1976; Kutzbach & Street-Perrott, 1885) and oceanic sediments (Damuth & Fairbridge, 1970; Pastouret et al. 1978; Imbrie, 1979; Rühlemann et al. 1999; Gasse, 2000; Peterson et al. 2000; Larrasoána et al. 2003; Li et al. 2016), and increased insight into tropical rain forest stability (Flenley, 1979; Behling et al. 2002; Ledru et al. 2005; Leite et al. 2016) suggests the role of the tropics in global climate change had previously been underestimated, and that the tropics directly affect global climate forcing (Kerr, 2001; Metcalfe & Nash, 2012). The magnitude and timing of Quaternary climate change in different parts of the tropics were also found to be significantly more complicated than initially thought (Metcalfe & Nash, 2012).

2.1.2: Quaternary environmental records from Central Mexico

In terms of what is understood about the late Quaternary environmental history of the North America tropics and sub-tropics (Figs 2.1 & 2.5), the lake systems that transect the Trans Mexican Volcanic Belt (Fig 2.2b), especially the Basin of Mexico (Fig 2.2a) are some of the most researched Quaternary sediments from the Northern

Hemisphere Tropics (Metcalf et al. 2000; Metcalfe, 2006; Caballero et al. 2010; Lozano et al. 2015; Metcalfe et al. 2015). Closed drainage basins situated at or close to climatic boundaries, like the Central Mexican basins (Fig 2.2a & b), are susceptible to climate change (Baturina et al. 2006; Roy et al., 2009; Borejsza & Frederic, 2010; Mueller et al. 2012; Tovar et al. 2014). The reactive nature of these basins to climate fluctuations means they have the potential to produce long, detailed records of local, regional and global climate-related changes (Metcalf, 1997; Lozano & Ortega, 1998; Enzel et al. 1999; Schuett, 2000; Sinha et al. 2006; Roy et al. 2008, 2009).

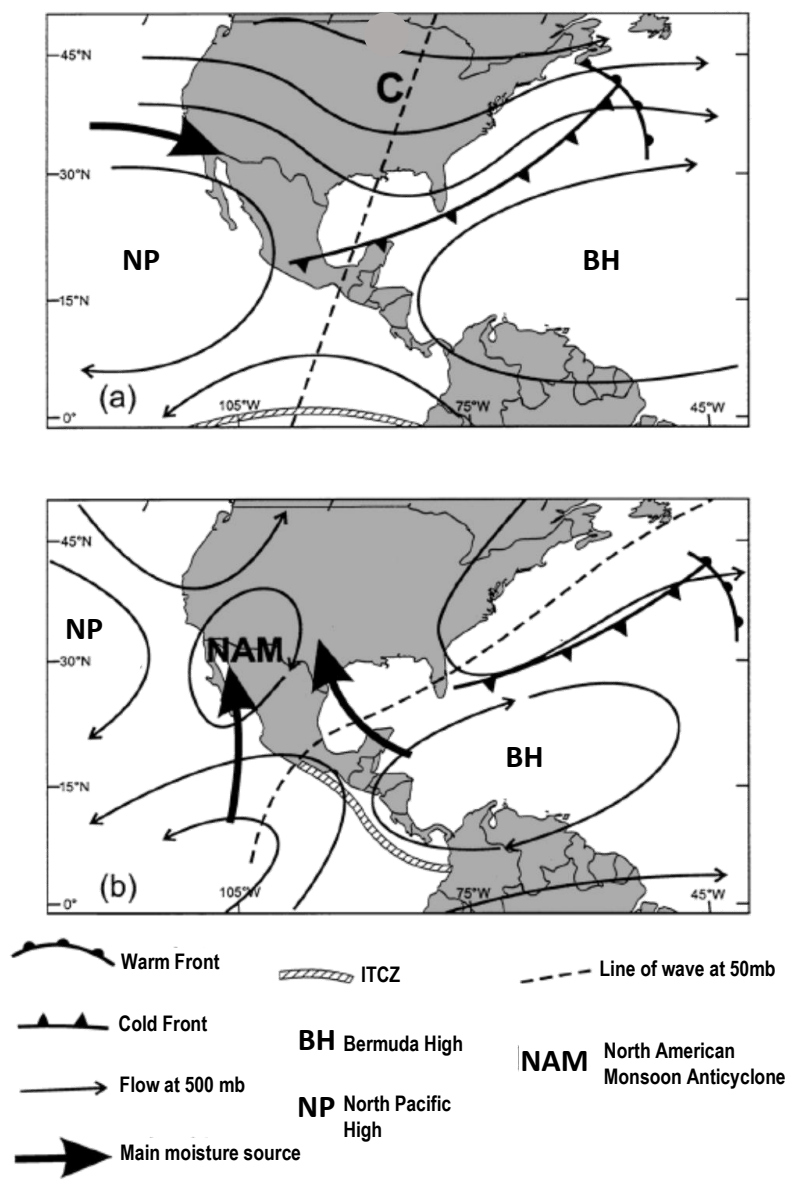


Figure 2.1: Climatology of the North American tropics and sub-tropics regions located within the North American Monsoon region today a) summer b) winter. (from Metcalfe et al. 2015).

The Trans Mexican Volcanic Belt (Figs 2.2a & b & 2.3) represents a transition zone between Northern Mexico's arid climate and the temperate, tropical climate of southern Mexico (see Section 2.4) (Douglas et al. 1993; Roy et al. 2009). Hence, these Central Mexican lake basins are likely excellent palaeoenvironmental research sites. However, of the records that are available today, site locations are distributed across niche geographic areas leading to poor spatial and temporally distributions of data (Metcalf et al. 2000; Metcalfe, 2006; Metcalfe & Nash, 2012; Metcalfe et al. 2015; Fig 2.7). The location of studied sites tends to be governed by the location lakes that hold suitable material to analyse, which ultimately leads to site clustering. Although lacustrine sediments have been the focus of palaeoenvironmental research across Central Mexico, abundant alluvial sequences are also present (see Borejsza & Frederick, 2010). Fluvial and paleosol sequences are increasingly being employed to understand long-term variations in hydrology (e.g. Vandenberghe & Maddy, 2001; Macklin et al. 2006; Borejsza & Frederick, 2010; Mueller et al. 2012; Tovar et al. 2014) and would be particularly useful where lacustrine sediments are dried, absent or limited, and evidence of glaciation is not present across Mexico (Roy et al. 2009). The advantage of using alluvial sediments from across Mexico in Quaternary research is their extensive geographical distribution. The distribution of alluvial sediments opens the possibility of exploring research areas away from the traditional lake basins (Borejsza & Frederick, 2010).

2.1.3: Forcing mechanisms of depositional change

Because the average basin elevation is above ca 2000 m a.s.l (Fig 2.5) across Central Mexico sea-level change has little impact on hydrological base-level changes. Instead, sedimentological research across Central Mexico has focused climatic forcing in core-based studies of Quaternary lake sediments. The focus on climatic forcing has a basis in the fact that moisture availability is the dominant cause of hydrological, sedimentological and vegetational change across tropical regions (Metcalf, 2006). Seismic activity, volcanic eruptions, and associated slope failures that have been occurring since the Miocene across Mexico (see Arreygue-Rocha, 1999; McGuire et al. 2000; Israde-Alcántara et al. 2005; Capra et al. 2013) have also had a significant impact on the configuration of hydrological networks, the availability of accommodation space, sedimentation, and vegetation cover (Arreygue-Rocha, 1999; McGuire et al. 2000; Israde-Alcántara et al. 2005; Ferrier, 2009; Ferrari et al. 2012; Capra et al. 2013; Lozano et al. 2015).

2.2: Physiography of Central Mexico

The Central Mexican lakes (Fig 2.2a & b) began to form around the time the Trans Mexican Volcanic Belt formed as Mexico's main volcanic arc during the Mid-Miocene (Fig 2.3). The transition, from the western Sierra

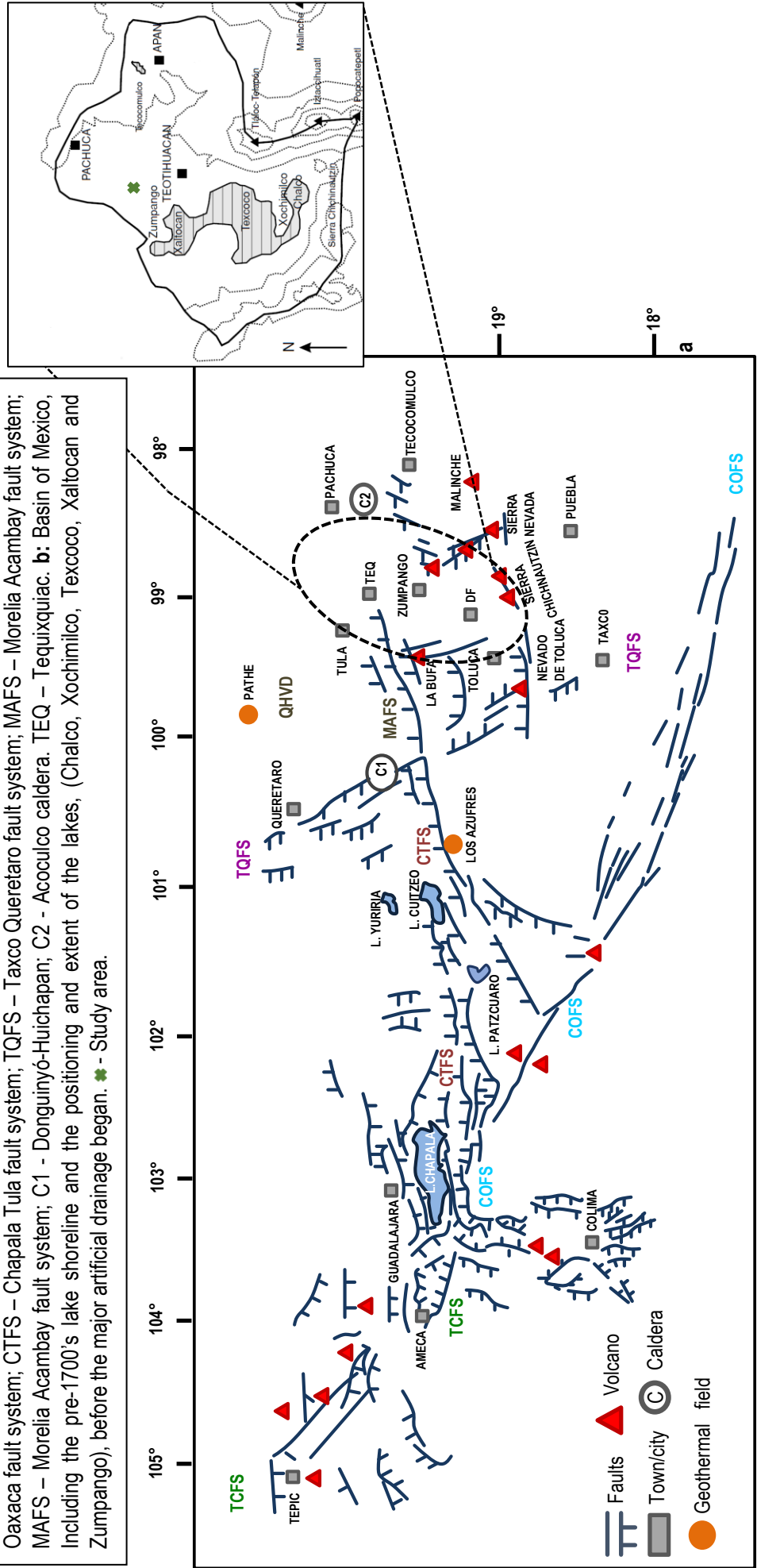
Madre Occidental volcanic arc, to the position of today's Trans Mexican Volcanic Belt (Fig 2.3) (Ferrier, 2009; Ferrari et al. 2012), coupled with intra-arch extension, restructured Central Mexico's surface hydrology. These events created fault-controlled sedimentary basins and volcanic topographic relief (Fig 2.2a) (Ferrari, 2009) that provided accommodation space for lacustrine sedimentation and created an altitude gradient of more than 5000 m east to west (Caballero et al. 2010). Intense volcanism along the Trans Mexican Volcanic Belt from the mid Miocene onwards has formed large stratovolcanoes (e.g. Pico de Orizaba, Popocatepetl, Iztaccihuatl, Nevado de Toluca, Tancitaro, Nevado de Colima, See Fig 2.2a & b and Caballero et al. 2010). In the Basin of Mexico, lacustrine, fluvial and volcanic sediments were deposited from the Pliocene into the Pleistocene (Ferrari, 2009). Around the early Pleistocene (1.2 – 0.78 Ma: Ortega et al. 2002; Arce et al. 2013) the emplacement of the Sierra Chichinautzin Monogenetic Volcanic Field hydrologically closed the Basin of Mexico to the south cutting off the basins only drainage outlet (Fig 2.2 & b) (Ortega & Farvolden, 1989; Ortega & Newton, 1998; Ferrari, 2009; Arce et al. 2013). Hydrological isolation allowed the development of an extensive lacustrine system within the Basin of Mexico that at one or more times likely merged to form a single deep-water body (Bradbury, 1989, Caballero & Ortega, 1998; Lonzano et al. 2015; Torres-Rodríguez et al. 2015). During the Quaternary, the lake system in the Basin of Mexico gradually receded to smaller areas forming a series of interconnected shallow lakes with Chalco and Xochimilco at the south; Zumpango and Xaltocan at the north and Texcoco at the centre, into which the other lakes drained (Fig 2.2b). See Chapter 3 for further discussion.

2.3: Quaternary Climate forcing across Mexico

Long-term global changes in the amount and distribution of incoming insolation are forced by the oscillatory nature of Earth's orbital and axial parameters (Milankovitch cycles; eccentricity (100kyr cycle), obliquity (41kyr cycle) and precession (23kyr cycle). These cycles have caused Earth's climate to alternate between warm (interglacial/interstadial) and cool (glacial/stadial) periods between which global temperatures differed by as much as c. 5°C+ (Delcourt & Delcourt, 1991). Across the Northern Hemisphere tropics (Fig 2.1), within which Mexico sits, precession has the most impact affecting the intensity of summer insolation leading to stronger seasonality which influences the position of the Intertropical Convergence Zone (ITCZ), see below and Figs 2.1 & 2.4 (Metcalf & Nash, 2012).

On shorter time scales, changes in the amount and distribution of precipitation across Mexico have been forced by shifts in the mean position of the ITCZ which in turn is affected by sea surface temperature (SST) latitudinal gradients, and atmospheric surface pressure gradients have (Chiang & Bitz, 2005; Hodell et al. 2008).

Figure 2.2: a: Simplified map of the fault controlled sedimentary basins, lake systems, neotectonic fault systems and active (in some cases inactive) volcanoes that transect E-W and NNW-SSE across Central Mexico (from: Johnson & Harrison, 1990; Ferrari et al, 2000; Alaniz & Nieto, 2007; Ferrari et al, 2012). TLPFS – Tenango – La Pera fault system; TCFS – Tepic Chapala fault system; COFS – Chapala Oaxaca fault system; CTFS – Chapala Tula fault system; TQFS – Taxco Queretaro fault system; MAFS – Morelia Acambay fault system; MAFS – Morelia Acambay fault system; TQFS – Taxco Queretaro fault system; MAFS – Morelia Acambay fault system; CTFS – Chapala Tula fault system; COFS – Chapala Oaxaca fault system; including the pre-1700's lake shoreline and the positioning and extent of the lakes, (Chalco, Xochimilco, Texcoco, Xaltocan and Zumpango), before the major artificial drainage began. * - Study area.



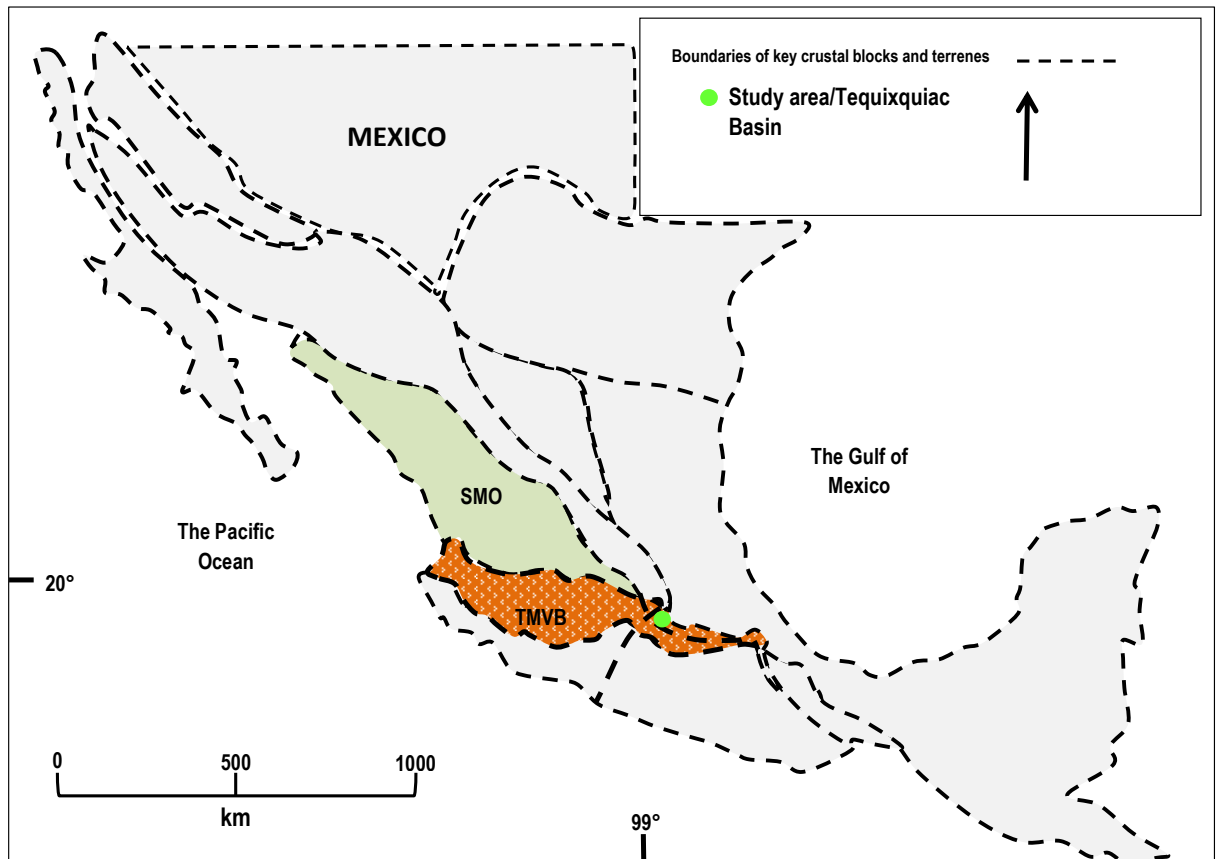


Figure 2.3: Simplified expression of the present volcanic arch, the Trans Mexican Volcanic Belt (TMVB) and Sierra Madre Occidental (SMO) which was the Mexican volcanic arch before the transition during the mid-Miocene. The TMVB represents the most recent episode of magmatic activity that has occurred in stages since the Jurassic Period (Ferrari et al. 2012). Also, see Figure 2.4.

Modelling has indicated that the position of the ITCZ has been highly sensitive to the extent of Northern Hemisphere land and sea ice cover during the Quaternary (Chang et al. 1997; Chiang et al. 2002, 2003; Chiang & Bitz, 2005; Hodell et al. 2008), and to changes to the Atlantic Meridional overturning circulation (Chang et al. 2007; Hodell et al. 2008). Faster Atlantic overturning, caused by strong bottom water formation, increases the cross-equatorial heat flux from the south to the north Atlantic. This forces the ITCZ to shift its mean position north (Figs 2.1 & 2.4) (Hodell et al. 2008), SST's to warm, trade wind strength to decline, and precipitation to increase in the Northern Hemisphere tropics (Hodell et al. 2008). The opposite happens if Atlantic overturning begins to slow down, which may result from the freshwater input, for example, from meltwater influx during Heinrich events (see below and Figs 2.1 & 2.4) (Hodell et al. 2008).

On millennial time scales, potential drivers of Central Mexican Quaternary climate include Dansgaard-Oeschger cycles (DO) and Heinrich Events (HE). DO cycles are short-lived, but rapid, global warming events that correlate with major interstadials in the Greenland summit ice core (Dansgaard et al. 1993; Andrews & Barber, 2002). DO cycles are related to unstable ice dynamics that affect the North Atlantic deep-water formation (above)

and Thermohaline Circulation (Broecker, 2003; Cantarero, 2013), evidence of which is found in low latitude terrestrial records (e.g. Cantarero, 2013, Lake Chalco, Basin of Mexico). Heinrich Events are related to colder intervals that occur in-between DO cycles. HE events are associated with episodes of escalated iceberg discharge from the Laurentide Ice Sheet into the Hudson Strait, and a southwards transgression of cold polar water allowing icebergs to travel further south towards the equator (Bond et al. 1992; Hemming, 2004). These events are linked to climatic shifts across the Northern Hemisphere. Across North America, they occurred during cold periods that preceded warming and the influx of meltwater into the Atlantic (Hemming, 2004).

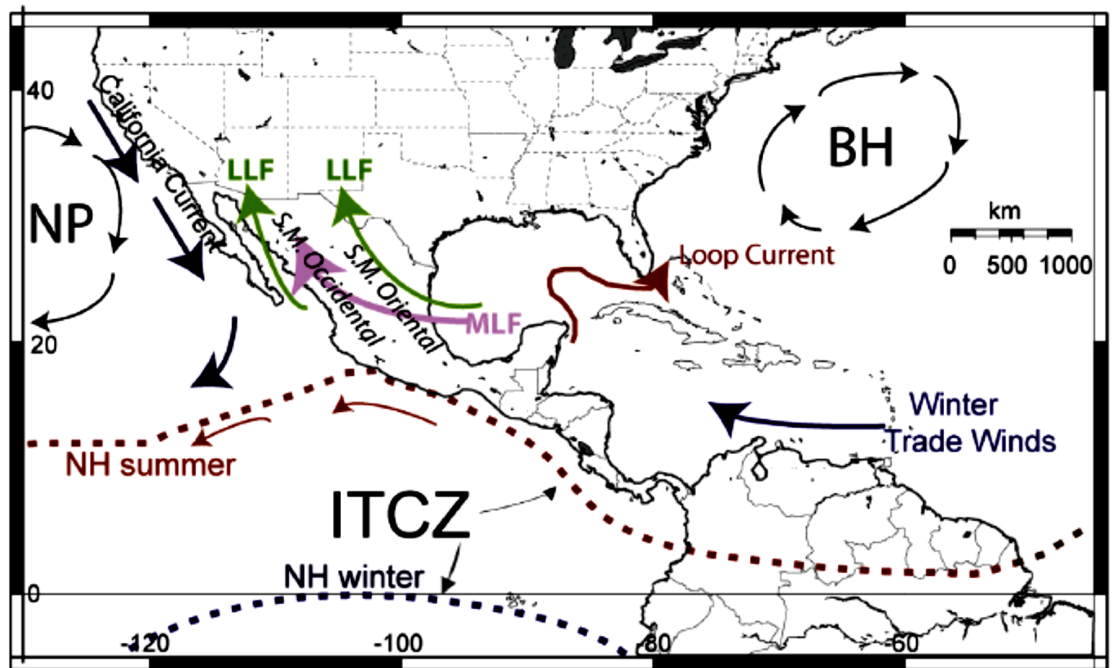


Figure 2.4: Contemporary climatology of Mexico (NAM region) (from Metcalfe et al. 2015). The movement of low-level moisture flow (LLF) moving north from the Gulf of Mexico and the Gulf of California which is blocked to the west and east by the Sierra Madre Occidental (see Fig 2.4) and Sierra Madre Oriental mountain ranges respectively. The movements of the mid-latitude Flow or mid-latitude Westerly depression (MLF). The northward movement of the ITCZ (NH Summer) drives tropical moisture. Tropical moisture is limited by the North Pacific (NP) and the Bermuda High (BH) high-pressure systems. Mid-level moisture from the Gulf of Mexico supplies much of the summer precipitation in Mexico and across the NAM region. The loop current is the primary surface-ocean current in the Gulf of Mexico that transports warm waters from the Caribbean Sea through the Yucatan Strait into the Gulf of Mexico (From Metcalfe et al. 2015).

During the Holocene, orbitally forced insolation changes across the Northern Hemisphere weakened and the NAM (North American Monsoon) (see Figs 2.1 & 2.4) gained strength as the interglacial period progressed (Knudsen et al. 2011; Metcalfe et al. 2015). In the absence of strong orbital forcing, the location and strength of integral atmospheric features became more critical in determining pressure distributions, and subsequently precipitation patterns across Mexico and the NAM region (see Figs 2.1 & 2.4, Metcalfe, 2006; Metcalfe et al. 2015).

Climatic anomalies that have altered precipitation patterns across the NAM regions from the Holocene up until today include El Niño Southern Oscillation (ENSO), the Pacific Decadal Oscillation (PDO), the North Atlantic Oscillation (NAO), and the Atlantic Multidecadal Oscillation (AMO). Briefly, during ENSO years precipitation decreases across Mexico except in the north-west (Magaña et al. 2003; Metcalfe, 2006), the opposite occurs during La Niña when the average annual summer rainfall increases (Metcalfe, 2006). This climate anomaly became more dominant after ca. 5000 cal BP and has since occurred every few years (Metcalfe et al. 2015).

PDO has ENSO characteristics but cycles over more extended periods. Positive (warm) PDO phases are like La Niña (eastern Pacific warm), and negative (cold) phases are like La El Niño (eastern Pacific cool) (Metcalfe, 2006; Metcalfe et al. 2015). Across central Mexico, El Niño cycles and positive phases of PDO reduce summer rainfall while the ITCZ remains close to the equator, and the thermal continental heat gradient is reduced (Castro et al. 2001; Magaña et al. 2003; Metcalfe et al. 2015). During La Niña cycles and negative PDO phases the average amount of annual of summer precipitation across the southern NAM region increases, coinciding with a strong ITCZ that relocates to the eastern tropical Pacific (Figs 2.1 & 2.4) combined with strong tropical convection (Metcalfe et al. 2015).

The NAO climate anomaly describes surface level pressure difference between the subtropical (Azores) high and the polar low-pressure system (Figs 2.1 & 2.4) (Metcalfe, 2006; Metcalfe et al. 2015). Positive phases of NAO display lower than average heights and pressures across North Atlantic high latitudes, and higher than average heights and over the central North Atlantic (Metcalfe, 2006; Metcalfe et al. 2015). Negative phases display the opposite trend of heights and pressure over the same regions (Metcalfe, 2006; Metcalfe et al. 2015). Both phases of the NAO reflect basin-wide (Atlantic Basin) changes in the strength and position of the North Atlantic jet stream, storm track, and to the usual pattern of zonal and meridional heat and moisture transport, which in turn results in changes in temperature and precipitation across the NAM region (Metcalfe, 2006; Metcalfe et al. 2015). The AMO represents a series of long-duration changes to SST in the North Atlantic consisting of alternative warm/cool phases that can last between 20-40 years with a difference of ca. 1°F between extremes (Delworth et al. 2008). The AMO climate anomaly has been active for around the last 1000 years (Delworth et al. 2008). Throughout the NAM region the AMO and the NAO are most influential during summer when positive (warm) AMO cycles create wetter summer seasons in Central and Southern Mexico when the ITCZ migrates north (Figs 2.1 & 2.4) and tropical cyclone activity increases (Sutton & Hodson, 2005; Metcalfe, 2006; Metcalfe et al. 2015)

2.4: Modern Climate of Central Mexico

Mexican climate today is governed by seasonal shifts in the position of the ITCZ (Figs 2.1 & 2.4), the position and intensity of the subtropical high pressure cells (Bermuda-Azores high: Fig 2.4), and the position and extent of the mid-latitude westerlies depression (Fig 2.4) (Metcalf, 2006, Metcalfe et al. 2015). Trade winds from the Gulf of Mexico, the Caribbean ocean, and the tropical Pacific supply the primary sources of moisture into eastern and northern Central Mexico by a monsoon type system (NAM; Figs 2.1 & 2.4) (Higgins et al. 1998; Caballero et al. 2010; Metcalfe et al. 2015). Low-level jets coming from the Gulf of Mexico also transport moisture through eastern Mexico towards the American Great Plains (Fig 2.4) (Higgins et al. 2003; Metcalfe et al. 2015). A north-south climatic gradient exists across the NAM (Figs 2.1 & 2.4) from the humid tropics to the dry subtropical regions in the north (Metcalf et al. 2015). Rainfall is highest in Central Mexico during the boreal summer when northern hemisphere insolation increases, and the ITCZ migrates north (Figs 2.1 & 2.4) (Cantarero, 2013; Metcalfe et al. 2015). Winter is characterised by the displacement of polar air masses across Central Mexico and the Gulf of Mexico, which reduces temperatures (Caballero et al. 2010). Average annual temperatures are strongly affected by topographic variations (Fig 2.5), but are generally between 12 ° and 18 ° C, with western areas being warmer (between 18° and 22° C) (Caballero et al. 2010) and spring being the warmest and driest season (Hernández-Cerda & Carrasco-Anaya, 2007; Caballero et al. 2010).

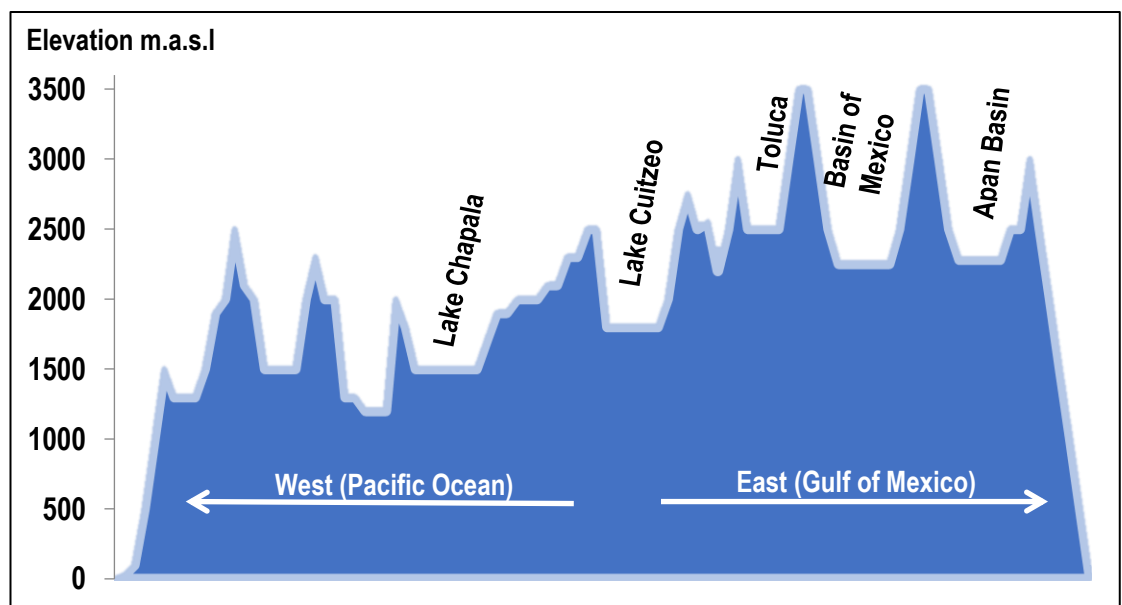


Figure 2.5: Sedimentary basins and topographic change east-west along the TMVB. Approximate altitude to illustrate change.

2.5: Quaternary lacustrine records from the Basin of Mexico

2.5.1: Introduction

The following Sections review, discuss and summarise most of the available records of Quaternary environmental change from the Lakes Chalco, Texcoco and Tecocomulco in the Basin of Mexico. Relevant records and reviews are also included from Eastern, Western, Northern and Southern Mexico to give a more comprehensive perspective of paleoenvironmental change during the Quaternary. From the summaries, gaps in current understanding are highlighted, and the research questions outlined in chapter one is further justified here.

2.5.2: Review of Quaternary records from the Basin of Mexico

Diatom ecology, palynological records, sedimentology, sediment geochemistry, magnetic susceptibility, charcoal particles, inorganic and organic carbon values, tephrostratigraphy, tephrochronology (see Appendix 1, Table 1), radiocarbon and U-series ages form the basis of palaeoenvironmental records from Lake Chalco (Fig 2.2a & b) (e.g. Bradbury, 1989; Caballero, 1997; Caballero & Ortega, 1998; Lozano & Ortega, 1998; Brown et al. 2012; Cantarero, 2013; Lozano et al. 2015). Limited stable isotope data and n-alkane biomarkers records are also available (Cantarero, 2013). Some of the most recent contributions include a 30,000 year-old record (Lozano et al. (2015) and drought and fire record that spans the last 85,000 years (Torres-Rodríguez et al. 2015). Records from Lake Texcoco (Fig 2.2a & b) are based on the multiproxy analysis of diatom ecology, sediment geochemistry, organic geochemistry, micromorphology, pollen analysis, magnetic susceptibility, LOI, stable isotopes, tephrochronology and radiocarbon and U-series dating (Bradbury 1971, 1989; Gonzalez & Fuentes, 1980; Lozano & Ortega, 1998; Bradbury, 1997; Sedov et al. 2001; Lamb et al. 2009; Sedov et al. 2010). Records mainly reconstruct paleolimnological and palaeoenvironmental data from Lake Texcoco (Bradbury 1971, 1989; Gonzalez & Fuentes, 1980; Lozano & Ortega, 1998; Bradbury, 1997; Sedov et al. 2001; Solleriro et al, 2006), while two focus on a section close to the Tepexpan Paleoindian site situated on the margin of Lake Texcoco's former shoreline (Fig 2.2b) (Lamb et al. 2009; Sedov et al. 2010). There are two paleolimnological records from the Lake Tecocomulco in the North-eastern Basin of Mexico (Fig 2.2a & b) that cover (approximately) the last 50,000 cal. BP (Caballero et al. 1999; Roy et al. 2009). Multiproxy evidence of environmental change includes palynology, diatom ecology, magnetic susceptibility, granulometry, multi-element geochemistry, loss on ignition and mineralogy.

In the following overview radiocarbon dates are given as uncalibrated ages (in brackets) the approximate mean calendar ages for the intervals were calculated in CALIB for this study (see Appendix 1, Table 2 - 4) and are reported in Caballero et al. (1999) and Roy et al. (2009).

2.5.2.1: The early-mid Glacial: MIS 5 – MIS 4, 85,000 – 29,000 cal. BP

Between 85,000 and 77,000 cal. BP drought conditions are reported at Chalco (Interval I, Fig 2.6) (Torres-Rodríguez et al. 2015) after which effective moisture availability increased (Interval II, Chalco 77,000 – 64,000 cal. BP) Fig 2.6). Climatic flips between wet to dry cycles during the early glacial in the southern Basin of Mexico are linked to Northern Hemisphere insolation and the mean position of the ITCZ (Figs 2.1 & 2.6) (Lozano et al. 2015; Metcalfe et al. 2015). After 64,000 Cal BP, the frequency of drought episodes increased in the Chalco record (Interval III, Fig 2.6) (Torres-Rodríguez et al. 2015), particularly after 42,000 cal. BP (Interval IV, Fig 2.6). Dry conditions are coupled with the increasingly unpredictable behaviour and Laurentide ice sheet during this interval (Torres-Rodríguez et al. 2015) which is supported by the increasing frequency between wet/dry cycles recorded from the Lake Petén Itzá, Peten sediment records, Guatemala (Hodell et al. 2008; Torres-Rodríguez et al. 2015).

Between 50,000 and 45,239 cal. BP Lake Tecocomulco was relatively deep, and the climate relatively cool and moist with some variation (Interval I, Fig 2.6) (Caballero et al. 1999). Between 48,387 and 41,918 cal. BP (sub-Interval IVa, Fig 2.6) a deep lake phase is also reported from Chalco (Fig 2.6) (Cantarero, 2013). The occurrence of the high lake stands in Chalco, and Tecocomulco possibly represents a temporary wet phase during a period of increased drought frequency based on the Chalco record (Torres-Rodríguez et al. 2015) (Intervals III-IV, Fig 2.6). Lake Tecocomulco was shallow after 45,239 cal. BP (Interval II, Fig 2.6) (Caballero et al. 1999), possibly in response to a slight temperature increase (Fig 2.6) (Caballero et al. 1999) suggesting a switch back to drought/dry conditions? Proxies indicating increased water depth in Lakes Chalco and Tecocomulco, and possibly the increase in the temperature recorded in Lake Tecocomulco (Fig 2.6), are thought to be a response to millennial-scale variations in precipitation trends linked to DO rapid warming cycles (events 12 or 13? Clement & Peterson, 2008), Laurentide ice sheet dynamics and the North Atlantic deep-water formation (Cantarero, 2013) which are all understood to affect precipitation patterns in the Basin of Mexico (Cantarero, 2013), exactly how is still unclear.

Depositional records from Lakes Chalco and Tecocomulco generally agree between 41,981 and 29,914 cal. BP with evidence of increased climate cycling between wet and dry phases and increased frequency of drought phases (Calco Interval IV, Fig 2.6), (Torres-Rodríguez et al. 2015) (Fig 2.6). Overall lake levels are reported to have been low, but fluctuating under a generally drying climate (Fig 2.6) (Caballero et al. 1999; Roy et al. 2009; Cantarero, 2013). Lake Tecocomulco was deeper at 40,646 cal. BP and again at 34,070 cal. BP (Intervals III & IV, Fig 2.6), but these appear to have been short-lived events within a shallowing trend (Fig 2.6) (Caballero et al. 1999;

Roy et al. 2009), although conditions were still deeper than today. Between 38,520 and 30,300 cal. BP (GBA ages, Appendix 1, Table 1) Lake Chalco may have become closed (Caballero, 1997; Caballero & Ortega, 1998) but likely maintained a seasonal connection with Lake Texcoco (Caballero, 1997). After 31,294 cal. BP, a significant decrease in lake level, is reported for lake Chalco (Cantarero, 2013), although this is not clear in all records (Fig 2.6).

Between 30,300 and 29,000 cal. BP, while the ITCZ remained south (Figs 2.1 & 2.4), the runoff signal in Lake Chalco is confused with data suggesting both increased (Lozano et al. 2015) and decreased runoff (Sub-Interval, IVc, Fig 2.6) (after 31,294 cal. BP, Cantarero, 2013). If runoff did increase, it remains unclear if this was because of higher summer insolation and temperatures in the Northern Hemisphere (Lonzano et al. 2015), or because of increased volcanic activity (Appendix 1, Table 1, Section 2.6). Consequently, understanding if this was a climatically wet or dry interval is difficult (Torres-Rodríguez et al. 2015). Drought conditions seem likely if increased glacial meltwater was the source of run-off into Chalco, as suggested by Lonzano et al. (2015). At the same time, Lake Tecocomulco maintained low lake levels which suggest a climatically dry episode, or a precipitation gradient from the dry north to the temperate-tropical south (should effective moisture have increased) but there no evidence to suggest this.

2.5.2.2: The Northern Hemisphere LGM: MIS 2, ca. 29,000 – 19,000 cal. BP

During this interval lacustrine records from Lakes Chalco, Texcoco and Tecocomulco agree that temperatures were cooler than at present and that lake levels were low, but in some records moisture and runoff levels fluctuate slightly (Fig 2.6) (Bradbury, 1971, 1989; Gonzalez & Fuenteo, 1980; Lozano et al. 1993; Lnzano & Ortega, 1998; Ortega et al. 2000; Marcías, 2007; Lamb et al. 2009; Lozano et al. 2015). After 28,000 cal. BP a long-term decrease in temperature set in across the Basin of Mexico that continued for the next 10,000 years (Calco Sub-Interval IVd, Fig 2.6) (Bradbury, 1989; Lozano et al. 2015). At 28,000 cal. BP volcanic activity (Appendix 1, Table 1) is thought to have altered hydrological networks feeding the Chalco sub-basin, with both decreased run-off (Lonzano et al. 2015) and increased runoff (see Caballero & Ortega, 1998; Lozano & Ortega, 1998) suggested (Chalco sub-interval IVd, Fig 2.6). After 27,330 cal. BP increased winter precipitation (Bradbury, 1971, 1989), periods of increased humidity (Bradbury, 1997; Lozano & Ortega, 1998; Sedov et al. 2001; Solleiro et al., 2006) and river input (Lamb et al. 2009), as well as dry conditions, are all suggested in the Texcoco record. Hence, while the temperature signal in the sedimentary records seems clear, the signal to reconstruct the amount and distribution of available moisture is not. After 27,000 cal. BP Torres-Rodríguez et al. (2015) interpret increased moisture or at

least decreased drought frequency in the Chalco record (Interval V, Fig 2.6). Lozano et al. (2015) suggest a shallowing trend with some fluctuation between 26,000 to 19,500 cal. BP (Chalco Sub-Intervals Va & Vb, Fig 2.6) (Lozano et al. 2015) which is also seen in the Lake Tecocomulco after 29,914 cal. BP, where the lake shallowed significantly (Interval V, Fig 2.6) (Caballero et al. 1999; Roy et al. 2009), humidity levels were slightly higher relative to Tecocomulco when the lake dried completely (Fig 2.6). Again this highlights the complexity of the moisture record.

Between 21,793 and 19,326 cal. BP Texcoco water levels were low, but runoff levels fluctuated (Lamb et al. 2009), possibly linked to intensified volcanic activity and increasing glacial meltwater during the latter half of this interval (Interval III, Fig 2.6). Conversely, cool, moist conditions are also reported (Gonzalez & Fuenteo, 1980), and warmer, less humid conditions with increased evapotranspiration at Texcoco (Sedov et al. 2010). Around 19,500 cal. BP runoff is thought to have increased into Lake Chalco (Fig 2.6) (Cantarero, 2013). Hence, there is some disagreement between the Chalco, Texcoco and Tecocomulco lacustrine records in terms of moisture and temperature which may well be because of different amounts of volcanically induced meltwater input into the separate basins rather than a confused climate signal, but there is no evidence of volcanic deposition during the latter half of this interval (Fig 2.6). Another alternative is that an increase in the ambient mean temperature may have also increased meltwater runoff into one or more sub-basin the Basin of Mexico.

The expansion of mountain glaciers across Central eastern Mexico during the LGM is thought to have followed the Northern American (mid-latitude) glacial regime, which suggests a synchronism of the main climatic events across Mesoamerica (Vázquez-Selem & Heine, 2011). Across central-eastern Mexico, the Late Pleistocene glacial maximum lagged the northern hemisphere LGM (Vázquez-Selem & Heine, 2011). The first advance (Hueyatlaco I: Fig 2.6) reached its maximum between 20,200 and 17,500 cal. BP, when Iztaccihuatl volcano was glaciated (Vázquez-Selem & Heine, 2011). Temperatures are estimated to have decreased by between 5 - 9°C based on the Hueyatlaco I (Fig 2.6) equilibrium ice-line altitudes which support pronounced cooling across tropical oceans and landmasses during the LGM (Vázquez-Selem & Heine, 2011).

Overall, available moisture in the Basin of Mexico between 29,000 – 19,000 cal. BP is linked to the expansion of the Laurentide Ice Sheet, the displacement of the westerlies, and the connectivity of the two. Suggestions of increased moisture availability during this period may have resulted from decreased evaporation instead of increased effective moisture caused by the cool glacial conditions (Brunner, 1982; Gonzalez & Fuentes, 1980; Van Devender & Burges, 1985; Metcalfe et al. 2000; Metcalfe, 2006). Alternatively, or additionally, runoff

may have also increased and decreased relative to meltwater generated by volcanic activity on Popocatepetl Volcano (around 27,330 cal. BP (Fig 2.6) (Appendix 1, Table 1) which may have selectively delivered meltwater to individual sub-basins (Chalco and Texcoco). The Tecocomulco record, because of its distance from the active volcanoes situated in the southern Basin of Mexico, probably gives a cleaner climatic signal rather than one that has been disturbed by volcanic events, although this record does not necessarily reflect conditions in the southern and central Basin of Mexico.

2.5.2.3: The Northern Hemisphere Deglaciation ca. 19,000 – 15,000 cal. BP

Temperatures remained cool during the Hueyatenco I glacial advance (ca. 20,200 - 17,500 cal. BP, Fig 2.6). Sedimentation in Lake Tecocomulco had ceased and the lake dried around 19,742 cal. BP corresponding to a hiatus at Lake Cuitzeo (west of the Basin of Mexico Fig 2.2a) between 21,345 – 8963 cal. BP (Fig 2.7). In the Chalco sub-basin runoff continued to decline further and littoral areas expanded (19,500 and 15,500 cal. BP, Sub-Intervals Vc & Vd, Fig 2.6) (Lozano, 1996; Lozano et al. 2015). Conditions in Lake Texcoco were also drying (19,326 and 16,992 cal. BP, Interval IV, Fig 2.6) (Bradbury, 1971, 1989; Lozano & Ortega, 1998; Lamb et al. 2009), possibly with slightly fluctuating humidity levels after 16,992 cal. BP (see below and Lamb et al. 2009). During this period, the central and southern Basin of Mexico were being subject to increased volcanic activity (Appendix 1, Table 1).

2.5.2.4: Pleistocene – Holocene transition ca. 15,000 – 11,000 cal. BP

During the Pleistocene – Holocene transition in the southern and central Basin of Mexico, volcanic activity continued to increase, obscuring the palaeoenvironmental record, particularly in Texcoco lake (Caballero & Ortega, 1998; Lamb et al. 2009). Between 16,992 and 11,445 cal. BP the Texcoco sub-basin is reported to have been initially humid, after which precipitation and evaporation decreased towards the Holocene (Interval V, Fig 2.6) (Lamb et al. 2009; Sedov et al. 2010). Precipitation levels are thought to have remained low until ca. 14,750 cal. BP according to Chalco records, after which orbital forcing increased Northern Hemisphere insolation. Increased insolation would have pushed the ITCZ northwards (Figs 2.1 & 2.4) intensifying and increasing the duration of the wet season in the Basin of Mexico (Cantarero, 2013). A relatively deep lake phase at Chalco around ca. 14,000 cal. BP (Lozano et al. 2015) also coincides with this period. The change in the position of the ITCZ is thought to have caused a massive ecological shift in the Basin of Mexico (Cantarero, 2013). The data presented for this interval broadly agree (i.e. Lamb et al. 2009; Cantarero, 2013; Lozano et al. 2015; Torres-Rodríguez et al. 2015), in that, there was decreased moisture availability in the Basin of Mexico until ca. 14,750 cal. BP after which precipitation levels began to increase and Lake Chalco was relatively deep.

Figure 2.6 Key

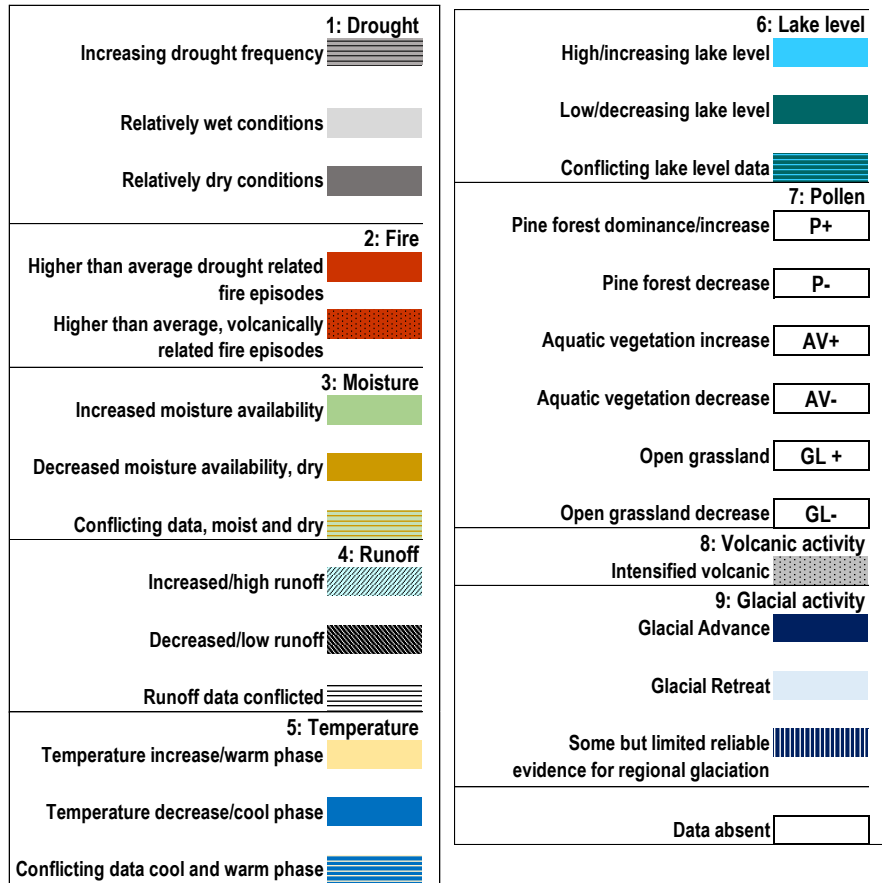


Figure 2.6: Synthesis of Quaternary records from the Basin of Mexico. (Bradbury, 1971; Gonzalez & Fuenteo, 1980; Heine, 1984; Bradbury, 1989; White, 1986; Lozano 1986; Lozano et al. 1993; Lozano & Ortega, 1994; Lozano, 1996; Bradbury, 1997, 1998; Caballero, 1997; Caballero & Ortega, 1998; Ortega & Newton, 1998; Lozano & Ortega, 1998; Caballero et al. 1999; Ortega, 2000; Gonzalez et al. 2001; Sedov et al. 2001; Nordt et al. 2002; Vázquez & Heine, 2004; Solleiro et al. 2006; Marcías, 2007; Lamb et al. 2009; Roy et al. 2009; Caballero et al. 2010; Sedov et al. 2010; Vázquez & Heine, 2011; In Ehlers et al. 2011; Roy et al. 2012; Cantarero, 2013; Lozano et al. 2015; Torres-Rodríguez et al. 2015; Siebe et al. 2017. * H: Hueyatlaco glaciation. M: Milpulco glaciation. Numbers 1 – 9 correspond to the figure key above. * The numbers at the top and bottom of the columns correspond to the number in the key below. Roman numerals indicate interval numbers related to each lake system.

Lake Tecocomulco (Interval VI) however remained dry until 3503 cal. BP. There is evidence of recessional moraine development between 14,000 and 13,000 cal. BP followed by an accelerated glacial retreat between 13,000 – 12,000 cal. BP (Vázquez-Selem & Heine, 2011), but no evidence of a Younger Dryas readvances. Instead, glaciers advanced around 12,000 cal. BP (Milpulco I, Fig 2.6).

2.5.2.5: Holocene

During the Early Holocene there is a general drying and warming trend with runoff gradually decreasing as evaporation increased in Chalco records (Interval X, Fig 2.6) (Caballero & Ortega, 1998; Lozano et al. 2015; Torres-Rodríguez et al. 2015), and Lake Texcoco records between 11,445 and 5693 cal. BP (Interval VI, Fig 2.6) (Bradbury, 1971, 1989; Gonzalez & Fuentes, 1980; Lamb et al. 2009). Sedov et al. (2010) contrarily suggest there is evidence of slightly increased moisture availability from Lake Texcoco and an eruption hiatus is present at 6,100 ka bp (Lozano & Ortega, 1998). At 8300 cal. BP and again at 7000 cal. BP glacial readvances (Milpulco II, Fig 2.6) corresponds to the Little Ice Age event at 8200 cal. BP (Vázquez-Selem & Heine, 2011). During the mid to late Holocene (Lake Texcoco, ca. 5693 and 0 cal. BP), low precipitation and evaporation values are reported from the Texcoco sub-basin by Lamb et al. (2009), while some records indicate a small increase in precipitation (Bradbury, 1997, 1989) and warmer temperatures (Lozano & Ortega, 1998). After 3503 cal. BP sedimentation began again in Lake Tecocomulco (Interval VI, Fig 2.6) (Caballero et al. 1999).

2.6: A broad overview of Mexico's Quaternary history

This overview is based on three reviews of Mexico's Quaternary climate (Metcalf et al. 2000; Metcalfe, 2006; Caballero et al. 2010 and references therein) and a paper that looked at the knowns and unknowns of the Holocene history of the NAM region (Metcalf et al. 2015 and references therein). From each region, additional studies are included when they are considered significant. Where radiocarbon ages are given as uncalibrated ages (in brackets) the approximate mean calendar ages for the intervals were calculated using CALIB for this study (see Appendix 1, Table 1.5) and are reported in Metcalfe et al. 2000, Metcalfe, 2006, Caballero et al. 2010 unless otherwise stated.

2.6.1: Northern Mexico

From across northern Mexico, pollen records indicate that vegetation communities developed that have no comparable modern analogue. *Pinyon* and *Juniper* covered vast regions of what is desert scrub today (Metcalf et al. 2000; Metcalfe, 2006). During the late Pleistocene, vast lakes and wetlands occupied basins that are the Chihuahuan and Sonoran Deserts today (Figs 2.7 & 2.8) (Metcalf et al. 2000; 2015, Metcalfe, 2006). Generally

across Northern Mexico during the late Pleistocene, there was a winter rainfall regime, with the modern summer rainfall regime not being established until after ca. 10,178 cal. BP (9000 ka bp: Metcalfe et al. 2000; 2015, Metcalfe, 2006). The Laurentide Ice Sheet is thought to have driven increased effective winter moisture sourced from the Pacific Ocean that was pushed south into Mexico (Metcalfe, 2006). Unpublished work from the Cuatro Ciénegas Basin in Northeastern Mexico (Fig 2.7) (Felstead, 2012) suggests that this region was wetter between 56,000 and 54,000 cal. BP, 37,000 – 31,000 cal. BP and between 28,000 – 12,000 cal. BP during stadial periods (Fig 2.8). Conditions were hydrologically variable between 84,000 – 56,000 cal. BP, 31,000 – 28,000 cal. BP and from 12,000 cal. BP because of strong seasonality between summer and winter moisture sources. High precipitation levels are reported during the late glacial and deglaciation, but the basin was drier during the Bølling Allerød warm interval (Felstead, 2012).

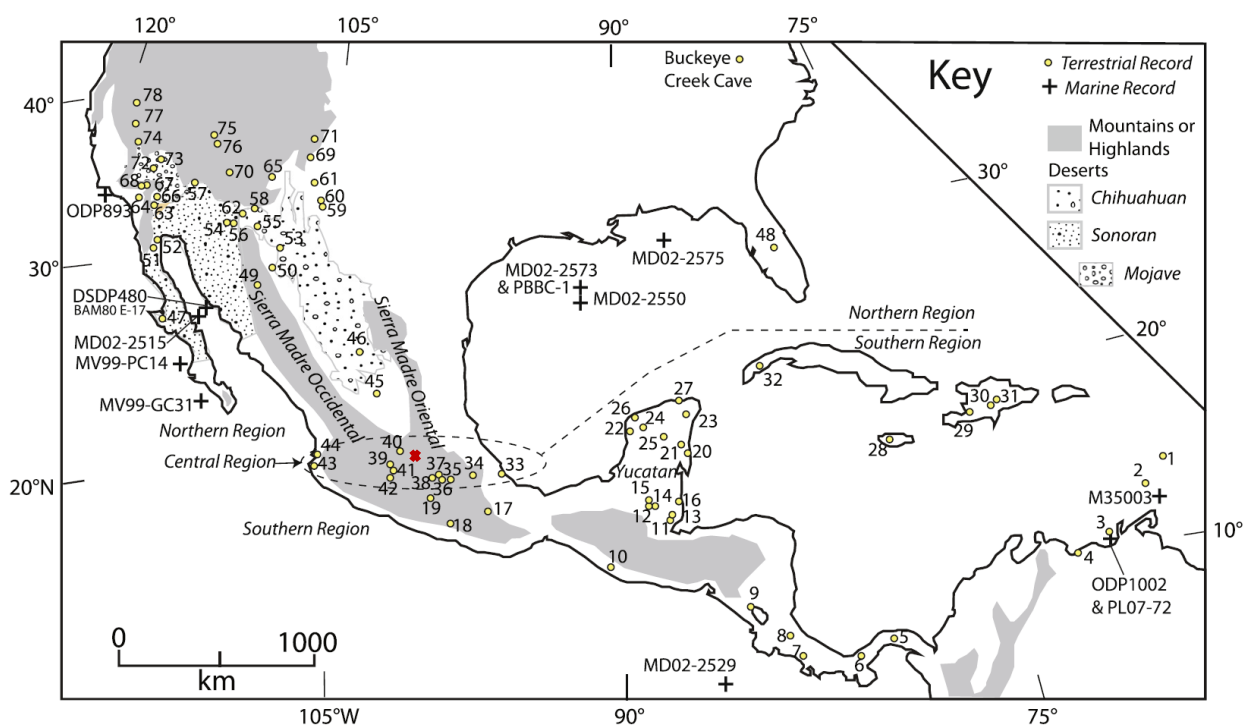


Figure 2.7: Mexican Quaternary environmental records from the NAM region (from Metcalfe et al. 2015). The figure highlights the uneven distribution of terrestrial records that predominantly come from the central and northern regions. For site names and references, see Metcalfe et al. (2015) and Appendix 1, Table 6. The red cross indicates the approximate location of the studies area.

Data from Alta Babicora Basin, central Northern Mexico, suggests a deep freshwater lake was present between 65,000 – 57,000 cal. BP, after which it shallowed (Metcalfe et al. 2002). The basin was hydrologically variable between 54,600 and 38,000 cal. BP with intervals of desiccation and deflation. The lake deepened again after 38,000 cal. BP up until 29,000 cal. BP (Metcalfe et al. 2002). Conditions were shallow during the LGM,

although deeper than at present, and around the time of deglaciation, the lake shallowed further (ca. 15,000 cal. BP). A shallow lake remained at the Holocene – Pleistocene transition, although levels continued to decline into the Holocene (Fig 2.8) (Metcalf et al. 2002).

During the LGM, temperatures were 5 - 6°C colder than today (Fig 2.8) (Metcalf, 2006) and conditions more variable. During the Younger Dryas, the Babicora site (Fig 2.7) had more effective moisture than at present, although conditions were still relatively dry (Metcalf et al. 2015). Moisture availability during deglaciation and the early Holocene is related to variations in the seasonality of precipitation across the NAM region (Fig 2.1), and the continued, but declining, presence and influence of the Laurentide Ice Sheet, particularly during the Younger Dryas, which allowed the westerlies to penetrate further south when the jet stream was relocated towards the equator (Metcalf et al. 2015). Wetter conditions after the Younger Dryas have been linked to the re-establishment of the NAM and increasing summer precipitation (Fig 2.8) (Metcalf et al. 2015).

Broadly, across northern Mexico, the late Pleistocene and early Holocene were wetter than the present (Fig 2.8) (Metcalf et al. 2000; 2015, Metcalf, 2006). From the early to mid-Holocene conditions were warmer, possibly by as much as 2°C, and wetter than today (Fig 2.8). Increased ambient temperatures are thought to have been forced by Milankovitch driven insolation changes, mainly precession, that started to increase summer precipitation and effective moisture (Fig 2.8) (Metcalf, 2006). The NAM strength peaked at 6000 cal. BP is bringing wetter conditions across Mexico (Fig 2.8) (Metcalf et al. 2015). Conditions began to dry, and precipitation decreased again around 5693 cal. BP (ca. 5000 ka bp) (Metcalf et al. 2000; 2015, Metcalf, 2006) with actual desert conditions not establishing until after 4465 cal. BP (4000 ka bp) (Fig 2.8) (Metcalf, 2006).

2.6.2: Central Mexico

During the early Pleistocene (ca. 120,000 – 90,000 cal. BP) Lake Cuitzeo, west of the Basin of Mexico (Fig 2.2a) was fresh and moderately deep with a transgression occurring at the end of the period (Fig 2.8) (Israde et al. 2002; Metcalf, 2006). After 90,000 cal. BP, there was a short-lived deep phase after which the lake shallowed and salinity increased until 39,556 cal. BP (35,000 ka bp) (Fig 2.8) (Israde et al. 2002; Metcalf, 2006) when the lake shallowed. After 39,556 cal. BP, moisture levels increased up until 26,199 cal. BP (22,000 ka bp), after which lake levels declined (Fig 2.8). During the LGM Lake Cuitzeo was relatively deep after which it shallowed (Fig 2.8). Determining if conditions were cool and dry or cool and moist is not presently possible. Moisture levels appear to have been cool and moist but subject to variability east to west, probably because of suppressed evaporation due to the lower glacial temperatures (Fig 2.8) (Metcalf et al. 2000). Caballero et al. (2010) suggest humidity was low,

but some records support dryer conditions during the LGM except for the Lake Pátzcuaro and Lake Cuitzeo records (Fig 2) (Caballero et al.2010).

Figure 2.8 Summary of Mexico's recorded Quaternary Environmental History. Northern Mexico (Metcalfe et al, 2002; Metcalfe et al. 2000, 2015; Metcalfe, 2006; Felstead, 2012): **Western Central Mexico**, predominantly Lakes Cuitzeo (Israde et al. 2002) and Pátzcuaro (Metcalfe et al. 2002, 2015; Metcalfe, 2006): **Eastern Central Mexico records mainly from the south and central Basin of Mexico** (Bradbury, 1971; Gonzalez & Fuenteo, 1980; Heine, 1984; Bradbury, 1989; White, 1986; Lozano 1986; Lozano et al. 1993; Lozano & Ortega, 1994; Lozano, 1996; Bradbury, 1997, 1998; Caballero, 1997; Caballero & Ortega, 1998; Ortega & Newton, 1998; Lozano & Ortega, 1998; Caballero et al. 1999; Ortega, 2000; Gonzalez et al. 2001; Sedov et al. 2001; Nordt et al. 2002; Vázquez & Heine, 2004; Solleríro et al. 2006; Marcías, 2007; Lamb et al. 2009; Roy et al. 2009; Caballero et al. 2010; Sedov et al. 2010; Vázquez & Heine, 2011; In Ehlers et al. 2011; Roy et al. 2012; Cantarero, 2013; Lozano et al. 2015; Torres-Rodríguez et al. 2015; Siebe et al. 2017). **General trends across Central Mexico** (Metcalfe et al. 2002, 2015; Metcalfe, 2006). **Pre-57,000 ca. BP Lake Chalco** (Lozano et al. 2015; Torres-Rodríguez et al. 2015); **Southern Mexico, Yucatán** (Metcalfe et al. 2002, 2015; Metcalfe, 2006). Numbers at the top of columns correspond to the key numbers below. SL: sea level, H: Hueyatenco glaciation. M: Milpulco glaciation, N1: Nexcoalango glaciation.

Figure 2.8 key

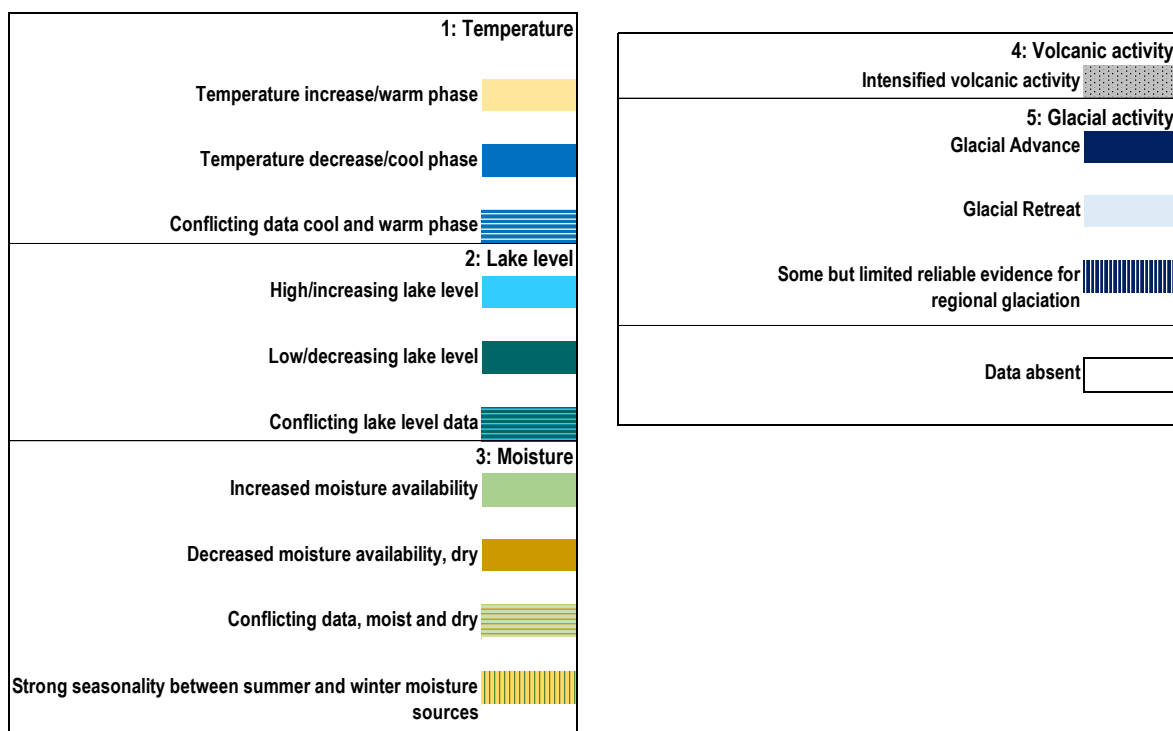


Figure 2.8: Summary of Mexico's recorded Quaternary Environmental History: present day to 29,000 cal. BP. * YD: Younger Dryas, BA: Bølling Allerød, H2: Hienrich 2 event, H: Hueyatlaco glaciation, M: Milpulco glaciation. Numbers 1 – 5 correspond to the Figure key

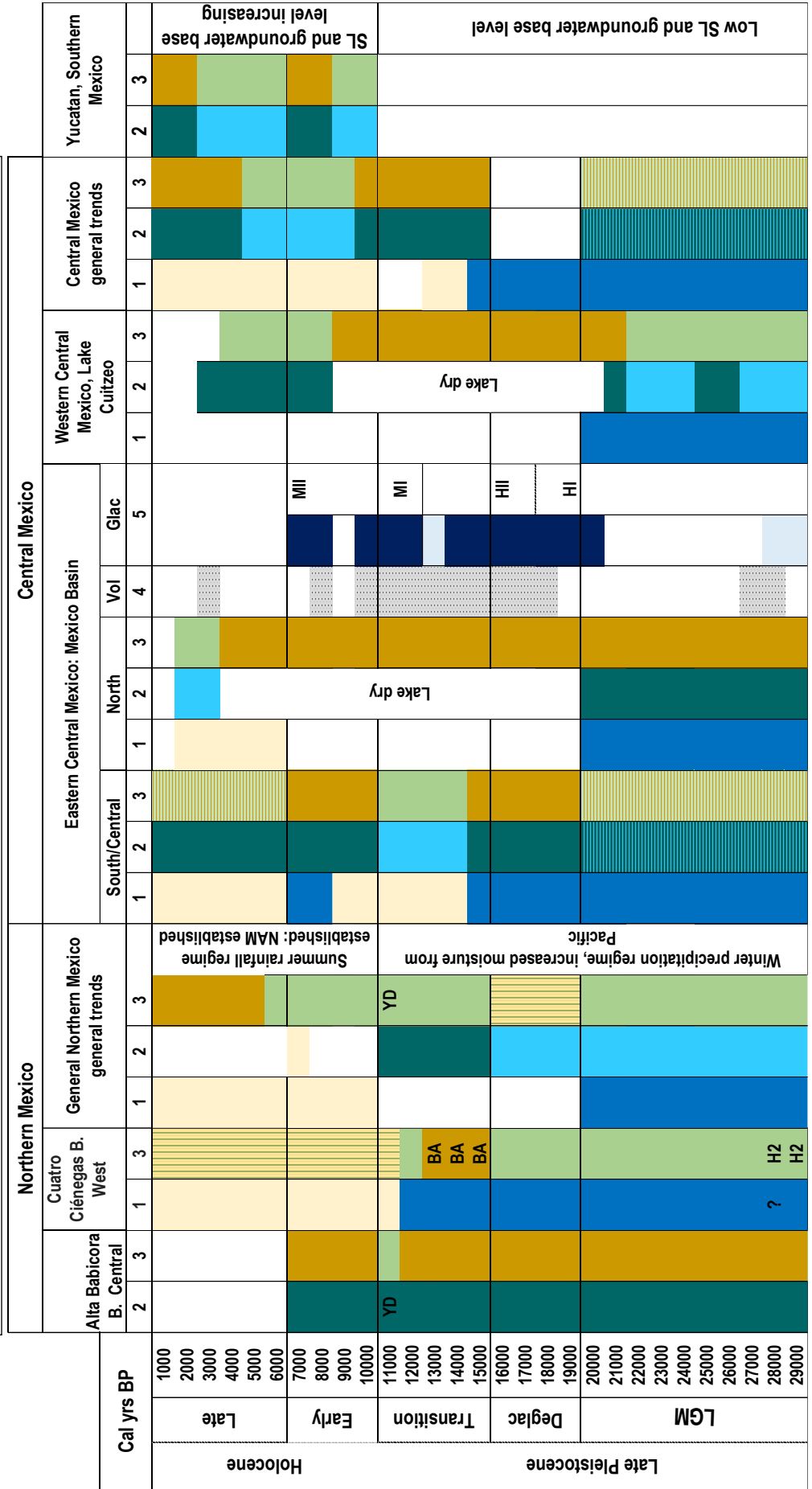
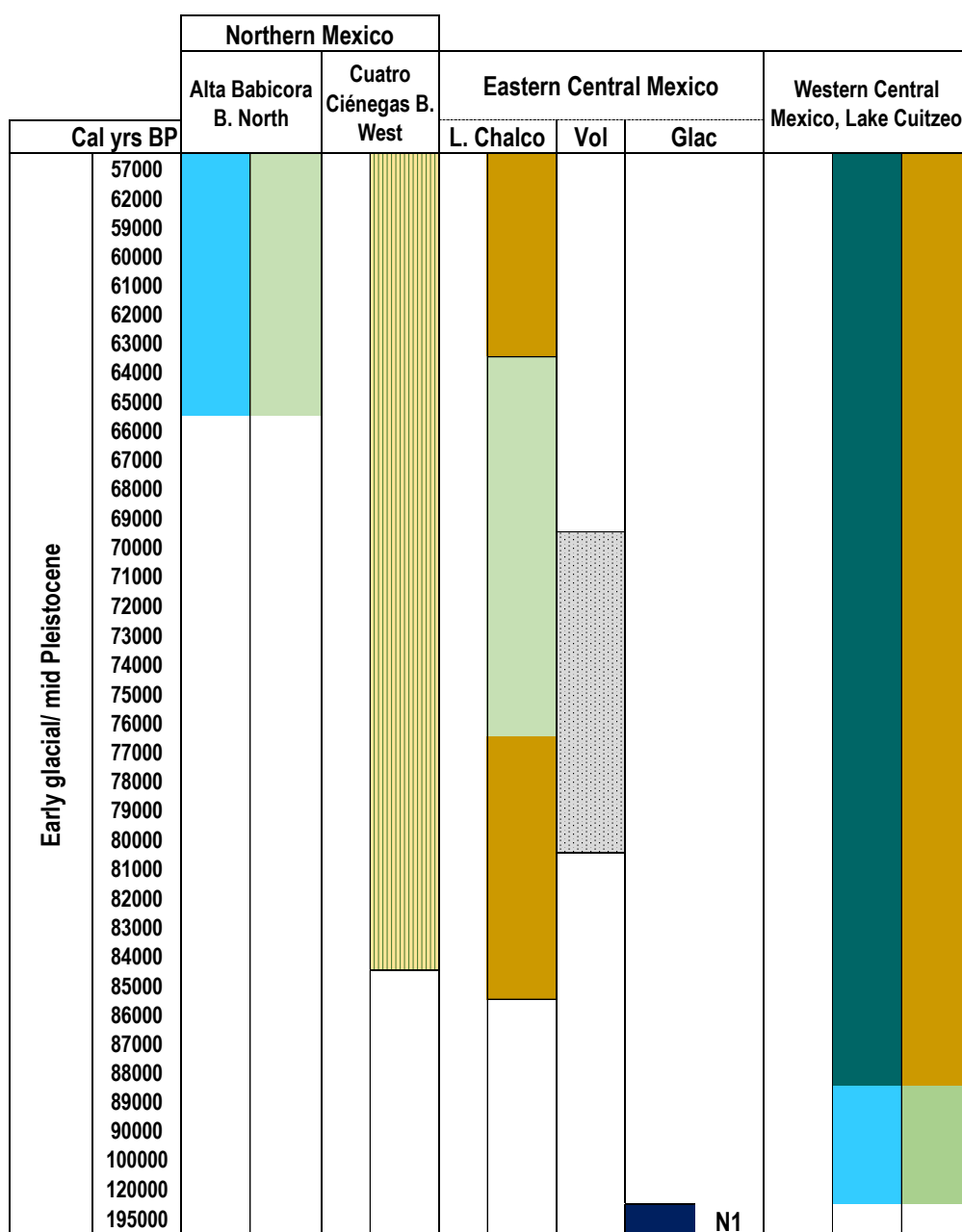


Figure 2.8 continued: Summary of Mexico's recorded Quaternary Environmental History: 57,000 – 195,000 cal. BP. N1: Nexcoalango glaciation



The variability found in records of effective moisture from across Central Mexico during the LGM appears to be related to the altitudinal difference of the depositing basins and the elevation and aspect of the volcanic topography surrounding the basins. All these factors impact moisture input into and out of sedimentary basins along the Trans Mexican Volcanic Belt which makes records particularly difficult to reconcile with each other and may suggest that there are marked differences between moisture inputs to sites (Caballero et al. 2010). The cooler LGM temperatures lasted until ca.15,000 cal. BP corresponding to the regional LGM (ca. 20,200 and 17,500 cal. BP) (Section 2.7; Figs 2.6 & 2.8). The regional deglaciation occurred around ca. 15 – 14,000 cal. BP and lasted until

ca. 12,500 cal. BP, by which time temperatures had increased by 2°C with vegetation changes reflecting the thermal increase (Fig 2.8) (Caballero et al. 2010).

The late-glacial was dry with the terminal Pleistocene excessively so (Metcalfe, 2006) and lake levels were low regionally (Caballero et al. 2010). The Younger Dryas was regionally dry except for Lake Pátzcuaro (Metcalfe et al. 2015) and this continued until ca. 9000 cal. BP, when lake levels started to increase (Fig 2.8) (Metcalfe et al. 2015). The climate was warmer and wetter during the early Holocene, although the Basin of Mexico was dry (see Section 2.8 and Figs 2.6 & 2.8). The NAM is thought to have peaked at 6000 cal. BP allowing wetter conditions to set in across Mexico (Metcalfe et al. 2015), although the Basin of Mexico appears dry, except in the north (Fig 2.8, see Section 2.8). Around 4000 cal. BP most sites along the Trans Mexican Volcanic Belt were dry as the monsoon strength decreased, Northern Hemisphere insolation decreased, and the ITCZ moved south (Fig 2.8) (Metcalfe et al. 2015).

2.6.3: Southern Mexico

There are comparably few records from southern Mexico mainly because of the impact of low glacial sea levels had on the regional water table during the last glacial, particularly during the LGM and the Younger Dryas (Metcalfe et al. 2000, 2015). Lake levels increased after 10,178 cal. BP (9000 ka bp) and again between 7888 and 3188 cal. BP (7000 – 3000 ka bp) possibly with a dry event between 6852 – 5639 cal. BP (6000 – 5000 ka bp) (Metcalfe et al. 2000). During the late Holocene, strong moisture fluctuations occurred with the driest period between 1500 and 900 ka bp, which correlates with the Mayan collapse (Metcalfe et al. 2000).

2.7: Summary

Reviews of Late-Pleistocene and Holocene climate-related data from across Mexico (Metcalfe et al. 2000; Metcalfe, 2006; Metcalfe et al. 2015) (Figs 2.6 & 2.8) indicate that there has been significant climate change during the Late Quaternary, but possibly less than in other parts of the Northern hemisphere tropics and sub-tropics (Street-Perrott & Perrott, 1993; Metcalfe et al. 2000). Early glacial and mid-Pleistocene conditions in Northern Mexico were strikingly different from today's conditions. Extensive forests, lakes and wetlands were present, some of which remained up until the early to mid-Holocene (Metcalfe, 2006). Increased moisture availability is related to the breakdown of the summer rainfall regime and increased winter precipitation sourced from the Pacific and delivered further south by southerly displaced westerlies and the jet stream. Western Central Mexico appears to follow the same moisture regime as northern Mexico (Fig 2.8). The Basin of Mexico (Central Eastern Mexico) follows the opposite trend, although the northern Basin of Mexico displays increased moisture availability. Holocene

records from southern Mexico suggest that Central Mexico may be climatically in phase with each with the Southern regions (see Fig 2.8).

Late Glacial and Early Holocene conditions in central and northern Mexico were dominated by the dynamics of the Laurentide ice sheet, and the Late Pleistocene saw the reorganisation of atmospheric circulation patterns which altered seasonality and precipitation regimes (Metcalf, 2006; Metcalf et al. 2015). Around the time of the Younger Dryas conditions across Mexico were colder and wetter in the north, drier in the south, and more variable centrally (Metcalf et al. 2015). During the transition from the Pleistocene into Holocene wetter conditions established in southern Mexico and migrated north as the NAM became more dominant (Metcalf et al. 2015) as deglaciation progressed. The Holocene shows insolation forcing of the NAM and the ITCZ with the monsoonal summer dominated precipitation regime reaching its peak and geographical extent around 6000 cal. BP (Metcalf et al. 2015). Around 4000 cal. BP there is an apparent climatological change in Northern Hemisphere summer when autumn insolation declined and the ITCZ moved south. At that time a bimodal precipitation pattern established between northern and southern Mexico with a summer rainfall regime continuing in the south and a winter regime in the north (Metcalf et al. 2015; see Fig 2.8). The bimodal pattern is thought to be related to the increasing influence of millennial climate forcing mechanisms like ENSO/PDO and AMO/NAO (Metcalf et al. 2015) with the Central Trans Mexican Volcanic Belt acting as a transition between the north and south and thus being subject to more significant variability.

2.8: Gaps and Questions about Central Mexican Quaternary Environments

Below open questions and gaps related to current research, and general problems associated with Central Mexican Quaternary records are considered.

2.8.1: Problems:

- LGM records from Central Mexico, particularly the Basin of Mexico, are complex and challenging to synthesise (Metcalf et al. 2000; Caballero et al. 2002; Metcalf, 2006; Metcalf et al. 2015) and this is evident in Figures 2.6 & 2.8.
- Hiatuses caused by volcanic and climatic episodes (Figs 2.6 & 2.8) (Bradbury, 1989; Caballero, 1997; Caballero & Ortega, 1998; Lonzano & Ortega, 1998; Brown; Lamb et al. 2009; et al. 2012; Lozano et al. 2015; Torres-Rodríguez et al. 2015), human influence and modification to the Late Pleistocene and Holocene stratigraphic sequence (Metcalf et al. 2015), a scarcity of datable organic material (Metcalf et

al. 2000; Metcalfe, 2006; Lamb et al. 2009; Metcalfe et al. 2015) coupled with old carbon in-fluxing into the system make finding a continuous sequence, that has a detailed chronological framework difficult (see Caballero et al. 1999; Metcalfe et al. 2000; Metcalfe, 2006).

- There are inconsistencies with terminology use and chronologies, i.e. referring to a period as the LGM or early/late-glacial does not represent a fixed point in time, and the definition of these terms probably varies from author to author and complicates comparisons between sites locally, regionally and globally.
- Most research agrees that reconstructing temperature is relatively straightforward but effective moisture/precipitation records are complex and highly variable between sites, especially along the Trans Mexican Volcanic Belt (Caballero et al. 2010).
- There is a consensus in the current research that more work needs to be carried out in areas that remain largely unstudied and unknown (e.g. areas between central and northern Mexico (see Fig 2.7)). Additional research is also required from heavily researched regions, but different field sites need to be found away from the traditional lake coring sites to extend the geographic distribution and coverage of data sets from region to region.

2.8.2: Gaps and open questions:

- No Central Mexican records are available for the early to mid-Pleistocene, and there are very few that cover the mid into the late Pleistocene.
- Very little information exists detailing the extent and timing of pre-Wisconsin glaciations (Vázquez-Selem & Heine, 2004, 2011).
- The nature of change from the last glacial into the Holocene interglacial and the impact of the Younger Dryas had in Central Mexico (if any) is not well understood. Questions remain about the lack of evidence to suggest that there were glacial advances across the highlands of Central Mexico during the Younger Dryas cold stage (Vázquez-Selem & Heine, 2004, 2011). It has been suggested that Youngers Dryas was too cold and dry for a glaciation to occur (Vázquez-Selem & Heine, 2004), or that the interval was warm because glacial water was being diverted away from the Mississippi River and the Gulf of Mexico (Nordt et al. 2002), and hence, the Gulf of Mexico didn't cool significantly.
- Its unclear if a winter dominated precipitation regime, when the westerlies were displaced further south into Mexico due to the expansion of the Laurentide Ice sheet (e.g. LGM and periods during the early

glacial, Fig 2.8), drove higher lake levels, or if there were additional factors forcing this change (Metcalf, 2006). It is also unclear how far south the precipitation moved into central and southern Mexico (Metcalf et al. 2015).

- Because records coming from Mexico are, for the most part, low resolution (mainly because cored lacustrine sediments lack varves; Metcalf, 2006; Metcalf et al. 2010), they fail to register millennial and seasonal scale changes in effective moisture. Subsequently, understanding the impact of ENSO/PDO and AMO/NAO in the past is difficult, which makes modelling future responses to moisture change more so. What is needed are chronologically constrained, high-resolution records that can be compared to oceanic records (Metcalf et al. 2015). Because of this, the balance between winter and summer precipitation is hard to understand presently.

2.9: Further justification of research aims and objectives

The Quaternary history of northern Central eastern Mexico, an area that lies between Central Mexico and the northern deserts, presently remains ambiguous, possibly because of the problematic and sometimes remote terrain, and its position at the semi-arid end of the north-south climatic gradient (see Fig 1.3). The arid climate and moisture deficit mean that few to none of the Pleistocene lake systems that are thought to have occupied the northern basins are present today. Globally, research that has looked at the timing and nature of Quaternary environmental change across dryland areas has been and still is challenging (Yang et al. 2011). Difficulties include a scarcity of high-resolution environmental records, the poor preservation of organic material at open-air sites because of low primary productivity, and a predominance of oxygen-rich conditions in the absence of long-lasting anoxic lakes and swamps (Yang et al. 2011). There are also problems with separating regional from local events, climatic forcing with other causes, and for some palaeoenvironments, there is no modern analogue (Metcalf, 2006; Metcalf et al. 2015). Collectively, these issues mean that the dating and interpretation of proxy data from areas such as these are precarious, and environmental reconstructions often have low temporal resolution giving only site-specific information (Yang et al. 2011). For these reasons the temperate and sub-tropical basins of Central Mexico (e.g. Basin of Mexico, the Lerma Basin, and Lake Pátzcuaro, Michoacán (Fig 2.2b) have been preferentially favoured over dry basins because of their potential to produce long, continuous records of environmental change from lake core sediments, persevered by long-lived anoxic conditions.

Despite the above, contemporary research in arid regions is evolving. Arid geomorphology that focuses on forms and processes like weathering, fluvial, lacustrine and aeolian systems is now being developed to look at the relationships that exist between these sub-components, and arid geomorphological systems (Tooth, 2009). Quaternary research in arid regions has been advanced by the realisation that these areas can make significant contributions to multi-disciplinary research themes including ecology, soil science, sedimentology and environmental geochemistry (Unkel et al. 2007; Oguchi et al. 2008; Nanson et al., 2008; Waters 2008; Tooth, 2009; Drake et al. 2011; Stojanowski et al. 2011; Yang et al. 2011).

The location of the sediments researched and discussed here, within Central eastern Mexico, places the study area within a climatological, geographical and geological boundary between northern and southern Mexico (Fig 2.2). The assumption is that sedimentation processes within the Tequixquiac Basin (Fig 2.2b) during the Quaternary will have been acutely sensitive to climate fluctuations. The aim is to construct a palaeoenvironmental record of these changes utilising the Quaternary sedimentary sequence in the Tequixquiac Basin to generate a new environmental record from Central Mexico. While this research is not proposing to address all the problems associated with Quaternary environmental research in Mexico, or to answer all or any of the open questions that exist after carers have been spent trying to answer them, it has the potential to assist by adding a new record of Quaternary environmental change from a study site in north-eastern Central Mexico from a region that is presently poorly understood.

2.10: Conclusion

In this chapter, the theoretical background of the research presented in this thesis has been set out. Problems exist with the understanding of several issues, especially in those records that span the last 50,000 years of palaeoenvironmental history of Central Mexico. There are problems with reconstructing effective moisture availability, and its distribution across Mexico during this period, environmental conditions remain unclear during the LGM, study sites are clustered with limited geographical distribution, and records can disagree, even from the same sites. Additionally, there is a deficit of data that explores environmental conditions throughout the early to mid-Pleistocene across Mexico. Consequently, the rest of the thesis is based on Quaternary sediments from the Tequixquiac Basin and the reconstruction of Quaternary Palaeoenvironments from this site in the northern Basin of Mexico. The aim is to produce a new data set, from a previously unstudied region of Central-eastern Mexico that has the potential extend what is currently understood for Mexico's Quaternary history. Chapter three describes the studied area.

Chapter Three: study area

3.1: Introduction

Very little information exists to define the physiographic characteristics of the study area situated between the Basin of Mexico (South) and the Mezquital Valley (North, Hidalgo) (Fig 3.1). Although the Tequixquiac Basin forms part of the State of Mexico (see Fig 1.1), it is hydrologically independent of the Basin of Mexico (Figs 1.1 & 3.1). Other than regional, predominantly pre-Quaternary geological maps (Segerstrom, 1952, 1956; Mooser, 1975), the Tequixquiac Basin is poorly characterised regarding its Quaternary geological, sedimentological, geomorphological, hydrological and structural features and its climate. This chapter describes the important physiographic features of the study area and Mexico.

3.2: Location

The town of Tequixquiac (19°54'29.14N - 99°08'44.64W) (Fig 3.1) lies within the northern hemisphere sub-tropics situated in Central-eastern Mexico, within the State of Mexico, (Fig 1.1). Tequixquiac town sits at the edge of a large depression known in this study as the Tequixquiac Basin (Fig 3.1). Within the Tequixquiac Basin, which lies between the Zumpango region of the Basin of Mexico (south, Mexico State) and the Mezquital Valley (north, Hidalgo region) (Fig 3.1), the towns of Hueyoptla and Tlapanaloya lie to the east, and Apaxco de Ocampo is to the northeast (Figs 3.1).

3.3: The Tequixquiac Basin

The Tequixquiac Basin lies at the semi-arid end of the climatic gradient that runs from the north to south in the Basin of Mexico (see Figs 1.3), although there is a degree of local variability between cool/warm and humid/dry conditions mainly related to altitude. There is a wet season between June and October and average annual temperatures are between 17 – 18 °C (Cervantes-Mendel & Armienta, 2004; Jiménez & Asano, 2008). Precipitation is around 400 – 536 mm in the lower catchment (Cervantes-Mendel & Armienta, 2004; Jiménez & Asano, 2008; Parsons 2008), 750 mm in the upper catchment (Cervantes-Mendel & Armienta, 2004) and evapotranspiration can be as much as 1750 mm yearly (based on Jiménez & Asano's (2008) study of the Mezquital Valley).



Figure 3.1: Google image of the study area, The Tequixquiac Basin, the dashed blue line indicates the limits of the basin

Rainfall is predominantly sourced from the Gulf of Mexico, but its delivery to the study area is restricted by regional (e.g. the Sierra Madre Oriental, Fig 3.2) and local (e.g. Sierra de Pachuca, Fig 3.2) mountains and hills (Segerstrom, 1962).

3.4: Topography

The topography of the study area corresponds to the physiographic province of the Trans Mexican Volcanic Belt where broad flat-floored valleys, between 1,600 – 2,400 m a.s.l. dominate (Segerstrom, 1962) and the Sierra Madre Oriental physiography in the far north (Segerstrom, 1962, Fig 3.3). The high basins of the Trans Mexican Volcanic Belt are commonly separated by hills and mountain ranges that can reach above 3,000 m a.s.l. Within the region of the study area, there are three major mountain ranges, the Sierra Nevada volcanic range to the southeast, the Sierra de Pachuca volcanic range to the northwest, and the Sierra de Las Cruces to the southwest (Fig 3.2).

3.5: Vegetation

The vegetation varies with altitude, climate and slope exposure. Where the average annual precipitation values are above 700 mm natural forest grows on north and south-facing slopes, usually at elevation. Precipitation values are between 500 – 700 mm restrict forest growth to north-facing slopes (Segerstrom, 1962). Below 500 mm, natural forest growth only occurs along streams and rivers (Segerstrom, 1962). On low slopes, and within uncultivated areas of the valley floor where the average annual rainfall is deficient (<400 mm) abundant desert flora dominate (Segerstrom, 1962). Native vegetation has been heavily disrupted by agricultural practice that was initially dry but has now become irrigation fed, with most of the water coming from the Agua Negra and the Rio Salado (see below).

3.6: Drainage

The drainage area of the Tequixquiac Basin is around 294 km², with relief reaching between 2350 – 3168 m.a.s.l. sloping towards the basin floor, at its lowest, 2197 m.a.s.l. (Fig 1.1). The catchment mainly has a dendritic drainage pattern and low drainage density (less than 2 km of stream length within a 2 km² portion of the 294 km² area of the drainage basin) (Topographic (1: 50 000) map of Zumpango De Ocampo (E14A19 INEGI)) (Fig). The basin is hydrologically open and drained by the Rio Salado River to the northeast (Fig 1.2). Further north, the Salado River merges with the Tula River (Jiménez & Chávaz, 2004) which later merges with the San Juan and Hondo (Jiménez & Asano, 2008). The Tequixquiac Basin forms part the Basin of Mexico 's extensive drainage

system via a 30.5 km tunnel and canal system, the Gran Canal del Desagüe along which the Agua Negra flows, that drains wastewater from the Basin of Mexico (Fig 1.2) along Barranca Acatlan (Fig 1.3 & Chapter 6).

3.6.1: Barranca and catchment draining

Small barrancas (gullies), between 2 – 6 km long, drain the upper and lower catchment (INEGI, 1997) (see Chapter 6). Morphologically barrancas have flat-bottoms and steep, near-vertical walls or cut banks and are essentially geo-fluvial/alluvial features that form in older unconsolidated sediments (see Chapter 6 and Heine & Schönhals, 1973; Borejsza & Frederick, 2010). Lateral confinement means vertical downcutting and backfilling are the primary responses to changes in discharge volumes and sediment load (Schumm, 1977 & 1999; Elliott et al. 1999; Waters & Haynes, 2001; Borejsza & Frederick, 2010). Barrancas are commonplace in arid and semi-arid environments where streams are ephemeral and fluvial systems alternate between two disequilibrium modes: stream channel erosion and incision (entrenchment) and infilling and back-filling (aggradation) (Bull, 1997). A knickpoint forms at some point along the shallow channel drainage pathway on a sloped surface. With repeated intermittent run-off or through-flow, head-cutting erosion occurs, causing the head of the barranca to migrate upslope which, through time and repetition, creates the barranca. With each rainfall and storm event runoff, erosion and the transport of materials expand the barranca in length and sometimes depth (Schumm, 1977 & 1999). Aggradation and erosion often occur together when the supply of sediment exceeds the capacity and availability of water to remove it from the barranca. In the Tequixquiac Basin barrancas have formed because of the large volume of underlying, unconsolidated easily erodible Quaternary clastic material (Borejsza & Frederick, 2010) and the positive topography created by the southern hydrological divide (see Chapter 8, Figs 8.14 – 8.16).

3.6.2: Natural springs

Today several active springs drain into the Tequixquiac Basin (see Appendix 10). Spring lines tend to develop where groundwater held in unconfined or artesian aquifers finds a route to the surface via, for example, fracture and fault systems. Springs can also be a product of perched aquifers where an impervious hydrostratigraphic unit (e.g. clay, basalt or granite) can hold infiltrated surface water and throughflow at elevation. The impermeable hydro-stratigraphic unit prevents groundwater from moving vertically downwards to join the main aquifer below the water table. Deep stream and river incision and barranca formation can expose a perched aquifer giving the stored water an exit at a perched point which appears to be the case in the study area.

3.6.3: Artificial drainage

The Rio Salado, Nochistongo and Tula Rivers today are almost exclusively carrying wastewater away from Mexico City (Jiménez & Asano, 2008). In the Tequixquiac Basin wastewater arrives through the Gran Canal de Desagüe which is drained by the Agua Negra River through Barranca Acatlan into the Rio Salado River (Fig 1.2). This water is then channelled and used for irrigation practices. Because of the wastewater drainage system and usage, the BGS (British Geological Survey, 1998) and The National Water Commission (1998) conducted a study in the Tula Valley North of the Tequixquiac Basin (Fig 1.2). They found that estimated aquifer recharge for one irrigation district in the Tula region was 25m³/s, 13 times the natural recharge rate (Jiménez & Chávez, 2004). The additional groundwater was found to have come from wastewater infiltrating down into the groundwater system recharging the aquifer with contaminated water pumped from the Basin of Mexico.

3.7: Geological setting

Geologically Mexico is composed of several crustal blocks that reached their current position after the Carboniferous (Dickinson & Lawton, 2009). During the Cretaceous (145 - 65 Ma) marine sediments (Fig 3.3) were deposited in epicontinental seas that centrally split North America and covered most of Central and Eastern Mexico. These deposits today form the elevated Mexican plateau that sits between different Sierras to the south, east and west (Fig 3.2). The southern end of the plateau is generally above 2000 m.a.s.l and dominated by volcanic deposits (Fig 3.2). Towards the North, there is an erosional trend and relief declines to below 2000 m.a.s.l (Alaniz & Nieto, 2007). During the Eocene (56 – 35 Ma) the Laramide Orogeny caused folding and faulting of the eastern continental shelf creating the Sierra Madre Oriental (SMO) which flanks the eastern side of the Mexican plateau. The orogeny elevated the eastern edge of Mexico, at its highest point, to around 3700 m.a.s.l and established a regional tectonic system of grabens centred in the Basin of Mexico spanning east-west across the country (see Fig 2.2 a) (Favolden, 1989). During the Cenozoic (65 Ma – to the present), due to subduction-related volcanism, two major volcanic arcs formed in Mexico; the NNW trending the Sierra Madre Occidental and the E-W trending Trans Mexican Volcanic Belt (Fig 3.2). The Sierra Madre Occidental occupies the western edge of Mexico today stretching north from the Pacific Coast where it overlaps with the Trans Mexican Volcanic Belt on the same latitude as Mexico City (Ferrari et al. 2000) (see Fig 3.2). The Trans Mexican Volcanic Belt represents the most recent episode of magmatic activity that has been on-going since the Jurassic period related to subduction along the Middle American Trench (Szykaruk et al. 2004; Ferrari et al. 2012; Fig 2.2). The Tequixquiac Basin and southwestern and central Hidalgo regions represent areas of transition between the Trans Mexican Volcanic Belt and the start of surface expressions

of the Cretaceous limestone basement in the north (Fig 3.1). In the Basin of Mexico, because of deformation and subsidence, the limestone basement is approximately 2240m below the present basin floor (Fig 3.) (Fig 8.14).

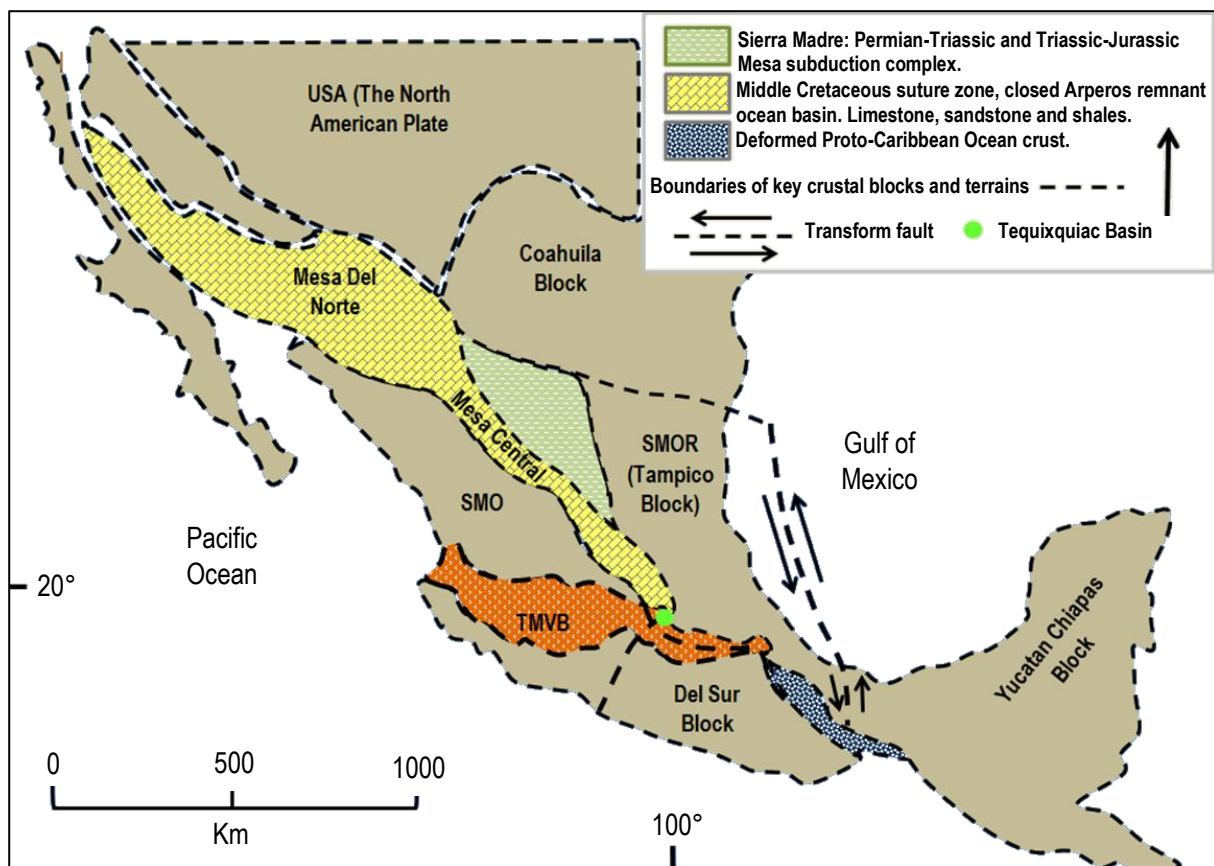


Figure 3.2: Simplified expression of the key crustal blocks and terranes that make-up Mexico (modified from Dickinson & Lawton, 2009). The Trans Mexican Volcanic Belt (TMVB) represents the most recent episode of long running and continual magmatic activity occurring in stages since the Jurassic Period (Ferrari et al. 2012). SMO: Sierra Madre Occidental. SMOR: Sierra Madre Oriental.

3.8: Surface geology in the study area

3.8.1: Introduction

Geological mapping in the south and central Hidalgo region and the northern Basin of Mexico was carried out by Segerstrom, (1952, 1956; 1962) and Mooser, (1975). These works involved extensive geological investigations of predominantly pre-Quaternary deposits and their resulting geological maps (Segerstrom, 1952, 1956; Mooser, 1975). The formations and units summarised below were mapped and defined by Segerstrom, (1952, 1956; 1962) and Mooser, (1975) and for full descriptions, refer to these works.

3.8.2: Cretaceous limestone system

3.8.2.1: El Doctor Limestone

Map Keycode: Ked (Fig 3.3).

Mid Cretaceous light to medium grey, relatively pure, medium to fine-grained marine limestone that has a range of textures. Chert lenses, dolomite, shale, limestone breccias, calcarenite and calcirudite interbeds, and gastropods and less common are corals, oysters and pelecypods also occur. Deposits directly overlie the lower Las Trancas or the Santuario formations. The maximum reported thickness is up to ca. 750 – 900 m. The El Doctor Limestone was deposited in shallow epicontinental marine environments suggested by biostromes, conglomerates, and thick limestone beds. Thin chert interbeds indicate increased water depth. In the study area, deposits occur in the northwest and south-east of Apaxco de Ocampo (Fig 3.3).

3.8.2.2: Cuautla Formation

Map key code: Kc (Fig 3.3).

Mid to the upper Cretaceous thick beds of calcarenite with biostromes and rudists that range in thickness up to 2 m with occasional thin lenses of chert. Some sections have a limestone conglomerate at the base, and volcanic rocks and terrestrial sediments underlie others. Reported maximum thickness is up to ca. 750 m and beds overlie the El Doctor Formation disconformably. The Cuautla Formation was deposited in a relatively narrow marine zone with the deposits lensing out towards the edges. These deposits occur in the study area to the northwest of Apaxco de Ocampo (Fig 3.3).

3.8.3: Cenozoic volcanic system

3.8.3.1: El Morro Formation (fanglomerate)

Map key code: Tem (Fig 3.3).

Eocene-Oligocene indurated limestone conglomerate consisting of various locally available (within 7 km) rock types (fine-grained – boulder size) deposited in alluvial fans. The matrix, if present, is reddish-grey and conglomerate units can be interbedded with siltstone, sandstone, andesite and basalt lava and tuffs depending on the section. Sorting is usually poor, tabular fragments are unoriented, and bedding is poorly defined although very occasionally sandstone lenses can be cross-bedded. The maximum formation thickness has been reported up to 400 m, and the lower contact represents an angular unconformity with the underlying marine beds.

The El Morro Formation is terrestrially formed and related to rapid sediment deposition from steep-sided highlands into the subsiding basins (Simons & Maps, 1956). In the study area, deposits occur in an isolated pocket to the southeast and northwest of Apaxco de Ocampo (Fig 3.3).

3.8.3.2: The Pachuca Group (Segerstrom, 1963) also known as the El Peñon Formation (Ledesma-Goerrror, 1987).

Map key code: Tpv (Fig 3.3).

Eocene-Miocene volcanic rocks that range in composition from basalt to rhyolite deposited by volcanic flows. The Pachuca Group is complexly faulted, indurated, hydrothermally altered, and mineralised. Clastic rocks within this group range from fine-grained tuff to coarse tuff breccias. Conglomerates also occur consisting of eroded volcanic rock, and occasionally lacustrine deposits, including shale. Fossil plants are present in some sections. Maximum thickness reach ca. 2000 m although this varies considerably because of lensing at the edges. Sections that overlie the El Morro Formation do so conformably. Other sections that overlie older rocks have a marked unconformity with the underlying beds. Within the group disconformities are variable and the youngest formation can overlie the oldest or any variation in-between. The Pachuca Group, for the most part, closes the eastern margin of the study area around the Tlapanaloya and Apaxco de Ocampo regions (Fig 3.3).

3.8.3.3: San Juan Group and the Jalpan Andesite

Map key code: Tsj (San Juan Group). Tj (Jalpan andesite) (Fig 3.3)

Middle to late Pliocene basaltic and andesite flows, water-laid tuffs, and a volcanic conglomerate composed of pebbles and cobbles of older andesite and rhyolite up to 400 thick. West and northwest of the Zumpango region the lithofacies change from basalt to hornblende andesite (Jalpan andesite) in the lower part of the section. Eroded cinder cones, basalt bombs, and composite cones are also associated with this group. Across the region volcanic eruptions and products associated with this group were quiet, probably occurring along fissures. The water-laid tuffs suggest lacustrine depositional environments and conglomerates fluvial and alluvial depositional environments. Basalt and andesite flows lie disconformably over older volcanic rocks, the Las Trancas formation, and the El Doctor limestone depending on the site. The San Juan Group occurs in the far south-west of the study area and to the southeast and southwest. The Jalpan Andesite occupies the western edge of the study area and forms the mesas that close the basin to the west (Fig 3.3).

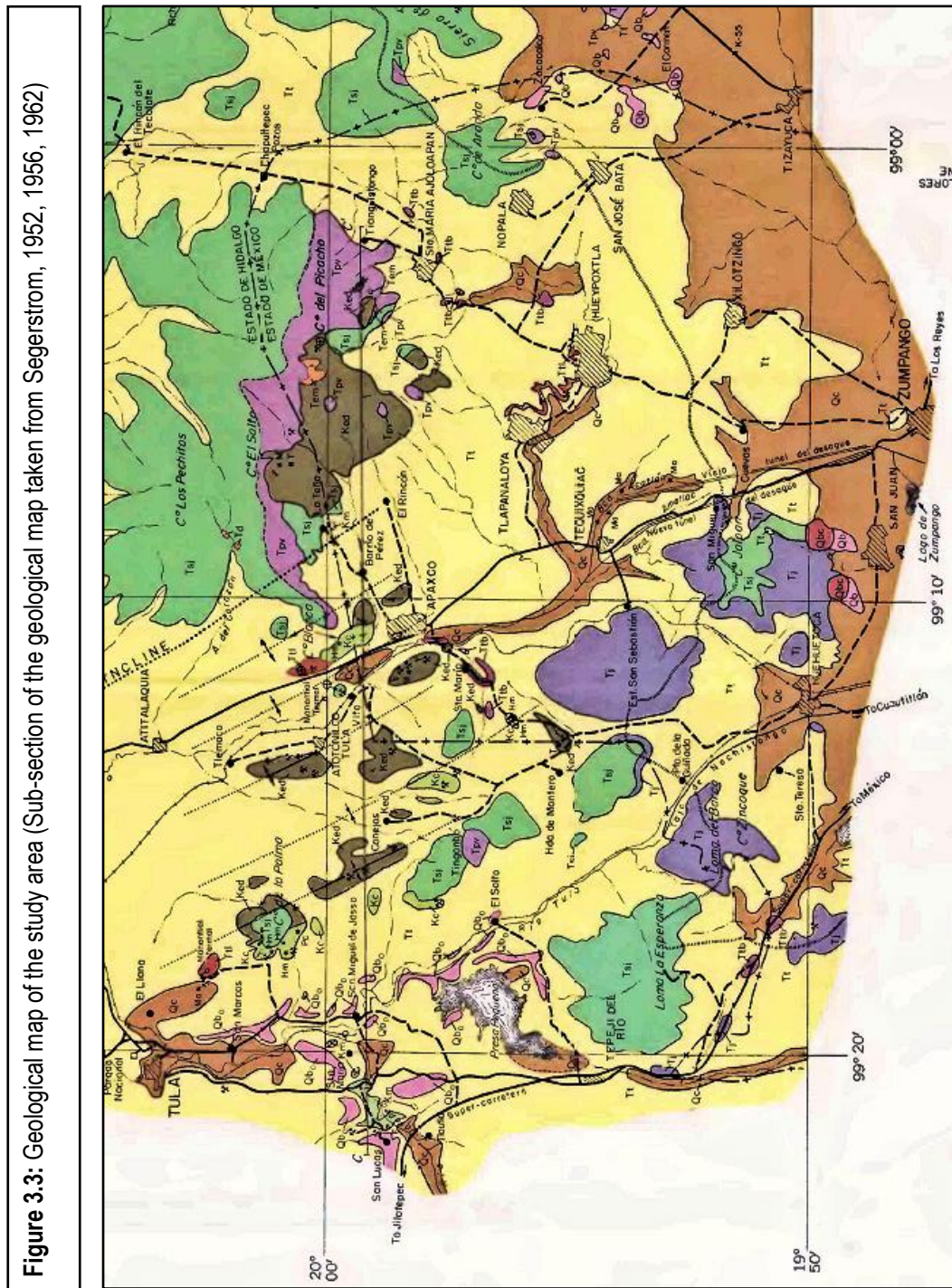
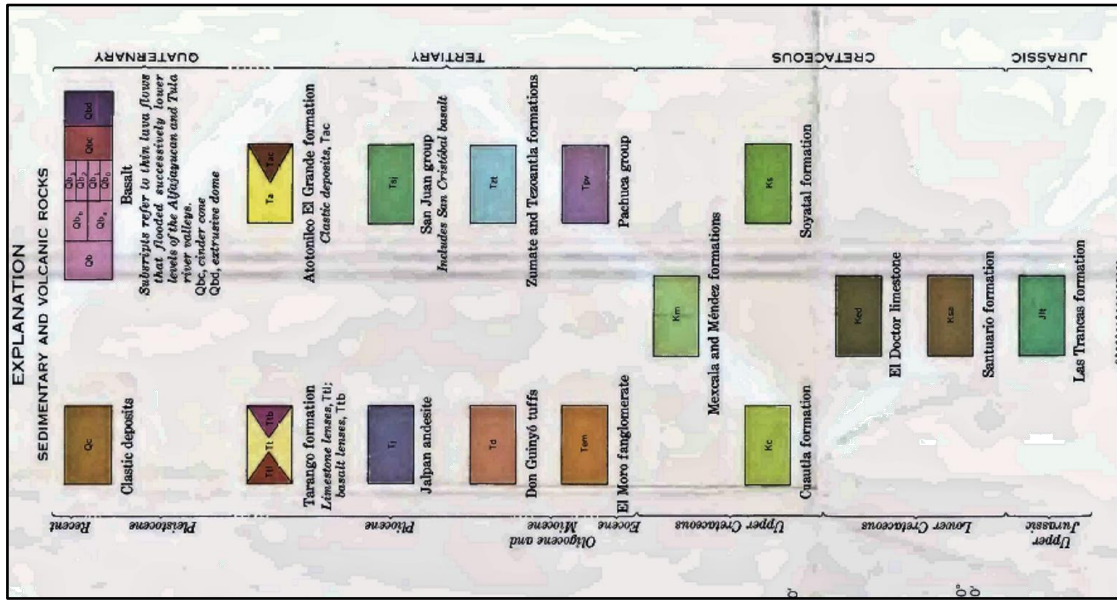


Figure 3.3: Geological map of the study area (Sub-section of the geological map taken from Segerstrom, 1952, 1956, 1962)



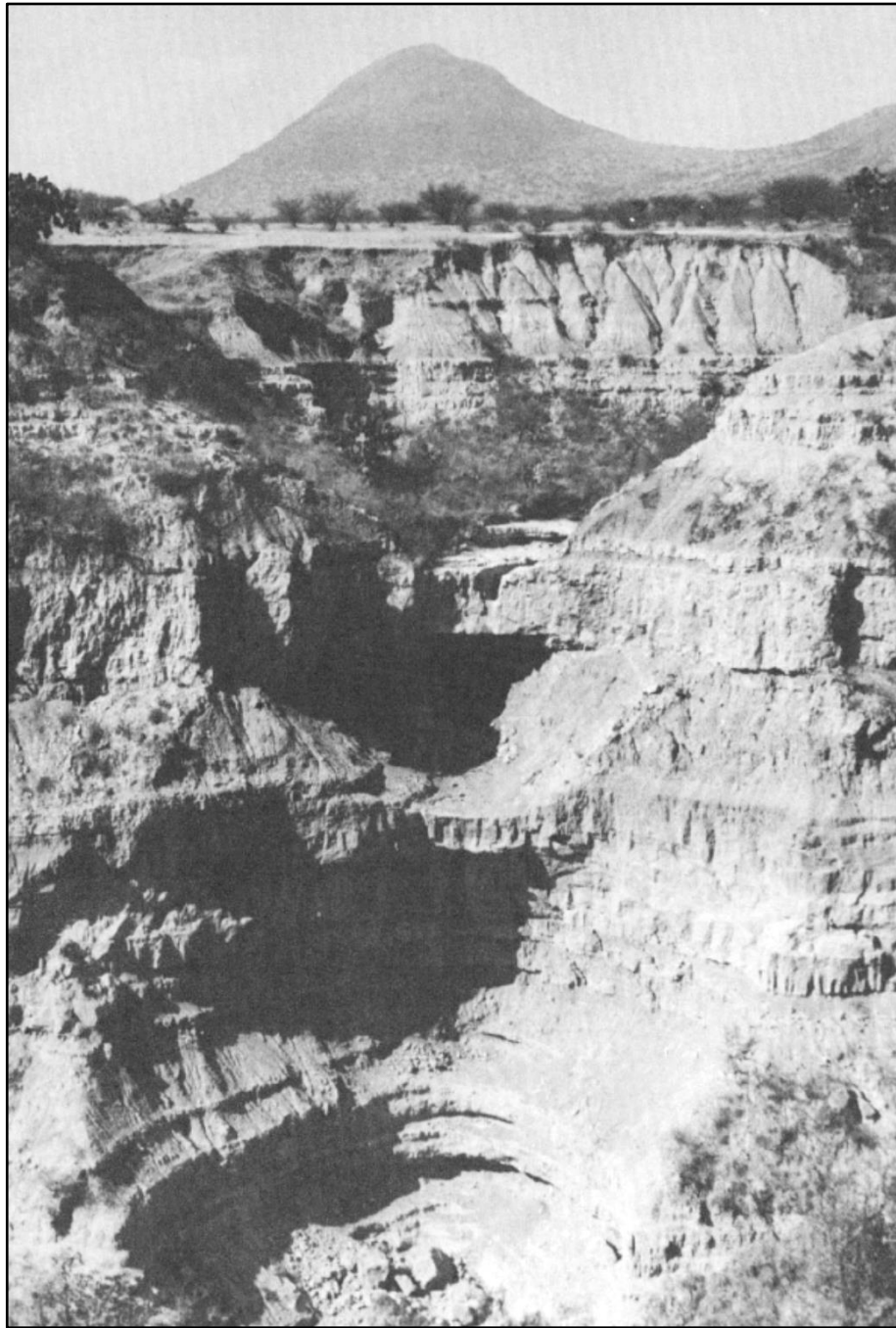


Figure 3.4: The Tarango Formation, over 150 m of exposed lacustrine muds, tephra and limestones that were exposed when the drainage channel was cut through San Mateo Hill (Site TB17) for the Nochistongo in the southwestern study area (see Chapter 6) (image taken from Segerstrom, 1962).

3.8.4: Late Pliocene – early Pleistocene system

3.8.4.1: The Trango and Atotonilco El Grande Formations

Map key code: Tt (Tarango Formation), Ttl (Tarango limestone lenses), and Ttb (Tarango basalt lenses) (Fig 3.3).

Pliocene to early Pleistocene formations thought to have been actively forming around the same time. The Tarango Formation, at type localities, consists of lacustrine deposits, mudflows, lahars and coalescing alluvial fans

and in some sections, limestone lenses up to 12 m thick, but with limited lateral extent (< km²). The Atotonilco El Grande Formation is like the Tarango Formation but has a high proportion of basalt lavas and basalt agglomerate related to eruptive vents in some areas. Formation thicknesses are > 150 m up to 600 m and sediments collected within lacustrine, fluvial, alluvial and lava flow depositional environments. Poorly preserved fossils associated with the Atotonilco El Grande Formation include Mastodon, horse molars and bones that are usually associated with clastic sediments interbedded with basaltic lava flows.

In the north (i.e. Huehuetoca) and northeast, these formations form low passes between the study area and the Pachuca sub-basin respectively. The low pass sits around ca. 2280 m a.s.l., ca 40 m above the lowest lake in the Basin of Mexico (Lake Texcoco). Early drainage works cut a path for the Tajo de Nochistongo (southwest of the study area; Fig 3.3) through the low pass in the north-western Basin of Mexico which exposed ca. 30 – 40 m of the Tarango Formation. The sequence includes water-lain yellow/brown silt, three beds (each ca. 3 m + thick) of sand-sized pumice and beds are horizontal and un-faulted. Between the study area and the Zumpango region of the Basin of Mexico (Fig 3.1), which is a higher pass than Tajo de Nochistongo, two further drainage channels were cut east of Zumpango to Tequixquiac. The western drainage cut is 12 km long and passes through > 150 m of the Tarango Formation, with occasional gravel beds with andesite cobbles.

3.8.5: The Quaternary system

Figure 3.3 only identifies basalt cinder cones from the Quaternary system. All other formations are grouped and only shown if the collective Quaternary system is thicker than 3 m. The Tacubaya, Younger Becerra, Older Becerra and Totolzingo Formations discussed below were identified by Furlong, (1925), Maldonado & Aveleyra, (1949), De Terra, (1949), Hibbard, (1955) and Aveleyra, (1955) (see Chapter 1 & Table 1.1).

3.8.5.1: Basalt

Map code: Volcanic cinder cones (Qdc). Basalt lava flows (Qb) (Fig 3.3).

Pleistocene age un-weathered basaltic cinder cones and basalt lava flows that follow the course of the Tula River. Variations include; black olivine basalt flow with olivine phenocrysts (2 – 3 mm) deposited under fluid flow conditions and cinder cones that are black ash and lapilli weathered to a yellow-brown soil. Close to the vents well cemented red scoriaceous rock is common (tezontle). Flow deposits are up to 10 m thick. Volcanic cinder cones (Qdc) and basalt lava flows (Qb) in various stages of erosion are found in the Zumpango region along the southwest margin of the study area (Fig 3.3).

3.8.5.2: Tacubaya Formation

Map code: Qa (Fig 3.3).

Pleistocene hard brown ochre clay coated in carbonate. Calcrete, or inter-formational caliche layers I and II (Table 1.1), are also common. Calcrete occurrence is related to the limestone bedrock, the height of the water table, erosion and the availability of unconsolidated sediment. The Tacubaya Formation is recorded in Barranca Acatlan, Barranca La Botica and Barranca El Salto (see Chapters 1 & 8)

3.8.5.3: Older Becerra Formation

Map code: Qc (Fig 3.3)

Pleistocene clastic deposits and soils including silt, clay, sand and ash deposited in lake systems, alluvium, and fanglomerates, talus and other locally sourced material deposited over short distances, predominantly from the surrounding sierras. Bentonite topped pink clays that grade into gravelly sands and yellow grey silts. Furlong (1925) previously identified two distinct Pleistocene gravel horizons and faunas (later named the Upper and Lower Breccia Formations). The Older Becerra Formation lies disconformably above the Tacubaya Formation and is recorded in Barranca Acatlan, Barranca La Botica and Barranca El Salto and other Barranca that feed into these (see Chapters 1 & 8).

3.8.5.3: Younger Becerra Formation

Map code: Qa (Fig 3.3)

Later Pleistocene fossil fauna rich gravel units with well-rounded and angular clasts overlain by greyish cross-bedded sand and gravel layers that grade to yellow-cream silts deposited in sediment gravity flow events. Calcrete is also common, and deposits contain Glyptodon, Gopher, Rodent, Wolf, Arctodus (bear), Mammoth, Horse, Camel, Bison, Shrub-Ox fossil bones (Hibbard, 1955). The younger Baccara Formation lies disconformably over the Older Becerra Formation. Positive topography is thought to have been created by up-lift related to fault movement. Changing climatic conditions are thought to have helped to destabilise slopes by reducing vegetation cover with entrainment and resedimenting occurring during short-lived flood events or under more sustained hydrological conditions.

3.8.5.3: Totolzingo Formation

Map code: Qa

Terminal Pleistocene Holocene dark silt and sand with caliche layers.

3.9: Central eastern Mexico fault systems

Recent crustal deformation in Central Mexico is mainly caused by faulting, rifting, transtension and shear (Johnson & Harrison, 1990). There are numerous fault systems concentrated across Central Mexico created by the fragmented nature of Mexico's continental crust (Figs 2.2 & 3.2). Crustal division means that at least three of the southern continental blocks (the Guerrero Block to the east, the central Michoacan-Oaxaca Block and the western Jalisco Block; Fig 2.2) are moving independently of each other and the North America Plate (Johnson & Harrison, 1990). The central and eastern parts of the Trans Mexican Volcanic Belt are predominantly influenced by the E-W trending Chapala - Tula fault system, the NNW – SSE Querétaro – Taxco fault system and to a lesser extent the Tepic - Chapala, and the Chapala – Oaxaca fault systems that run along the western edge of Mexico (Fig 2.2) (Johnson & Harrison, 1990).

3.9.1: Faulting associated with the Basin of Mexico

The Basin of Mexico is an Eocene/Oligocene tectonic depression over 2km deep (Ferrari et al. 2003; Álvarez & Nieto, 2007) which has sixteen NE – SW lateral displacement and/or normal faults that have been active since the Miocene (see Fig 8.14 and Mooser, 1975; Marín-Córdova et al. 1986; De Cserna et al. 1988; Marín-Córdova et al. 2004). Marín-Córdova et al. (2004) propose the existence of a NW 35° – SE distensive fault axis, related to the NW 35° – SE and the NE – SW faults, that joins Popocatepetl Volcano (southeast), the Tequixquiac - Huehuetoca zone (northwest), the lowest portion of the Basin of Mexico including Lake Texcoco and the Peñon de Los Baños zones (see Chapter 8). Faulting is proposed to be caused by deformation forcing blocks to pull apart in NW-SE directions creating new deformation in the Basin of Mexico (Marín-Córdova et al. 2004 (see Chapter 8)). The southern Basin of Mexico is bordered by the Chapala-Tula Fault System (Fig 2.2) and the Taxco-Queretaro Fault system (see Fig 2.2) which is thought to control the monogenetic volcanism of the Sierra Chichinautzin (Garcia-Palomo et al. 2000; Ferrari et al. 2003; Álvarez & Nieto, 2005; Gómez et al. 2007).

3.9.5: Faulting associated with the Mezquital Valley

The Mezquital Valley (Hidalgo, Fig 1.1) lies immediately north of the study area (Fig 1.1) and has been characterised as a Miocene fault-bounded graben/lacustrine basin comprising a single tectonic depression (Campos & Sánchez 2000; Gómez et al. 2007; see Fig 8.14). Within the Mezquital Valley master faults place Cretaceous Limestone against Late Miocene – Early Pliocene alluvial and lake deposits thought to belong to the Tarango Formation (Tt, Fig 3.3 & 3.4) dated to be between 7.1 – 4.6 Ma (Kowallis et al. 1998; Suter et al. 2001).

The Cardonal fault limits the northern end of the Mezquital Valley and cuts rock dated to 4.6 Ma vertically displacing the Tarango Formation sediments by 300m. This implies that the fault system has been inactive since the early Pliocene and two recent earthquakes (magnitude (M_w) 5) indicate the fault is still active (Suter et al. 1991, 1996 & 2001; Quintanar et al. 2004). Towards the southern margin of the Mezquital Valley, there are two E-W trending normal faults moving at a rate of 0.02 mm/yr (Suter et al. 2001).

3.10: Faults influencing the Tequixquiac Basin

From a regional perspective Figure 2.2 shows most major faults systems found across Central Mexico do not have any direct influence on the Tequixquiac Basin other than the Chapala-Tula Fault system. The Chapala-Tula Fault system flanks the Tequixquiac Basin along its western edge (see Figs 2.2) and may have influenced rates of deformation and subsidence in the study area. A northwest-southeast distensive axis linking Popocatepetl Volcano to the Tequixquiac – Huehuetoca zone is currently causing new deformation and subsidence in the region of Tequixquiac and possibly has done for a significant portion of its past. Faulting associated with northern horst of the Cuautitlan graben in the Basin of Mexico may influence the Tequixquiac Basin along its southern margin due to its position immediately north of this end of the graben system in the Basin of Mexico (Fig 8.14). From a local perspective, the North and North-eastern margins of the Tequixquiac Basin are lined by faulted Cretaceous limestone that separates the study area from the Mezquital Valley (Fig 3.3). The Pliocene - Quaternary Mesa Grande lava flow and volcanic cone (Fig 3.3) closes the Tequixquiac Basin to the west and may have been controlled by a fault, fracture and structural weakness along the western side of the Tequixquiac Basin.

3.11: Summary and conclusion

Here the physiography of the study area has been outlined and indicates that the Tequixquiac Basin is a hydrologically independent, temperate semi-arid basin. This chapter has also demonstrated that the study area has a complicated geological history (see Figs 3.3, 8.9, 8.1). Around the Tequixquiac region folding and faulting associated with the Laramide Orogeny and its position at the northern edge of the graben system in the Basin of Mexico (see Chapter 8) has caused Quaternary volcanic and clastic deposits, and Cretaceous limestone to sit adjacent to each other. To the north, northeast and northwest, the Tequixquiac Basin is limited, in parts, by exposures of basement limestone that are lifted in structural blocks limited by faults (Marín-Córdova et al. 2004). Pliocene/Pleistocene basaltic and andesitic lava flows and volcanic cones close the basin to the West. In the northeast, Eocene-Oligocene andesitic and rhyolitic volcanic sierras reach 3168 m.a.s.l and stretch 11km to the east towards the Sierra Madre Oriental. Low hills (c.2300 – 2400 m.a.s.l) limiting the southern Tequixquiac Basin

comprise an early Pliocene volcanic material overlain by Quaternary alluvial deposits (Durazo & Farvolden, 1989, Mooser, 1975). The Tequixquiac Basin, along with the Tula, Nochistongo and the Mezquital basins, are filled with Pliocene (possibly as old as Miocene and as young as Pleistocene) lake clays combined with soils, pumice and tuffs derived from tephra fallout that collectively form the Tarango Formation (Mooser, 1975) (see Figs 3.3, 8.9, 8.1).

Chapter 4 follows and outlines the methods used by this research to achieve the aims and objective discussed in chapter 1.

Chapter four: Methods

4.1: Introduction

The PhD research aims to reconstruct the Mid to Late Quaternary palaeogeographic and palaeoenvironmental history of the Tequixquiac Basin. The field and laboratory methods used to address these research aims are justified and explained below.

4.2: Fieldwork

The field strategy was designed to address the objectives 1 - 4 set out in Chapter 1. Specifically, the mapping and the characterisation of the Quaternary sedimentary succession in the study area (objective 1) and the collection of representative sediment and rock samples (objective 2). A first field season in the Tequixquiac Basin was carried out by the author, Professor Silvia Gonzalez, Professor David Huddart, and Dr Nicholas Felstead in December 2009. A second field season was carried out during 2010 by the author, Professor Silvia Gonzalez, Professor David Huddart and Dr Hannah O'Regan. Subsequent visits to the study site occurred during 2012 and 2013 that enabled follow up fieldwork to be carried out.

4.2.1: Mapping

To satisfy objective 1 (Chapter 1), mapping in the Tequixquiac Basin started with a desk-based study of available publications discussing the geological, sedimentological and structural features and history of the Mexico Basin, the Mezquital Valley (Hidalgo), and the surrounding areas to help understand these features in the study area (Fig 1.1). Previously documented field sites thought to cover the Late Pleistocene to Holocene, (Chapter 1 & 3), were initially targeted. The focus of the second field season was to recognise and map the vertical and lateral extent of the defining sequences of Quaternary sediment in the study area. Geomorphological features in the study were initially located using Google Earth, and a 1: 50 topographic maps (INEGI, E14A19, 1994) which enabled suitable large-scale Quaternary geomorphic features to be located.

4.2.2: Detailed sedimentological investigation

To establish a Pleistocene to Holocene representative sequence of deposition, and a stratigraphic framework for the study area (objective 1, Chapter 1) 58 stratigraphic sections were described and logged at 27 different sites, across a 226.6 km² area with an altitude range between 2100 and 2314 m.a.s.l (meters above sea level) (see Chapter 5). Viable stratigraphic sections were measured in the field using a 30 m tape and drawn to

scale. The criteria used to identify observable erosional, depositional, and syndepositional sedimentological, and biological features, and textures related to clastic, mixed clastic and carbonate, and carbonate depositional systems in the study area are outlined in Tables 4.1, 4.2 & 4.3. By these criteria, recognisable lithological and biological features including; composition, grain size, shape and arrangement, bedding, biological content, and primary and secondary sedimentary structures were described and classified.

| Table 4.1: Hydrodynamic erosional structures. The description, defined by Boggs, 2006; Nichols, 2009 and Miall, 2016, outlines the criteria used for the identification of similar deposits in the study area. | |
|---|---|
| Facies | Description |
| Fluvial channels | Present as channel forms infilled with sediment with grain sizes and bedding structures distinctly different from the incised units they cut. Coarse fills can indicate energy increases. Abandoned channels can be filled with fine sediment and coal under low energy conditions. |
| Low relief erosion surfaces | Encompass entire surfaces |
| Intraformational breccias | Angular clasts larger than 2mm with varying degrees of matrix. Form with minimal transport, or by in-situ fragmentation of the same geological sequence (post-depositional). |

4.2.3: Sediment sampling

Based on preliminary C¹⁴ dates, and geochemical analysis, sediment and rock sampling during the 2010 field season were focused at sites that had indicated viable sediments suitable for carbonate micromorphological analysis, geochemical (¹⁸O/¹³C_{CARBONATE}), ⁸⁷S/⁸⁶Sr_{CARBONATE & TEPHRA}), ICP – OES sediment mineralogy and tephra bulk oxide content and LOI. Samples were collected from sections after cutting the face back at least 10 cm, when possible, to avoid contamination from organic oxidation. Lithified hand specimens were collected using a chisel and hammer at measured depths, and marked with an orientation arrow. Rock sub-samples, collected for analysis, were taken from unweathered surfaces.

4.3: Petrographic analysis of hand specimens and sediment samples

For terrestrial carbonate sediments, the criteria employed by this PhD research for the petrographic identification of carbonate sediment grains (Table 4.4), the classification of terrestrial carbonate deposits (Table 4.5), and for the determination of microfacies (Table 4.6) is outlined below. For carbonate and limestone terminology; spring, lacustrine, palustrine, marsh (paludal), fluvial and water-lain (when there is no discernable origin) carbonates subdivisions are used to describe carbonates deposited in and around these environments. The subdivisions are applied irrespective of the water source temperature, CO₂ carrier and mechanism of precipitation (after Brasier, 2011). The term pedogenic calcrete is used to define the terrestrial pedogenic (soil) build-up of surface or near-surface calcium carbonate. Groundwater calcrete defines the none-pedogenic, groundwater build-up of carbonate (see Alonso-Zarza & Wright, 2010b; Brasier, 2011).

Table 4.2: Hydrodynamic depositional structures. The description, defined by Boggs, 2006; Nichols, 2009 and Miall, 2016, outlines the criteria used for the identification of similar deposits in the study area.

| Mass gravity transport | Facies | | Description |
|------------------------|-------------------------------------|--|---|
| | | Normal grading | |
| | Massive (structureless) beds | | Liquefaction, rapid deposition from suspension or rapid deposition by sediment gravity flow (e.g. flash flooding, gravity flows, fault movement) can create massive deposits. |
| By non-cohesive flow | Laminae (<1cm) | | Short-lived depositional changes create variations in grain size, organic content, mineral composition and microfossil content. Form from suspension sedimentation (low energy, e.g. a deep lake) and via traction transport of sand in water (higher flow velocities, e.g. fluvial). Structures can be destroyed by burrowing and feeding activities. |
| | Crossbedding | Cross-bedded ripples, < 4 – 5 cm | Bedding features that require moderate flow velocities, regardless of water depth, and a hydrodynamically smooth bed to develop. Restricted to sands with grain sizes <0.6mm (coarse), coarser grades create bed roughness and turbulent mixing, which restricts the small scale flow separation needed for ripple formation. |
| | | Cross-bedding dunes, >5 cm | Related to large scale turbulence within the whole flow. Low velocities and weak roller vortices mean sand on the lee slope of the dune is not reworked, deposition occurs building angular based beds into the trough (planar or tubular cross-bedding). Higher flow velocities create stronger roller vortices that scour a pit at the reattachment point. If the roller vortex counter flow is strong enough ripples can form and migrate up the lee slope (trough cross-bedding). |
| | Clast Imbrication | | Traction transport or transport within sediment gravity flows. With traction, platy clast can be stacked up with the flattest surface dipping downstream. Fluvial depositional environments. |

4.4: Framework for the identification of depositional environments

To reconstruct Quaternary palaeogeography and palaeoenvironments for the study area lithofacies were identified (see Chapter 5) and combined with petrographic (Section 4.3), and geochemical data (Section 4.5).

4.4.1: Methodology used to describe the sediments

In the study area, localised depositional environments are characterised based on the presence or absence of the main facies types known to be related to each other, and recognised for a particular depositional environment. The concept here is based on Walker & James, (1992) and Miall, (2016), but generally facies models have been widely used for the classification of lacustrine sediments (Olsen, 1990; Garcés & Aguilera, 1992; Carroll & Bohacs, 1999; Tanner, 2000; Freytet, 2002; Benvenuti, 2003; Anadón et al. 2009; Platt & Wright, 2009; Ghinassi et al. 2015), palustrine deposits (Platt & Wright, 1992; Armenteros et al. 1997; Freytet & Verrecchia, 2002; Gulbranson, 2004; Tófaló & Pazos, 2010; Ghannem et al. 2016), tufa deposits (Glover & Robertson, 2003; Arenas et al. 2007; Garcés et al. 2008; Linares et al. 2009; Guerreiro et al. 2011; Guo & Chefetz, 2012; Norwak & Weiss, 2013; Henchiri, 2014a; Camuera et al. 2015; Pellicer et al. 2016), calcretes (Theriault & Desrochers, 1993; Horbury & Adams, 1996; Dhir et al. 2004; Durand et al. 2007; Khalaf & Gabar, 2008; Adamson et al. 2015; Valero et al. 2015; Abed et al. 2016), paludal deposits (Pedley et al. 2003; Pedley & Hill, 2003; Koşun, 2012; Henchiri, 2014b),

and in fluvial and alluvial depositional settings (Cant & Walker, 1976; Miall, 1980; Singh & Bhardway, 1991; Boyd et al. 2006; Fielding et al. 2009; Dalrymple, 2010; Weissmann et al. 2010; Zhang et al. 2011; Miall, 2016). Aside from the fluvial (see Section 4.4.2) depositional model, the facies models used for the identification of continental carbonates and clastic deposits in the study area are taken from a review and compilation of available research published in 2010. (Carbonates in Continental Settings In developments in sedimentology, Alonso-Zarza, & Tanner. 2010). From these, depositional systems were defined for the study area and combined with the available chronology to reconstruct the depositional environments that were active in the study area during the Quaternary (see Chapters 5 & 6).

4.4.2: Fluvial facies and depositional model

A synthesised version of Miall's fluvial facies model (Miall, 1985; 1996; 1997; 2016) has been used as a framework of reference to identify fluvial successions in the study area (Table 4.8) (e.g. Cant et al. 1976; Singh et al. 1991; Gani & Alam, 2004; Gosh et al. 2014; Rivas et al. 2015; Scherer et al. 2015; Mukhopadhyoy et al. 2016). Miall's facies scheme is combined with Pedley (1990 & 2009), Pedley et al. (2003) and Ford & Pedley, (1996) carbonate fluvial facies model to expand the model to include carbonate sediments for this PhD research. The addition of a carbonate fluvial facies model forms part of the tufa classification system advocated by the Jones and Renaut (2010) review of calcareous spring deposits in continental settings (Section 4.4.5).

| Table 4.3: Syndepositional deformation structures. The description, defined by Boggs, 2006; Nichols, 2009 and Miall, 2016, outlines the criteria used for the identification of similar deposits in the study area. | |
|--|---|
| Facies | Description |
| load casts, mm - cm | Irregular lobes projecting from the base of overlying beds. Form when coarser sediment overlays fine sediment through the sinking of a denser sediment layer into a less dense underlying, fluidised bed. Can occur via gravitational instability. |
| Ball and pillow, cm - m | Hemispherical to kidney-shaped forms of sand encased within a stratigraphically lower sediment layer. Associated with the breakup of semi consolidated sand or lime-mud due to partial liquefaction of the underlying muds. |
| Faults and slumps | Develop on saturated clay deposits, particularly those deposited on a sloping surface. Form through a combination of fluid saturation, low cohesion, overstepping and shocking (e.g. earthquake or fault movement). |
| Growth faults 1 – 50 m | Surfaces within a sedimentary succession along which there has been displacement. They can form through gravitational instabilities. Failure occurs along weak horizons and progrades upwards forming a spoon-shaped fault within the succession. |
| Desiccation cracks, mm - m | Identified by polygonal, vertically tapering cracks that are usually 5 – 7 sided. They are often cast in the lower bounding bed by the overlying bed. They develop through the subareal drying and desiccation of a clay-rich sediment layer. |
| Mud lumps | Balls or lumps of cohesive sediment that are roughly spherical of variable size. They are usually minor, isolated structures made of clay or mud lumps that have been gouged out of the bed surface within a high - energy environment (e.g. shoreline or fluvial channel). |

Table 4.4: Carbonate grain (allogenic) classification. The description, defined by Flügel (2010) and combined with Tucker & Wright, 1990; Nichols, 2009 and Brasier, 2011 outlines the criteria used for the identification of similar deposits in the study area. Also, see Table 4.9.

| Carbonate grains | | |
|--------------------------------------|---|--|
| Micrite < 4µm in diameter. | Microcrystalline calcite (micritic or calc-mud). Micrite can be bioclastic, made up of shell fragments/bioclasts or formed in-situ via physiochemical processes (e.g. supersaturation of Ca) or microbial activity (e.g. photosynthetic processes). Associated with low energy lake, pond and marsh environments. | |
| Peloids <0.02 to 1mm | Small micritic grains, no internal structure. Ellipsoidal, sub-rounded, spherical, ovoid, or irregular in shape. Peloids are polygenetic and form several ways, for example from the shallow burial, compaction and micritization of faecal pellets or from the micritization of abraded grains (e.g., shell fragments and ooids) with the original grain being micritized by endolithic (rock-dwelling) micro-organisms. (Flügel, 2010). | |
| Coated grains | Oncoids <1mm - 5 mm in diameter | Oncoids have a nucleus around which partially overlapping, irregular, non-concentric laminae develop. Laminae can be biochemically (e.g. cyanobacteria, algae or microbes generated in non-skeletal forms (without visible organic microstructures), skeletal (have preserved tubular microstructures) or combined (two or more encrusting organisms) conjoin. Abiologically coated (e.g. micrite) grains have no clear lamination. Spheroidal forms are linked with rivers; oblate spheroidal forms with slow-flowing water and free forms are associated with static water environments. |
| | Ooids <2 mm in diameter | Concentrically laminated spheroids/ovoid grains. Laminae is regular, smooth and, successive forming around a nucleus (e.g., carbonate grain, a sand grain or pollen). Laminated micro-fabrics can be tangential (aragonite grains with their long axis parallel to the ooid laminae), Radial (aragonite needles fanning out from the nucleus) or, random and mixed coatings can occur. |
| | Pisoids <2 mm to >1 cm in diameter | Large subspherical/irregularly shaped grains with a mainly non-biogenic nucleus surrounded by a thick cortex that often has densely spaced laminae showing tangential and radial microfabrics (see above). |
| Lithoclast 0.5 to 2mm | Grains consisting of one or more of the above/below definitions that are cemented together. Void spaces are filled with micrite or spar cement. | |
| Intraclasts (size variable) | Synsedimentary or post-sedimentary carbonate clasts that are reworked partly consolidated sediment or re-worked lithified carbonate material. Mainly form in lake, pond and marsh environments. | |
| Bioclasts (size variable) | Fragmented or complete micro-organisms remains e.g. ostracods and diatoms. | |
| Phytoclast | Carbonate encrusted plant fragments, typically transported plant fragments. | |
| Cyanolithic carbonates | Oblate to sub-spherical stromatolites are composed of cyanobacterial/cement fringes associations. High sphericity is linked to river systems, and oblate forms are linked to sluggish flow (marsh?), freeforms develop in static conditions. Can be grain supported and mixed with smaller intraclasts and micrite. | |

4.4.3: Lacustrine carbonate facies and depositional model

The identification of Lacustrine facies in the study area is based on a carbonate database built from facies information gathered from nearly 250 lakes and lake basins after Gierlowski-Kordesch, (2010), and Pedley's (2009) lacustrine tufa depositional model (Tables 4.10 & 4.11 and Fig 4.2) The description, defined by Flügel (2010) and combined with Tucker & Wright, 1990; Nichols, 2009; Brasier, 2011, classification used in this PhD research. Also, see Table 4.9.

Table 4.5: Carbonate grain classification and definitions. Adapted from Flügel (2010) and combined with Tucker & Wright, 1990; Nichols, 2009; Brasier, 2011 for this study.

| Depositional | | | | Biological | | | Diagenetic | | | |
|---|--------------|-----------------|-------------|--------------------------|------------------------------|-------------------------|--------------------------|---|---|----------------------------------|
| Matrix-supported clay and silt-sized grains | | Grain-supported | | In situ organisms | | | Non-obliterate | | | Obliterate |
| <10% grains | >10% grains | With matrix | No Matrix | Rigid organisms dominant | Encrusting binding organisms | Organisms act to baffle | Main component in cement | Many grain contacts are micro-stylolite | Most grain contacts are micro-stylolite | Crystals >10 µm |
| Calci-mud stone | Wackestone | Pack stone | Grain stone | Frame stone | Bound stone | Baffle stone | Cement stone | Dense Grainstone | Fitted Grainstone | Sparstone |
| | Floatstone | Rudstone | | | | | | | | Crystals <10 µm: Micro-sparstone |
| | Grains > 2mm | | | | | | | | | |

Table 4.6: Visual petrographic characteristics of spring, stream and lacustrine (SSL) carbonates and calcretes used for identification (from Brasier, 2011). Alpha refers to the micromorphological features of calcrete discussed in Section 4.4.8.

| Fabric | Spring, stream, lake (SSL) or calcrete | Description | Diagram |
|---------------------------|--|---|---|
| Nodules | Calcrete Alpha | Spherical to irregular, indurated, mm - cm in size. Abiological |  |
| Laminar crusts | Calcrete Alpha | Laminar crusts found in association with (1), mm – cm in size. Abiological |  |
| Rhizoliths | Calcrete | Organosedimentary root structures |  |
| None-marine stromatolites | SSL | Laminar microbial carbonates. Cyanobacterial in origin |  |
| Peloids | Calcrete Alpha & SSL | Round micrite grains. Can be faecal (biological or abiological) |  |
| Pisoliths | Calcrete Alpha & SSL | Concentrically laminated spheroids > 2mm. Abiological, downslope movement and biological (fungi and lichen) |  |
| Ooids | Calcrete Alpha & SSL | Concentrically laminated spheroids < 2mm |  |
| Coated Macrophyte stems | SSL | Carbonate cast of plant stems (e.g. framestone) |  |

Table 4.7: The defining characteristic of tufa and travertine, from Capezzuoli et al. (2014) (numerical data is taken from Pentecost. 2005; Gandin & Capezzuoli. 2008 and the references within these papers.

| | Travertine | Tufa |
|-------------------------------|--|---|
| Deposition | Mainly abiotic | Mainly biotic |
| HCO ₃ ⁻ | >7 | <6 |
| δ ¹³ C (PDB‰) | -1 to +10 | <0 |
| DIC (mmol/l) | >10 | <8 |
| Water temperature | Thermal, >30°C | Ambient <20°C |
| Minerology | Calcite, aragonite | Calcite |
| Depositional rate | High, cm/year | Lower, mm |
| Fabric | Bedded to laminated | Micritic to micro sparitic |
| Primary porosity | Low (<30%) | High (>40%) |
| Biological content | Low (bacterial) | High (micro to macrophytes) |
| Depositional morphologies | Multi-symmetrical bodies (e.g. mounds etc) | Axial-symmetrical bodies (cascade dams etc) |
| Distinctive morphologies | Coated bubbles and shrubs | Phytoherms |
| Hydrological setting | Generally permanent flow | Variable, rainfall-dependent |
| Climatic control | Less dependent | Strictly dependent |
| Tectonic relationship | Always present | Often absent |

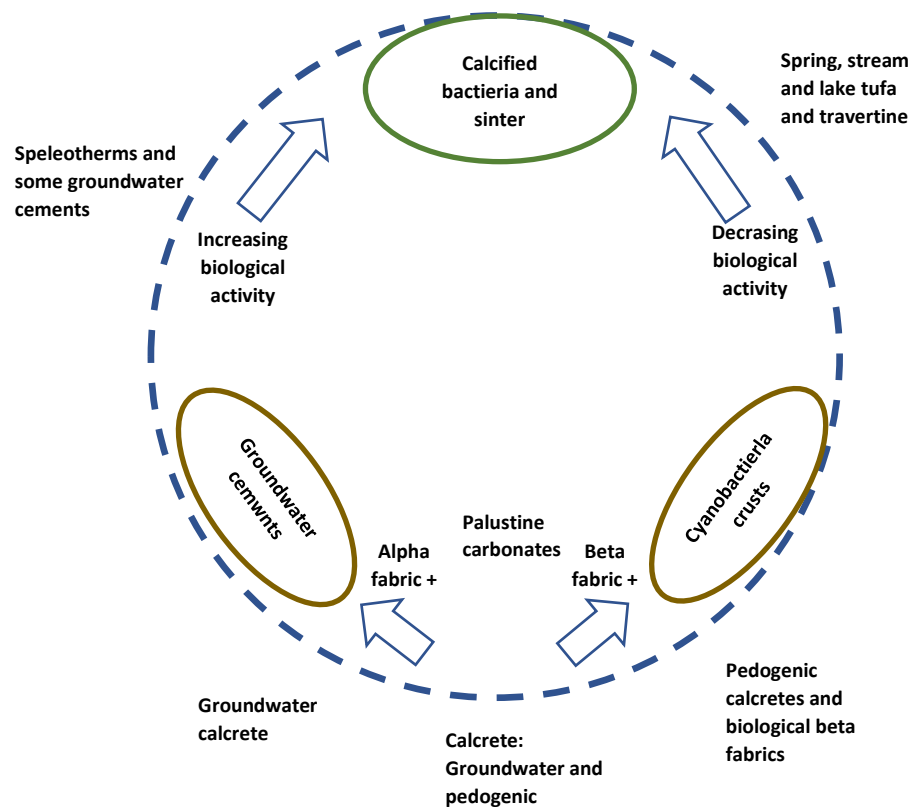


Figure: 4.1 Conceptual model of the degree of a continuum between different terrestrial carbonate depositional environments (adapted from Brasier, 2011). See section 4.4.8

Table 4.8: Fluvial facies model. The description, defined by Miall, 1977; 1996; 2016 and combined with Pedley (2009) and Arenas-Abad et al. 2010, outlines the criteria used for the identification of similar depositional environments in the study area. See also Tables 4.1, 4.2 & 4.3.

| Log Code | Facies | Sedimentary structure | Interpretation |
|----------|---|--|---|
| FGmm | Massive, matrix-supported gravel, very poorly sorted | Weak to no grading | Plastic debris flow deposit (high strength, viscous) |
| FGmg | Matrix-supported gravel | Inverse to normal grading | Pseudoplastic debris flow (low-strength, viscous) |
| FGci | Clast – supported gravel | Inverse grading | Clast-rich debris flow (high - strength) or, pseudoplastic |
| FGcm | Clast-supported massive gravel | None | Pseudoplastic debris flow (internal bedload, turbulent flow) |
| FGh | Clast-supported, crudely bedded gravel | Horizontally bedded, imbrication | Longitudinal bars, lag deposits, sieve deposits |
| FGt | Gravel stratified | Trough cross-beds | Minor channel fill |
| FGp | Gravel stratified | Planar cross-beds | Transverse bars or deltaic growths from older remnants |
| FSt | Sand, medium to very coarse, maybe pebbly | Solitary or grouped trough cross-beds | Sinuuous-crested and linguoid bedforms (3D dunes) lower flow regime |
| FSp | Sand fine to very coarse, maybe pebbly. | Solitary or grouped planar cross-beds | Linguoid traverse bars, sand waves (2D dunes) |
| FSr | Sand, very fine to coarse | Ripple marks, cross-lamination | Ripples (lower flow regime) |
| FSh | Sand, very fine to very coarse, maybe pebbly | Horizontal lamination, parting or streaming lineation | Planar bed flow (critical flow regime) |
| FSI | Sand fine | Low angle (<15%) cross-beds | Scour fills, crevasse splays, antidunes, humped or washed out dunes. |
| FSe | Erosional scours containing intraclasts with silt or intraclasts lag deposits. | Crude cross-bedding | Scour fills |
| FFSs | Sand, fine to coarse, maybe pebbly | Board, shallow scours some cross-bedding | Scour fills |
| FFSm | Sand, fine to coarse | Massive, or with faint laminations | Sediment gravity flow |
| FFI | Sand, silt and mud | Massive to fine lamination, very small ripples | Overbank, waning flood, abandoned channel or drape deposits |
| FFsc | Silt, mud and clay | Horizontally laminated to massive | Back swamp deposits |
| FFms | Mud and silt | Massive with freshwater molluscs | Back swamp pond or abandoned channel deposits |
| FFm | Mud and silt | Massive with desiccation cracks (red to brown) | Overbank, abandoned channel or drape deposits |
| FFr | Mud and silt | Massive with roots and bioturbation | Root beds, incipient soil |
| FP | Paleosol, carbonate (calcite or siderite) | Pedogenic features (nodules and filaments (Figs 4.3 & 4.4) | Soil, with chemical precipitation and post-depositional alteration |
| FGwc | Groundwater carbonate | Massive, soft nodules and lobes of altered sediment (Fig 4.3 & Table 4.16) | Sediment profiles with chemical precipitation and post-depositional alteration |
| FC | Coal, carbonaceous mud | Plants, muds and films | Vegetated swamp deposits |
| FBlS | Braided fluvial limestone. Intraclasts and oncoids, interbedded with phytoclast lenses. Small marginal micritic phytoherm and flow-aligned boundstone on the stream bed (Tables 4.4 & 4.9). | Boundstone (Tables 4.5 & 4.15) on the stream bed. Low-angle climbing ripples and laminae that makeup low – domes (microherms) associated with stromatolite growth. | Develop in areas of unimpeded active fluvial flow under relatively constant velocity. |

| Table 4.8: Continued | | | |
|-----------------------------|---|---|---|
| Code | Facies | Sedimentary structure | Interpretation |
| FpBlS | Barrage limestone. Down-stream facing, transverse phytoherms that dam streams with macrophytes (Framestone) (Tables 4.5, 4.14 & 4.15). Lime-mud in ponded up-stream areas with local phytoherm development. | The upstream: sharp contact with fine, uncemented lake or pool carbonate with intraclasts. Downstream: clinofom beds associated with deeper water. | Develop on low gradient watercourses at pinch point along the course of the river (lighted areas). Phytoherm deposits also develop in slow-flowing and calm dammed fluvial areas. |
| FpChls | Charophyte phytoherm limestone (framestone) (Tables 4.5, 4.14 & 4.15). | Alteration of layers of the in-situ brushes and layers of fragments charophytes. Lenses and patches up to several meters thick and 10s of meters wide. | Slow-flowing and calm dammed fluvial areas. |
| F/LpStls | Phytoherm stems dominate, forming cliffs and brushes (framestone) (Tables 4.5, 4.14 & 4.15). | Interbedded with cm-dm layers of rudstone, phytoclasts and boundstone mosses. Tabular to lenticular, domed, cm-dm thick and laterally extensive, 10s of meters | Palustrine setting on fluvial banks, floodplains, inter-channel areas and lake shorelines |
| FInls | Intraclastic limestone. Rudstone, packstone or grainstone. Rounded to angular clasts. | Unorganised or with planar or trough-cross-beds. Lenticular to tabular cm-dm in thickness and lateral extent. | Flood events that erode and re-work previously deposited limestone deposits |
| Fstmls | Stromatolitic limestone. Alternating layers <10.5 mm of different colours and thicknesses. (Tables 4.5, 4.14 & 4.15). | Fstmls 1: Tabular, stepped and hemidomic deposits dm to m thick and 10s of meters in lateral extent. Fstmls 2: Planer and undulatory layers. Bioherms. Variable thickness and lateral extent. | Fstmls 1: Fast flowing areas on the river bed F/Lstmls 2: Calm fluvial and lacustrine areas. |
| F/LMls | Massive or laminated marls (Table 4.10). | Structureless or with horizontal laminations, with or without biota. Geometry: Mostly lenses or patches dm up to 2 m high and laterally extensive. Molluscs. | Settle out in ponds, on floodplains and offshore lake areas |

4.4.4: Palustrine carbonate facies and depositional model

Palustrine carbonates in the study area have been identified based on palustrine facies described by Alonso-Zarza, (2003) and summarised in Alonso-Zarza & Wright, (2010a), with “true” palustrine lithofacies outlined in Table 4.12, and lithofacies that are closely linked palustrine depositional systems in Table 4.13.

4.4.5: Spring carbonate facies and depositional model

The classification used to identify spring carbonate depositional environments (see Tables 4.4, 4.6 & 4.13 – 4.15 for common facies), and morphologies is based on the extensive work of Capezzuoli et al. (2014), Pedley, (1990, 1992, 2009), Ford and Pedley, (1996), Pedley and Rogerson (2010), and Pedley et al. (1996, 2000, 2003 & 2009) (see Table 4.15). The models focus on the geometry and profile aspects of tufa outcrops and typically found bed associations that have defining facies for each depositional environment (Pedley, 2009b). Models commonly overlap with one another due to a continuum of depositional environments (Brasier, 2011; see Fig 4.1), but each is said to be recognisable based on one dominant facies (Pedley, 1990, 1992, 2009; Ford and Pedley, 1996; Pedley and Rogerson, 2010; Pedley et al. 1996, 2000, 2003 & 2009; see Table 4.15).

Table 4.9: Architectural elements in fluvial deposits. The description, defined by Miall, (1985), outlines the criteria used for the identification of similar depositional environments in the study area. See Table 4.8.

| Feature | Principle facies | Geometry and relationship | Interpretation |
|---|--|---|---|
| CH: Channels | Any combination | Finger, lens or sheet; concave-up erosional base. Scale and shape highly variable. | Erosive fluvial/alluvial features |
| SG: Sediment gravity flow | FGmm, FGmg, FGci, FGcm | Lobe, sheet typically interbedded with GB. Internal bedding: none, weak, and normal or reverse grading bedding. | Plastic and pseudoplastic, high strength debris flow. Clast rich to matrix-supported. |
| GB: Gravel bars and bedforms | FGp, FGt, FGh | Lens, blanket. Usually tabular bodies. Commonly interbedded with SB and SG. | Longitudinal bars, lag deposits, sieve deposits, minor channel fill, transverse or deltaic growths. |
| SB: Sandy bedforms | FSt, FSp, FSh, FSI, FSR, FSe, FFs, FFsm, FBls, FPIs, F/LOnls | Lens, sheet, blanket, wedge shapes occurring as channel-fills, crevasse splays, minor bars. | 3D dunes, 2D dunes, ripples (lower flow regime), planar bed flow (critical flow regime, scour fills, crevasse splays, washed out dunes, and gravity flows. |
| DA: Downstream accretion macro forms | FSt, FSp, FSh, FSR, FSe, FFs, FInls, FStmls (1) | Lenses resting on flat or channelised base, with convex-up 3 rd -order internal erosion surfaces and upper 4 th -order bounding surfaces. | 3D dunes, 2D dunes, ripples (lower flow regime), planar bed flow (critical flow regime), and scour fills. |
| LA: Lateral accretion macro forms | FSt, FSp, FSh, FSI, FSe, FFs, occasionally FGmm, FGt, FGp | Wedge, sheet, lobe structures characterised by internal lateral-accretion 3 rd -order cycles. | 3D dunes, 2D dunes, planar bed flow (critical flow regime), scour fills, crevasse splays, washed out dunes, and occasionally vicious, plastic debris flows, and minor channel fill, transverse or deltaic growths |
| LS: Laminated sand sheet | FSh, FSI, and minor FSp, FSR, F/LMls | Sheet or blanket. | Planar bed flow (critical flow regime), scour fills, crevasse splays, washed out dunes, 2D dunes and ripples (lower flow regime). |
| OF: Overbank fines | FFm, FFI, FP, FFr, FFsc | Thin to thick tabular blankets cm up to m thick. Ochre, red and grey. Commonly interbedded with SB, may fill abandoned channels. | Overbank, waning flood, abandoned channel or drape deposits, root beds and incipient soils, and soil with chemical precipitation. Settling out of fines. |
| BS: Back swamps and pools | FFsc, FFms, FP, FFr, Fc, F/LOnls, F/LpStls, F/LMls | Sheet or blanket | Organic-rich fines with root beds and incipient soils, and soil with chemical precipitation |

4.4.6: Pedogenic calcrete

Several classification systems identify the morphological features of pedogenic calcrete formation (Gile et al. 1966; Allen, 1986; Steel, 1974; Machette, 1985). Per Wright & Tucker (1991), the most comprehensive classification is given by Machette (1985) (Fig 4.4). Consequently, this was used here. Pedogenic calcrete (or caliche, Goudie et al. 1975) horizons develop through chemical and physical weathering of the carbonate host rock, by soil development and the accumulation of calcium carbonate within the soil profile via evaporation and; by

saturated pore water being driven to the surface by capillary forces. Under these circumstances, physicochemical and microbial activity within the soil profile can lead to the development of a hard crust on the surface of the ground or in the upper soil horizon (Watts, 1980; Goudie, 1996; Wright & Tucker, 1991; Nash & Smith, 2003; Flügel, 2004; Alonso-Zarza & Wright, 2010b; Brasier, 2011).

4.4.7: Groundwater calcrete formation

The identification of groundwater calcrete is based on facies types outlined by Alonso-Zarza & Wright (2010b) (Table 4.16). Within sedimentary basins, phreatic water chemistry has control of groundwater mineralogy where calcite is the main precipitant and groundwater has low salinity levels (Alonso-Zarza & Wright, 2010b). Evaporation, evapotranspiration, CO₂ degassing and the common ion effect are the main reasons for carbonate deposition (Mann & Horwitz, 1979; Arakel, 1986; Tandon & Gibling, 1997; Wright & Tucker, 1991; Alonso-Zarza & Wright, 2010b).

Table 4.10: Common carbonate and clastic lacustrine facies, The description defined by Gierlowski-Kordesch, 2010 (and references therein), outlines the criteria used for the identification of similar depositional environments in the study area.

| Code | Facies | Depo -Zone | Description |
|------|---------------------|--|--|
| LMS | Massive | Nearshore to basinal areas | Structureless fine-grained carbonate or clastic sediments with or without flora and fauna. Occurs as calc-mudstone, wackestone, packstone, grainstone, marlstone, fine carbonate siltstone (Table 4.5) or the equivalent clastic grain sizes. Oxygenated waters, low sedimentation rates, bioturbation, and sediment churning can erase sedimentary structures (Gierlowski-Kordesch, 2010). See also Table 4.5 and Figure 4.3. |
| LMi | Microbial | Shallow lake margins or shallow lakes < 5 m (Photic) | Defined by macro and microphytes, oncoids, ooids, pisoids, algal bioherms, and laminated, flat-topped stromatolites and create hanging ledges (see Pedley., 2009 & Tables 4.3, 4.4, 4.14 & 4.15). Alga <i>Chara</i> and micrite (Table 4.4) are common. Algal and bacterial mats influence sedimentation patterns on deformation and erosion surfaces. Beds can also contain, tufa mounds, and microbial algal crusts (e.g. Schneider et al., 1983; Lindqvist, 1994). Form as fixed growths on fossils, sediment grains and plant material as well as transported crusts, intraclasts (Table 4.4), or form as microbial laminae (Gierlowski-Kordesch, 2010). Fluvial, ground a spring (e.g. Casanova & Thouin, 1990) promote microbial carbonates development. |
| LMa | Marginal | Littoral | Sedimentary structures, grains and intraclasts (Table 4.4) are present due to wave and current action. Can contain shells, ooids, carbonate or clastic silts and sands, charophyte stems, pisoids and terrace gravels (Table 4.5). Small to large scale cross-stratification, ripple cross-lamination, and horizontal lamination formed under upper and lower flow regimes are common (see Table 4.2). Encrusted intraclasts (Table 4.2) and fossils are common. See also Figure 4.3. |
| LOw | Open water | Sublittoral to profundal | Deposited by current or density flows in open lake waters with grain sizes from silt to cobble. Turbidity currents and debris flows (overloading) move sediment distally (Gruszka, 2007; Gierlowski-Kordesch, 2010). Tectonic activity (e.g. Rodríguez-Pascua et al. 2003) and large waves (seiches) (Schnellman et al. 2006) can deform sedimentary layers, cause brecciation and resuspension (e.g. Moretti & Sabato, 2007) |
| LP | Exposed lake margin | Eulittoral zone | Lake marginal areas that become vegetated. Carbonaceous muds can develop (FC: Table 4.8). There can be further desiccated and pedogenised, eroded and re-worked or re-submerged. |

Table 4.11: Lake margin facies model for partially and dominantly carbonate lakes that develop with a surface input of carbonate. The description, defined by Gierlowski-Kordesch, (2010), outlines the criteria used for the identification of similar deposits in the study area. See also Table 4.10).

| Facies code | Lake margin type | Depositional environment | Facies description |
|-------------|------------------------------|--|--|
| LLeb | 1: Low - energy bench (X11) | Steep littoral to sublittoral zones. Restricted wave action. | Massive, microbial and bedload transported carbonate with slumps, turbidites and grain flows containing re-sedimented carbonate from the littoral zone. |
| LHeb | 2: High - energy bench (X12) | Steep slope margins that typically get sediments from shallow water. | Topset beds develop in the photic zone where sediments are displaced downslope and along-shore by reworking, grain flow, turbidity currents, and slumping onto cross-stratified forest beds. Bottom sets can contain microbial carbonates from the littoral zone interbedded with laminated and bedload transported carbonate. |
| LLer | 3: Low - energy ramp (X13) | Margin subject to fluctuating water levels. | Palustrine facies are typical, and high productivity adds diagenetically altered carbonate (Table 4.5) sediments to palaeosols when lake levels decline. Sublittoral to profundal zones develop massive, and bedload transported carbonates. Deepwater zones can also develop laminated carbonates |
| LHer | 4: High - energy ramp (X14) | Marginal areas dominated by wave activity | Bedload-transported carbonates accumulate on exposed surfaces while sheltered littoral and sublittoral zones develop massive carbonates. Microbial carbonates are also found in the littoral zone, and laminated carbonates can develop in the profundal zone. |

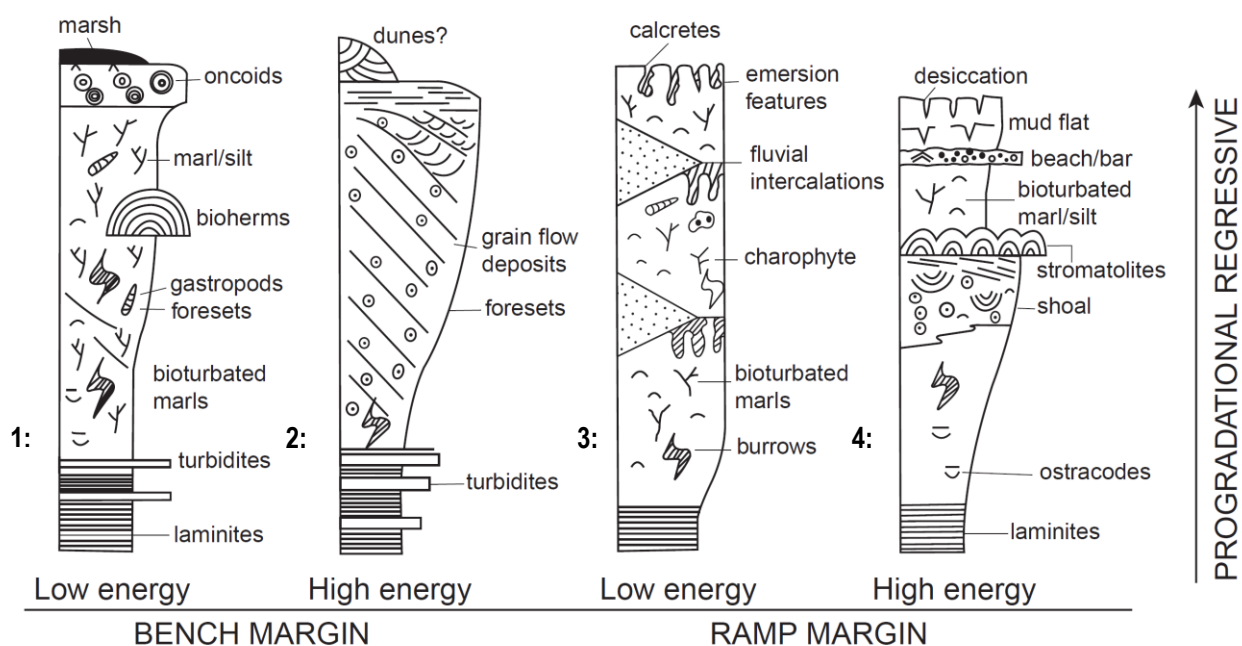


Figure 4.2: Bench and ramp lake margin facies models for partially and dominantly carbonate lakes (from Platt & Wright, 1992. In: Gierlowski-Kordesch, 2010, see also Table 4.11).

Table 4.12: Palustrine facies, defined by Alonso-Zarza, 2003 & Alonso-Zarza & Wright, (2010a) and references therein), outlines the criteria used for the identification of similar depositional environments in the study area.

| Code | Facies | Formation | Description |
|----------|--------------------------------------|---|--|
| PMot | Mottled carbonate | Water table fluctuations change groundwater Eh and remobilise iron in sediments with <2% iron, manganese and calcium. | Yellow-orange-red mottling outlined by desiccation cracks (Tables 4.4 – 4.6). Ferruginous nodules, tubular voids, concretions and crusts can be present (Freytet & Verrecchia, 2002). |
| PNod/Bre | Nodular and brecciated carbonates | Nodules form when desiccation creates planar and curved fissures that are later infilled under vadose and phreatic oxidising conditions (Freytet, 1973). | Centimetre scale irregular nodules often within a chalky micritic matrix or interspaced by cracks filled with microspar (Table 4.5) and sparry calcite (Table 4.6). The matrix can be detrital grains and whole or fragmented charophytes, ostracods and molluscs. Deposits can show mottling. Meter – thick beds can indicate that a significant portion of the lacustrine sequence exposed in one or several events. Short-lived subaerial exposure and rewetting of lake sediments can sandwich lacustrine deserts with brecciated or nodulised deposits. |
| PRm | Carbonates with vertical root moulds | Calcification around vertical root systems in clayey or soft carbonate sediments. Indicates well-developed vegetation cover during formation. | Matrix dominated deposit with gastropod shells, charophytes, ostracods, desiccation cracks, and fenestral and alveolar structures. Root voids (Table 4.6) are irregular, vertical (decimetre scale) and up to several centimetres in width. Structures are wider at the top and can be empty or infilled by micrite, microspar, peloids, intraclasts, bioclasts and spar (Table 4.4) cement. Host sediment can also become brecciated and nodulised in the areas around rhizospheres, especially in marl. |
| PMk | Microkarst | Voids develop networks via root activity, desiccation, and to a lesser extent, dissolution. | Carbonate with irregular and intricate voids that are small (few cm), circular, and elongated joining to form part of a larger network. Voids have sharp boundaries, and rounded margins indicate dissolution (Platt, 1989). The primary muddy structure is lost. |
| PGran | Granular carbonates | Develop in shallow marginal areas. Form at the top and bottom of packets of lacustrine sediment via repeated wetting and drying of carbonate muds. Root activity causes advanced fragmentation. | Made up of peloidal, coated grain and intraclast carbonates (Tables 4.4 & 4.6) in a calcite mosaic cement (microspar to coarsely crystalline) (Table 4.4). Sediments sit within different types of voids, forming an intricate network that show evidence of multiple phases of fragmentation, coating, internal sedimentation, microspar silt and blocky calcite cementation (Table 4.4). Fluctuations in the water table can cause reworking, concentration and coating on mud fragments. |

4.5: Geochemical analysis of sediment samples

Ground and surface water flowing into a basin move various clastic materials and soluble ions into, around and sometimes out of the basin, depending on its hydrological state (closed or open). The ion concentration of water can cause the chemical precipitation of autogenic salts, carbonates and clays. Understanding these processes elucidates to the environmental conditions at the time of deposition, helping to reconstruct the palaeoenvironmental conditions at the time formation (e.g. Ebro Basin, Spain (Schuett, 1998, 2000); Thar Desert playa lakes, India (Enzel et al. 1999); Lake Tecocomulco, The Basin of Mexico (Roy et al. 2008, 2009).

For this PhD research, the geochemical analysis of key, representative sections of the stratigraphic sequence were carried to build a isotopic ($\delta^{18}\text{O}$, $\delta^{13}\text{C}$) and geochemical (ICPMS) records for depositional episodes in the study area which fulfils Objective 2 (Chapter 1) and is used to compare with data collected to meet objective

Table 4.13: Interchangeable lacustrine, palustrine and fluvial facies defined by Alonso-Zarza, (2003) & Alonso-Zarza & Wright, (2010a) and reference therein, outlines the criteria used for the identification of similar depositional environments in the study area.

| Code | Facies type | Formation | Facies |
|-------|---|---|---|
| IOlsc | 7: Organic marl and clay (stone) | Fluctuating water levels | Massive to poorly laminated organic-rich marls and clays with varying amounts of fragmented plant remains, gastropod shell, carbonate nodules, carbonate and clay intraclasts (Alonso-Zarza & Wright, 2010a). Interbedded with clastic deposits or sandwiched between lacustrine/palustrine carbonates with sharp transitional boundaries. |
| ICh | 8: Carbonate and clastic filled channels | Develop during prolonged periods of desiccation. Fluvial incision and reworking of the lacustrine and palustrine sequences. | Irregularly bedded deposits with erosive upper and lower planar surfaces that have root traces leading to prismatic structures. Channels infilled with oncoids, bioclasts, phytoclasts and reworked micritic grains. Can also contain clastic sediments. |
| IPm | 9: Green to brown marl (stone) | Develop in vegetated marsh and wetlands with high water tables. Distal fan, lake margin or mudflat areas. | Green to brown massive or slightly laminated marl that can contain micritic nodules (mm in diameter) and root casts (Table 4.6). Often found interbedded with clastic sediments, carbonate sediments and small silt ripple beds. Root activity and desiccation lead to brecciation and colour changes indicative of ground and surface water changes. |
| — | 12: None - palustrine facies | Associated with marginal lake areas, ponds and pools | None carbonate evaporates, dolomites, clays and dolomitic muds. Bioturbated, modified (plants and animals) lenticular gypsum formed in marginal lake areas is common. |

4.5.1: ICP – OES $\delta^{18}\text{O}$ and $\delta^{13}\text{C}$ stable isotope carbonate geochemistry

Freshwater carbonates hold a record of the $\delta^{18}\text{O}$ and $\delta^{13}\text{C}$ characteristics of the water they precipitated from (Fig 4.5), and are environmental, hydrological, tectonic and climatological records of the time span of which they formed (eg Talbot, 1990; Winnograd, 1992; Chivas et al. 1993; Edwards, 1993; Andrews et al. 1997; Bar-Matthews et al. 1997; Wei & Gasse, 1999; Matsuoka et al. 2001; Rosenmeier et al. 2002; Leng & Marshall, 2004; Andrews, 2006; Colman et al. 2006; Leng et al. 2006; O'Brian et al. 2006; Viles & Pentecost, 2007; Zanchetta et al. 2007; Pedley, 2009; Arenas-Abad et al. 2010; Brasier, 2010; De Filippis et al. 2012; Vázquez-Urbez et al. 2012; Gandin & Capezzuoli, 2014; Adamson et al. 2015; Candy et al. 2015; Tonker et al. 2015; Candy et al. 2016; Kämpf et al. 2016; Wendt et al. 2016).

4.5.1.1: Isotope terminology

Here the terms positive higher (+) and negative lower (-) to report the stable isotope ratios of samples (see Clark & Fritz, 1997; Kendall & McDonnell, 1998; Tucker & Wright, 2004; Leng, 2006; Sharp, 2007). The delta sign (δ) used is the standard notation for reporting the ratio of abundance of the heavy to light isotope in parts per mil (‰) (Clark & Fritz, 1997; Kendall, 1998; Sharp, 2007).

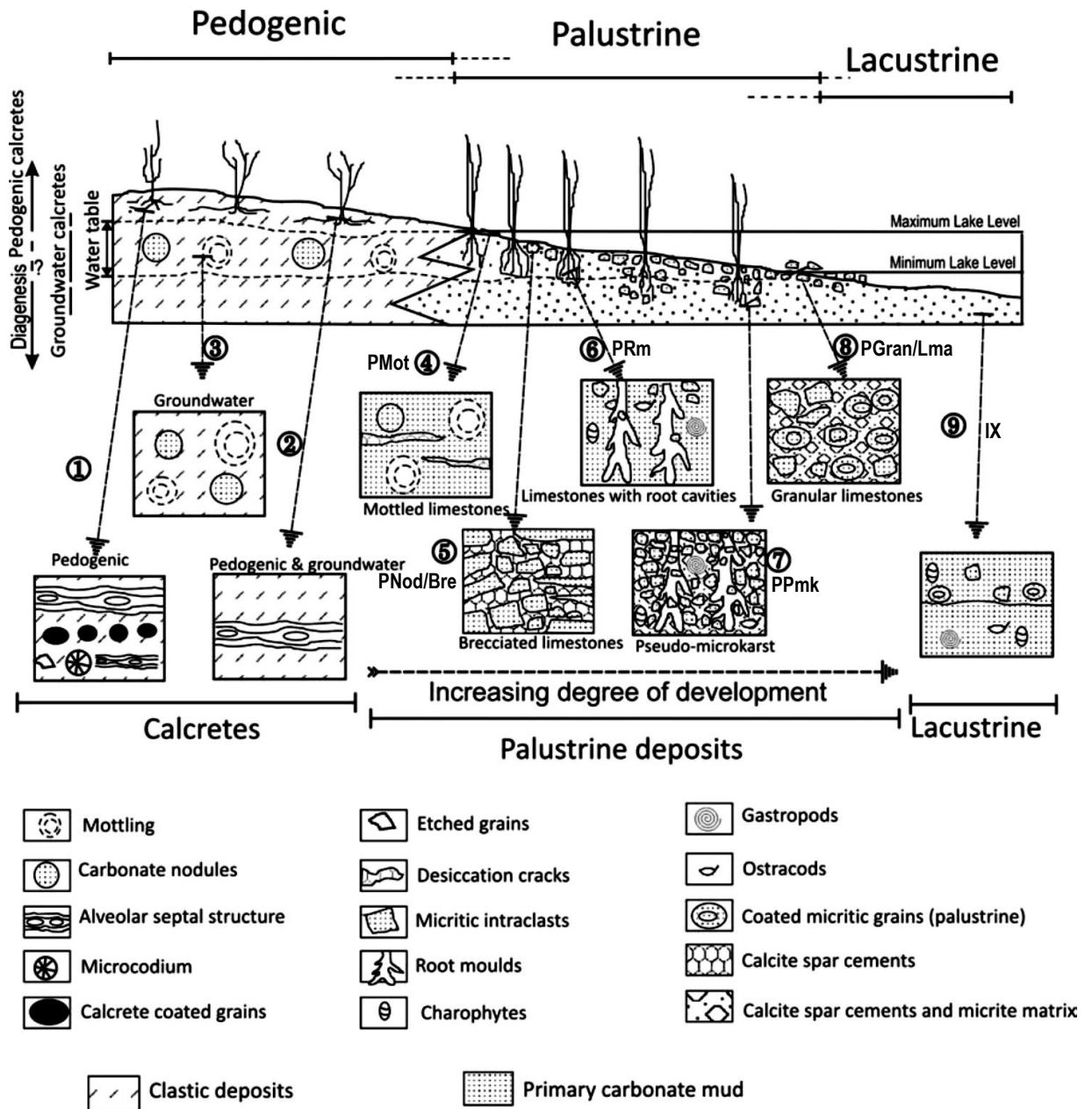


Figure 4.3: Transitional pedogenic – palustrine – lacustrine facies associations. Calcrete (1 – 3); palustrine carbonates (4 – 8), from the less developed (4) to more mature deposits (8); and none pedogenically altered lacustrine carbonates (9) (from Alonzo-Zarza, 2003; Alonzo-Zarza & Wright, 2010b). Facies in 1 – 3 are described in Figure 4.4 and Table 4.16. 5 – 8 facies codes are defined in Tables 4.12 and 4.13. Facies 9 is described in Table 4.10.

4.5.1.2: Oxygen isotopes in lacustrine and marsh limestone carbonate deposits

Oxygen isotopes are reported relative to Vienna standard mean ocean water (VSMOW) for water samples and Vienna PDB or VPDB (belemnite calcite from the Pee Dee Formation) for carbonate samples (Eq 4.1).

Equation 4.1: $\delta^{18}\text{O} = 1000 * \frac{(^{18}\text{O}/^{16}\text{O} \text{ sample} - ^{18}\text{O}/^{16}\text{O} \text{ standard})}{^{18}\text{O}/^{16}\text{O} \text{ standard}}$

Table 4.14: Classification of autogenic, freshwater carbonate that displays an organic in-situ framework. Defined by Cipriani et al. (1977), Pedley, (1990 & 1992) and Ford & Pedley, (1996), outlines the criteria used for the identification of similar depositional environments in the study area.

| Facies Code | Phytoherm deposit name | Facies |
|-------------|-------------------------------|--|
| StrLs | 2: Stromatolitic (Boundstone) | Sheets of micrite and peloids (Tables 4.4 & 4.6) (e.g. Stromatolitic tufa). Can be dominated by the heads of skeletal stromatolite consisting entirely of cement fringes associated with oscillatoriacean cyanobacteria. Can include coarse, detrital intraclasts and oncoids (Tables 4.4 & 4.6). |
| FraLs | 3: Framestore | Living anchored framework of vertical and horizontal hydrophytes and macrophytes (aquatic/semi-aquatic plants (Table 4.6)) with matted microfilms of bacteria (e.g. cyano or fungi). Held in a low – Mg calcite cement fringe. Cavities are filled with phytoclasts, micrite (peloidal), and lithoclasts (Tables 4.4 & 4.6). Has a wide fauna diversity (e.g. larvae & mollusc). Framework decays readily leaving distinctive porous and permeable fabric. |

Table 4.15: Carbonate depositional models defined by Capezuoli et al. (2014), outlines the criteria used for the identification of similar marsh depositional environments in the study area. Also, see Tables 4.8 & 4.10.

| Model | Dominant facies | Depositional environment | Facies code | Description |
|-----------------|--------------------|--|-------------|--|
| Paludal (marsh) | Photoherm cushions | Low gradient valley floors that have sluggish drainage | TPal | Spring fed water seeps through bryophyte carpets, and between reed and bryophyte cushions leaving a carbonate coating. Cushions may maintain their original structure or collapse. Poorly cemented “spring chalk” can collect in pools, cylindrical oncoids can also form. Water level fluctuations can allow palaeosol development. Deposits can be crudely laminated and include clastic layers. |

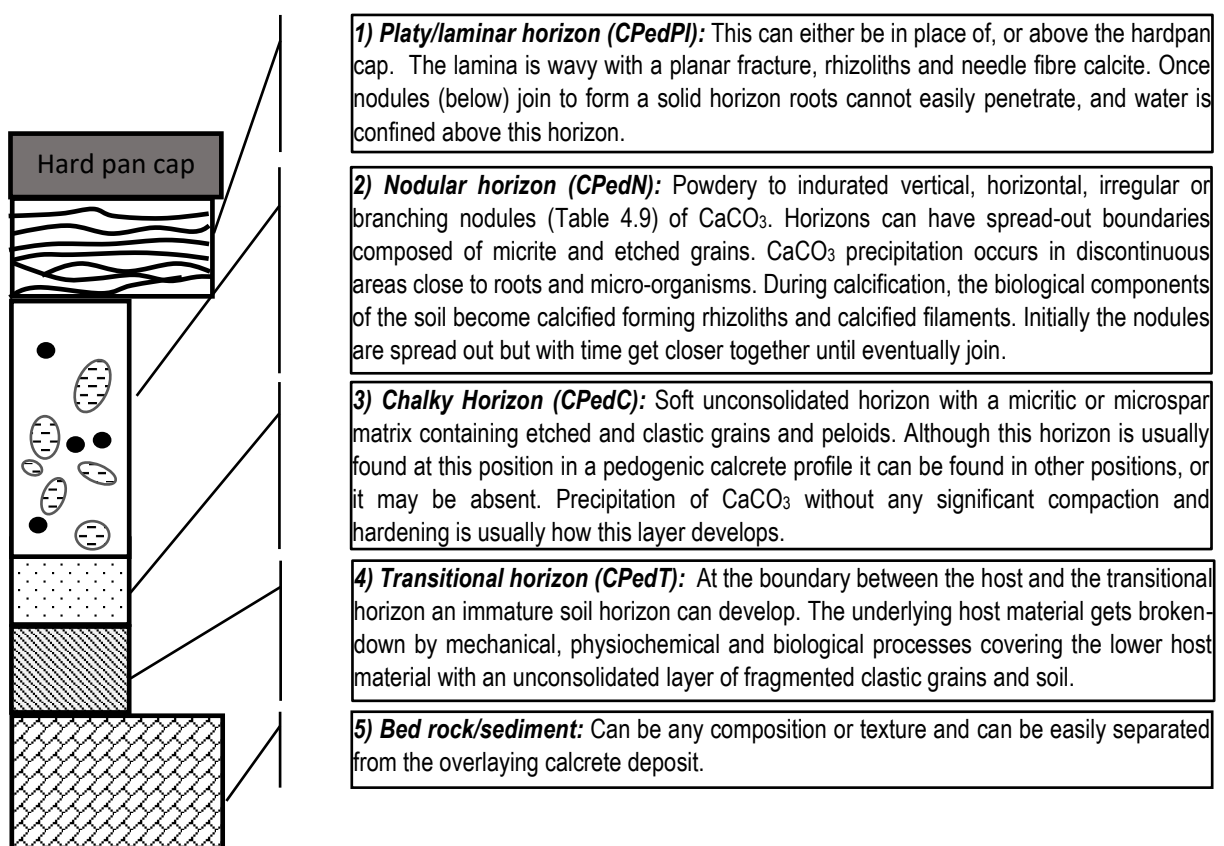


Figure 4.4: Idealised pedogenic calcrete profile development based on Manchette, (1985) from Esteban & Klappa, (1983) and Alonso-Zarza & Wright, (2010b).

Table 4.16: The six main types of Groundwater calcrete facies (adapted from Alonso-Zarza & Wright, 2010b and references therein).

| Code | Facies | Description |
|---------------|------------------------------|---|
| CGwMa | Massive beds | Thick massive beds of carbonate deposited by the lateral flow of groundwater usually >1.5m in thickness (Wright & Tucker, 1991; Mack et al. 2000; Jutras et al. 2007; Alonso-Zarza & Wright, 2010b). Alpha fabrics (Table 4.9) dominate, and upper and lower boundaries are sharp. |
| CGwNod | Soft nodular layers | Contains layered soft carbonate nodules with dispersed boundaries that follow the stratification of the sediment body or the convex nature of channel fill deposits (Khadkikar et al. 1998). |
| CGwcl | Cemented layers | Cemented layers that form lenses up to 20 cm thick and 3 m wide with solitary, vertically elongated nodules (Tandon & Gibling, 1997). Some deposits have an upper curtain of nodules and tubules precipitated at the interface between the water table and the capillary fringe (Mack et al. 2000). Found in proximal and medial alluvial fan deposits as well as in fluvial channels (Tandon & Narayan, 1981; Nash & Smith, 1998). |
| CGwRo | Root mats | Calcified root mats, here because they can develop by phreatophytes (deep-rooted plants that draw water from the phreatic zone or the capillary fringe) mostly in relation to perched groundwater tables (Semeniuk & Meagher, 1981). |
| CGwsh | Thin carbonate sheets | Thin sheets (10 - 50cm) of carbonate in the subsurface of fluvial-aeolian sands. These sheets are made up of calcium carbonate aggregates that develop just above the water table, and deposits can transect stratigraphic boundaries and unconformities (Semeniuk & Meagher, 1981). |

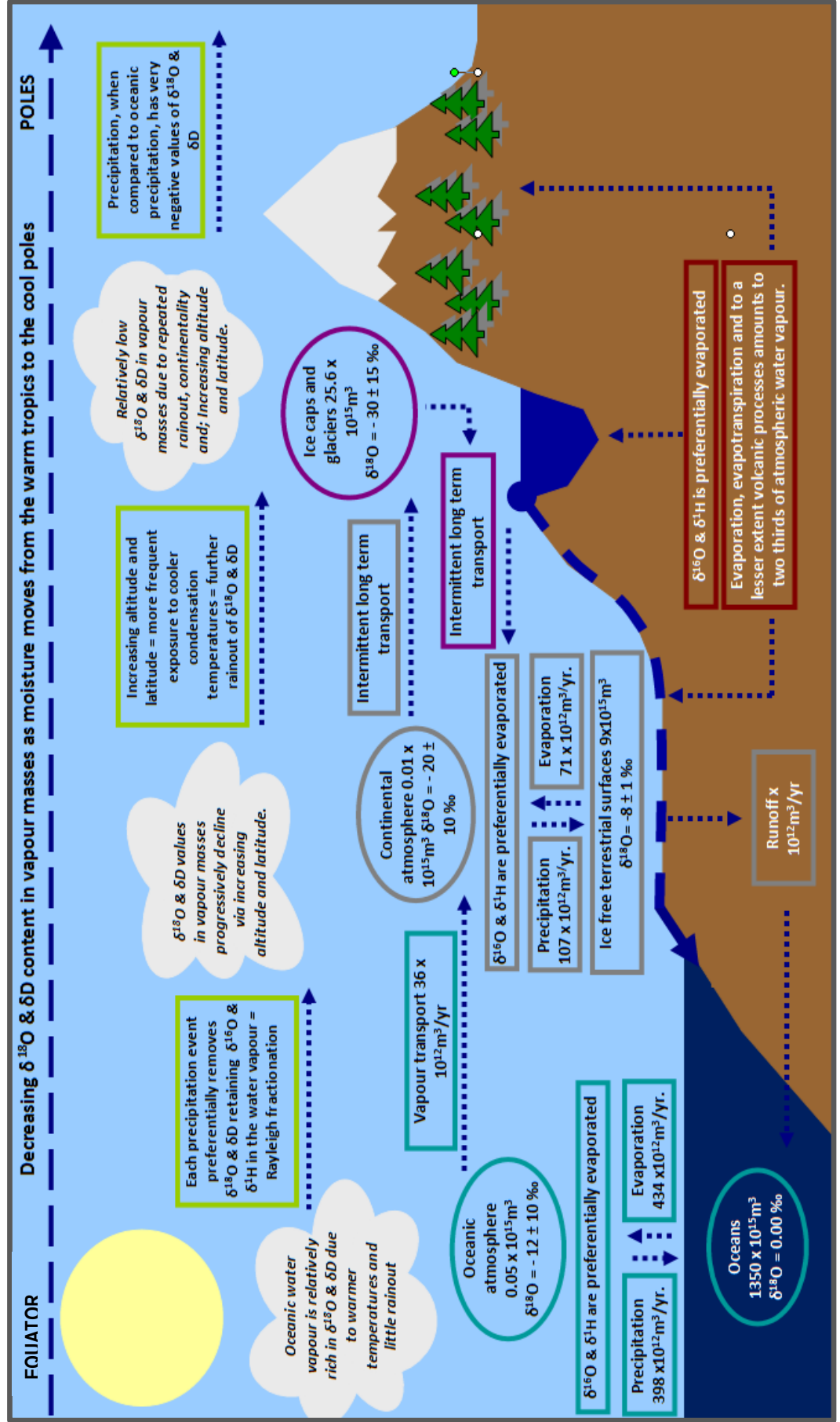
The oxygen isotope content of lacustrine, marsh and fluvial sediments is calculable by thermodynamic correlation which is understood to be equilibrium mineral precipitation (Leng, 2005; Sharp, 2007 Hoefs, 2009, Felstead, 2012). Carbonate precipitation under equilibrium conditions is mainly caused by the removal of CO₂ (Eq 4.2).



Precipitation occurs under ambient temperatures in calcium-bicarbonate waters when dissolved CO₂ in source waters, with high PCO₂ (P= partial pressure), encounter lower PCO₂ pressures and de-gassing occurs, for example, when spring waters emerge at the surface. This forces disequilibrium conditions and carbonate precipitation until the system achieves equilibrium (Eq 4.1). Under equilibrium conditions temperature and water isotope conditions can be linked to the isotope composition of calcite by the Craig (1965) palaeotemperature equation (Eq 4.3) with a 0.24‰ δ¹⁸O shift (+ or -) in the precipitating calcite parallel to a temperature change of 1°C (+ or -) (Craig, 1965; Andrews, 2006). In this PhD research, the Hays and Grossman (1991) equation is used (Eq 4.3) as it was created for use on meteoric cement of which Facies 1-7 (Chapter 5) are arguably a sub-group.

Equation 4.3: $T = 15.7 - 4.36 (\delta^{18}\text{O}_{\text{calcite}} - \delta^{18}\text{O}_{\text{water}}) + 0.12 (\delta^{18}\text{O}_{\text{calcite}} - \delta^{18}\text{O}_{\text{water}})$.

Figure 4.5: The hydrological cycle, including fluxes for meteoric water between the oceans, atmosphere, terrestrial land surface and the ice caps expressed in m^3/yr (modified after Sharp, 2007). The behaviour of the stable isotopes of deuterium and oxygen within the water cycle, during the flux of meteoric waters between phase changes and different water stores and, the effects of temperature, altitude and continentality are also shown (adapted after, Brasier, pers comm, 2011).



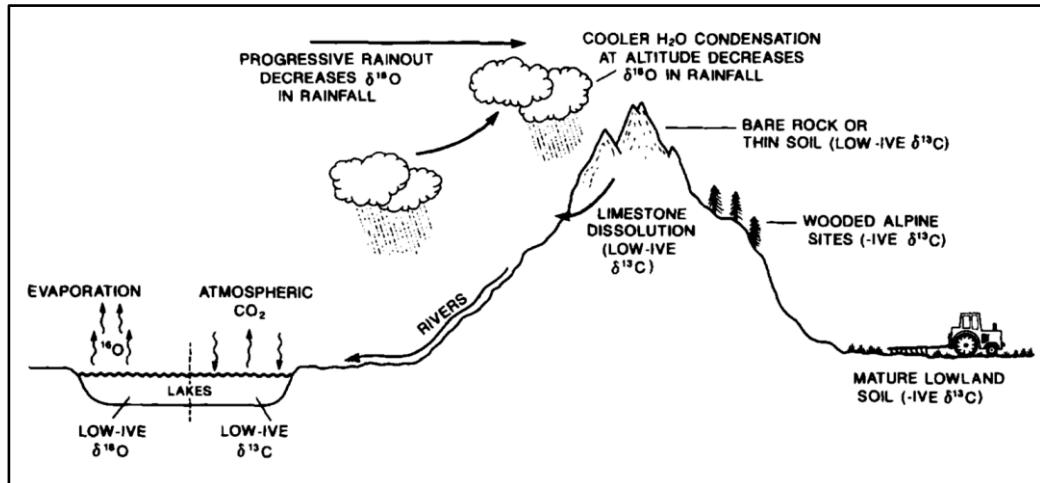


Figure 4.6: Main regional-scale environmental factors which affect the $\delta^{18}\text{O}$ and $\delta^{13}\text{C}$ of microbial carbonates (from Andrews et al. 1997).

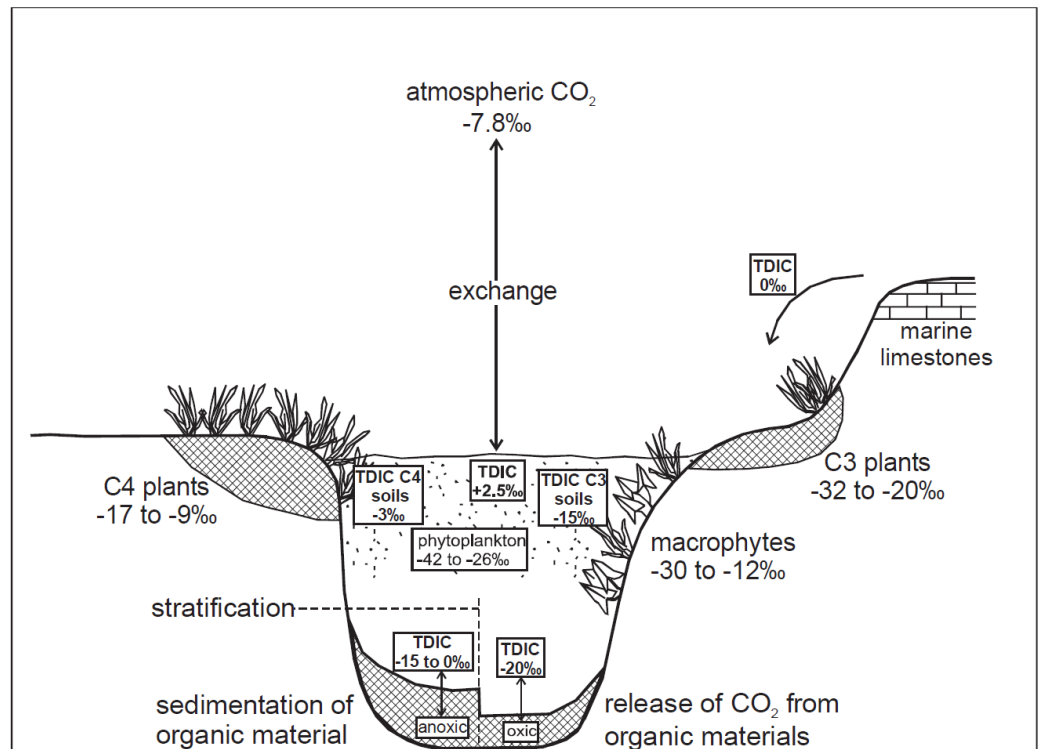


Figure 4.7: Carbon isotope values of carbon sources into lakes resulting in $\delta^{13}\text{C}$ TDIC (Total dissolved inorganic carbon). From Leng and Marsahll, (2004).

Knowledge of what may have affected the composition of the source water is vital to the interpretation of $\delta^{18}\text{O}$ ratios in the mineral precipitate (Figs 4.5 – 4.7). Most of these effects, like the amount effect and variations in air mass trajectories, are short-lived over periods of hours to weeks and have little effect on the stability of groundwater $\delta^{18}\text{O}$ values that are relatively constant $\delta^{18}\text{O}$ over time (Fig 4.5 & 4.6, Chafetz et al. 1991 a & b;

Andrews et al. 1993; Arenas et al. 2000; Matsuoka et al. 2001; Andrews, 2006). This relationship can be more complicated in arid and semi-arid regions where evaporative processes are intense, and groundwater mixing is frequent (Gat & Issar, 1974; Clark & Fritz, 1997; Andrews, 2006). Within streams and marsh settings these processes are likely to be expressed in the $\delta^{18}\text{O}$ vs $\delta^{13}\text{C}$ carbonate record by significant covariance (Smith et al. 2004), just as it does in hydrologically closed lakes (Talbot, 1990; Lang & Marsahll, 2004).

Kinetic or disequilibrium effects are linked to incomplete or modified mineral precipitation. Disequilibrium mineral precipitation impacts the $\delta^{18}\text{O}$ ratios of a mineral outside of the usual thermodynamic effect. Instead, this can be associated with differing rates of mineral precipitation, pH, speciation controls (vital effects) and microenvironmental fluctuations (Leng & Marshall, 2004; Leng et al. 2006; Sharp, 2007). However, the systematic nature of some species-specific carbonate minerals means that disequilibrium effects can be offset (see Holmes & Chivas, 2004; Leng & Marshall, 2004). This means that, as long as the factors that offset the isotopic equilibrium are corrected for or accounted for when interpreting palaeoenvironmental data, they appear not to pose a problem (Holmes & Chivas, 2004; Leng & Marshall, 2004).

Like for this PhD research, palaeoclimatic studies commonly use a bulk carbonate sample for stable isotope analysis (Leng & Marshall, 2004) which likely represents the relative abundance of source components (e.g. biogenic vs authigenic) rather than reflecting climatic or hydrologically induced changes. While this can cause issues, the change in source components will often be related to a change in the water body source components like pH and depth which can be a direct function of climatic or hydrological change. Plus, bulk authigenic bulk carbonate samples give an integrated climate signal of the whole sample that can span 1 – 100 years subject to sedimentation rates (Leng & Marshall, 2004). For the bulk carbonate samples collected from lacustrine, marsh and stream limestone deposits in the study area micromorphological analysis helped to distinguish between authigenic sediments and allogenic, terrestrially derived sediments, the former being preferentially selected for analysis (see Leng & Marshall, 2004). Additionally, fractionation effects associated with different calcite crystal faces (Dickson, 1991) are assumed not to be a problem for the samples collected from the study areas as sample sizes were larger than individual crystal sizes (Brasier pers comm. 2010).

4.5.1.3: Carbon isotopes in lacustrine and marsh limestone carbonate deposits

As with oxygen isotopes; carbon isotope lacustrine, marsh and stream limestone data are reported here in the delta notation relative to Vienna PDB standard (Eq 4.4).

Equation 4.4: $\delta^{13}\text{C} = 1000 * \frac{(^{13}\text{C}/^{12}\text{C} \text{ sample} - ^{13}\text{O}/^{12}\text{O} \text{ standard})}{^{13}\text{O}/^{12}\text{O} \text{ standard}}$

Dissolved inorganic carbon (DIC) in waters can indicate catchment environmental changes that are usually forced by climate (Fig 4.6 & 4.7) (Drummond et al. 1995; Li & Kim, 1997; Leng & Marshall, 2004; Leng et al. 2006). The factors that affect the $\delta^{13}\text{C}$ composition of the biogenic or authigenic stream, lacustrine or marsh carbonates are those that affect the $\delta^{13}\text{C}$ composition of DIC in the precipitating waters (Fig 4.7). Inorganic carbonate isotopes are mainly derived from HCO_3^- (bicarbonate) which becomes incorporated into the precipitating carbonate with the ratio of $\delta^{13}\text{C}/\delta^{12}\text{C}$ relative to the standard reflecting the depositional environment (Leng & Marshall, 2004; Leng, 2005; Leng et al. 2006). Temperature change has a negligible effect on the $\delta^{13}\text{C}$ of calcium carbonate precipitated by HCO_3^- supersaturated waters (Romanek et al. 1992; Brasier, pers comm, 2010). The predominant source of bicarbonate in lacustrine, marsh and stream environments is sourced from groundwater interactions with catchment soils and rocks (Andrews et al. 1993; Leng & Marshall, 2004; Andrews, 2006). Hence, the $\delta^{13}\text{C}$ record deposited along with carbonate sediments is typically a reflection of the sources of carbon that contributed DIC to the precipitating waters.

4.5.1.4: Composition of source waters

Plant respiration and CO_2 production by organic matter decay are responsible for most of the carbon found in inflowing waters (Leng & Marshall, 2004). HCO_3^- derived just from C3 dominated soils will have $\delta^{13}\text{C}$ values between -10‰ and -22‰. HCO_3^- derived just from C4 dominated soils will have $\delta^{13}\text{C}$ values between -7‰ and 0‰, possibly as high as -6‰ to +2‰ (Smith et al. 2004; Andrews, 2006). The resulting $\delta^{13}\text{C}$ values in the precipitated carbonate would be within the range of the parent water source (Leng & Marshall, 2004; Andrews, 2006). Based on Romanek et al. (1992), ground and river waters that have HCO_3^- values sourced from terrestrial soil environments should have a $\delta^{13}\text{C}$ range of between -22‰ and 0‰.

The biological productivity of a water body can change its DIC, particularly during photosynthesis, when aquatic plants preferentially up-take ^{12}C (Fig 4.7). This process is escalated during periods of increased productivity (e.g. seasonally), or when there is significant biomass. In both cases, the DIC $\delta^{13}\text{C}$ values increases within the water body and consequently, in precipitated carbonates (Leng & Marshall, 2004). However, oxidation of bulk organic matter can create $\delta^{13}\text{C}$ DIC lake water stratification, which causes lower DIC $\delta^{13}\text{C}$ values to occur with increasing water depth (Fig 4.7) caused by a localised availability of ^{12}C in CO_2 form respiring sinking organic matter (Leng & Marsahll, 2004). While the above may present a problem when interpreting DIC records the influence of

biological activity within a water body in a carbonate record of $\delta^{13}\text{C}$ values is not yet fully understood and is also debated (see Andrews, 2006). Changes in topography and altitude may lead to vegetation and soil changes from sparse to abundant or vice versa (Figs 4.6 & 4.7) (see Catalan Coastal Ridges, Zamarreño et al. 1997; Andrews, 2006). The CO_2 exchange between the atmosphere and water DIC usually leads to increased $\delta^{13}\text{C}$ DIC that has a covariance with high $\delta^{18}\text{O}$ in carbonate sediments because of the tendency of water to equilibrate with atmospheric CO_2 , which has $\delta^{13}\text{C}$ values of ca. - 8‰ (Fig 4.7) (Leng and Marsahll, 2004). This is especially evident in hydrologically closed systems where ^{16}O , is preferentially evaporated off (Leng & Marsahll, 2004).

4.5.1.5: Sample preparation for ICP – OES $\delta^{18}\text{O}$ and $\delta^{13}\text{C}$ analysis

Before sub-samples were collected the carbonate samples were examined for evidence of diagenetic alteration and these areas were avoided. The author prepared sediment samples at Liverpool John Moores University. From each sample, a 1mg subsample was collected and dried overnight in a 105°C oven, in pre-marked crucibles. After drying samples were transferred to labelled sample bags for transport to SUERC, Glasgow. At SUERC organic matter was removed from the calcites (by the author) by low temperature (<80°C) oxygen plasma ashing (Bio-Rad PT 7300 plasma barrel etcher) for 3 hours, at 300w forward power. Stable isotopes were measured from CO_2 evolved from reacting the sample with 103% H_3PO_4 overnight at 70°C before analysis (after Garnett et al. 2006) by the author.

4.5.1.6: Sample analysis for ICP – OES $\delta^{18}\text{O}$ and $\delta^{13}\text{C}$

The relative abundances of masses 44, 45 and 46 in the gas are compared with those of a working standard reference gas of known isotopic composition. In practice this is achieved by automatic valve switching and data collection whereby reference gas (in this case NBS – 18 calcite) and sample gas are alternately bled into the mass spectrometer switching ten times over a period of several minutes thus obtaining a mean delta value for the sample with respect to the reference gas using the delta notation shown below where R is the 45/44 ratio (to get $\delta^{13}\text{C}$) and δ is in units of per – mil, below:

Equation 4.5:
$$\delta_{s-r} = \left(\frac{R_{sample}}{R_{ref}} - 1 \right) \times 10^3$$

The 46/44 ratio was used to get the $\delta^{18}\text{O}$ of the sample on the reference gas. Contributions to the 45 and 46 peaks from minor isotope combinations (e.g. ^{17}O) in the CO_2 molecules are corrected for using “Craig corrections” in the software (Craig, 1957) giving the raw delta values for the internal reference gas. Adjusting the deltas to get values relative to the international standards (V -PDB & V - SMOW) involves the equation below, where A is the sample gas, B is the internal reference gas, and C is the international standard below:

Equation 4.6: $\delta_{A_C} = \delta_{A_B} + \delta_{B_C} + 10^{-3} \delta_{A_B} \delta_{B_C}$

The internal reference gas was pre-calibrated using carbon dioxide sample gases of the known isotopic composition produced from International Reference Material, NBS – 18 calcite. The carbon dioxide evolved from the dissolution of both the reference material and samples was isolated, purified and then analysed at SUERC on PRISM III and AP2003 mass spectrometers. The mean value of repeat analysis of NBS – 18 (calcite standard) and internal calcite standards MAB – 2 calcite (Carrara Marble) were better than $\pm 0.2\text{‰}$ for carbon and 0.03‰ for oxygen (SUERC per comm, 2011). All samples were corrected as calcite because of the temperature-dependent acid fractionation factors for dolomite and calcite (within experimental uncertainty) (after Rosenbaum & Sheppard, 1986). Analysis of the first batch of carbonate sediment samples was carried by the author under the guidance and supervision of Dr Alex Brasier at SUERC. The second batch of carbonate sediment samples was prepared at Liverpool John Moores University and sent to Dr Alex Brasier at SUERC for analysis at SUERC.

4.5.2: Terrestrial carbonate ICP – OES geochemistry

Palaeoclimatic and environmental information generated from the geochemistry of terrestrial carbonate deposits is now an established branch of Quaternary environmental research (e.g. Platt, 1989; Talma & Vogel, 1992; Quade et al. 1995; Liutkus et al. 2005; Ortiz et al. 2009; Candy et al. 2012; Bertini et al. 2014; Pla-Pueyo et al. 2015; Toker, 2016). Alongside stable isotopic analysis, the geochemical records of terrestrial carbonate sediments can also document palaeoenvironmental information (Andrews, 2006). The rationale for the geochemical analysis of carbonate sediments in the study area was to support stable isotope data. The aim is to build a palaeoenvironmental record from a representative sample set to address objective 4, Chapter 1

4.5.2.1: Methodology

All ICP-OES data from sediment samples was scaled to the mass of the dissolved sample, with no adjustment made for the small insoluble component of the mass. One week was spent at SUERC preparing sediment samples for analysis within an ultra-clean lab and sample preparation, and analysis methods were set out by Professor Rob Ellam. Samples were ground using an agate pestle and mortar and sieved (2 mm) with the fine fraction being used for analysis. Approximately 0.1 mg of each sample was placed into pre-labelled Teflon containers.

The wet, open container digestion method was used, and samples were submerged in 2 ml of 5 % HCl overnight in a fume cupboard. If the samples were still reacting after 12 hours, they were heated to 90°C for 30

mins while maintaining a 2 – 5 ml covering of 5% HCl until the reaction subsided. After this, any excess HCl was evaporated off at 90 °C without boiling for as long as needed. The sample was continuously kept in solution by topping up with ultrapure MilliQ™ water (\pm 5 ml) leaving the sample in a covering of ultrapure MilliQ™ water at the end of the process (\pm 2 ml). If the sediment was not completely digested (this was the case with silica-rich samples), samples were treated with 40% HF. In a specified fume cupboard 5 ml of 40% HF was added to the Teflon containers which were left to stand for up to one hour. If needed, the samples were heated to 90°C for 30 mins and occasionally mixed with a polyethylene rod. The evaporation process was repeated to remove the HF solution, and samples were again left in solution in 1 – 2 ml of ultrapure MilliQ™ water. After the HF stage, samples were washed and evaporated a further two times. Samples were then transferred to 50 ml polyethylene test tubes and topped up with 10 ml of ultrapure MilliQ™ water. Preparation of blanks and reference materials along with sample analysis was carried out by Anne Kelly at SUERC.

4.5.3: Tephra geochemistry

Volcanic ash deposits produced during eruptions have unique geochemical and lithological characteristics that can be used to reconstruct the origin and eruptive mechanism of the tephra (Ersoy, 2006). The correlation and dating of tephra layers can give precise stratigraphic time-markers that cover broad geographic regions, and they are important in understanding volcanic (Ortega & Newton, 1998) and palaeogeographic histories (Objective 4, Chapter 1).

4.5.3.1: Methodology

Five bulk tephra samples were sent to the litho-geochemistry lab, Activation Laboratories, Ancaster, Ontario, Canada. Package 4B, (Lithium Metaborate /Tetraborate Fusion – ICP/OES) was used to obtain the bulk major oxide content of the samples (see Chapter 7 and Actlabs., 2016). The samples are run for major oxides and selected trace elements (Code 4B) on a combination simultaneous/sequential Thermo Jarrell-Ash ENVIRO II ICP or a Varian Vista 735 ICP. Calibration is performed using seven prepared USGS and CANMET certified reference materials. One of the seven standards is used during the analysis for every group of ten samples. Totals were between 98.5% and 101%. If results are lower, samples are scanned for base metals. Low reported totals might indicate sulphate being present or other elements like Li. Samples with low totals, however, are automatically re-fused and reanalysed (Actlabs, 2016).

4.5.4: Loss on ignition (LOI)

LOI analysis of Quaternary sediments provides an inexpensive and easy way to investigate past environmental change (Shuman, 2003). The method used here is based on the initially published methodology of Dean (1974), adapted by Berglund (1986), and later adapted by Lamb, (2004). LOI was calculated as weight loss (g) as a % of loss after ignition of approximately 1 g of sediment.

4.5.4.1: Methodology

The sample was first broken up using an agate pestle and mortar, placed in pre-washed (in deionised water), pre-dried (in a 105°C oven overnight), pre-marked (using a graphite pencil) and pre-weighed crucibles (using a four-point balance) and heated to progressively higher temperatures to measure water loss % (g) (105°C 12 hours), organic loss % (g) (two hours at 550°C) and carbonate loss % (g) (four hours at 950°C) from the sample. After each ignition, the sample and crucible were cooled to room temperature in a desiccator and weighed on a four-point balance (after Dean, 1974; Lamb, pers comm). Gloves and tweezers were used to avoid transferring moisture from skin contact with the crucibles. Bulk carbonate includes calcium carbonate and dolomite, as CO₂ evolves from dolomite at lower temperatures than calcium carbonate. Although the two have different CO₂ evolution temperatures, it is not possible to separate the carbonate species. Consequently, weight loss (g) between 550°C and 950°C is considered a bulk carbonate weight rather than a calcium carbonate weight. Additionally, carbonate-poor, clay-rich samples can give inaccurate results due to clay minerals containing up to 5% lattice OH water (e.g. a false positive of up to 5% weight loss). This is removed between 550°C - 1000°C, which can give a false positive to the results as it decreases the weight of the sample (see Dean, 1974; Lamb, pers comm).

4.6: Dating of the Quaternary sequence

Multidisciplinary dating methods were used to obtain the age of the Quaternary sequences found in the study area. The aim of dating viable sediments from the study area was to build a geochronological framework of depositional events addressing Objective 3 (Chapter 1).

4.6.1: AMS radiocarbon dating

The AMS radiocarbon method of dating measures the residual radioactivity in the sample to be dated. By knowing how much Carbon¹⁴ remains fixed in an organism or organic material at the time of dating the time of death and discovery can be determined (see Libby, 1949; Godwin, 1962; Stuiver & Polach, 1977; Ramsey, 2008; BETA, pers comm, 2015). Radiocarbon ages can be reported in their raw (uncalibrated) state or as calibrated ages. Raw radiocarbon ages are converted (calibrated) to account for fluctuations in the radiocarbon content of carbon dioxide

over time (Klein et al. 1982) which, makes raw ages comparable to calendar dates. Calibration curves that are based on independent dating methods like dendrochronology can be combined with radiocarbon dating to transform raw, uncalibrated dates into correct calendar year dates.

4.6.1.1: Sample preparation

¹⁴C AMS dating for the study area was carried out on five bulk organic sediment samples, two gastropods, and two bivalve shells (see Appendix 9, Table 2). Samples were sent to BETA Analytic, Miami, USA for analysis. The bulk organic sediment samples were dated as macrofossils (e.g. seeds, roots, plant matter) were absent or too few to use independently. Consequently, 2 g of well-humified bulk organic sediment was sub-sampled for each of the five organic samples and contaminated (e.g. modern root systems were removed if present) were removed using a binocular microscope and tweezers. Eight shells (two from each sample site) were photographed and cleaned using a binocular microscope and a fine paintbrush to remove any contaminants before being sent for dating.

4.6.1.2: Gastropod and bivalve samples

Samples (see Appendix 9, Table 2) were collected from fluvial and alluvial sediments found in cut channels (see Chapter, 6). ¹⁴C AMS dates from fossil bivalve, and gastropod shells are known to be problematic, and the following precautions were either adhered to in the field or considered when interpreting results. As seen in Figure 4.9, only intact shells were sent for AMS ¹⁴C dating. There was no abrasion or chipping on the shells, which is another good indication that the shells had not been transported and reworked. No evidence of burrowing could be seen in the sedimentary units from which the bivalves were collected.

Bivalve and Gastropod shells that form in open systems, like the silts, sands and gravels of Facies Group 5 (Chapter 8), can incorporate dissolved carbon dioxide and bicarbonates from older waters that are not in equilibrium with the atmosphere during shell formation (reservoir effect) (Price et al. 2011). Old carbon up-take can cause radiocarbon ages to be 200 – 3000 yrs older than their actual age (see Goodfriend & Stipp, 1983; Pilcher, 1991; Hedges, 1992; Pigati et al. 2010). Recently Pigati et al. (2010) measured the ¹⁴C activity of a range of small gastropods living in alluvium dominated by Palaeozoic carbonate rocks, and they found that 22% of the small species of gastropod shells did incorporate older carbon and 78% did not. They also found that ¹⁴C ages of 173 late Pleistocene fossil gastropod shells were indistinguishable from the ages of well-preserved plant macrofossil remains. Within sediment horizons, the recrystallisation and replacement of the original (fossil) aragonite bivalve or gastropod shell with neomorphic calcite can also occur after burial, giving a younger ¹⁴C AMS age (see, Magnani

et al. 2007; Webb et al. 2007; Pigati et al. 2010; Price et al. 2011). Where neomorphic calcite can be proved to be absent, fossil bivalve shells are considered reliable sources for ^{14}C ages (see Gillespie, 1997; Price et al. 2011).

BETA Analytic acid etch shells to remove contamination via carbon exchange with ambient water bicarbonate ions (Bowman, 1990). As a caveat, an acid etch will not help when aragonite has been replaced with neomorphic calcite. There was no visible sign of recrystallisation on the shells sent to BETA for dating (Fig 4.8). Gastropod shells sent for dating were within the limits of what was considered small by Pigati et al. (2010). The ^{14}C AMS ages for the bivalves (Fig 4.8) and gastropods (Fig 4.8: 7 & 8) are taken as an approximate age for the deposition of the sedimentary unit and were interpreted with the understanding that there is a broad margin for error above or below the reported date. For example, fossil gastropods shells from arid regions tend to be problematic when ages are over 30,000 yrs BP (Pigati et al. 2010).

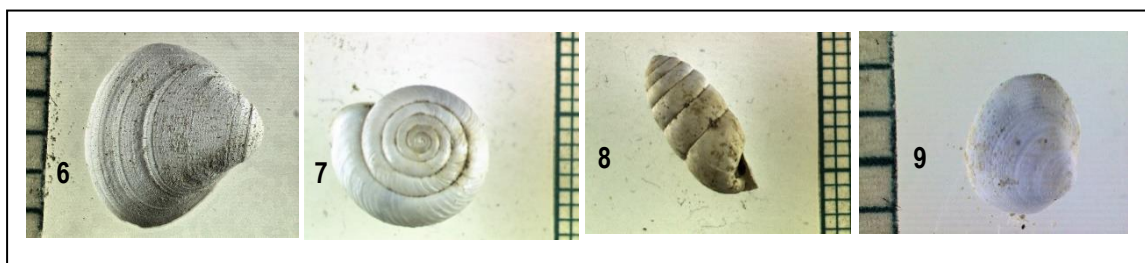


Figure 4.8: AMS Radiocarbon dated sample images, the image number, is related to sample numbers see Appendix 9, Table 2 and Chapters 6 & 8. Samples 6 (Site TB1) and 9 (Site TB3) are aquatic species, and samples 7 (Site TB10, Log 4) and 8 (Site TB9, Log 5) are land species.

4.6.1.3: Bulk organic sediment concise

Sediment samples 1 – 5 (Appendix 9, Table 2 and Chapters 6 & 8) accumulated in fluvial to meadow (see Chapter 8) depositional environments. Hence, the major organic components in samples 1 - 5 is semi-aquatic fluvial, meadow and floodplain vegetation. These environments will have allowed fluvial fines to be trapped, enriching the sediments with organic matter. Possible sources of contamination that were considered when dating the bulk sediment samples included: carbon from older or younger stratigraphic units being reworked into, and mixed with, the dated stratigraphic layer; older or younger dissolved carbonate in groundwater percolating through the sediments; modern root systems penetrating older stratigraphic units, and younger or older micro and macrofossils becoming incorporated into dated deposits. Samples were selected for dating from logged sections when: the sediment sequence was well stratified and visually appeared undisturbed, there was no obvious evidence of modern root system penetration, there was no evidence of oxidation, and when there were no apparent fissures indicating water movement vertically through the sequence. Further measures to reduce possible contamination by

BETA Analytic include, sieving the bulk samples to remove larger detritus like roots and micro and macrofossils and an acid washing to dissolve carbonates.



Figure 4.9: Modern analogue conditions for fluvial and marsh environments and organic carbon sources in clastic sediments. Barranca La Macura (Site TB5).

4.6.1.4: Reporting Radiocarbon results

All AMS Radiocarbon ages for the study area are reported as calibrated ^{14}C AMS Radiocarbon ages within the body of the text. Uncalibrated and calibrated ^{14}C AMS radiocarbon ages for all samples are given in Appendix 9, Table 2. Samples 7 - 9 are outside of BETA's calibration range and are only reported in their conventional radiocarbon date by BETA Analytic. The calibrated (calendar) ages for samples 7, 8 & 9 have been calculated using the INTCAL13 curve (Reimer et al. 2013) in CALIB (Stuiver et al. 2017) (see Table 2, Appendix 9).

4.6.2: $^{40}\text{Ar}/^{39}\text{Ar}$ dating

The basic principle of this dating method is based on the accumulation of radiogenic ^{40}Ar from ^{40}K by an electron-capture decay. The $^{40}\text{Ar} / ^{39}\text{Ar}$ dating method has its foundations in the K / Ar dating method but allows the dating of a wider range of samples that contain acceptable levels of K. The $^{40}\text{Ar} / ^{39}\text{Ar}$ method of dating can be applied to any mineral or rock that contains measurable amounts of potassium (e.g. sanidine and mica) with an age range of a few thousand years to the age of the Solar System (see Bogard, 1995; Renne et al. 1997; McDougall & Harrison, 1999). Age calculations require knowledge of the parent (K) and daughter (Ar) isotope abundances within a sample, as with the K / Ar dating method (see McDougall & Harrison, 1999). However, with the Ar / Ar

method, to avoid measuring the level of K, the sample is irradiated by fast neutrons within a nuclear reactor. The neutron flux (in the order of 10^{12} n/cm²s) produces ³⁹Ar from ³⁹K by an (n,p) nuclear reaction (McDougall & Harrison, 1999). After irradiation, the argon is thermally extracted from the samples within an ultra-high vacuum (UHV) system using either an IR laser or a furnace system. After cleaning, the isotope ratios of Ar are measured, and from the ⁴⁰Ar/³⁹Ar ratio, the age of a sample can be calculated (McDougall & Harrison, 1999). Because this dating method has such a wide application, it was particularly well suited to the study area to date samples that were expected to be older than the range of the radiocarbon and OSL dating methods. It was used here to date two tephra layers (See Table 1, Appendix 9).

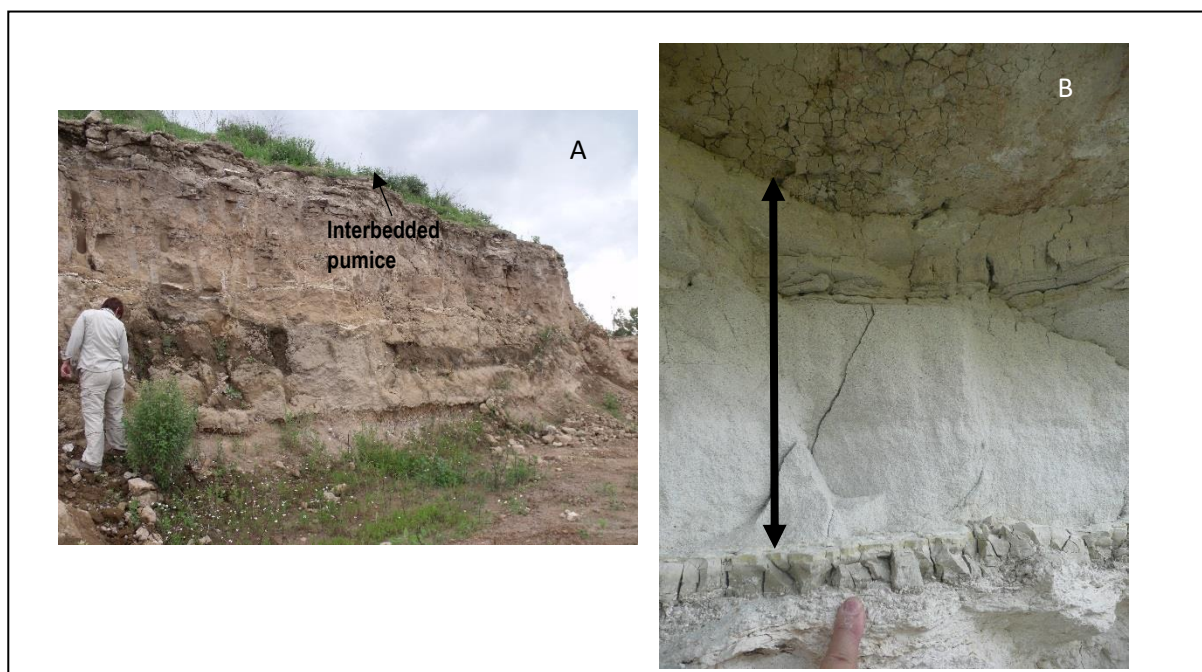


Figure 4.10: A: Facies 18d (Table 5.23) medium light grey coarse ash to lapilli from San Mateo Hill (SMH, Site TB17). B: Facies 18c (Table 5.23) white fine dacitic sandy ash, from Barranca de Colores (BC, Site TB9).

4.6.2.1: Sample preparation and measurement

The author prepared two tephra samples, one medium-light grey coarse ash to lapilli (Facies 18d, Table 5.23) collected from San Mateo Hill (Site TB17, Section 6.3) and one in-situ white fine dacitic sandy ash (Facies 18c, Table 5.23) collected from Barranca de Colores (Site TB9, Section 6.6) (Fig 4.9 and see Chapters 5 & 6), at the Scottish Universities Environmental Research Centre (SUERC). Detailed methodology for preparation for Ar/Ar of the samples can be found in Mark et al. (2011), and a summary of this is presented here. Samples of pumice (San Mateo Hill) and dacitic tephra (Barranca de Colores) collected from the field were broken up using a jaw crusher. A disc mill was used to disaggregate material and concentrate crystal sizes between 500 and 1500 μ m.

Samples were washed, sieved, magnetically separated (using a Franz Magnetic Separator) and density separated (using sodium poly tungstate at an LST of 2.63) to produce a sanidine-rich sub-sample. Sanidine (250-500 μm) was handpicked under a binocular microscope using the methods of Hynek et al. (2010) to ensure a pure separate. After leaching in dilute HF (in sealed Teflon pb beakers) and rinsing in deionised water and methanol, the grains were parcelled into Cu packets and positioned within an Al holder for irradiation. An international standard, Alder Creek Tuff sanidine (ACs, 1.2056 ± 0.0019 Ma, Renne, et al. 2011), a secondary standard referenced against the Fish Canyon sanidine age (FCs) (28.294 ± 0.036 Ma, Renne, et al. 2011), were loaded adjacent to the samples of unknown age.

Samples were irradiated for 0.17 hours in the CLICIT facility of the OSU reactor in USA. ACs grains ($n = 20$) were analysed by total fusion with a focused CO_2 laser. The J-parameter was determined from ACs. FCs was also loaded adjacent to the samples to check J-parameter accuracy. Using J-parameter measurements from ACs, and the standard ages and decay constants of Renne et al. (2011), the age for FCs overlap with the age as defined by Renne et al. (2011) indicating appropriate measurements of the J-parameter from ACs for the determination of unknown ages. Single grains of sanidine were loaded into Cu planchettes in ultra-high vacuum laser cells with double pumped ZnSe windows. Argon was released using a CO_2 laser. All gas fractions were subjected to 180s of purification with two SAES GP50 getters (one at room temperature, the other at 450°C) and a cold finger maintained at -95.5°C using a mixture of dry ice ($\text{CO}_{2[\text{s}]}$) and acetone. Argon isotope ratios (i.e., ion beam intensities) were measured using a MAP 215-50 mass spectrometer in peak jumping mode. The mass spectrometer has a measured sensitivity of 1.13×10^{-13} moles/volt. Both the extraction and clean-up processes were automated, as were the mass spectrometer peak jumping routines and data acquisition. For the proximal samples, full system blanks were measured after every two analyses of unknowns. Improved blank control was required for the distal samples, and complete system blanks were run after every single analysis (unknown and calibration). Average full system blanks \pm standard deviation ($n = 62$) from the entire run sequence was used to correct raw isotope measurements of unknowns.

Mass discrimination ($D: 1.012928 \pm 0.0007595$) was monitored by analysis of air pipettes after every five analyses ($n = 15$). The argon isotope data were corrected for backgrounds, mass discrimination, and reactor-produced nuclides and processed using standard data reduction protocols. The decay constants of Renne et al. (2011) and atmospheric argon ratios of Lee et al. (2006), the latter independently verified by Mark et al. (2011), were employed. The BGC software *MassSpec* was used for data regression. Data are displayed on ideograms and

isotope correlation plots (inverse isochron plots). The standard error on the mean (SEM) was determined for all samples that displayed a Gaussian (normal) distribution with a mean square weighted deviation (MSWD) < 1 (Chapter 6). Data were not rejected by %⁴⁰Ar*. Using these criteria, no data from all runs were dismissed.

4.6.3: Uranium-series (U - series) dating

The principle of U – series dating is based on the measurement of both the parent, ²³⁴U and daughter, ²³⁰Th, products along the decay chain of uranium (Cheng et al. 200; Frank et al. 2006). The process of decay from ²³⁴U to ²³⁰Th is part of a much larger decay chain that starts with ²³⁸U and ends in ²⁰⁶Pb. For U - series dating the ratio of ²³⁰Th/²³⁴U that was present during the samples deposition must be known or calculated (Frank et al. 2006). As time passes, the amount of ²³⁰Th increases in the sample via radiometric decay along the chain. Sample age is based on the difference between the starting ratio and the end ration of ²³⁰Th/²³⁴U measured in or calculated for the sample. Uranium isotopes are easily released, via weathering and erosional processes, from an aquifer host rock (mainly limestone) and remobilised in groundwater. Unlike uranium, the radioactive daughter product ²³⁰Th is highly reactive and not abundant in groundwater (Frank et al. 2006). As part of the process of secondary terrestrial carbonate precipitation, uranium is co-precipitated along with the carbonate (Frank et al. 2006). Within the laminations, beds and sequences of terrestrial carbonate that is deposited ²³⁴U, the decay chain starts with deposition (Frank et al. 2006). If carbonate deposition is assumed to have occurred within a closed system, and there are no starting traces of ²³⁰U, the age of the carbonate deposit can be calculated accurately (Frank et al. 2006).

The above is ideal, but, terrestrial carbonates can contain aluminosilicate, limestone particles and organic matter, which all alter the concentration of U-series nuclides in a deposit (Frank et al. 2006). Other potential problems come from none – detrital ²³⁰Th input via karstification and third-generation carbonate precipitation or, the infilling of void spaces with detritus. This method of dating was chosen because there is an abundance of carbonate deposits in the study area (see Chapter 5). Three lithified carbonate hand samples were sent to Dr Gilbert Price, University of Queensland, Australia, for U-series dating. No preparation was carried out by the author (see Section 6.6). The samples were collected from Barranca de Colores, Site TB9, Logs 1 & 2. The raw data is reported in Appendix 9, Table 3 and the results are discussed in Section 6.6.

4.7: Conclusion

The methods outlined in this chapter were applied in the study area and the laboratory. The lithostratigraphy and geochemical results can be seen in Chapters 5 - 7 and palaeoenvironmental interpretations and discussions are reported in Chapter 8. Chapter 5 characterises and describes the facies that have been identified from the Quaternary stratigraphy from the study area.

Chapter Five: Tequixquiac Facies Descriptions

5.1: Introduction

This chapter focuses on giving detailed facies type descriptions from the Quaternary sedimentary sequence that has been recorded by this research in the Tequixquiac Basin to stratify the aims and objective set out in Chapter 1. Sample by sample, bed by bed logging have been avoided within the main body of the thesis because of time limitations unless it is needed to generate a more detailed palaeoenvironmental picture. Detailed sedimentological descriptions of each of the logged sequences are however provided in Appendix 3 – 8 and interpretations of depositional environments are given in Chapters 6 – 8.

5.1.1: Facies analysis

A system of deposition develops when a specific set of environmental conditions prevail at a depositional setting (e.g. fluvial, lacustrine, marine, aeolian, glacial). Facies models encompass multiple facies datasets from “type” depositional environments allowing facies groups to be associated with a given depositional system based on the identification of a specific and limited number of facies. This is possible because depositional settings produce a unique range of three-dimensional assemblages of strata. Assemblages have characteristic geometry and facies that facilitate the identification, interpretation and reconstruction of palaeo-depositional environments (Catuneanu, 2006). Depositional systems form the building blocks of recognisable depositional environments that can be stratigraphically correlated and used to reconstruct the genetic origin of sedimentary basin fill sequences (Catuneanu, 2006).

5.2: Tequixquiac Basin sediment types and facies

Here, an example of each identified facies type is given with descriptions that include (when applicable) colour (Munsell notations added; see Appendix 2, Table 1), lithology, texture, boundary surfaces, structures, micromorphology and geometric relationships. Changes in sediment type, colour, grain size and sorting, and grain type were used to differentiate between sedimentary units and to identify a change in sedimentation, indicating changing depositional conditions. Field observations were based on sediment body form, stratigraphic position, landscape relationship, colour, lithofacies (codes Table 5.1), grain size (Fig 5.1, Table 5.2), maturity, hardness, texture, bedforms (Table 5.3), and fossil content following the criteria set out in Sections 4.2 – 4.5, Tables 4.1 – 4.16 and Figs 4.1 – 4.4). Additional micromorphological analysis of carbonate and mixed clastic-carbonate sediments (Tables 5.4 & 5.5), that again looked at the characteristics listed above, was a further step taken in the

laboratory to identify different facies types correctly. Abbreviations used throughout the following chapters to characterise bed types and sedimentary structures are explained in Chapter 4 and Tables 5.1 – 5.5.

| PARTICLE DIAMETER | | | | CLASTICS | | |
|-------------------|---------|--------|-------------------------------|-----------|----------|--------|
| m | mm | Φ | | | | |
| 10^0 | 2048 | -11 | micrometres (μm) | v. large | boulders | gravel |
| | 1024 | -10 | | large | | |
| | 512 | -9 | | medium | | |
| | 256 | -8 | | small | | |
| 10^{-1} | 128 | -7 | | large | cobbles | |
| | 64 | -6 | | small | | |
| | 32 | -5 | | v. coarse | | |
| 10^{-2} | 16 | -4 | | coarse | pebbles | |
| | 8 | -3 | | medium | | |
| | 4 | -2 | | fine | | |
| | 2 | -1 | v. fine | | | |
| 10^{-3} | 1 | 0 | v. coarse | sand | | |
| | 0.5 | +1 | coarse | | | |
| | 0.25 | +2 | medium | | | |
| 10^{-4} | 0.125 | +3 | fine | | silt | |
| | 0.0625 | +4 | v. fine | | | |
| | 0.0312 | +5 | v. coarse | | | |
| | 0.0156 | +6 | coarse | | | |
| 10^{-5} | 0.0078 | +7 | medium | clay/mud | | |
| | 0.00390 | +8 | fine | | | |
| | 0.00195 | +9 | v. fine | | | |
| | | | 2 | | | |

Figure 5.1: Grain size classification used by this research for carbonate and clastic rocks (from Miall, 2016).

| Bed code | Description |
|----------|---------------------|
| C | Clay |
| Si | Silt |
| sSi | Sandy silt |
| M | Mud (clay and silt) |
| sM | Sandy mud |
| S | Sand |
| siS | Silty sand |
| G | Gravel |

| | |
|----|-------------|
| vf | Very fine |
| f | Fine |
| m | Medium |
| c | Course |
| vc | Very coarse |
| s | Small |
| lg | Large |
| vl | Very large |

| Structure | | Feature | |
|-----------|--|---------|------------------|
| mcl | Micro cross-lamination < 1 mm thick | cv | Calcite vein |
| mch | Micro channel form < 10 mm wide | nod | Carbonate nodule |
| mif | Micro-fault/fracture < 3 mm thick | ruc | Rip-up clast |
| fc | Fluvial channel | wr | Wave rippled |
| tcb | Trough cross bedding | ext | Extraclasts |
| hcs | Hummocky cross-stratification | int | Intraclasts |
| ch | Chaotic bedding | mot | Mottling |
| lca | Load casts | | |
| dc | Desiccation cracks (vertical jointing) | | |
| imc | Infilled mud crack | | |

| | |
|--------|--------------------------------------|
| CmLs | Calc-mudstone |
| miM | Micritic mudstone |
| miS | Micritic sand |
| Mmi | Muddy Micrite |
| SMi | Sandy Micrite |
| PeLs | Peloidal Limestone (pelleted) |
| PiLs | Pisolitic Limestone |
| InclLs | Intraclastic Limestone |
| BrLs | Brecciated Limestone |
| ShBLs | Shocked-brecciated Limestone |
| StagLs | Agglutinated Stromatolitic limestone |
| StmLs | Stromatolitic Limestone |
| FraLs | Framestone Limestone |
| CalLs | Calcrete |

5.3: Terrestrial limestone facies

Carbonate sediments collected from the study area are classified based on the textural, compositional, and petrographic analysis. Micromorphological data is supported by geochemical and LOI analysis. A sedimentary deposit is classified as a limestone here if its TIC is > 50% (per Tucker, 2003). Limestone samples collected from the study area have TIC percentages (g) between 50 – 90% and TOC between 5 – 17% (see Chapters 6 & 9 and Appendices 11). Most of the hand samples collected for analysis show a degree of post-depositional alteration and in some cases tertiary karst features. Examples of the Tequiquiac Basins Limestone facies are given below.

5.3.1: Facies 1, Framestone limestone

5.3.1.1: Description

Framestone limestones (see Table 4.14 for facies definition and D'Argenio et al. 1981; Pedley, 1992; Golubic et al. 1993) are freshwater, autogenic carbonate deposits that have an organic macrophytic in-situ framework (Cipriani et al. 1977; Pedley, 1990, 1992; Ford & Pedley, 1996; Flügel, 2010; Capozzoli et al. 2013).

They form through continuous freshwater circulation conditions that provide nutrients and replenish CaCO₃ enabling the precipitation of low-Mg calcite cement around an organic framework that preserves deposits (Flügel, 2010). Secondary framework structures come from organisms colonising exposed surfaces (e.g. Oscillatoriaceae cyanobacteria, diatoms, insect larvae) (Flügel, 2010). Shelly fauna is common (e.g. ostracods, gastropods and bivalves (Flügel, 2010)). Calcite fringe cement and peloids are related to biological activity linked to prokaryote-microphyte biofilms (see Pedley, 1990) and the presence of organic detritus (Flügel, 2010). Deposits are commonly associated with shallow fluvial (see Table 4.8), marginal lacustrine (Table 4.10 & 4.11, Figs 4.2 & 4.3) marsh and spring depositional environments (see Tables 4.8, 4.10, 4.11, 4.13, 4.15 and Pedley, 1992, 1999, 2009; Ford & Pedley, 1992; Pedley et al. 1996; Pedley et al. 2009; Flügel, 2010; Capezzuoli et al. 2013).

| Table 5.5: Suffixes used for carbonate and mixed carbonate and clastic sedimentary structures and grains (see Table 4.4 & 4.6) | |
|---|--|
| mi | Micritic |
| mfc | Micritic fringe cement |
| pe | Peloid |
| on | Oncoid |
| oo | Ooid |
| pi | Pisoid |
| inc | Intraclasts (can include bio (bic), litho (lic) and phytoclasts (phy)) |
| spc | Sparry calcite cement |
| dr | Drusy calcite cement |
| bf | Biofilm |
| stm | Stromatolitic layers |
| ibf | Incipient biofilm laminae |
| bbf | Broken biofilm fragments |
| bl | Broken micritic silt laminae |
| bi | Bioturbation |
| sh | Gastropod shell |
| rc | Root casts |
| rv | Root Void |
| rt | Root trace |
| mcms | Micrite coated macrophyte stems |
| od | Organic detritus |
| mg | Manganese |
| mlp | Moldic porosity |
| bv | Bubble voids |
| shb | Shocked brecciated |
| br | Brecciated |
| mif | Micro-fault/fracture |
| cv | Calcite vein (secondary) |
| hpc | Salt hopper crystal |
| vol | Volcaniclastics |
| kst | Karstification |
| lc | Lamina calcrete crust |
| nod | Nodules |

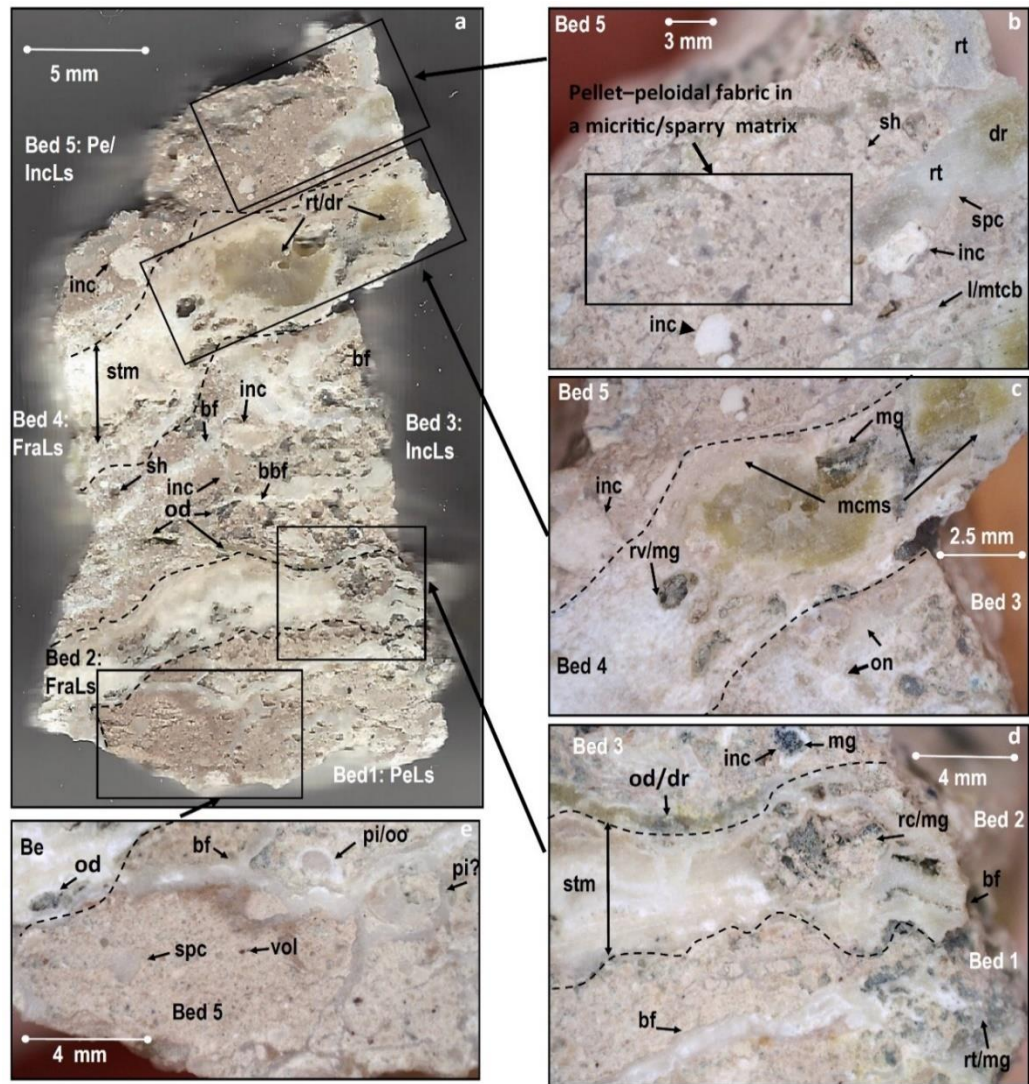


Figure 5.2: Example of framestone facies from Site TB9 a) Bed 19, Barranca de Colores (BDC) sample BDC T2 (see Chapter 6, Fig 6.33, and Appendix 4, Table). See Table 5.6 for bed descriptions.

5.3.1.2: Defining characteristics

Under fast freshwater flow conditions; micrite fringe cement (around root stems and interbedded within biofilm layers), biofilms, peloids (see Figs 4.4 & 4.6), root moulds, casts and voids (see Table 4.6), and vegetation litter or detritus (Flügel, 2010) define deposits. Biofilms can be poorly developed because of increased water velocity (Lorch & Ottow, 1985; Pedley, 1990; Flügel, 2010) and micritic fringes can be absent or weakly formed (Pedley, 1992; Flügel, 2010). Under sluggish water flow conditions; thick micritic fringes and bladed calcite fringes are narrow or absent (Pedley, 1992; Pedley, 2009; Flügel, 2010).

Table 5.6: Example of framestone facies from Site TB9. Bed descriptions from site TB9, Log 2, sample BDC T2, (see Fig 5.2, Fig 6.33 and Appendix 4, Table 2).

| Facies name | Facies description | Sub-facies description | Post depositional facies |
|---|---|--|---|
| Bed 5: Pelleted-peloidal | Greyish-pink (5R 8/2) micritic matrix with irregularly shaped peloids (<1 mm in diameter) (Fig 5.2 a & b). Large intraclasts at the base of the bed up to 3 mm in diameter and some micro trough cross-bedding. | Silt intraclast (<3 mm in diameter), gastropod shell, macrophyte traces with very light grey (N8) sparry calcite fringe cement, and volcanoclastic input (2 - 5%). | Drusy calcite cement. Sparry cement patches (<5%). |
| Bed 4: Micro-framestone limestone (immature). | Very light grey (N8) wavy, biofilm layers that have outer micritic cement fringes. Contains large (3 - 4 mm) micrite coated macrophyte stem (Fig 5.2 a & c). | Volcanoclastic input (2 - 5%) | Drusy calcite and root voids coated or partially filled manganese |
| Bed 3: Intraclastic limestone | Yellowish-grey (5Y 8/1) lithoclasts <3 mm in diameter within a greyish-pink (5R 8/2) silty micritic matrix. The bed contains organic detritus (Fig 5.2 a & c). | Gastropod shell, oncoids, biofilm laminae and volcanoclastic input (2 - 5%) | Organic detritus has been replaced by either manganese or drusy calcite. Sparry cement (<5%). |
| Bed 2: Framestone limestone (immature). | Very light grey (N8) biofilm build-ups around macrophyte root casts (Fig 5.2 a & d). | Volcanoclastic input (2 - 5%) | Macrophyte roots have been lined or filled with manganese. |
| Bed 1: Pelleted-peloidal | Greyish-pink (5R 8/2), micritic silty fine sand matrix. Pisoids are irregularly shaped (<1 mm in diameter). Fine biofilm laminae (<2 mm) (Fig 5.2 a, d & e). | Volcanoclastic input (2 - 5%) Peloids and ooids. | Manganese. Sparry cement patches (<5%). |

5.3.1.3: Tequixquiac Framestone deposits (See Table 5.9 for facies summary)

Framestone deposits in the study area consist of peloidal textures (Fig 5.2 a & b), micro and macrophyte root traces, voids, and root casts with micritic and sparry (less common) fringe cement (Fig 5.2 a – d, Fig 5.2 a - d), organic detritus, biofilms and gastropod shell intact and fragmented (Fig 5.2 a & b). The matrix can be calc-mudstone (Facies 3) or mixed carbonate-clastic (Facies 8 – 10). Micro and macrophyte root systems and organic detrital components are usually replaced with drusy calcite or sparry calcite cement and micritic silt. Peloidal fabrics are pelleted to clotted, and within these, there can be occasional micritic silt intraclasts (< 5 mm in diameter). Volcanoclastics are found in most deposits (2 - 5%), and there are varying degrees of clastic silt input (2 - 50%). Deposits are often interbedded with calc-mudstones (see Fig 5.3), Intraclastic limestones (see Fig 5.2 a & c and Section), peloidal pack and wackestone (see Fig 5.2 a & b), stromatolitic limestone (see Fig 5.4), paleosols, calcrete (Section 5.7), siltstones, claystone (see Section 5.5) and basaltic-andesite (Facies 15), andesitic (Facies 16) and dacitic (Facies 17) tephra layers (Chapter 7). Deposit thickness range from centimetres (Figs 5.2 a & c, Table 5.6; Fig 5.6, Table 5.10), up to one meter (Fig 5.3). Deposits are laterally discontinuous and occur as outcrops that pinch out towards the lateral limits of sequence.

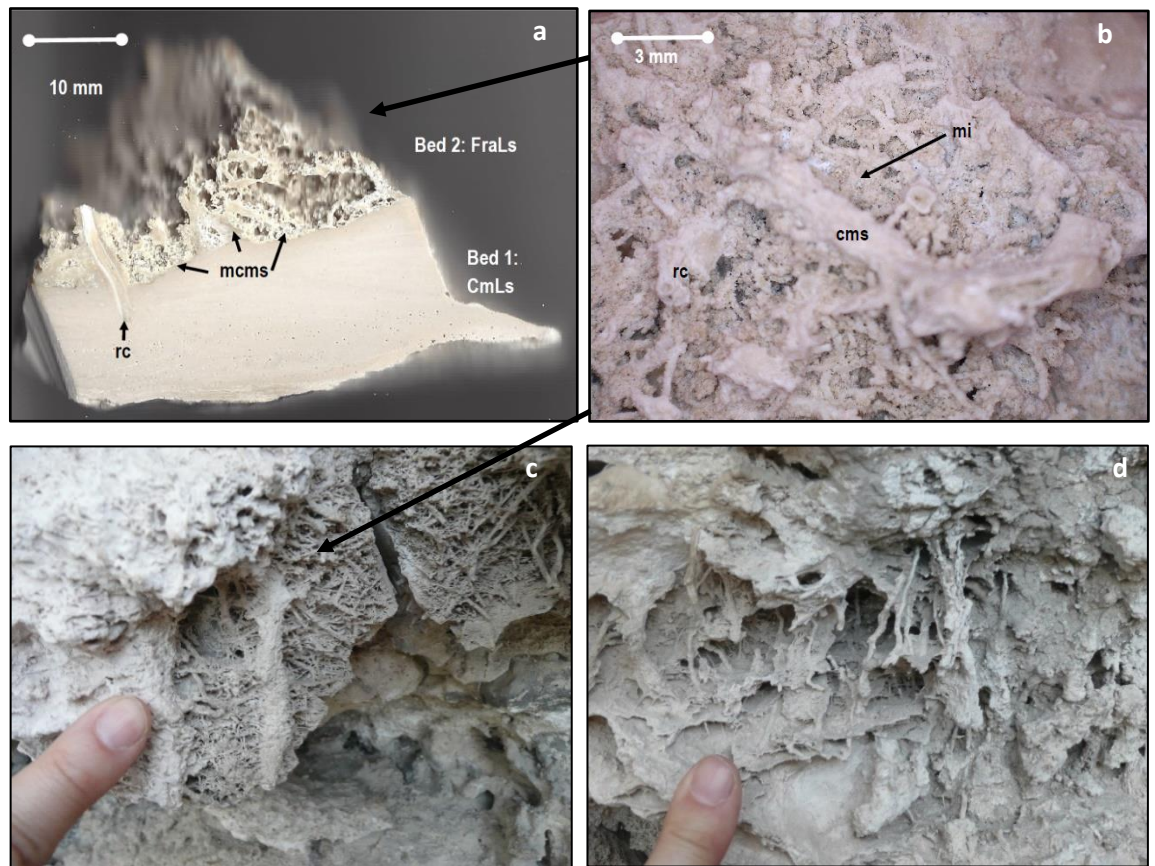


Figure 5.3: Examples of **a)** Microdetrital limestone (Bed 2), Framestone limestone (bed 1) (Bed 5, sample ASH T7) **b)** Framestone limestone (sample ASH T7). **c)** The upper surface of sample ASH T7 (bed 2 a & b) in-situ before collection (see Table 5.7 for bed deceptions). **d)** section above sample ASH T7, Log 2 (samples ASH T8 to T10). Sample and images are from site TB12, Log 2 (Appendix 4, Table 6).

Table 5.7: Examples of bed descriptions from site TB12, Log 2, sample ASH T7, (Appendix 4, Table 6). See Figure 5.3 a, b & c images of the beds.

| Facies name | Facies description | Sub-facies description | Post depositional features |
|--|---|---|---|
| Bed 2: Framestone limestone (top) | Micro and macrophytic root casts that sit on top of and penetrate the surface of bed 1 (Fig 5.3 a). Micritic silt infill the void spaces (Fig 5.3 a, b & c) | Volcaniclastic input (2 - 5%) | Organic material replacement with micritic silt |
| Bed 1: Sparse biogenic Calc-mud stone (base) | Microdetrital carbonate silt with micro-laminations, although they are poorly formed (Fig 5.3 a). | Volcaniclastic input (2 - 5%). Shell fragments (see Fig 5.7). Root penetration of the upper surface of the bed. | None-visible |

5.3.2: Facies 2 a & b, Stromatolitic limestone

5.3.2.1: Description

Carbonate stromatolites are laminated, benthic, microbial mediated (biofilms, mats) build-ups of carbonate that differ markedly in origin, constituents and laminae quality (Riding, 2000). Bacterial biofilms have habitat tolerances that are suited to stressed environments and harsh environmental conditions, for example, hypersaline

ponds, hot springs, intertidal sediments, exposure to high UV and alkaline lakes and springs (Deho, 1994; Costerton et al. 1995; Westall et al. 2000). Stromatolitic laminations usually consist of siliciclastic and carbonate particles (variable sizes but predominantly silt) trapped or blocked by microbial build-ups (i.e. biofilms, mats) as sediment passes across the uneven surface of the biofilm or mat (Riding, 2000; Westall, 2000). Hiatuses in clastic sedimentation encourage microbial colonisation and growth (Noffke, 1998; Riding, 2000). Development is affected by the type and species of microbe present in the biofilm, the type and bulk medium of the substrate, fluid flow rates, temperature, pH, and nutrient supply (Westall, 2000). Within depositional settings, even ephemeral accretion can promote layering and laminae related to seasonal growth, periodic sedimentation or both (Braga et al. 1995; Riding, 2000). Deposits are commonly associated with fluvial (see Table 4.8 and Pedley, 1990; Pedley, 2009; Arenas-Abad et al. 2010) and nearshore lacustrine (see Table 4.10, 4.11 and Fig 4.2 and Pedley, 1990; Pedley, 2009; Gierlowski-Kordesch, 2010) depositional environments (see also Tables 4.8 & 4.10).

5.3.2.2: Defining characteristics

Biofilm fabrics can be smooth, ropy, fibrillar (cell fibres and filaments), mamillated or granular, all of which can build complex microstructures (see Tables 4.8, 4.10, 4.11, Figs 4.14, 4.15 and Westall, 2000) and consist mainly of skeletal heads centimetres to meters in diameter (see Tables 4.5, 4.6, 4.7, Fig 4.1 and Pedley, 1990). The heads are made up of cement fringes (sparry and micritic) that form in close cooperation with Oscillatoriaceae cyanobacteria layers (Table 4.6). Coarse detrital carbonate intraclasts and oncoids (Table 4.6 & 4.4) are often associated (Pedley, 1990; Riding, 2000). Wavy and ruffled laminae can suggest sub-areal exposure, drying and desiccation of the sequence (Riding, 2000; Westall, 2000). Some stromatolitic sequences are purely precipitated (no binding or baffling) and made up of microbial laminae with precipitation substrates provided by bacteria that degrade organic matter below the mat surface (Riding, 2000) (e.g. Tufa).

5.3.2.3: Tequiquiac Stromatolitic limestone (See Table 5.9 for facies summary)

Deposits thicknesses in the study area range from millimetres up to 1 m. They can have wavy to horizontal (Fig 5.4 a, d & e), sparry (<1 mm), and micritic laminae (<2 mm) that can alternate with red-brown to olive clastic clayey and silt (mixed carbonate-clastic and clastic beds Fig 5.5 b) (< 3 mm) and micrite fringe cement (<5 mm) (Facies 2a). The alternations likely represent seasonal deposition (Facies 2b) with vertical jointing suggesting exposure. Bed thicknesses are < 2 m (see Fig 5.5 a & b) and interbeds of mixed carbonate-clastic and clastics (see Fig 5.17, Table 5.17) are common.

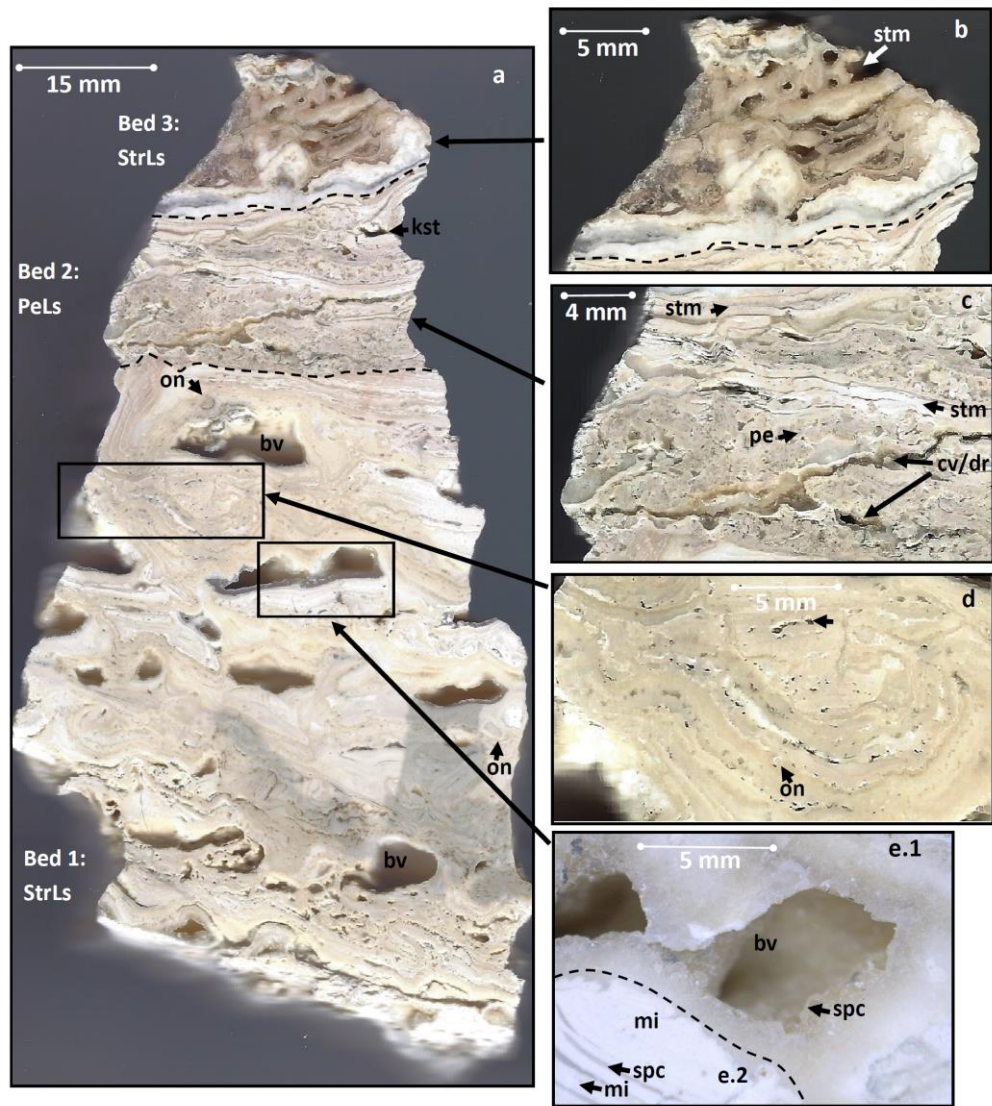


Figure 5.4: Example of stromatolitic limestone from the study area. Site TB12, Log 2, Bed 5, corresponding to sample ASH T11 (Appendix 4, Table 6). See Table 5.8 for bed descriptions.

5.3.3: Facies 3, Calc-mudstone

5.3.3.1: Description

The term micrite was originally proposed to be a generic term used to describe lithified, mechanically deposited lime mud (Folk, 1959). Today the term is used by most authors to describe non-genetic rock composed of fine-grained calcite crystals and particles formed in place, or through the accumulation of fine-grained pre-existing carbonate material. This includes microcrystalline, and micrite cement precipitated as micron-sized Mg-calcite (see Table 4.4 and Wilber & Neumann, 1993; Flügel, 2010).

5.3.3.2: Defining characteristic

Micrite is primarily formed by accumulations of microdetrital carbonate particles of varied origins (Tables 4.4, 4.5 and Flügel, 2010). Deposits are closely associated with lake (sublittoral to profundal zone) (Tables 4.10 &

4.11 and Figs 4.2 & 4.3 and Gierlowski-Kordesch, 2010), pond, marsh (Table 4.15 and Pedley, 2009) and fluvial floodplain environments (see Table 4.8 and Arenas-Abad, 2010). Micrite forms in thick sheet deposits on slopes and infilling framestone (Facies 1) bio-frameworks (Flügel, 2010). Fabric textures can be grainy or clotted (Pedley, 1990). Deposits can form through physiochemical precipitation, biologically induced precipitation, biologically controlled precipitation, the disintegration of benthic and pelagic biota, erosion and abrasion, and through diagenesis (Arenas-Abad, 2010).

Table 5.8: Example of stromatolitic limestone bed descriptions from the study area, site TB12, Log 2, Bed 5, corresponding to sample ASH T11, stromatolitic limestone, (Appendix 4, Table 6). For images of beds, see Figure 5.4.

| Facies name | Facies description | Post depositional features |
|-----------------------------------|---|--|
| Bed 3: Stromatolitic limestone | Bed 3 is like bed 1. Stromatolitic laminae that appear to have had more clastic silt input because of the greyish pink (5R 8/2) hue to the laminations (Fig 5.4 a & b). | None |
| Bed 2: Peloidal limestone | Greyish pink (5R 8/2) and yellowish-grey (5Y 8/10) peloids <1 mm in diameter within a yellowish-grey (5Y 8/10) micritic matrix (<5%) (Fig 5.4 a & c). | The lower stromatolitic layer has been replaced post-depositionally by sparry, slightly drusy calcite, possibly under vadose conditions. There is some early-stage karstification along the edges (Fig 5.4 a & c). Sparry patches (<3%). |
| Bed 1: Stromatolitic limestone | Biofilm laminae alternate between yellowish-grey (5Y 8/1), slightly granular layers >4 mm, pale greenish-yellow (10Y 8/2) laminae <4 mm and clearer, white (N8), laminae <0.5 mm, there are also very fine (< 0.1 mm) black (N1) laminae that may be voids (Fig 5.4 d). Bubble voids create moldic porosity related to degassing and photosynthetic processes. Void spaces range in diameter from 0.2 mm – 15 mm (Fig 5.4 a & e). | Post-depositional bubble void lining with sparry calcite, and partial infill with laminated micrite >2 mm and sparry calcite laminae < 1 mm thought to be related to microbes (Fig 5.4 a & e 1 & 2). |

5.3.3.3: Tequixquiac calc-mudstone deposits (See Table 5.15 for facies summary)

In the study area, micro detrital carbonate in the form of calc-mudstone and unlithified micrite occurs in all logged limestone and unlithified carbonate deposits (see Fig 5.2 – 5.8 and Tables 5.6 – 5.10). Deposits can be laterally extensive or terminate in an outcrop and form layer-cake stratigraphy with plane to wavy contacts that can be graded or disconformable or paraconformable. The homogenous beds likely represent stable physical, chemical and biological conditions. Beds thicknesses range from 1 mm up to 0.50 m. Thicker beds tend to be massive with occasional faint laminations, bioturbation, root traces and shell (Figs 5.6 - 5.8, Table 5.10) and this is thought to represent more constant physical, chemical and biological deposition under low energy condition conditions (e.g. nearshore to basinal lacustrine or pool environments and calmer fluvial environments). Beds with internal bedding structures and with or without root traces, shell and dissolution features suggest shallow ephemeral, more changeable depositional environments.



Figure 5.5: Field examples of stromatolitic limestone from the study area **a: Facies 2a, Greyish pink (5R 8/2) stromatolitic limestone with peloidal beds** Site TB12, Log 2, Bed 5 (see Appendix A4, Table 6). Hand sample collected from the bed is shown in Figure 5.4 and bed descriptions are given in Table 5.8. **b: Facies 2b, Greyish yellow green (5GY 7/2) agglutinated (?) stromatolitic limestone.** Site TB9, Log 2, Bed 1, BDC T32 (see Appendix 4, Table 2 and Chapter 6, Fig 6.33). **c & d:** Barranca la Botica (Figs 8.1 & 8.9) fluvial tufa? (see Table 4.8) lining the bottom of the barranca (Site TB6).

5.3.4: Facies 4, Peloidal limestones

5.3.4.1: Description

Peloidal limestone is associated with algal remains, faecal remains and physiochemical processes (see Tables 4.4 & 4.6 for description) (Tucker & Wright, 1990). Peloidal build-ups are often interbedded with and infill the framework of phytomerms (see Section 5.3.1).

| Table 5.9: Summary of the recorded Tequiquiac bio-mediated limestone and carbonate facies, formed in-situ (see Table 5.4 for bed codes) | | | | | |
|---|--|---|---|--|--------------------------|
| Facies name | Key facies description | Range of sub-facies description | Range of post-depositional features | Associated facies | Stratigraphic facies key |
| Facies 1, Framestone limestone (FraLs). | <ul style="list-style-type: none"> -Can be yellowish grey (5Y 8/1), white (N9), moderate pink (5R 7/4) calc-mudstone and peloidal matrix. -Macrophyte root and leaf traces and casts (1 – 10 mm in diameter). -Micritic fringe cement (white (N9)) -Isolated biofilm lamina -Peloids in a micritic matrix -Deposits are laterally discontinuous (e.g. localised fluvial, marsh and lacustrine deposits) -Internal bedding can be massive or comprise simple or composite bed sets | <ul style="list-style-type: none"> -Occasional oncolites and ooids -Volcaniclastics 5-10% -Moldic porosity -Shell fragments -Micritic silt filled micro-channels -Organic detritus replaced by drusy calcite -Sparry calcite fringe cement occur around macrophytes but are less frequent than micrite fringe cements <1 mm | <ul style="list-style-type: none"> -Clastic silt infills along weaknesses and joints. -Brecciation through wetting and drying? -Calcite vein re-precipitation and replacement of the original sediment along weaknesses in the bed, i.e. bedding planes and root traces. -Sparry and drusy cements occur infilling or lining; drusy calcite is sometimes brilliant green (5G 6/6) -Root voids coated with manganese or sparry calcite. | <ul style="list-style-type: none"> -Calc-mudstone -Stromatolitic boundstone -Intraclastic limestone -Peloidal limestone -Muddy micritic that replaces the calc-mudstone matrix -Muddy micrite -Mudstone | |
| Facies 2a, Stromatolitic limestone (StmLs) | <ul style="list-style-type: none"> -Bio-mediated lamina can be alternations of yellowish grey (5Y 8/1), moderate pink (5R 7/4), pale red (5R 6/2), greyish pink (5R 8/2), greenish yellow (10Y 8/2), and yellowish grey (5Y 8/1) beds (usually <5 mm) of: - Micritic (calc-mud) fringe cements (<5 mm) - Sparry calcite fringe cements (<1 mm) -Moldic porosity (bubble voids) created by degassing. -Gypsum layers that have been replaced -Wavy to horizontal continuous and discontinuous lamina - Deposits are laterally discontinuous (e.g. localised fluvial, marsh and pond deposits) - Internal bedding can be massive or comprise simple or composite bed sets | <ul style="list-style-type: none"> -Root traces, casts and voids -Channel forms -Micro cross-bedding -Pisoliths -Sparry calcite crystals in cement -Chert formation through tephra alteration -Intraclasts -Gypsum formation | <ul style="list-style-type: none"> -Brecciation -Shock brecciation -Later clastic silt infill along weaknesses and joints. -Micritic silt and sparry calcite development in void spaces -Replacement of gypsum layer with calcite cement or drusy calcite cement -Vertical jointing and desiccation of silts and clays | <ul style="list-style-type: none"> -Calc-mudstone -Biogenic calc-mudstone -Framestone -Mud -Muddy micrite -Micritic mud | |
| Facies 2b, Agglutinated, stromatolitic limestone (StagLs) | <ul style="list-style-type: none"> -Bio-mediated lamina that can be yellowish grey (5Y 8/1), moderate pink to white (N9) (<5 mm) alternate with: -Greyish yellow green (5GY 7/2) and moderate red (5R 5/4) sandy or muddy micrite, and sand or mud lamina (< 10 mm thick). - Wavy and horizontal continuous and discontinuous lamina | None-observed | <ul style="list-style-type: none"> Vertical jointing and blocky texture to the clastic and mixed carbonate - clastic sediments. Some of which are small balls that have been coated with micrite. | <ul style="list-style-type: none"> -Mud -Muddy micrite -Micritic mud -Calc-mudstone -Biogenic calc-mudstone -Framestone | |

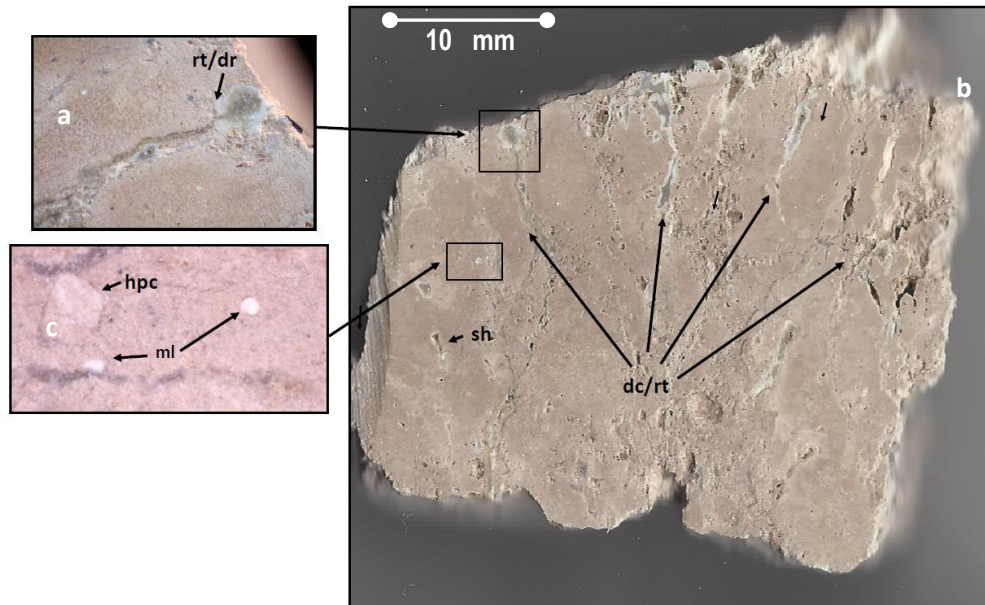


Figure 5.6: Example of calc-mudstone from the study area, site TB9, Log 2, Bed 16, BDC T5 (see Appendix 4, Table 2, and Chapter 6). For bed descriptions, see Table 5.10.

| Facies name | Facies description | Sub-facies description | Post-depositional features |
|----------------------|---|---|--|
| Bed 1: Calc-mudstone | Greyish-pink (5R 8/2) fine, massive mud (Fig 5.6 c). (Fig 5.6 c). | The mid-bed has a shell fragment (Fig 5.6 c). The speckled texture seen in Fig 5.6 b suggests aeolian fall-out. | Salt hopper crystal, desiccation features (ca. 7 mm thick) (Fig 5.6 a & c), and root penetration mostly in the upper bed (Fig 5.6 b & c). The desiccation cracks have been infilled with sparry and in some cases drusy calcite cement. There is probably some karstification around the outer edges of the sample along weaknesses created by desiccation and roots; this is presumed to be a much later feature. |

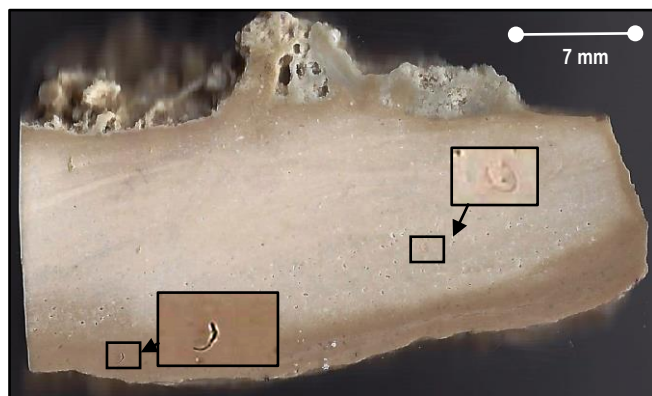


Figure 5.7: Example of calc-mudstone from the study area, sparse biogenic calc-mudstone, with shell (enlarged). Sample from site TB12, Log 2, Bed 4, sample ASH T7 (Appendix 4, Table 6). See Figure 5.3 also which shows the other half of this cut hand sample and Table 5.7 for bed descriptions.

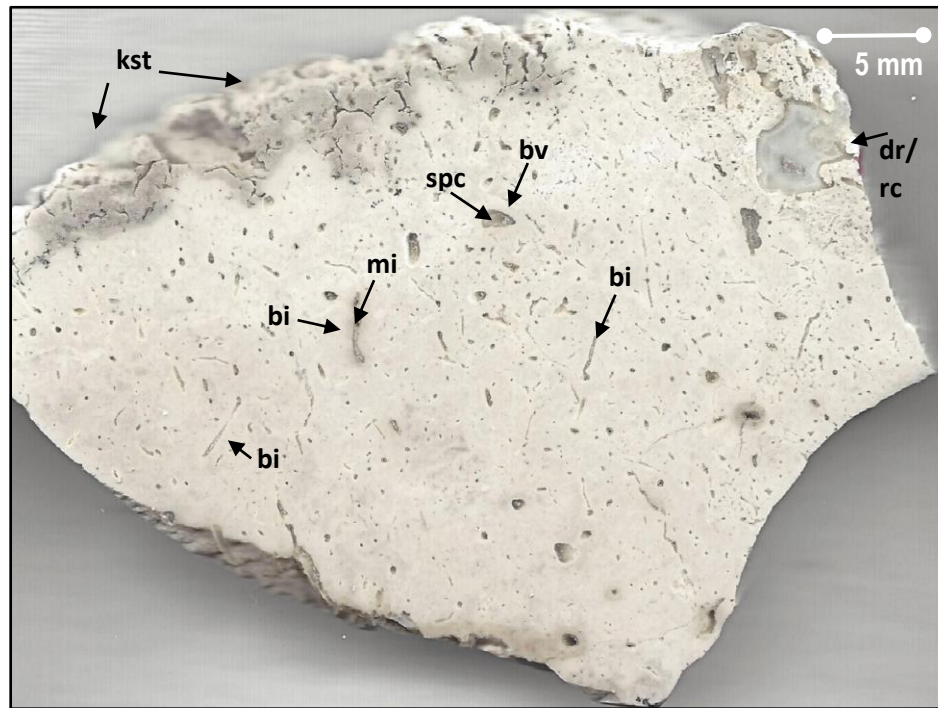


Figure 5.8: Example of calc-mudstone from the study area. White (N9) to very light grey (N8) biogenic calc-mudstone. Calc-mudstone with scattered bioturbation burrows (<1 mm in diameter), and organic detritus that are represented as void spaces with sparry calcite fill. The upper bed (5 mm) is medium grey (N5) and has desiccation features and manganese clusters. The upper right-hand side of the sample has a large (6 mm in diameter) root trace filled with drusy cement. Sample from Site TB13, Log 1, Bed 8 TLAP (Tlapanaloya) T31 (see Appendix 4, Table 7).

Peloids are found in most terrestrial carbonate depositing systems including, palustrine and lacustrine (see Tables 4.10 to 4.13, Figs 4.2 & 4.3 and Alonso-Zarza & Wright, 2010; Gierlawski-Kordesch, 2010); spring systems (see Table 4.15 and Ford & Pedley, 1996; Jones & Renault, 2010), fluvial (see 4.8 and Manzo et al. 2012), and calcrete (see Fig 4.4, Table 4.16 and Alonso-Zarza & Wright, 2010).

5.3.4.2: Defining characteristics

Peloids (smooth to free-form, see Table 4.6) are frequently found grouped in polynucleate masses 10 – 70 µm in diameter (Pedley, 1990). Beds can be grain-supported (particularly within phytoherm frameworks), but compacted textures can appear clotted and fused (Pedley, 1990).

5.3.5.3: Tequixquiac peloidal limestone (see Table 5.15 for facies summary)

In the study area, peloidal fabrics are pelleted to clotted, and grain supported to matrix-supported with varying amounts of sparry cement (usually <10%) (Figs 5.9 & 5.10, Tables 5.11 & 5.10). Beds are horizontal, and contacts are straight to wavy. Bed thicknesses vary but are usually < 0.05 m, and they occur as part of layer-cake stratigraphy associated with limestone sequences. Peloidal deposits in the study area are found in association with

framestone (Facies 1) stromatolitic (Facies 2) and pisolitic (Facies 5) limestone deposits (see Sections 5.3.1, 5.3.2 & 5.3.5).

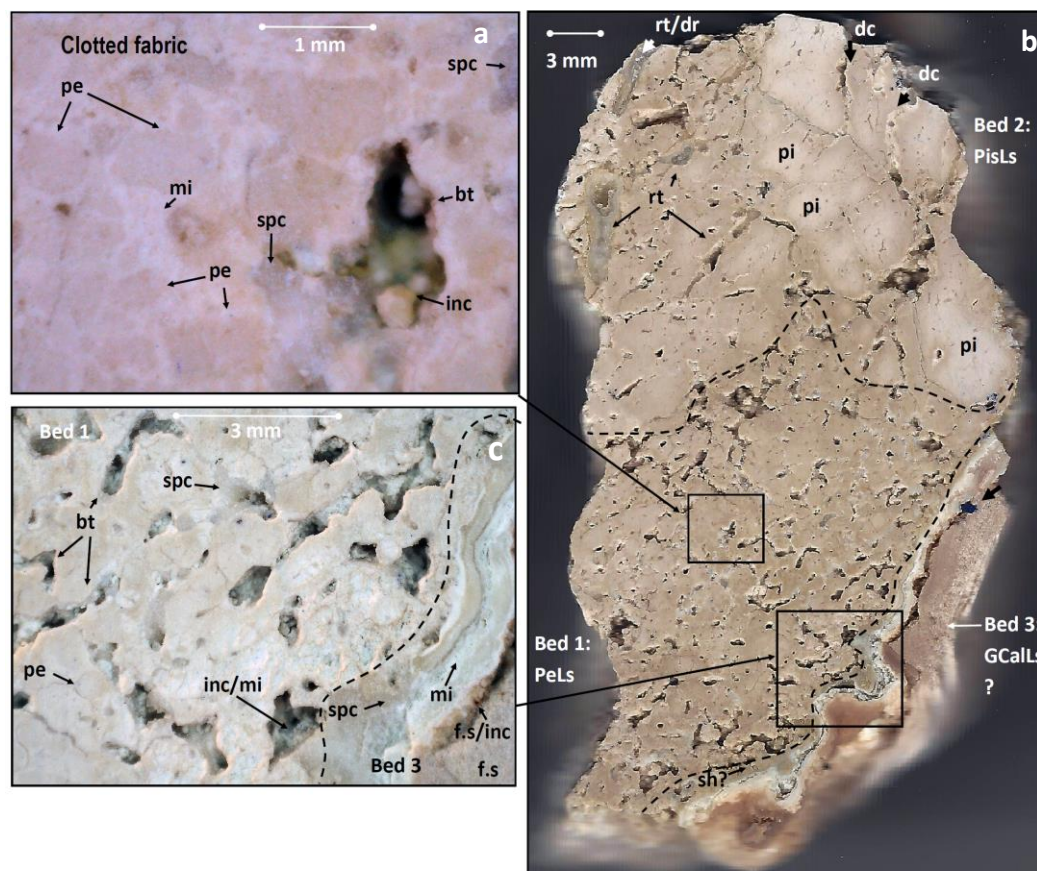


Figure 5.9: Example of peloidal limestone and associated facies from the study area. Sample from Site TB9, Log 2, Bed 11, BDC T13 (Appendix 4, Table 2 and Fig 6.33). See Table 5.11 for bed descriptions.

Table 5.11: Example of peloidal limestone bed descriptions and associated facies from site TB9, Log 2, Bed 11, BDC T13 (Appendix 4, Table 2 and Chapter 6). See Figure 5.9 for images of the beds.

| Facies name | Facies description | Sub-facies description | Post depositional facies |
|-------------------------------|--|-----------------------------|--|
| Bed 3: Calcrete | None | None | Desiccation cracks infilled with layers of reprecipitated white (N9) micrite and pinkish-grey (5YR 8/1) clastic silty fine sand (Fig 5.9 b & c). |
| Bed 2: Pisolitic limestone | Large, white (N9) freeform pisoids that are <5 mm in diameter within a pinkish-grey (5YR 8/1) micritic (mi) cement (Fig 5.9 b). | None | Post-depositional root penetration and root cast infilled with drusy calcite. Desiccation cracks are present in the upper bed (fig 5.9 b). |
| Bed 1: Peloidal limestone | Rounded to irregular yellowish-grey (5Y 8/1) peloids (<1 mm in diameter) that form a clotted fabric. Matrix is white (N9) - pinkish-grey (5YR 8/1) bioturbated micritic silt (Fig 5.9 a, c & d). | Occasional shell fragments. | None |

5.3.5: Facies 5, Pisolitic limestone

5.3.5.1: Description

In terrestrial settings, pisoids can be used as indicators of water energy and salinity. Variations to the shape and lamination of pisoids can indicate continuous and discontinuous flow regimes and changes between high and low water energies (Flügel, 2010). Pisolitic deposits are also commonly associated with elevated salinity levels in freshwater environments that have evolved to brackish conditions (Flügel, 2010).

5.3.5.2: Defining characteristics

In lacustrine settings, pisoids can be related to the activity of algae and microbes and spring orifices on lake bottoms with deposits consisting of calcite rays, intraclasts and pisoids. Pisoids are also common in sublittoral lacustrine zones (see Tables 4.4, 4.6 & 4.10 and Gierlowski-Koresch, 2010). Concentrically laminated pisoids are associated with turbulent waters and inorganic processes (Guo & Riding, 1998; Jones & Renaut, 2010). Radial shrub pisoids can be bacterial in origin and are associated with periodically agitated pools (see Table 4.15 and Folk & Chafetz, 1983; Guo & Riding, 1998; Jones & Renaut, 2010). Stromatolitic, mamillated pisoids have been linked to cyanobacteria (Koşun et al. 2005).

5.3.5.3: Tequiquiac pisolitic limestone (see Table 5.15 for facies summary)

Pisolitic deposits in the study area are held within a micritic matrix (see Figs 5.9 & 5.10 and Tables 5.11 & 5.12). Bed thickness tends to be < 20 mm up to 0.5 m. Collectively deposits form part of the layer-cake, composite stratigraphy associated with outcrops of laterally discontinuous tufa found in the study area. Beds usually have even to wavy parallel contacts. Deposits are thought to represent relatively turbulent saline waters.

5.3.6: Facies 6, Intraclastic limestone

5.3.6.1: Description

Intraclastic limestone (see Table 4.4) consists of eroded and redeposited particles supplied by currents and waves (storm events), fluvial flood events, the desiccation of muds (e.g. lithoclasts), localised sliding, and by the burrowing and grazing activities of organisms (Pedley, 1990, 2009; Flügel, 2010). Intraclasts are also sourced from the breakup and re-deposition of carbonate muds (lithoclast), bioconstructions (e.g. phytoclasts see Table 4.4), and bioclasts like shell and microorganisms (Pedley, 1990, 2009; Flügel, 2010). Diagenetic changes in the sediment volume during dehydration, compaction and leaching can also produce Intraclastic material (Pedley, 1990, 2009; Flügel, 2010). Intraclastic deposits will differ significantly having varying percentages of lithoclasts (carbonate and clastic), bioclasts and phytoclasts (see Tables 4.4 & 4.6) and deposition can be related to temporary

increases in depositional energy. Exceptions to this would be, for example, the decay of bioconstructions in static water conditions under low energy conditions (see Table 4.8 & 4.14 and Pedley, 1990; 2009).

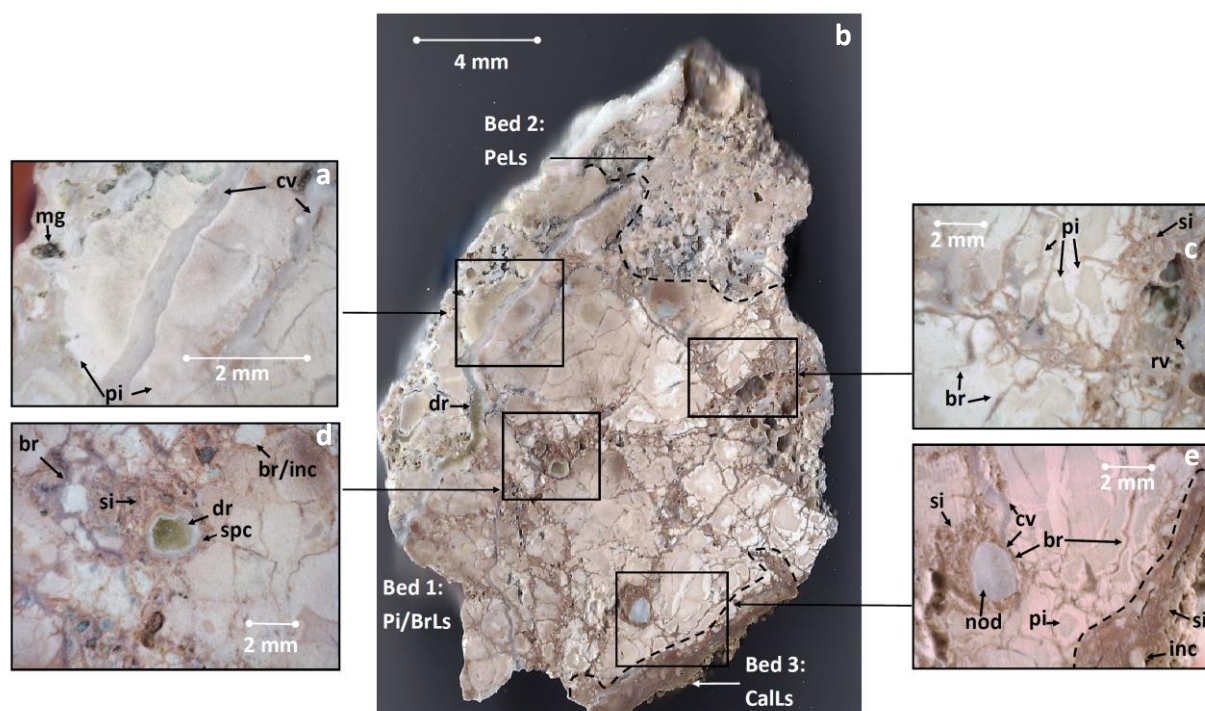


Figure 5.10: Example of pisolitic (brecciated) limestone from the study area. Sample from site TB9, Log 2, Bed 19, BDC T3 (Appendix 4, Table 2 and Fig 6.33). See Table 5.12 for bed descriptions.

Table 5.12: Example of pisolitic limestone bed descriptions from the study area, site TB9, Log 3, Bed 19, BDC T3 (Appendix 4, Table 2 and Fig 6.33). See Figure 5.10 for images of the beds.

| Facies name | Facies description | Sub-facies description | Post depositional facies description |
|--|--|--|--|
| Bed 3: Silt | Greyish-pink (5R 8/2) silt matrix with occasional white micritic intraclasts | None | |
| Bed 2: Peloidal packstone limestone | Greyish-pink (5R 8/2) grain supported peloidal (<1mm) packstone. | Moldic porosity < 30%. | |
| Bed 1: Brecciated, Pisolitic limestone | Greyish-pink (5R 8/2) pisoids (2-4 mm in diameter) have a maximum of two, relatively concentric coatings that mainly consist of darker and lighter white (N9) layers of micrite. Pisoids are set within a greyish pink (5R 8/2) to white (N9) matrix (Fig 5.10 a – e). | Infilled desiccation crack or remobilised silt and fine sand under vadose conditions | Calcite veins have replaced or been reprecipitated along joint weaknesses and cracks created by desiccation and root penetration. Root penetration, desiccation and potentially much later microkarst features have allowed groundwater to move light red (5R 6/6) clastic silt through the deposit that has replaced micrite along weaknesses or infilled void spaces. All the above have caused the brecciation of the original pisolitic limestone. Organic material has been replaced by drusy calcite, and in places coated with manganese (mg) (Fig 5.10). |
| | | Calcite vein development. | |

5.3.6.2: Defining characteristics

In palustrine environments, intraclasts can infill desiccation cracks and microkarst features, or form beds with clast sizes that range from millimetres to centimetres in diameter, rounded to angular, usually poorly sorted, in a micritic matrix (see Tables 4.12 & 4.13 and Wright, 1990; Alonzo-Zarza & Wright, 2010). In fluvial settings, during flood events, old deposits are eroded, and new intraclastic deposits build up (see Table 4.8).

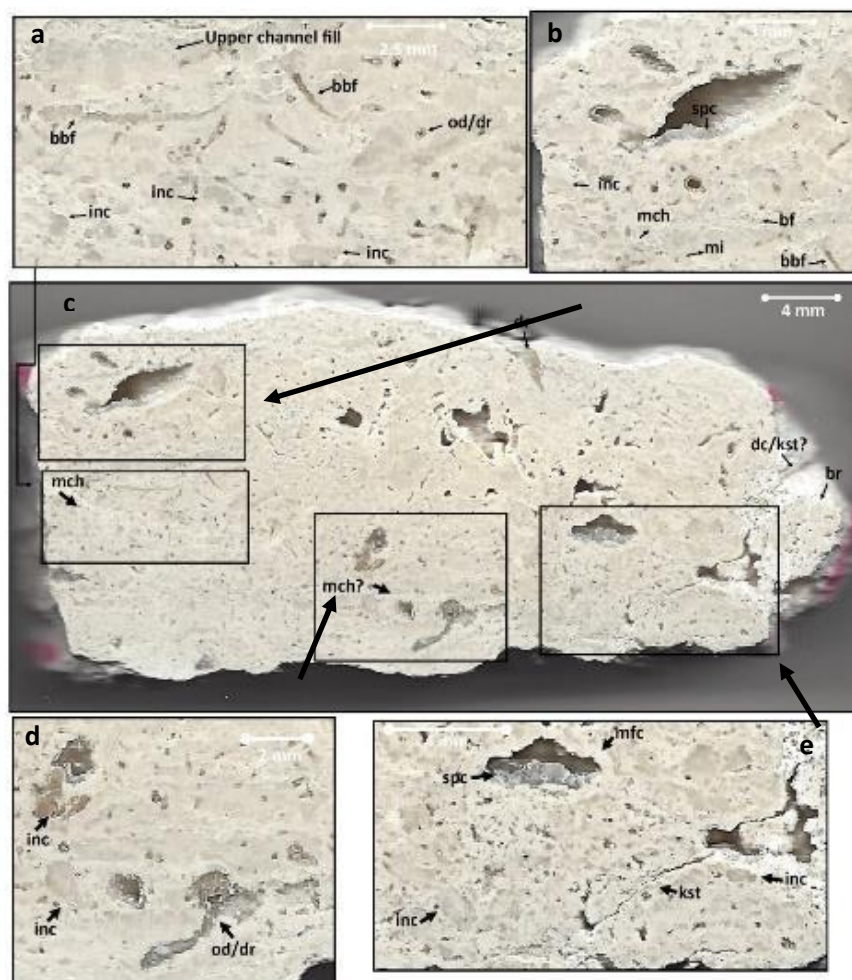


Figure 5.11: Example of intraclastic limestone from the study area. Sample is from site TB13 Log 2, Bed 15, TLAP T16 (Appendix 4, Table 7). See Table 5.13 for bed descriptions.

| Facies name | Facies description | Sub-facies description | Post depositional facies description |
|------------------------|--|--|---|
| Intraclastic limestone | Greyish-pink (5R 8/2) to white (N9) litho, bio and phytoclasts that range from coarse sand (0.5 mm) to fine pebbles (4 mm) in diameter. White (N9) micritic to sparry matrix (Fig 5.11 a - e). | Micro-channel forms that grade from coarse sand to medium pebbles at the base to a micrite infill topped by biofilm lamina (Fig 5.11). | Karst or desiccation features that are infilled with white (N9) micritic silt (Fig 5.11). |

Photoclasts can also accumulate in agitated and slow-flowing waters in barrage and palustrine environments (see Tables 4.2, 4.10 & 4.11 and Arenas-Abad et al. 2010). In Lacustrine settings, Intraclastic build-ups accumulate in marginal areas where wave action and higher energy conditions are concentrated, and re-working is common (Gierlowski-Koresch, 2010).

5.3.6.3: Tequixquiac intraclastic limestone (for facies summary see Table 5.15)

Intraclastic deposits were identified in the Tequixquiac basin when there was a predominance of intraclasts making up the deposit (see Table 4.5). Intraclasts were usually a mixture of carbonate silt, and clastic mud clasts, bioclasts and phytoclast held within a micritic matrix with varying degrees of sparry cement (see Figs 5.2 & 5.11 and Tables 5.6 & 5.13). Fine fraction volcanoclastics (<0.5mm) are common in all deposits, but usually only made up <5% of the matrix.

5.3.7: Facies 7, Laminated limestone deposits

5.3.7.1: Description

Beds that consists of simple laminated/bedded bed sets that are composite or have multiple interbeds with different textures, grain sizes or structure. Composite beds consist of laminae/beds that have a different composition, texture and internal structure but that are associated genetically (Boggs, 2006; Nichols, 2009). Changes to beds types and internal bedding are evidence of long and short-term changes in sedimentation caused by climatic and hydrological variations (Arenas-Abad et al. 2010). Biological activity can also be directly or indirectly responsible for sedimentation changes, bed types and internal bedding structures creating varying bedforms (Pentecost, 2005; Arenas-Abad et al. 2010; Jones & Robin, 2010).

5.3.7.2: Defining characteristics

Variable flow regimes dominate arid and semi-arid surface waters (e.g. fluvial, lacustrine) and desiccation, erosion and clastic sediment, that alternate with aqueous carbonate sediments, are common (Viles et al. 2007; Arenas-Abad et al. 2010). Laminated bioclastic limestones are common in ponded areas and along shallow lake shorelines (Arenas-Abad et al. 2010).

5.3.7.3: Tequixquiac laminated limestone (for facies summary see Table 5.15)

In the study area, laminated or bedded limestone (e.g. Figs 5.12, 5.13, & 5.14 and Table 5.14) are made up of simple and composite bed sets including any of the facies defined in Section 5.3, 5.4, 5.5 and 5.6.

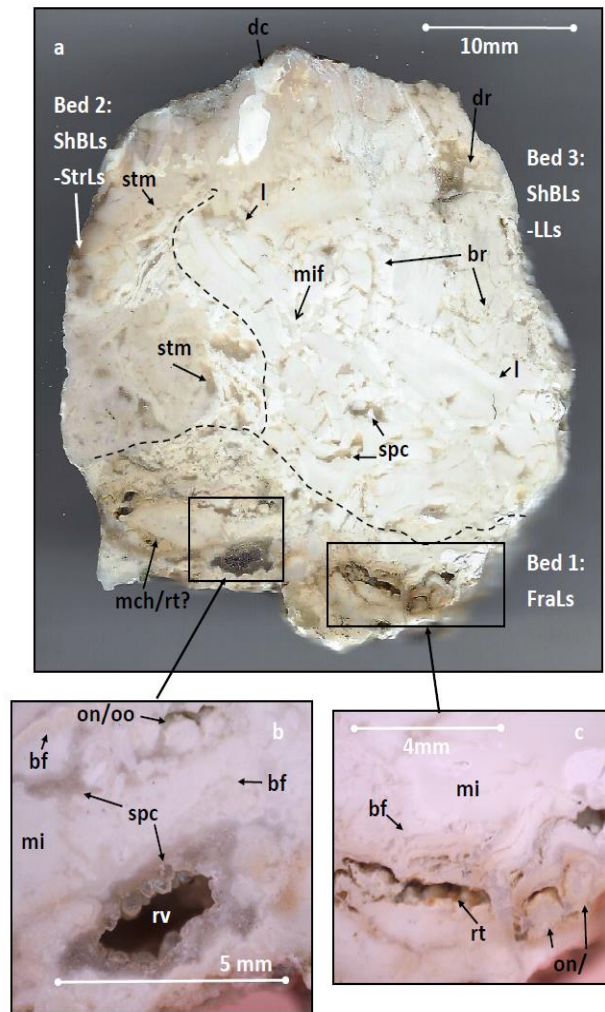


Figure 5.12: Example of laminated limestone despoths and associated facies from the study area. Site TB12, Log 2, Bed 5, ASH T8 (see Appendix 4, Table 6). See Table 5.14 for bed descriptions.

Table 5.14: Examples of bed descriptions for laminated limestone and associated facies from the study area. Site TB12, Log 2, Bed 5, sample ASH T8 (see Appendix 4, Table 6). See Figure 5.12 for sample images.

| Facies name | Facies description | Sub-facies description | Post-depositional facies |
|--|---|---|--|
| Bed 3: Shocked-brecciated laminated limestone (top). | White (N9), laminated (>3mm thick) calc-mud (see Fig 5.12 a). | None | Shocking and brecciation. Occasional pockets (<10%) of drusy and sparry calcite cement. In the upper bed, there is a large (3mm wide, 7mm thick) desiccation fracture with a micritic silt infill. |
| Bed 2: Shocked-brecciated stromatolitic limestone | White (N9) stromatolitic limestone (see Fig 5.12 a). | None | Shocking and brecciation. The bed appears to be pushed into bed 3. Calc-mud laminations in bed three have been compressed. |
| Bed 1: Framestone limestone (base). | Yellowish-grey (5Y 8/1), framestone limestone (base) with biofilms, calc-mud and macrophytes interbeds (see Fig 5.12 a, b & c). | Peloids, pisoliths and occasional biofilm lamina (see Fig 5.12 a, b & c). | Root voids and traces are either infilled with drusy calcite cement or micritic mud, or they are lined with sparry calcite or void. |



Figure 5.13: Barranca de Colores site showing a field example of interbedded and laminated **(1)** Greyish yellow-green (5GY 7/2) and moderate-pink (5R 7/4) mud; Pale, greenish-yellow (10Y 8/2) fine sand; Yellowish-grey (5Y 8/1) and white (N9) calc-mud; **(2)** Greyish yellow-green (5GY 7/2) and moderate pink (5R 7/4) micritic mud; White (N9), yellowish-grey (5Y 8/1) and moderate pink (5R 7/4) muddy micrite. All the above can be poorly lithified, massive or vertically jointed. Site TB9, Logs 1 and 2 (see Appendix 4, Tables 1 & 2 and Chapter 6 Figs 6.26 – 6.34).



Figure 5.14: Example of laminated limestone deposits from the study area. Greyish-pink (5R 8/2), laminated muddy micrite. Site TB12, Log 2, Bed 3, sample ASH T3 (see Appendix 4, Tables 5 & 6).

Table 5.15: Summary of the recorded, carbonate grain (allogenic) limestone and carbonate facies (see Table 5.4 for bed codes)

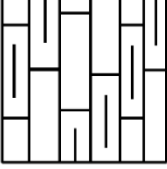
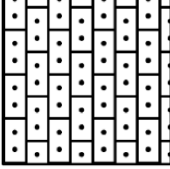
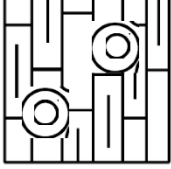
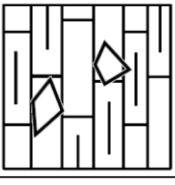
| Facies Name | Main facies description | Range of sub-facies description | Range of sedimentary structures | Range of post-depositional facies | Associated facies | Stratigraphic facies key |
|--|--|--|---|--|--|---|
| Facies 3, Microdetrital limestone and carbonate (CmLs & BmLs) | <p>-White (N9), greyish pink (5R 8/2), moderate pink (5R 7/4), yellowish grey (5Y 8/1), pale greenish yellow (10Y 8/2) micritic silt</p> <p>-Moldic porosity (5-60%)</p> <p>-Beds are between 0.02 – 1m in thickness</p> <p>a: laterally continuous (e.g. lacustrine deposits)</p> <p>b: laterally discontinuous (e.g. fluvial, marsh and pond deposits)</p> | <p>-Volcaniclastic input (10 – 5%)</p> <p>- Sparse intraclasts (e.g. shell, mud clasts organic detritus)</p> <p>-Clotted fabric</p> <p>-Bioturbation</p> <p>-Intact, incipient and broken biofilm lamina</p> <p>-Peloids</p> <p>-Intraclasts</p> | <p>-Micro-laminations (incipient).</p> <p>-Internal bedding can be massive or comprise simple or composite bed sets</p> | <p>-Brecciation</p> <p>-Shocked (e.g. tectonized) brecciated beds</p> <p>-Calcite veins</p> <p>-Salt hoppers (halite crystals)</p> <p>-Root penetration</p> <p>-Karsification</p> <p>-Clastic silt infill of void spaces</p> <p>- Drusy (brilliant green 5G 6/6) and sparry (white N9 to light grey N8) calcite void infills and organic replacement</p> <p>-Void coatings and traces of manganese indication of the decay of organic material</p> | <p>All other carbonate facies (see this table and Table 5.9)</p> <p>-Silty fine sand</p> |  |
| Facies 4, Peloidal limestone (PeLs) | <p>-Yellowish grey (5Y 8/1) and greyish pink (5R 8/2)</p> <p>Pelleted to clotted fabric.</p> <p>-Clotted tends to have fused edgings.</p> <p>-If there is a matrix, it is either yellowish grey (5Y 8/1), greyish pink (5R 8/2)</p> <p>Peloidal fabrics are pelleted to clotted, and within these, there can be occasional micritic silt clasts (< 5 mm in diameter)</p> <p>-Beds are between 0.02 – 0.10 m in thickness</p> <p>-Deposits are laterally discontinuous (e.g. fluvial, marsh and pond deposits)</p> | <p>-Pisoliths</p> <p>-Shell</p> <p>-Volcaniclastic (5 – 10%).</p> <p>- Macrophyte root traces (rt)</p> | <p>-Bioturbation</p> <p>-Massive</p> <p>-Grain supported</p> <p>-Matrix supported</p> | <p>-Macrophyte root replacement with drusy calcite, and sparry calcite cement coatings.</p> <p>-Calcite veins</p> <p>-Desiccation cracks</p> <p>-Karsification around the edges of deposits</p> | <p>-Framestone limestone</p> <p>-Stromatolitic limestone</p> <p>-Pisolitic limestone</p> <p>-Calc-mudstone</p> |  |
| Facies 5, Pisolitic limestone (PiLs) | <p>-Greyish pink (5R 8/2), white (N9) pisoliths are up to 4 mm in diameter with at least two concentric lamina coatings</p> <p>-Pisoliths are sub-rounded to free form.</p> <p>-Micritic matrix, greyish pink (5R 8/2), white (N9)</p> <p>-Deposits are laterally discontinuous (e.g. fluvial, marsh and pond deposits)</p> | <p>-Volcaniclastic (5 – 10%).</p> <p>-Peloids</p> | <p>-Massive</p> | <p>-Brecciation</p> <p>-Karsification</p> <p>-Desiccation cracks</p> <p>-Root penetration and replacement with drusy calcite (brilliant green 5G 6/6) and sparry (white N9 to light grey N8) calcite void infills and organic replacement</p> | <p>-Calc-mudstone</p> <p>-Peloidal limestone</p> <p>-Mudstone</p> |  |

Table 5.15 continued: Summary of the recorded, carbonaceous limestone and carbonate facies (see Table 5.4 for bed codes)

| Facies Name | Main facies description | Range of sub-facies description | Range of sedimentary structures | Range of post-depositional facies | Associated facies | Stratigraphic facies key |
|---|---|---|---|--|---|---|
| Facies 6, Intraclastic Limestone (Incls) | <ul style="list-style-type: none"> -Lithoclasts of clastic mud, sand and micrite yellowish grey (5Y 8/1). -Bioclasts of shell and broken biofilms -Phytoclasts, mostly of organic detritus -Matrix, micrite with sparry patches (< 10%), usually white (N9) or greyish pink (5R 8/2). -Peloids -Deposits are laterally discontinuous (e.g. fluvial, marsh and pond deposits) | <ul style="list-style-type: none"> -Volcaniclastic input throughout -Occasional peloids -Incipient biofilm lamina -Moldic porosity (<5%) -Gastropod shell -Oncoids | <ul style="list-style-type: none"> -Fluvial grading in some beds. - Sub-angular to sub-rounded clasts <1mm – 0.5m -Micro-channel forms (<20 mm in diameter | <ul style="list-style-type: none"> -Replacement with drusy calcite, Drusy (brilliant green 5G 6/6) and sparry (white N9 to light grey N8) calcite void infills and organic replacement -Secondary micritic precipitation in void spaces and sparry fringe void coatings -Manganese indicating the decay of organic material | <ul style="list-style-type: none"> -Framestone limestone -Calc-mudstone |  |
| Facies 7, Laminated carbonate deposits | <p>Mostly simple and composite bed sets that can be repetitions of a single facies type or, a combination of related facies types.</p> | <p>Any</p> | <p>Any</p> | <p>Any</p> | <p>Any</p> | <p>Any</p> |

5.4: Mixed clastic and carbonate deposits

A deposit is classified as mixed carbonate-clastic here if more than 10% of the sample volume is made up of the opposing component. Sparry and crystalline cement were not counted as these are a post-depositional carbonate sub-category (Mount, 1985). A series of yes or no questions were posed (see Fig 5.15) to classify mixed sedimentary deposits (as proposed by Mount, 1985) (see Fig 5.15). Allochem refers carbonate grain larger than 0.05 mm that has been transported, or that form organised aggregates (e.g. ooids, intraclasts, bioclasts and peloids). Sandy allochems, sandy micrite, muddy allochems and muddy micrite were identified based on grain size and TIC (>25% - < 50 % TIC). Allochem sands, micritic sands, allochem mud and micritic mud were identified by grain size and TIC (>10% and <25 % TIC).

5.4.1: Tequixquiac mixed clastic and carbonate deposits (for facies summary see Table 5.20)

In the study area mixed clastic and carbonate deposits include muddy micrite (Facies 8) (Figs 5.16 & 5.16, Tables 5.17 & 5.17), sandy micrite (Facies 10) (Fig 5.18, Table 5.18), and micritic mudstone and mud (Facies 9) (Fig 5.19, Table 5.19). Deposits often contain intraclasts and are associated with each other, limestone deposits (Section 5.3), or clay, mud and sand deposits that have undergone varying degrees of lithification. Thicker beds (>0.50 m) are predominantly planar to wavy. Smaller beds (<0.50 m) can be parallel to non-parallel and curved.

Figure 5.15: Mixed carbonate and siliciclastic sediment deposit classification used by this PhD research (after Mount, 1985).

| Q1: Is the total siliciclastic % larger than the carbonate %? | Q2: Of the siliciclastic sediment, is the amount of sand greater than mud? | Q3: Of the carbonate, sediment is the volume (%) of allochems greater than micrite? | Sediment or rock name | |
|---|--|---|--------------------------------------|---|
| Yes → No → | Yes → No → | Yes → | 1: Allochem Sand 2: Micritic Sand | |
| | | No → | | |
| | Yes → No → | Yes → | 3: Allochem Mud 4: Micritic Mud | |
| | | No → | | |
| | Yes → No → | Yes → No → | Yes → | 5: Sandy Allochem carbonate 6: Sandy Micrite |
| | | | No → | |
| | | Yes → No → | Yes → | 7: Muddy Allochem carbonate 8: Muddy Micrite |
| | | | No → | |

| Table 5.16: Examples of muddy micrite bed descriptions and associated facies. Site TB12, Log 2, Bed 3, ASH T4, (see Appendix 4, Table 6). See Figure 5.16 (a - e) for images of the beds. | | | |
|--|---|---|---|
| Facies name | Facies description | Sub-facies description | Post depositional features |
| Bed 2: Biogenic muddy micrite (sparse) | White (N9) micritic silt that in places has a clotted texture and occasional sparitic cement (Fig 5.16 c). Within the silt matrix there are scattered shell fragments (Fig 5.16 a & c), broken biofilm fragments (Fig 5.16 c), and small (<1 mm in diameter) micritic mud clasts. | Moldic porosity (10%) and volcanoclastic input (<10%) (Fig 5.16 b & e). | Occasional patches of manganese within void spaces that suggest organic detritus was also incorporated into the matrix and was later replaced (Fig 5.16 b). |
| Bed 1: Framestone | Large macrophyte with leaf traces that penetrates, and are surrounded by, stromatolitic biofilm lamina (<1 mm) that alternate with micritic silt (<3 mm). Moldic porosity (50%) (Fig 5.16 c & d). | Volcanoclastic input (<3%) (Fig 5.16 e). | Void spaces remain void or have been partially infilled or lined with sparitic calcite, micritic silt, or manganese (Fig 5.16 e). |

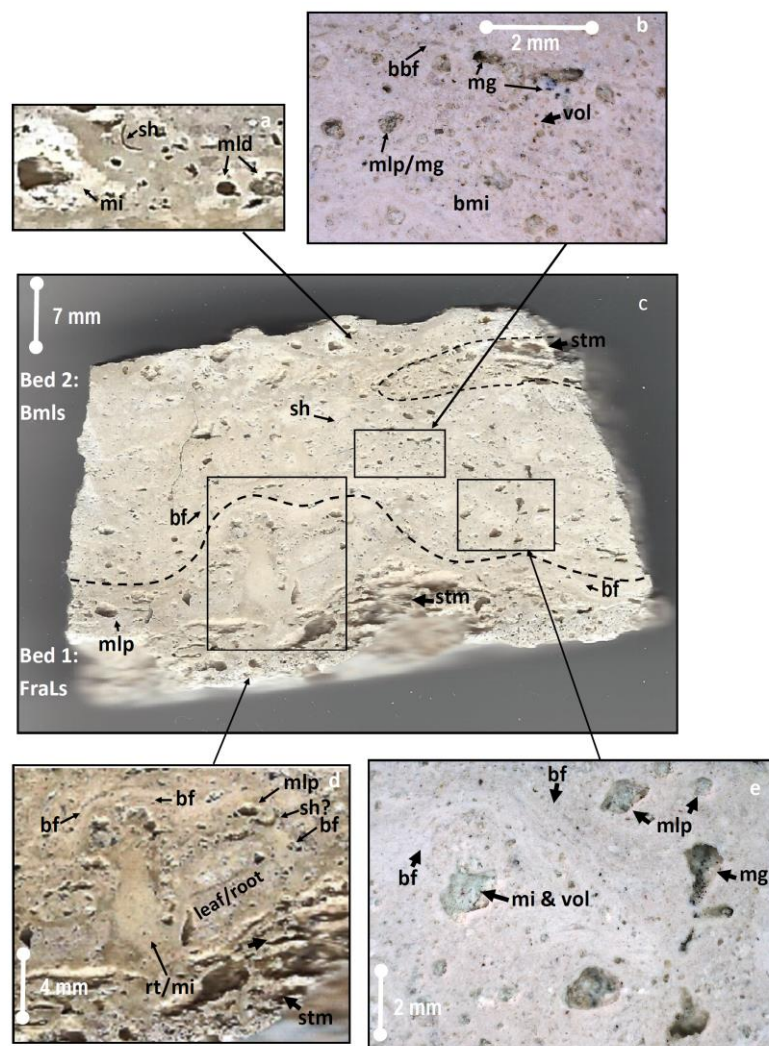


Figure 5.16: Example of muddy micrite from the study area and associated facies. Bed descriptions are given in Table 5.16. Sample from site TB12, Log 2, Bed 3, ASH T4. (See Appendix 4, Table 6).

Table 5.17: Example of muddy micrite from the study area. Site TB12, Log 2, Bed 3, ASH T5 (See Appendix 4, Table 6). See Figure 5.17 for images of beds.

| Facies name | Facies description | Sub-facies description | Post depositional facies |
|----------------------------|--|--|---|
| Intraclastic muddy micrite | White (N9) micritic silt with sparry patches (30%). Within the matrix there are intraclasts (<5%) (sub-angular to sub-rounded carbonate mud/silt clasts <1 mm in diameter (Fig 5.17 c), broken biofilms, organic detritus (<4 mm) and oncoids (Fig 5.17 b & c). Moldic porosity (60%) (Fig 5.17 a -c). The first 7 mm of the bed has a higher percentage (30%) of lithoclasts. | In-situ (top and bottom) and incipient, (2—0.2 mm) biofilms (Fig 5.17 a & b) that have associated, localised bubble voids (<0.5mm). Volcaniclastic input 2-5% (Fig 5.17 a). Shell fragment in the base of the bed. | Void spaces are very occasionally infilled with drusy calcite suggesting the presence of decayed organic matter (waterweed?). Clastic and micritic silt infilling some of the void spaces may suggest groundwater moving through the deposit later, after lithification (Fig 5.17 a & c). |

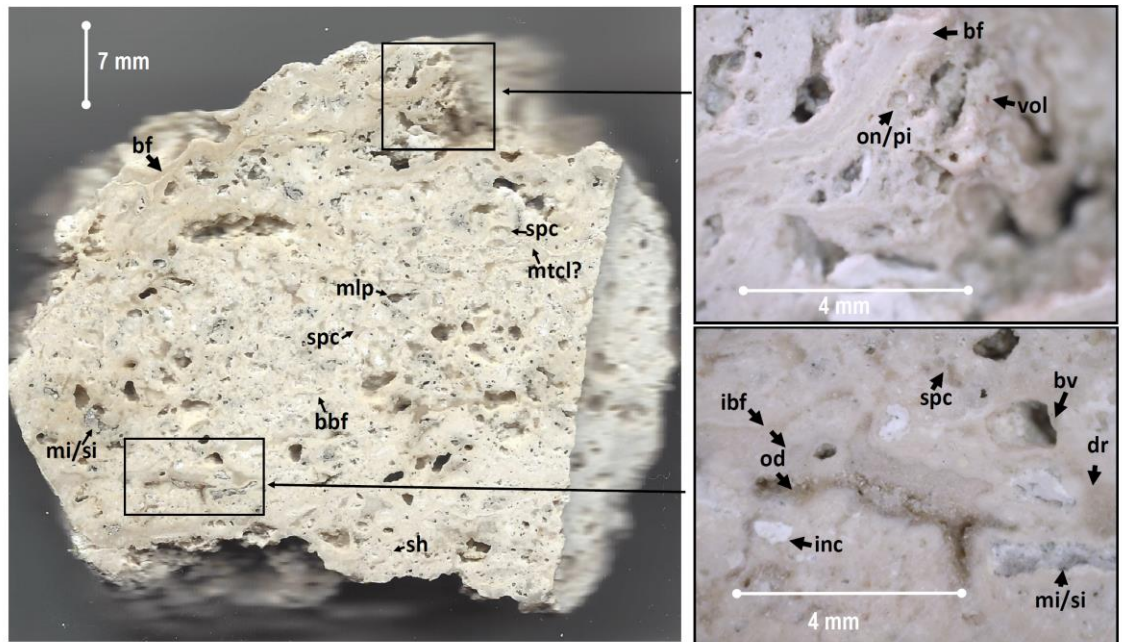


Figure 5.17: Example of intraclastic muddy micritic and associated, Sample from site TB12, Log 3, ASH T5, Bed 3 (See Appendix 4, Table 6). Bed description is given in Table 5.17.

Beds that occur in an outcrop are laterally discontinuous and can be massive, laminated, cross-bedded and cross-rippled. These beds are usually composite beds-sets that can consist of limestone (Section 5.3), tephra (Section 5.6) and clastic deposits (Section 5.5) and show evidence of subaerial exposure, desiccation and erosion with occasional channel forms, micro-scale (<10 mm wide). Within the sequence large-scale channels (1 m+) cut some sections (Figs 5.20 & 5.21). Matrix and clast-supported intraclastic gravels made up of mixed lithologies are also commonly interbedded (Figs 5.17, 5.18 & 5.20; Tables 5.17 & 5.18). These beds are associated with marginal lacustrine and pool areas, tufa deposits and alluvial and fluvial sequence. Laterally continuous mixed clastic-carbonate deposits are found along the southern, south-east and southwest basin and upland areas (see Chapter 8) in thicknesses up to 10 + m. Internal bedding is commonly massive, and contacts appeared graded (see Fig 5.21) except at the top of shallowing upwards cycle (see Chapter 6) (e.g. desiccation cracks).

Table 5.18: Example of an intraclastic sandy micrite bed description. Site TB13, Log 2, Bed 6, Sample TLAP L2 (see Appendix 4, Table 7). See Figure 5.18 for the image of beds.

| Facies name | Facies description | Sub-facies description | Post depositional facies |
|---|---|--|--|
| Bed 1: Intraclastic fine sandy micritic. | Greyish pink (5R 8/2) fine sandy micritic matrix with yellowish-grey (5Y 8/1) sub-angular micritic silt clasts (< 4 mm in diameter) and dark greenish-yellow (10Y 6/6) angular mud clasts (< 3 mm in diameter). Collectively lithoclast account for < 30% of the sample and the deposit is poorly sorted. | Void spaces account for <10% of the fabric and they can be up to 3 mm in diameter but are mostly ca. < 1 mm. The sample has occasional manganese clusters assumed to be related to organic detritus. | Most voids are empty, one or two have a sparry lining. In the upper sample, desiccation fractures are relatively deep (>20 mm), post-depositional feature related exposure, wetting and drying of the upper surface. |

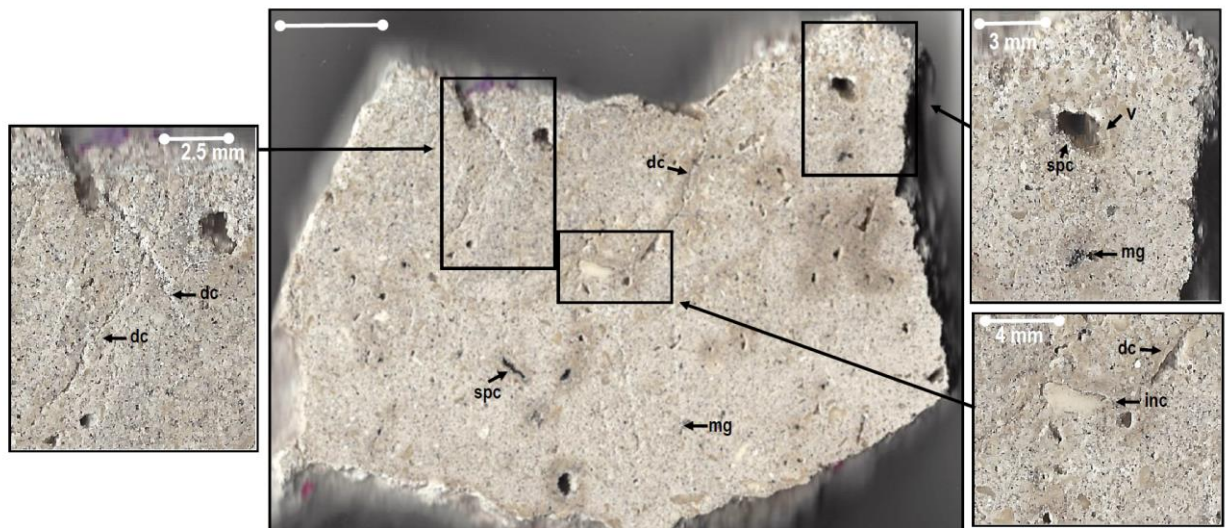


Figure 5.18: Example of intraclastic fine sandy micritic and associated facies, site TB13, Log 2, Bed 6, TLAP L2 (Appendix 4, Table 7). Bed description is given in Table 5.18.

Bed sets occur in laterally continuous sequences are usually simple consisting of cycles of calc-mudstone, muddy micrite, sandy micrite, micritic mud, mud and clay.

5.5: Clastic sedimentary facies

Terrigenous clastic material predominantly comes from the weathering breakdown and erosion of bedrock and the detritus is primarily composed of silicate minerals (Nichols, 2009). The textures and structures of sediments and sedimentary rock can provide valuable information about the nature of sediment transport and the depositional setting. Within the study area, terrigenous material has been classified based upon the characteristics discussed in Tables 4.1 to 4.16 and 5.1 to 5.5 and Figures 4.1 to 4.4. A large proportion of the siliciclastic deposits recorded from the study area are water-lain, or slope and pyroclastic material that has been eroded and reworked by fluvial and alluvial processes with various degrees of aeolian sorting. The following section gives examples of type deposits of Quaternary siliciclastic facies that have been recorded for this PhD research from the study area.

Table 5.19: Example of a micritic mud bed description Site TB9, Log 2, Bed 13, Sample BDC T10 (see Appendix 2, Table 4 and Chapter 6, Fig 6.33). See Figure 5.19 for the sample image.

| Bed name | Facies description | Sub-facies description | Post depositional features |
|--|---|-----------------------------|---|
| Bed 3: Immature laminar calcrete horizon (top). | Very light grey (N8) calcrete laminar feature, possibly with a lower nodular horizon directly below. | None | None |
| Bed 2: Micritic mudstone | Moderate red (5R 5/4) fine-grained low energy mud that has areas of increased energy micritic sand in-wash. | Volcaniclastic input (15%). | The post-depositional movement of water through the deposit, probably under vadose conditions has removed the primary sediment and replaced this with calcite veins infilling the conduits. |
| Bed 1: Stromatolitic micritic mudstone (bottom). | Fine alternating parallel lamina of blocky moderate red (5R 5/4) micritic mud and indurated, greyish pink (5R 8/2) hard micritic lamina (< 2 mm). | Volcaniclastic input (15%). | |

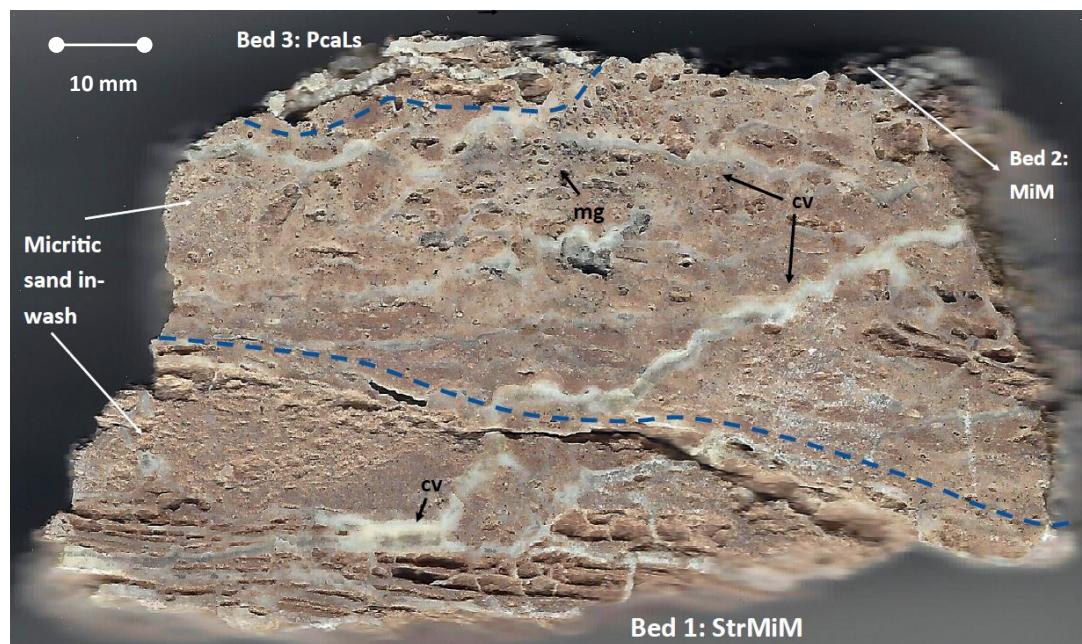


Figure 5.19: Example of micritic mud deposits and associated facies from the study area. Site TB9, Log 2, Bed13, BDC T10 (see Appendix 4, Table 2 and Chapter 6, Fig 6.33).

5.5.1: Facies 11 (a-c), Clay

5.5.1.1: Description

Clay and claystone are textural terms defining the finest grade of clastic sediments (Table 5.1) and roc, which forms from the breakdown of feldspars and other silicate minerals (Boggs, 2006). Clay particles are present in the suspended load of most air and water currents and stay so until the flow velocity decreases (Nichols, 2009). When deposited, particles tend to become cohesive because of an electrostatic effect, and their platy particle shape.

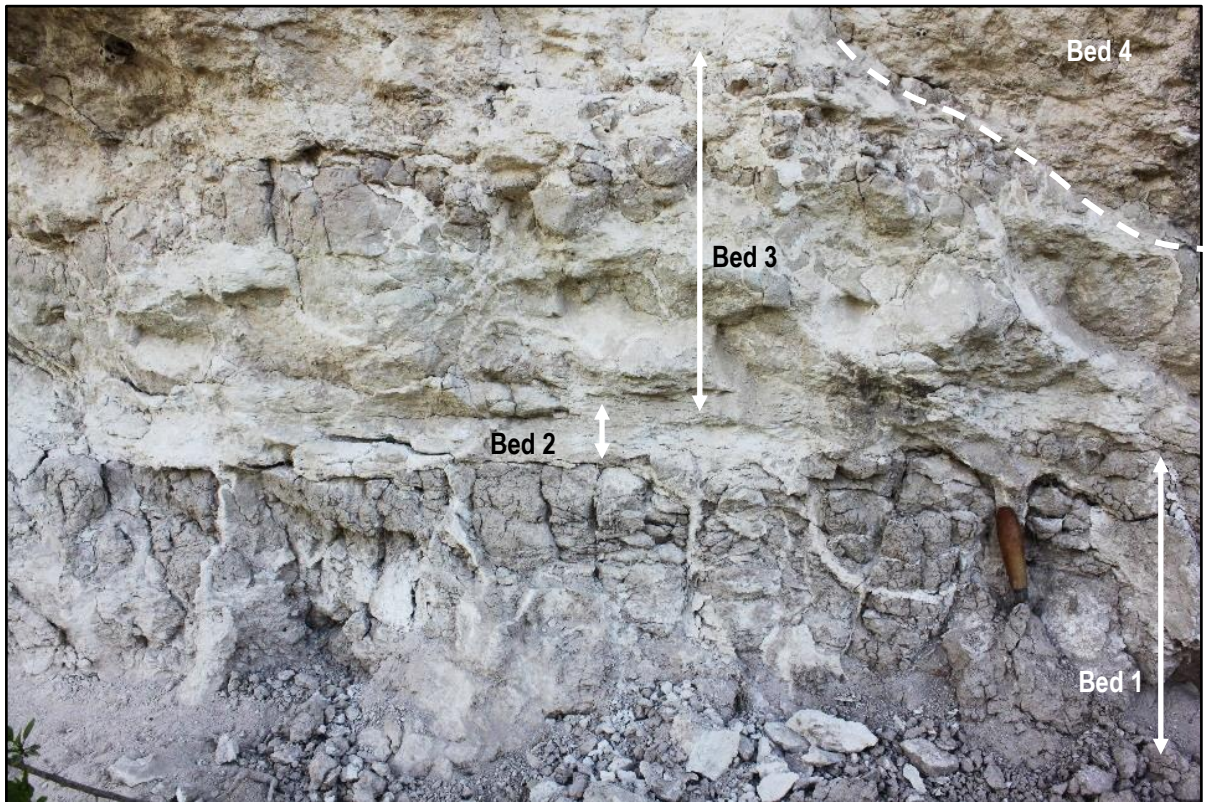


Figure 5. 20: Field examples of laterally discontinuous, mixed carbonate and clastic sediments. **Bed 1: Moderate red (5R 5/4) muddy micrite (L28).** Laterally continuous, blocky in appearance and the bed, before desiccation, had horizontal to wavy, very fine lamination. Along brecciated jointing fractures secondary white (N9) silt (micrite) in-fill has occurred. **Bed 2: Yellowish grey (5Y 8/1) clay (L27).** Very blocky in appearance and the bed, before desiccation, had horizontal to wavy, very fine lamination and trough-cross bedding. **Bed 3: Moderate red (5R 5/4) muddy gravel (L24-L27).** Bed contains sub-angular to sub-rounded mud and muddy micrite lithoclasts < 5 mm – 0.40 m in diameter. Limestone gravel with sub-angular to sub-rounded clayey silt balls and rip-up clasts < 0.20 m in diameter. **Bed 4: Moderate red (5R 5/4) gravel.** Gravel contains a relatively high proportion of volcanoclastics (10%) and angular, greyish pink (5R 8/2) rip-up clasts (<5 mm in diameter). Site TB10, Barranca del Muerto, the upper contact of Log 1 overlain by Log 3 (Figs 6.15, 6.16a & b, 6.18, 6.19).

5.5.1.2: Defining characteristic

Clay is fine-grained (see Fig 5.1) and plastic when wet, and its volume decreases if air-dried leading to shrinkage features like desiccation cracks (UCL, 2017).

5.5.1.3: Tequixquiac clay deposits (for facies summary see Table 5.21)

Massive clay deposits are found interbedded with massive mud, muddy micrite, sandy micrite, micritic mud and limestone (e.g. F/LMIs, LMs) along the southern, south-east and southwest basin and upland areas of the study area with bed thicknesses that range from a few mm up to several meters (see Fig 5.21) (Facies 11a). Laterally discontinuous clay beds (e.g. FFsc, FC) from 2 mm up to 2 m thick and up to 200 m wide (e.g. abandoned channel or back swamp), occur in association with silt, mud and sand deposits, and gravel. Thin beds can be

massive, faintly laminated, organic-rich and occur with or without molluscs (see Fig 5.22). Deposits are vertically jointed in some sections and can have occasional carbonate nodules (<2 mm) (Facies 11b). The geometry of the beds is mainly sheet, or blanket and contacts can be gradational, sharp or disconformable (Fig 5.22).

5.5.2: Facies 12 (a-c), Mud

5.5.2.1: Description

Mud (Table 5.1) is composed of mixtures of clay minerals and fine-sized quartz and feldspars (Boggs, 2006). Mud forms in an environment that has an abundance of fine sediment and low energy conditions that allow suspension sedimentation (Boggs, 2006). Deposits are particularly common on river floodplains and in lakes, both along low-energy margins and in deeper basinal lacustrine areas (Tucker, 2006).

5.5.2.2: Defining characteristic

Mud is essentially a mixture of clay and silt, but in unknown proportions and nodules are a common feature, usually of calcite, dolomite, siderite and pyrite (Tucker, 2006).

5.5.2.3: Tequiquiac mud deposits (for facies summary see Table 5.21)

In the study area, mud deposits can occur as isolated or laterally extensive beds with gradational, paraconformable or disconformable contacts. Larger beds (<10 m) (e.g. F/LMIs, LMs) are massive, plane tabular beds that are concentrated across the southern, south-east and southwest basin (see Fig 2.21 and Chapter 6) (Facies 12a). Smaller beds (<0.30 m) tend to be interbedded within tufa sequences (see this chapter and Chapter 6) and are massive, laminated to rippled tabular to wavy beds that terminate in out-crop, sometimes pinching out in sequence (Facies 12b) (e.g. F/LMIs, IOm, Im) and these have a wider distribution across the study area (see Figs 5.13, 5.5 and Chapter 6).

5.5.3: Facies 13 (a & b), Silt

5.5.3.1: Description

In aqueous or air currents, silt remains suspended until low energy flow conditions or standing water has been achieved (e.g. deeper lacustrine, fluvial floodplains or loess deposits) (Boggs, 2006; Tucker, 2006; Nichols, 2009).

5.5.3.2: Defining characteristics

Most other minerals have been broken down chemically before they reach a silt-sized grain because the most common constituent of silt is quartz (Boggs, 2006; Nichols 2009).

| Table 5.20: Summary of the recorded, mixed carbonate and clastic facies recorded in the study area. | | | | | |
|---|--|--|--|---|--------------------------|
| Facies Name | Main facies description | Range of sedimentary structures | Post depositional facies | Associated facies | Stratigraphic facies key |
| Facies 8, Muddy micrite | <p>a) Laterally extensive beds can be: -Between 10 m to 0.50 m thick -Moderate red (5R 4/4) -Greyish yellow green (5GY 7/2) -Pale red (5R 6/2)</p> <p>b) Laterally discontinuous beds can be: -Lamina to 0.50 m thick -Moderate red (5R 4/4) -Moderate pink (5R 7/4) -Pale rec 5R 6/2 -Greyish yellow green (5GY 7/2)</p> | <p>a) Laterally extensive beds -Massive -Plane, straight bedding planes -Contacts are mainly grades -Mainly unconsolidated</p> <p>b) Laterally discontinuous beds -Massive -Sand-sized silt intraclasts -Fine pebble gravel rip-up clasts -Faint ripple-cross lamination -Lensing</p> | <p>a) None-observed b) -Vertical jointing -Carbonate nodules (sand-sized) -Manganese</p> | <p>-Micritic mudstone -Sandy micrite -Calc-mudstone -Mud and mudstone</p> | |
| Facies 9, Micritic mud | <p>a) Laterally extensive beds can be: -Between 10 m to 0.50 m thick -Greyish yellow green (5GY 7/2) -Pale red (5R 6/2) -Pinkish grey 5RY 8/1 Moderate pink 5R 7/4</p> <p>b) Laterally discontinuous beds can be: -Moderate red (5R 4/4) -Greyish pink (5R 8/2) -Greyish yellow green (5GY 7/2) -Moderate pink (5R 7/4) -Pale red (5R 6/2)</p> | <p>a) Laterally extensive beds -Massive -Plane, straight bedding planes -Contacts are mainly grades -Mainly unconsolidated</p> <p>b) Laterally discontinuous beds -Plane, straight bedding planes -Ripple cross-lamina and beds -Lenticular lamina and bedding -Laminations -Sand-sized silt intraclasts -Massive -Very coarse pebble gravel diamict</p> | <p>a) None-observed b) -Vertical jointing -Carbonate flecks < 5 mm in diameter -Nodules</p> | <p>-Sandy micrite -Calc-mudstone -Mud and mudstone -Muddy micrite</p> | |
| Facies 10, Sandy micrite | <p>a) Laterally extensive beds can be -Between 10 m to 0.50 m thick -Pale pink (5R 8/2)</p> <p>b) Laterally discontinuous beds can be: -Very fine pebble gravel diamict -Moderate red (5R 4/4) -Greyish yellow, green 5GY 7/2)</p> | <p>a) Laterally extensive beds -Massive -Plane, straight bedding planes -Mainly unconsolidated -Occasionally some vague bedding</p> <p>b) Laterally discontinuous beds -Massive -Ripple cross-lamina and beds -Lenticular lamina and bedding -Carbonate nodules < 5 mm in diameter</p> | <p>a) None-observed b) -Vertical jointing -Carbonate nodule</p> | <p>-Calc-mudstone -Micritic mudstone -Mud and mudstone</p> | |



Figure 5.21: 1: Field example of mixed clastic and carbonate deposits from Site TB9. 1, Log 1. 2: Gravels, Log 5 cutting Log 1. (see Appendix 4, Tables 1, & 4 and Chapter 6).

5.5.3.3: Tequixquiac silt deposits (for facies summary see Table 5.21)

Silt in the study area is found occasionally interbedded with smaller (<0.50 m) beds of massive mud (Facies 12 a-c), muddy micrite (Facies 8), sandy micrite (Facies 10) and micritic mud (Facies 9) along the southern, south-east and southwest basin and upland areas of the study area (see Figs 5.13, 5.21) (e.g. F/LMIs, LMa, Facies 13a), these deposits terminate in outcrop. Beds, from 2 mm up to 2 m also occur in association with silt, mud and sand deposits that can be organic-rich to organic poor (see Fig 5.22). These beds are vertically jointed in some sections and can have occasional carbonate nodules (<2 mm) and calcified roots (e.g. FFsc, FFms, FFr, Facies 13b).

5.5.4: Facies 14 (a-d), Sand

5.5.4.1: Description

Sand forms through the breakdown of pre-existing rock via weathering and erosion of the material from within the depositional environment, and in some cases outside this environment depending on the clastic transport into and out of the basin (Boggs, 2006, Tucker, 2006; Nichols, 2009). In terrestrial environments, sand and sandstone deposits are commonly found in fluvial and alluvial fan deposits as well as marginal and basinal lacustrine environments (Boggs, 2006; Tucker, 2006; Nichols, 2009).

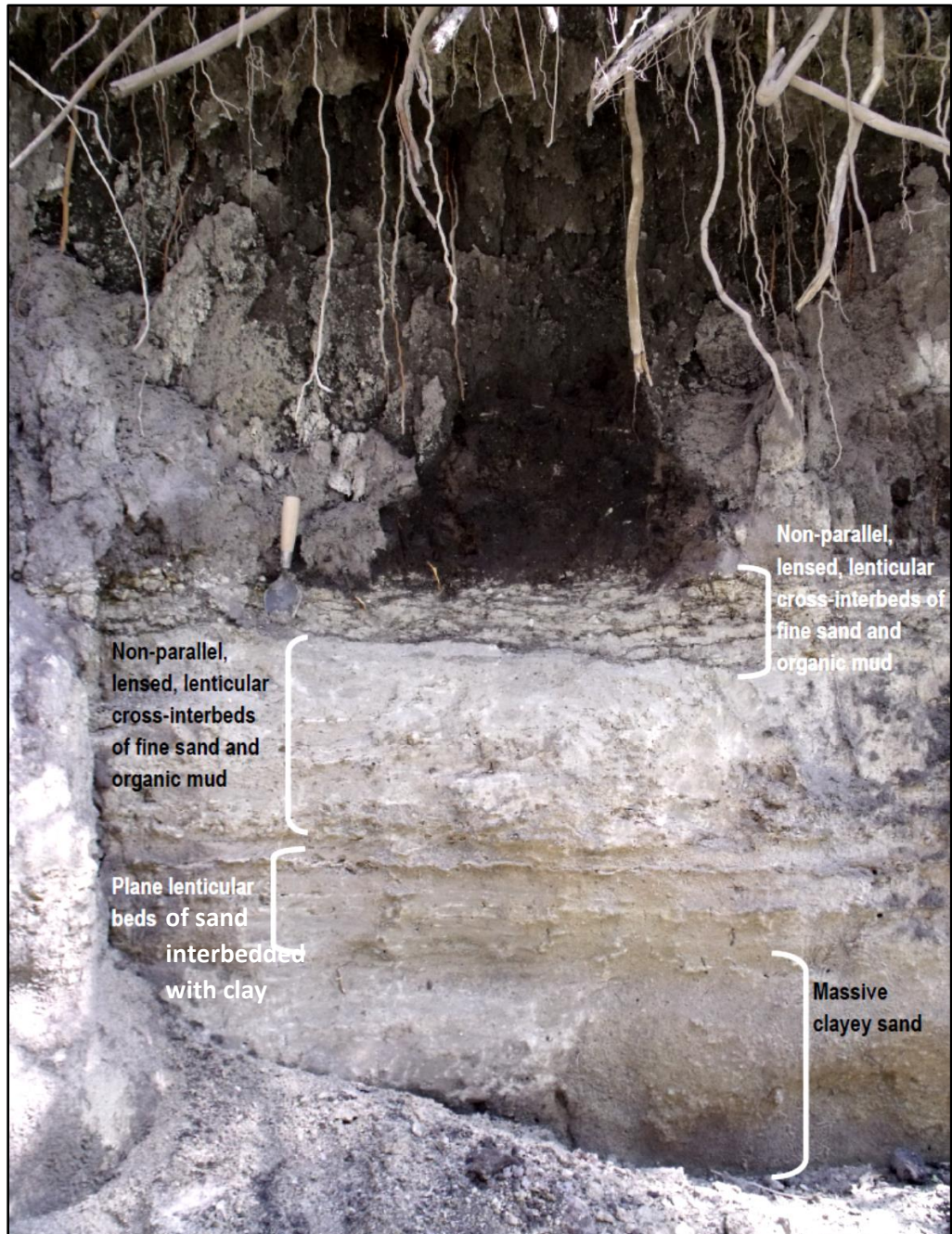


Figure 5.22: Field examples of clay, silt and sand beds from the study area. Site TB2, Log 3, Beds 1, 2, 3 and 4 (see Appendix 8, Table 15).

5.5.4.2: Defining characteristics

Sand, like gravels, can have variable degrees of matrix, and this is expressed as degrees of maturity. Immature sand has a high percentage of clay, unstable grains that have yet to be broken down chemically and poorly sorted angular grains. Mature sand has little to no clay, relatively well-sorted grains and sub-rounded clasts. Super-mature sand has virtually no clay and is well-sorted with rounded clasts (Boggs, 2006; Tucker, 2006; Nichols, 2009).

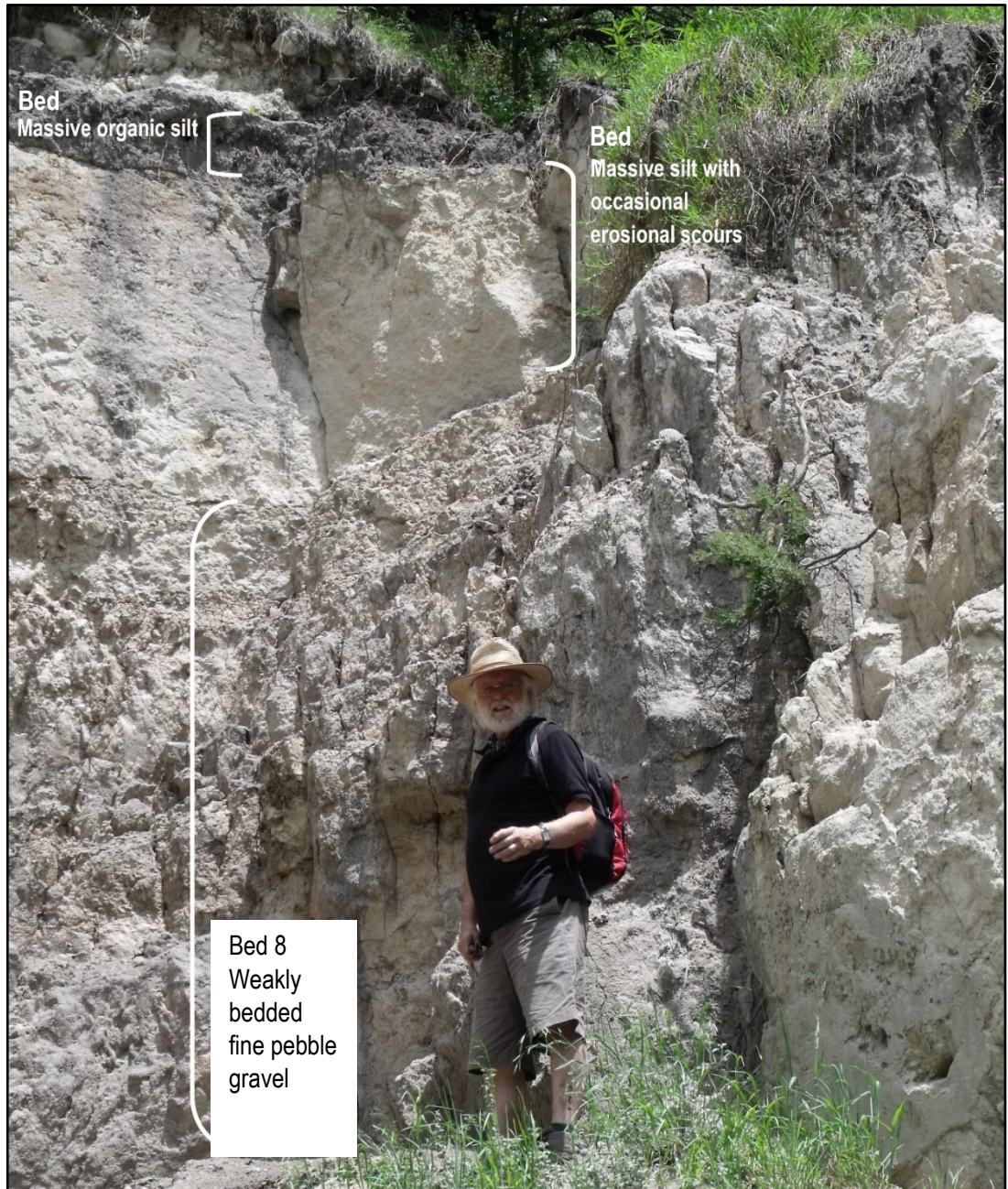


Figure 5.23: Field examples of silt and angular-rounded gravels (Facies 17). Massive organic silt, Bed 9. Massive silt with erosional scours, Bed 8. Weakly bedded pebble to cobble angular to rounded gravel (Facies 17), Bed 6. Site TB1, Log 7 (see Appendix 8, Table 12).

5.5.4.3: Tequixquiac sand deposits (for facies summary see Table 5.21)

Within the study, there is a wide and varied range of sandy deposits (see Table 5.21). Most beds terminate in outcrop (Fig 5.13) with a variable gross geometry from lensed, sheet, blanket or wedge shapes and channel fills (e.g. FSt, FSp, FSr, FSh, FSI, FFSm, FFI or LMa) (Facies 14a).



Figure 5.24 (above): Field examples of silt, sand and gravel deposits from the study area. Extraformational, massive, fine to medium sand fine pebble, polymictic gravel (Bed 1 base of section). Composite bed sets of tabular cross-bedded coarse sand and upper ripple cross-laminated to plane cross-bedded and trough cross-bedded medium sand (Bed 2 of log). Example from site TB1, Log 1 (see Appendix 8, Table 6).



Figure 5.25: Field example of Facies 15, massive gravel. Site TB1, Logs 5 & 6 (see Appendix 8, Tables 10 & 11).

Large beds (up to 2 m) are not typical but when they do occur they are massive and tabular and interbedded with massive mud (Facies 12 a & b), muddy micrite (Facies 8), sandy micrite (Facies 10), micritic mud (Facies 9) (e.g. LMa, LMs, LOw), again along the southern, south-east and southwest basin and upland areas of the study area (see Fig 5.21) (Facies 14b).

5.5.5: Gravels Facies 15 – Facies 17

Gravel deposits commonly occur in alluvial fan depositional settings and braided stream sequences and are a standard feature of turbidity currents (Boggs, 2006; Tucker, 2006; Nichols, 2009). All gravels found within the

study area are found in close association with active and inactive barranca, rivers, streams and floodplains (Fig 5.26) forming erosive channels that incise the underlying beds which comprise any of the facies described here (Tables 5.9, 5.15, 5.20, 5.21 & 5.23) besides Facies 12b, and Facies 11c.

5.5.5.1: Description

Unlithified, usually poorly sorted, matrix or clast supported deposits with rounded to angular clasts (Boggs, 2006).

5.5.5.2: Tequiquiac gravel deposits (for facies summary see Table 5.21)

Facies 15 has angular to rounded clasts above 2 mm in diameter that makes up < 30% of the deposit. Beds are matrix-supported, massive and poorly sorted (FGmm, Table 4.8). Deposits can be normally graded (FGmg, Table 4.8) and occur as sheet flow deposits and cut channel infills (Fig 5.25). Facies 16 has angular clasts larger than 2 mm that make > 30% of the deposits. Facies 17 has angular to rounded gravels here have >30% clasts above 2 mm in diameter. In the study area both Facies 16 and Facies 17 can be massive, poorly sorted and matrix (FGmm, FGmg, Table 4.8) or clasts supported (FGcm) and occasionally cross-bedded (Fig 5.26).



Figure 5.26: Field examples of Facies 16, massive matrix supported gravel (Facies 16). Site TB10, Log 3.



Figure 5.27: Field example of poorly sorted, matrix-supported angular-rounded gravel (Facies 17). Site TB5, Log 7.

5.6: Facies 18 a - d, Volcanic tephra deposits

This section focuses on pyroclastic deposits made up of volcanic rock fragments and minerals that form a volcanic ash matrix. Tephra forms when a combination of ash, rock and mineral fragments (< 4mm) (pyroclastic and tephra fragments), are blasted into the air and fall to the ground as a mixed deposit (USGS, 2017).

5.6.1 Tequixquiac volcanic tephra deposits (see Table 5.23 for facies summary)

The principal oxides and trace elements concentrations of several tephra deposits from the study area were measured (see Chapter 7, Table 7.2) these include; course to fine basaltic-andesite ash (Facies 18a), fine andesitic ash (Facies 18b), and fine dacitic ash (Facies 18c). Other tephra deposits were observed and logged in the field, and these have been classified by grain size (Table 5.22), colour and sedimentary structures (Fig 5.28). Tephra deposits in the study area range fine ash to lapilli with or without pumice fragments (Facies 18 d & e), and they have usually undergone a degree of reworking (Table 5.23). Deposits are usually wide-spread and mantle the topography.

5.7: Facies 19, Calcrete

5.7.1: Tequixquiac pedogenic calcrete facies (see Table 5.24 for facies summary)

Pedogenic calcrete formation, facies and facies architecture are discussed in Chapter 4 and outlined in Tables 4.13 and Figures 4.3 and 4.4. In the study area, pedogenic features mainly consist of laminar crusts

Table 5.21: Summary of the recorded, clastics deposits found within the study area

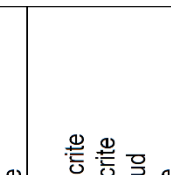
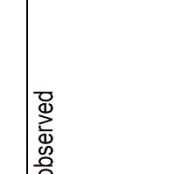
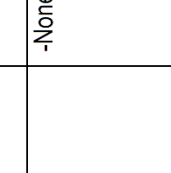
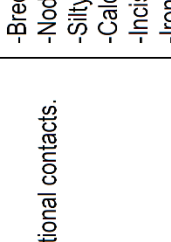
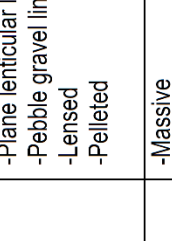
| Facies Name | Main facies description | Range of sub-facies description | Range of sedimentary structures | Post depositional facies | Associated facies | Stratigraphic facies key |
|-------------------------|--|----------------------------------|---|---|---|--|
| Facies 11a, Clay | -Beds thicknesses are < 0.10 m. -Greyish yellow green (5GY 7/2). -Light brown (5YR 5/6). -Moderate red (5R 5/4) -Dark reddish brown (10R 3/4) | -None | -Massive -Tabular plane beds -Disconformable and gradational contacts | -Vertically jointed -Nodules -Silty joint infill | -Mud -Muddy micrite -Sandy micrite -Micritic mud -Limestone |  |
| Facies 11b, Clay | -Beds thicknesses up to 7 m. -Greyish yellow green (5GY 7/2). -Pale yellowish green (10GY 7/2). | -None | -Massive -Tabular plane beds -Disconformable and gradational contacts | -None-observed | -Mud -Muddy micrite -Sandy micrite -Micritic mud -Limestone |  |
| Facies 11c, Clay | -Bed thicknesses are between 0.10 – 1 m. -Brownish black (5RY 2/1) -Dark grey (N3) -Black (N1) | -Molluscs in-tact and fragmented | -Massive -Faintly laminated | -Soft, mm scale, aligned flecks of fine white sand, high water table and ground water deposition? | -Silt -Mud -Sand -Gravels |  |
| Facies 12a, Mud | -Bed thicknesses from 0.10 m to 3 m. -Pale yellowish green (10GY 7/2) -Greyish yellow green (5GY 7/2) -Moderate pink (5R 7/4) -Light greyish green (5G 8/1) -Pale red (5R 6/2). -Moderate red (5R 4/4) -Pale reddish brown (10 5/4) | -None | -Massive -Poor to moderate sorting -Plane tabular -Disconformable and gradational contacts -Lenticular cross-bedded ripples | -None-observed | -Mud -Muddy micrite -Sandy micrite -Micritic mud -Limestone |  |
| Facies 12b, Mud | -Black (N1) or greyish black (N2) mud. -Bed thicknesses range from 0.03 m – 2 m. | -Organic | -Massive -Faintly laminated -Disconformable, sometime gradational contacts | -Root penetration -Vertical jointing | -Clay -Silt -Sand -Gravels |  |

Table 5.21: Summary of the clastics facies recorded from the study area

| Facies Name | Main facies description | Range of sub-facies description | Range of sedimentary structures | Post depositional facies | Associated facies | Stratigraphic facies key |
|---|---|---------------------------------|---|---|--|---|
| Facies 12c, Mud | <ul style="list-style-type: none"> -Bed thicknesses are < 0.20 m. -Moderate red (5R 5/4). -Dark reddish brown (10R 3/4). -Greyish yellow green 5GY 7/2). -Light brown (5RY 5/6). | -None | <ul style="list-style-type: none"> -Massive -Faintly laminated -Disconformable, sometime gradational contacts. -Lensed. -Bioturbation/Burrows -Pelleted mud-lumps | <ul style="list-style-type: none"> -Vertically jointed -Brecciation -Nodules -Silty joint infill -Calcified root system -Incision -Iron staining | <ul style="list-style-type: none"> -Limestone -Muddy micrite -Sandy micrite -Micritic mud -Sand -Gravels -Breccia |  |
| Facies 13a, silt | <ul style="list-style-type: none"> -Bed thicknesses range from 2 – 4 m. -Moderate red (5R 5/4). -Yellowish grey (5Y 8/1). -Light brown (5YR 5/6) silt. -Pale red (5R 6/2). -White (N9). | -None | <ul style="list-style-type: none"> -Massive -Straight upper and lower contacts -Cross-ripple lamination -Plane lenticular lamina -Pebble gravel lined scours -Lensed -Pelleted | <ul style="list-style-type: none"> -None | <ul style="list-style-type: none"> -Limestone -Muddy micrite -Sandy micrite -Micritic mud -Sandy silt |  |
| Facies 13b, silt | <ul style="list-style-type: none"> -Bed thicknesses variable up to 4 m. -Moderate red (5R 5/4). -Moderate brown (5RY 3/4). -Light brown (5YR 5/6). -White (N9). -Light red (5R 6/6) | -None | -Massive | <ul style="list-style-type: none"> -Vertically jointed -Brecciation -Nodules -Silty joint infill -Calcified root system -Incision | <ul style="list-style-type: none"> -Clay -Fine sand | |
| Facies 14a, fine silty sand to fine sand | <ul style="list-style-type: none"> -Bed sizes variable. -Moderate red (5R 5/4) -Dark reddish brown (10R 3/4) | -None | <ul style="list-style-type: none"> -Massive -Poorly sorted | <ul style="list-style-type: none"> -Vertically jointed -Brecciation -Nodules -Silty joint infill -Calcified root system -Incision -Iron staining Fine sand -None | Any |  |

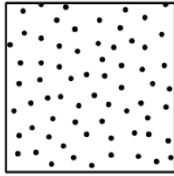
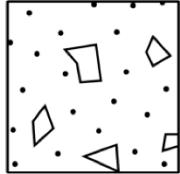
| Table 5.21: Summary of the recorded, clastics deposits found within the study area | | | | | | |
|--|--|---|---|--|--|---|
| Facies Name | Main facies description | Range of sub-facies description | Range of sedimentary structures | Post depositional facies | Associated facies | Stratigraphic facies key |
| Facies 14b, fine silty sand to fine sand | <ul style="list-style-type: none"> -Bed thicknesses are between 0.10 – 5 m -Pinkish grey (5RY 8/1). -White (N9) | <ul style="list-style-type: none"> -Molluscs -Megafaunal bones | <p>Silty fine sand to fine sand</p> <ul style="list-style-type: none"> -Usually poorly sorted -Massive -Channel scours that have trough cross-beds and plane laminations. Scours can be lined with pebble gravel lag deposits. -Cross ripple-lamina -plane cross-beds -Plane lamination -Load structure -Cross bedding | -Nodules | <ul style="list-style-type: none"> -Clay -Silt -Sand -Gravels -Calcrete -Micrite |  |
| Facies 14c, fine to medium sand | <ul style="list-style-type: none"> -Light brown (5YR 5/6) -Medium grey (N5) -Pale reddish brown (10R 5/4) -Yellowish grey 5Y (8/1) -Dusky yellow green (10GY 3/2). -Pale red (5R 6/2). | <ul style="list-style-type: none"> -Molluscs -Megafaunal bones -Pebble gravel clasts | <p>Fine to mediums sand</p> <ul style="list-style-type: none"> -Usually poorly sorted -Cross beds -Lenticular tough cross-beds -Plane lamination -Plane cross lamination -Trough cross beds | <ul style="list-style-type: none"> -Nodules -Vertical jointing | <ul style="list-style-type: none"> Clay -Silt -Sand -Gravels -Calcrete | |
| Facies 14d, medium to coarse sand | | <ul style="list-style-type: none"> -Megafaunal bones | <p>Medium to coarse sand</p> <ul style="list-style-type: none"> -Usually poorly sorted -Cross-bedded ripples -Plane lamination -Plane cross beds -Tabular plane cross-beds channels infill -Massive with pebble gravel lined scours -Trough cross-beds | -Nodules | <ul style="list-style-type: none"> Clay -Silt -Sand -Gravels -Calcrete | |

Table 5.21: Summary of the recorded, clastics deposits found within the study area

| Facies Name | Main facies description | Sub-facies description | Range of sedimentary structures | Post depositional facies | Associated facies | Stratigraphic facies key |
|---|--|--|---|---|--|---|
| Facies 15, Gravel, matrix dominated and clast poor | Pebble to boulder gravel. Clasts include mud and silt rip-up clasts, volcanoclastics and limestone. Matrix: clay, silt or sand or a mixture. Yellowish grey (5Y 8/1), Dusky yellow green (5GY 5/2), Pale reddish brown (10R 5/4), Moderate reddish brown (10R 4/6), Greyish pink (5R 8/2), Light grey (N8), and Moderate red (5R 5/4) | -Molluscs -Megafauna bones (fragmented) | -Massive -Can be normally graded -Poorly sorted -Range of gravel sizes -Angular to rounded clasts -Polymictic -Monomictic -Intraformational - Extraformational -Blanket deposit -Can infill cut-channel -Very occasional bed forms | -Vertical jointing -Brecciation -Root penetration | -Laminated, ripple-cross laminated to cross-bedded sands that follow bed -Muddy micrite, micritic mud, sandy micrite. |  |
| Facies 16, Angular gravel | Pebble to boulder sized clasts. Clasts include mud and silt rip-up clasts, volcanoclastics and limestone. Matrix: clay, silt or sand or a mixture. Yellowish grey (5Y 8/1), Dusky yellow green (5GY 5/2), Pale reddish brown (10R 5/4) or Moderate reddish brown (10R 4/6) | -Megafauna bones (fragmented) | -Massive -Can be normally graded -Poorly sorted -Range of gravel sizes -Angular clasts -Polymictic -Monomictic -Intraformational - Extraformational -Blanket deposit -Can infill cut-channel -Some bedding structures -Very occasional bed forms | -Vertical jointing -Brecciation -Root penetration | -Laminated, ripple-cross laminated to cross-bedded sands that follow bed |  |
| Facies 17, Angular – rounded gravel | Pebble to boulder angular – rounded gravel. Clasts include mud and silt rip-up clasts, volcanoclastics and limestone. Matrix, clay, silt or sand or a mixture. Yellowish grey (5Y 8/1), Dusky yellow green (5GY 5/2), pale reddish brown (10R 5/4) or moderate reddish brown (10R 4/6) | -Megafauna bones (fragmented) | -Massive -Can be normally graded -Poorly to relatively well sorted -Range of gravel sizes -Can be crudely bedded -Angular to rounded clasts -Polymictic -Monomictic -Intraformational - Extraformational -Blanket deposit -Can infill cut-channel -Very occasional bed forms | -Vertical jointing -Brecciation -Root penetration | - Laminated, ripple-cross laminated to cross-bedded sands that follow bed |  |

| Grain size mm | Tephra fragments |
|---------------|------------------|
| | Blocks and bombs |
| 64 | Lapilli |
| 2 | Coarse Ash |
| 1/16 | Fine Ash |

Table 5.22: Grain-size classification for tephra fragments used in the study area (Mullineaux, 1996).



Figure 5.28: Field example of Fine light grey (N7) ash interbedded with coarse sand sheets (CGwsh?). Site TB15 (see Chapter 6 and Appendix 5, Table 1)

(CPedPI, Fig 4.4) and nodular (CPedN, Fig 4.4) horizons. For a petrographic example of laminar crusts, see Figure 5.19 and Table 5.19. For a field example of pedogenic calcrete root-nodular horizon, see Figure 5.29.

5.7.2: Groundwater calcrete facies found in the Tequixquiac Basin (see Table 5.24 for facies summary)

Groundwater calcrete formation, facies and facies architecture are discussed in Section 4.4.8 and outlined Table 4.16. In the study area, groundwater calcrete beds are thought to be either soft nodular layers (CGwNod, Table 4.16, Fig 5.30) or thin carbonate sheets that transect stratigraphic boundaries in fluvial-aeolian sands (CGwsh, Table 4.16, Fig 5.31).

5.7.3: Calcite cement

The precipitation of cement in carbonate sediments is a diagenetic process that occurs when pore-fluids are supersaturated during the cement phase when there are no kinetic factors inhibiting precipitation (Tucker & Wright, 1990). Cement precipitate into open cavities within the sediment body, between grains and many cement crystals, show typical fabrics that indicate void infill (e.g. drusy) (Tucker & Wright, 1990).

Table 5.23: Summary of recorded volcanoclastic facies recorded from the study area (also Chapter 7 and Table 7.2)

| Facies name | Facies description | Sedimentary structure | Stratigraphic key |
|--|---|---|-------------------|
| Facies 18a: Basaltic-andesite (see Table 7.3 – 7.5, Figs 7.3 – 7.5, Figs 7.3 – 7.5) | -White (N9) to greyish yellow-green (5GY 7/2) coarse to fine ash. -Bed thicknesses from 0.10 up to 0.30 m. | -Massive -Lamented -Normally graded -Tabular bed | |
| Facies 18b: Andesite (see Table 7.4 – 7.5, Figs 7.3 – 7.7) | -White (N9) fine ash up to 0.50 m thick. | -Massive -Normally graded -Tabular bed -Bioturbation/burrows -Ungulate hoof prints | |
| Facies 18c: Dacite (Tables 7.4 – 7.5, Figs 7.3, 7.4 & 7.7) | -White (N9) to greyish pink (5R 8/2) fine ash. -Bed thicknesses range from 0.15 – 0.30 m. | -Massive -Lamented -Normally graded -Re-worked in channel form | |
| Facies 18d: Medium-light grey coarse ash to lapilli (Figs 5.28 & 5.31) | -Medium-light grey (N6) coarse ash to lapilli -Bed thickness < 2 m. -Can contain pumice fragments | -The bed has boundary and channel form or is massive to laminated with thin sandy interbeds -In places, chaotic bedding -Contacts are gradational, or erosive channel scours. | |
| Facies 18d: Black fine to coarse ash | -Black (N1) -This deposit is reworked and occurs as interbeds | -Massive -Laminated -Cross-laminated -Cross-bedded | |



Figure 5.29: Field example of pedogenic root-nodules. Site TB16, Log 1, bed 1 (see Appendix 6, Table 1 and Chapter 6).



Figure 5.30: Field example of soft nodular groundwater calcrete horizon that join to form thin (<5 mm) lamina in places. Site TB9, Log 1, bed 19 1 (see Appendix 4, Table 1 and Chapter 6). Arrows indicate examples.



Figure 5.31: Field example of coarse sand sheets containing sandy calcified horizons that transect stratigraphic boundaries (CGwsh?) (<15 mm). Site TB17, Log 1, bed 4 (see Appendix 3, Table 1 and Chapter 6). Arrows indicate examples.

| Table 5.24: Summary of recorded calcrete facies recorded from the study area. See Figure 4.4 & Table 4.16. | | | |
|---|---|---|--------------------------|
| Facies name | Facies description | Sedimentary structure | Stratigraphic key |
| Facies 19a: Pedogenic laminar calcrete horizon | Very light grey (N8) micrite to micritic sand | -Fine lamina | |
| Facies 19b: Pedogenic nodular horizon | Moderate red (5R 4/6) silt matrix | -Massive -Sub-rounded carbonate (max 0.24 m in diameter) nodules and vertically elongated carbonated nodules (max 0.25 m in diameter and 0.50 m thick) -Vertical jointing | |
| Facies 19c: Groundwater calcrete soft nodular bed | Greyish yellow-green (5GY 7/2), massive micritic mud. | -Small carbonate flecks (<.10 mm) -Flecks are soft, aligned with sedimentary bedding, and the edges of the nodules are defused | |
| Facies 19d: Groundwater calcrete thin carbonate sheets | White N9 indurated micritic carbonate with sand inclusions (0.10 – 0.03 m thick). | Coarse to fine sand beds that sit at the boundaries of sandy bedforms associated with fluvial and alluvial environments. | |

Table 5.25: Sedimentological symbol key for stratigraphic logs

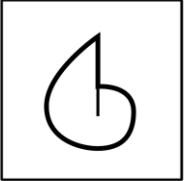
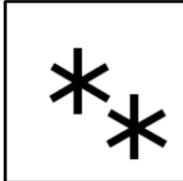
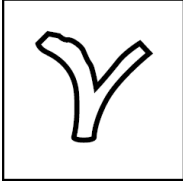
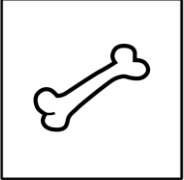
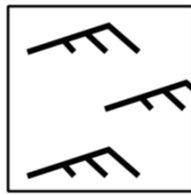
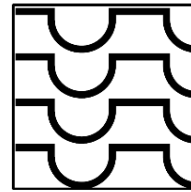
| | | | |
|---|-----------------|---|-----------------------|
|  | Shells |  | Bioturbation |
|  | Gastropods |  | Manganese |
|  | Biofilm laminae |  | Calcite vein |
|  | Stromatolites |  | Halite crystal moulds |
|  | Vertebrates | | |
|  | Plant material | | |
|  | Roots | | |

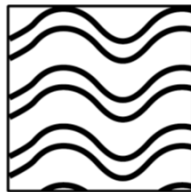
Table 5.25: Continued



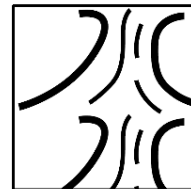
Current ripple cross-lamination



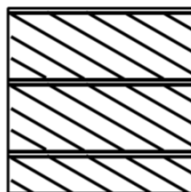
Load casts



Wave ripple cross-lamination



Water structures

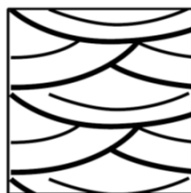


Planar cross bedding

Base Boundaries



Erosion



Trough cross bedding



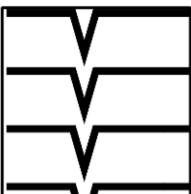
Gradational



Horizontal planar lamination



Sharp



Mudcracks

5.7.3.1: Sparry calcite cement

Sparry calcite cement consists of translucent and equant (roughly cubic or spherical) calcite crystals (0.02 – 0.1 mm). They form during diageneses, and their presence within pore spaces suggests that the grain framework voids were empty when the deposit accumulated. Voids within carbonate or mixed carbonate-clastic deposits tend to indicate rapid deposition under high energy conditions.

Sparry crystals also form through the recrystallisation of the primary deposit during diageneses (Boggs, 2006). In the study area, sparry cement is a common feature of carbonate and mixed carbonate and clastic deposits these infill fabric void spaces and precipitate along fractures and weaknesses (calcite veins). For petrographic examples and descriptions, see Sections 5.3 and 5.4.

5.7.3.2: Drusy calcite cement

Drusy calcite cement line the pore walls of limestone with increasing crystal sizes that radiate inwards. Usually, there is an increase in crystal size and a decrease in number towards the centre of the void (Tucker & Wright, 1990). Drusy calcite is a primary pore-filling cement in the study area. For petrographic examples and descriptions, see Sections 5.3 and 5.4.

5.7.4: None-carbonate evaporite deposits

Evaporation and freezing can cause crystals of evaporitic salts and water to develop, respectively. These features are standard on alluvial floodplains and lake margins (Meurant, 1976). The crystals can be preserved or replaced by pseudomorphs or dissolved, and the remaining cavity filled (e.g. silt, sand or sparry calcite) with the infill casting the shape of the crystal (Meurant, 1976). These structures signify sub-area exposure and drying of a sedimentary sequence but do not necessarily imply long-term exposure (Meurant, 1976). From the original volume of a water body, when 50% is remaining, carbonate precipitates, when 20 % is remaining gypsum precipitates, and when 10% is remaining halite precipitates (Boggs, 2006). In the study area, halite hopper crystal moulds occasionally occur in micritic mud and mudstone beds (Facies 3) suggesting robust evaporitic processes were occurring, and the 90% of the volume of the water body had been evaporated (Meurant, 1976). For petrographic example and description, see Table 5.10 and 5.6.

5.8: Conclusion

Here identified Quaternary facies that have been observed and recorded in the study area have been described, identified, separated into facies and summarised in Tables 5.9, 5.15, 5.20, 5.21 and 5.23. Table 5.25 gives the sedimentological symbol key for the stratigraphic logs presented in Chapter 6.

Chapter Six: Tequixquiac Basin Stratigraphy

6.1: Introduction

In this chapter, examples of the stratigraphy recorded at the studied sites are described, and depositional environments are interpreted. The stratigraphic logs and sedimentological descriptions follow the facies nomenclature proposed in Chapters 4 & 5. Specifically Table 5.9, Facies 1 – 2, Bio-mediated limestone, Table 5.15, Facies 3 – 7, Carbonate grain limestone; Table. 5.20, Facies 8 – 10, Mixed carbonate-clastic deposits, Table 5.21, Facies 11 – 17, Clastic deposits, and Table 5.23, Facies 18, tephra deposits should be referred to for facies codes.

6.2: Barranca el Pocito, Site TB14

Barranca el Pocito is located in the far south-western study area in between the Mesa Grande and San Mateo Hill (Table 6.1, Figs 6.1, 8.1 & 8.9). Both hills are thought to exist because of the aggradation of the Tarango Formation and Quaternary alluvial sediments (see Moser, 1975; Segerstrom, 1952, 1956, 1962; Bradbury, 1998, Chapter 3, Chapter 8 and Figs 3.3, 8.1, 8.9 & 8.14). The Barranca has an approximate length of 1.34 km and an altitude range of 2314 - 2268 m a.s.l. Today the barranca is dry with ephemeral flow occurring during the wet season which drains into the Rio Salado River (Figs 6.1 & 6.2). There is very little vegetation on the barranca floor, but the slopes are partially vegetated, providing some slope stability (Fig 6.3).

6.2.1: Geomorphology, Site TB14

The barranca is flat bottomed and deeply incised (<150 m) into unconsolidated, horizontally stratified clastic material. The walls are near vertical with gully incision and debris cone development evident (Fig 6.3). There are no visible terrace deposits preserved along the length of the barranca, and currently, within its life cycle, it appears to be infilling and back-filling slowly.

6.2.2: Sedimentological description, Log 1, Site TB14

The lower 12 m of Log 1 (Figs 6.1, 6.3 & 6.4) is made up of thick interbeds (<3 m) of (from the base) massive carbonate-rich mud (Facies 9a), massive mud (Facies 12a) and massive silt (Facies 13b) beds that are separated by thinner beds (<0.25 m) of carbonate-rich mud (Facies 3a). The boundary contacts between beds are gradational and straight. In the upper 3 m, average bed thickness decreases to < 1 m. Bedding contacts are uneven, and in some cases erosive and disconformable.

Figure 6.1: Location map for Site TB14, Barranca el Pocito and Site TB17, San Mateo Hill. a) The green dashed line indicates the general location of the studied sites. b) Location of stratigraphic logs. L = Log. See also Figures 8.1 & 8.6.

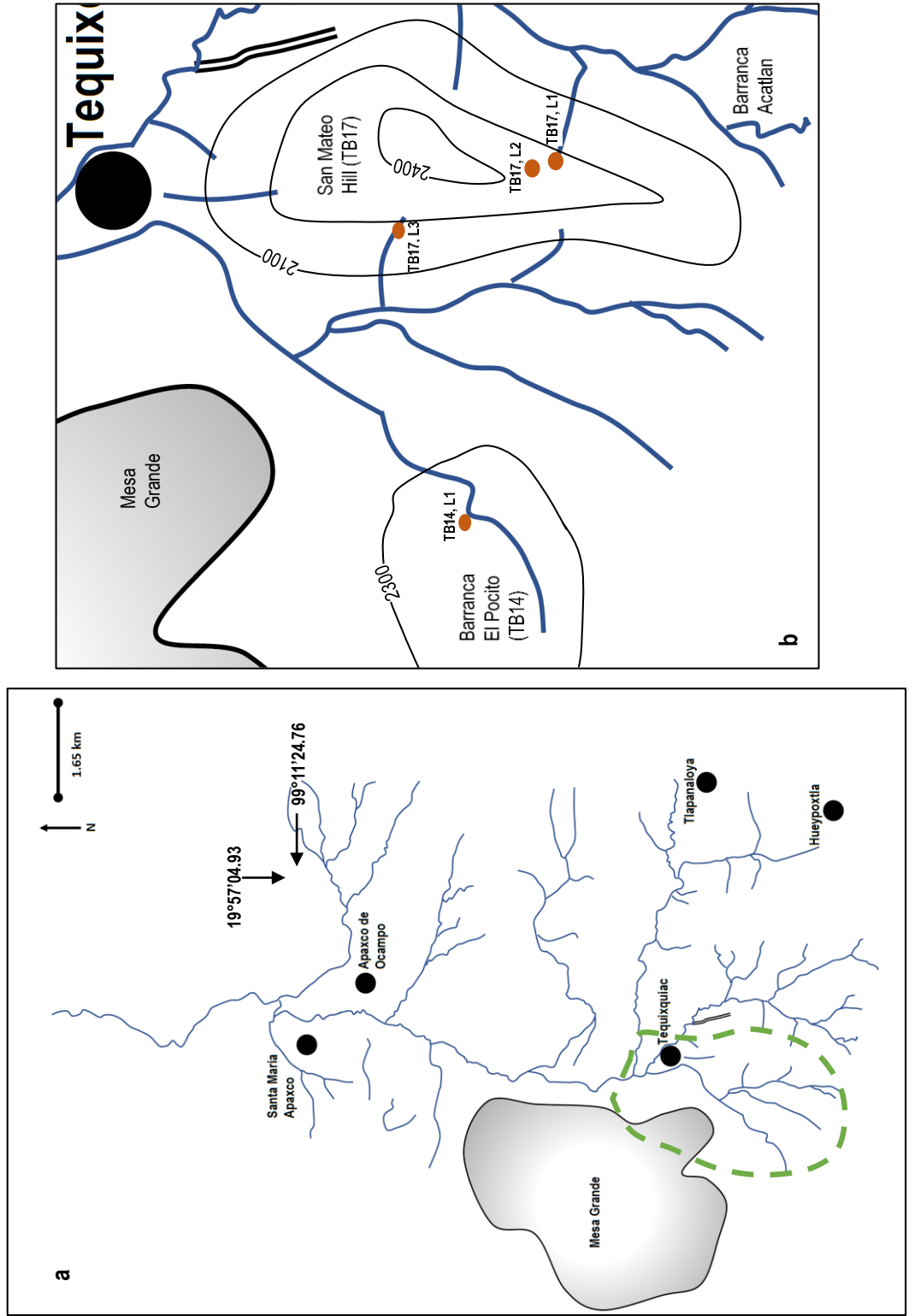


Table 6.1: Site information. Altitude recorded from the base of logged sequences. See Figures 6.1, 6.2, 8.1 & 8.9.

| Log Num. | Latitude | Longitude | Altitude m a.s.l | Location |
|-------------------------------|-----------|-----------|------------------|------------------------------------|
| Site TB14, Barranca el Pocito | | | | |
| L1 | 19 52.491 | 99 09.060 | 2275±4 | Right side of barranca half way up |
| Site TB17, San Mateo Hill | | | | |
| L3 | 19 53.632 | 99 08.150 | 2260±4 | San Mateo Hill barranca |
| L2 | 19 53.312 | 99 07.542 | 2318±3 | San Mateo Hill Corn Field |
| L1 | 19 53.342 | 99 07.496 | 2300±4 | San Mateo Quarry |

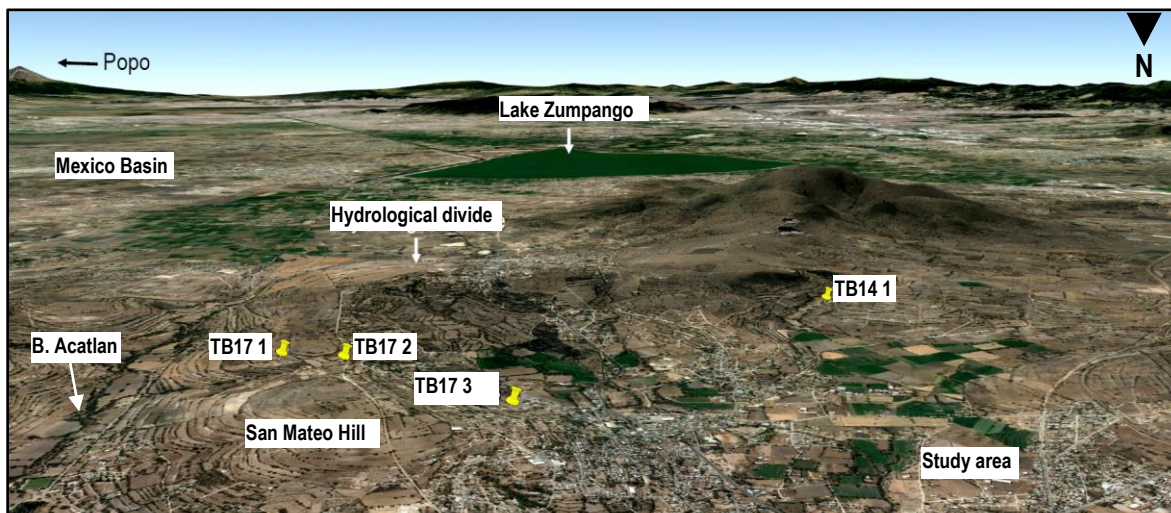


Figure 6.2: Location map for Site TB14 and Site TB17. Source, Google Earth. Popo: Popocatepetl volcano. B. Acatlan = Barranca Acatlan.



Figure 6.3: Site TB14, Log 1. See Figure 6.4 for stratigraphic log (see Figs 6.1, 6.2, 6.3, 8.1 and 8.9).

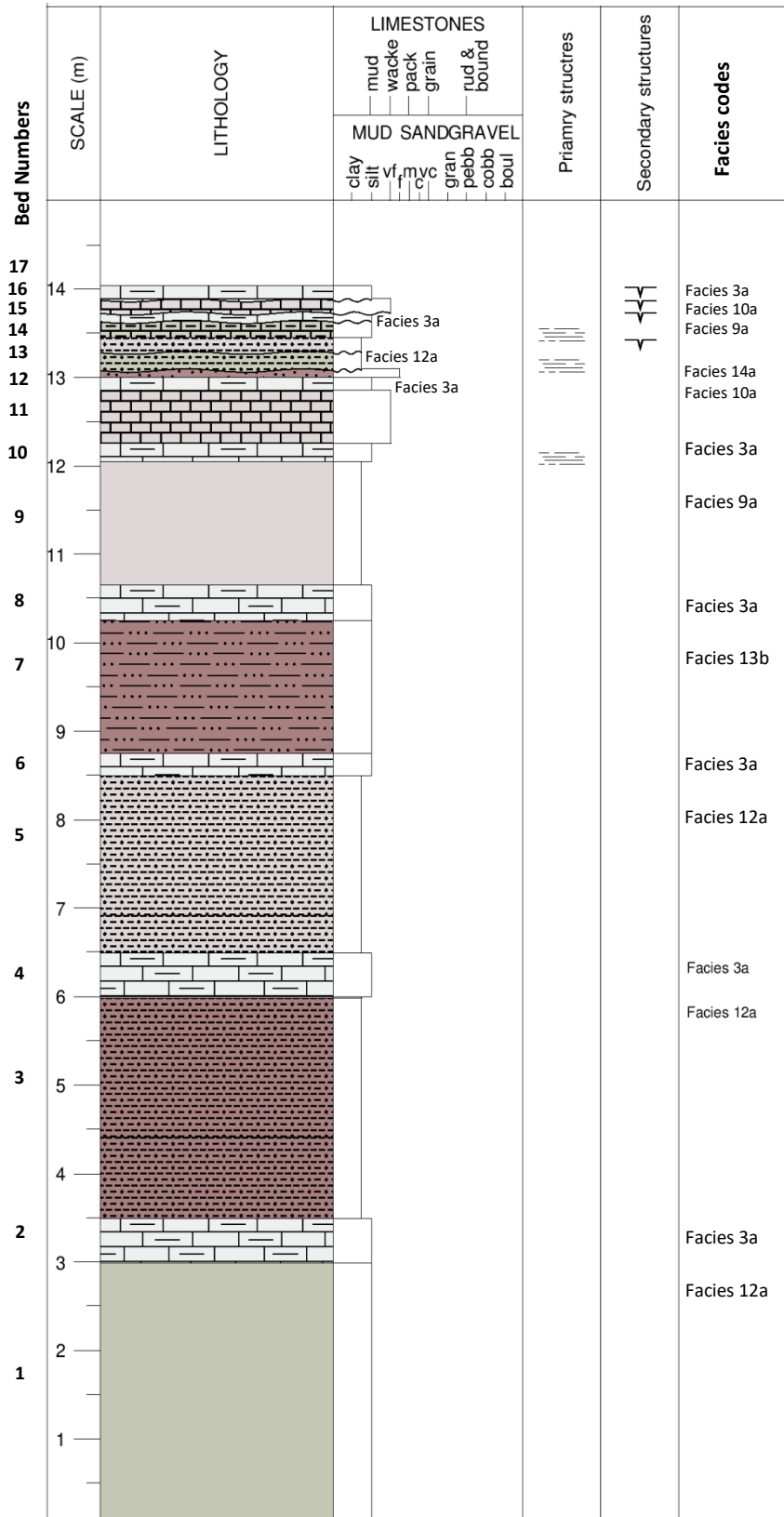


Figure 6.4: Site TB14, Log 1. See Figure 6.3 for a photograph of the logged site. See also Figures 8.1, 8.3, 8.11 & 8.12.

6.2.3: Interpretation, Log 1, Site TB14

Log 1 (Figs 6.4, 8.1 & 8.9) represents massive nearshore to basinal lacustrine sediments that collected in shallow lacustrine depositional environments (e.g. F/LMIs, Table 4.8; LMs, Table 4.10, LHer – LHer, Table 4.11) (Figs 6.15b, 6.16a & 6.18). The first 12m (Facies 9a, 12a & 13b, Beds 1 – 10; Fig 6.4) and is interpreted as massive nearshore to basinal lacustrine depositional deposits (e.g. F/LMIs to LMs, Tables 4.8 & 4.10) suggested by the absence of sub-areal exposure and bedding features, and the laterally extensive and plane nature of the beds. Thinner beds, larger clast size (e.g. Facies 10a, 14a & 10a), erosional bedding contacts, laminations and exposure features in the upper log (Fig 6.4) suggest a shallowing water body subject to temporary hydrological fluctuations (see PNod/Bre, Table 4.12) (Fig 6.4). Clastic beds (Facies 14a, 12a) indicate increased terrestrial clastic input that suppressed carbonate precipitation with carbonate beds representing the opposite (Facies 3a). The stratigraphic sequence recorded in Log 1 (Fig 6.4), Site TB14 has no chronological context other than similarities between this site and Barranca de Colores (Site TB9, Section 6.6) which is known to older than MIS 12c. Because these sequences sit stratigraphically below Logs 1 and 2, Site TB17 it is likely older than MIS 14.3 (see Section 6.3).

6.3: San Mateo Hill, Site TB17

San Mateo hill is a flat-topped mesa-like outcrop that straddles the hydrological divide between the Basin of Mexico and the Study area (see Figs 6.1, 6.2, 8.1, 8.9 & 8.14). At its highest, the hill sits 2311 m a.s.l. At Log 1 records sediments exposed at a quarry site located on the eastern side of the hill 2300 m a.s.l (Figs 6.1, 6.2, 6.5 & 6.8). Log 2 was recorded from the top of the hill from sediments exposed by a road cutting (Figs 6.1, 6.2, 6.6, 6.9, 8.1 & 8.9). Similar sediments to those recorded in Logs 1 & 2 have also been recorded at sites TB1 (Log 1, Appendix 8, Table 6, Figs 8.1, 8.8 & 8.9) and site TB15 (Logs 1 – 4, Appendix 5, Table 1, Figs 8.1, 8.5, 8.9 & 8.13). Log 3 records sediments exposed in a barranca on the western side of the hill (Figs 6.1, 6.2, 6.7 & 6.11). Sequences comparable to these are recorded in sections 6.2.3, 6.4, 6.5 and 6.6.

6.3.1: Geomorphology, Site TB17

The barranca is ca. 25 m deep and densely vegetated which provides slope stability and indicates that water flow is very infrequent, less so than at site TB14. (Fig 6.7 & 6.11). Within its current lifecycle, there is no active incision. Instead, backfilling is occurring.



Figure 6.5: Site TB17. **a)** Log 1 (see Figs 6.1, 6.2, 6.8, 8.1 and Appendix 3, Table 1). **b)** Nodule. Bed 2 (Fig 6.8). **c)** Carbonate nodules in-situ Bed 2 (Fig 6.8). **d)** Sandy carbonate layer (Facies 19d). Upper bed 4 (Fig 6.8).

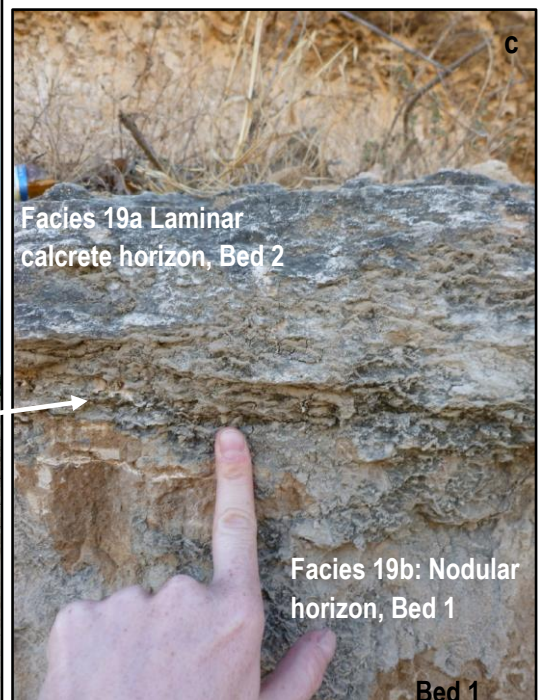
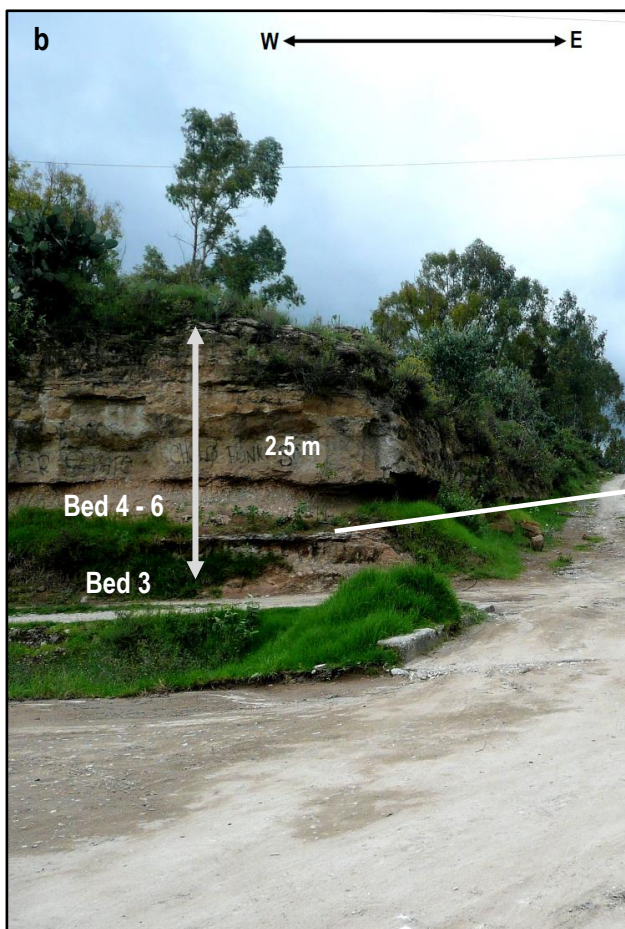
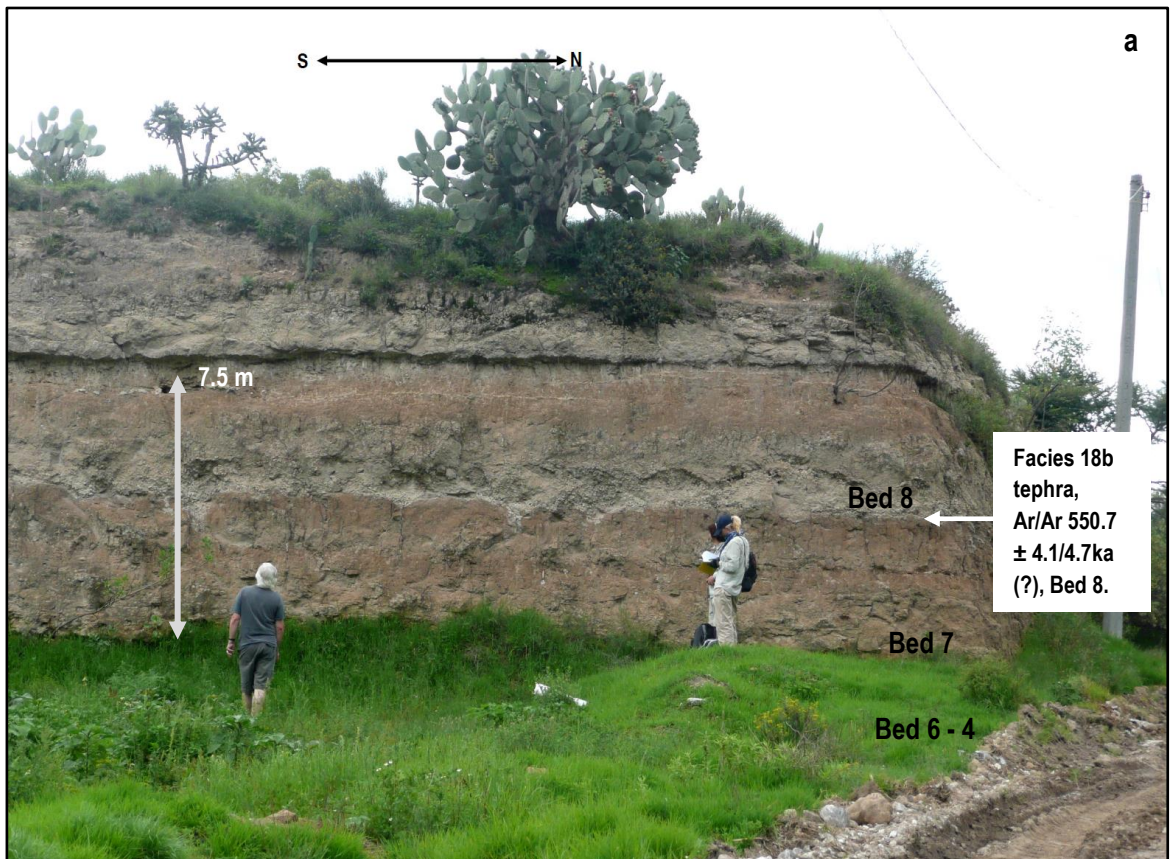


Figure 6.6: Site TB1, Log 2 (see Figs 6.1, 6.2, 8.1). **a:** Upper section of composite sequence. **b:** Lower section of composite log. Log locations indicated by grey arrows. See Figure 6.4. for stratigraphic log. **c:** 19 b & c: Pedogenic calcrete horizon. See Figure 6.9 for stratigraphic log.

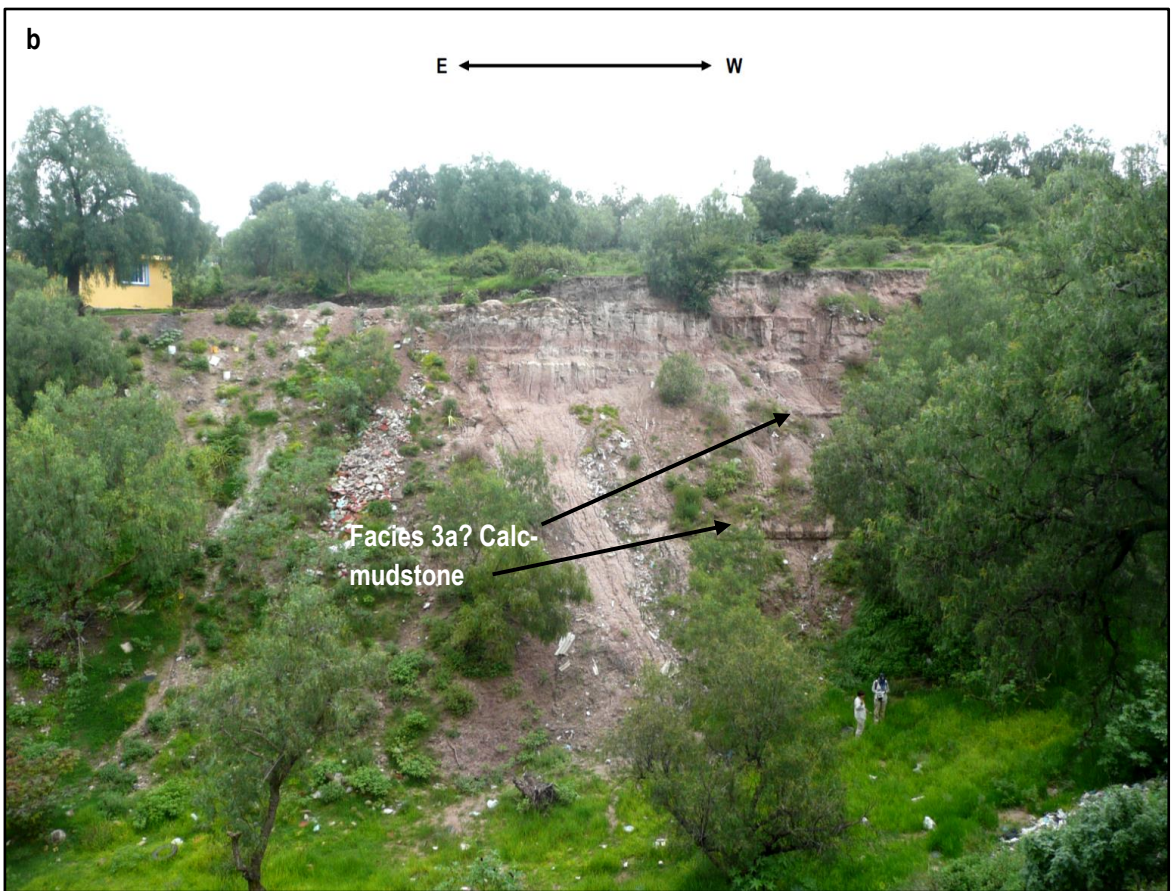


Figure 6.7: Site TB17 **a:** Log 3, Barranca (see Figs 6.1 & 6.2). White lines indicate Log 1 location, is a composite section, see Figure 6.11 for the stratigraphic log. **b:** Southern wall of the barranca were interbedding of Facies 3a can be seen.

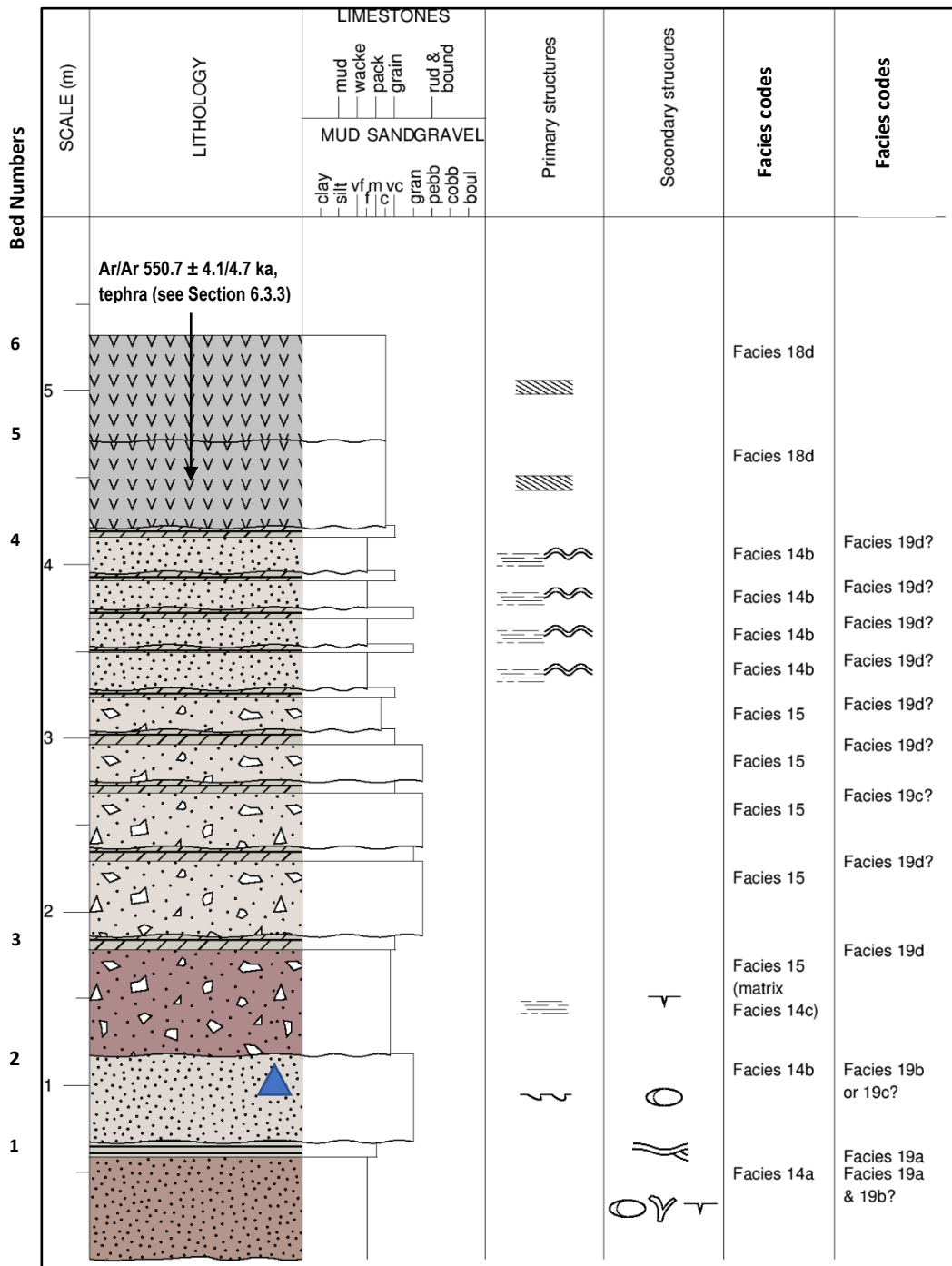


Figure 6.8: TB17, Log 1, see Figure 6.5 for a photograph of log site. For a sedimentological description of this sequence, see Appendix 3, Table 1. See Figure 6.5 a, b & c for Bed 2 and Figure 6.5 d for Bed 4. See also Figures 8.1, 8.5, 8.10. The blue triangle indicates the area highlighted in Figure 6.5 b & c.

6.3.2: Sedimentological description, Site TB17

6.3.2.1: Logs 1 and 2, Site TB17

Sedimentological descriptions for Site TB17, Logs 1 (Fig 6.8) & 2 (Fig 6.9) are given in Appendix 3, Tables 1 & 2; a summary is given here. Logs 1 & 2 both have basal massive, vertically jointed, moderate reddish-

brown (10R 4/6), silty fine sand beds (Facies 14a). Secondary features include vertical jointing, brecciation, carbonate vein and nodule development. In both sections, the upper contact is disconformable. Log 1, Bed 1 (upper) and Log 2, Bed 2 both consists of an unevenly laminated micrite with fine to medium sand (Facies 19a). In Log 2, this bed has a maximum thickness of 0.30 m, in Log 1, bed thickness is < 0.20 m. These beds are followed by 1 m of massive to cross-bedded pinkish-grey (5RY 8/1) fine silty sand (Facies 14b) with nodules in both logs. Locally sourced rip-up clasts form the nodule nucleus coated by sandy carbonate layers (Figure 6.5 b & c). Beds 3 and 4, Log 1 and Bed 6, Log 2 comprise bed set cycles of massive pinkish-grey (5RY 8/1) coarse to fine sand with poorly sorted, angular pebble gravel clasts (Facies 15). This grades into wavy to plain laminated pinkish-grey (5RY 8/1) silty fine with small-scale cross-beds and very occasional small pebble gravel intraclasts (Facies 14b). The same sequence cycle is repeated in the upper section of Log 2, Bed 9. At most of the boundary contacts in Logs 1 and 2, between beds, there is a thin deposit of massive, white (N9) indurated sandy carbonate. These deposits follow the erosive bases of the gravel beds and are usually < 0.05 thick. In both Logs (Bed 5 & 6, Log 1, Fig 6.8 and Bed 8, Log 2, Fig 6.9), there is a thick (<1.5 m) deposit of medium-light grey (N6), medium-coarse fine sand with very fine medium pebble gravel-sized pumice clasts (Facies 18d). This deposit is poorly sorted and sits within boundary and channel forms (max 0.10 m thick).

6.3.2.2: Log 3, Site TB17

Sedimentological descriptions for Site TB17, Logs 3 (Fig 6.11) are given in Appendix 3, Table 3; a summary is given here. The base of Log 3 (Beds 1 – 6) is made up of thick (up to 3 m), vertically jointed (Beds 4 & 5), plane massive interbeds of mud (Facies 12a), silt (Facies 13b), fine silty sand (Facies 14a) and smaller (0.30 m thick), laminated carbonate-rich silt (Facies 3a) in the first 11 m. Bed contacts appear straight and gradational between the clastic beds. The upper and lower contacts of Bed 5, laminated carbonate-rich silt (Facies 3a) are disconformable. The average bed size decreases in the upper 5 m of the sequence (<0.30 m) with interbeds of massive, plane bedded mud (Facies 9a), silt (Facies 13b) and carbonate-rich siltstone (Facies 3a). In the upper log, there is cross-bedded and laminated (see Fig 6.11) interbeds of clay (11b), silt (Facies 13b) and carbonate-rich mud (Facies 9a?). Vertical jointing is common throughout the upper sequence.

6.3.3: ⁴⁰Ar/³⁹Ar age, tephra Facies 18d, Site TB17

A sample of the medium-light grey (N6) coarse ash to lapilli (SMH: San Mateo Hill) (Facies 18d, Logs 1 and 2, Site TB17 (Figs 6.8 & 6.9; Appendix 3 & Appendix 9, Table 1) was submitted to SUERC for Ar/Ar dating (see Chapter 4). Sample (SMH) defines a single age population with an Ar/Ar age of $550.7 \pm 4.1/4.7$ ka. The

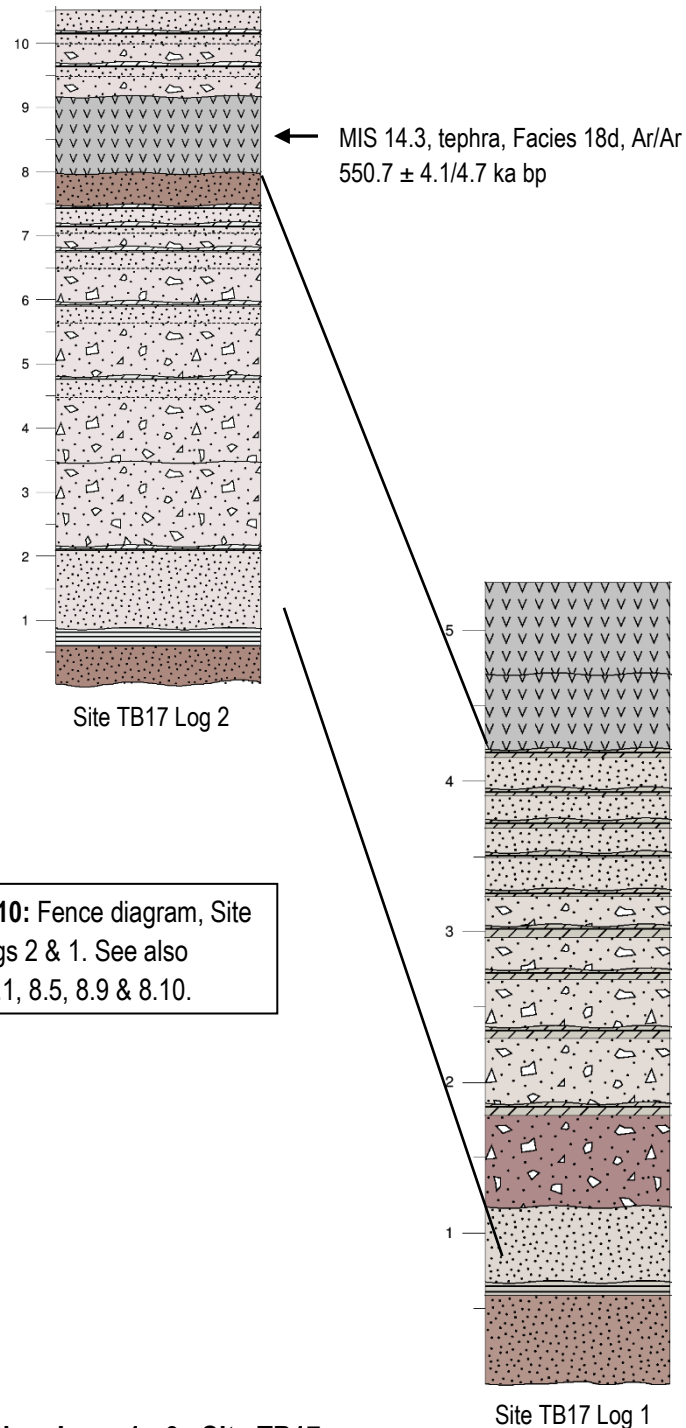


Figure 6.10: Fence diagram, Site TB17, Logs 2 & 1. See also Figures 8.1, 8.5, 8.9 & 8.10.

6.3.4: Interpretation, Logs 1 - 3, Site TB17

6.3.4.1: Logs 1 & 2, Site TB17

Bed 1 (Log 1) and Beds 1 & 2 (Log 2) are interpreted as a pedogenic calcrete profile with a nodular horizon at the base (FP, Table 4.8, 4.9; PNod/Bre Table 4.12) overlain by a laminar horizon (Facies 19a) (CPedPI; Fig 4.4). Massive to bedded gravel and sand beds (Facies 15 & 14b) in Logs 1 & 2, including Facies 18d, likely accumulated during pulses of plastic and pseudoplastic sediment gravity flow (FFSm, FGmm and FGmg, Table 4.8 & 4.9). Ripple-cross to plane laminated fine silty sand beds (Facies 14b, Fig 6.8 & Fig 6.9) (FSr,

FSp, FFSm, FSt Table 4.8 & 4.9) are thought to be fluviually reworked sediments developed during semi-permanent flow, or waning flood conditions (e.g. FFSs, FFI, Table 4.8).

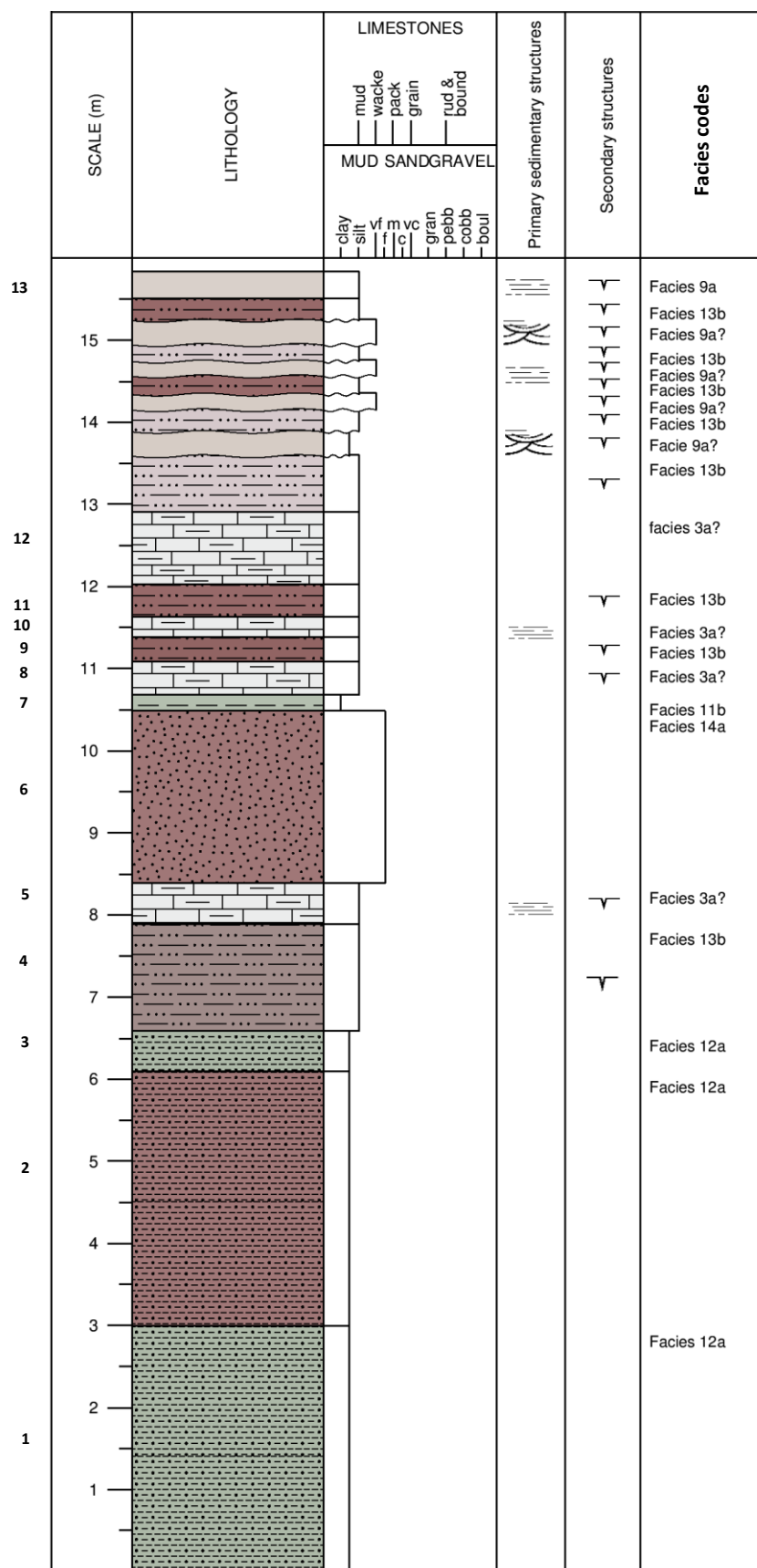
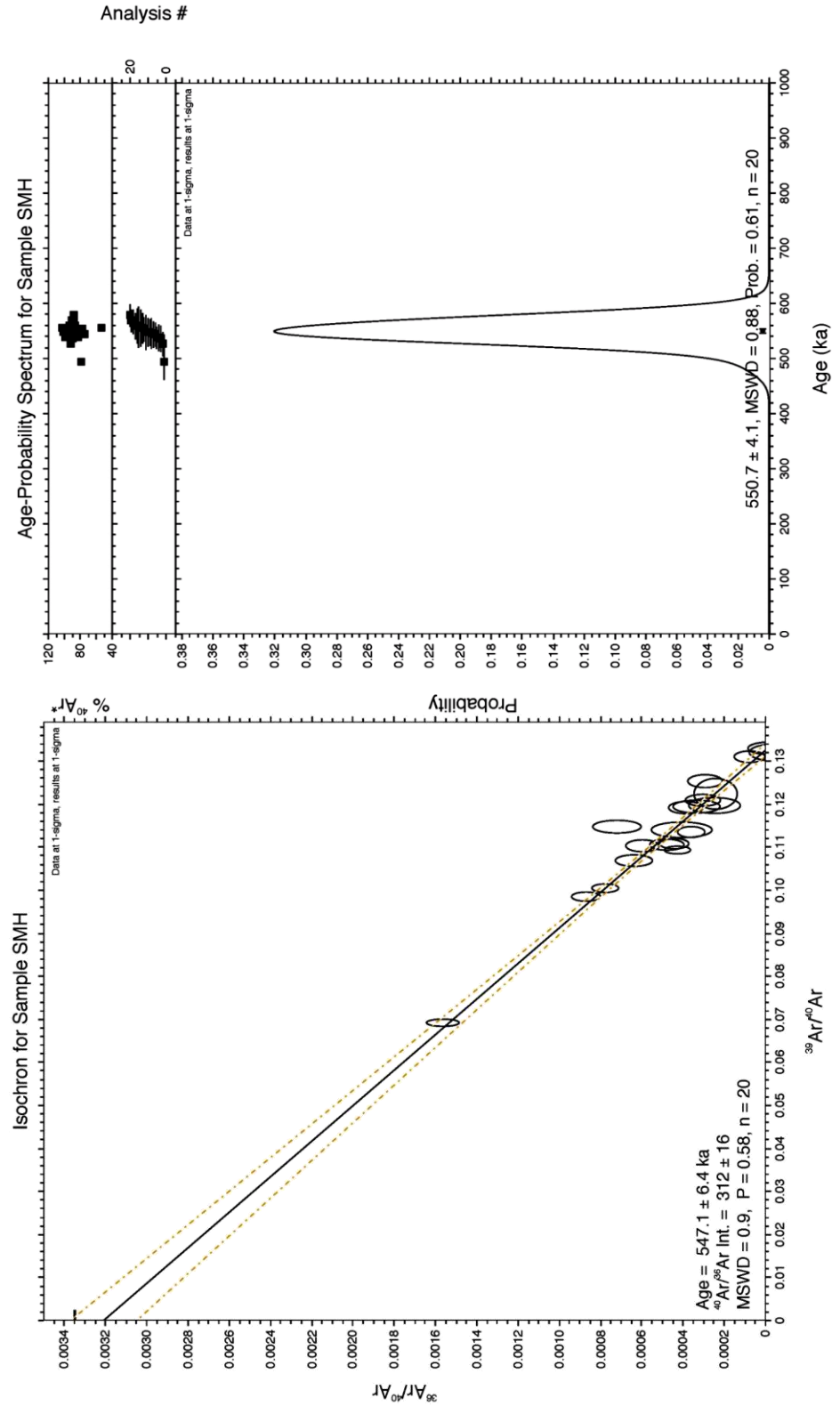


Figure 6.11: TB17, Log 3, San Mate, composite log. Lower and upper and lower log (Fig 6.7). Sedimentological descriptions are given in Appendix 3, Table 3. See also Figs 8.1, 8.3, 8.9, 8.11 & 8.12

Figure 6.12: Right graph: Ar/Ar dating of volcanic ash at San Mateo Hill: Inverse Isochron for Facies 18d (tephra sample SMH). The x-axis plots the $^{39}\text{Ar}/^{40}\text{Ar}$ ratios and $^{36}\text{Ar}/^{40}\text{Ar}$ ratios of the individual heating steps. The best line fit through the data set gives the trapped $^{40}\text{Ar}/^{36}\text{Ar}$ values from the y intercept and the $^{40}\text{Ar}/^{39}\text{Ar}$ age value from the x – intercept (McIntosh et al. 2015). **Left graph:** Age probability spectrum for Facies 18d (tephra sample SMH). Data at 1 – sigma and results at 1 – sigma.



The grey tephra deposit recorded in Log 1, (Beds 5 & 6, Facies 18d, $550.7 \pm 4.1/4.7$ ka BP) was deposited around MIS 14 and stratigraphically links Logs 1 and 2 (Figs 6.8, 6.9, 6.10, 8.1, 8.5, 8.9 & 8.13) at Site TB17 (Fig 6.10). Facies 18d at Site TB17 potentially correlates to similar sediments recorded at Site TB1, Log 1 (Fig 8.5, Appendix 8; Table 6) and Site TB15, Log 1 (Fig 8.5, Appendix 5; Table 1). Both sites TB17 and TB1 sit around the same altitude, towards the southern end of Barranca Acatlan (Figs 8.1 & 8.9) and record similar stratigraphy. Site TB15 (Appendix 5, Table 1) also has a dominance of massive to cross-bedded gravels (Facies 15) interbedded massive, laminated and cross-bedded sand (Facies 14), but lies ca. 30 m below Sites TB17 & TB1.

Because Logs 1 & 2 (Site TB17), and the sequences recorded at Sites TB1 and TB15, sit stratigraphically above sections interpreted as lacustrine sediments (see Sections 6.2.2 and 6.3.4.1; Figs 6.4, 6.11, 6.18, 6.19, 6.29, 6.30, 6.33, 6.34, 8.1, 8.5 & 8.10) these sediments are thought to be younger. The elevation of the gravels may indicate the palaeo-basin floor elevation at the time deposition. Together the gravels and sandy beds indicate a period of environmental instability when reduced vegetation cover exposed unconsolidated slope material that could be easily eroded and resedimented (see Chapter 8, Figs 8.1 & 8.9).

6.3.4.2: Interpretation, Log 3, Site TB17

The stratigraphic sequence recorded in Log 3 (Fig 6.11), Site TB17 has no chronological context other than similarities between this site and Site TB9, (Section 6.6) and Site TB12, (Appendix 4, Table 5) which is known to be older than MIS 13 (see Section 6.6, Chapter 8 & Figs 8.8, 8.10 & 8.11). The facies identified for Log 3, like in Log 1 Site TB14, suggest lacustrine intersectional shallowing cycles and an overall shallowing water body (Fig 6.11). For example, Beds 1 – 3 (mud, Facies 12a) imply a relatively stable water body, Beds 4 – 5 silt (Facies 13b) to calc-mudstones (Facies 3a) suggest a shallowing water body, Beds 6 – 7, fine silty sand (Facies 14d) to clay (Facies 11b) suggest increasing water depth (see Fig 6.11 and LMs, LM_i, LM_a, Table 4.10; PNod/Bre, Table 4.12). The lower 10.5 m are massive, with predominantly gradational contacts and no evidence of sub-areal exposure (Fig 6.10) indicating nearshore to basinal lacustrine depositional environments (LMs, Table 4.10). The upper 6 m of the sequence shows evidence of fluctuating water levels and sub-areal exposure (Fig 6.10). These beds are interpreted as marginal lacustrine deposits (LM_a, Table 4.10; LL_{er}, Table 4.11 and Fig 4.2).

6.4: San Jose Hill

The San Jose Hill (Fig 6.13), like San Mateo Hill (Fig 6.1), is a flat-topped mesa-like outcrop that straddles the south-eastern hydrological divide between the Basin of Mexico and the Study area (see Figs 6.1, 6.13 & 6.14, Table 6.2). Before fluvial incision, there was likely no topographic separation between the San Jose and San Mateo hills (see Fig 8.14). The flat mesa top of the hill sits, at its highest, 2340 m a.s.l towards at the southern limit of the divide (See Figs 6.13 & 8.1). Again, the hill is thought to exist because of the aggradation of large volumes of Tarango Formation and Quaternary alluvial sediments (see Moser, 1975; Segerstrom, 1952, 1956, 1962; Bradbury, 1998, Chapter 3, Chapter 8 and Figs 3.3, 8.1, 8.9 & 8.14). Barranca and gully incision into the unconsolidated Tarango Formation occurs below ca. 2300 m. a.s.l. Modern drainage through the barrancas is ephemeral, and precipitation dissipates downslope percolating into the alluvium before it has a chance to reach the Agua Negra and Salado Rivers (Fig 6.13) (INEGI, 1997) unless rainfall is heavy. Some sites have active springs flowing from barranca heads suggesting a perched or pressurised ground-water source. All the barrancas drain into either the Agua Negra or the Rio Salado rivers.

Sites TB10 (Figs 6.13, 6.14, 8.1, 8.8, 8.9), and TB9 (Figs 6.13, 6.14, 8.1, 8.8, 8.9; Appendix 4, Tables 1 – 4) are discussed here as they represent sedimentological type sections for the study area, particularly the southwestern study area (Figs 6.13, 6.14, 8.1 & 8.9). Additional sites from San Jose Hill that show similar sedimentological sequences included sites; TB7 (Appendix 4, Tables 8 & 9, Figs 6.13, 6.14, 8.1, 8.8 & 8.9), TB12 (Appendix 4, Tables 5 & 6, Figs 6.13, 6.14, 8.1, 8.8 & 8.9), TB13 (Appendix 7, Table 7, Figs 6.13, 6.14, 8.1, 8.9, 8.10 & 8.12), TB16 (Appendix 6, Table 3; Fig 8.1, 8.5 & 8.6), TB3 (Appendix 6, Tables 1 & 2; Figs 6.13, 8.1, 8.9 & 8.13), TB1 (Appendix 8, Table 12; Figs 6.13, 8.1, 8.6, 8.9, 8.11 & 8.13), TB4 (Appendix 8, Tables 17 & 18; Figs 6.13, 8.1, 8.5, 8.9 & 8.12) and TB6 (Appendix 8, Table 6; Figs 8.1 & 8.8). Northern sites include, TB11 (Appendix 7, Table 1; Figs 8.1, 8.6 & 8.9), TB18 (Appendix 7, Table 3; Figs 8.1, 8.3 & 8.9) and TB8 (Appendix 7, Table 2; Figs 8.1, 8.4 & 8.9); and sites on and around San Mateo Hill (Sections 6.2 & 6.3) also have similar sedimentological successions to those recorded from Sites TB10 and TB9.

6.5: Barranca del Muerto, Site TB10

Logs 1 & 2 are from a composite section close to the head of the barranca (Figs 6.13, 6.14, 6.15b, 6.16 a & b, 6.18, 6.19 & 8.1). Log 3 records a erosive channel-fill sequence located opposite Logs 1 & 2 (Figs 6.13, 6.14, 6.16c, 6.20, 6.22 & 8.1). Log 4 was logged further west of Log 3 towards the outlet of the barranca (see Table 6.2 and Figs 6.13, 6.14, 6.15a, 6.17, 6.21 & 6.22, 8.1 & 8.9).

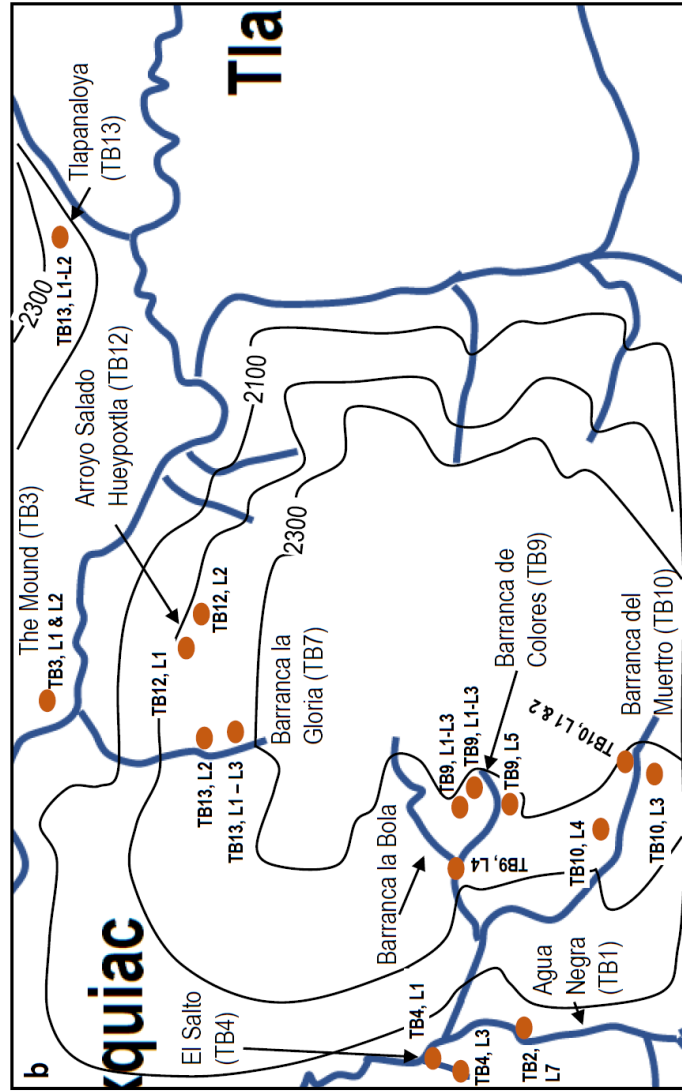
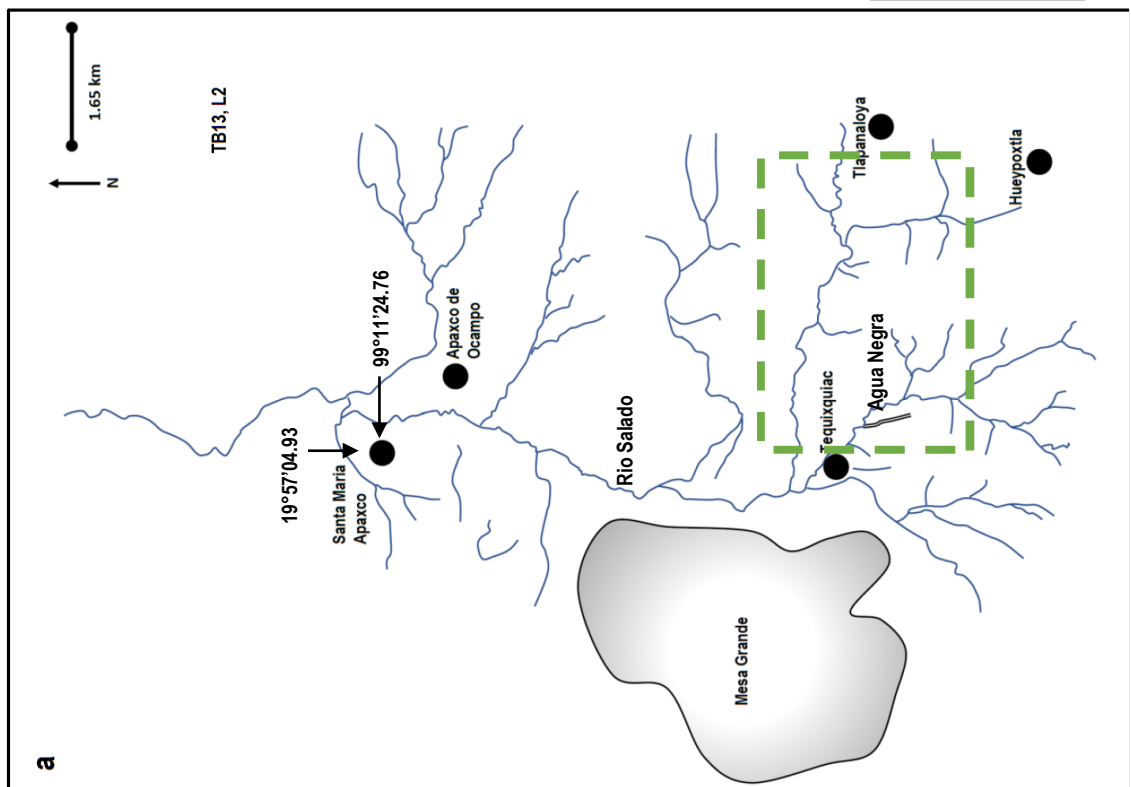


Figure 6.13: Location map for Sites TB1 Agua Negra, TB3 The Mound, TB4 El Salto, TB7 Barranca la Gloria, TB9 Barranca de Colores, TB10 Barranca del Muerto, TB12 Arroyo Salado de Hueyepoxtia, TB13 Tiapanaloya. a) The green dashed line indicates the general location of the studied sites. b) Indicates the location of the studies sites. L = Log. See Figure 8.1 & 8.9 for the location of all logged sites and study area.



Figure 6.14: Location map, Sites TB9 and TB10. Log sites indicated. Source, Google Earth. See also Figure 8.1.

Table 6.2: Site TB10, Log site location. Altitude recorded from the base of the logged sequence. Also, see Figure 8.1 & 8.9.

| Log Num. | Latitude | Longitude | Altitude m.a.s.l | Location/Sediment type |
|----------|--------------|--------------|------------------|---|
| L4 | 19 54'29.15" | 99 06'41.62" | 2264±8 | Right side of barranca, opposite Logs 1 & 2 |
| L3 | 19 54'30.56" | 99 06'38.78" | 2270±8 | 200 m west of Logs 1 & 2, left side of barranca |
| L2 | 19 54'31.67" | 99 06'39.16" | 2287±8 | Facing the head of the barranca, left side. Above Log 1 |
| L1 | 19 54'31.67" | 99 06'39.16" | 2267±8 | Facing the head of the barranca, left side |

6.5.1: Geomorphology, Site TB10

Barranca del Muerto (Table 6.2, 6.13 & 8.9) runs east to west along the western flank of San Jose Hill (Figs 6.13 & 6.14) and is 20 m deep (Fig 6.14 & 6.15b). When compared to other barrancas (e.g. Site TB9, Section 6.6) Barranca del Muerto is a relatively shallow and narrow "V" shaped incision, ca. 50 m wide suggesting that barranca incision is at a relatively youthful stage, or that previous aggregational infills have been left in-situ, helped the vegetation cover. There is a small spring-fed (?) pool centrally shown in Figure 6.15a and at least one terrace deposit that cuts into and stacks above the underlying beds (Fig 6.15). According to previous geological mapping, barranca incision cuts the Pliocene-Quaternary Tarango formation (see Moser, 1975; Segerstrom, 1952, 1956, 1962; Bradbury, 1998 and Chapter 3).

6.5.2: Sedimentological description Site TB10

6.5.2.1: Log 1, Site TB10

Sedimentological descriptions for Log 1 are given in Appendix 4, Table 10, a summary is given here.

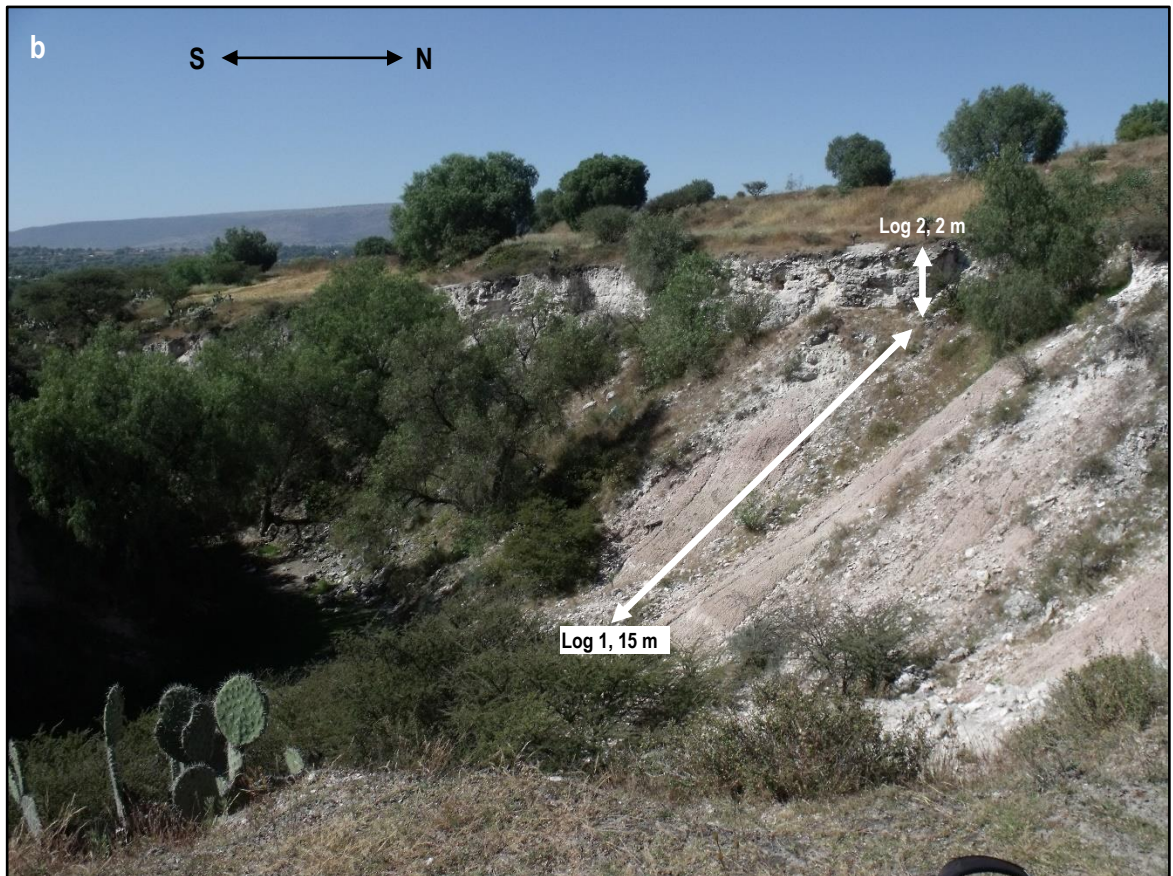
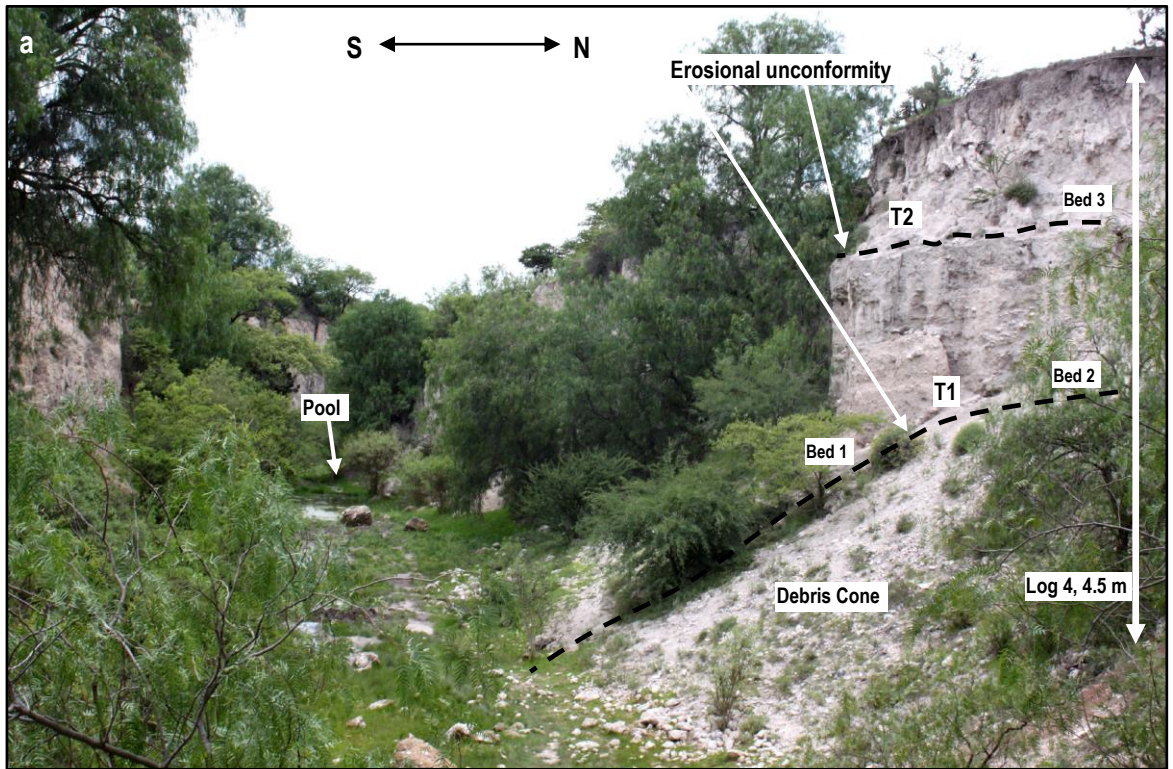


Figure 6.15: Site TB10. a) Log 4, b) Logs 1 & 2. Photograph was taken looking west, close to the head of the barranca. Also see Figure 6.13, 6.16 b & c & 8.1.

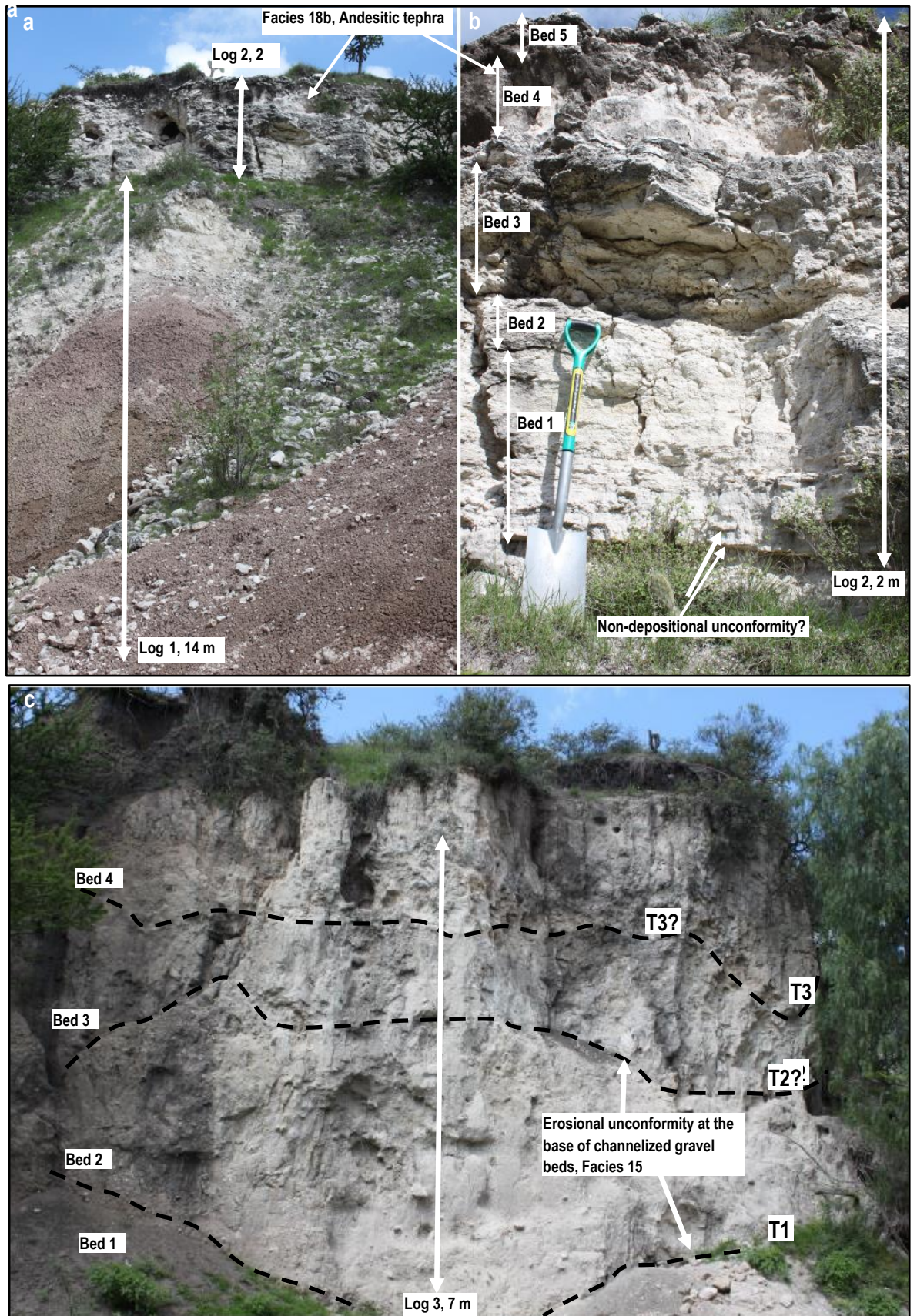


Figure 6.16: Site TB10. a) Logs 1 & 2 b) Log 2, see also Figure 6.17b c) Log 3.

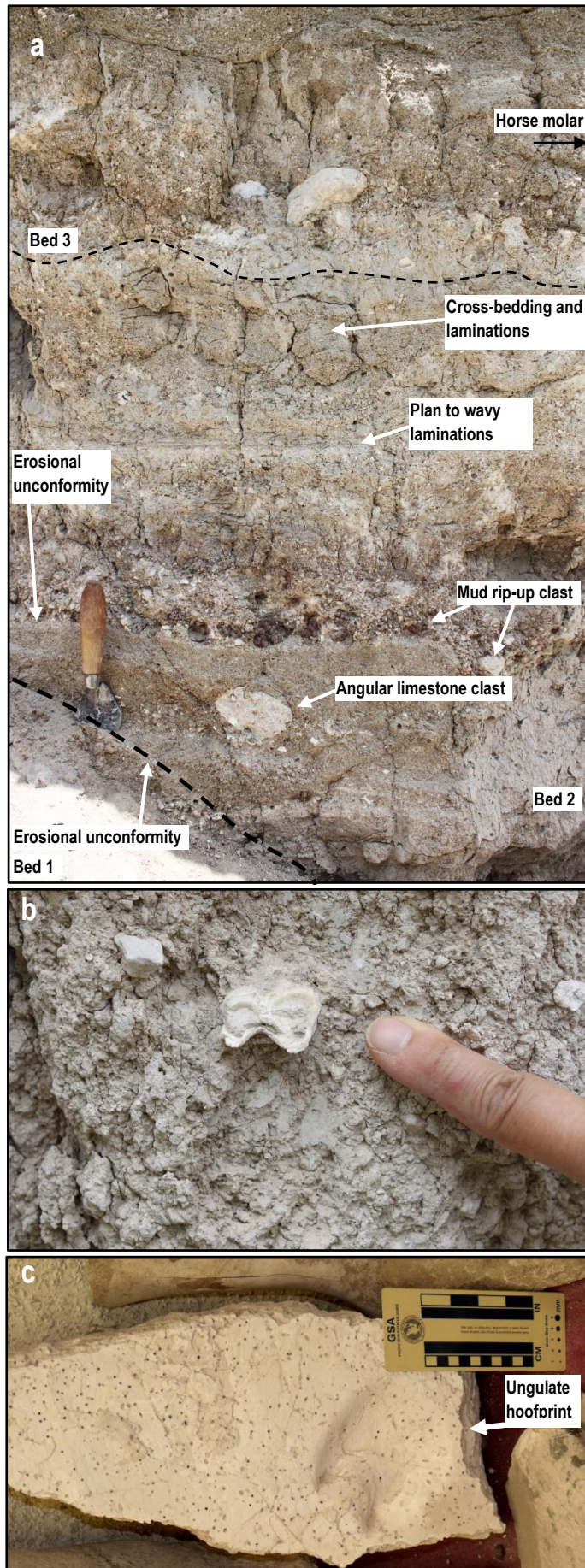


Figure 6.17: a) The base of Log 4, terrace one, see Figures 6.15a and 6.22. b) Horse molar found in-situ. The black arrow in the image (a) c) Facies 18b, andesitic tephra.

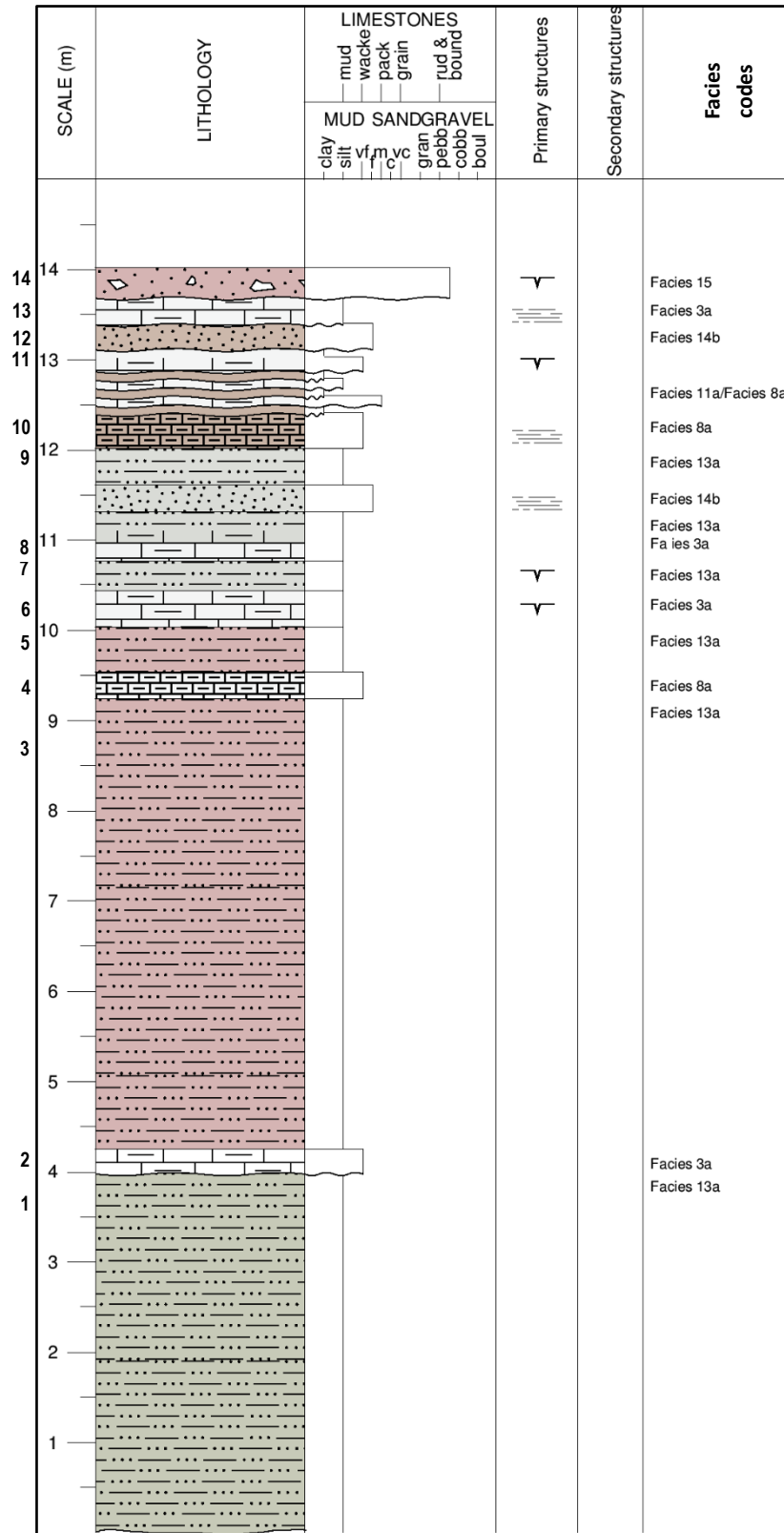


Figure 6.18: Log 1, Site TB10. See Figure 6.16 a & b for photographs of logged sequence and Figure 6.19 for the upper section of the sequence (also see Figs 6.13, 8.1 & 8.9).

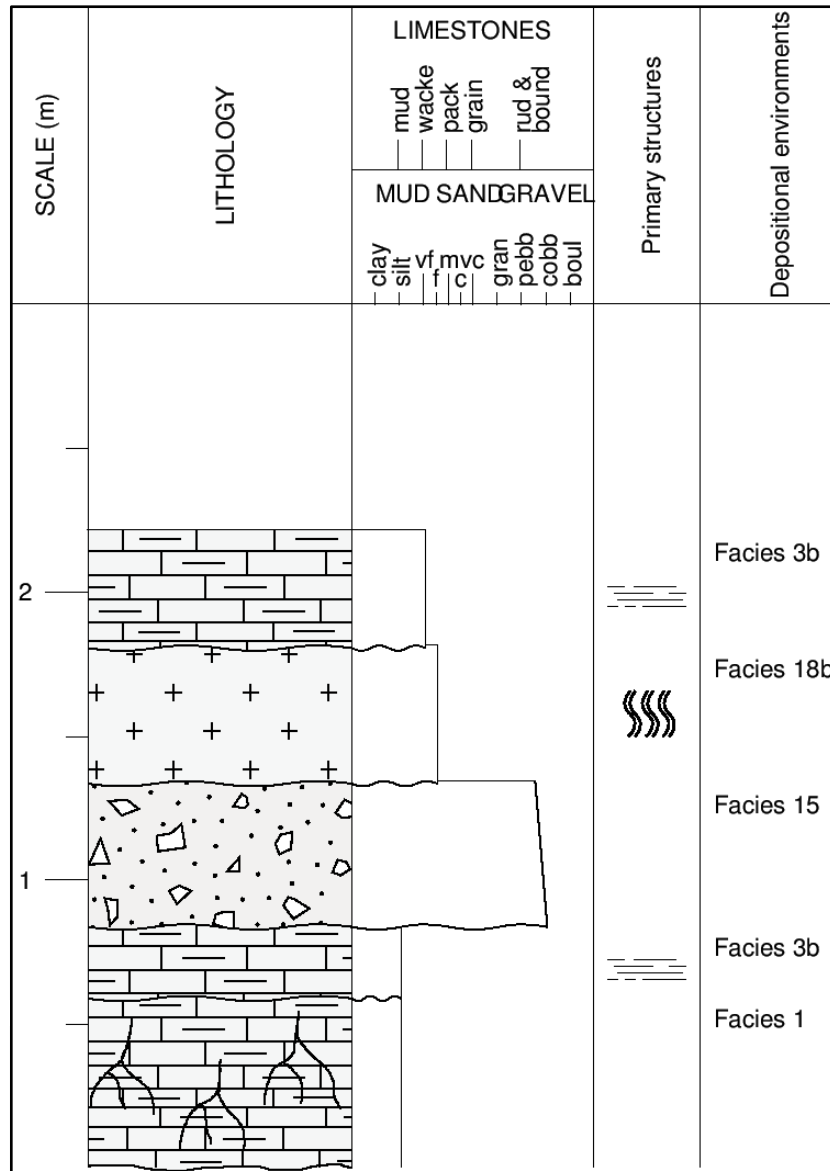


Figure 6.19: Log 2, Site TB10. See Figure 6.16 a & b for photographs of logged sequence and Figure 6.18 for the lower section of the sequence (also see Figs 6.13, 8.1 & 8.9).

Log 1 repeats similar stratigraphy to that described from Site TB14, Log 1 (Section 6.2), Site TB17, Log 3 (Section 6.3) and stratigraphy from Site TB9 discussed in Section 6.6 (Fig 6.29). The Lower 10 m consist of massive, plainly bedded silts (Facies 13a; Fig 6.18, Beds 1, 3 & 5) up to 5 m thick. Separating the silt beds are thin interbeds (<0.20 m) of carbonate-rich indurated silt (Facies 3a and Facies 8a; Fig 6.18, Beds 2, 4 & 5) (Fig 6.18) that have straight to uneven boundaries. In the upper 5 m, the average bed size thins to <0.50 m, vertical jointing is present and the contacts between these beds vary but are mostly erosive (Figs 6.16a & b, 6.18). The interbeds are made up of silt (Facies 13a), carbonate-rich silt (Facies 3a; Fig 6.18 Beds 6, 8, 11 &

13), fine silty sand (Facies 14b), clay (Facies 11a), and muddy micrite (Facies 8a) and matrix-supported gravel (Facies 15) (Fig 6.18), and Log 2 (6.19).

6.5.2.2: Log 2, Site TB10

Sedimentological descriptions for Log 2 (Figs 6.19 & 6.16b) are given in Appendix 4, Table 11, a summary is given here. Bed 1, carbonate-rich silt with vertical calcified root structures (0.01 – 0.03 m wide) (Facies 1). Bed 2, is made up of laminated carbonate-rich mud (Facies 3b).

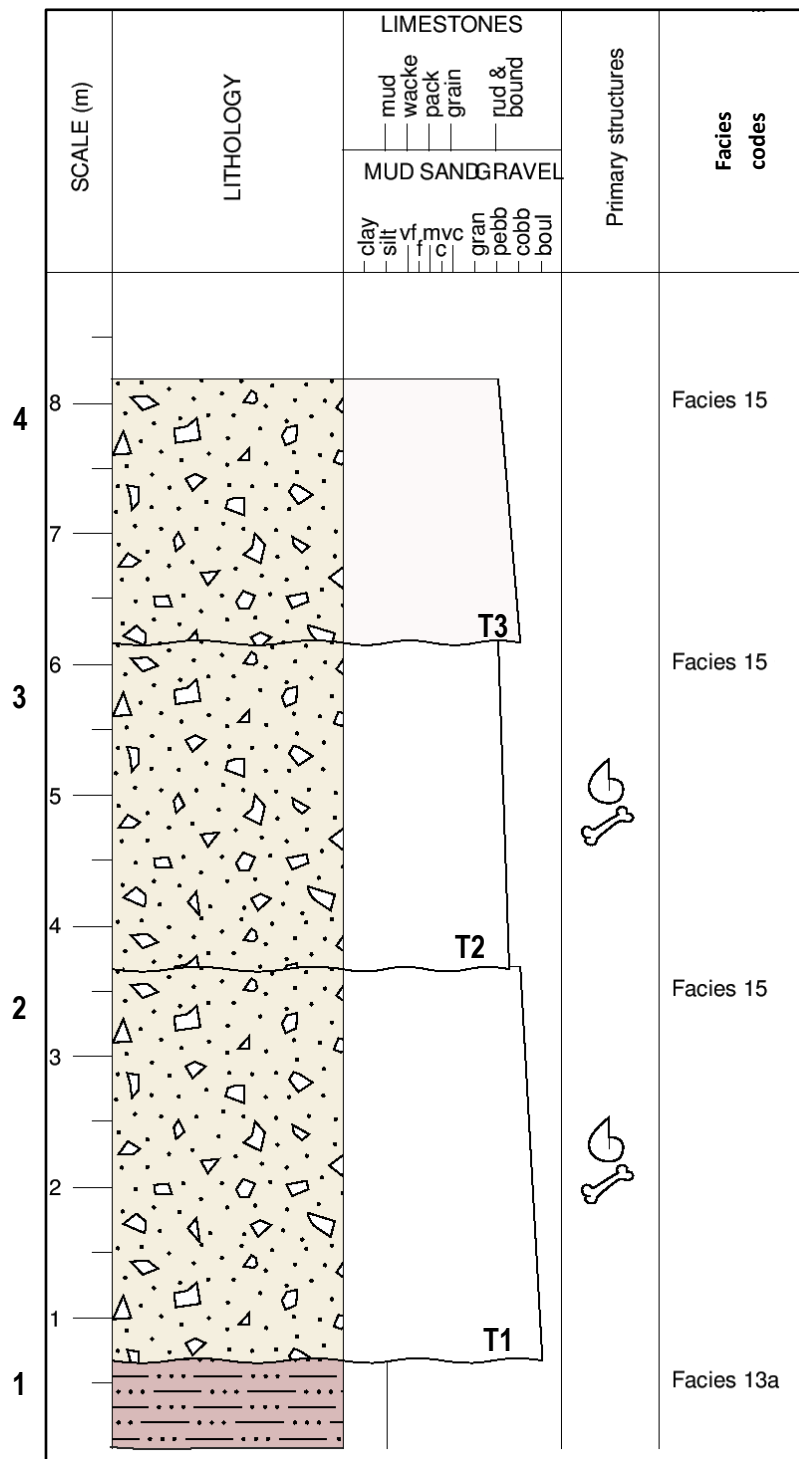


Figure 6.20: Log 3, Site TB10. For photograph of log see Figure 6.16c. T1: Terrace 1. For location see Figures 6.13, 8.1 & 8.9.

Bed 3 has erosive upper and lower contacts and is dominated by silt with angular brown silt clasts and limestone clast >0.15 m in diameter (Facies 15). Bed 4 is a thick silt bed that has bioturbation burrows throughout (Fig 6.17c, Facies 18b, also see Chapter 7). The upper bed in Log 2 is made up of laminated carbonate-rich silt. The sequence recorded in Log 2 is isolated along the to the western edge of the barranca towards the head and is heavily weathered and eroded (Figs 6.15b, 6.16a & b & 6.19).

6.5.2.3: Logs 3 and 4, Site TB10

Sedimentological descriptions for Log 1 are given in Appendix 4, Tables 12 and 13; a summary is given here. Logs 3 and 4 (Figs 6.15a, 6.16c, 6.17 a & b, 6.20 - 6.22) are very similar, and both occur in the same stratigraphic position, incising into the unconsolidated clastic and carbonate sediments recorded in Log 1 (Figs 6.15a, 6.16c, 6.17, 6.21 - 6.22). Both sequences include matrix-supported gravel deposits that are less than 3 m thick (Facies 15 – 17). In Log 4 gravel beds (Facies 15) are followed by plane laminated to ripple-cross laminated fine silty sand (Facies 14b) that contains mud- rip-up clasts and angular limestone intraclasts. In Logs 3 and 4, the gravel beds commonly contain intact and fragmented terrestrial gastropod and aquatic bivalve shells (see Section 6.5.4 and Fig 6.23c). Fragmented and scattered large mammal fossil bones also commonly occur in these sequences, examples of fossil bones that have been recovered from alluvial deposits, like those in Logs 3 and 4, are described in Table 6.3 and shown in Figures 6.17c and 6.23. The horse molar shown in Figure 6.17c was found in-situ by the author while recording Log 4; its stratigraphic position is indicated in Figure 6.17a. This sample was not collected and was left in-situ.

6.5.4: Radiocarbon dating, Site TB10

One terrestrial gastropod shell was selected for dating (sample BDM2TEQ, see Appendix 9, Table 2 and Section 4.6). The gastropod shell (see Fig 4.8 (7)) was collected 2.5 m from the base of Log 4 (Fig 6.21 & 6.22) (Facies 14b). The shell that was sent to BETA Analytic, Miami, USA for analysis was selected by field-picking pristine complete shells that had the potential to be suitable for dating. The precautions to mitigate the known issues of radiocarbon dating shells are discussed in Section 4.6, and these were followed before sending this sample for dating. The uncalibrated radiocarbon age ($40,100 \pm 500$, Appendix 9, Table 2) for sample BDM2TEQ was outside of BETA's calibration range, so the INTCAL13 curve (Reimer et al. 2013) in CALIB (Stuiver et al. 2017) was used to generate a 2-sigma calibrated age range of ^{14}C 43,349 to 44,038 cal. BP, with an average of $43,694 \pm 500$ cal. BP (Appendix 9, Table 2). Both the uncalibrated and calibrated ages are

considered a maximum possible age. This is because of the potential for hard water effects, which will make the measured age of the shell older than a direct date generated for the terrestrial material the shell was collected from. Hence, all the ages (calibrated and uncalibrated) associated with sample BDM2TEQ may be accurate, or a finite maximum age because of older carbonate up-take or an infinite age with minor contamination with the measured age pushing the limits of the radiocarbon dating method.

6.5.5: Interpretation, Site TB10

6.5.5.1: Log 1, Site TB10

The lower 9 m of Log 1 is made up of massive, plane, thick-bedded (<5m) massive silt beds (Facies 13a) that are thought to represent shallow nearshore to basal lacustrine type depositional environments (e.g. F/LMIs, Table 4.8; LMs, Table 4.10, Ller – Lher, Table 4,11) (Figs 6.15b, 6.16a & 6.18).

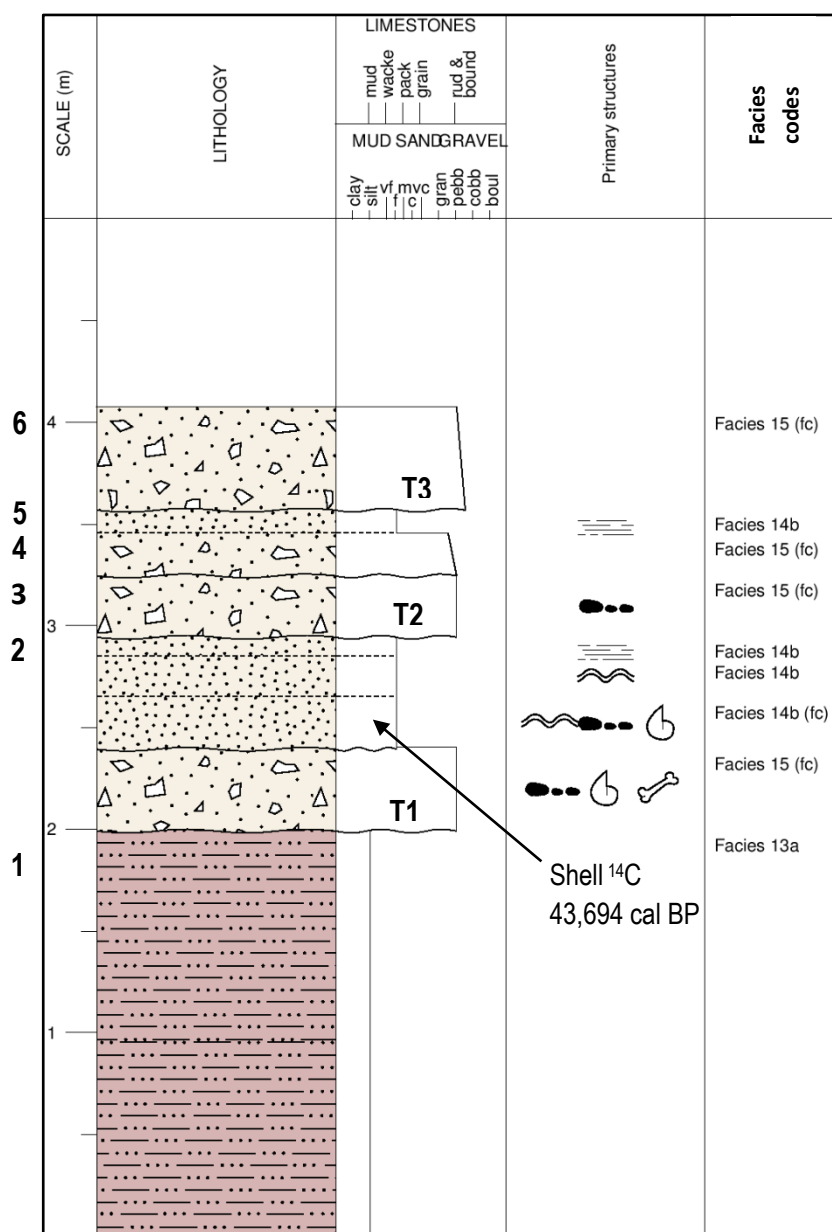


Figure 6.21: Log 4, Site TB10. For images of the log see Figures 6.15a, 6.17 a & b.

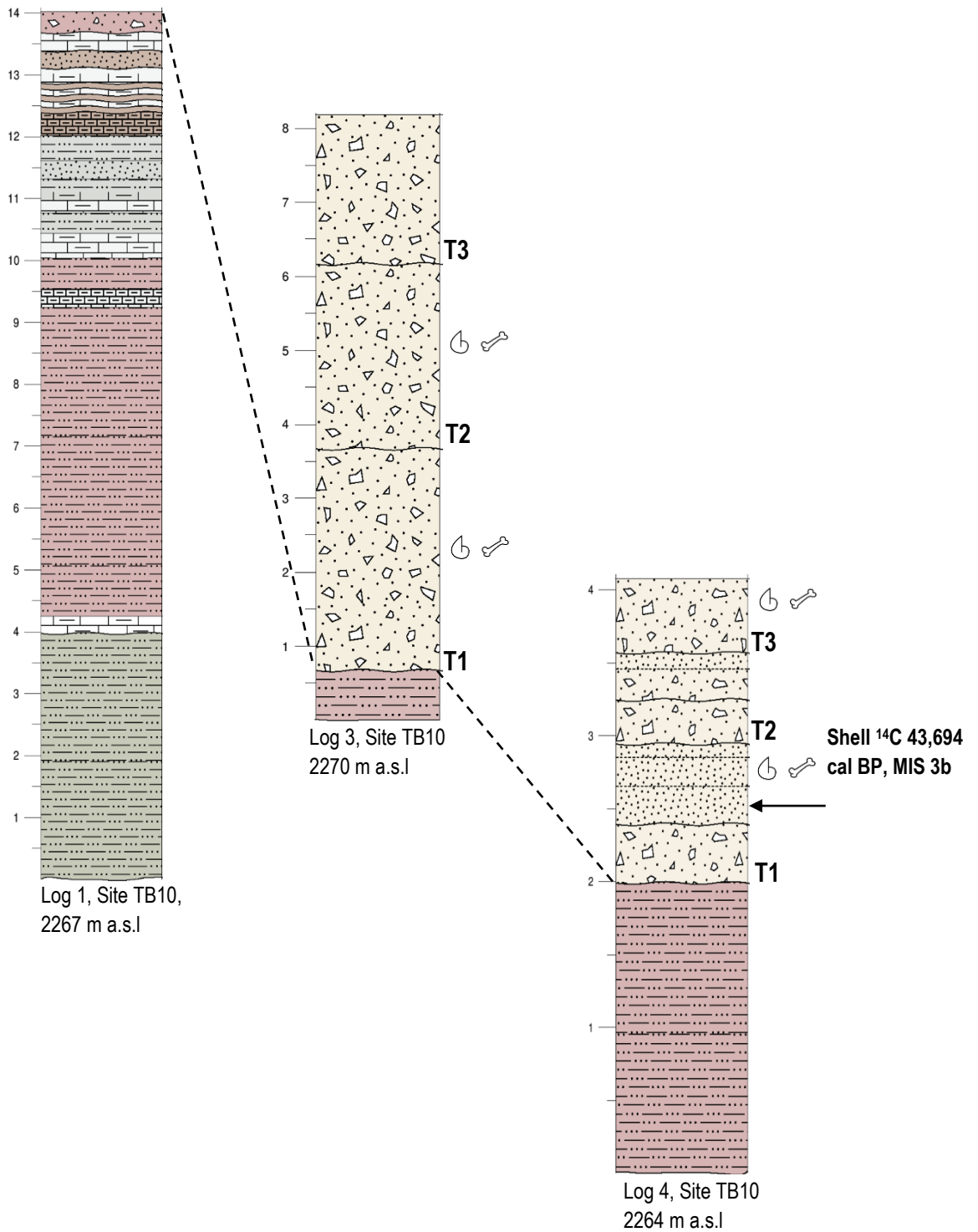


Figure 6.22: Fence diagram for site TB10, Logs 1, 3 and 4. For log site locations see Figures 6.13, 8.1 and 8.9.

Thinner calc-mudstone (Facies 3a) beds indicate occasional short-lived increases carbonate precipitation (e.g. LMs, Table 4.10, or F/LMs, Table 4.8) and reduced clastic sedimentation. Thicker silt (Facies 13a) dominated beds suggest deposition during suppressed carbonate precipitation (e.g. LMs to IMa, Table

4.10, or F/LMIs, Table 4.8). The upper thinner interbeds of gravel (Facies 15), calc-mudstone (Facies 3a), fine silty sand (Facies 14b), massive clay (Facies 11a), muddy micrite (Facies 8a) and silt (Facies 13a) follow a similar depositional pattern to the thicker lower beds, but suggest that conditions were more changeable, and that hydrological variation occurred over much shorter time periods (e.g. Flns, Table 4.8; LMa, Table 4.10; PGran, Table 4.12) probably with some depositional hiatuses in-between beds. The desiccation features indicate shallowing and exposure (see Table 4.12) in the upper 4 m of the sequence (Fig 6.18). The sediments recorded in Log 1 (Figs 6.13, 6.14 – 6.16, 6.18 & 6.22) have no chronological control except that they are positioned stratigraphically below Log 4 (Fig 6.22) that was deposited around MIS 3 (see Section 6.5.4). Like at Sites TB14 (Log 1, Figs 6.2) and TB17 (Log 3, Fig 6.3), Log 1 has a facies group that is very similar to Log 1 recorded at Site TB9 (Section 6.6) that is known to predate the MIS 12c glacial period (See Section 6.6 and discussion, Chapter 8. These sediments are also identical to sequences photographed by Segerstrom, (1962) (Fig 3.4) in the southwestern study area.

Table 6.3: Examples of fossil fauna collected from gravels (Logs 3 and 4 Figs 6.20 – 6.22) at Site TB10. Mammalian Fauna collections housed at the Museum del Pueblo, Temoatzin totals. See Figure 6.23 for Photographs of some of the samples.

| Specimen number | Body part | Identification |
|---------------------------------|---|--------------------------|
| Tx5 | Molar | <i>Mammuthus columbi</i> |
| Tx6 | Molar | <i>Mammuthus columbi</i> |
| Tx37 | Antler fragment | Cervid |
| Tx105a+b+c, Tx107a+b, Tx109 | Rib fragments | unknown |
| Tx113 | - | Snail |
| Tx115, Tx116, Tx122a+b+c, Tx127 | Tibia, femur, tusk (in 3 pieces), scapula | <i>Mammuthus columbi</i> |
| Tx123 | Mandibular symphysis only | <i>Mammuthus columbi</i> |
| Tx126 | Innominate fragment | Large mammal |
| Tx129 | Carapace scute (small) | Glyptodont |
| Tx130 | Carapace scute | Glyptodont |
| Tx143 | Vertebral centrum | <i>Very large</i> |
| Tx146 | Vertebra | |
| Tx147 | Vertebra | |

6.5.5.2: Log 2, Site TB10

Log 2 sits directly above Log 1 at site TB10 (Figs 6.13, 6.14, 6.15b, 6.16 a & b, 6.19, 8.1 & 8.9). The framestone (Facies 1) limestone (e.g. FpChls, Table 4.8) at the base of Log 2 is thought to represent a marginal pool depositional environment (F/LMIs, Table 4.8), LMs (Table 4.10). This deposit could have developed along fluvial banks or in inter-channel areas, but it seems more likely that it developed in a shallow lacustrine to marsh environment (Log 1, Fig 6.18) (e.g. F/LpStls, Table 4.8: LLeR – LHeR, Table 4.11 & Fig 4.15). Massive to laminated carbonate-rich beds (Fig 6.19 Beds 2 & 5) are interpreted as calc-mudstones (Facies 3b) deposited

by suspension sedimentation in pool or floodplain environment (F/LMIs, Table 4.8) and LMs & LMa, Table 4.10). Anoxic conditions limiting biological activity combined with a high sedimentation rate may have preserved laminations. Alternately, these deposits may indicate higher energy depositional conditions within marginal lacustrine or fluvial environments (e.g. LMs, Table 4.10 or F/IMIs, Table 4.8) (See Fig 6.18).



Figure 6.23: Examples of fossil funa bones associated with gravels (Figs 6.20 – 6.22), Site TB10. See Table 6.3 for descriptions

The central section of Log 2 (Fig 6.19, Bed 3) is made up of a massive, matrix-supported gravel (Facies 15, e.g. Table 4.8, FGmm) thought to have accumulated during a high energy flood event that occurred during low or absent water levels allowing the erosion, incision and redepositing of the gravel limestone bed (e.g. ICh, Table 4.13). Bed 3 suggests a depositional hiatus likely occurred between the gravel and the lower laminated calc-mudstone bed (Bed 2, Fig 6.19). Bed 4, andesitic tephra (Facies 18d see Chapter 7) signals that a large eruption occurred with the resulting air-fall tephra deposit either falling into standing water or that the surface of the deposit was flooded post-depositionally allowing bioturbation to occur (Figs 6.17c & 6.18). The ungulate footprint on the upper surface of the tephra suggests that animals were grazing around a pool environment before paleo-barranca incision (Logs 2 & 3). The upper laminated calc-mudstone beds also suggest water levels had increased and that a pool had developed again (Fig 6.18) (F/LMIs, Table 4.8; LLam, Table 4.10).

6.5.5.3: Logs 3 and 4, Site TB10

Log 4 was deposited around MIS 3, and by association, Log 3 is thought to be of a similar age (Fig 6.22). Both logs incise the sequence recorded in Log 1 (Fig 6.22) and include at least two pulses of sediment gravity flow (e.g. FGmm, plastic debris flow deposit, Table 4.8). The gravel beds represent remnants of alluvial aggregational fill cycles, and palaeo-barranca floor elevation after the previous barranca cut and fill events. Log 3, in the upper reach of the barranca (Figs 6.13, 6.14, 6.16c & 6.20) is 7.5 m thick and its upper surface is elevated 15 m above the modern barranca floor. Log 4, which is nearly 100 m west of Log 3 towards the centre of the barranca, thins to 3 m. The upper surface of this deposit is elevated 9 m above the modern barranca floor (Figs 6.13, 6.14, 6.16c & 6.21). It is likely that the gravels and sands are palaeo-floodplains, cut through by ephemeral flow and left standing above the present barranca floor level. The degree of incision and fill is indicated by the depth of the deposit marked by the terrace bases (Figs 6.20, 6.21 & 6.22, T1 – T3). Stratigraphic and sedimentological similarities between Logs 3 & 4 (Fig 6.22), their stratigraphic position (Figs 6.15a, 6.16b, 6.17a, 6.20, 6.21 & 6.22), and their biostratigraphy (Figs 6.17b, 6.20, 6.21, 6.22 & 6.23) suggests a correlation.

6.6: Barranca de Colores, Site TB9

Barranca de Colores is situated along the western flank of San Jose Hill (Figs 6.13 & 6.24), has an approximate length of 66 km and ranges in altitude from 2220 to 2280 m a.s.l (Table 6.4 & Fig 6.24). Towards the barranca outlet, at the co-joins with Barranca la Bola (Figs 6.13, 6.24, 8.1 & 8.9, Site TB18), barranca floor elevation increases again to 2230 m a.s.l (Fig 6.24). As with most of the other barrancas described in Chapter 6, there is no surface water. Occasionally, spring activity is reactivated with ephemeral resurgences in the limestones which outcrop in the barranca (Figs 6.25, 6.26, 6.31 - 6.34). At the junction between the two barrancas (Fig 6.24), the drainage network flows towards the Agua Negra River, which joins the Rio Salado River to the North (Fig 6.13).

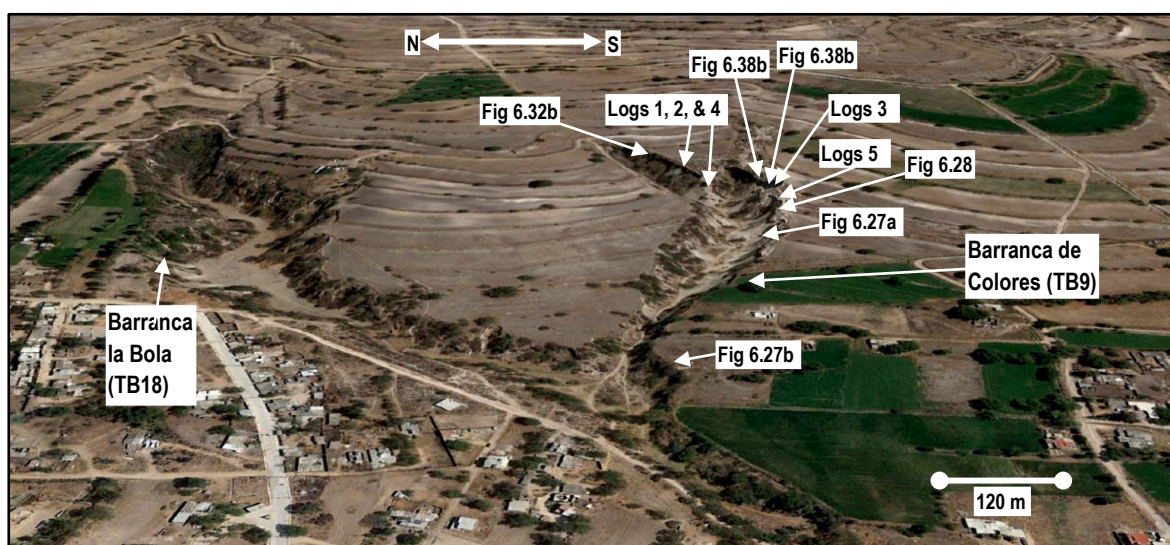
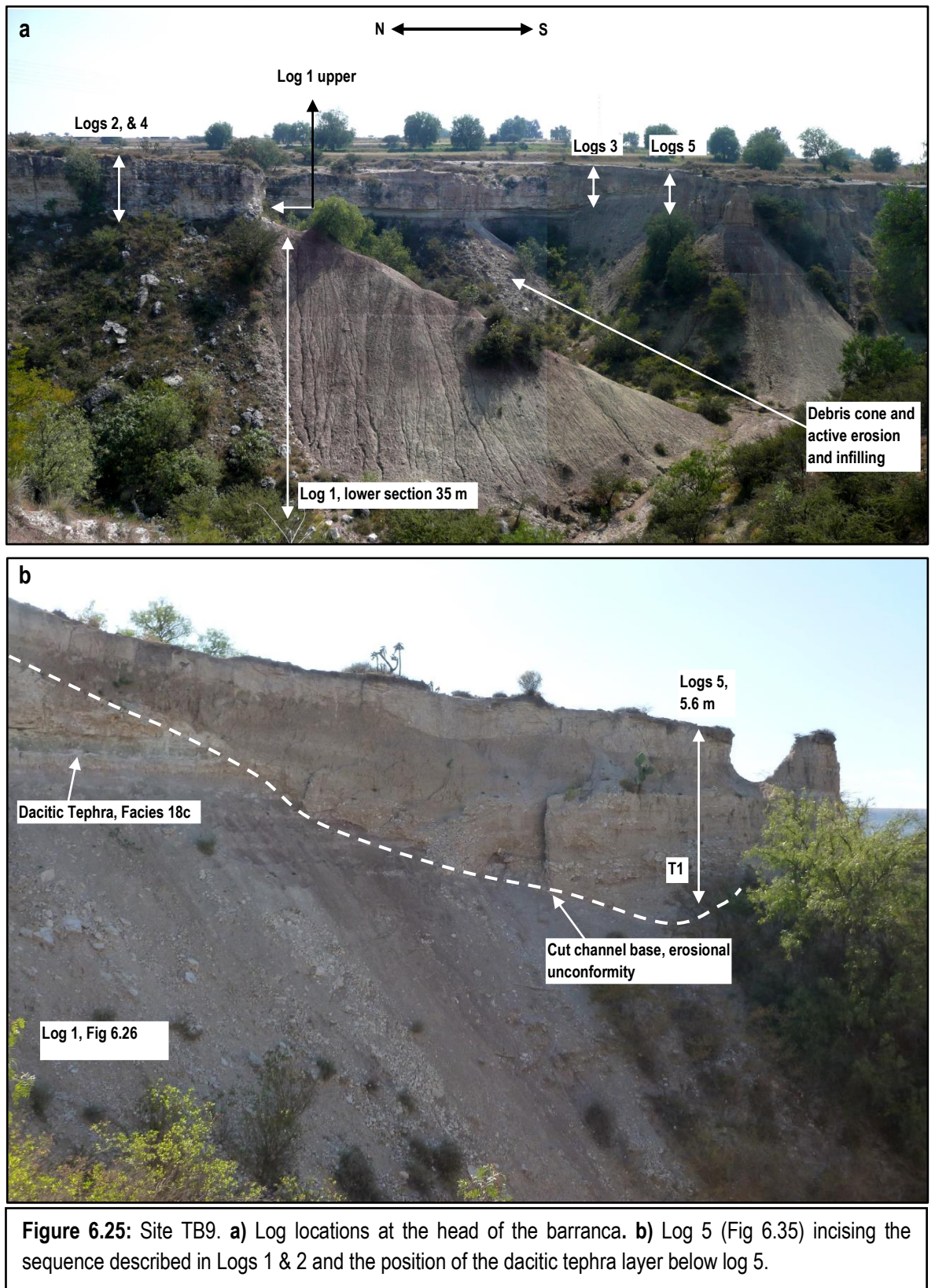


Figure 6.24: Location map for Site TB9, Barranca de Colores and Barranca la Bola. Google Earth image.

Table 6.4: Site TB9, Barranca de Colores, altitude recorded at the base of logged sequence (see Figs 6.13, 6.24, 8.1 & 8.9)

| Log number | Latitude | Longitude | Altitude m.a.s.l | Location |
|------------|-----------|-----------|------------------|--|
| L5 | 19 54.752 | 99 06.931 | 2266±14 | The cut channel at the barranca head, gravels, silt and sand |
| L4 | 19 54.752 | 99 06.931 | 2268±14 | Head of the barranca, basaltic-andesitic tephra (see Chapter 7). The northern side of the barranca. |
| L3 | 19 54.752 | 99 06.931 | 2266±14 | Head of the barranca, limestone sequence, dacitic and basaltic-andesitic tephra. The southern side of the section. |
| L2 | 19 54.752 | 99 06.931 | 2266±14 | Head of the barranca, limestone sequence and Basaltic-andesitic tephra layer. The northern side of the section. |
| L1 | 19 54.752 | 99 06.931 | 2229±14 | Head of the barranca, unconsolidated clastic material northern side of the section. Composite section. |



Five stratigraphic sections were logged from Site TB9 (Fig 6.24). Logs 1, 2 & 4 together make up a composite section logged at the head of the barranca (Figs 6.24, 6.25a & 6.36 and Table 6.4). Log 3 (Fig 6.34) records the upper bed described in Log1 (Bed 15, Fig 6.29) and the lower portion of Log 2 (Beds 1 – 5, Fig 6.33) (Figs 6.24, 6.25, 6.34 & 6.36 and Table 6.4). Log 4 (Figs 6.25 a & b, 6.38a) gives a detailed description

of the basaltic-andesite tephra layer (Facies 18a, see Chapters 5 & 7, Fig 7.2 & Table 7.3) interbedded within Logs 2 & 3 (Fig 6.33, bed 5). Log 5 (Fig 6.35 & 6.36) records gravels, sands and silt that incises Logs 1 – 4 (Figs 6.25 & 6.27a).

6.6.1: Geomorphology, Site TB9

The incision at the head of Barranca has exposed up to 40 m of unconsolidated clastic material and limestone. Like at Barranca del Muerto (Site TB10; Section 6.3), the sediments recorded in Logs 1 – 4 have been cut (<15 m thick) by thick sand, silt and gravel beds that track along the edges of the barranca (Log 5; Figs 6.25b, 6.27a, 6.35 & 6.36) representing at least one alluvial terrace deposit (T1, Figs 6.25b & 6.27a).

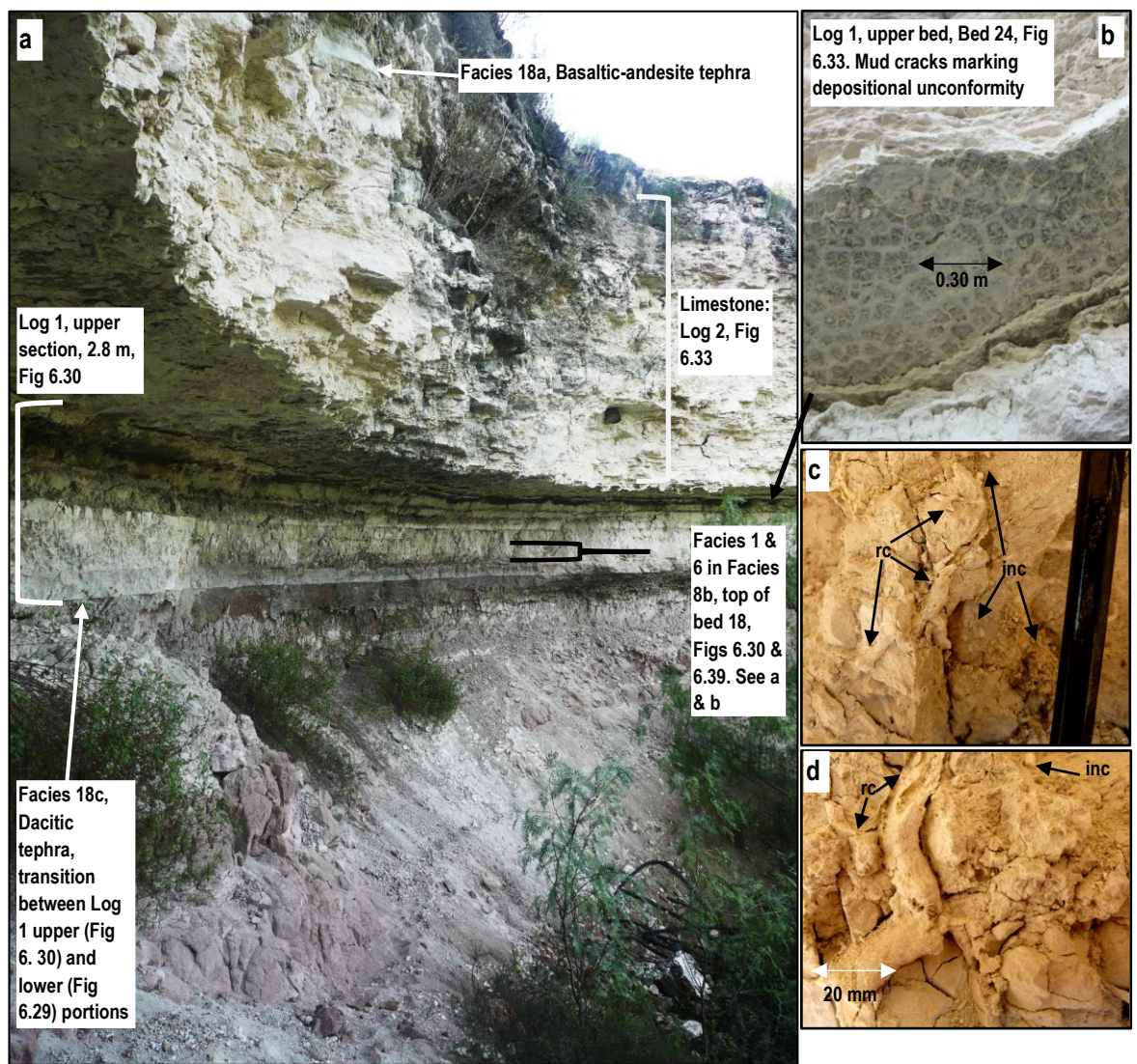


Figure 6.26: a: Site TB9, Logs 1 & 2, see Figure 6.30. c & d: Bed 18, Log 1, Fig 6.30

6.6.2: Sedimentological descriptions, Site TB9

6.6.2.1: Log 1, Site TB9

Sedimentological and petrographic descriptions for Log 1 (Fig 6.29 & 6.30, Table 6.4) are given in Appendix 4, Table 1 and the geochemical characteristics of sampled beds is given in Appendix 11, (see Figs 6.25 – 6.30 & 6.39). The lower portion of Log 1 (Figs 6.25 a & b, 6.27a, 6.28 a & b, 6.29) is made up of greyish yellow-green (5GY 7/2), pale-red (5R 6/2), moderate-pink (5R 7/4), massive, horizontally stratified beds of calc-mudstone (Facies 3a, Fig 6.28), mixed carbonate-clastic sediments (Facies 8a, 9a & 10a) mud (Facies 12a), silt (Facies 13a) and fine silty sand (Facies 14a) (Figs 6.29 & 6.35). The beds have no exposure features and have mainly gradational contacts. Bed thicknesses vary between 1 and 6 m thick, and the whole sequence is interbedded with thin (<0.50 m thick) white (N9) massive carbonate-rich mudstone beds (Facies 3a and Facies 8a) that have varying degrees of biological input (<0.10 m) (Fig 6.28). Beds can be traced along the length of the barranca, with or without interbedded silty fine sand lenses (Facies 14 a & b) (< 0.10 m) (Fig 6.28). The upper contact of Bed 14 (Fig 6.26) has extensive mud cracks and vertical jointing on the surface of the bed.

The upper portion of Log 1 (Figs 6.25a, 6.26 & 6.30) has bed thicknesses below 0.30 m, and beds commonly show exposure features (mud-cracks, Figs 6.26 and 6.30, Bed 24) and vertical jointing (e.g. Facies 19b & 19c, Fig 6.30). Interbeds comprises white (N9) carbonate-rich mudstone (Facies 3b) and greyish yellow-green (5GY 7/2), pale-red (5R 6/2), moderate-pink (5R 7/4) and greyish-pink (5R 8/2) mud (Facies 12 a & b), clay (Facies 11b), mixed carbonate-clastic beds (Facies 8a & Facies 9b), matrix-supported pebble gravel (Facies 15), and intraclastic beds (Facies 6). The transition between the upper and lower sections (Figs 6.29 & 6.30) of Log 1 is marked by a dacitic tephra deposit (Facies 18c) (Figs 6.26, 6.29, 6.30; Chapter 7, Tables 7.2, 7.4 & 7.5 and Figs 7.3, 7.4 & 7.7).

6.6.2.2: Log 2, Site TB9

Sedimentological descriptions for Log 2 (Fig 6.33, Table 6.4) are given in Appendix 4, Table 2, and the geochemical characteristics of sampled beds are given in Section 6.6.7 (see Figs 6.24, 6.25a, 6.26 a & b, 6.27 a, 6.31, 6.32, 6.33, 6.36 & 6.40). Log 2 (Figs 6.24, Table 6.4) sits stratigraphically above Log 1 (Figs 6.35 & 6.36) and the contact between the two logs likely represents a none depositional or erosional unconformity (Bed 25, Log 1, upper, Figs 6.26 & 6.30). The sequence thins and lenses out towards the northern and southern limits of the deposit at the head of the barranca (Figs 6.25a, 6.31 & 6.32). The logged sequence includes white (N9), greyish-pink (5R 8/2) and moderate-red (5R 5/4):

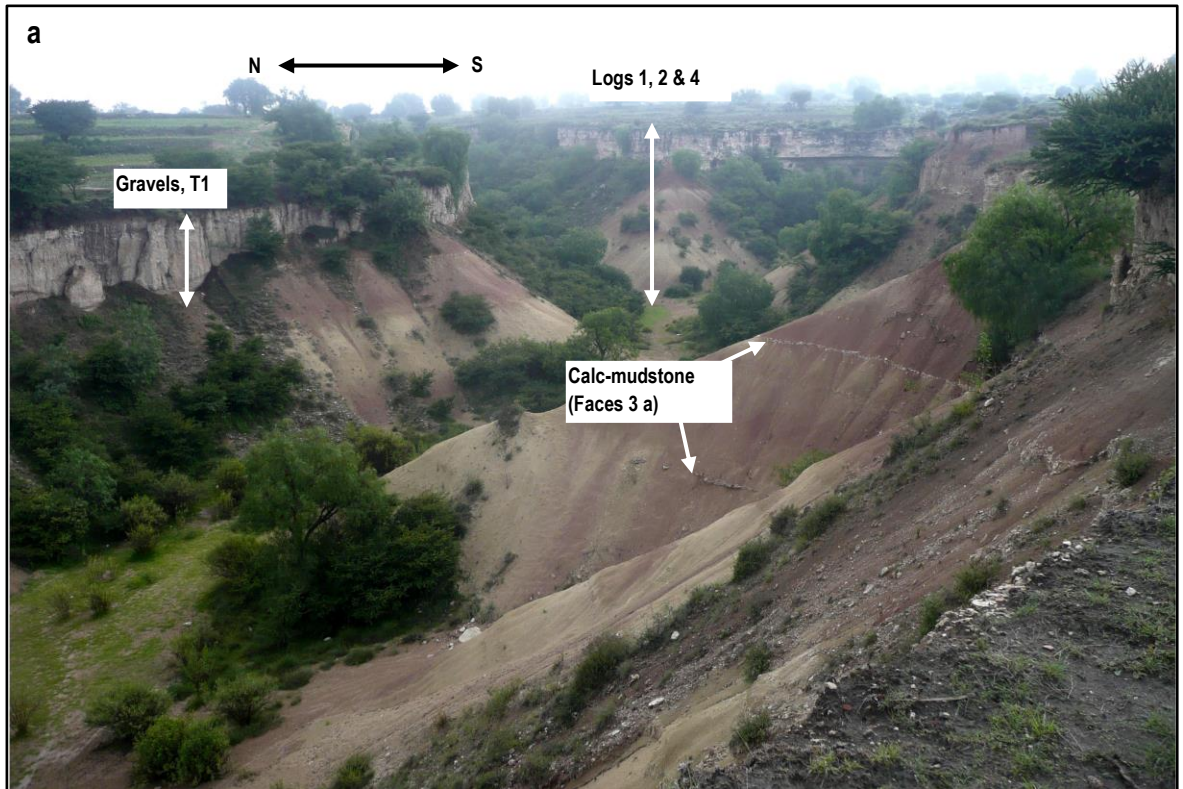


Figure 6.27: a) View of Site TB9 from the western end of the barranca. Locations of photographs indicated on Fig 6.24. T1 = gravel terrace 1, see Log 5, Figure 6.35. b) Thick beds of unconsolidated clastic material located at the junction between Barrancas de Colores and la Bola

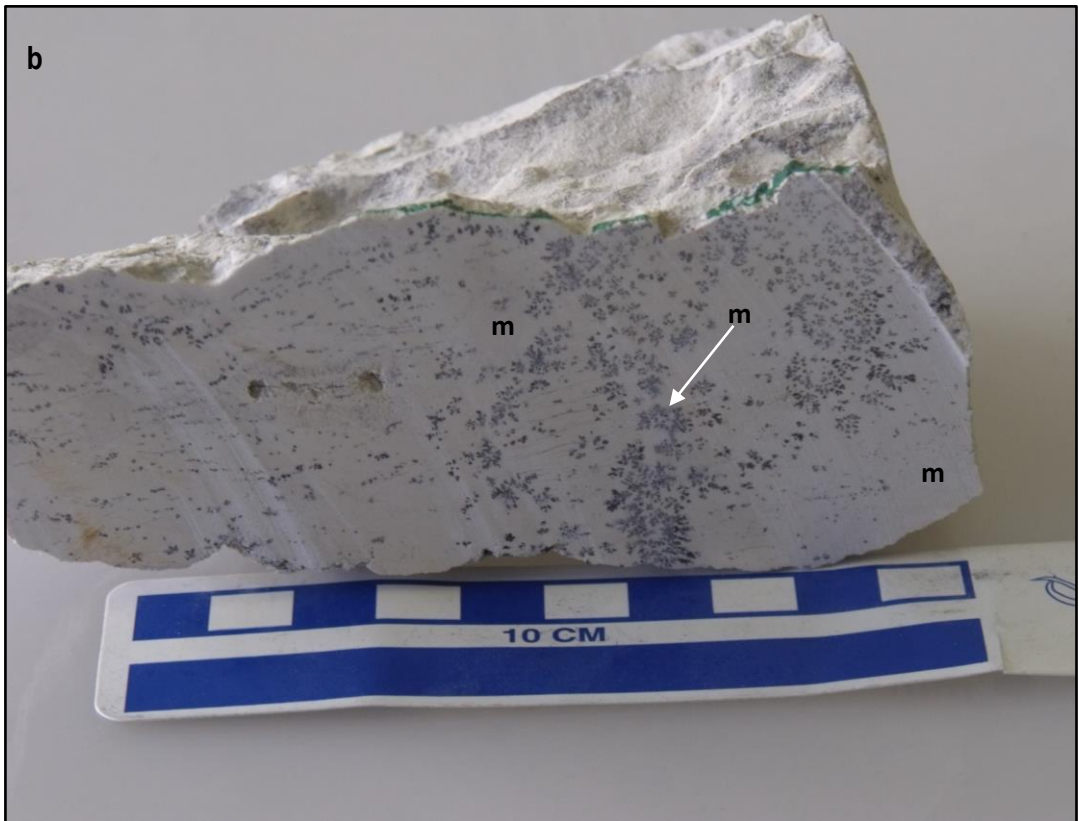
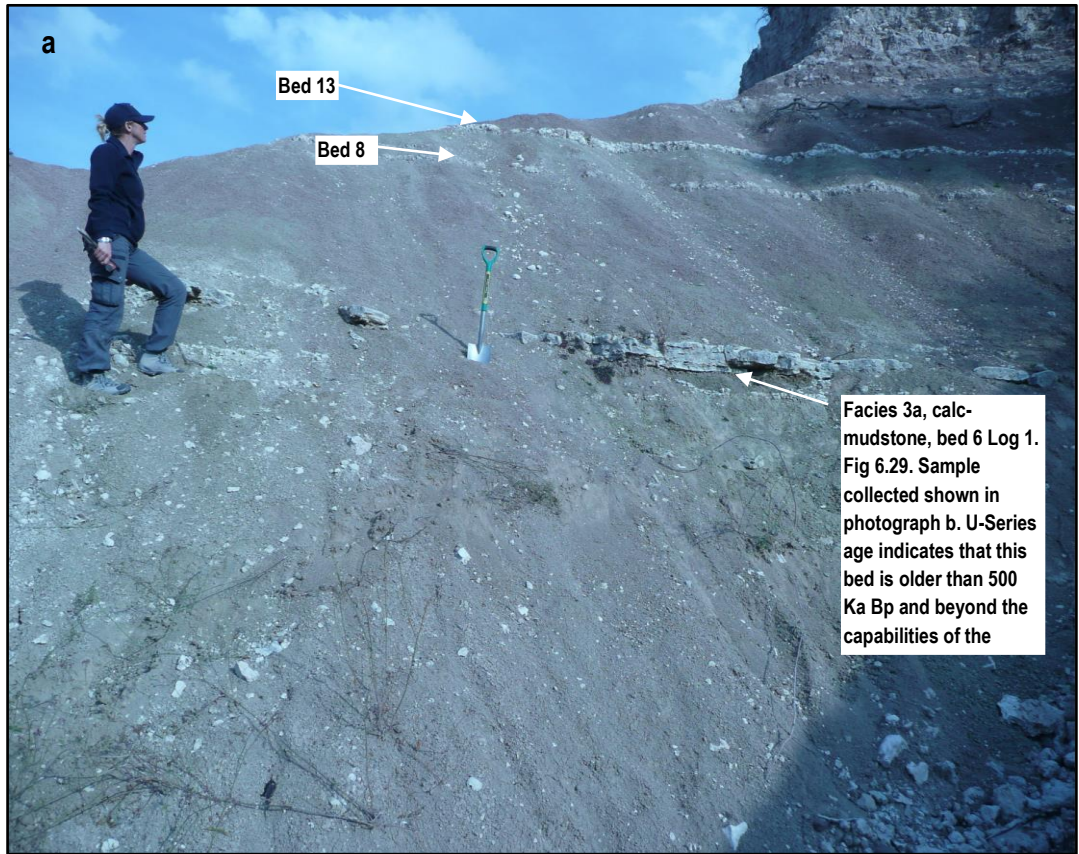


Figure 6.28: Log 1 lower; Site TB9 Log 1 (Fig 6.29). **a**) In-situ calc-mudstone interbedded within the unconsolidated clastic and mixed carbonate-clastic beds (for the location of photograph see Fig 6.24, for the stratigraphic sequence see Log 1, Fig 6.29). **b**) Calc-mudstone sample collected for U-series dating, sample C1 (see Section 6.6.7.3), the photographed bed is equivalent to bed 8, Log 1 (Fig 6.29).

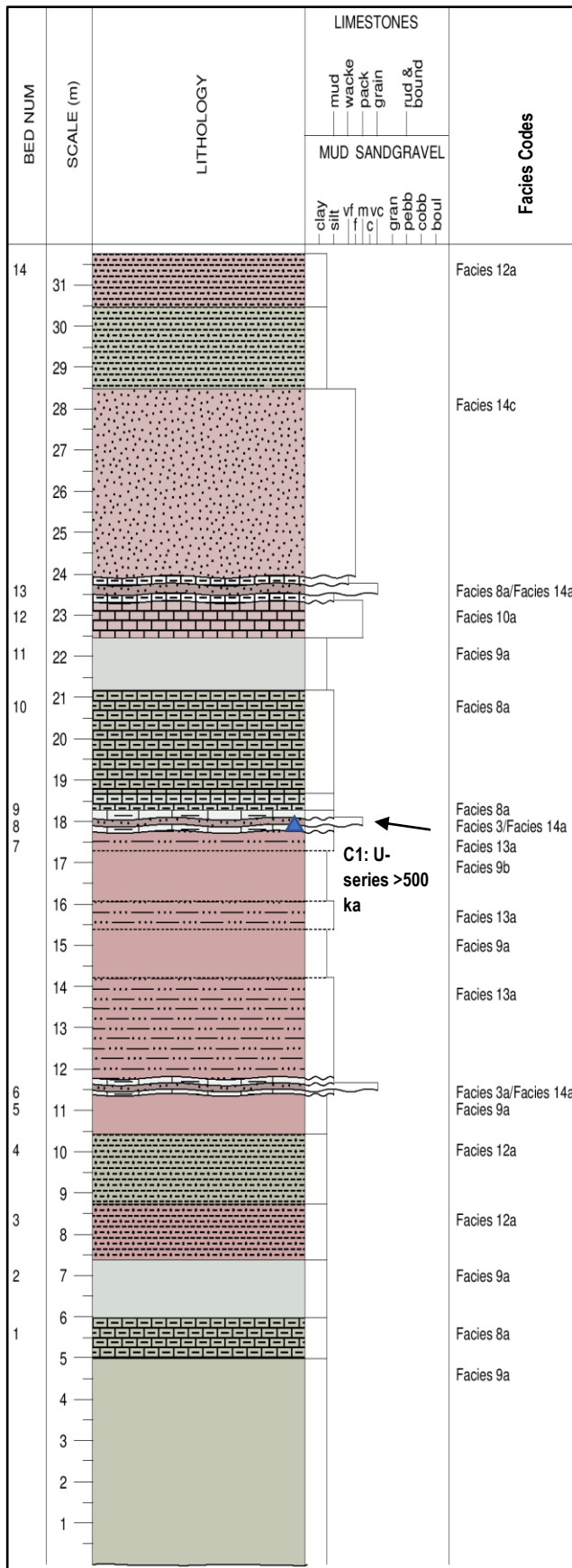


Figure 6.29: Site TB9, Log 1, lower section (Figs 6.24, 6.25a, 6.26, 6.27a, 6.28, Table 6.4). For a photograph of the logged section, see Figure 6.25a. For U-Series age data see Section 6.6.7.3. ▲ Micromorphological analysis of sample BDC 56 (see Fig 6.36, Bed 6 and Appendix 4, Table 1, Bed 6)

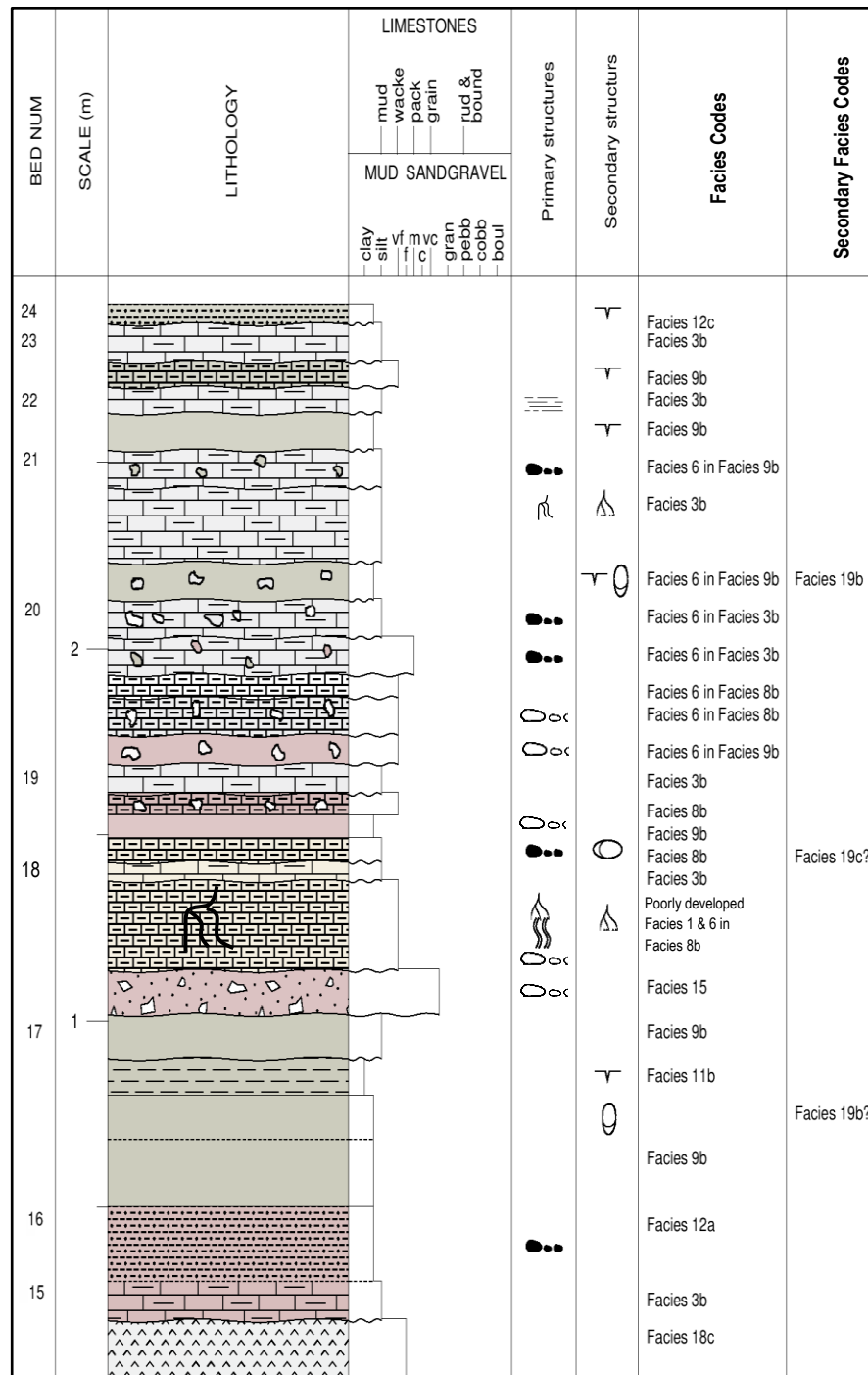


Figure 6.30: Site TB9, Log 1, upper section (Figs 6.24, 6.25a, & 6.36, Table 6.4). For a photograph of the logged section see Figure 6.26.

1) Massive to faintly laminated carbonate-rich mudstones sediments (Facies 3a & 3b) (e.g. Beds 1, 6, 8, 10, 12, 14, 15, Fig 6.33 and Table 5.10, Appendix 4, Table 2) and commonly contain aquatic mollusc and land snail shells (see Chapter 5). Organic (e.g. waterweed, T24, Table 2, Appendix 4) material replacement with manganese and drusy calcite cement is frequent (see Chapter 5). Bioturbation burrows and isolated biofilm (<1 mm), or thicker stromatolitic layers (< 6 mm) can also occur (see Section 5.3.3).

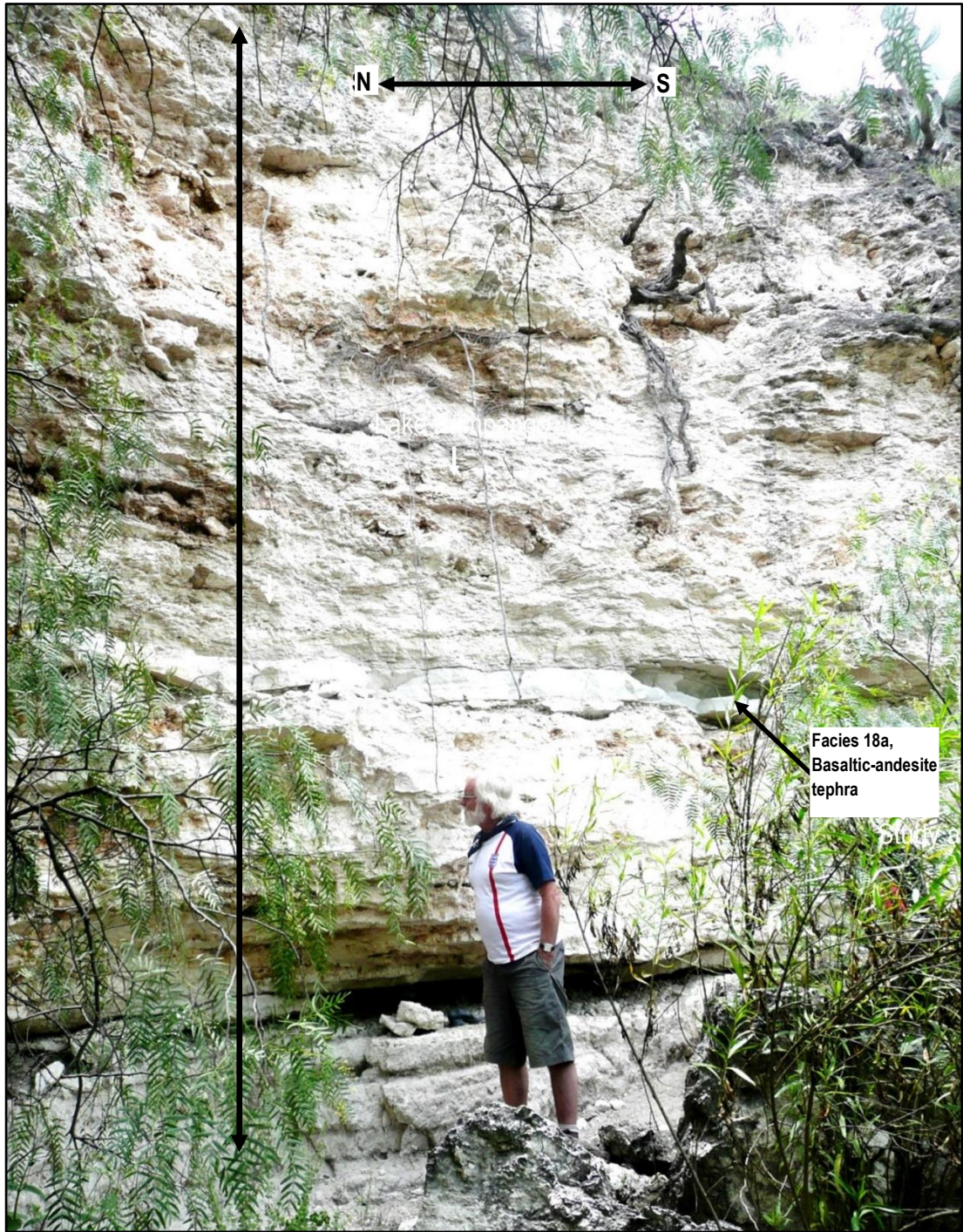


Figure 6.31: Site TB9, Log 2, logged and sampled limestone section at the head of the barranca (Fig 6.24, 6.25a & 6.36). see Figure 6.33

Sparry calcite cement infilling interparticle spaces and bubble voids within the micritic matrix, calcite vein development, root penetration and desiccation features frequently occur (See Chapter 5, Fig 5.6, Table 5.10 and Appendix 4, Table 2). Salt hopper crystals occur far less frequently.

2) The pisolitic limestone deposits reported in Log 2 and recorded in Beds 3, 12 and 18 (Fig 6.33) are shown in Figures 5.9 & 5.10 and described in Tables 5.12 & 5.13 in Chapter 5.

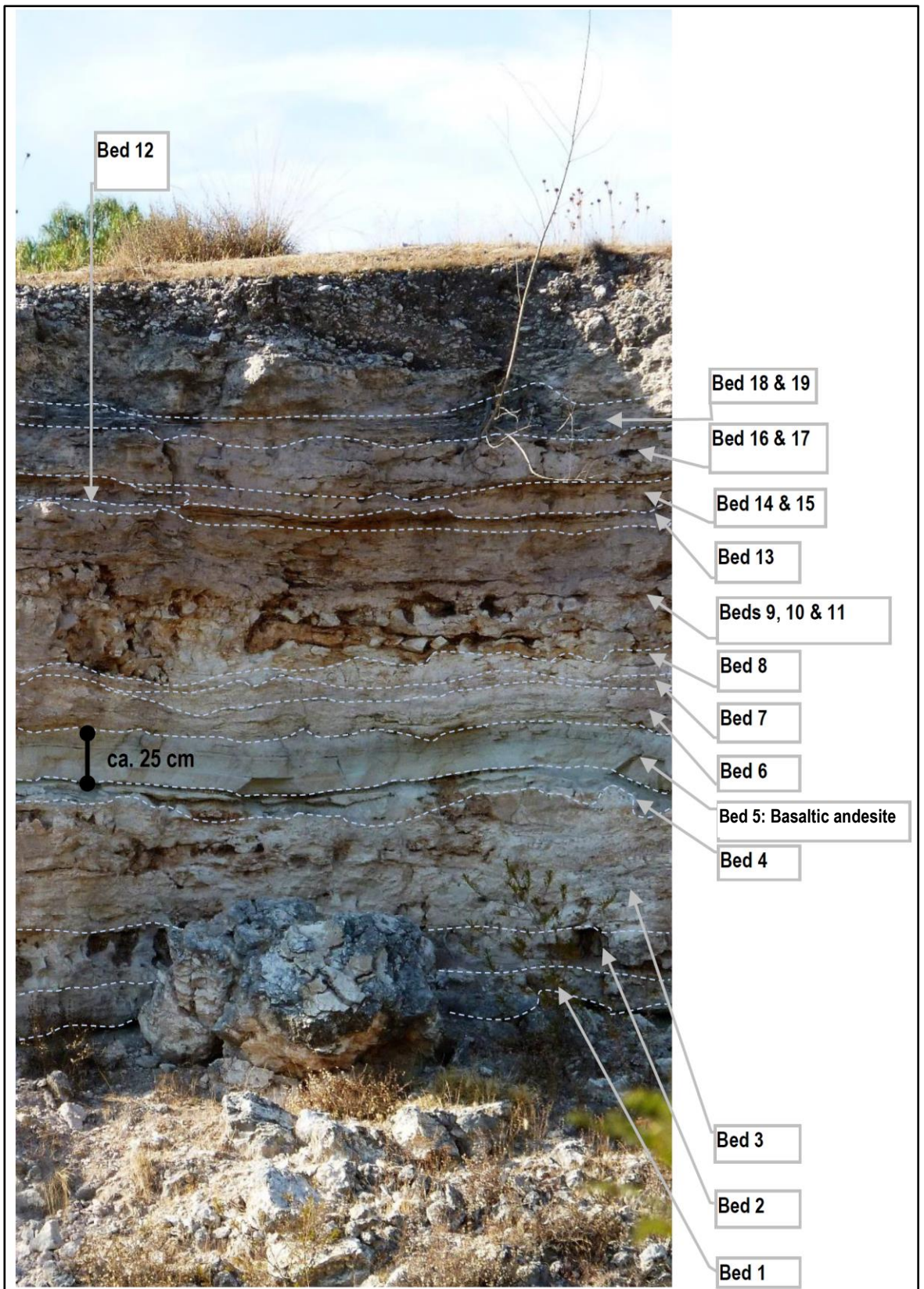


Figure 6.32: Site TB9, field example of the freshly exposed section recorded from the northern end of the limestone sequence logged at the head of the barranca (Fig 6.24). Beds that are indicated in Log 2 (Fig 6.33) can be traced along from the central section (Fig 6.33) to the lateral limits of the sequence where they thin and lens out. Basaltic-andesite (Facies 18a). See Appendix 4, Table 1.

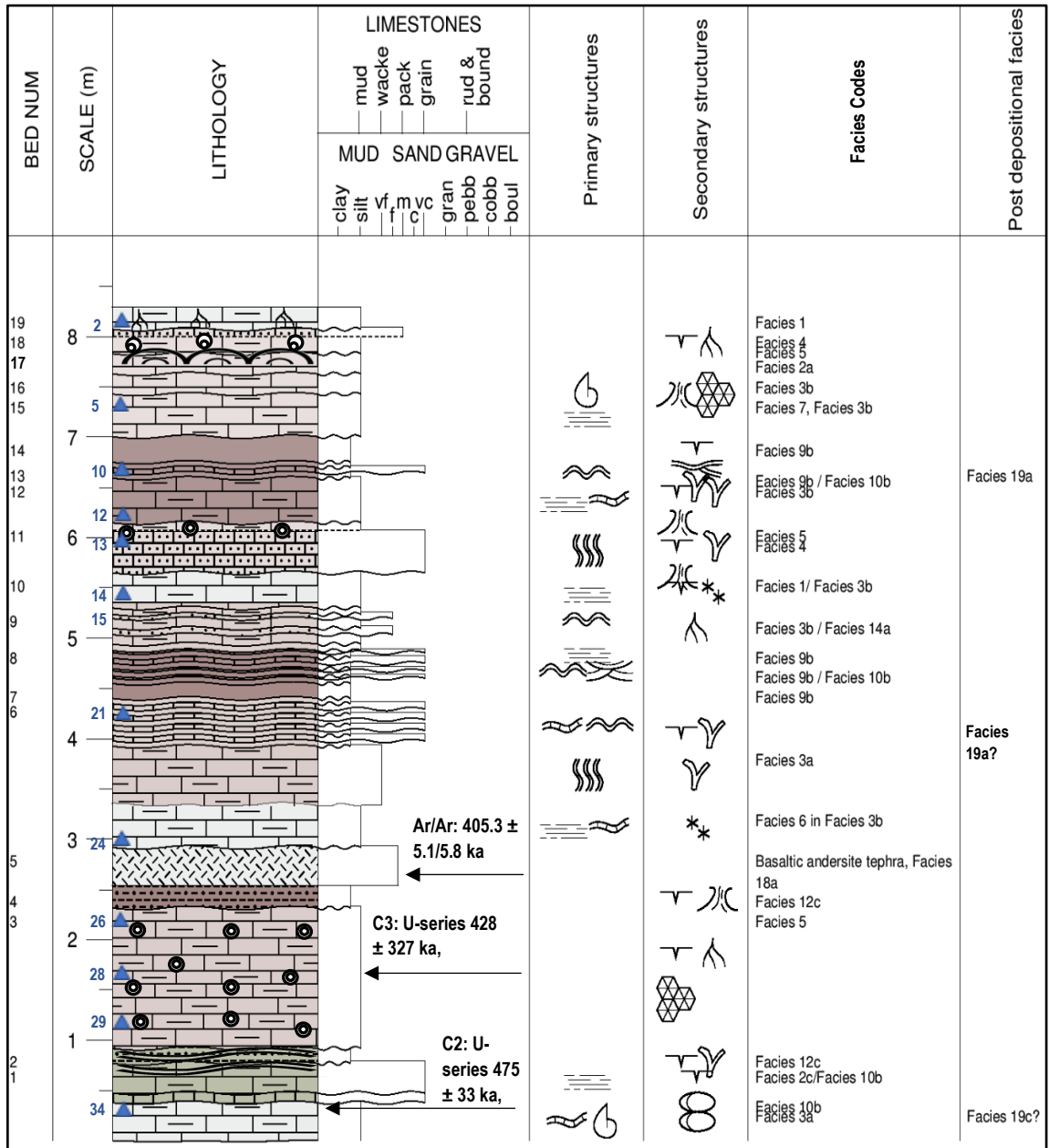


Figure 6.33: Site TB9, Log 2, limestone sequence, (Figs 6.24, 6.25a, 6.27a & 6.31, Table 6.4, Appendix 4, Table 3 and section 6.6.6 onwards. For a photograph of the logged section, see Figure 6.31.

Within beds, there is a lack of biological material, and pisoliths are elliptical, usually with no more than two layers, and they are < 6 mm wide. They sit within a calc-mudstone (Facies 3) matrix and are often associated with peloidal beds. Roots traces and calcite veins (Facies 19a) can cut through the original depositional features (Tables 4.12 & 4.13 also see Figs 5.9 & 5.10, Tables 5.12 & 5.13) and deposits can have secondary silt infills and drusy calcite replacing post-depositional root stems. Occasionally some sparry calcite cement infills interparticle spaces within the micritic matrix (see Fig 5.10, Table 5.12).

3) Peloidal limestones (Facies 4) fabrics are mostly pelleted, and bioturbation shell fragments, mud-lumps and organic detritus (indicated by manganese) are common (e.g. Beds 12, 17, Fig 6.33). Sparry and

drusy cement can occur (Fig 5.2, Table 5.6, Appendix 4, Table 2), and samples can show post-depositional features, like mud-cracks and root penetration (see Chapter 5 for examples).

4) Bedded clastic, intraclastic, carbonate and mixed carbonate-clastic beds (Facies 6) encompass laminated to cross-ripple laminated calc-mudstone and packstone that can have coarser wackestone, grainstone and sandstone cross-lamina and micro-channelised in-wash beds (< 0.10 m thick) (see Beds 6, 8 and 10, Fig 6.33, Table 2, Appendix 4 and Chapter 5). Incipient and isolated biofilm lamina occasionally occur (see Facies 6, Chapter 5). Interbed thickness vary but are <0.10 m thick.

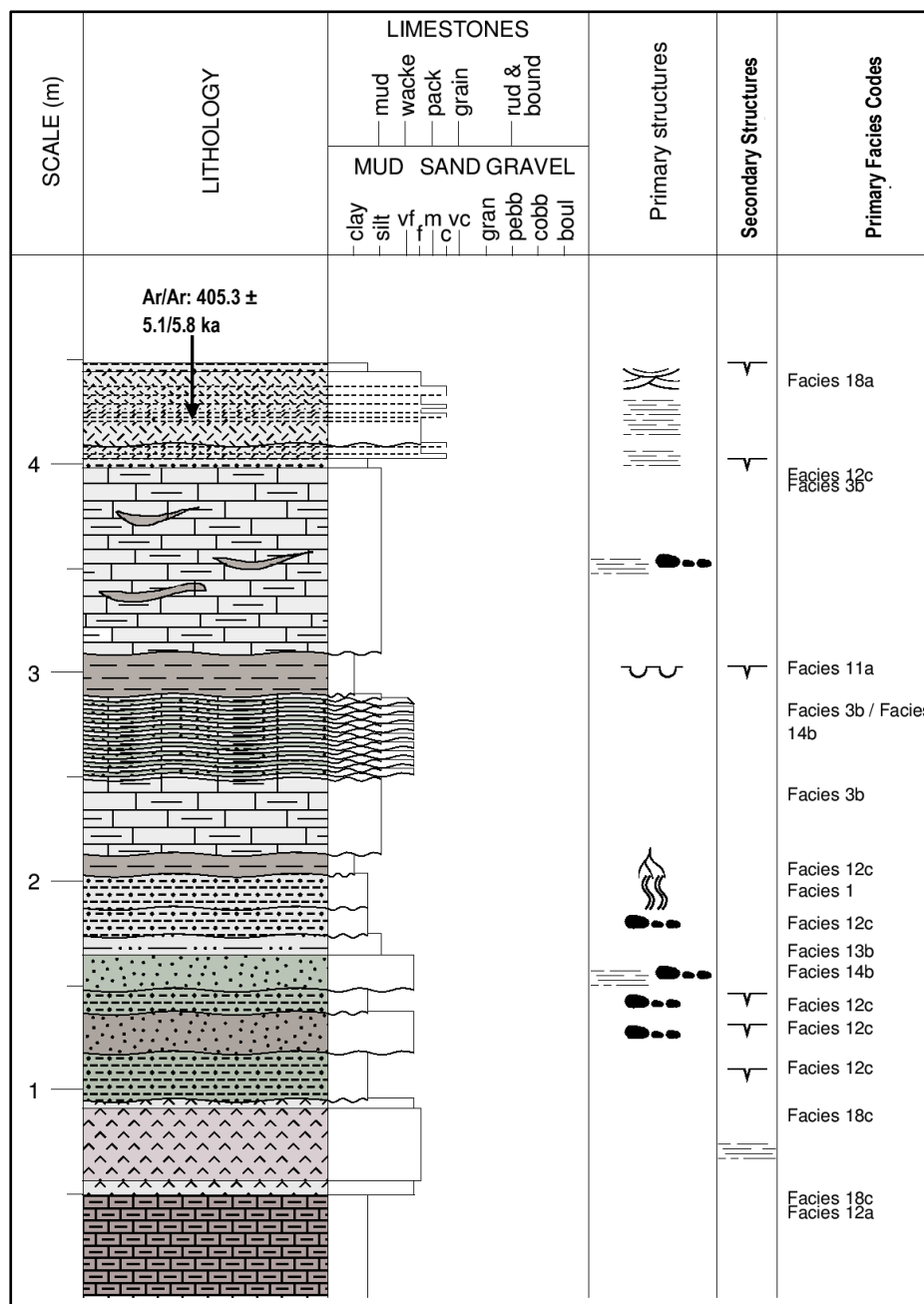


Figure 6.34: Site TB9, Log 3 (Figs 6.24 & Table 6.4). See Figure 6.39 for an image of the logged section.

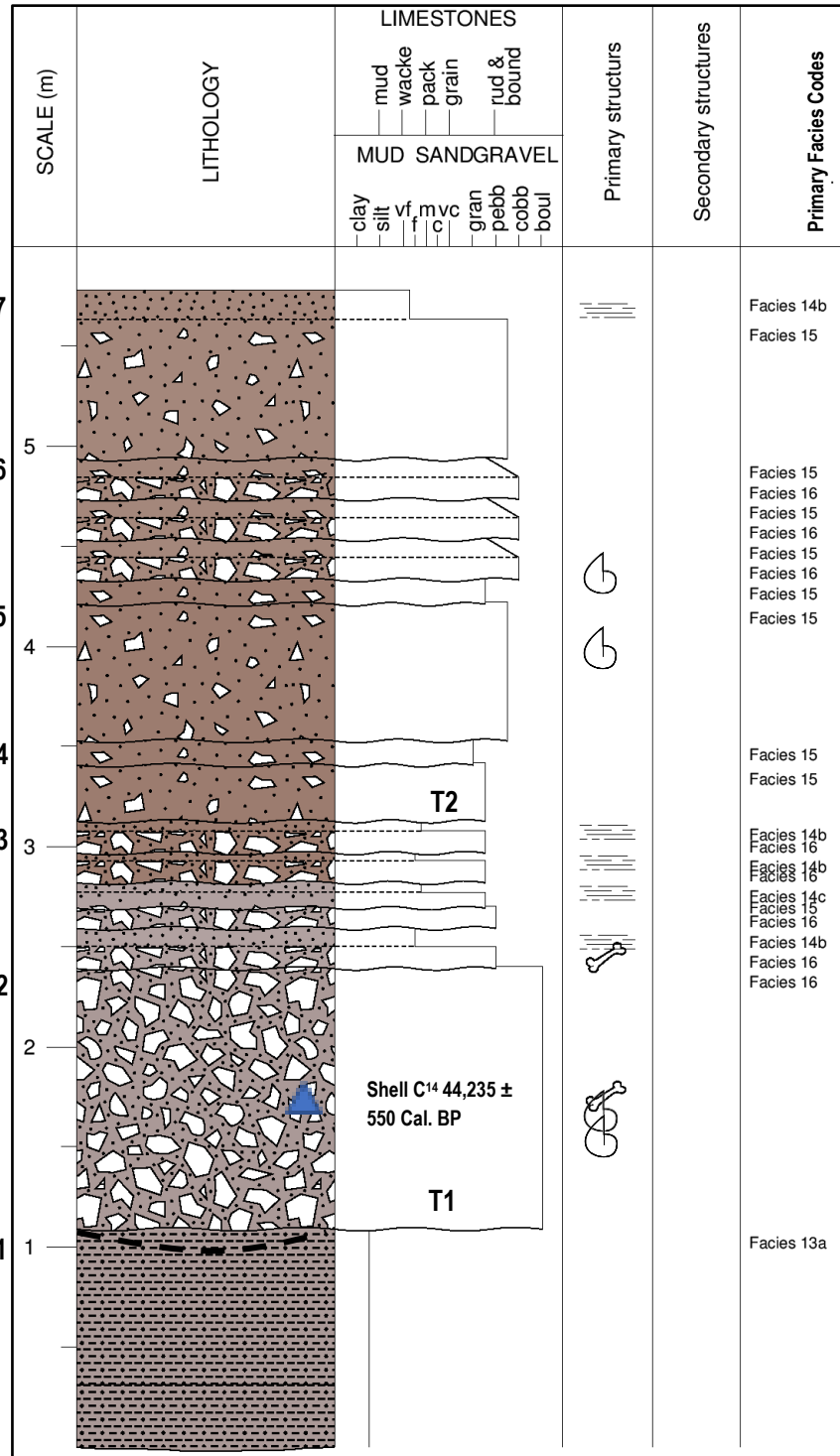


Figure 6.35: Site TB9, Log 4, (Figs 6.24, 6.25b, 6.36, Table 6.4). T1 = Terrace 1. For a photograph of the logged section see Figure 6.25b. See Section 6.6.6 the details of the ¹⁴C age.

5) Framestone limestone (Facies 1) One thin (0.20 m) framestone limestone occurs in Log 2 (Bed 19, Fig 6.33; see Fig 5.2 also) and is defined by vertical root structures in a carbonate mud matrix. For a full description of these beds, see Table 5.6.

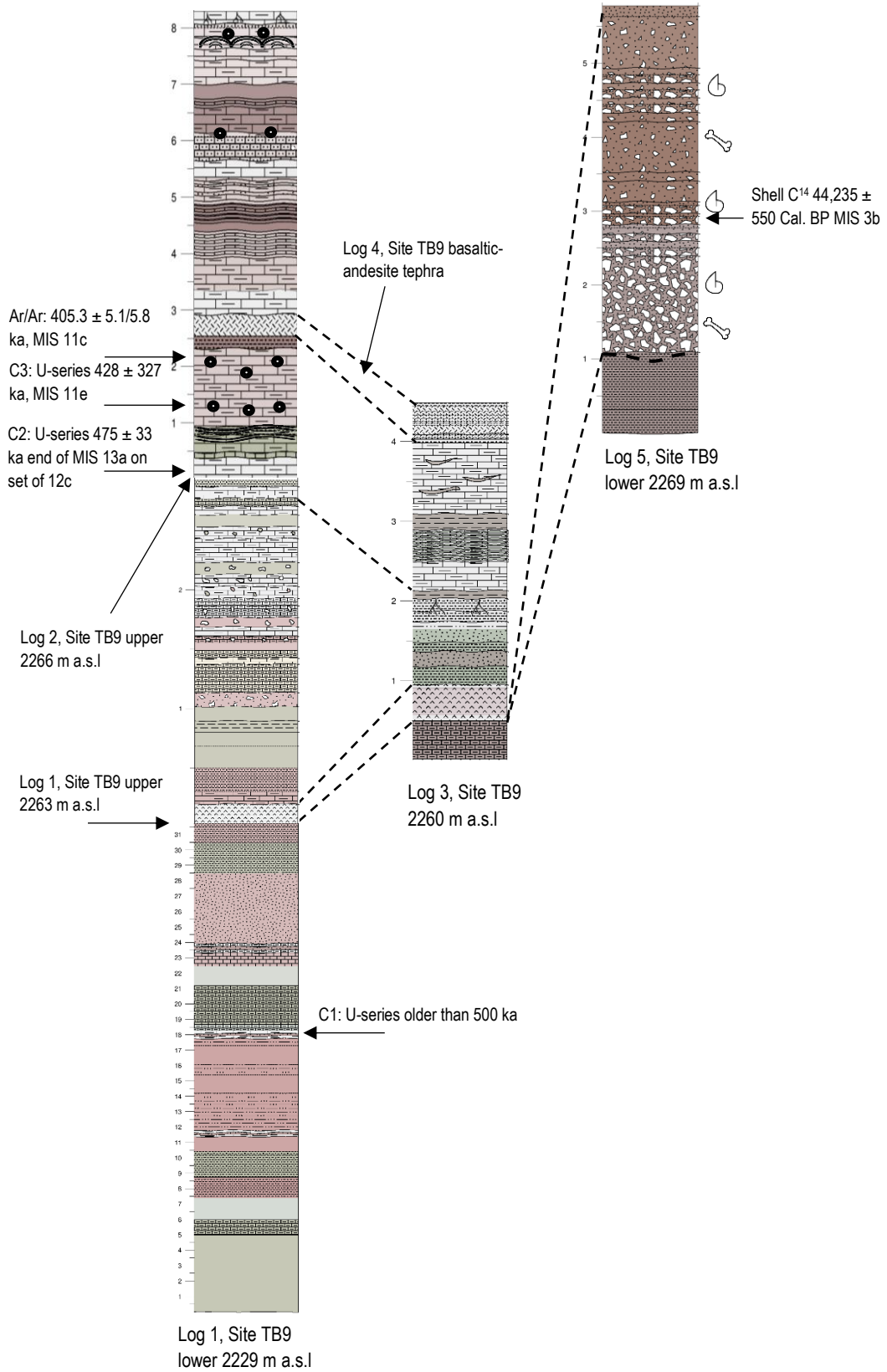


Figure 6.36: Barranca de Colores, Site TB9, Fence diagram Logs 1, 2, 3, 4 and 5. See Section 6.6.6 for details of the chronology (see Appendix 9 chronology). Numbers to the left of logs indicate meaters, logs to scale.



Figure 6.37: Images of TX89 Mammoth molar collected from gravel, sand and silt deposits like those recorded Logs 5 (Fig 6.35) at Site TB9. See Table 6.5 for descriptions of specimens

Table 6.5: TX89 Mammoth molar collected from T1 type deposits, Log 5 (Figs 6.24, 6.25a, 6.35 6.36), Site TB9. See Figure 6.37.

| Locality | Specimen number | Body part | Identification |
|---------------------|-----------------|-----------|----------------------|
| Barranca de Colores | Tx26a+b | Molar | <i>Mammuthus</i> sp. |
| Barranca de Colores | Tx89 | Molar | <i>Mammuthus</i> sp. |

6) Stromatolitic limestone has wavy, discontinuous sub-parallel white (N9) biofilm laminae (<5mm thick) that can be interbedded with clastic or mixed carbonate-clastic deposits greyish yellow-green (5GY 7/2) blocky, fine muddy micrite (Facies 2c in Facies 12c) (Figs 5.5 b). Incipient or isolated biofilm lamina are also common.

7) Mixed carbonate-clastic (Facies 9b & 10b) and clastic (Facies 12 b & c) sediments include greyish yellow-green (5GY 7/2) micritic mudstone (e.g. Facies 9b, Bed 7, 0.15 m, T20), mudstone (Facies 12b) beds that have total organic carbon (TOC) values between 11 and 15 % (Fig 6.40), massive sandy micrite with sand-sized intraclasts (Facies 10b, Log 2, Bed 1, Fig 6.33), and mudstone (Bed 2, Fig 6.33). Post-depositional root penetration and vertical jointing are also common.

6.6.2.3: Log 3, Site TB9

Log 3 (Fig 6.34, Table 6.4) records portions of Log 1 (upper, Beds 14 – 24, Fig 6.30) and Log 2 (Beds 1 – 5, Figs 6.30, 6.33 & 6.36). At the base, there is a massive muddy micrite (Facies 8a) followed by the dacitic tephra layer (Facies 18c, Log 1, upper section, Fig 6.30, Bed 14, Fig 7.2). Above this are massive mud beds

(Facies 12c) with desiccation features, silt (Facies 13b), and laminated fine silty sand with mud-lumps (Facies 14b).

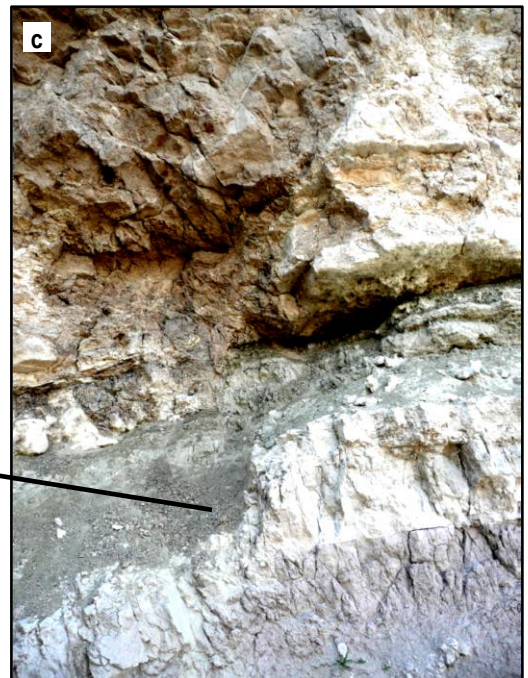
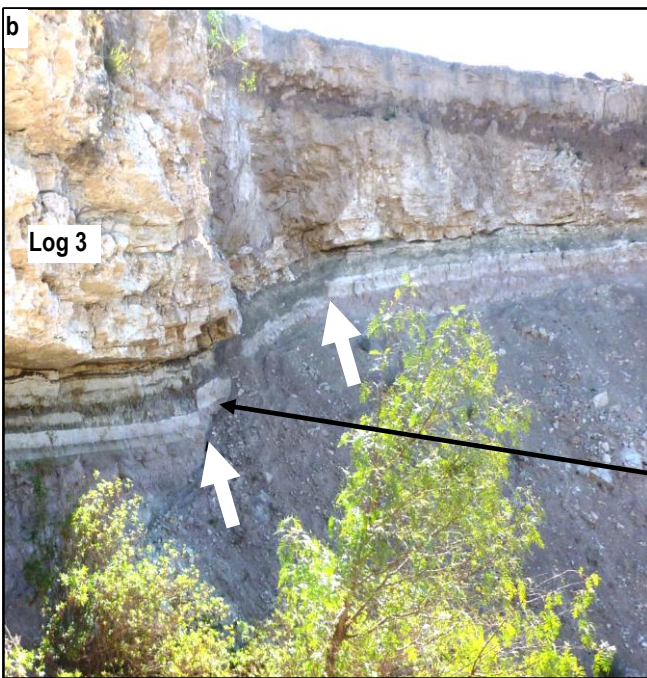


Figure 6.38: a - c) Displaced beds in Barranca de Colores (Site TB9) that correspond to the upper portion of Log 1 located at the southern end of the sequence at the head of the Barranca, the position of Log 3 is also indicated (see Fig 6.24 for location. b) Slumping sediments, basal contacts indicated by the black arrows. These sediments correspond to the top of lower the portion of Log 1. Location of photo indicated on Fig 6.24.

Above these are laminated calc-mudstones (Facies 3b) that have occasional mud-clasts, and channel scours (Facies 3b/14b) with or without wavy interbeds of fine silty sand, bioturbation and root casts and vertically jointed silt (Facies 11a) that load on to the lower bed and. At the top is the basaltic-andesitic tephra layer (Log 4, Facies 18a; Figs 3.26, 6.31 – 6.34).

6.6.2.4: Log 4, Site TB9

The sedimentology, geochemistry and Ar-Ar age for this tephra deposit are reported in Chapter 7 (see Tables 7.2 – 7.5, Figs 7.2, 7.3, 7.4, 7.6, 7.7 and Appendix 4, Table 3).

6.6.2.5: Log 5, Site TB9

Sedimentological descriptions for Log 5 are given in Appendix 4, Table 4 and (see Fig 6.35) a summary is given here. Log 5 incises Logs 1, and 2 and the whole sequence sits within gravel (Facies 16) lined cut channel (erosional unconformity) (Fig 6.25b & 6.35, Beds 1 & 2). Above the unconformity, four cycles of thinner (<0.40 m) gravel (Facies 15 and Facies 16), that grade into laminated fine sand (Facies 14c and Facies 14b) (<0.25 m thick) follow. Four matrix-supported gravel beds (1.7 m) (Facies 15) follow, each with an erosive channel base (Fig 6.35) overlain by three cycles (each <0.40 m thick) of clast supported gravel (Facies 16) that grade to poorly sorted, matrix-supported gravel (Facies 15). The gravels comprise locally sourced angular limestone clasts, fragmented terrestrial gastropod and aquatic bivalve shells (see Section 6.5.4). Poorly preserved megafaunal fossil bones have also been collected from these sediments, and examples of specimens from Barranca de Colores are shown in Figure 6.37 and described in Table 6.5.

6.6.3: Soft-sediment deformation features, Site TB9

Slump scars that correspond to the upper portion of Log 1 have also been recorded at Site TB9 and are thought to be related to faulting and soft sediment displacement (e.g. Table 4.3, fsl & gf), (see Fig 6.38d). At the head of the barranca, in-between Logs 3 & 5, the beds that correspond to the upper portion of Log 1 have been pushed upwards, and the entire section has been elevated above equivalent beds by 0.30 m. The offset can be seen in Figure 6.38 a, b & c.

6.6.4: Sediment geochemistry, Logs 1 & 2, Site TB9

The $\delta^{18}\text{O}$ and $\delta^{13}\text{C}$ isotope ratios, Ca, Mg, Sr, K, Na, Fe, Mn, Al ppm concentrations, molar ratios of Mg/Ca and Sr/Ca (see Fairchild et al. 200; Ihlenfeld et al. 2004 for their application), and organic, and inorganic carbon loss on ignition (LOI) is reported here from Logs 1 & 2 (see Figs 6.39 & 6.40 & Chapter 4). These data are presented to meet objectives 1- 4 set out in Chapter 1. Significant gaps exist in the data sets because the number of samples the author was able to run, and the number of samples suitable for this type of analysis was restricted. In some cases no data was not returned (see Appendix 11, Tables 1 & 2, Figs 39 & 40).

6.6.4.1: Log 1, Combined geochemical results, Site TB9

The $\delta^{18}\text{O}$ values in Log 1 (Fig 6.29 & 6.39) range from -4.6 to -11.0‰ (VPDB) and $\delta^{13}\text{C}$ values range between -1.9 to -5.3‰ (VPDB). In Figure 6.39, the $\delta^{18}\text{O}$ values become negative with increasing depth, and $\delta^{13}\text{C}$ follows the opposite trend. TOC decreases steadily with decreasing sample depth, and TIC follows the opposite trend (Fig 6.39). In the lower section of Log 1 (Fig 6.39, Zones 1 – 6) peaks of TIC in the upper portions of the allocated zones correspond to calc-mudstone interbeds (Samples BDC L56, L50, L36 & L20, Facies 3a; Fig 6.39). TIC values range between 2.3% to 73.3%, with a mean of 15.7%. TOC values range between 44.60% and 2.17% with a mean of 14.81%. In Zone 1 the $\delta^{18}\text{O}$ and $\delta^{13}\text{C}$ ratios (samples BDC L64 to L48) positively covary (R^2 0.68), $\delta^{13}\text{C}$ values range between -5.07‰ to -3.13‰, with a mean of -3.52‰ and $\delta^{18}\text{O}$ values range between -7.55‰ to -4.6‰ with a mean of -5.78‰ (Fig 6.39).

In the upper section of Log 1 (Fig 6.39, Beds 18 – 1, Zones 7 - 10), $\delta^{18}\text{O}$ and $\delta^{13}\text{C}$ ratios show no covariance. TOC values are variable and lower than in Zones 1 – 6 (range 3.80% to 18.06%, mean 12.79%). TIC values are higher than in Zones 1 – 6 (range 6.88% to 82.51%, mean 39.10%), but variable (Fig 6.39). There is a negative correlation (R_2 values between 0.40 and 0.63) between Ca vs Mg, TOC, Na, Fe, Mn and Al. Mg/Ca, and Sr/Ca ratios positively trend together (R_2 0.94), and all the above show a high degree of variability (Fig 6.39). Values of Mg, K, Fe, Al, Ca/Mg, Ca/Sr, and $\delta^{18}\text{O}$ positively covary with Na (R^2 above 0.47) (Fig 6.39, Appendix 11, Table 1). In Zones 7 – 10 values Ca, Mg, Fe, Sr, Na, K, Al TOC, TIC, Mg/Ca, and Sr/Ca show large swing in values relative to the sediment type. For example; In Zone 8, values of Ca vs Mg, Na, K, Fe and Al in calc-mudstone beds all negatively covary (R^2 0.68 to 1), and Ca vs Sr positively, but weakly, covary (R^2 0.33). In micritic mud and muddy micrite beds (BDC L15 & L14) Na vs K, Fe, Mn, Al, Mg/Ca and Sr/Ca all positively correlate (R_2 0.33 to 1) and are higher in these beds.

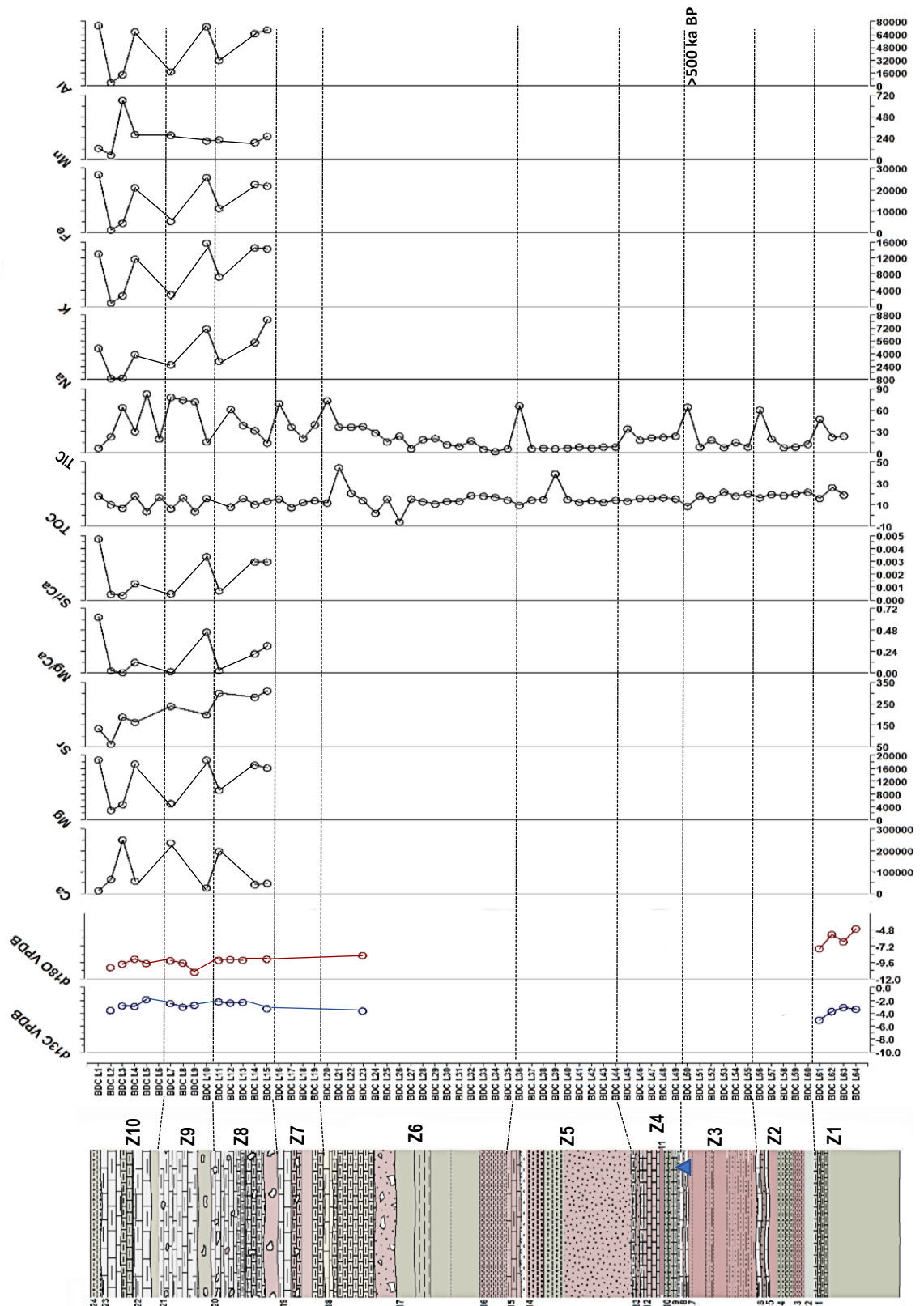


Figure 6.39: Geochemistry and stratigraphy, Log 1, Site TB9, composite section, 55 m. Beds 1 - 14 lower log (Fig 6.29). Beds 15 – 24 upper log (Fig 6.30). Mineral concentrations, ppm, TOC and TIC % (g), Mg/Ca and Sr/Ca molar concentrations (Appendix 11, Table 1). Facies key, Figs 5.25, 6.29 & 6.30. Z = Zones. Bed numbers on the left-hand side of log. ▲ = Bed 5, Sample BDC L58; Micromorphological analysis (Appendix 4, Table 2) and U-Series age of >500 ka BP, which is beyond the capabilities of the dating method.

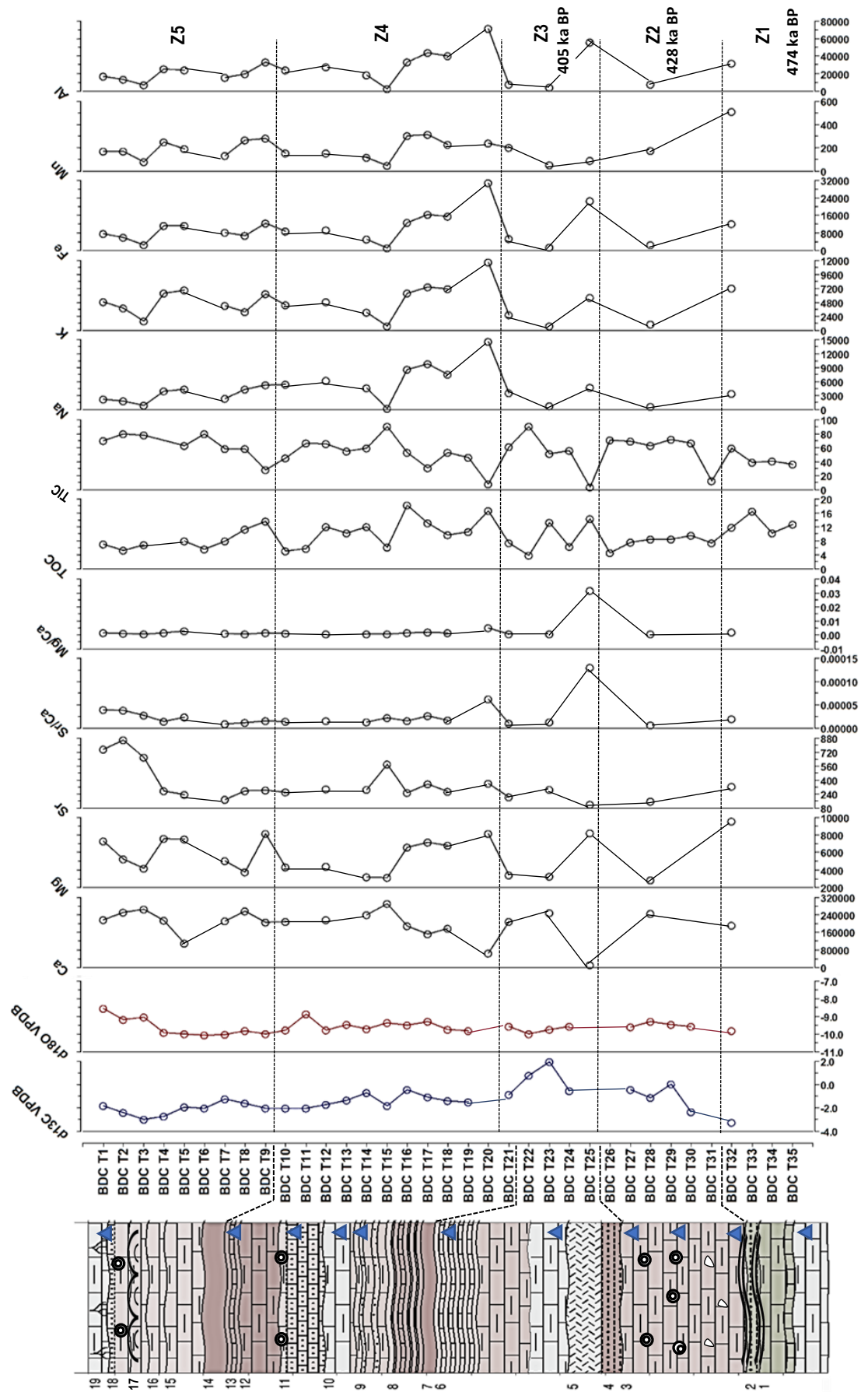


Figure 6.40: Geochemistry and stratigraphy Log 2, Site TB9, 8.5 m. Mineral concentrations, ppm. TOC and TIC % (g). Mg/Ca and Sr/Ca molar concentrations. Facies key Figs 5.25 & 6.33. Z = Zones. Bed numbers on the left-hand side of log. ▲ = Bed 5, Sample BDC L58; Micromorphological analysis (Appendix 4, Table 2).

In Zone 10, values of $\delta^{18}\text{O}$ vs Mg, Sr, Na, K, Fe, Al, Mg/Ca and Mg/Sr all positively covary (R_2 values between 0.50 to 0.91) within the zone. Lower values are associated with calc-mudstone beds, and higher values are associated with mixed clastic-carbonate beds. Values of Na vs Mg, Ka, Fe, Al TOC, TIC Mg/Ca and Mg/Sr all positively covary and higher values are associated with muddy micrite and mud beds.

6.6.4.2: Log 2, Combined geochemical results, Site TB9

The $\delta^{18}\text{O}$ values in Log 2 (Fig 6.40) range from -8.5‰ to -10.1‰ (VPDB) with a mean of -9.58‰. Values of $\delta^{13}\text{C}$ range from 1.9‰ to -3.3‰ (VPDB) with a mean of -1.38‰. TIC ranges between 3.5% to 90.5% with a mean of 59% and TOC ranges between 3.5% to 18.2%, with a mean of 9.0%. In Figure 6.40 values of the $\delta^{18}\text{O}$ trend to more positive values in the upper log (BDC T4 to T1, Zone 5, Fig 6.40) and between samples BDC T18 and T4 (Zones 3 & 4) values are stable, except in sample BDC T11 (0.05 ‰ positive shift; Fig 6.40). There is more variability in values of $\delta^{13}\text{C}$ with higher values in Zones 2 and 3 and more negative values in Zones 1 and 5 (Fig 6.40). There is no covariance between $\delta^{18}\text{O}$ and $\delta^{13}\text{C}$ in Log 2 (Fig 6.40). Ca negatively covaries with Mg, Na, K, Fe, Al, Sr/Mg and Mg/Ca (R_2 above 0.40). Molar concentrations of Mg/Ca vs Sr/Ca positively tend (R_2 0.85) and are stable between samples BDC T18 to T1 (Zones 4 & 5, Fig 6.40); below this, there is more variability. Values of Na positively trend with K, Fe, Al, TOC (R_2 above 0.72) and again samples below BDC T18 show more variability.

6.6.5: Dating of the logged sections, Site TB9

6.6.5.1: Radiocarbon ages

One terrestrial gastropod shell was selected for dating, sample BC1TEQ. (see Appendix 9, Table 2 for BETA Analytics report and Fig 4.6 (8)). The shell collected from Log 5, Barranca de Colores was collected from Bed 9 (Figs 6.35 & 6.36) (Facies 15). The uncalibrated radiocarbon result for sample BC1TEQ (40,670 \pm 550 bp; see Table 2, Appendix 9) was outside of BETA's calibration range, so the INTCAL13 curve (Reimer et al. 2013) in CALIB (Stuiver et al. 2017) was used to generate a 2 Sigma calibrated age range of ^{14}C 43,905 - 44,564 cal. BP. The average value of these ages, 44,235 \pm 550 cal BP, is shown in Figures 6.35 and 6.36 (see Appendix 9, Table 2, for full details). Both the uncalibrated and calibrated ages are considered a maximum possible age (see Section 6.5.4 and Appendix 9).

6.6.5.2: $^{40}\text{Ar}/^{39}\text{Ar}$ ages

The data for the age of the basaltic-andesite tephra layer (Facies 18a) recorded in Logs 2 & 4 (Figs 6.36, 6.41, 6.42 & 6.36, see also Chapter 7) define a single age population with a date of 405.3 \pm 5.1/5.8 ka.

The data cast on an isotope correlation plot define an inverse isochron with an age that is indistinguishable from the ideogram age and an initial trapped component that is indistinguishable from the atmosphere (Lee et al. 2006), showing the data to be robust (see Appendix 3, Table 1; Figs 6.41 & 6.42). The age data for the basaltic-andesite tephra layer (Facies 18a) was run through the Optimisation Model of Renne et al. (2011) to determine the full uncertainty (including decay constant) to allow comparison of the $^{40}\text{Ar}/^{39}\text{Ar}$ age data with other chronometers. Data are reported on all figures as Age \pm Analytical/Full Uncertainty (1 sigma). When comparing the Ar/Ar data, one sigma is appropriate given the reproducibility between the single data populations and the normal distribution that the data sets have around the mean (Figs 6.41 & 6.42) (Mark pers comm. 2015).

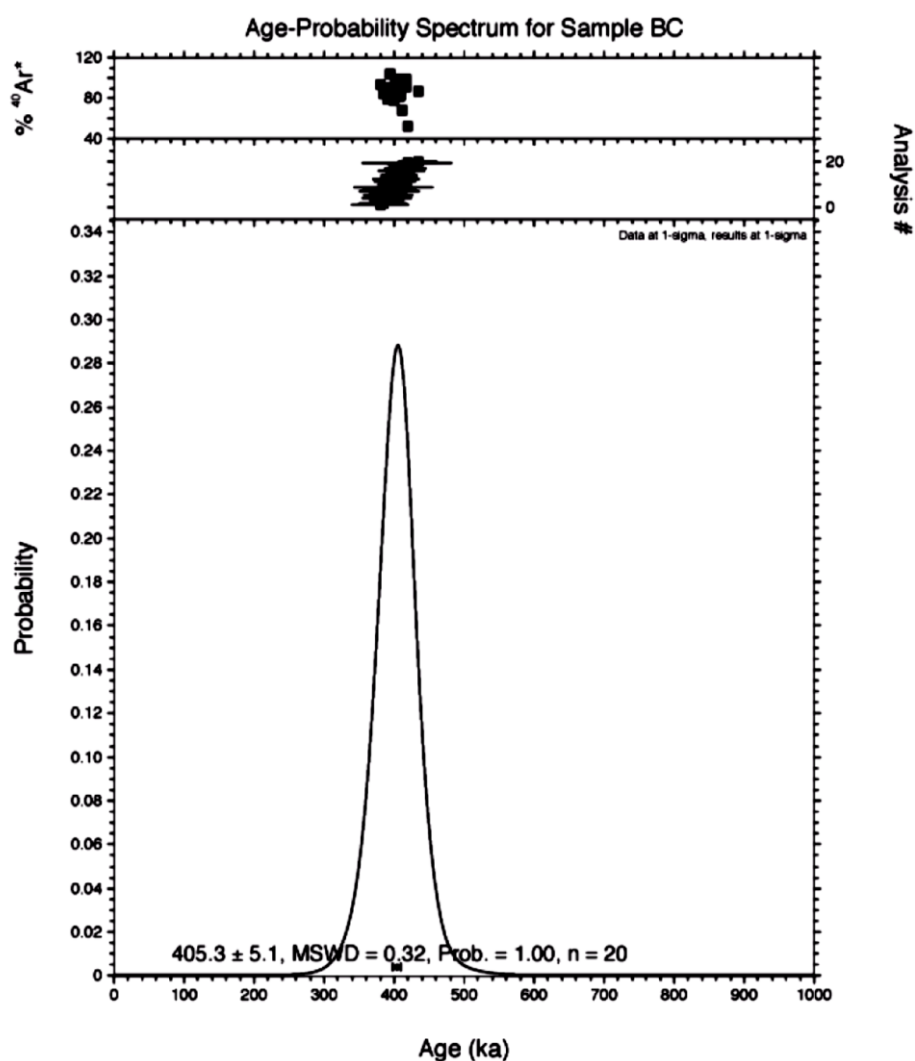


Figure 6.41: Age probability spectrum for the basaltic-andesite tephra layer, Barranca de Colores, Site TB9, Logs 2 & 4 (Figs 6.33, 6.34 & 6.36) Data at 1 – sigma and results at 1 – sigma.

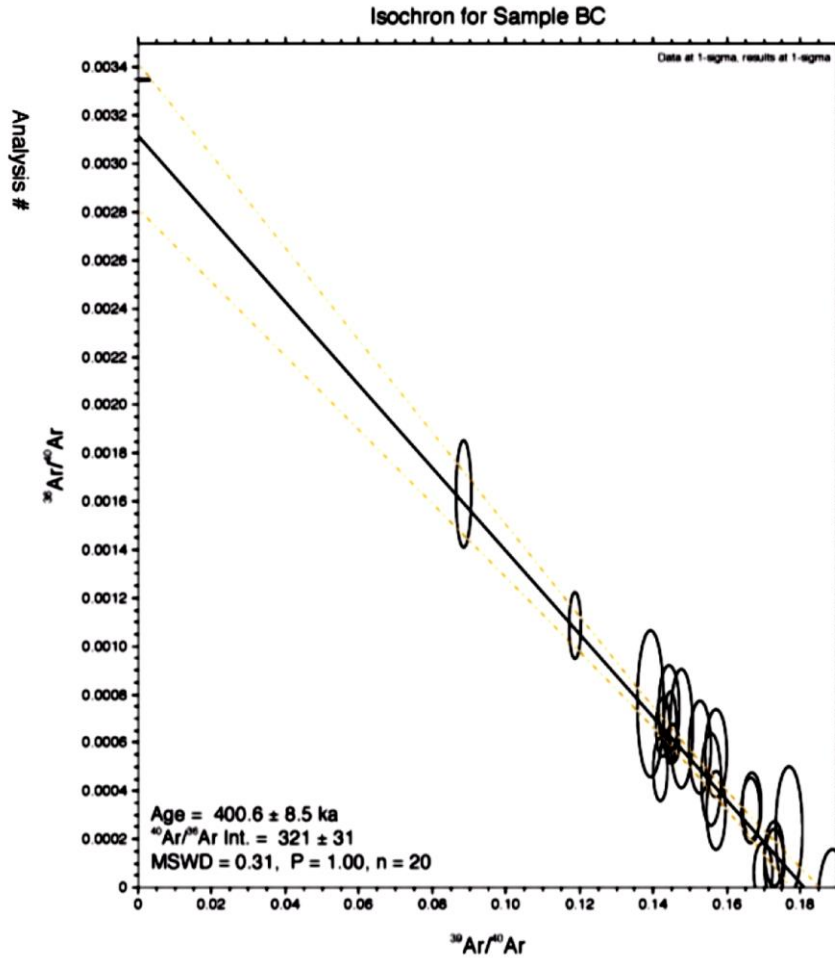


Figure 6.42: Inverse Isochron for the basaltic-andesite tephra layer barranca de Colores, Site TB9 Logs 2 & 4 (Figs 6.33, 6.34 & 6.36). The x-axis plots the $^{39}\text{Ar} / ^{40}\text{Ar}$ ratios and $^{36}\text{Ar} / ^{40}\text{Ar}$ ratios of the individual heating steps. The best line fit through the data set gives the trapped $^{40}\text{Ar} / ^{36}\text{Ar}$ values from the y-intercept and the $^{40}\text{Ar} / ^{39}\text{Ar}$ age value from the x-intercept (McIntosh et al. 2015).

6.6.5.3: U -Series ages

U – series ages obtained for the Barranca de Colores Log 2 (C2 (474 ± 33 ka BP) & C3 (428 ± 428 ka BP); Table 3, Appendix 9, Fig 6.33 & 6.40) and Log 1 (C1 (>500 ka BP), Table 3, Appendix 9, Figs 6.29 & 6.39) are used with extreme caution as part of the chronology due to the following issues: a) In all of the samples uranium counts were low, between $0.4187 - 1.1990$ ng/g when counts above $2000 - 3000$ ng/g are really needed to date accurately. b) All samples have extremely high ^{232}Th counts ($183.41 - 697.20$ ng/g), which suggests that the samples are dirty and contaminated by the detrital ^{230}Th input. Any ^{232}Th counts above >50 ng/g are considered uncertain. c) $^{230}\text{Th} / ^{232}\text{Th}$ activity ratios should be >30 ng/g combined with a high U count.

Where this is not the case, ^{232}Th detrital contamination is too significant which makes calculating a decay constant from $^{230}\text{Th} - ^{232}\text{Th}$ very difficult (Price, pers comm, 2011; Felstead pers comm, 2015). Hence, significant measurement errors make the U – series ages potentially unreliable (Price pers comm, 2011). The $^{40}\text{Ar}/^{39}\text{Ar}$ age of $405.3 \pm 5.1/5.8$ ka (see Section 6.6.7.2) however gives some chronological reassurance and control to the u-series ages generated from calc-mudstone (>500 ka BP) from Bed 8, Log 1 (Figs 6.29 & 6.39, Table 3, Appendix 9, sample 03 SG-C3), from Bed 1, Log 2 (Figs 6.33 & 6.40, Appendix 9, Table 3 sample 02 SG-C2, 475 ± 33 ka BP) and from pisolithic limestone, Bed 3, Log 2 (Figs 6.33 & 6.40, Table 3, Appendix 9, sample 01 SG-C1, 428 ± 327 ka BP), and so they are used tentatively here.

6.6.6: Combined seismological and geochemical Interpretation, Log 1, Site TB9

The sequence recorded in Log 1 is understood to be older than 474 ± 33 ka BP based on u-series age from the base of Log 2 (Fig 6.40, Section 6.6.7.3). Overall Log 1 shallows upwards from open water lacustrine conditions (Zones 1 – 6) to shallow ephemeral conditions in Zones 7 – 10 (F/LMLs (Table 4.8), LMs, LMi (Table 4.10), LHer, (Fig 4.2) and Fig 4.3).

6.6.6.1: Green mud and mixed carbonate-clastic beds Zones 1 – 5

In Zones 1 – 5 Greyish yellow-green (5GY 7/2) and light greyish green (5GY 8/1) fine-grained micritic mud (Faceis 8a) and muddy micrite (Facies 9a) with occasional mud interbeds (Facies 12a) have high TOC (39.1% – 0.9%) and TIC (24.2% - 6.4%) values relative to the red beds (Section 6.6.8.1), although this varies from zone to zone (see Fig 6.39). These beds are interpreted as being deposited in relatively deep (but fluctuating), low-energy, oxygen-poor and nutrient-rich lacustrine to wetland/marsh environments (see Tables 8.1 – 8.3). In Zone 1 for example, the negative covariance between $\delta^{18}\text{O}$ and $\delta^{13}\text{C}$ in Log 1 (Fig 6.39), suggests a hydrologically closed water body (e.g. LMs, LMa, Table 4.10; F/LMIs, Table 4.8), although the data is limited (Fig 6.39). The mean of $\delta^{18}\text{O}$ ratios (-5.98 ‰, Zone 1, Fig 6.39) is up to 5‰ more positive than the mean of contemporary precipitation and groundwater values recorded from the study area and surrounding areas (Cortez & Favolden, 1989, see Appendix 10). Negative covariance between $\delta^{18}\text{O}$ and TIC suggests that temperature-driven change is unlikely. Instead, high nutrient levels within the waterbody encouraging accelerated biological activity and biogenic carbonate precipitation via photosynthesis is interpreted. The decomposition of organic matter would have increased the biological demand for oxygen, increasing carbonate precipitation and decreasing water oxygen levels, causing a shift towards a reducing state and eutrophication of the water body. The result is an enrichment of ^{13}C (^{12}C preferentially taken removed during photosynthesis,

Leng & Marshall, 2004) in the carbon-pool and increased ^{13}C DIC incorporation into carbonate precipitants (Leng, 2006).

By the same principle, more $\delta^{16}\text{O}$ would be incorporated into the precipitated mineral suppressing the $\delta^{18}\text{O}$ signal in the bulk carbonate sample (Fronval et al. 1995; Leng, 2006). Consequently, negative shifts of $\delta^{18}\text{O}$ and ratios and comparably high TIC and TOC values (Fig 6.39) are associated with eutrophication of the precipitating water body (e.g. LMs to IM, Tables 4.10 and 4.13). It follows that as productivity decreased, more negative ^{13}C DIC values would be expected, which is likely the case in Zone 1, where values of $\delta^{13}\text{C}$ decrease from the base upwards, overall by 3‰. The range of $\delta^{13}\text{C}$ values (-3.2 to -5.1‰, see Section 6.6.8.1) indicate C4 type vegetation dominated the catchment (Andrews, 2006) although the relatively negative $\delta^{13}\text{C}$ values, compared to the values in the upper portions of Log 1 (Fig 6.39), also support higher available moisture levels.

6.6.6.2: Red mud, silt, sand and mixed carbonate-clastic Zones 1 – 5

Pale red (5R 6/2) and moderate pink (5R 7/4) massive mud (Facies 12a), silt (Facies 13a), fine-medium sand (Facies 14c), muddy micrite (Facies 8a), micritic mud (Facies 9a) and sandy micrite (Facies 10a) beds in Zones 1 – 5 (Figs 6.29 & 6.39, Tables 8.1 – 8.3) indicate relatively shallow (compared to green beds, Section 6.6.8.1) low to moderate energy, well-oxygenated playa-type environments (Figs 6.29 & 6.39) (e.g. Smoot & Olsen, 1988; Talbot et al. 1994). At Site TB9 these beds generally have lower TOC values (21.5% - 2.3%) and TIC (21.5 – 2.3%) compared green beds (see Zone 3, Log 1, Fig 6.39 and Section 6.6.8.1) which is thought to be a function of reduced available moisture, a decrease in the lateral extent of the water body and/or its depth, weathering and terrigenous and organic in-wash from the catchment. The absence of exposure features again suggests that, although shallowing may have occurred (relative to green beds), there was still a perennial playa type water body (e.g. F1:1, Mercia Mudstone Group, Porter & Gallois, 2008; the Provence Basin, France, Colson et al. 1998). Sandy beds are taken to indicate periods of littoral zone expansion and a further reduction in the lateral extent of the water body (e.g. the Serinhisar-Acipayam Basin, Denizli, southwest Turkey, Akbulut & Kadir, 2003), or possibly rapid deposition during a flood event (e.g. Mercia Mudstone Group, Porter & Gallois, 2008).

6.6.6.3: Calc-mudstone and muddy micrite beds: Zones 1 – 6

Thin (< 0.50 m) massive calc-mudstone (TIC > 50%, Facies 3a) and muddy micrite (TIC 25 % - 50%, Facies 8a) beds with thin (<0.05) fine silty sand interbeds (Facies 14b) that cap Zones 1 – 6 (Figs 6.25 - 6.28, 6.29, 6.30, 6.39) indicate shallow, fresh-brackish water (e.g. sample BDC 57, Zone 2). Values of TOC are between 13.5% and 2.2%, indicating nutrient-poor conditions relative to red and green beds, except in Zones 1

& 2 (Fig 6.39). The absence of evaporitic fabrics indicates a perennial water cover, and manganese clusters suggest some biological activity (see Appendix 4, Table 1, Figs 6.29 & 6.39). They are interpreted as brackish-freshwater semi-arid deposits developing in response to suppressed terrestrial clastic input and fluctuating humidity levels (see Talbot et al. 1994). Interbeds of sand within these beds suggests short-lived shallowing and/or flood events in both cases, an increase in energy is associated.

6.6.8.4: Mud, silt, sand and carbonate and mixed carbonate-clastic: Zones 7 – 10

In Zones 7 – 10, like in Zones 1 – 6, micritic mud (Facies 9a), muddy micrite (Facies 8a), sandy micrite (Facies 10a), mud (Facies 12a), silt (Facies 13a), fine to medium sand (Facies 14c), muddy micrite (Facies 8a) and green (Section 6.6.8.1), red (Section 6.6.8.2) and white (N9) calc-mudstone (Facies 3a) (Section 6.6.8.3) interbeds occur. Unlike Zones 1 – 6, bed thicknesses are < 0.10 m indicating high-frequency changes over relatively short depositional episodes. Bedding contacts are mainly disconformable and erosive. Ratios of $\delta^{18}\text{O}$ (-11.0‰ to -9.1‰) in Zones 8 - 10 fall within the range of $\delta^{18}\text{O}$ values known for Central Mexican ground and surface waters today (see Tables 1- 6 and Figs 1 – 7, Appendix 11). Values of $\delta^{13}\text{C}$ (-2.75‰) indicate that C4 vegetation still dominated, but a positive shift from Zone 1 of -3.23‰ indicates that catchment had significantly less available moisture.

Green beds recorded in Zones 7 - 10 are thought to represent shallow, oxygen-poor mud-flat to marsh depositional environments (e.g. Myrow, 1990; Potter et al. 2005; the Eocene Green River Formation, Remy & Ferral, 1989; Pietras & Carrol, 2006). High Mg/Ca and Sr/Ca molar concentrations (Fig 6.39) that can be associated with these beds is possibly related to accelerated in-aquifer mineral leaching during dry intervals. For example, in Zone 8 positive covariance (R_2 0.33 to 1) between Na vs Ka, Fe, Mn, Al, Mg/Ca and Sr/Ca values in the basal micritic mud and muddy micrite beds (BDC L15 & L14) suggest the same process is controlling all variables. Higher molar ratios of Mg/Ca imply dry conditions, less groundwater availability, longer groundwater residence times and less through-flow (see Huang & Fairchild, 2001; Ihlenfeld et al. 2003; Garnett et al. 2004; Forbes, 2010).

In the upper zone the trend is reversed in samples BDC L13 to BDC L11) where Mg/Ca concentrations decrease, and values of Ca, Sr, TIC and TOC dominate. Increased TOC suggests that the water body and catchment had become more productive, which is thought to have caused a positive shift in $\delta^{13}\text{C}$ values (see Section 6.6.6.1). The above suggests increased available moisture, shorter groundwater residence times and associated rapid through-flow, fresher groundwaters with lower TDS values and lower Mg/Ca concentrations.

Red beds (Section 6.6.8.2) are thought to represent a nutrient deficient, oxygen-rich (Myrow, 1990; Carroll & Bohacs, 1999; Potter et al. 2005; Pietras & Carroll, 2006), shallow, but hydrologically variable waterbody that allowed sediments to oxidise (e.g. Newark Supergroup, Smoot & Olsen, 1988). Dry (warm/cool) conditions are interpreted coupled with reduced biological activity and biogenic carbonate precipitation relative to green beds.

For Example, pale red (5R 6/2) massive mud (BDC L55, Facies 12a), micritic mud (BDC L54 & L52, Facies 9b) and silt (BDC L53 & L51, Facies 13b) beds in Zone 3 are thought to have been deposited in a semi-arid, shallow playa type system (e.g. LMs, LMa to IOm Tables 4.10 to 4.13). Cyclicity between clastic beds (high TOC & low TIC; BDC L55, L53, L51) and mixed carbonate-clastic and calc-mudstone beds (low TOC and high TIC; BDC L54, L52, L50) suggests shifts in the lateral extent and productivity of the water body and catchment (e.g. LMs, Table 4.10). Similar stratigraphy has been recorded in the Mercia Mudstone Group where massive, structureless red dolomitic mudstones, siltstones, limestone, sandstone and evaporites are linked to playa-lake depositional environments on vast alluvial plains. The massive fine-grained sediments are associated with shallow low energy water that had a broad lateral extent in an area of low topographic relief within a semi-arid interior basin (Talbot et al. 1994), like the study area.

White carbonate-dominated beds are thought to indicate decreased moisture and suppressed clastic input (Section 6.6.8.2) into a low energy fluvial-lacustrine environment (e.g. F/LMIs, LMs, LMi, LMa Tables 4.8, 4.10). Intraclastic beds (FInIs, LMs, LLer. Tables 4.8, 4.10 & 4.11), brecciation and exposure features, (e.g. Beds 17 – 24, Fig 6.30 Facies 6 and 15; PNod/Bre, Table 4.12.) reflect increased energy, flooding, erosion, incision and reworking in littoral to eulittoral lacustrine zones, or marginal fluvial environments (e.g. Freytet & Plaziat, 1982; Tucker & Wright, 1990; Pietras & Carroll, 2006). (e.g. Beds 17 – 24, Fig 6.30). At the top of Zone 10 (Site TB9, Fig 6.30; e.g. PNod/Bre, Table 4.12) there are extensive and established mud cracks (Fig 6.26) indicating that water body at the depositional completely dried pre-MIS 12c (Fig 8.8). Because of this a significant depositional hiatus and none-depositional unconformity are proposed between Logs 1 and 2 at Site TB9.

6.6.7: Combined sedimentological and geochemical Interpretation, Log 2, Site TB9

The $\delta^{18}\text{O}$ values recorded from Log 2 fit within the current range of values known for the study area today and fall within Groups 1 and 2 comfortably, which were also found to be similarly evolved from regional and local precipitation values (see Appendix 10). When compared to the upper portion of Log 1 (Fig 6.39) values

of $\delta^{13}\text{C}$ (-3.3‰ to 1.9‰) and TIC (mean 59%) are correspondingly high and TOC (mean 9.0%) low indicating that the increasing aridity recorded in the upper portion of Log 1 continued into Log 2 (Fig 6.40). Very occasional low values of TIC and high clastic signals are associated with mudstone and micritic mudstone beds at the base of identified zones (Figs 6.33 & 6.40). Negative shifts in $\delta^{18}\text{O}$ values and low molar concentrations Sr/Ca and Mg/Ca (Fig 6.40) suggest that there was either a fresh surface water source or that there was rapid throughflow compared to some beds (e.g. Bed 4, Log 2, Figs 6.33 & 6.40). The base Log 2 was deposited around 475 ± 33 ka BP, (Bed 1, Fig 6.33 & 6.39, Section 6.6.7.3) after which there is assumed to be a depositional hiatus. Bed 2 was deposited around 428 ± 327 ka BP (BDC T29, Fig 6.33 & 6.40, Section 6.6.7.3). The Basaltic-andesitic tephra layer recorded in Bed 5 (Fig 6.33) indicates deposition continued up to and beyond $405.3 \pm 5.1/5.8$ ka BP (Section 6.6.7.2).

6.6.7.1: Massive to faintly laminated calc-mudstone sediments (Facies 3a & 3b)

Calc-mudstone beds indicate deep but hydrologically variable, low energy fresh to brackish fluvial-lacustrine depositional environments (see Figs 6.33 & 6.40, see also Table 2, Appendix 4). For example; the massive to laminated calc-mudstone beds recorded for samples BDC T8 to T5 (Beds 15 & 16, Zone 5) are interpreted as being deposited though settle out in fresh, clear, relatively deep-water environments (e.g. F/LMIs, LMa, Tables 4.8 & 4.10). Shell fragments within the beds and the lowest values of Mg and clastic minerals recorded in Zone 5 (Fig 6.40) support this. Negative $\delta^{18}\text{O}$ (-9.8 to -10.1‰) values also suggest increased available moisture or decreased evaporation relative to Beds 17 – 19 (samples BDC T4 – T1). On the upper surface of Bed 16 (BDC T5), a salt (halite) hopper crystal mould (see Fig 5.6 & Table 5.10) and minor microkarst features (e.g. PMk, Tables 4.12 & 4.13) suggest sub-areal exposure and intense evaporation occurred post-depositionally. A depositional hiatus is interpreted between Beds 16 and 17 because of this (Figs 6.33 & 6.40).

6.6.7.2: Pisolitic limestones (Facies 5)

The pisolitic limestone beds indicate shallow, evaporitic, but hydrologically variable, moderate to low energy, saline fluvial-lacustrine depositional environments (e.g. F/LMIs, LMa, LMs, Tables 4.8 & 4.10). For example; the transition from calc-mudstone at the base of Zone 2 to brecciated pisolitic limestone (Bed 3, Fig 6.40, BDC T31 – T26) represents the evolution from relatively deep freshwater, to shallow, turbulent/flowing, saline water (Johns and Wilkinson 1978; Folks & Chavetz, 1983; Hunt pers comm, 2017), although pisoliths can also be biologically mediated in standing water (see Table 4.15 and Folk & Chafetz, 1983). Lower levels of

available moisture are indicated by the positive shift in $\delta^{13}\text{C}$ values within Zone 2 (-2.4 to 0.00‰), and from Zones 1 to 2 (Fig 6.40) and TOC values are the lowest recorded from Logs 1 (Fig 6.39) and 2 (Fig 6.40) indicating nutrient-poor environments. Relative to Zone 1 (Log 2, Fig 6.40) there is a 0.04‰ positive shift in the mean $\delta^{18}\text{O}$ value suggesting that the precipitating water body was more evolved and subject to more intense evaporation. Secondary root traces cutting pisolith forms signify sub-areal exposure and drying (e.g. PBre, PRm Tables 4.12 & 4.13 also see Figs 5.9 & 5.10, Tables 5.12 & 5.13). A salt hopper casts in the upper zone indicates a period of exposure (Meurant, 1976) and that 90% of the original water body had likely evaporated allowing halite to precipitate (Boggs, 2006). The precipitating water body was saline, similar to a playa-type environment heading towards a shebka like conditions (BDC T29 and T28; Fig 6.33 & 6.40) towards the upper zone (e.g., Mercia Mudstone Group, Talbot et al. 1994).

6.6.7.3: Peloidal limestones (Facies 4)

Peloidal beds are thought to represent moderate energy depositional environments (Tucker & Wright, 1990) where bioturbation was occurring (Fig 5.9) within the photic environment. Assuming a faecal origin of the peloids, biological activity is implied within relatively fresh to brackish fluvio-lacustrine pool environments (Figs 6.33 & 6.40). For example, in Zone 4, the bioturbated peloidal limestone (Bed 11, BDC T13) suggests increased biological activity and relatively well-oxygenated fresh waters compared to Bed 9 (Figs 6.33 & 6.40). In Zone 4, there is no relationship between $\delta^{13}\text{C}$ vs $\delta^{18}\text{O}$ or between $\delta^{13}\text{C}$ and $\delta^{18}\text{O}$ vs Mg/Ca in Zone 4 suggesting that $\delta^{13}\text{C}$ values are not groundwater driven. Molar concentrations of Mg/Ca, and Sr/Ca are low, indicating groundwaters were not held in storage for extended periods or that there was a surface water source feeding the pool.

6.6.7.4: Framestone deposits (Facies 1)

Only one thin framestone deposit occurs in Log 2, and it is thought to represent either marginal pool or fluvial environments (e.g. F/LpStLs, LMa, Tables 4.8 & 4.10, Figs 6.33 & 6.40). In Zone 5 the framestone limestone deposit is interbedded with a pelleted-peloidal limestone and intraclastic rudstone (see Fig 5.2 and Table 5.6 for a description). The bed contains organic detritus, shell, oncoids, biofilm laminae and volcanoclastic input (2 - 5%) suggesting freshwater conditions (shell) that were occasionally evaporitic (biofilm) (Bed 19, BDC T2, and T1, Fig 6.2 & Table 5.6). A shallower water body is supported by a positive shift in $\delta^{18}\text{O}$ values and clastic input.

6.6.7.5: Stromatolitic deposits (Facies 2)

Stromatolitic beds are thought to represent seasonal deposition (Facies 2b) in marginal to shallow fluvial-lacustrine environments. Biofilm lamina within beds suggests short-lived hydrological changes, i.e. inter-seasonal drying, flooding and re-working as some lamina are in-situ, and others are intraclastic (see Sections 6.6.9.6 & 6.6.9.7). For example, the agglutinated stromatolitic in the upper portion of Zone 2 (Bed 2, 6.33 & 6.40) consists of wavy, discontinuous sub-parallel white (N9) biofilm laminae (<5mm thick) interbedded with greyish yellow-green (5GY 7/2) blocky, muddy micrite laminae (<10 mm) that contains brecciated silty clay balls (of the same sediment) (Facies 2c in Facies 8b) (Figs 5.5 b, 6.33 & 6.40). Overlaying this is 0.05 m of greyish yellow-green (5GY 7/2), vertically jointed micritic mud with calcified roots and carbonate nodules. Marginal fluvial-lacustrine environments are interpreted with cycles between high energy (muddy micrite: Facies 8b) and low energy conditions, allowing microbial growth (see Fig 5.5b). Ephemeral conditions are supported by vertical jointing in the upper section of Bed 1 and Bed 2 (6.33 & 6.50).

6.6.7.6: Mixed carbonate-clastic (Facies 8 – 10)

Mixed carbonate-clastic beds indicate hydrologically variable, low-moderate energy fluvial-lacustrine depositional environments (Figs 6.33 & 6.40, see also Table 2, Appendix 4) and deposits are transitional between clastic and carbonate beds. For example, the basal muddy micrite (Fig 6.33, lower Bed 1, BDC T35 & T34) at the base of Zone 1 likely developed via suspension sedimentation in relatively deep standing water. Shell fragments suggest freshwater conditions (e.g. F/LMIs, LMs, Tables 4.8 & 4.10) (see Flügel, 2010). Void spaces suggest rapid lithification (Flügel, 2010). Biofilm lamina in the upper deposit suggest shallowing and abnormal salinity levels (Fig 6.40) (e.g. Fstmls2, Table 4.8; LMi, Table 4.10) (Deho, 1994; Costerton et al. 1995; Westall et al. 2000). Post-depositional silt infill of void spaces in the lower bed is related to groundwater movement (Hunt, pers comm, 2017). High TOC at the top of Bed 1 (BDC T33, 16.5%), and sediment colour suggest a marsh to wetland type environment had developed (e.g. F/LMIs, Table 4.8; LMa, Table 4.10) (e.g. Zone 1).

6.6.7.7: Intraclastic beds (Facies 6 - 15)

Intraclastic beds can be laminated, wave-rippled and can have micro-channelised in-wash beds that indicate relatively short-lived hydrological fluctuations between higher and lower energy conditions (e.g. FInIs, F/LMIs, FFsc, FFm, FFr and FGwc Table 4.8, or LMs, LMi, LMa & Lp, Table 4.10). The micro cross-bedded ripples and coarser sediment in-wash within micro-channels suggest higher energy environments (see Chapter

5 and Figs 6.33 & 6.40) and flood events, but mostly under a lower flow regime (e.g. FSr, FNls, LMa, Tables 4.8 & 4.10; Fig 6.33, beds 2, 6, 9, and 13). These deposits suggest fluctuating hydrological conditions caused by water fluctuations driven by changes to flow volume, intra-drainage networks and the extent of the littoral zone of the depositing water body. For example, In Zone 4 (Beds 8, 10 & 12) calc-mudstone was likely deposited in low energy ponds on floodplains (e.g. F/LMls, LMa, LMi, Tables 4.8 & 4.10). Hydrological fluctuations (e.g. FSr, FNls, LMa, Tables 4.8 & 4.10) and reworking are indicated by wave-rippled intraclastic interbeds and sandy lenses (Bed 8, BDC T17 & Bed 9, BDC T15 & T16).

6.6.7.8: Paleosol deposits

Paleosol deposits occur in Beds 4 and 14 (Figs 6.33 & 6.40, Appendix 4, Table 2). The upper and lower contacts of these beds are disconformable, suggesting depositional hiatuses. They are thought to have formed in response to hydrological variations. Erosion, downcutting, re-working and brecciation in the upper bed occurs, suggesting that conditions were dry, and the bed was exposed for a prolonged period. For example, in Zone 3 (Bed 4) the massive mudstone is thought to be either a drape or paleosol deposit (TOC 15%) (e.g. FFm, FP Table 4.8, LP Table 4.10). Either way, the bed represents the evolution of the robust evaporitic processes seen in the upper portion of Zone 2 with a depositional hiatus between Beds 4 and 5 (see Pnod/Bre, PMk, Table 4.12; lom, Rm, Table 4.13; Figs 6.33 & 6.40). The peak in molar concentrations of Sr/Ca, and Mg/Ca (Fig 6.40) also suggests decreased available moisture (see Zone 2).

6.6.7.9: Tephra deposits

The basaltic-andesite volcanic ash (Facies 18a, Bed 5) corresponds to MIS 11c with deposition occurring between 428 ± 327 ka and BP – $405.3 \pm 5.1/5.8$ ka BP (see Figs 6.33 & 6.40).

6.6.8: Equilibrium $\delta^{18}\text{O}$ carbonate precipitation, Logs 1 & 2, Site TB9

The mean temperature of the modern surface and groundwater collected from the study area is 20°C (see Appendix 10). For temperature (a) (Appendix 11, Tables 1 & 2), the Hay's and Grossman, (1991) (see Appendix 11) palaeotemperature equation was used with the mean $\delta^{18}\text{O}$ water value for Central Eastern Mexico (-8.1‰, Appendix 11, Tables 1 & 2) based on data from the Global Network of Isotopes in Precipitation (GNIP) and the Global Network of Isotopes in Rivers (GNIR) (IAEA, 2018), and the $\delta^{18}\text{O}$ values of each sample from Log 2 (Figs 6.39 Appendix 11, Table 1). The resulting mean temperature of 21.6°C suggests that equilibrium precipitation of carbonate sediments likely occurred. The temperatures are not included in Figure 6.40 because direct comparisons are not very robust since there is no active carbonate precipitation at Site TB9; they are

given in Tables 1 and 2, Appendix 11. The data for Log 2, is promising, and with more data, this sequence or sections of it have the potential to produce a detailed averaged and possibly annual palaeo-temperature record.

6.6.9: Interpretation, Logs 4 and 5, Site TB9

6.6.9.1: Log 4, Site TB9

The sediments, geochemistry and interpretations discussed for Logs 1 and 2 (Figs 6.39 & 6.40) are the same or similar for Log 4. The section recorded in Log 4 covers the uppermost bed of Log 1 and the lower portion of Log 2. Primarily, the sequence records high-frequency cycles between carbonate depositing pool environments subject to fluvial reworking and mudflat to marsh development (Fig 6.34).

6.6.9.2: Log 5, Site TB9

The logged section incises Logs 1 – 4 (Figs 6.29, 6.33, 6.39, 6.40) in Barranca de Colores and includes at least nine sediment gravity flow deposits (FGmm: alluvial plastic debris flow deposit or FGcm: pseudoplastic, turbulent debris flow, Table 4.8) and gravel bars and bedforms (FGh: Fluvial/alluvial lag deposit, Table 4.8) that can grade into laminated waning flood or drape deposits (FFI, Table 4.8). Like at site TB10 (Logs 3 & 4). Log 5 represents a remnant cycle of alluvial incision and aggregational fill and at its base indicates the palaeo-barranca floor elevation that has been exposed by modern incision. Like at Site TB10, that these gravels are thought to represent an old floodplain, cut through by ephemeral flow and left standing above the present barranca floor. The degree of incision and infill (<12 m) is indicated by the depth of the deposit marked by the terrace bases (Figs 6.24, 6.25 a & b, 6.27 a, 6.35, 6.36 & 6.38). Fossil megafaunal remains associated with the gravel deposits recorded from Barranca de Colores are shown in Figure 6.37 and reported in Table 6.37 (Figs 6.17b, 6.20, 6.21, 6.22 & 6.23). Radiocarbon ages from the gravels recorded at Sites TB9 (¹⁴C 44,235 cal. BP) and TB10 (¹⁴C 43,694 cal. BP) suggests a similar age for deposition (see Appendix 9, Fig 8.8) at both sites.

6.10: Summary and conclusion

Five primary depositional environments were identified for the study area. 1) Relatively deep-water lacustrine to wetland environments. 2) Marginal lacustrine to playa-type environments that display high-frequency wet and dry cycles between with exposure, desiccation and erosion features. 3) Thick, localised limestone sequences that display complex carbonate-dominated facies deposited under high-frequency cycles between flooding, shallowing, exposure, desiccation and erosion. 5) Alluvial and fluvial debris flow beds that occur in isolated outcrops disconformably incising environments 1 - 4. Chapter 7 details the geochemical results from tephra deposits recorded from the study area.

Chapter Seven: Tephra geochemistry

7.1: Introduction

An extensive Late Quaternary tephrochronology, stratigraphy and geochemical record now exists for the southern and central Mexico basins (e.g. Ortega & Newton, 1998; Newton & Metcalfe, 1999; Capra et al. 2002; Siebe & Macías, 2003; Arce et al. 2005; Lozano et al. 2015; Siebe et al. 2017). Comparably little is understood for the northern Basin of Mexico and its sub-basins (Roy et al. 2008, 2009, 2010, 2012). Here, geochemical data from seven tephra layers (Tables 7.2 - 7.5) and one Ar-Ar dated tephra layer are presented from the study area. The data is compared with the existing tephrochronology and tephra geochemistry presented by Roy et al. (2012) (Table 7.1 and Figs 7.2 & 7.4) to address Objectives 1 – 4 outlined in Chapter 1.

7.2: Regional Volcanic setting

Possible sources of tephra deposits found in the study area include Tláloc volcano (Sierra Nevada volcanic range), La Bufa volcano (Sierra de Las Cruces volcanic range), the Apan-Tezontepec monogenetic volcanic field (in the Pachuca sub-basin), and the Donguinyó-Huichapan (north-west) and Acoculco calderas (south-east) (Fig 7.1 a & b). The Pliocene to Late Pleistocene aged Tláloc stratovolcano sits at the northern end of Sierra Nevada volcanic range is ca. 75 km south-east of the study area (Fig 7.1 a & b) (Vázquez-Sánchez & Jaimes-Palomera, 1989; García-Palomo et al. 2002; Rueda et al. 2006, 2007). Geochemically products associated with Tláloc are dacitic to rhyolitic (Macias, 2008). La Bufa volcano marks the northern tip of the Sierra de Las Cruces volcanic range (García-Palomo et al. 2008) located ca. 60 km southwest of the study area (Fig 7.1 a & b). The structure is dated to 3.7 Ma (Osete et al. 2000) and has geochemical compositions that range between andesite to dacite (Rodríguez-Saavedra, 2007). The northern end of the Apan-Tezontepec monogenetic volcanic field (ATVF) in the Pachuca Basin (Fig 7.1 a & b) is located within 20 km of the study area (Fig 7.1a & b). The volcanic field is made up of over 295 volcanic structures (García-Palomo et al. 2002; Roy et al. 2012) with mafic volcanism occurring between 1.50 and 0.47 Ma (Cantagrel & Robin, 1979; López-Hernández & Castillo-Hernández, 1997; García-Palomo et al. 2002; Roy et al. 2012). The Donguinyó-Huichapan Caldera complex is located north-west of the study area (Fig 7.1 a & b) and formed between and erupted andesite to trachydacitic pyroclastics ca. 5.0 Ma, several small shield volcanoes and cinder cones built up the caldera rims and basaltic-andesite to andesitic lava flows occurred around Around 4.6 Ma (Aguirre-Díaz & McDowell, 1999). The Huichapan caldera and Huichapan Tuff

were deposited around ca. 4.2 Ma (Aguirre-Díaz & McDowell, 1999; Aguirre-Díaz & López-Martínez, 2009; Roy et al. 2012; see Fig 7.6). The Nopala volcano, which forms part of the Jiltepec volcanic (Fig 7.6), which is part of the Donguinyó-Huichapan Caldera complex (Aguirre-Díaz & McDowell, 1999) formed around 2.5 Ma.

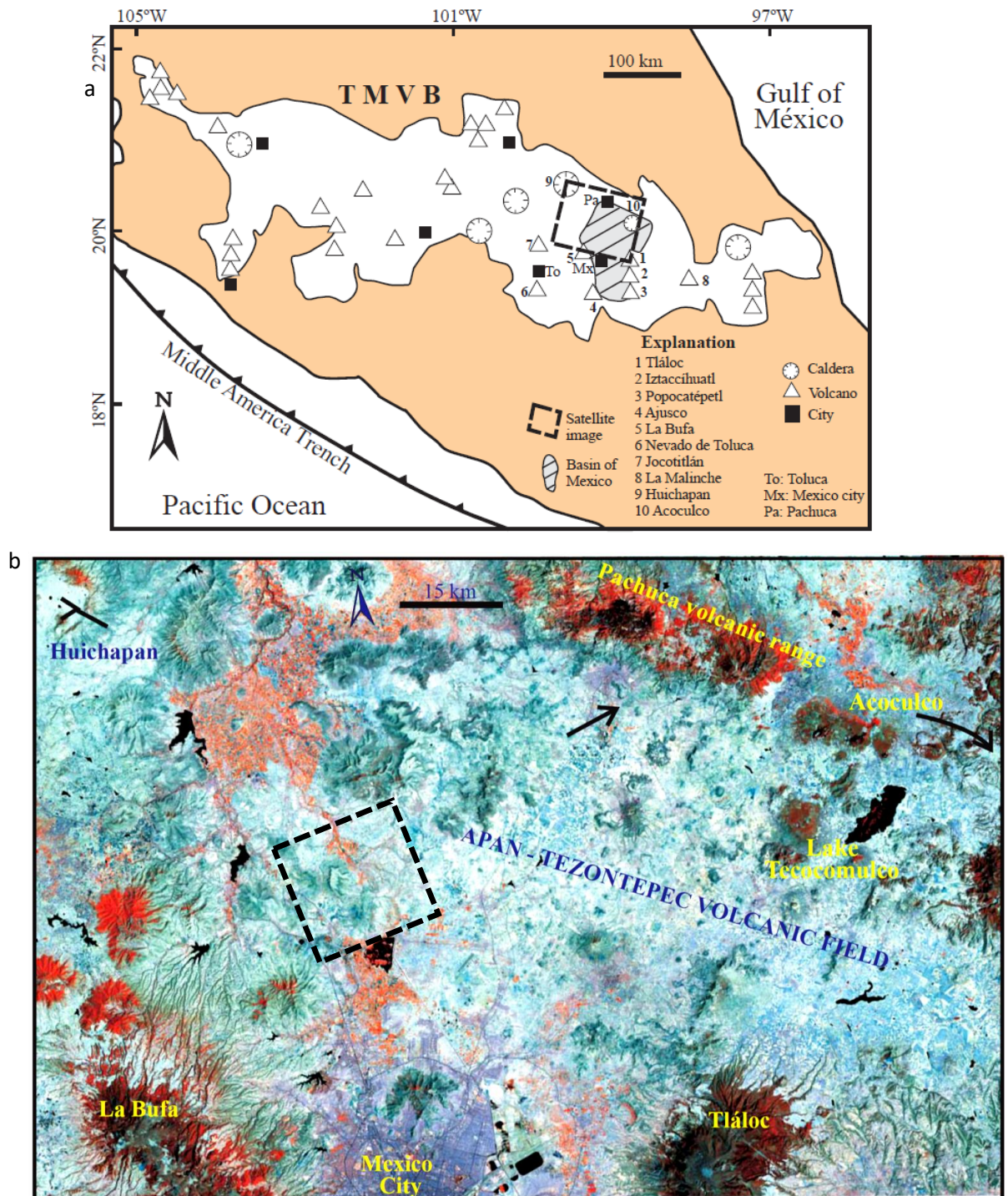


Figure 7.1: a) The Trans Mexican Volcanic Belt with the dashed black box: study area from Roy et al. (2012 (see b). b) Roy et al. (2012) study area (see a) and the volcanic structures that lie within that area. The Black arrow represents the location of Roy et al.'s core site. (image was taken Roy et al. 2012 and annotated for this study).

Table 7.1: Tephra samples from Roy et al. 2012. Samples were collected from a 30 m thick tephra sediment sequence, exposed in different parts of a mine exposure in the Pachuca sub-basin (see Fig 7.1).

| Name | Thickness | Description | Composition |
|------|-----------|--|-------------------------------|
| Tr8 | 2 m | Light colored lapilli sized pumice fall | Rhyolite |
| Tr7 | 0.5 m | Dark coarse to fine ashfall | Basaltic-andesite |
| Tr6 | 0.5 m | Dark coarse to fine ashfall | Basaltic-andesite |
| Tr5 | 0.8 m | Light grey pumice-rich lapilli | Rhyolite |
| Tr4 | 1.2 m | Light grey pumice-rich lapilli | Rhyolite |
| Tr3 | 0.6 m | White-beige fine to medium ash | Rhyolite-Trachydacite |
| Tr2 | 3 m | Beige fine to medium ash | Dacite-rhyolite |
| Tr1 | 2.8 m | Black-brown multilayered lapilli to coarse ash | Basaltic to basaltic-andesite |

The Acoculco caldera (ca. 120 km east of the study area) has a basaltic-andesitic to rhyolitic eruptive history dated to between 3.0 and 0.24 Ma (Fig 7.6) (López-Hernández & Castillo- Hernández, 1997; Aguirre-Díaz & McDowell, 1999; López-Hernández, 2009).

7.3: Previous work on tephra deposits associated with north-eastern Central Mexico

This record is predominantly based on a study by Roy et al. (2012) of a volcanic-sedimentary sequence in the Pachuca sub-basin in the northeastern Basin of Mexico (Fig 7.1 a & b). The study found at least eight tephra layers that range from basalt to rhyolite representing eight different volcanic events (Table 7.1) (Roy et al. 2012). The tephra layers outlined below are used for comparison with the tephra layers deposited within the study area (Table 7.2). The findings of Roy et al. (2012) are as follows

7.3.1: Mafic tephtras

Three basaltic to basaltic-andesite (mafic) tephtras layers were recorded (Tr1, Tr 6 and Tr7 Table 7.1). Tr1 consists of multilayered lapilli (grain size 2 – 64 mm) to coarse ash. Tr6 and Tr7 are fine ash (Roy et al. 2012, Table 7.1, Fig 7.4). Compositionally the mafic tephtras layers are like the Apan-Tezontepec monogenetic volcanic field volcanic products (Figs 7.1 & 7.4) (Roy et al. 2012). K/Ar dates from the volcanic field suggested activity at 1.50 ± 0.7 Ma (Cantagrel & Robin, 1997), 0.80 ± 0.2 Ma (López-Hernández & Castillo- Hernández, 1997), and 0.47 ± 0.7 Ma (Garcia-Palomo et al. 2002). Although there were no direct dates on the tephra layers, the study suggests they are linked to the three periods of activity dated above based on geochemical comparisons (Roy et al. 2012). Mafic volcanic activity supplying tephra layers to the Pachuca sub-basin is thought to have occurred between 1.50 and 0.47 Ma BP (Roy et al. 2012).

7.3.2: Felsic tephtras

Light coloured felsic tephtras (Fig 7.4) include Tr3 – Tr5 that are grain supported lapilli deposits and Tr2 (dacite) and Tr 8 (rhyolite) that are fine-grained ashfall deposits (Roy et al. 2012). Felsic tephra layers were found

to be geochemically comparable to Acoculco Caldera volcanic products (Fig 7.4, Roy et al. 2012). The volcanic products of the Acoculco Caldera range in age from 3.0 – 0.24 Ma (Garcia-Polomo et al., 2002) with the felsic products being deposited during the later part of the activity period (Roy et al. 2012). Rhyolites in the Acapulco sequence occur from ca. 1.7 ± 0.4 Ma (K/Ar) (Hernández & Hernández, 1997). Roy et al. (2012) suggest that the four rhyolite layers represent four volcanic events associated with the Acoculco Caldera that occurred between 1.50 and 0.24 Ma.

7.4: Results and interpretation

Sedimentological descriptions and facies codes (Facies 18a-d) are given in Chapter 5, Table 5.23. Here, the geochemical composition of the analysed tephra layers (Table 7.2), their possible provenance based on their main oxide geochemistry (Tables 7.4 & 7.5) and the available chronology from these tephra layers (also see Appendix 9, Table 1) are discussed.

7.4.1: Basaltic-andesite (TEQ 4)

One basaltic-andesite tephra layer was sampled from the study area (TEQ 4, Tables 7.2 - 7.5, Figs 7.2 - 7.7 and 7.6 & 7.7, also see Table 5.23, Facies 18a) which is composed of white, fine to coarse-grained sand and in some sections greyish yellow-green silt and sand (see Fig 7.2 and Table 7.3). TEQ 4 is sub alkaline (Figs 7.2 & 7.4a) and has a SiO₂ concentration of 55.01 (wt%) and total alkalis 4.26 (wt%) (Table 7.4, Fig 7.4 a & b). Strontium values are the highest in this sample (Table 7.5) when compared to the other tephra layers sampled from the study area. The basaltic-andesitic tephra layer occurs at Site TB9 (TEQ 4, Figs 6.33 & 6.34). At Site TB7 (Figs 6.13, 8.1 & 8.9) a similar deposit occurs in the same stratigraphic position, although there is no geochemical evidence to support that they are genetically related. TEQ 4 is sub-alkaline and groups with the volcanic products of the Apan-Tezontepec monogenetic volcanic field (Fig 7.1, Table 1.7, Tr1 and Tr6) and the Donguinyó-Huichapan Caldera complex (Fig 7.4a). The age of TEQ 4 places its deposition into the same timeframe as activity occurring along the Apan-Tezontepec monogenetic volcanic field (1.50 Ma and 0.47 Ma (Roy et al. 2012)). However, there are separations in the bivariate plots of silica vs aluminium oxide (Fig 7.4c), calcium oxide (Fig 7.4d), magnesium oxide (Fig 7.4e), and titanium oxide (7.4f). In plots e-f (Fig 7.4) TEQ 4 values are lower (ca. 6 – 7 %) than the average values of the Apan-Tezontepec monogenetic volcanic field, and Tr1 and Tr6 which are associated with this volcanic field. In Figure 7.4 c, (silica vs aluminium) TEQ 4 has higher (ca. 4%) values than all other samples plotted. Hence, the bivariate diagrams (Fig 7.4 c-f) do not support a genetic connection.

Table 7.2: Tephra samples geochemically analysed from the study area. For the location of the sampled tephra layers, see Chapters 6 & 8.

| Name | Thickness | Description | Location | Composition |
|-------|-------------|--|---|--------------------------------|
| TEQ 1 | 0.50-0.60 m | White (N9) coarse-fine ash with bioturbation | Site TB10, Log 2, (Facies 18b) (Figs 6.18, 8.8). | Andesite (Facies 18b) |
| TEQ 2 | 0.25-0.30 m | White (N9) to greyish pink (5RY 8/2) fine ash | Site TB12, Log 2, (Facies 18c) (Appendix 4, Table 6). | Dacite (Facies 18c) |
| TEQ 3 | 0.10-0.15 m | White (N9) fine ash | Site TB9, Log 3 (Facies 18c) (Figs 6.33, 6.34, 8.8, 8.10, 8.11). | Dacite (Facies 18c) |
| TEQ 4 | 0.40-0.50 m | White (N9) to greyish yellow-green (5GY 7/2) coarse to fine ash. | Site TB9, Log 3, (Facies 18a) (Figs 6.34, 8.8, 8.10, 8.11). | Basaltic-andesite (Facies 18a) |
| TEQ 5 | 0.10-0.15 m | White (N9) fine ash | Site TB9, Log 2, (Facies 18c) (Figs 6.33, 6.34, 8.8, 8.10, 8.11). | Dacite (Facies 18c) |
| ASH 1 | 0.25-0.30 m | White (N9) to greyish pink (5RY 8/2) fine ash | Site TB12, (Facies 18c) (Figs 8.8, 8.12; Appendix 4, Table 6). | Dacite (Facies 18c) |

Table 7.3: The lithology of TEQ 4, Basaltic-andesite, Barranca de Colores. Site TB 9, Logs 2 & 4. See Section 6.6

| Bed Number | Bed Size | Description (Bed 1: base of the logged sequence, Bed 9: top of logged sequence) | Bed name |
|------------|----------|--|---|
| 13 | 0.02 m | Greyish yellow-green (5GY 7/2), mud with vertical jointing and small (< 5 mm) carbonate nodules. Thickness varies. | Mudstone (Facies 12a) |
| 12 | 0.07 m | Greyish yellow-green (5GY 7/2) ripple cross-lamination and plane laminations fine sand | Ripple cross-laminated to plane fine laminated sand |
| 11 | 0.04 m | White (N9) massive fine sand with coarser sand inclusions | Massive fine-coarse sand |
| 10 | 0.04 m | White (N9), plane laminated fine sand | Laminated fine ash |
| 9 | 0.01 m | White (N9) massive fine sand with coarser sand inclusions. Ar/Ar date $405.3 \pm 5.1/5.8$ ka bp | Massive fine-coarse sand |
| 8 | 0.01 m | White (N9), plane laminated fine sand. | Laminated fine ash |
| 7 | 0.02 m | White (N9), massive silty fine sand with coarse sand inclusions | Massive fine-coarse sand |
| 6 | 0.02 m | White (N9), plane laminated fine sand | Laminated fine ash |
| 5 | 0.10 m | Greyish yellow-green (5GY 7/2) massive fine sand with black flecks | Massive fine ash |
| 4 | 0.02 m | White (N9) massive fine sand with coarser sand inclusions | Massive fine-coarse sand |
| 3 | 0.03 m | White (N9), plane laminated fine silt | Laminated fine ash |
| 2 | 0.02 m | White (N9), massive very fine sand | Massive fine ash |
| 1 | 0.02 m | Greyish yellow-green (5GY 7/2) massive mud with vertical jointing | Mudstone (Facies 12a) |

Reported activity along the Donguinyó-Huichapan Caldera complex (Fig 7.1) (5.0 ± 0.3 Ma to 2.5 ± 0.1 Ma, Aguirre-Díaz & López-Martínez, 2009) is older than the Ar-Ar age for TEQ 4, although a later eruptive phase is entirely possible. Again, in Figure 7.4 there are separations in the bivariate plots of silica vs aluminium oxide (Fig 7.4c), calcium oxide (Fig 7.4d), magnesium oxide (Fig 7.4e), and titanium oxide (7.4f) when compared to Roy et al. (2012). When TEQ 4 is plotted with calcium oxide (Fig 7.7a), and titanium oxide (7.7b) and magnesium oxide (Fig 7.7c) from the Donguinyó-Huichapan Caldera complex and the Jiltopec volcanic field that sample groups with the products of the Jiltopec volcanic field (Le Bas et al. 1986; Aguirre-Díaz & López-Martínez, 2009; Diaz & Martinez, 2009).

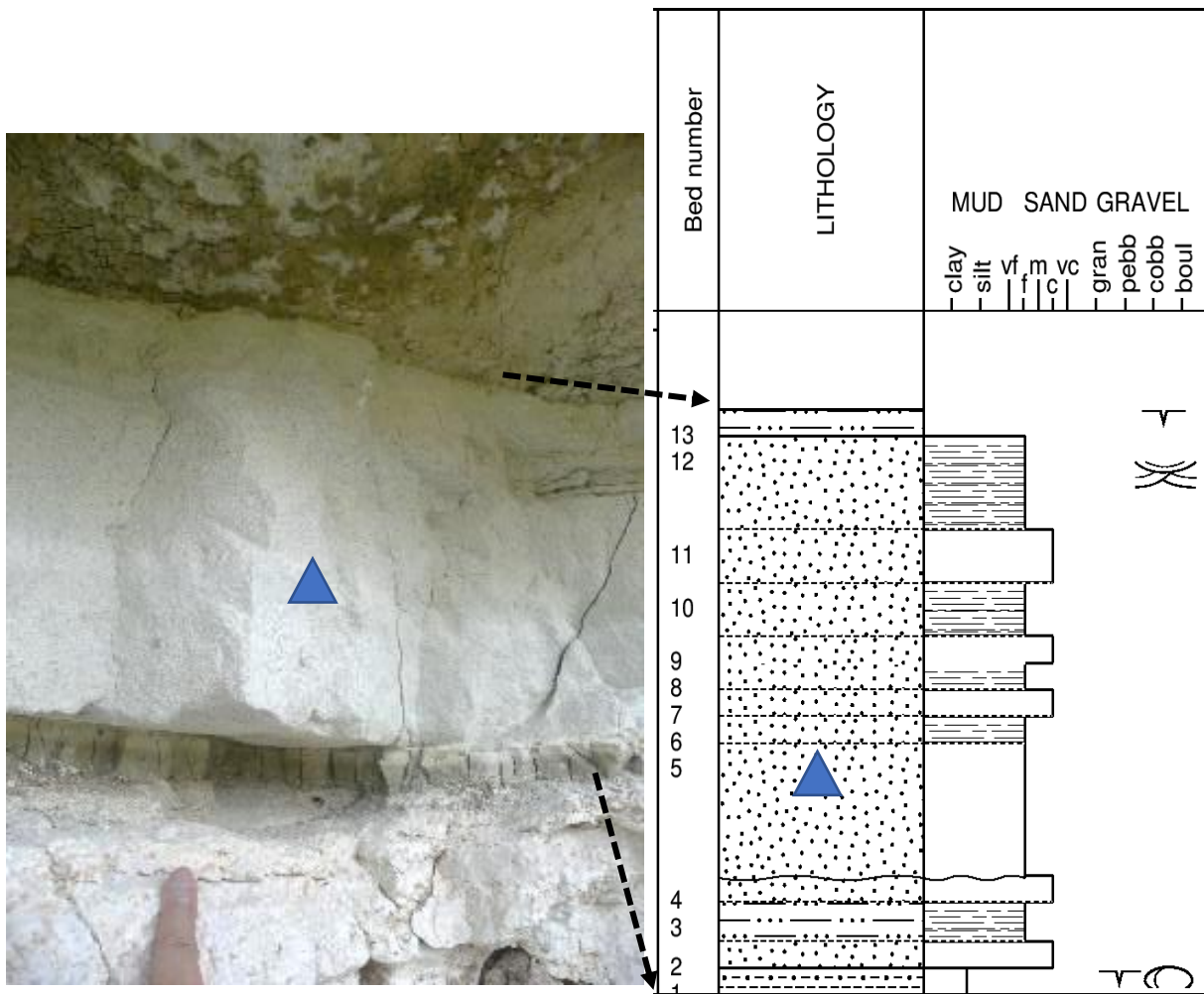


Figure 7.2: TEQ 4, Barranca de Colores basaltic-andesite tephra layer. Site TB 9, Logs 2 & 4, Figs 6.33 & 6.34. Scale 1:10. See Table 7.3 for beds descriptions. Blue triangle Ar/AR date $405.3 \pm 5.1/5.8$ ka bp (see Chapter 6)

For a genetic relationship to be possible, a later eruptive phase of the Huichapan caldera would have to have occurred which is possible also. The Nopala shield volcano that was emplaced on the Huichapan rim is reported to have marked the demise of the Huichapan caldera system around 2.5 Ma hence, for TEQ 4 to be linked to this system it would have had to have erupted around 1.6 Ma years after the Nopala shield volcano formed based on the age of TEQ 4 (405 ka BP). Unfortunately, there is limited data available for the field Jiltopec volcanic field and the Nopala volcano, but the basaltic-andesitic tephra layer reported from the study area helps by adding a new dated tephra layer to the record which indicates that volcanic activity to the west of the study area continued much later into the Pleistocene than was previously thought.

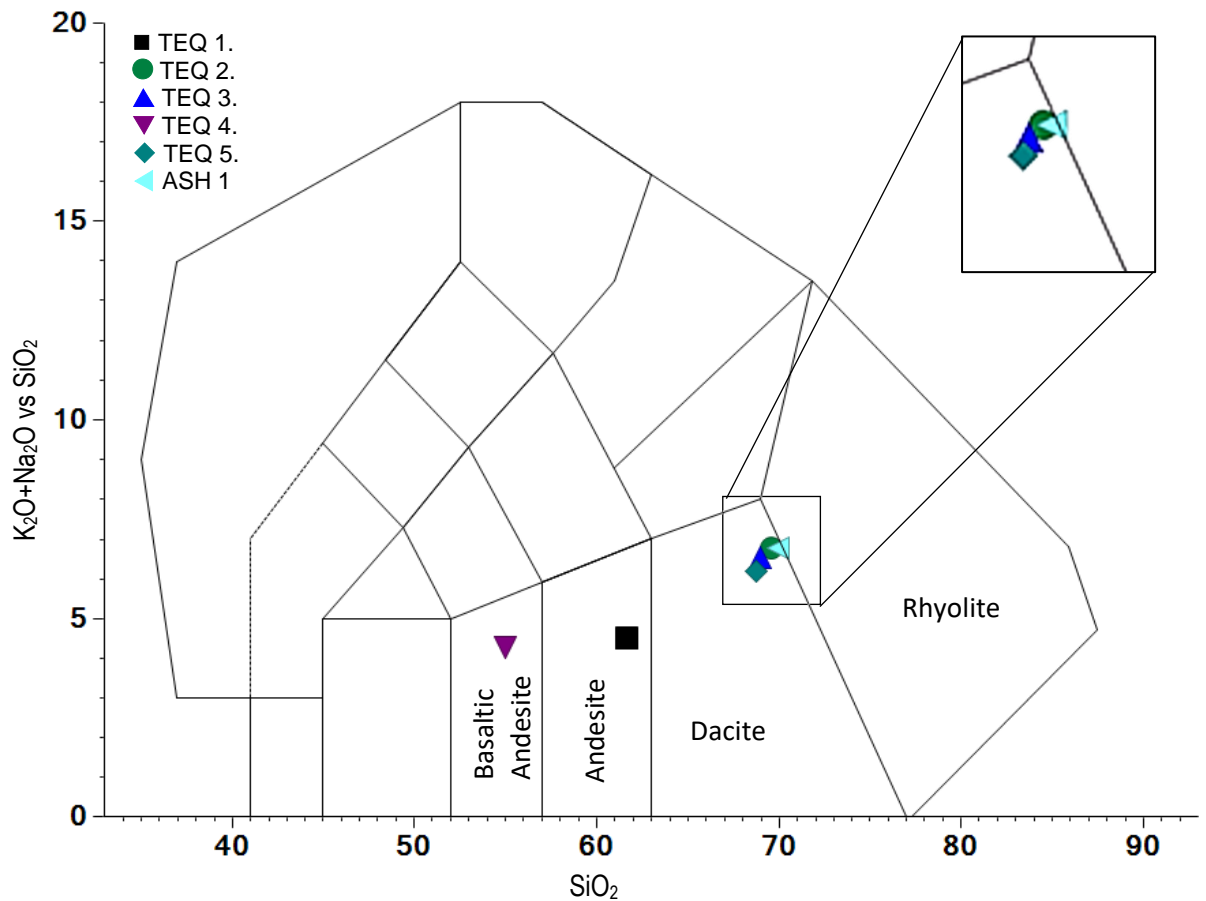


Figure 7.3: Average K_2O+Na_2O vs SiO_2 (TSA) geochemical data for samples TEQ 1 – 5 and ASH 1 (see Tables 7.4). See Table 7.2 for sedimentological descriptions and sample site details and see Figs 6.13 and 8.1 for a location map of sample sites (Chapter 6). TEQ1; Andesite. TEQ 2, TEQ 3, TEQ 5, ASH 1; Dacite. TEQ 4; Basaltic-andesite.

Table 7.4: Major main oxide concentrations (%) of the Tequixquiac tephra layers (see Table 7.2)

| Sample | SiO ₂ | Al ₂ O ₃ | Fe ₂ O ₃ (t) | MnO | MgO | CaO | Na ₂ O | K ₂ O | TiO ₂ | P ₂ O ₅ | LOI | Total |
|--------|------------------|--------------------------------|------------------------------------|-------|------|------|-------------------|------------------|------------------|-------------------------------|------|-------|
| TEQ 1 | 61.67 | 14.7 | 4.67 | 0.05 | 1.99 | 2.26 | 2.19 | 2.3 | 0.324 | 0.07 | 9.54 | 99.77 |
| TEQ 2 | 69.57 | 14.01 | 2.04 | 0.05 | 0.72 | 2.25 | 2.8 | 3.98 | 0.256 | 0.09 | 4.14 | 99.91 |
| TEQ 3 | 68.96 | 14.05 | 1.65 | 0.043 | 0.78 | 2.21 | 2.67 | 3.87 | 0.25 | 0.08 | 5.19 | 99.75 |
| TEQ 4 | 55.01 | 23.88 | 1.78 | 0.02 | 1.13 | 5.66 | 4.02 | 0.24 | 0.508 | 0.08 | 8.39 | 100.7 |
| TEQ 5 | 68.79 | 13.88 | 1.65 | 0.043 | 0.79 | 2.33 | 2.39 | 3.79 | 0.253 | 0.09 | 5.74 | 99.75 |
| ASH 1 | 69.94 | 14.22 | 1.60 | 0.05 | 0.49 | 2.44 | 2.75 | 4.03 | 0.24 | 0.09 | 4.03 | 99.88 |

Table 7.5: Trace element concentrations (ppm) of the Tequixquiac tephra layers (Table 7.2).

| Sample | Ba | Sr | Y | Sc | Zr | Be | V |
|--------|------|-----|----|----|-----|----|----|
| TEQ 1 | 532 | 323 | 9 | 6 | 103 | 1 | 42 |
| TEQ 2 | 528 | 312 | 11 | 3 | 105 | 1 | 23 |
| TEQ 3 | 2163 | 317 | 10 | 3 | 108 | 1 | 30 |
| TEQ 4 | 196 | 815 | 2 | 3 | 102 | 1 | 47 |
| TEQ 5 | 4657 | 320 | 9 | 3 | 109 | 1 | 29 |
| ASH 1 | 550 | 288 | 11 | 3 | 60 | 1 | 21 |

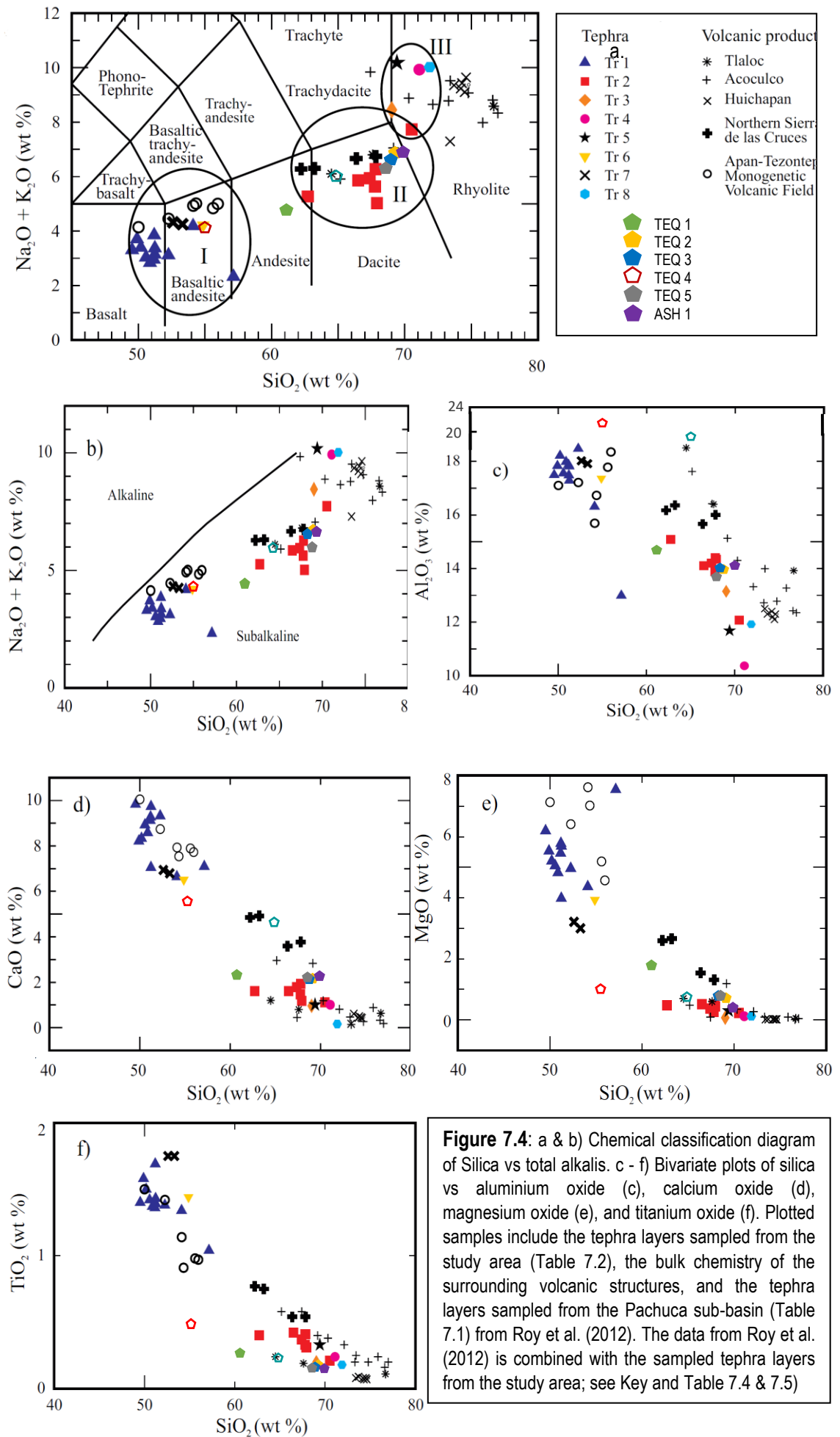


Figure 7.4: a & b) Chemical classification diagram of Silica vs total alkalis. c - f) Bivariate plots of silica vs aluminium oxide (c), calcium oxide (d), magnesium oxide (e), and titanium oxide (f). Plotted samples include the tephra layers sampled from the study area (Table 7.2), the bulk chemistry of the surrounding volcanic structures, and the tephra layers sampled from the Pachuca sub-basin (Table 7.1) from Roy et al. (2012). The data from Roy et al. (2012) is combined with the sampled tephra layers from the study area; see Key and Table 7.4 & 7.5)

7.4.2: Andesitic tephra layer (TEQ 1)

The andesite tephra layer (TEQ 1) (Table 5.23, Facies 18b (Chapter 5), Fig 7.5) is a white (N9) massive coarse to fine sand with what appear to be bioturbation burrows that pass through the deposit (Tables 7.2) (site TB10, Log 2, see Chapter 6). TEQ 1 is sub-alkaline (Figs 7.3 & 7.4) and has SiO₂ vs total alkali values of 61.67 (wt) % and 4.49 (wt) % respectively (Table 7.2). TEQ 1 is relatively isolated in all the bivariate plots in Figure 7.4. The sample loosely plots around one of the outliers from sample Tr2 (Pachuca sun-basin, Roy et al. 2012) in the chemical classification and bivariate diagrams (Table 7.1, Fig 7.4 a - f) which is associated with Acoculco Caldera (Fig 7.1) (Roy et al. 2012). When plotted on TAS diagram by Le Bas et al. (1986) with the main products of the Donguinyó-Huichapan Caldera TEQ 1 tends to group with the products of the rim dome complex, particularly the Donguinyó Tuff (see Fig 7.8 a-d) and to a lesser extent the products of the Jiltepec Volcanic field (see Fig 7.7 and Le Bas et al. 1986; Aguirre-Díaz & López-Martínez, 2009; Díaz & Martínez, 2009). The similarities between Tr2 and TEQ 1 seen in Figure 7.4 (a-f) suggest the products are similar and related to the Acoculco Caldera system which is the suggested provenance of Tr2 (Roy et al. 2012). If this is the case, the deposition could be constrained to between 1.5 and 0.47 Ma. Roy et al. (2012), indicate that rhyolitic eruptions dominated that latter part of this activity period so TEQ 1 may be older than the estimated age of the rhyolitic tephra layers recorded from the Pachuca sun-basin (see Figure 4 and Roy et al. 2012). TAS diagram comparisons with the products of the Donguinyó-Huichapan and the surrounding volcanic structures also suggest a genetic correlation (Fig 7.7). As there is no age assigned to TEQ 1, it is possibly related to the Acoculco Caldera suggesting an age of between 5.0 ± 3 and 2.5 ± 0.1 Ma, and is comparable with the Donguinyó Tuff, at 5 Ma. It is also possible that TEQ 1 represents a later eruptive phase from both suggested sources.



Figure 7.5: Example of andesitic coarse to fine ash (TEQ 1, Andesite) collected from Barranca del Muerto, Site TB10, Log 2. Ungulate imprint can be seen on the righthand side photograph.

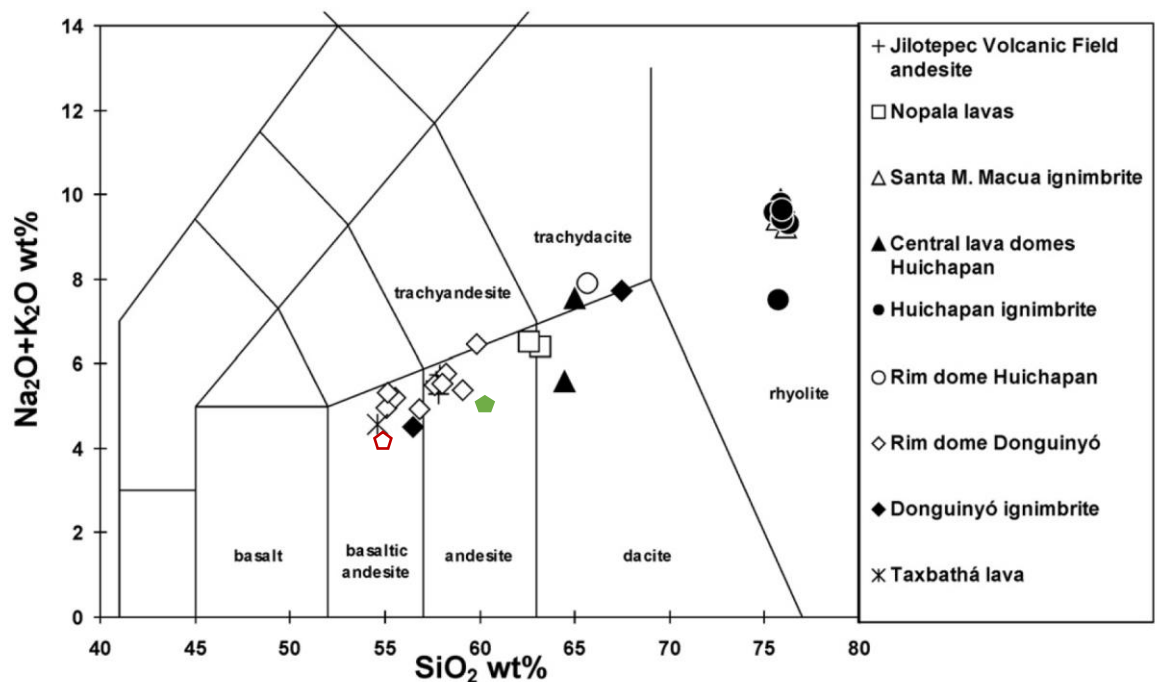


Figure 7.6: Total alkali vs Silica (TAS) diagram based on the classification from Le Bas et al. (1986) (In Aguirre-Díaz & López-Martínez, 2009). Main products of the Donguinyó-Huichapan caldera complex and the surrounding volcanic structures see (Fig 7.1). $\color{red}\blacklozenge$ TEQ 4, Basaltic-Andesite: $\color{green}\blacklozenge$ TEQ 1, Andesite.

7.4.3: Dacitic tephra Layers

TEQ 2, TEQ 3, TEQ 5 and ASH 1 (Table 5.23, Facies 18c, Fig 7.2, Table 7.2) are made up of fine white to a greyish pink fine ash. The tephra layers are found in Barranca de Colores (site TB9, Logs, 2 - 4, Figs 6.13, 8.1 & 8.9), Arroyo Salado Hueypoxtla (site TB12, Appendix 4, Table 6), and possibly in Barranca la Gloria (Site TB7, Figs 8.1 & 8.9, Appendix 4, Table 9). TEQ 2 and ASH 1 are separate samples, collected from different points, at the same stratigraphic sequence, in the same stratigraphic position, from site TB12 (Arroyo Salado Hueypoxtla) (see Appendix 4, Table 6). TEQ 3 and TEQ 5 are again separate samples, collected from different points along a cross-section from the same stratigraphic position in the Barranca de Colores (site TB9, see Chapter 6). TEQ 2 has Silica values of 69.57 (wt) % and total alkali values of 6.78 (wt) %. ASH has Silica values of 69.94 (wt)% and total alkali values of 6.78 (wt) %, which are nearly identical for each sample (Figs 7.2, 7.4 a-f and Tables 7.1, 7.4 & 7.5). Total silica vs total alkali values are 68.96 (wt)% vs 6.54 (wt)% for TEQ 3 and 68.70 (wt) % vs 6.18 (wt) % for TEQ 5, and are again practically identical (Figs 7.4 a-f and Tables 7.2, 7.4 & 7.5) and both samples have similarly high levels of Ba (see Table 7.5). In Figures 7.2, 7.4 (a - f) and 7.7 all four samples are so closely grouped they are identified as the same deposit and the product of the same volcanic event.

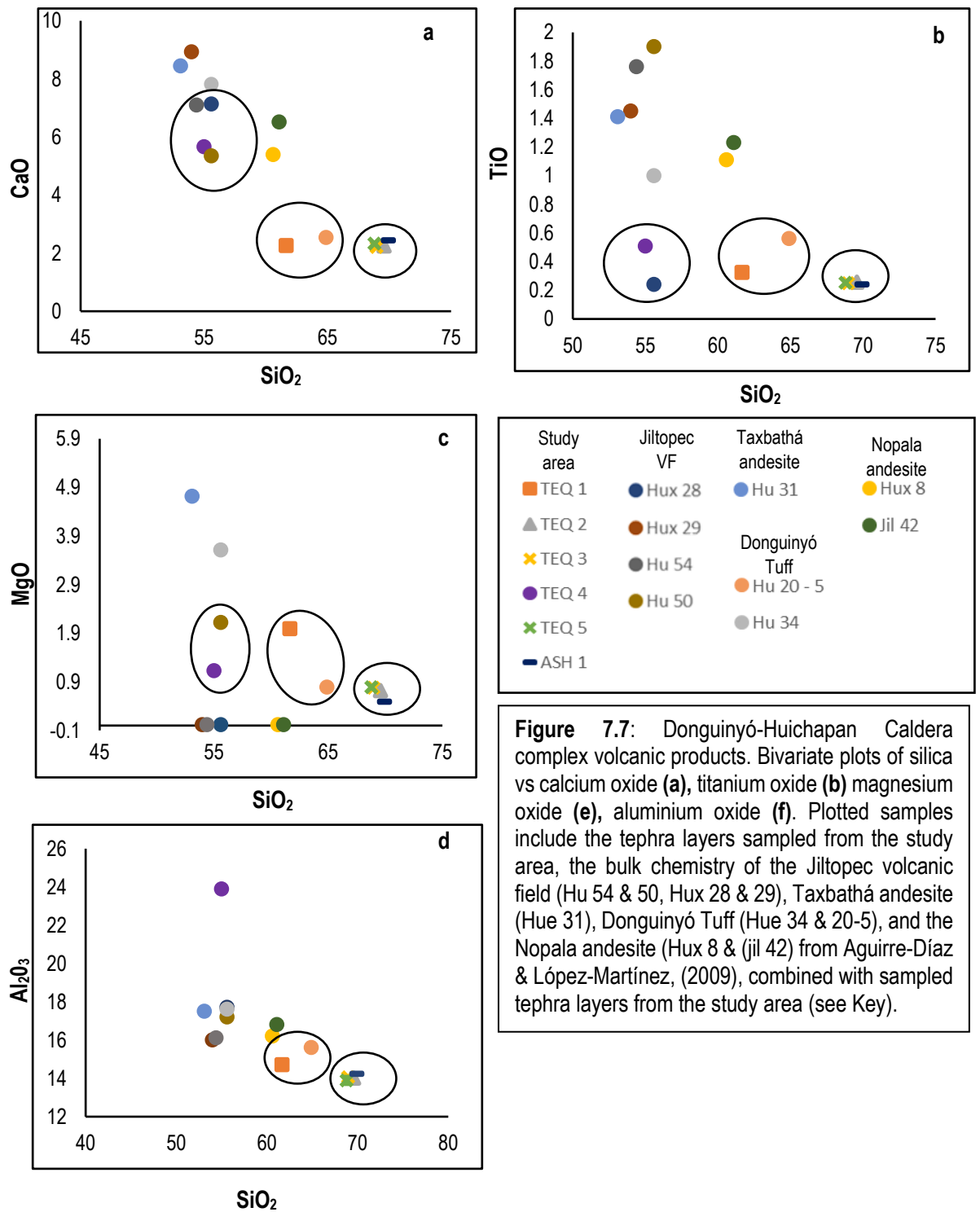


Figure 7.7: Donguinyó-Huichapan Caldera complex volcanic products. Bivariate plots of silica vs calcium oxide (a), titanium oxide (b) magnesium oxide (c), aluminium oxide (d). Plotted samples include the tephra layers sampled from the study area, the bulk chemistry of the Jiltopec volcanic field (Hu 54 & 50, Hux 28 & 29), Taxbathá andesite (Hue 31), Donguinyó Tuff (Hue 34 & 20-5), and the Nopala andesite (Hux 8 & (jil 42) from Aguirre-Díaz & López-Martínez, (2009), combined with sampled tephra layers from the study area (see Key).

On the silica vs total alkali diagram (Fig 7.4 a & b) values of all four samples group with the volcanic products of La Buff volcano (northern Sierra de Las Cruces), the Aocolco Caldera complex and Tlaloc volcano (northern end of the Sierra Nevada volcanic range (Fig 7.1), and tephra layer Tr2 (dacite, Table 7.1) from the Pachuca sub-basin (Roy et al. 2012). Bivariate diagrams (Fig 7.4c-f) indicate that silica vs Al_2O_3 , CaO, MgO and TiO values group with the Aocolco volcanic products rather than La Buff products (Fig 7.1b-f). Tephra layer Tr2 has also been interpreted (Roy et al. 2012) as being one of several plinian eruptive phases of the Aocolco Caldera,

and it seems likely that TEQ 2, 3, 5 and ASH 1 have the same provenance, and are the same event (see Figs 8.1, 8.8, 8.10, 8.11 & 8.12). Because of the stratigraphic position of TEQ 2, 3, 5 and ASH 1 (see Chapter 8), below TEQ 4 dated at $0.405.3 \pm 5.1/5.8$ Ma (see Chapter 5 & 8), these samples are known to be older than this date.

Tlaloc is ruled out as a potential source because of this age despite some of the geochemical similarities (Fig 7.4 a-f) as Tlaloc's activity started around ca. 50,000 bp (Ortega et al. 1999; Roy et al. 2009). Roy et al. (2012) suggest the Acuculco caldera was active between 3.0 and 0.24 Ma (Garcia-Polomo et al. 2002), and that rhyolitic volcanism dominated the latter part of this time (between 1.7 – 0.24 Ma). This combined with the fact that the deposit is known to be older than $0.405.3 \pm 5.1/5.8$ Ma suggests that deposition occurred between this date and 3.0 Ma. Alternatively, if the time frame assigned to the deposition of felsic tephra layers in the Pachuca sub-basin are taken into account (see section 6.3.2) possibly between 1.7 and $0.405.3 \pm 5.1/5.8$ Ma.

7.5: Summary

The basaltic-andesite ash found in the study area, and reported here, is a sub-alkaline tephra layer that was deposited during the peak of the MIS (Marine Isotope Stage) 11.3 interglacial around $405.3 \pm 5.1/5.8$ ka and is linked to the products of the Donguinyó-Huichapan Caldera and the Jiltepec volcanic field. The andesitic tephra layer (TEQ 1) has genetic similarities to the Donguinyó rim dome complex, mainly the Donguinyó Tuff that dated to 5 Ma. TEQ 1 may be related to a later eruptive phase indicating that volcanic activity continued much later into the Quaternary than previously thought. The dacitic tephra layers recorded and analysed from the study area (TEQ 2, TEQ 3, TEQ 5 and ASH 1) are genetically related to each other and are interpreted as the same deposit. They are also very similar to the Tr2 dacitic-rhyolite tephra layer from the Pachuca sub-basin (Roy et al. 2013) and are all thought to have been produced by the same volcanic eruption. The geochemistry of the dacitic tephra layer is comparable with the Acoculco Caldera, and deposition is thought to have occurred between 1.7 and $0.405.3 \pm 5.1/5.8$ Ma based on its stratigraphic position below TEQ 4 and the age estimates provided by Roy et al. (2010). In Chapter 8, the palaeoenvironmental and palaeogeographic reconstruction for the study area is presented.

Chapter Eight: Discussion

8.1: Introduction

This chapter develops the palaeoenvironmental and palaeogeographic framework for the study area, considering the environmental interpretations of the stratigraphy and formation processes identified in Chapters 5, 6 and 7 to create a history of mid to late Pleistocene environmental and geographic change.

8.2: Tequiquiac Basin Quaternary stratigraphy

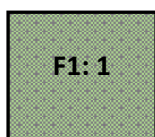
This section summarises groups of associated facies that have distinctly different but recognisable sedimentary characteristics identified for the study area. The characteristics of the facies (Chapter 5) and the depositional environments interpreted for them (Chapters 6 & 7) are developed into facies groups here (Figs 8.1 – 8.16). Within the study area, five primary depositional environments were identified; these are summarised below.

8.2.1: The Lower Colores Formation, > MIS 12c, Interval 1 (Figs 8.15a - 8.16a): Facies group 1

Facies group 1 (F1) is associated with the Tarango Formation (Tt) (Figs 3.3, 8.1 & 8.9) (Segerstrom, (1952, 1956; Mooser, 1975). Specifically, the horizontally stratified, water-lain, poorly indurated silt interbedded with pumice, sand, clay and lacustrine limestone. The group is defined by a type section recorded from Site TB9 (Section 6.6, Fig 6.29 and Fig 6.39, Zones 1 – 6) and is redefined here as the Lower Colores Formation.

8.2.1.1: Lacustrine to wetland environments, Facies Group 1.1

Stratigraphic key (Figs 8.1 & 8.2).



At Site TB9 (Figs 8.8, 8.10 & 8.11) Facies Group 1:1 (F1:1) is defined by high TOC values, (39.1% – 0.9%), negative mean $\delta^{13}\text{C}$ (-3.52 ‰, C4 type vegetation) and positive mean $\delta^{18}\text{O}$ (-5.98 ‰) values compared to Facies Groups 2 and 4 (Section 6.6.6, Zones 1 – 6, Figs 6.39). Covariance between $\delta^{13}\text{C}$ and $\delta^{18}\text{O}$ indicates a hydrologically closed water body and $\delta^{18}\text{O}$ ratios have no modern analogue (Log 1, from Zones 1 – 5, Fig 6.39, Sections 6.6.8.1). Across the study area Facies Group 1:1 (F1:1) is represented by thick (< 5 m) massive, green, fine-grained, organic-rich, clay (Facies 11a), mud (Facies 12a) and mixed carbonate-clastic sediments (Facies 8a & 9a) associated with a lacustrine-wetland system (or systems). F1:1 is thought to have developed during periods of increased moisture availability relative to F2 – F5 (Figs 8.1 - 8.6, 8.8 – 8.12). The sediments indicate periods of perennial high-lake stand mainly expressed as a lateral expansion rather than vertical expansion. Associated higher

TOC values indicate a combination of primary productivity, low-oxygenation, increased preservation and limited dilution by inorganic sedimentation (Bohacs, 1998; Myrow, 1990; Potter et al. 2005; Pietras & Carroll, 2006). F1:1 reflects increased humidity, weathering, and nutrient loading of the water body leading to saline, eutrophic like conditions (see Sections 6.2, 6.4 & 6.6 & Figs 8.1 – 8.6, 8.8 – 8.12, 8.15a & 8.16a). The absence of laminations or bedding structures presumably reflects benthic organism activity during the periods of increased oxygenation (e.g. Green River Formation, Wyoming, Pietras & Carroll, 2006).

8.2.1.2: Lacustrine to playa environments, Facies Group 1:2

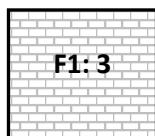
Stratigraphic Key (Figs 8.1 & 8.2).



At site TB9 Facies Group 1:2 (F1:2) has high TOC (by up to 5%, Zones 1 – 6, Log 1, Site TB9, Fig 6.39 and Sections 6.6.4.2 & 6.6.6.2) values relative to F1:1 indicating reduced humidity and shallowing, possibly seasonally and/or in response to decadal or orbitally driven change, allowing oxidation (e.g. Qa el Azraq playa, Jordan, Hunt & Garrard, 2013). Within the study area F1:2 is defined by thick (< 5 m), massive, red, mud (Facies 12a), silt (Facies 13a), sand (Facies 14 b & c) and mixed carbonate-clastic beds (Facies 8a – 10a) associated with a playa type depositional system (or systems) (Sections 6.2, 6.4 & 6.6 & Figs 8.1 – 8.6, 8.8 – 8.12, 8.15a & 8.16a). F1:2 developed during periods of decreased available moisture, decreased in-water nutrients and decreased nutrient inflow from the catchment, reduced biological activity and, for the most part, reduced carbonate precipitation relative to F1:1 (for example Site TB9, Log 1, Zone 5, Figs 6.29 & 6.39) (Meyers & Teranes, 2001; Myrow, 1990; Potter et al. 2005; Cantarero, 2013).

8.2.1.3: Lacustrine limestone interbeds, Facies Group 1:3

Stratigraphic key (Figs 8.1 & 8.2).



The low TOC values associated with Facies Group 1:3 (F1:3) relative to F1:1 & F1:2 at Site TB9 (2.2% - 13.5%, Fig 6.39) indicate relatively nutrient-poor conditions, although manganese clusters suggests macrophytic vegetation and algae were present (Figs 6.25 - 6.28, 6.29, 6.30, 6.39 & Section 6.6.6.3). Across the study area F1:3 includes massive to laminated calc-mudstone interbeds (Facies 3) deposited in low energy, oxygenated,

shallow water that was subject to relatively short-lived periods of higher energy deposition and reworking (Facies 14b). Bed development was likely helped by suppressed terrestrial clastic input into the water body (see Section 6.6.6.3 & Figs 6.2, 6.4 & 6.6, 8.1 – 8.6, 8.8 – 8.12, 8.15a & 8.16a).

8.2.1.4: Geographical distribution, Facies Group 1

Along the southern margin of the study area thick (>6 m) sequences of F1 are elevated above the basin floor by up to 66 m (Fig 8.4). Study sites include TB9, (Section 6.6 & Figs 8.1, 8.2, 8.8 – 8.11), TB10 (Figs 6.15b, 6.16 a & c, 6.18, 6.22, 8.1, 8.8 & 8.9), TB1 (Log 7, Appendix 8, Table 12, Figs 8.1, 8.6, 8.9 & 8.11), TB14 (Figs 6.3, 6.4, 8.1, 8.3, 8.9, 8.11 & 8.12), TB12 (Appendix 4, Table 5, Figs 8.1 8.8, 8.9 & 8.12), TB17 (Log 3; Figs 6.7, 6.11, 8.1, 8.4, 8.9 & 8.11). Truncated sections of Facies Group 1, that are up to 66 m below the above mentioned sites are recorded at Sites TB2 (Appendix 8, Tables 13 – 15, Figs 8.1, 8.7 & 8.9), TB3 (Appendix 6, Tables 1 & 2, Figs 8.1, 8.9 & 8.13), TB4, (Appendix 8, Tables 17 & 18, Figs 8.1, 8.5, 8.9 & 8.12), TB5, (Appendix 8, Table 19, Figs 8.1, 8.7 & 8.9), TB7, (Appendix 4, Table 9, Figs 8.1, 8.8, 8.9 & 8.12), TB11, (Appendix 7, Table 1, Figs 8.1 & 8.6), TB13, (Appendix, 4, Table 7, Figs 8.1, 8.10, 8.9 & 8.13), TB16, (Appendix 6, Tables 2 & 3, Figs 8.1, 8.5 & 8.6), TB17, (see Section 6.3 & Fig 8.5), TB1, (Appendix 8, Table 6, Fig 8.5), and TB15 (Appendix 5, Table 1, Figs 8.1, 8.5, 8.9 & 8.13).

8.2.1.5: Age, Facies Group 1

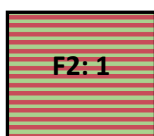
The deposition of the F1 at Site TB9 pre-dates MIS 12c (475 ka BP \pm 33, Fig 6.36), with the lower portions of the sequences known to be older than 500 ka bp (MIS 13a) (Fig 6.39). Despite Facies Group 3 having the oldest direct date (MIS 14d), F1 is thought to be the oldest depositional episode recorded from the study area based on their stratigraphic position below F3 and F4 (Figs 8.8, 8.10 & 8.11).

8.2.2: Mid Colores Formation, > MIS 12c, Interval 2 (Figs 8.15b & 8.16b), Facies group 2

Facies Group 2 (F2) is associated with the Tarango Formation (Tt) (Figs 3.3, 8.1 & 8.9) (Segerstrom, (1952, 1956; Mooser, 1975). Specifically, the horizontally stratified, water-lain, poorly indurated silt interbedded with pumice, sand, clay, tephra and lacustrine limestone. The group is defined by a type section recorded from Site TB9 (see Section 6.6, Log 2, Figs 6.30 and 6.39, Zones 7 – 10) and is redefined as the Mid Colores Formation.

8.2.2.1: Shallow lacustrine marsh, mud-flat and playa environments, Facies Group 2:1

Stratigraphic key (Figs 8.1 & 8.2).



At Site TB9, Zones 7 – 10 (Log 1, Figs 6.25a & b, 6.26, 6.27a, 6.28, a & b, 6.29, 6.39, 8.1, 8.8 - 8.11 & 8.14) show a 3.23‰ positive shift in the mean ratio of $\delta^{13}\text{C}$ (-2.75‰, Log 1, Fig 6.39) indicating that the catchment had dried significantly from F1 into F2:1. The $\delta^{18}\text{O}$ values associated with this facies group (Fig 6.39) (mean -9.3‰) at Site TB9 closely reflect the range of $\delta^{18}\text{O}$ values found in Central Mexico meteoric waters today (see Zone 7- 10, Section 6.6.8.4 and Appendix 8). Across the study area Facies Group 1:2 (F2:1) is defined by thick (< 5 m), massive, red, mud (Facies 12a), silt (Facies 13a), sand (Facies 14 b & c) and mixed carbonate-clastic beds (Facies 8a – 10a) associated with lacustrine, marsh, mud-flat (green beds) and playa (red beds) depositional environments. F2:1 is differentiated from F1 by an overall decrease in bed size (<0.50 m), erosive boundary contacts and exposure features (see Sections 6.2, 6.4 & 6.6 & Figs 6.26, 6.29 & 6.30). Root systems, vertical jointing, intraclasts and carbonate nodule formation suggest periods of sub-areal exposure, erosion and palustrine alteration within shallow water littoral to eulittoral zones (8.3 - 8.6, 8.8, 8.10 - 8.13, 8.15 b & 8.16 b) (see Freydet & Plaziat, 1982; Tucker & Wright, 1990; Pietras & Carroll, 2006). These types of sequences are expansive in low gradient basins, where minor changes in water inflow can result in high-frequency wetting and drying across extensive areas (Pietras & Carroll, 2006). In the Tequixquiac Basin, similar processes are thought to have been occurring supported by a locally high groundwater table, and perhaps spring activity. F2:1 represents nutrient-poor, oxygen-rich, shallow, but hydrologically variable water that allowed sediments to oxidise. The depositional conditions interpreted for F2:1, and the recorded stratigraphy and geochemistry shares commonalities with the Newark Supergroup (Smoot & Olsen, 1988, Myrow, 1990; Carroll & Bohacs, 1999; Potter et al. 2005; Pietras & Carroll, 2006; Hunt & Garrard, 2013) which had been used for reference to help define F2:1.

8.2.2.2: Tephra, Facies Group 2:2

Stratigraphic key (Figs 8.1 & 8.2).



Facies Group 2:2 (F2:2) represents the greyish pink dacite tephra layer (F2: 1, Facies 18c) thought to be related to the Tr2 dacitic-rhyolite tephra recorded from the Pachuca sub-basin (see Chapter 7 & Roy et al. 2013). F2.2 is recorded at Site TB9 (Logs 1 & 4, Figs 6.26, 6.30, 6.34, 6.36, 8.1, 8.8, 8.10 & 8.11), Site TB12 (Logs 1 & 2, Appendix 4, Tables 5 & 6, Figs 8.8, 8.9 & 8.12) and is also thought to be recorded at Site TB7 (Appendix 4, Table 9, Figs 8.1, 8.8 & 8.12). Consequently, the three sites were actively depositing contemporaneously when the Dacitic tephra was deposited (Figs 8.2 & 8.8).

8.2.2.3: Geographical distribution, Facies Group 2

F2:1 has been recorded at sites TB14 (Figs 6.2, 6.3, 6.4, 8.1, 8.3, 8.9, 8.11 & 8.12), TB17 (Log 3, Figs 6.2, 6.7 a & b, 6.11, 8.1, 8.8, 8.9 & 8.11), TB10 (Logs 1 & 2, Figs 6.14, 6.15b, 6.18, 6.22, 8.1, 8.8 & 8.9), TB7 (Appendix 4, Table 9, Figs 8.1, 8.8 & 8.12), TB13 (Appendix 4, Table 7, Figs 8.1, 8.10, 8.9 & 8.13), TB18 (Appendix 7, Table 3, Figs 8.1, 8.3 & 8.9) and TB16 (Appendix 6, Table 3, Figs 8.1, 8.9, 8.10 & 8.13). There are elevation differences between logged sections (see Figs 8.5, 8.6, 8.8 and 8.11). For example, ca. 24 m of elevation difference between Sites TB14 and TB9 (Fig 8.11) and 39 m between Sites TB14 and TB12 (Fig 8.12).

8.2.2.4: Age, Facies Group 2

F2 pre-dates MIS 12c based on its stratigraphic position below Log 2 at Site TB9 (Figs 6.30, 6.39, 8.8, 8.10 & 8.11). The Group is likely of a similar age, or older than F3, deposited around MIS 14, as F2 sits stratigraphically below F3 (Figs 8.1, 8.2, 8.5, 8.6 & 8.10). F2:2 has a geochemistry that is comparable with the Acoculco Caldera volcanic deposits, and deposition is thought to have occurred between 1.7 Ma and $475.33 \pm \text{ka}$ BP based on the stratigraphic position of F2:2 below Log 2 (6.33 & 6.36) at Site TB9 (see F4 and Fig 8.2), and the age estimate for the Tr2 dacitic-rhyolite tephra layer (Roy et al. 2010) (see Chapter 7).

8.2.3: San Mateo Formation, MIS 14d, Interval 3 (Fig 8.15c & Fig 8.16c): Facies Group 3

Facies Group 3 (F3) is associated with the Tarango Formation (Figs 3.3, 8.1 & 8.9), specifically the poorly indurated tuff, tuff-breccia and volcanic gravel associated with fluvial and alluvial depositional systems (Seegerstrom, 1952, 1956; Mooser, 1975). Type sections for these deposits were recorded at Site TB17, San Mateo Hill, Logs 1 & 2 (Figs 6.1, 6.2, 6.5, 6.6, 6.8, 6.9, 6.10). It is proposed here that these sections be redefined as the San Mateo Formation.

8.2.3.1: Fluvial and alluvial environments, Facies Group 3:1

Stratigraphic key (Figs 8.1 & 8.2).



Facies Group 3:1 (F3:1) at Site TB17 is represented by gravels (Facies 15 – 17) deposited as pulses of plastic and pseudoplastic sediment gravity flow (Figs 6.8, 6.9 & 6.10). Massive and bedded sandy bedforms (Facies 14) with gravel (Facies 15v- 17) at Sites TB1 (Log 1, Appendix 8, Table 6, Fig 5.24) and TB15 (Logs 1, Appendix 5, Table 1, Figs 8.1, 8.6, 8.9 & 8.13) indicate ephemeral, low to moderate fluvial flow regimes interspaced by sediment gravity flow events (Section 6.4, Figs 8.1, 8.2, 8.4 – 8.6, 8.9 & 8.13). The deposition of F3:1 at Site TB1

is related a cut and fill cycle (or cycles) and the incision along Barranca Acatlan (Figs 8.1, 8.5, 8.9, 8.15c & 8.16c). Site TB17 (Logs 1 & 2) is thought to be a marginal environment to Site TB1 (see Section 6.3 and Figs 8.1, 8.5, 8.9 & 8.15c), and together, the two sites are thought to represent proximal deposits relative to Site TB15 which is situated north of Sites TB17 and TB1 (Figs 8.1, 8.9 & 8.13). Site TB15 represents more basinal (distal) environments (see Appendix 5, Table 1) with a lacustrine limestone at the base of the sequence cut by an erosional unconformity, above which fluvial sandy bedforms (Facies 14b) and occasional gravels (Facies 15) occur. Site TB15 is thought to have formed in association with incision occurring along the course of the Rio Saldo (see Figs 8.1, 8.5, 8.9, 8.13 & 8.15). Calcrete profiles recorded at the three sites (Facies 19a & b) likely indicate warm evaporitic conditions and periods of stability under these conditions.

8.2.3.2: Tephra, Facies Group 3:2

F3: 2: Stratigraphic Key (Figs 8.1 & 8.2)



Facies Group F3:2 (Facies 18d, In Log 1, Site TB17, Section 6.2) comprises thick (<0.70 m), medium light grey (N6), medium-coarse ash (Figs 6.8, 6.9, 6.10, 8.1, 8.5, 8.9 & 8.13 see Section 6.4). Depositional environments are the same as those described for the gravels in F3:1 (e.g. Facies 15 - 16, Tables 4.8, 4.9 & 8.3) except that some beds may be laharic in origin, but still deposited under sediment gravity flow to fluvial conditions. Facies 18d recorded in Log 1 (Facies 18d) stratigraphically links Logs 1 and 2 (Figs 6.8, 6.9, 6.10, 8.1, 8.5, 8.9 & 8.13) at Site TB17 (Fig 6.10) and potentially correlates to similar sediments recorded at Site TB1, Log 1 (Fig 8.5, Appendix 8; Table 6) and at Site TB15, Log 2 (Fig 8.5, Appendix 5; Table 1).

8.2.3.3: Geographical distribution, Facies Group 3

Sites TB1 (Log 1, Appendix 8, Table 6, Figs 8.1, 8.8 & 8.9) and TB17 (Section 6.2, Figs 8.1, 8.5, 8.9 & 8.3) are in the upper reaches of Barranca Acatlan, elevated 54 m above Site TB15 (Logs 1 – 4, Appendix 5, Table 1, Figs 8.1, 8.5, 8.9 & 8.13). Site TB15 is located distally at the outlet of Barranca Acatlan, along the banks of the Rio Saldo close to where it joins the Agua Negra (an outlet for Barranca Acatlan) (Figs 8.1, 8.9 & 8.15c).

8.2.3.4: Age, Facies Group 3

The age of F3:2 recorded in Log 1, Beds 5 & 6 (Facies 18d, Ar/Ar $550.7 \pm 4.1/4.7$ ka, MIS 14d) suggests deposition occurred around MIS 14. The fact that the tephra has been resedimented suggests that the actual eruption date may be younger than the recorded age (Figs 8.5, 8.6, 8.10 & 8.13).

8.2.4: Upper Colores Formation, MIS 12c – MIS 11, Interval 4, (Fig 8.15d & 8.16d), Facies Group 4

Facies group 4 (F4) is associated with the Tarango Formation (Tt) (Figs 3.3, 8.1 & 8.9). Specifically, ash deposits and thicker lacustrine limestone sequences (relative to F1) up to 12 m thick and less than a km² (Segerstrom, (1952, 1956; Mooser, 1975). The group is defined by a type section recorded from Site TB9 (see Section 6.6, Log 2, Figs) and is redefined as the Upper Colores Formation.

8.2.4.1: Fluvial-lacustrine to marsh environments, Facies Group 4:1

Stratigraphic key (Figs 8.1 & 8.2)



At Site TB9 (Log 2, Sections 6.6.4.2 & 6.6.7; Figs 6.33 & 6.40) the recorded $\delta^{18}\text{O}$ values fit within the modern range of values known for Central Mexico today (see Appendix 10). Isotopic ratios of $\delta^{13}\text{C}$ (-3.3‰ to 1.9‰), supported by similarly high TIC values (30.9% to 90.4%), indicate significantly drier and likely warmer conditions than during the deposition of F1 and F2. Very occasional low TIC values, high clastic signals, and low Sr/Ca and Mg/Ca molar concentrations in mud and micritic mud beds at the base of zones (Figs 6.33 & 6.40) suggest a fresh surface water source, and/or rapid throughflow relative to the other beds (e.g. Bed 4, Log 2, Sections 6.6.4.2 & 6.6.7, Figs 6.33 & 6.40) and likely cooler ambient temperatures. Across the study area Facies Group 4:1 (F4:1) represents fresh relatively small, at times saline to hypersaline evaporitic fluvial-lacustrine pools that developed in close association to barranca heads, localised water availability, spring activity and/or high groundwater tables (Figs 8.3, 8.5, 8.6, 8.8, 8.10 - 8.13, 8.15d & 8.16d). The sequences are complex, and between sites, there is a range of fabrics and facies (Facies 1 – 6 with elements of Facies 7 – 16) that represent slightly different sub-depositional environments from fluvial to ephemeral marginal pool to relatively deep standing water. For example, the dominance of framestone (Facies 1) and stromatolitic (Facies 2) limestone at Site TB12 (Appendix 4, Table 6) indicate mainly relatively freshwater fluvial-lacustrine environments (e.g. micrite fringe cement (around root stems and interbedded within biofilm layers), biofilms, peloids, root moulds, casts and voids, and vegetation litter or detritus, see Appendix 4, Table 6) (Lorch & Ottow, 1985; Pedley, 1990; Flügel, 2010). Occasional massive micrite beds indicate low energy depositional environments within standing water (Facies 3b). In comparison, conditions at Site TB9 (Fig 6.40) were more saline and dominated by pisolitic limestone (Facies 5,) which likely indicate that there was flowing water, or standing water that was occasionally turbulent (Folk & Chafetz, 1983; Guo & Riding, 1998; Koşun et al. 2005; Jones & Renaut, 2010).

8.2.4.2: Tephra layers, Facies Group 4:2 and 4:3

Stratigraphic key (Figs 8.1 & 8.2)



During this depositional period the study area was impacted by sub-alkaline volcanic activity indicated by the basaltic-andesitic tephra layer (Facies 18a) recorded at Site TB9 (Logs 1 & 4, Figs 6.31 - 6.34 & 6.36) Facies Group 4:2 (F4:2) related to the Donguinyó-Huichapan Caldera system or the Nopala Shield volcano (see Chapter 7, Fig 7.1, TEQ 4). Between sites stratigraphic, and in some cases geochemical correlation of tephra layers (F4:2) links Sites TB9 and Site TB7 indicating they were active contemporaneously.

Facies Group 4:2: Stratigraphic key (8.1 – 8.2)



The thick white, bioturbated, andesite tephra (Facies Group 4:3, (F4: 3)) Facies 18b) recorded at Site TB10 (Log 2, Figs 6.19 & 8.8) also suggests volcanic input into the study area. Its age is estimated to be between 470 ka bp and 5 Ma bp dependent on the source of the tephra (see Chapter 7). The ungulate hoofprint on the surface of this tephra deposit suggests that animals were grazing around the pool the tephra was deposited in (Fig 7.7). Hence, this is taken to indicate the base level for the pool before the first cycle of palaeo-barranca incision had occurred in Barranca del Muerto (Site TB10). The absence of F4:3 from other sites indicates Site TB10 was active before or after deposition occurred at Sites TB9 & TB7 (Figs 8.1, 8.8 & 8.9).

8.2.4.3: Geographic distribution, Facies Group 4

Deposits are recorded at Sites TB10 (Log 2, Section 6.4), TB12 (Log 2, Appendix 4, Table 6; Fig 5.3, 5.4, 5.7, 5.14, 5.16, 5.17, 6.13, 8.1, 8.8, 8.9 & 8.12, Tables 5.7, 5.8, 5.16 & 5.17), TB13 (Log 1; Appendix 4, Table 7; Figs 5.8, 5.11, 5.18, 6.13, 8.1, 8.10, 8.12 & 8.10, Tables 5.13 & 5.18), TB7 (Appendix 4, Table 9; Figs 6.13, 8.1 8.8, 8.9 & 8.12), TB4 (Appendix 8, Table 18; Figs 8.1, 8.9 & 8.12), TB16 (Appendix 3, Table 3; Figs 8.1, 8.5, 8.6 & 8.9), TB11 (Appendix, Table 2; Figs 8.1, 8.6 & 8.9 and TB18, (Appendix 7, Table 3; Figs 8.1, 8.3 & 8.9). Between Sites TB10 and TB9, an offset of ca. 7 m between Facies Groups 1, 2 & 4 suggest that there is possibly a normal fault separating the two barrancas (Fig 8.8). Slump scars corresponding to the upper portion of Log 1 (Fig 6.30) have also been recorded at Site TB9 and are possibly related to mass movement and sediment displacement (e.g. Table

4.3, fsl & gf), both of which are associated with gravitational instability and failure along weak bedding horizons (see Figs 6.38d & 8.8).

8.2.4.4: Age, Facies Group 4

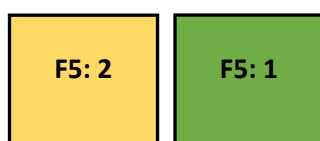
At Site TB9 the base of F4 is associated with MIS 12c (475 ± 33 ka BP, Bed 1 Log 2, Figs 6.33 & 6.39) after which there is assumed to be a depositional hiatus, possibly with occasional deposition represented by Bed 2 (see Figs 6.33 & 6.39). The site flooded again around the onset of MIS 11 (Bed 3, Log 2, Fig 6.33) and deposition continued during the interglacial based on the Ar/Ar date of $405.3 \pm 5.1/5.8$ ka BP from the Basaltic-andesitic tephra layer recorded in Bed 5 (Log 2, Fig 6.33).

8.2.5: Quaternary fluvial - alluvial deposits, <MIS 3, Interval 5, (Figs 8.15e & 8.16e) Facies Group 5

Facies Group 5 (F5) is associated with the fossil fauna rich gravels, sands and silts belonging to the Younger Becerra Formation and Totolzingo Formation (Furlong, 1925; Maldonado & Aveleyra, 1949; De Terra, 1949; Hibbard, 1955; Aveleyra, 1955; see Table 1.1) and Quaternary clastic deposits identified (Figs 3.3, 8.1 & 8.9, Qc; Segerstrom, 1952, 1956; Mooser, 1975).

8.2.5.1: Fluvial and alluvial depositional environments, Facies Group 5

Stratigraphic key (Figs 8.1 & 8.2)



Facies Group 5 (F5) represents alluvial and fluvial terraces marking stages of incision along the Agua Negra river (Terrace 3 (T3), Figs 8.1, 8.6, 8.7, 8.10, 8.9, & 8.11, see Section 8.2.5.1), and its elevated feeder barrancas (Terrace 2 (T2), Figs 8.1, 8.8, 8.10, 8.9, 8.11 & 8.12, see Section 8.2.5.1). Facies Group 5:2 (F5:2) T2 deposits consist of plastic, pseudoplastic and turbulent sediment gravity flow gravels (Facies 15 – 17). Occasional gravel bar and bedforms (Facies 14, FGh: Fluvial/alluvial lag deposit, Tables 4.8 & 8.1 – 8.4) that grade into laminated waning flood drape deposits (Facies 14, FFI, Tables 4.8 & 8.3) also occur (see Sections 6.6.2.5 & 6.5.3.3). Facies Group 5:2 T3 deposits, in addition to the features described above for T2 deposits, contain thin diatomite and fine sand (Facies 14a) beds inferring fresh-saline marsh to fluvial environments. Massive clay (Facies 11c) beds represent pond, marsh and/or floodplain environments that were strongly evaporation and brackish at times (based on diatom data, Appendix 8, Table 11). Capping sequences recorded at Sites TB1, TB2 and TB5 (Figs 8.1, 8.6, 8.7 & 8.9) are dark (dark grey (N3), dusky brown (5YR 2/2), black (N1) massive to laminated sand (Facies 14 b - d) with fine pebble gravel (Facies 15 & 16), clay (Facies 11c) and mud (Facies 12b) with or without

molluscs (Facies Group 5:1 (F5.1)). Deposition (based on diatom, pollen and sedimentological data, see Appendix 8, Table 15) occurred within ephemeral marsh/pond environments within a meadow to floodplain setting. Water chemistry fluctuated between alkaline, saline and acidic. Within the pollen assemblage regional tropical forest taxa and local shrubs and herbs are the main contributors with occasional evidence of increased wetland pollen taxa, macrophytes and temperate forest taxa (see Appendix 8).

8.2.5.2: Geographic distribution, Facies Group 5

Feeder barrancas that drain towards Angua Negra include Sites TB9 (Log 5, Fig 6.35, 6.36, 8.8, 8.9, 8.10 & 8.11), TB10 (Logs 3 & 4, Figs 6.20, 6.21, 8.1, 8.8 & 8.9), TB4 (Appendix 8, Table 17; Figs 8.1, 8.9 & 8.12) and TB6 (Appendix 8, Table 16; Figs 8.1, 8.8 & 8.9). Site TB7 (Appendix 4, Table 8; Figs 6.13, 8.1, 8.8, 8.9 & 8.12) drains towards the Rio Salado. Basinal and northern sites include TB8 (Appendix 7, Table 2) and TB16 (Appendix 6, Table 3; Figs 8.1, 8.5, 8.6 & 8.9). Lower elevation sites that form part of Barranca Acatlan include Agua Negra include; TB5 (Appendix 8, Table 29; Figs 8.1, 8.7 & 8.9) and TB2 (Appendix 8, Table 12 – 14; Figs 8.1, 8.7 & 8.9).

8.2.5.3: Fossils, Facies Group 5

Mammoth, glyptodont and small deer were found associated with the gravels in T2 and T3 deposits (see Chapter 6).

8.2.5.4: Age, Facies Group 5

Radiocarbon dates, because they push the boundary of the method, are assumed to have substantial error bars. The land snails dated were probably re-sedimented, which causes uncertainty (e.g. see Hunt et al. 2015). Radiocarbon ages from the gravels recorded at Sites TB9 (^{14}C 44,235 cal. BP) and TB10 (^{14}C 43,694 cal. BP) suggests a similar age for deposition (see Appendix 9, Fig 8.8) at both sites during MIS 3. These deposits are recognised as T2 deposits (F5:2) (Figs 8.5, 8.8, 8.10, 8.8 & 8.12). F1 deposits along the Agua Negra (Site TB1) recorded a younger age at the lower incisional contact of ^{14}C 17,695 cal. BP and these are recognised as T3 deposits (F5:2). Organic-rich silt and clay that overlie the gravels at Site TB1 (Facies 11c, 12b, 14a - 14d & 15 – 16) date to 12,354 cal. BP at the lower contact (see Appendix 9 and Fig 8.6). At Site TB2 (El Tajo) similar organic deposits, stratigraphically above the silts and sands and gravels associated with T3, have a basal date of ^{14}C 11,440 cal. BP (Fig 8.7). These deposits are associated with T3 (F5:1) deposits and represent the youngest cycle of erosion and deposition recorded here (Figs 8.6, 8.7, 8.10 - 8.12).

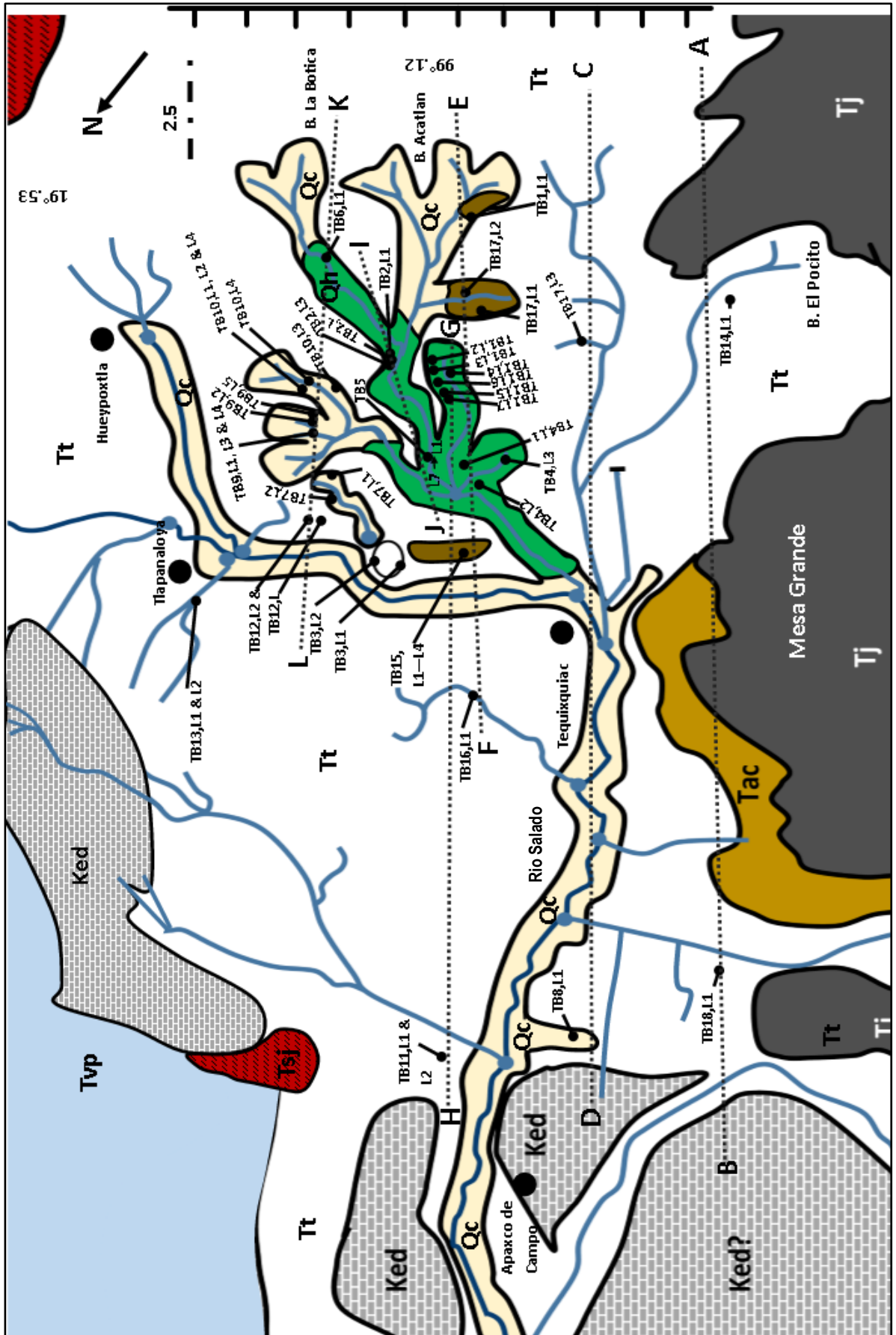
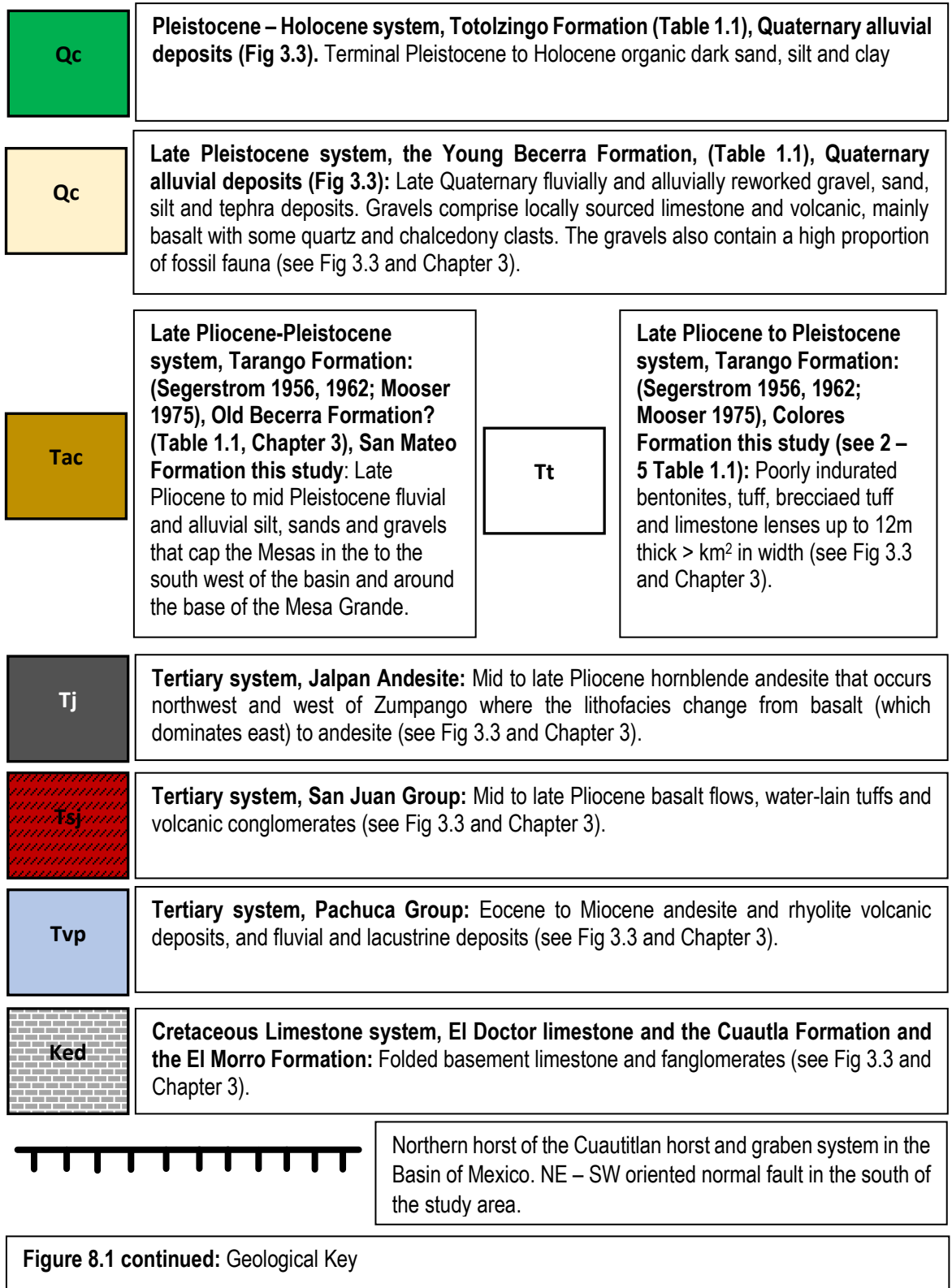
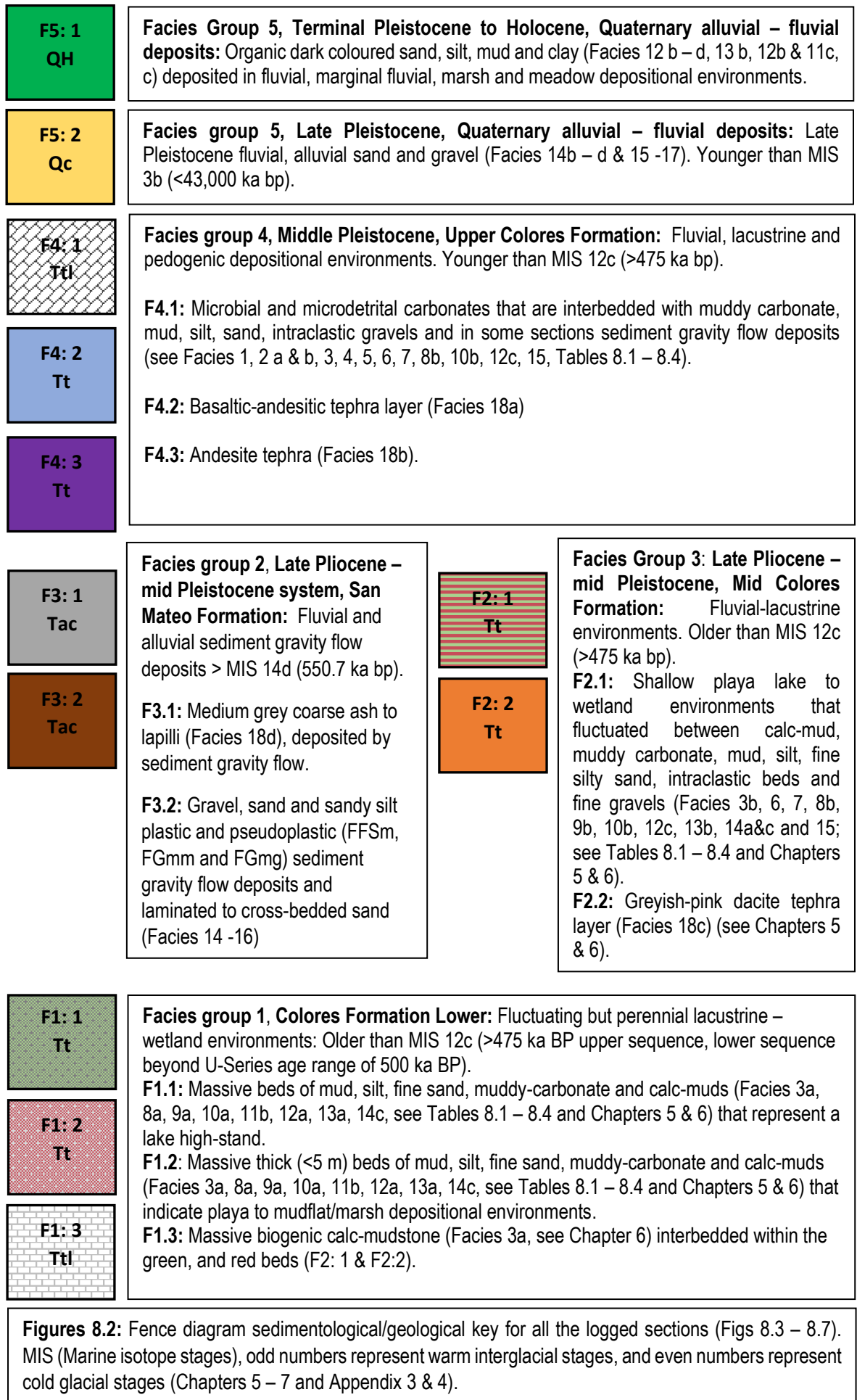


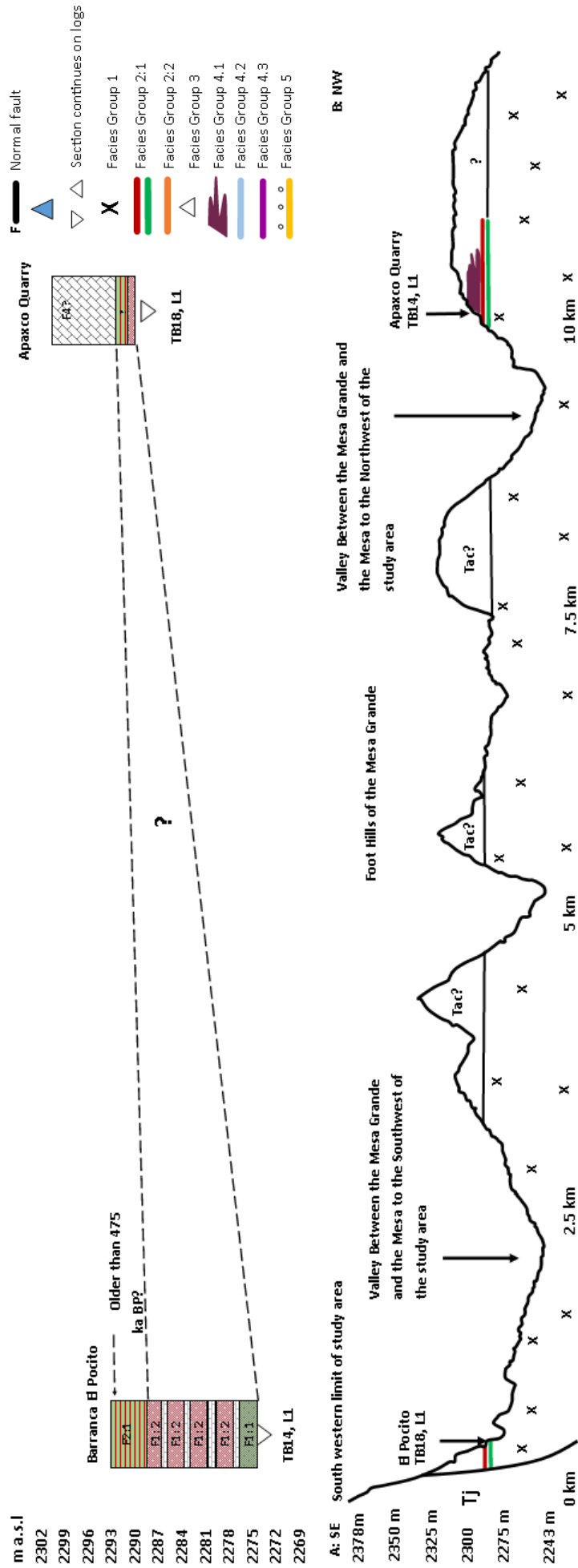
Figure 8.1: Geological map of the study area and location sites of logged sequences. Modified after Mooser (1975) and Segerstrom, (1956, 1962) to include the results of this PhD Research. Position of SE – NW in Fence diagrams shown in Figures 8.3 – 8.7.

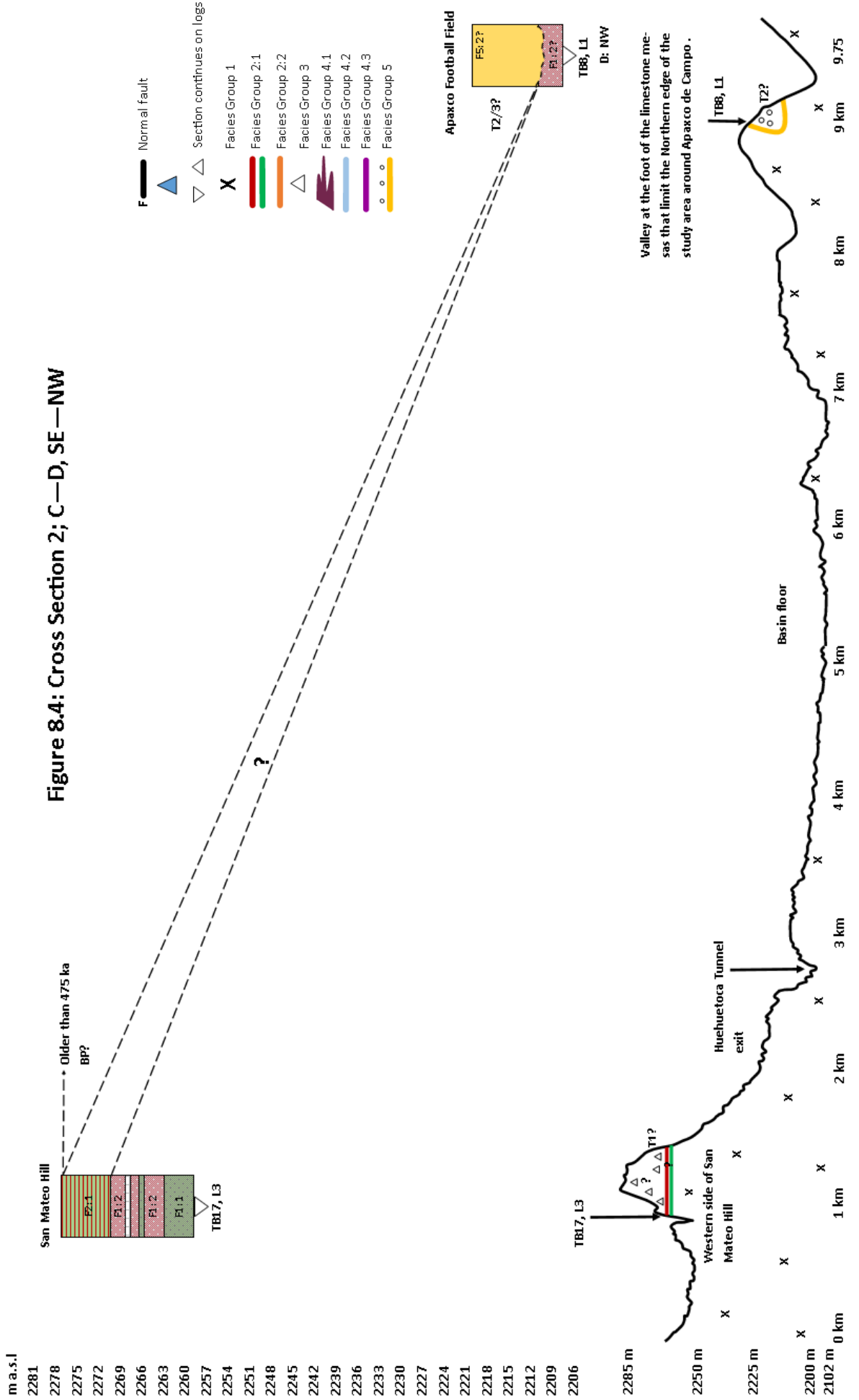




Figures 8.2: Fence diagram sedimentological/geological key for all the logged sections (Figs 8.3 – 8.7). MIS (Marine isotope stages), odd numbers represent warm interglacial stages, and even numbers represent cold glacial stages (Chapters 5 – 7 and Appendix 3 & 4).

Figure 8.3: Cross Section 1; A—B, SE—NW





m
2335
2332
2329
2326
2323
2320
2317
2314
2311
2308
2305
2302
2299
2296
2293
2290
2287
2284
2281
2278
2275
2272
2269
2266
2263
2260
2257
2254
2251
2248
2245
2242
2239
2236
2233
2230
2227
2224
2221

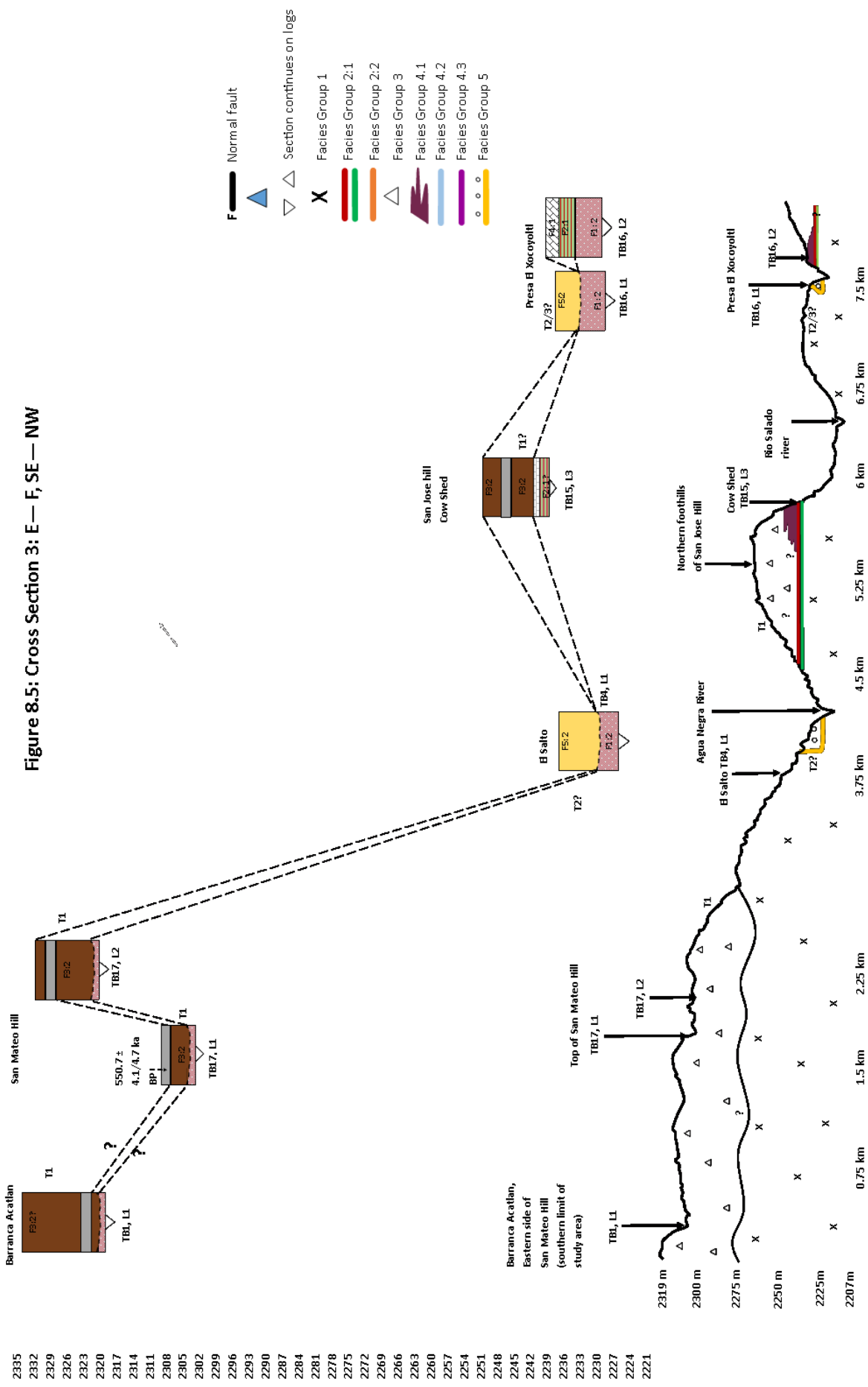
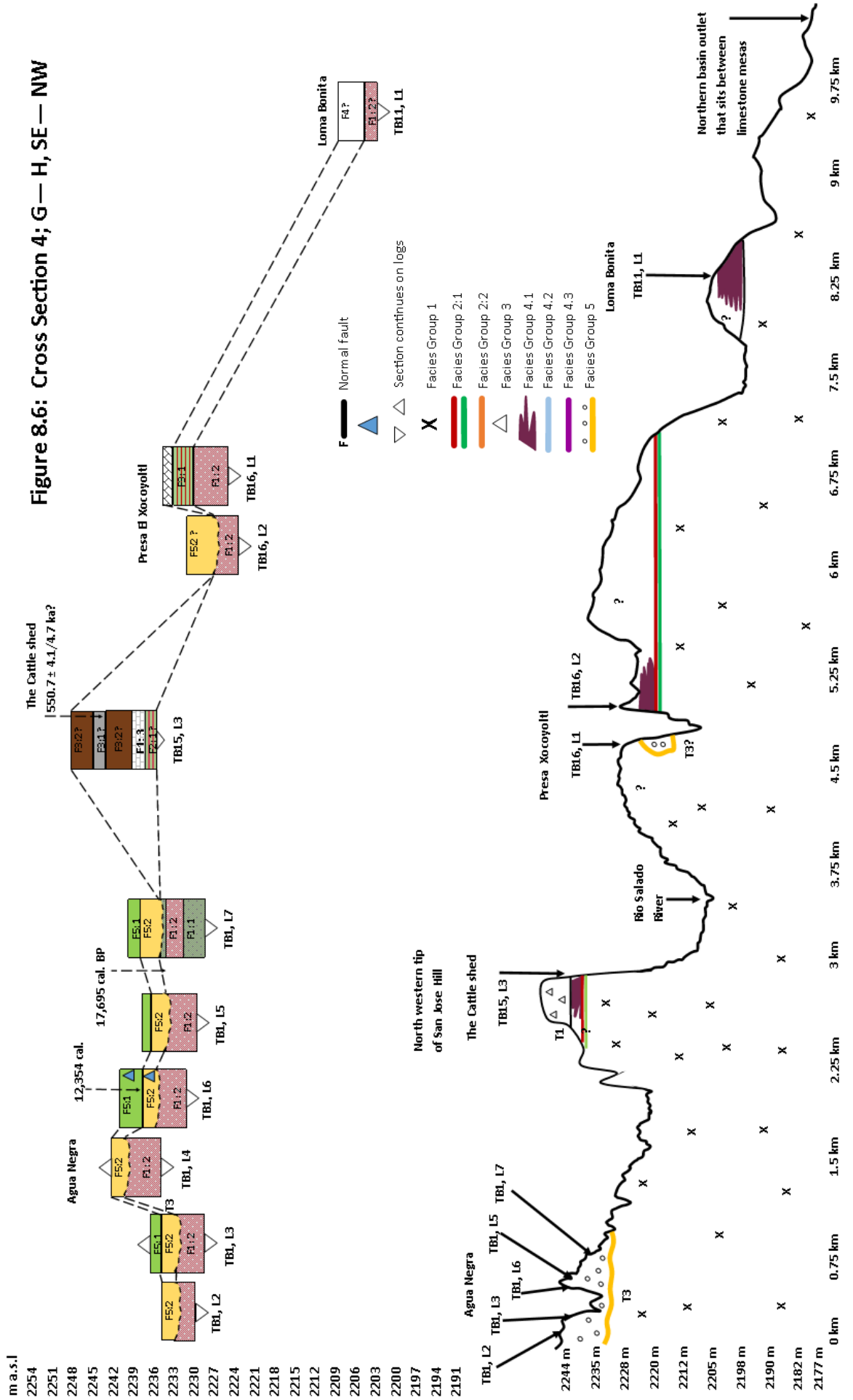
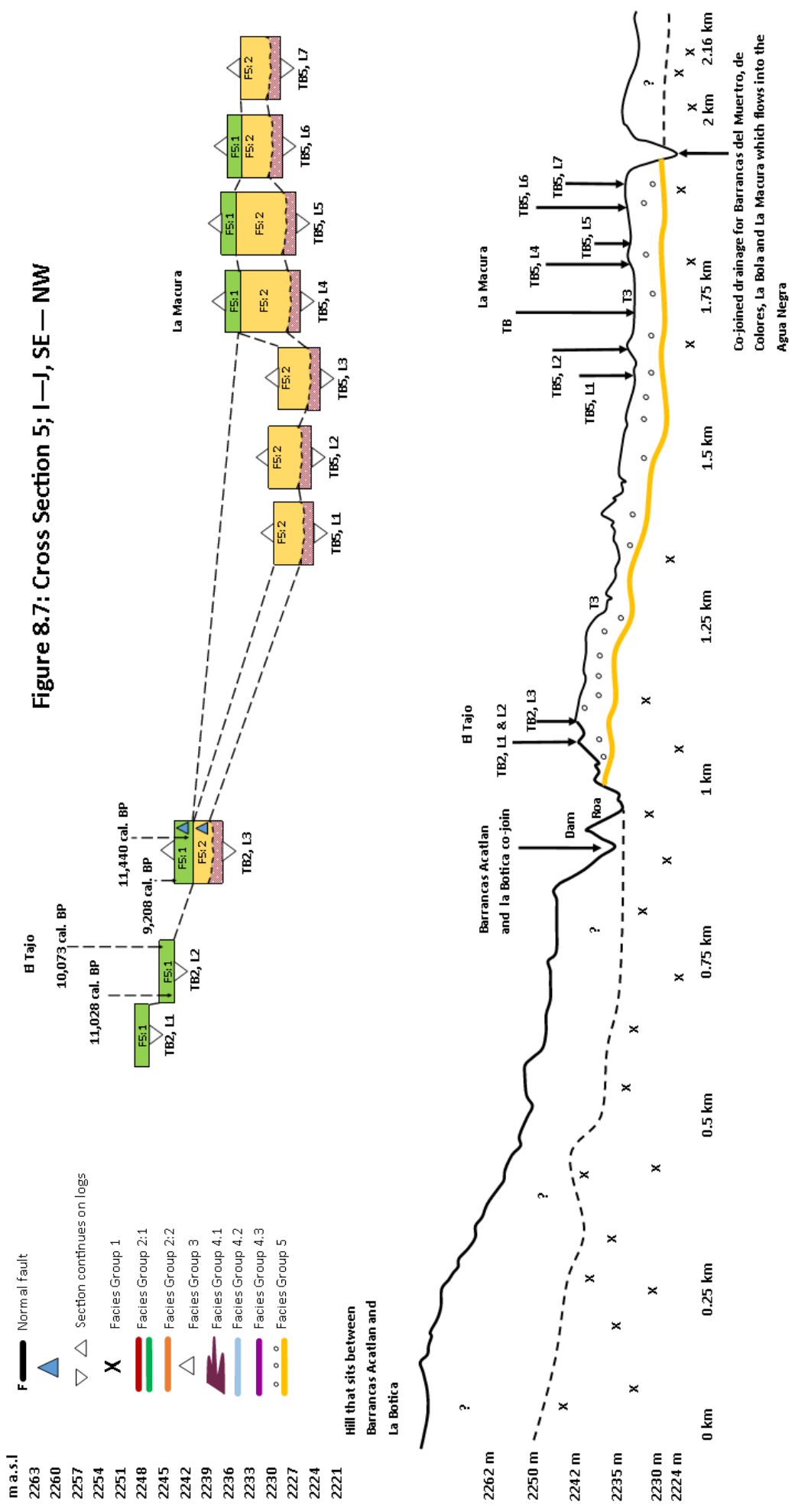


Figure 8.6: Cross Section 4; G—H, SE—NW





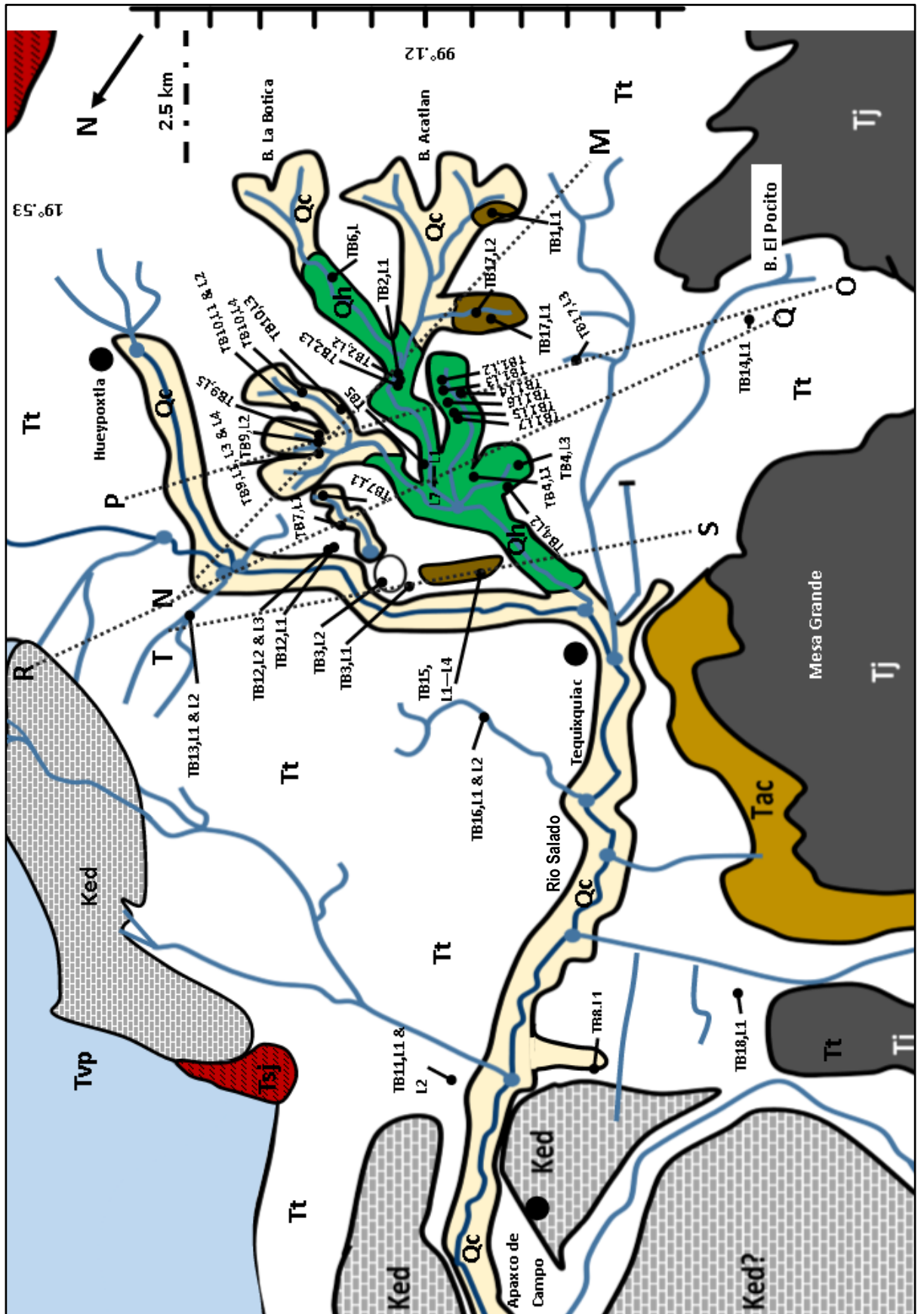
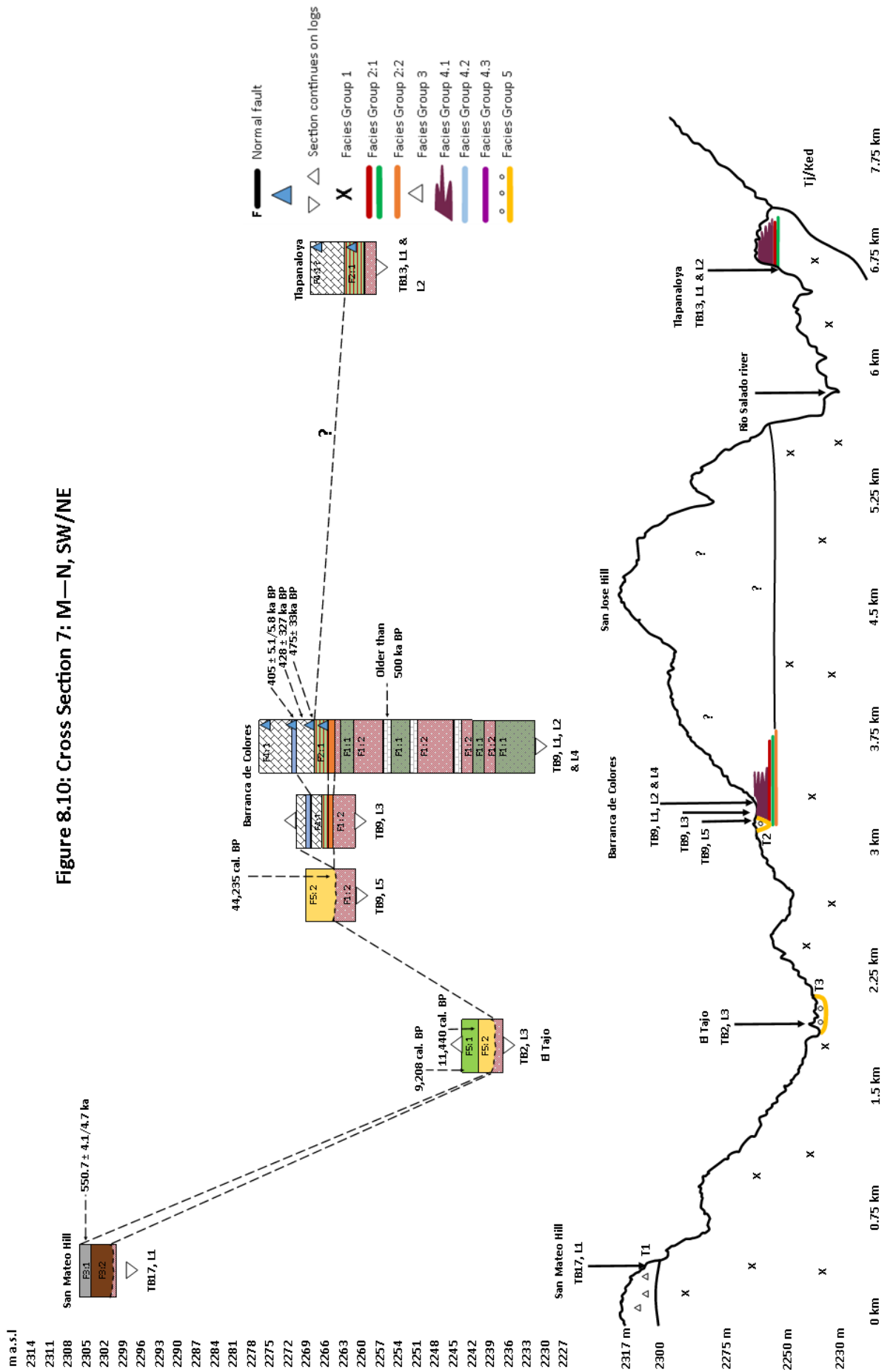
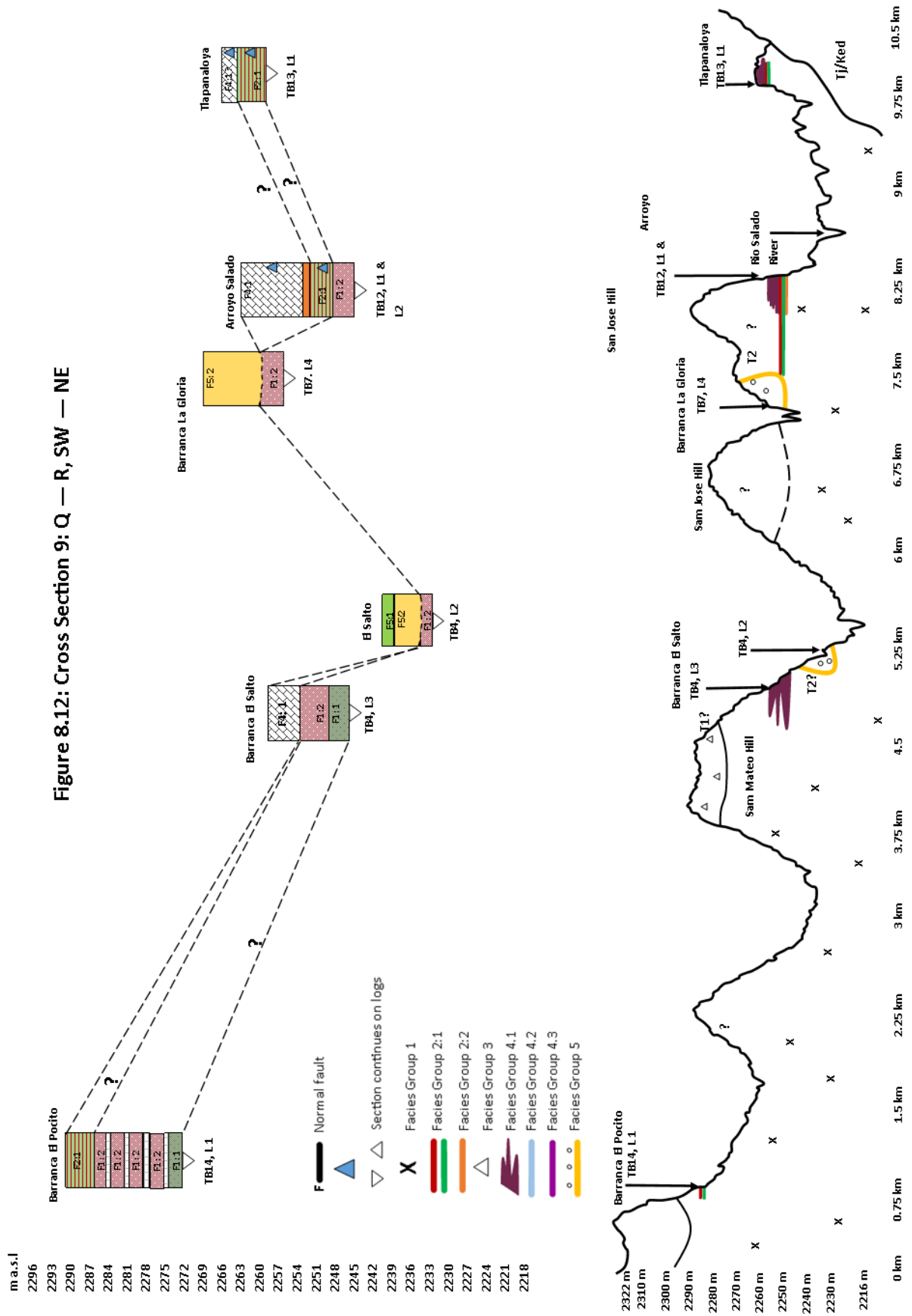


Figure 8.9 (see Fig 8.1 for geological key): Geological map of the study area and location sites of logged sequences. Modified after Mooser (1975) and Segerstrom, (1956, 1962) to include the results of this PhD Research. Figure also shows SW – NE cross sections. Fence diagrams shown in Figures 8.10 – 8.13).





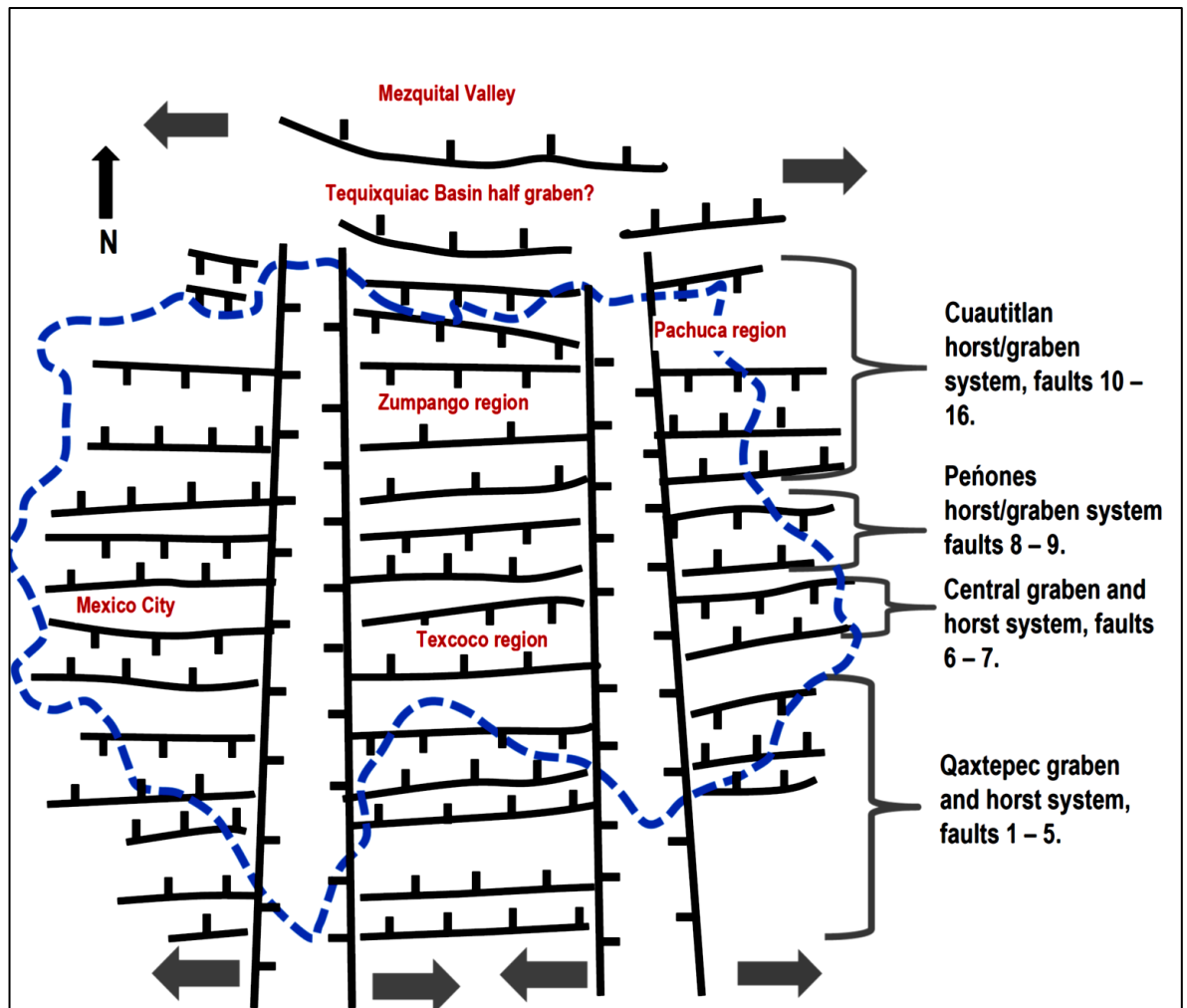


Figure 8.14: A conceptual model for the geological formation of the study area related to extensional deformation and subsidence in the Basin of Mexico. These are 16 NE – SW normal and/or strike-slip faults that form horst and graben structures. Figure from Marín-Córdova et al. (2004) adapted to include the study area and based on geological studies of the Basin of Mexico by Mooser (1975); Marín-Córdova et al. (1986); De Cserna et al. (1988) and the Mezquital Basin by Suter et al. (2001); Medel & Armienta (2004). All the graben basins orientated NE – SW. Black arrows represent distensive axis and extensional faulting that, to the west of the figure, join Popocatepetl Volcano, the Teixiquiac - Huehuetoca zone, the lowest portion of the Basin of Mexico (central lakes) including Lake Texcoco and the Peñón de los Baños zones. To the east, extensional faulting (orientation is NW –SE) joins the Ixmiquilpan (Hidalgo) valley, the Apizaco region of Tlaxcala and the La Malinche Volcano. The blue dashed line represents the watershed of the Basin of Mexico. The half graben indicated for the study area is based on this PhD research and is the proposed working hypothesis of basin formation and evolution. Not to scale.

8.3: Paleogeographic and palaeoenvironmental evolution of the study area

8.3.1: Basin formation and subsidence

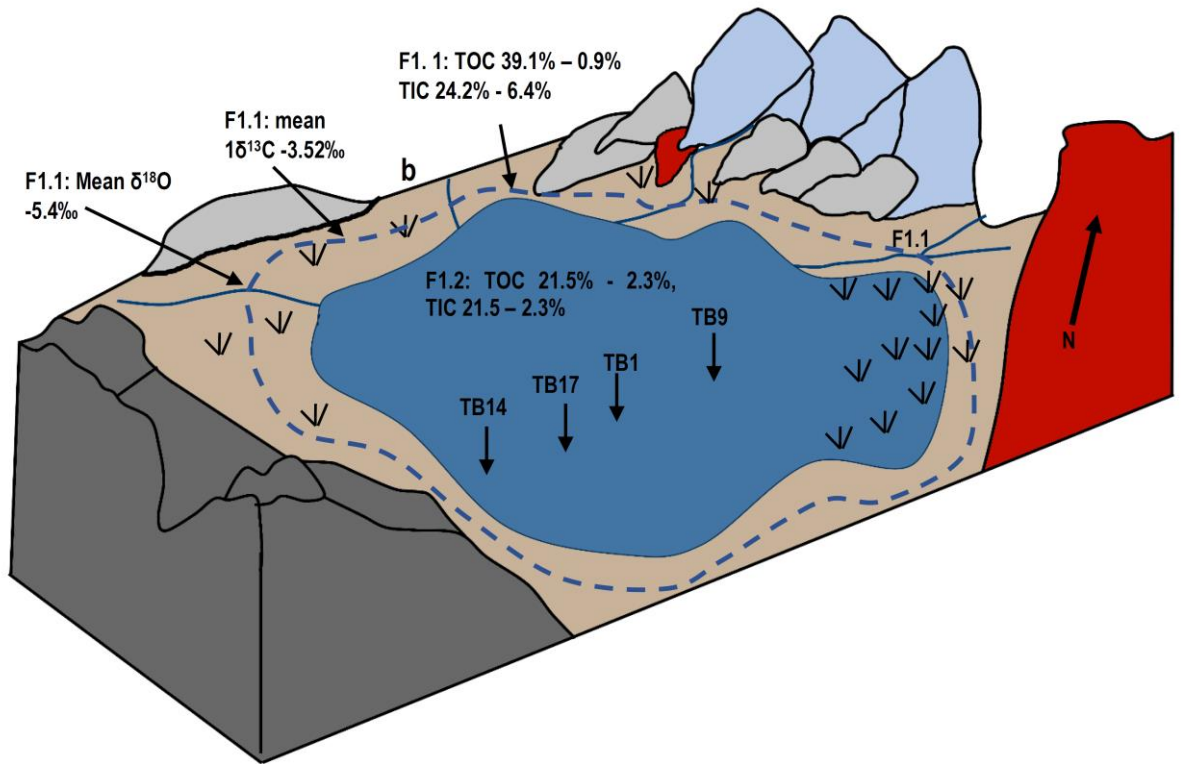
Basin formation and subsidence in the study area likely started during the Eocene/Oligocene and developed further during the mid-Miocene (Campos & Sánchez 2000; Ferrari et al. 2003; Álvarez & Nieto, 2007; Gómez et al. 2007). The estimation of a Pliocene age for the onset of the deposition of the Tarango Formation

(Mooser, 1975) seems realistic with sedimentation continuing into the early to mid-Pleistocene, and it is these later sediments that have been recorded and reported by this research (Facies Groups 1, 2 & 4). Accommodation space was potentially generated by subsidence connected to the NW 35° – SE distensive fault axis in the Basin of Mexico (Marín-Córdova et al. 2004, Fig 8.14), or in relation to the formation of a southward-dipping half-graben (Fig 8.1, 8.9, 8.14 & 8.16), connected to the Cuautitlan horst and graben system in the Basin of Mexico (Marín-Córdova et al. 2004: NE – SW oriented normal fault, Figs 8.14 – 8.15a).

| | |
|-------------|---|
| F5:2 | Late Pleistocene fluvial to marginal fluvial environments |
| F5:1 | Late Pleistocene alluvial and fluvial deposits |
| F4 | Mid Pleistocene fluvial-lacustrine pool environments: Upper Colores Formation |
| F3 | Mid pleistocene fluvial/alluvial environments: San Mateo Formation |
| F1 | Mid Pleistocene fluvial-lacustrine pool environments: Lower and mid Colores Formation |
| Tj | Tertiary system, San Juan Group, Jalpan Andesite |
| Tsj | Tertiary system, San Juan Group |
| Tvp | Tertiary system, Pachuca Group |
| Ked | Cretaceous Limestone system, El Doctor limestone and the Cuautla Formation and the El Morro Formation: |

Figure 8.15: Geological Key

Figure 8.15 a) Interval 1: Facies Group 1, MIS 15 – 14 (?) lacustrine environments. An aggregational lacustrine system, climate warm and humid, initial active subsidence followed by sediment loading and reduced accommodation space (Fig 8.16a)



Facies 8.15 b) Interval 2: Facies Group 2, MIS 15 - 14 shallow marsh to playa lacustrine environments. Reduced available moisture, likely related to the onset of MIS 13, intermittent subsidence followed by sediment loading (Fig 8.16b). End of interval water body dried. Possible uplift along the southern margin (Fig 8.16b).

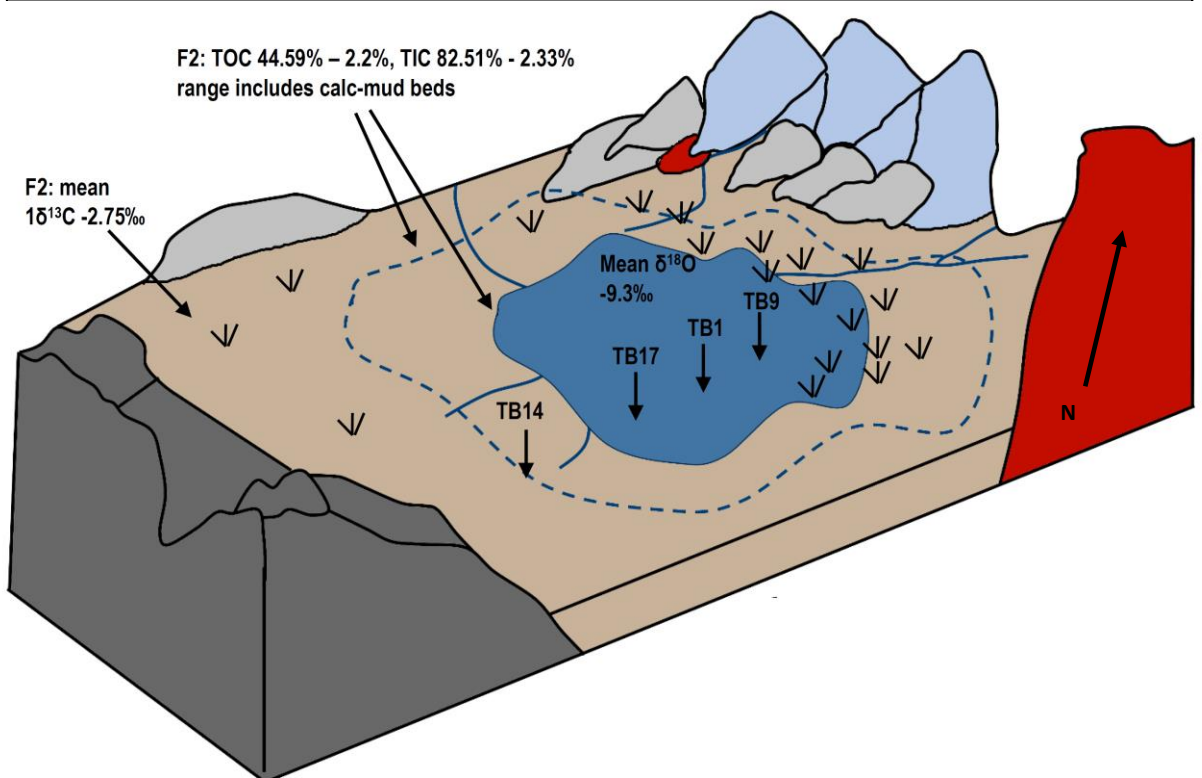
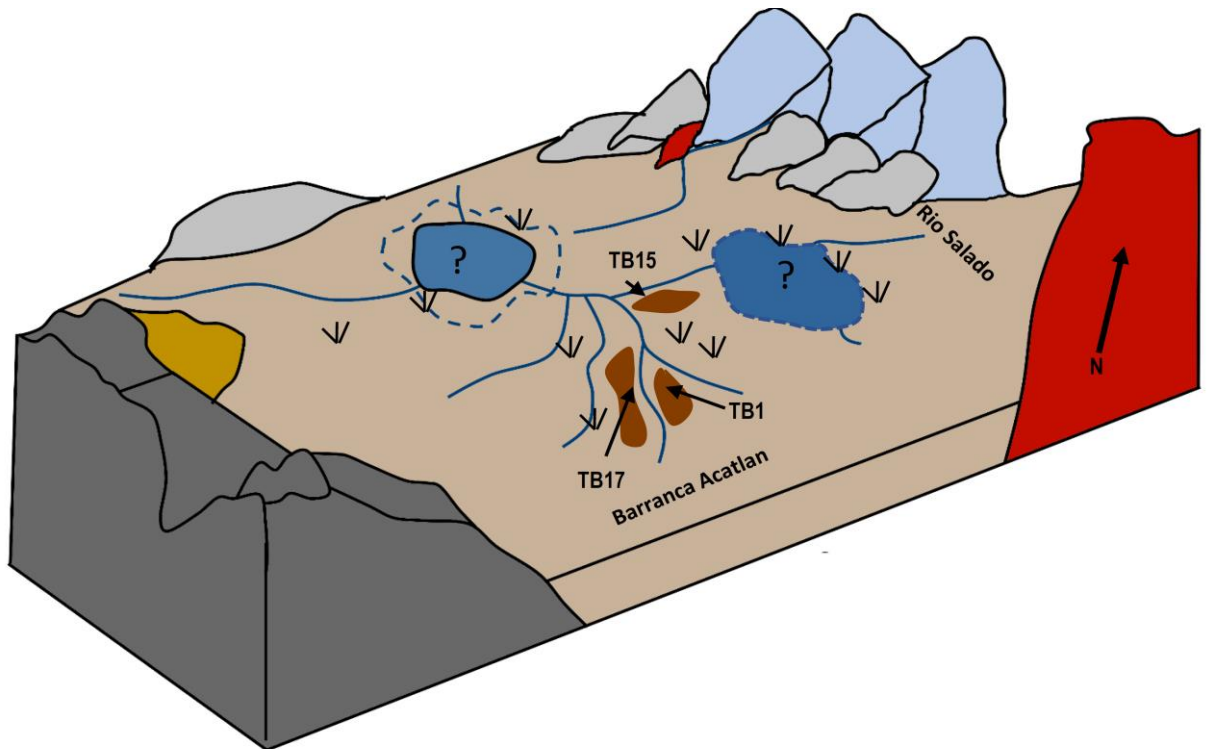


Figure 8.15 c) Interval 3, Facies Group 3, MIS 14d Fluvial-alluvial environments, possibly with sub-basinal lacustrine environments (Fig 8.16c). End of lacustrine aggregational phase (sediment loading exceeded capacity) and the onset of alluvial-fluvial aggradation, incision and erosion. Localised deformation may have allowed standing water bodies to develop (Fig 8.16c).



d) Interval 4, Facies Group 4, MIS 12 & 11, fluvial-lacustrine pool to marsh environments, possibly with sub-basinal lacustrine environments. Dry conditions and hydrological change in the study related the MIS 11 interglacial climates, reduced accommodation space and localised deformation and faulting. Alluvial-fluvial aggradation, incision and erosion continue. Potential for 30 m + of incision, deformation and/or uplift to have occurred between interval 3 and interval 4.

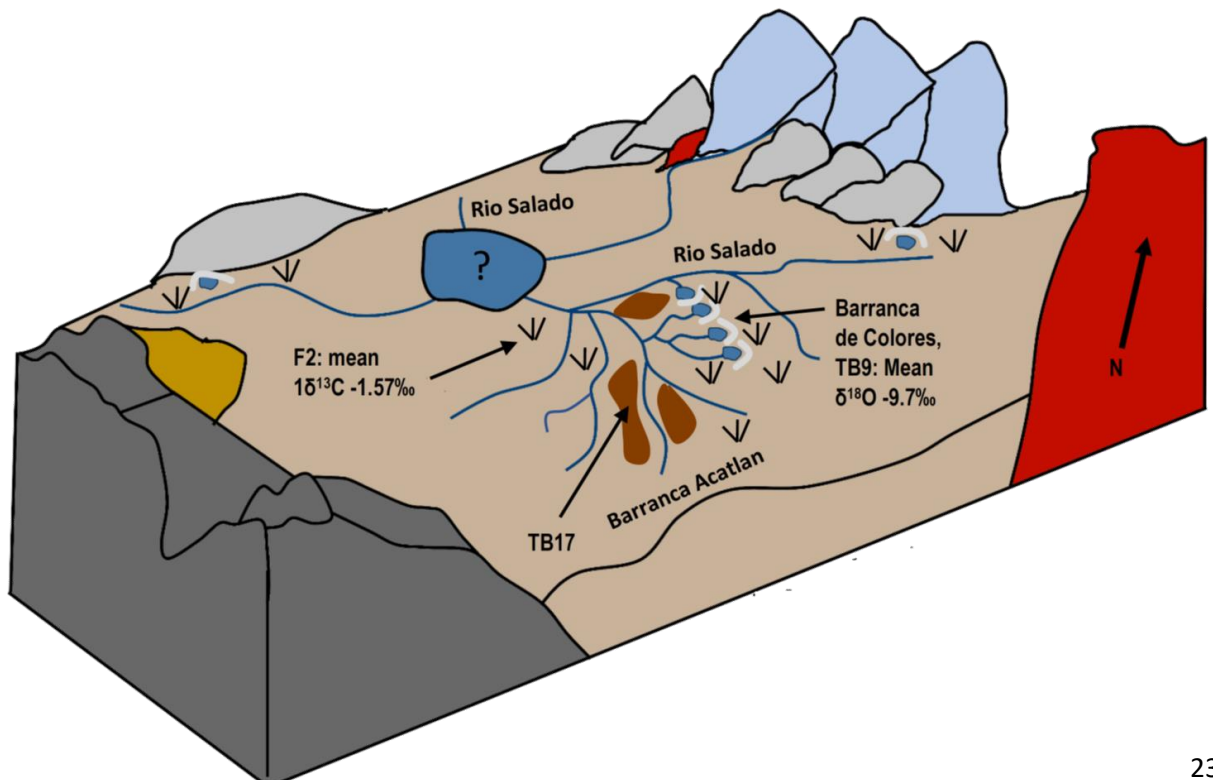
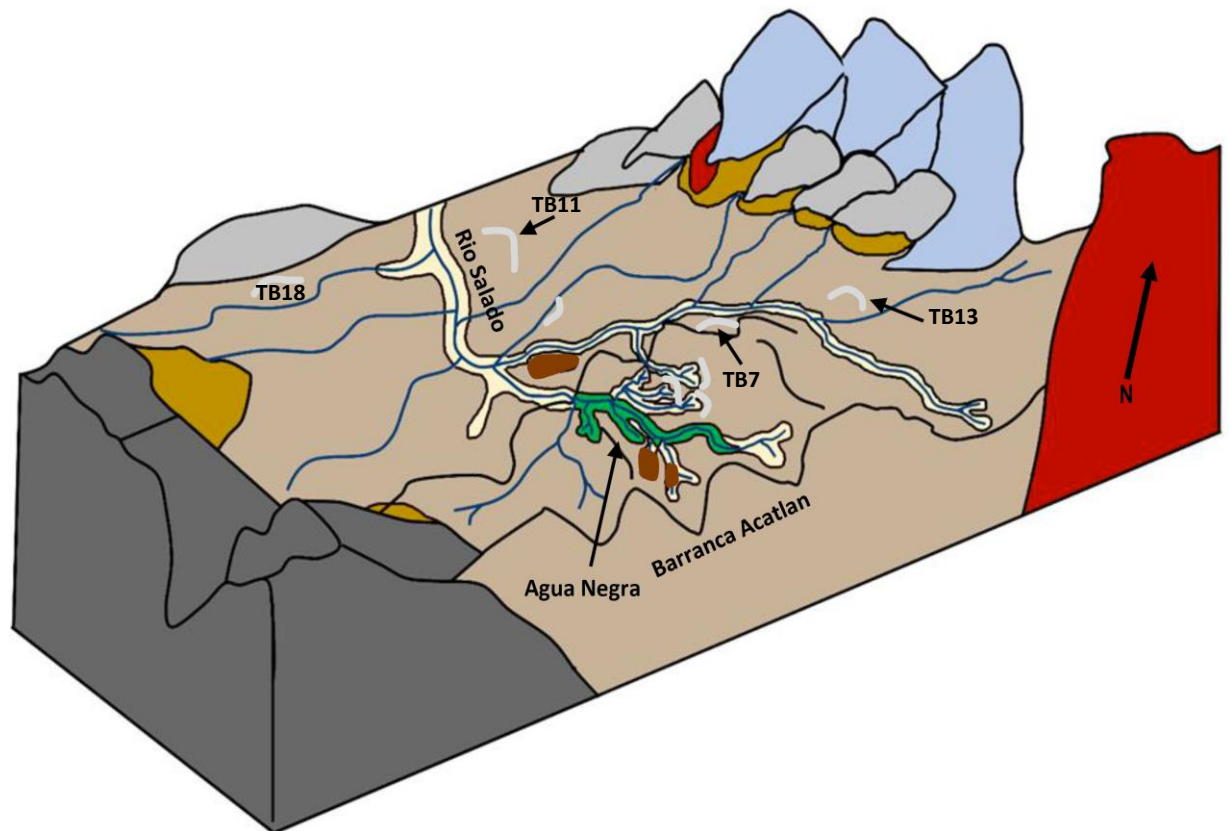


Figure 8.15 e) Interval 5, Facies Group 5, MIS 3 – 1. Fluvial-Alluvial depositional environments: Changeable late glacial climates related to ITCZ, DO and HE climate anomalies. Alluvial-fluvial aggradation, incision and erosion continue. Potential for 60 m + of incision, deformation and/or uplift to have occurred between interval 4 and interval 5.



It is hypothesised that a half-graben developed, with its hinge towards Mezquital valley (Fig 8.14) represented by the outcropping basement limestone which is absent in the southwest of the study area (Figs 3.3, 8.1, 8.9 & 8.14). During the late-Pliocene and early-Quaternary, the partial closure of the western edge of the study area by the Pliocene lava flow (Mesa Grade, Tj, Figs 3.3, 8.1 & 8.9) may have redirected drainage towards the study area enabling any lacustrine system to deepen. Alternatively, it may have altered the hydrology of the basin leading to reduced fluvial inflow and connectivity to surrounding lake basins (Figs 1.1, 8.1, 8.9 & 8.14).

8.3.2: Interval 1, > MIS 12c Perennial lacustrine environments, Facies Group 1

The deposition of F1 (Section 8.2.1) is thought to have occurred during MIS 15 and MIS 14, although the lateral extent of the water body appears to have declined, with fluvial incision associated with F3 occurring around MIS 14d (Interval 3, Figs 8.15 c & 8.16 c). During MIS 15e – 13a precessional climate patterns across low latitude regions were interrupted by an abnormally warm and humid period during the MIS 14 glacial (Wang et al. 2004; Prokopenko et al. 2006; Sun et al. 2006; Clemens et al. 2008; Yu & Chen, 2011). Between MIS 15 – 13, these conditions are thought to have helped a perennial water body to occupy the study area (Figs 8.15a & 8.16a).

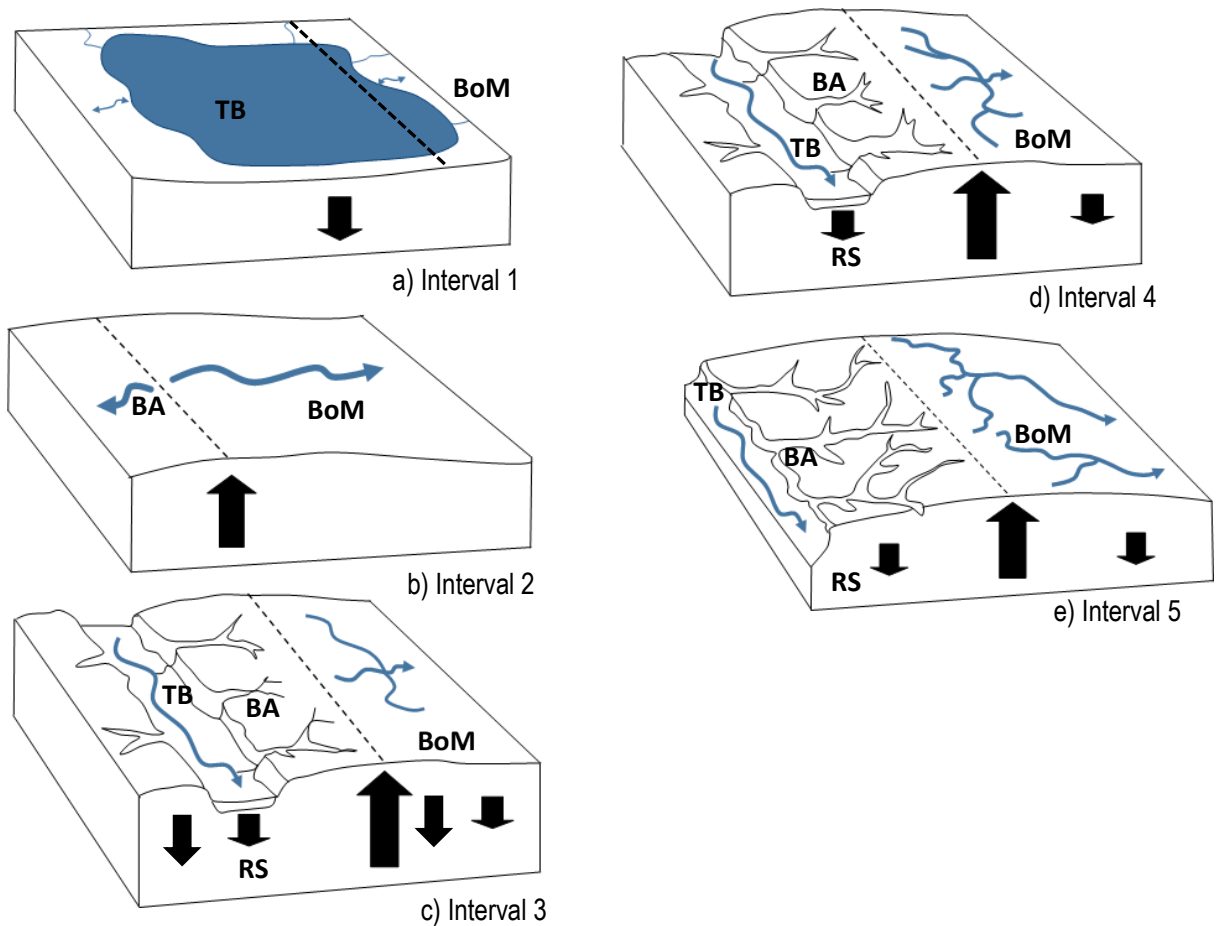


Figure 8.16: Potential tectonic and incisional evolution along of the study area between the Basin of Mexico and the southern hills in the Tequiquiac Basin. Up-lift and/or deformation related to NE – SW oriented normal fault associated with the Cuautitlan horst in the Basin of Mexico (Figs 8.14) likely influenced the study area along its southern margin due to its position immediately north of this end of the horst graben system in the Basin of Mexico. See Fig 8.15 for descriptions of intervals a – e. BA = Barranca Acatlan. RS = Rio Salado. TB = Tequiquiac Basin. Image adapted from Summers, (1991).

Climatic fluctuations will have augmented humidity levels, expressed as depositional cyclicity (Figs 8.3, 8.4, 8.8, 8.10 – 8.12). Potential forcing mechanisms include precessional fluctuations to insolation levels, and on shorter time-scales, changes in the mean position of the ITCZ related to SST, latitudinal gradients, atmospheric surface pressure gradients (Chiang & Bitz, 2005; Hodell et al. 2008), the extent of Northern Hemisphere land and sea ice cover (Chang et al. 1997; Chiang et al. 2002, 2003; Chiang & Bitz, 2005; Hodell et al. 2008), and oceanic circulation patterns (Chang et al. 2007; Hodell et al. 2008). Fluctuations in the TOC content of sediments is possibly a response to climatic anomalies like El Niño (dry) and La Niña (wet) events (e.g. Lake Mono, California, Meyers & Lallier-Vergés, 1999). Increased sediment loading, because of periods of accelerated weathering (F1:1), would have significantly impacted a shallow, laterally expansive water body or bodies causing progressive shallowing during the deposition of F1 (Interval 1, Figs 8.1 - 8.6, 8.8 – 8.12, 8.15a & 8.16a). Without continued deformation, or a rate

of deformation that could keep up with sedimentation (e.g. the Wind River Basin; Carroll & Bohacs, 1999) climate-driven sediment loading would have been exaggerated. It is also possible that localised uplift had started to isolate the water body (Figs 8.14 & 8.16a) hydrologically. The elevation differences (50 m +) between the recorded sections of F1 (Figs 8.1, 8.4, 8.9, 8.10, 8.11 & 8.12) suggest post-depositional uplift, localised deformation and/or that significant erosion of these sediments occurred post-depositionally (Figs 8.1, 8.8, 8.9, 8.14). The elevation differences between the logged sites could represent a palaeo-lake basin profile (Figs 8.11 & 8.12) and a deep palaeolake system that was 66 m ± deep based on the elevation differences of sequences (see Section 8.2.1.4). The sediments documented Facies Group 1 however, do not support this type of depositional system and water depth (see Section 8.2).

8.3.3: Interval 2, > MIS 12c, Playa to mud-flat/marsh environments, Facies Group 2

Depositional episodes in F2:1 (Fig 8.15b & 8.16b, Section 8.2.2) indicate high-frequency changes over relatively short depositional episodes with periods of flooding, standing water, exposure, incision and palustrine alteration (Fig 6.30 & 6.39) suggesting the waterbody was hypersensitive to hydrological change (Freynet & Plaziat, 1982; Tucker & Wright, 1990; Pietras & Carroll, 2006). Sequences like F2 are often found to be expansive in low gradient basins where minor changes to the hydrology of the basin produce high-frequency wetting and drying cycles under climatic and/or tectonic controls (Pietras & Carroll, 2006). In the Teruel Graben, Spain, periods of subsidence enabled basin flooding indicated by sharp erosive basal contacts. A preceding tectonic stasis or equilibrium between subsidence and sediment loading led to marsh development followed by facies that indicate shallow lacustrine environments that were occasionally sub-aerially exposed and altered by palustrine processes (Alonso-Zarza & Calvo, 2000). Similar cyclic conditions would explain F2 where; subsidence and flooding allowed playa type and shallow lacustrine (like F1:2 or F1:3) conditions to develop (like F1:2) followed by sediment loading and mud-flat/marsh (like F1:1) development. Alonso-Zarza & Calvo (2000) relate sub-aerial exposure to depression sediment infill and climate-driven hydrological fluctuations (Figs 8.14 – 8.15a) In the Teruel Graben, which is plausible for the study area. It is also possible that further localised uplift continued to isolate the water body (Fig 8.16b) hydrologically.

Portions of F2 may have been deposited into and during MIS 13 within sub-basinal areas. However, records from the Valles Caldera, New Mexico, show low TOC values and mud cracks related to recurring episodes of high temperature and aridity (Williams, 2011). MIS 13 records indicate conditions were warmer and drier than during MIS 11 (Williams, 2011) which, based on the mud-cracks in the upper facies group suggest similar conditions

across the study area, possibly around the same time. The higher molar ratios of Mg/Ca that are associated with increases in $\delta^{18}\text{O}$ ratios at Site TB9 (e.g. Zone 8, Log 1 Fig 6.39) may indicate less groundwater availability overall, increased ambient temperatures and longer groundwater residence times (Garrett, 2004). A positive shift in $\delta^{13}\text{C}$ values of 3.23‰ from F1 indicates that catchment was significantly drier during the deposition of F2 (Fig 6.39). Consequently, it is possible that conditions were too dry during MIS 13 for deposition to occur based on the Valles Caldera record (Williams, 2011) and geochemical data from Site TB9, and that the drying surface recorded across the south-eastern study area (Zone 10, Fig 6.39) is related to the onset of MIS 13. During this depositional interval, a large Plinian type dacitic eruption impacted the study and the Pachuca sub-basin (Section 8.2.2.2)

8.3.4: Interval 3, MIS 14 d, Alluvial to fluvial environments, Facies Group 3

Together gravels (Facies 15 – 17), sandy beds (Facies 14b) and tephra deposit (Facies 18d) recorded in F3 (Figs, 8.15 c & 8.16 c, Section 8.2.3) are thought to represent fluvial and alluvial terraces (T1) and a switch from an aggradational lacustrine system to a degradational alluvial/fluvial system and the onset of the palaeo-basin incision (Figs 8.14, 8.15c & 8.16c). F3 follows on logically from the shallowing sequence recorded in F1 & F2. For example, in the Wind River Basin (Green River Formation), decreased basin subsidence or equilibrium conditions between subsidence and sedimentation, and a reduction of the tectonic drainage divides, caused sediment loading and a lacustrine regression which allowed throughgoing river systems to develop (Carroll & Bohacs, 1999). Similar conditions are interpreted for the study area. Across Central Mexico, late Pliocene to early Pleistocene fluvial sequences are associated with the disappearance of large lacustrine systems (Israde-Alcantara & Garduño-Monroy, 2010) that were fragmented by Pliocene to Pleistocene tectonism and the establishment of more arid conditions (Israde-Alcantara & Garduño-Monroy, 2010). In the Cuitzeo Basin in central-western Mexico, similar sequences to those recorded in F3 marked the beginning of an erosive episode that co-occurred with block tilting, the onset of fault-controlled fluvial drainage and the demise of the lacustrine system (Israde-Alcantara & Garduño-Monroy, 1999).

8.3.5: Interval 4, < MIS 12c, Fluvio-lacustrine environments, Facies Group 4

The deposition of F4 is associated with the end of MIS 12c and MIS 11 (Fig 8.15 d & 8.16 d, Section 8.2.4). Sequences represent relatively small, ephemeral, evaporitic saline to fresh fluvial-lacustrine pool environments that developed in association to spring activity and elevated groundwater tables. The group is defined by microbial and microdetrital carbonates that are interbedded with muddy carbonates, muds, silts sands and intraclasts and in some sections, sediment gravity flows. During this depositional period, sub-alkaline volcanic was

occurring regionally (F4: 2. Facies, 18a). Moreover, an andesite eruption (F4: 3) (Site TB10, Log 2, Fig 6.19) occurred between 470 ka bp and 5 Ma bp dependent on the source of the tephra (see Chapter 7). Sequences from across the study area show similar depositional characteristics to F1 and F2 (Section 8.2) but F4 suggests that the overall drying trend in the study area continued (TIC 30.9% to 90.4% and $\delta^{13}\text{C}$ -3.3‰ to 1.9‰, Log 2 Site TB9, Fig 6.40) (see Figs 8.15 & 8.16d). F4 is taken to represent the elevation of palaeo-water tables, rather than ambient temperatures, (Capezzuoli et al. 2014), that was a function of water availability controlled by a tectonic and/or climatic influence (Pedley and Rogerson, 2010). Climatic conditions during MIS 11 were unusually long and warm (Farrell & Prell, 1989; Droxler & Farrell, 2000; Tzedakis et al. 2010; Fawcett et al. 2011; Williams, 2011) and circulation patterns were fundamentally different than during any other interglacial. The tropical Pacific was isolated from southern waters and strong El Niño-like and La Niña-like conditions interrupting the normal precessional driven climatic cycles (Mohtadi et al. 2006). During MIS 11 stronger El Niño-like may have supported the drying trend seen in F4 (Figs 8.15 d & 8.16 d). Hydrological variability likely came from La Niña-like cycles (wet), the strength and distribution of other atmospheric pressure systems and precipitation patterns and the mean annual position of the ITCZ (see Chapter 2). While climate is thought to have been a critical factor in the development and demise of these pools, they may also indicate a tectonic signal related to uplift, expressed as normal faulting (Fig 8.8) along the southern margin of the study area, changing paleo-water tables and the isolation of portions of San Jose Hill from the palaeo-water tale.

8.3.6: Interval 5, < MIS 3 Alluvial – fluvial environments, Facies Group 5

It is presupposed that the deposition of the F5 gravels occurred as part of on-going basin-wide incision that removed large portions the Facies Groups 1, 2 & 4 (Figs 8.4, 8.15e & 8.16e). A regional climatically generated signal likely helped the T2 incisional phase during MIS 3. Overall a high degree of climatic variability appears to have occurred between 50,000 and 34,070 cal. Bp with conditions cycling between wet and dry (see Chapter 2, Figs 2.6 & 2.7) seemingly with the T2 gravels (Fig 8.15e & 8.16e) being deposited during vegetation low when slopes were exposed and unstable, maybe during Heinrich Event 2 (Figs 2.6 & 2.7). Similar deposits associated with extreme rainfall, laharic events and limited vegetation cover either in response to climatic aridity and low moisture and/or land clearing have been recorded in Central Mexico, (Borejsza & Frederick, 2009; Solleiro-Redolledo et al. 2011; Mueller et al., 2012).

During MIS 2, around the time T3 was deposited (^{14}C 17,695 cal. BP) conditions were dry across the Basin of Mexico, and temperatures remained cool (Figs 2.6 & 2.7). Early during MIS 1 data from the Basin of Mexico broadly agree (Lamb et al. 2009; Cantarero, 2013; Lozano et al. 2015; Torres-Rodríguez et al. 2015) that precipitation levels began to increase after ca. 14,750 cal. BP in the Basin of Mexico, which corresponds to the ephemeral meadow to marsh conditions interpreted for the upper sections of T3.

While climate is thought to have been a contributing factor for the hydrological base-level change, F5 may indicate a period of incision related to localised uplift, deformation, and/or localised normal faulting (Fig 8.8, 8.14, 8.15e, 8.16b). In Mezquital Valley, there are two east-west trending normal faults moving at a rate of 0.02 mm/yr that currently have 30 m of Quaternary throw (Suter et al. 2001) along the southern margin (Fig 8.14). The Tarango Formation, which covers the lower basin and extends partway up the surrounding slopes and mountains, has been rapidly dissected by the Rio Tula and its tributaries. In some sections, the Tarango Formation exposes a maximum thickness of 400 m in escarpments (Segerstrom, 1962) suggesting an equal degree of the incision. Thus, the removal of the Pliocene/Pleistocene basin-fill sequence (Tarango Formation) in the Mezquital Valley is thought to have occurred through a combination of faulting (Kowallis et al. 1998; Suter et al. 2001) and hydrological incision and erosion (Segerstrom, 1962) and the same is probably accurate for the study area. Since MIS 14 (Site TB17, Logs 1 & 2, T1) there have been 105 m+ of incision based on the elevation difference between Site TB17 (T1) and the elevation of the Rio Salado, at its lowest ca. 2200 m a.s.l (Figs 8.1, 8.5, 8.9 8.15 e & 8.16 e). The incision is thought to have occurred via a combination of deformation and uplift, providing relief coupled with climate-driven degradation (Figs 8.14 – 8.16).

8.6: Conclusion

The five main facies groups with distinctly different and recognisable sedimentary characteristics have been characterised and interpreted. Chapter 9 summarises and concludes these findings.

Chapter Nine: Conclusions

9.1: Original thesis aims and research outcomes

Research for this thesis carried out in the Tequixuiac Basin aimed to establish a Quaternary depositional history from a previously unstudied area in eastern Central Mexico. From the depositional history, the research aimed to interpret a palaeogeographic and palaeoenvironmental history for the study area (e.g. Table 1.1 & Figs 2.6 & 2.8) to reconstruct the basins evolution throughout the Quaternary. A further aim was to examine if the Quaternary sedimentary succession had the potential to extend the Central Mexican environmental record beyond the last 90,000 years. The following objectives were developed to achieve the thesis aims:

- 1: To carry out basin-wide stratigraphic logging, focused on the Quaternary succession, to establish a mid to late Pleistocene to early Holocene lithostratigraphic record of deposition for the study area.
- 2: To select key, representative stratigraphic sections of the logged sequence to build a detailed sedimentological, isotopic ($\delta^{18}\text{O}$ & $\delta^{13}\text{C}$) and geochemical record for depositional episodes.
- 3: To date, available material to build a geochronological framework for the study area to allow the identification of the timing of depositional events.
- 4: To combine objectives one to three to develop a spatial and temporal Palaeogeographic and Palaeoenvironmental model for the study area.

By these objectives, a mid to late Pleistocene palaeoenvironmental and palaeogeographic history for the study area has now been established which extends the current knowledge of Quaternary environmental change beyond MIS 5 to at least MIS 15, although significant depositional gaps exist in the record. Five primary depositional environments and facies groups have been characterised (Figs 8.1 - 8.15). The first four are associated with the Tarango Formation and the fifth the later Quaternary alluvial deposits, both of which had previously been reported for the study area (see Chapters 1 & 3). The geochronological framework established here has constrained the depositional episodes and allowed facies groups to be linked spacially across the study area (Figs 8.1 – 8.16). The five identified depositional environment include:

Facies Group 1) Perennial lacustrine conditions associated with the Lower Colores Formation deposited before MIS 12c (likely before and during MIS 15 up to MIS 14) that cycled between an oxygen-rich playa type lake, oxygen-poor, occasionally eutrophic wetland, and relatively fresh clear waters (Facies Group 1, Section 8.2.1, Fig 8.15 a & 8.16 a). Positive values of $\delta^{18}\text{O}$ with a mean of -5.4‰ (Fig 6.39) also suggest that palaeo-airmasses were

different from those recognised for today (Fig 8.15a). Controls on water depth and lateral extent are thought to have been a combination of climate-driven hydrological change and weathering, coupled with a deformational stasis, or a slowing of subsidence rates that caused sediment loading into a shallow water body and possible faulting affecting drainage divides and hydrological connectivity. Overall these environments show decreasing available moisture and represent a shallowing lacustrine system.

Facies Group 2) Before MIS 12c, likely from MIS 14 until MIS 13, a shallow ephemeral water body or bodies occupied the study area (Facies Group 2, Section 8.2.2, Fig 8.15b & 8.16b). Decreasing moisture availability follows on from F1, and the stratigraphy represents periodic subsidence, flooding, infill, exposure and erosion cycles that created the relatively thin beds deposited over shorter/ephemeral depositional episodes (Section 8.2.2). The $\delta^{18}\text{O}$ values associated with F2 (Fig 6.39) indicate that precipitation reaching the study area during this depositional interval was similar to today. Sub-alkaline volcanic activity linked to the Donguinyó-Huichapan Caldera system was occurring regionally.

Facies Group 3) During MIS 14d fluvial and alluvial deposition associated with the onset of palaeo-basin incision were active. The resulting deposits suggest a major hydrological and depositional shift from aggradational lacustrine system to an alluvial-fluvial system, and they mark the onset of a significant incisional and erosional phase that is still ongoing today. Incision (15 m +) that occurred during Interval 3 (Fig 8.15c & 8.16c) could be related to 1) a reduction of the drainage divides, 2) the establishment of a low hydrological divide to the south (Fig 8.16c) causing down-cutting, 3) the warm humid conditions interpreted for MIS 14 (Wang et al. 2004; Yu & Chen. 2011) possibly under La Niña-like conditions.

Facies Group 4) Relatively small, ephemeral, evaporitic pools developed in the study area during MIS 11. The pools formed in close association with barranca heads linked to spring activity and high groundwater tables that promoted microbial and microdetrital carbonate formation (Facies Group 4). During MIS 11 warm-arid conditions are linked to stronger El Niño-like climate cycles F4 (Figs 8.15 d & 8.16 d) with hydrological variability recorded in the study area possibly coming from La Niña-like phases (see Section 8.3.5). While climate is thought to have been critical to the development of F4, deposits may also indicate a tectonic signal related to localised uplift, normal faulting (Fig 8.8) and/or deformation. These factors are expected to have caused changing paleo-water table elevations and the isolation of portions of San Jose Hill away from the palaeo-water table (Figs 8.15 d & 8.16 d). During this period the basin was under the influence of sub-alkaline volcanic activity related to the

Donguinyó-Huichapan Caldera system indicated by the basaltic-andesitic tephra layer (F4: 2) and andesitic volcanic activity (F4: 3).

Facies Group 5) Between MIS 3 and MIS 1 the deposition of the fluvial and alluvial sands and gravels associated with F 5 (T2 & T3) occurred as part of on-going basin-wide incision that removed large portions the Facies Groups 1, 2 & 4 (Figs 8.4, 8.15e & 8.16e). During the deposition of T2, the regional climate was variable (50,000 and 34,070 cal. Bp) and deposition coincides with Heinrich Event 2 (Figs 2.6 & 2.7). During the deposition of T3 (MIS 2: ^{14}C 17,695 cal. BP), conditions were cool and dry (Figs 2.6 & 2.7) until early during MIS 1 when precipitation levels began to increase in the Basin of Mexico after ca. 14,750 cal. BP. While climate is thought to have been a contributing factor for the hydrological base-level change, F5 may indicate a period of incision related to localised uplift, deformation, and/or localised normal faulting (Fig 8.8, 8.14, 8.15e, 8.16b). Between MIS 14 and MIS 3, 33 m + of incision occurred along Barranca Acatlan (Site TB1) and Agua Negra (Site TB2) based on the elevational difference between T1 deposits and T2 deposits (Figs 8.1, 8.9, 8.10, 8.15 e & 8.16 e). By MIS 2 a further 30 m + of incision had occurred between, for example, Sites TB9 and TB2 (Fig 8.10: T3). The base level of the palaeo-barrancas indicates the degree of incision that was available to be filled at these sites during MIS 3 (ca 8 m, Site TB9). Since then, until today, over 60 m of Facies Groups 1, 2, 4 & 5 have been exposed at several locations in the study area (see Figs 8.1 – 8.13, 8.15e & 8.16e). The incision has helped create a significant unconformity in the basin and a stratigraphic gap between MIS 14 and MIS 3 that separates the Facies Group 3 and from Facies Group 5.

9.2: Limitations

The primary limitation placed upon this research was the absence of previous research both from the study area and from across Mexico that covered the same period. Having this would have given the research a platform from which to launch and a foundation from which to work. Regarding the study area, difficulty dating the sequence was a significant problem and one that has made interpreting the depositional history of the study area complicated in terms of the depositional period and potential hiatuses.

9.3: Future work

Further work in the Tequixquiac Basin is undoubtedly warranted as the sedimentological work carried out here has indicated. There are several sequences of terrestrial limestone that, because of the dating and geochemical characterisation of interbedded tephra layers here, have the potential to produce high-resolution,

annual-scale $\delta^{18}\text{O}$ and $\delta^{13}\text{C}$ records of paleoenvironmental change for MIS 13 & 11 that could also be combined with other proxy data from the limestone sequence, i.e. pollen and diatoms. Several tephra layers could be analysed, characterised and used in the same way as those identified by this research to build a more robust tephrochronology for the study area and give a better understanding of Pliocene – Quaternary volcanism in the northern sub-basins of central-eastern Mexico, which is still poorly understood. This is important as, based on the Ar/Ar ages of the tephra layers recorded by this research, Pliocene – Quaternary volcanism was occurring north of the Basin of Mexico much later than was previously thought. Because of the absence of previous work, and limitations placed on the number of samples that could be analysed, this research spread a blanket out over the research areas to test the viability of the Quaternary sequences to provide a chronologically controlled record of palaeoenvironmental change.

At the Site TB9, a 55 m vertical section was sampled at low-resolution for stable isotope and geochemical analysis, and the resulting findings and interpretations of these have yielded the oldest record of paleolimnological change from Mexico. There are several similar sequences exposed in the study area that could also be analysed in detail, and at a better resolution, in addition to the sequence at Barranca de Colores. This would likely provide a detailed record of Pliocene-Pleistocene environmental. Looking at the C/N ratios of the lake sediments, for example, would give more information about the productivity of the catchment and the lake supporting the TIC and TOC values and making the record more robust. Within these sequences, the muddy carbonate beds, calc-muds and limestone interbed could also provide a higher resolution $\delta^{18}\text{O}$ and $\delta^{13}\text{C}$ record of palaeoenvironmental change that could offer an annual or interannual temperature record.

9.4: Conclusions

This thesis has demonstrated the potential of the Quaternary sediment sequences in the Tequixquiac basin to contain detailed palaeoenvironmental data. The abundance of exposed sedimentary sequences that span at least as far back as MIS 14 suggests that records older than 500 ka bp are easily obtainable and that they would cover multiple glacial and interglacial cycles. Terrestrial sequences that cover MIS 11, 13 - 15 are sort after, mainly from low-latitude regions and multiple sections from the study area could be examined and correlated with tephra stratigraphy and chronology. Further, from a local perspective, this study has challenged previous assumptions that during the Quaternary, the north-eastern sub-basins of Mexico were tectonically stable, and that fault movement and volcanic activity had mostly ceased.

- Adamson, K., Candy, I. and Whitfield, L., 2015. Coupled micromorphological and stable isotope analysis of Quaternary calcrete development. *Quaternary Research*, 84(2), pp.272-286.
- Aguirre-Díaz, G.D.J., ZÚÑIGA DÁVILA, F.R., Pacheco Alvarado, F.J., Guzmán Speziale, M. and Y NIETO OBREGÓN, J., 2000. El graben de Querétaro, Mexico, observaciones de fallamiento activo. *Unión Geofísica Mexicana, Geos*, 20(1), pp.2-7.
- Alaniz-Álvarez, S.A., Nieto-Samaniego, Á.F. and Mexicana, S.G. eds., 2007. *Geology of México: Celebrating the centenary of the Geological Society of México* (Vol. 422). Geological Society of America.
- Alaniz-Álvarez, S.A., Nieto-Samaniego, Á.F., 2007. The Taxco-San Miguel de Allende fault system and the Trans-Mexican Volcanic Belt: two tectonic boundaries in central Mexico active during the Cenozoic., In: Alaniz-Álvarez, S.A., Nieto-Samaniego, Á.F., (Eds.), *Geology of Mexico: Celebrating the Centenary of the Geological Society of México: Geological Society of America Special Paper*, 422: 301 - 316.
- Alberdi, M.T., Arroyo-Cabrales, J., Marín-Leyva, A.H. and Polaco, O.J., 2014. Study of Cedral Horses and their place in the Mexican Quaternary. *Revista Mexicana de Ciencias Geológicas*, 31(2).
- Allen, J.R.L., 1986. Pedogenic calcretes in the Old Red Sandstone facies (late Silurian-early Carboniferous) of the Anglo-Welsh area, southern Britain. *Paleosols. Their recognition and interpretation*, pp.58-86.
- Alonso-Zarza, A.M. and Tanner, L.H., 2010. *Carbonates in continental settings: facies, environments, and processes* (Vol. 61). Elsevier.
- Alonso-Zarza, A.M. and Wright, V.P., 2010a. Palustrine Carbonates. *Developments in Sedimentology*, 61, pp.103-131.
- Alonso-Zarza, A.M. and Wright, V.P., 2010b. Calcretes. *Developments in Sedimentology*, 61, pp.225-267.
- Alonso-Zarza, A.M., 1999. Initial stages of laminar calcrete formation by roots: examples from the Neogene of central Spain. *Sedimentary Geology*, 126(1), pp.177-191.
- Alonso-Zarza, A.M., 2003. Palaeoenvironmental significance of palustrine carbonates and calcretes in the geological record. *Earth-Science Reviews*, 60(3), pp.261-298.
- Alonso-Zarza, A.M., Sanz, M.E., Calvo, J.P. and Estévez, P., 1998. Calcified root cells in Miocene pedogenic carbonates of the Madrid Basin: evidence for the origin of *Microcodium* b. *Sedimentary Geology*, 116(1-2), pp.81-97.
- Alonso-Zarza, A.A., Calvo, J.P. and Del Cura, M.G., 1992. Palustrine sedimentation and associated features-grainification and pseudo-microkarst-in the Middle Miocene (Intermediate Unit) of the Madrid Basin, Spain. *Sedimentary Geology*, 76(1-2), pp.43-61.
- Anadón, P., Cabrera, L. and Kelts, K. eds., 1991. *Lacustrine Facies Analysis*. Blackwell.
- Anderson, N.J. and Leng, M.J., 2004. Increased aridity during the early Holocene in West Greenland inferred from stable isotopes in laminated-lake sediments. *Quaternary Science Reviews*, 23(7), pp.841-849.
- Anderson, R.S., Jiménez-Moreno, G., Ager, T. and Porinchu, D.F., 2014. High-elevation paleoenvironmental change during MIS 6-4 in the central Rockies of Colorado as determined from pollen analysis. *Quaternary Research*, 82(3), pp.542-552.
- Anderton, R., 1985. *Clastic facies models and facies analysis*. Geological Society, London, Special Publications, 18(1), pp.31-47.
- Andrews, J.E. 2006. Palaeoclimatic records from stable isotopes in riverine tufas: Synthesis and review. *Earth-Science Reviews Isotopes in Palaeoenvironmental reconstruction (ISOPAL)*, 75: 85-104.
- Andrews, J.E. and Brasier, A.T., 2005. Seasonal records of climatic change in annually laminated tufas: short review and future prospects. *Journal of Quaternary Science*, 20(5), pp.411-421.
- Andrews, J.E., 2006. Palaeoclimatic records from stable isotopes in riverine tufas: synthesis and review. *Earth-Science Reviews*, 75(1-4), pp.85-104.

- Andrews, J.E., Riding, R. and Dennis, P.F., 1997. The stable isotope record of environmental and climatic signals in modern terrestrial microbial carbonates from Europe. *Palaeogeography, Palaeoclimatology, Palaeoecology*, 129(1-2), pp.171-189.
- Andrews, J.T. and Barber, D.C., 2002. Dansgaard-Oeschger events: is there a signal off the Hudson Strait Ice Stream?. *Quaternary Science Reviews*, 21(1), pp.443-454.
- Arakel, A.V., 1982. Genesis of calcrete in Quaternary soil profiles, Hutt and Leeman lagoons, Western Australia. *Journal of Sedimentary Research*, 52(1).
- Arce, J.L., Cervantes, K.E., Macías, J.L. and Mora, J.C., 2005. The 12.1 ka Middle Toluca Pumice: A dacitic Plinian-subplinian eruption of Nevado de Toluca in central Mexico. *Journal of Volcanology and Geothermal Research*, 147(1), pp.125-143.
- Arce, J.L., Layer, P.W., Morales-Casique, E., Benowitz, J.A., Rangel, E. and Escolero, O., 2013. New constraints on the subsurface geology of the Mexico City Basin: The San Lorenzo Tezonco deep well, on the basis of $^{40}\text{Ar}/^{39}\text{Ar}$ geochronology and whole-rock chemistry. *Journal of Volcanology and Geothermal Research*, 266, pp.34-49.
- Arce, J.L., Macías, J.L. and Vázquez-Selem, L., 2003. The 10.5 ka Plinian eruption of Nevado de Toluca volcano, Mexico: Stratigraphy and hazard implications. *Geological Society of America Bulletin*, 115(2), pp.230-248.
- Arenas, C., Cabrera, L. and Ramos, E., 2007. Sedimentology of tufa facies and continental microbialites from the Palaeogene of Mallorca Island (Spain). *Sedimentary Geology*, 197(1), pp.1-27.
- Arenas-Abad, C., Vázquez-Urbez, M., Pardo-Tirapu, G. and Sancho-Marcén, C., 2010. Fluvial and associated carbonate deposits. *Developments in Sedimentology*, 61, pp.133-175.
- Armenteros, I., Daley, B. and García, E., 1997. Lacustrine and palustrine facies in the Bembridge Limestone (late Eocene, Hampshire Basin) of the Isle of Wight, southern England. *Palaeogeography, Palaeoclimatology, Palaeoecology*, 128(1-4), pp.111-132.
- Arp, G., Reimer, A. and Reitner, J., 2001. Photosynthesis-induced biofilm calcification and calcium concentrations in Phanerozoic oceans. *Science*, 292(5522), pp.1701-1704.
- Arreygue-Rocha, E., 1999. Le condizioni di pericolosità idrogeologica nella città di Morelia, Michoacan (Messico). Tesi di dottora to XI Ciclo 1995-1998, Università degli studi di Perugia. 171pp.
- Arroyo-Cabrales, J. and Polaco, O.J., 2003. Caves and the Pleistocene vertebrate paleontology of Mexico. *Ice Age cave faunas of North America* (BW Schubert, JI Mead, and RW Graham, editors). Indiana University Press, Bloomington, pp.273-291.
- Arroyo-Cabrales, J., Polaco, O.J. and Johnson, E., 2006. A preliminary view of the coexistence of mammoth and early peoples in Mexico. *Quaternary International*, 142, pp.79-86.
- Assereto, R.L. and Kendall, C.G., 1977. Nature, origin and classification of peritidal tepee structures and related breccias. *Sedimentology*, 24(2), pp.153-210.
- Asta, M.P., Auqué, L.F., Sanz, F.J., Gimeno, M.J., Acero, P., Blasco, M., García-Alix, A., Gómez, J., Delgado-Huertas, A. and Mandado, J., 2017. Travertines associated with the Alhama-Jaraba thermal waters (NE, Spain): Genesis and geochemistry. *Sedimentary Geology*, 347, pp.100-116.
- Aveleyra Arroyo de Anda, L., 1950. Prehistoria de Mexico. Ediciones Mexicanas, SA Mexico City, Mexico, 167.
- Aveleyra de Anda, L.A.A., 1965. The Pleistocene Carved Bone from Tequixquiac, Mexico: A Reappraisal. *American Antiquity*, pp.261-277.
- Aveleyra, L., 1964. El sacro de Tequixquiac. *Cuadernos del Museo Nacional de Antropología*, 2, pp.9-52.
- Avilés, J. and Pérez-Rocha, L.E., 2010. Regional subsidence of Mexico City and its effects on seismic response. *Soil Dynamics and Earthquake Engineering*, 30(10), pp.981-989.
- Báez, A., Belmont, R., García, R., Padilla, H. and Torres, M.D.C., 2007. Chemical composition of rainwater collected at a southwest site of Mexico City, Mexico. *Atmospheric Research*, 86(1), pp.61-75.

- Bárcena, M., 1882. Antropología.-Descripción de un hueso labrado, de llama fósil, encontrado en los terrenos postterciarios de Tequixquiac, Estado de México.-Estudio. *Anales del Museo Nacional de México, primera época (1877-1903)*, 2, pp.439-444.
- Barker, P., Gasse, F., Roberts, N. and Taieb, M., 1990. Taphonomy and diagenesis in diatom assemblages; a Late Pleistocene palaeoecological study from Lake Magadi, Kenya. In *Environmental History and Palaeolimnology* (pp. 267-272). Springer Netherlands.
- Barker, P., Telford, R., Gasse, F. and Thevenon, F., 2002. Late Pleistocene and Holocene palaeohydrology of Lake Rukwa, Tanzania, inferred from diatom analysis. *Palaeogeography, Palaeoclimatology, Palaeoecology*, 187(3), pp.295-305.
- Bar-Matthews, M., Ayalon, A. and Kaufman, A., 1998. Middle to Late Holocene (6,500 yr. period) paleoclimate in the Eastern Mediterranean region from stable isotopic composition of speleothems from Soreq Cave, Israel. In *Water, environment and society in times of climatic change* (pp. 203-214). Springer Netherlands.
- Barnes CJ, Allison GB (1988) Tracing of water movement in the unsaturated zone using stable isotopes of hydrogen and oxygen. *J Hydrol* 100:143-176.
- Battarbee, R.W., Jones, V.J., Flower, R.J., Cameron, N.G., Bennion, H., Carvalho, L. and Juggins, S., 2002. *Diatoms* (pp. 155-202). Springer Netherlands.
- Behling, H., 2002. Carbon storage increases by major forest ecosystems in tropical South America since the Last Glacial Maximum and the early Holocene. *Global and Planetary Change*, 33(1), pp.107-116.
- Beier, J.A., 1987. Petrographic and geochemical analysis of caliche profiles in a Bahamian Pleistocene dune. *Sedimentology*, 34(6), pp.991-998.
- Benvenuti, M., 2003. Facies analysis and tectonic significance of lacustrine fan-deltaic successions in the Pliocene-Pleistocene Mugello Basin, Central Italy. *Sedimentary Geology*, 157(3), pp.197-234.
- Berglund, B.E. and Ralska-Jasiewiczowa, M., 1986. *Handbook of Holocene palaeoecology and palaeohydrology*. Handbook of Holocene palaeoecology and palaeohydrology.
- Bershaw, J., Penny, S.M. and Garzione, C.N., 2012. Stable isotopes of modern water across the Himalaya and eastern Tibetan Plateau: Implications for estimates of paleoelevation and paleoclimate. *Journal of Geophysical Research: Atmospheres*, 117(D2).
- Bertini, A., Minissale, A. and Ricci, M., 2014. Palynological approach in upper Quaternary terrestrial carbonates of central Italy: anything but a 'mission impossible'. *Sedimentology*, 61(1), pp.200-220.
- Bibliography**
- Bogard, D.D., 1995. Impact ages of meteorites: A synthesis. *Meteoritics & Planetary Science*, 30(3), pp.244-268.
- Boggs, S., 2006. *Principles of sedimentology and stratigraphy*, fourth edition. Pearson prentice Hall, Upper Saddle River, New Jersey, US.
- Bond, G., Heinrich, H., Broecker, W., Labeyrie, L., McManus, J., Andrews, J., Huon, S., Jantschik, R., Clasen, S., Simet, C. and Tedesco, K., 1992. Evidence for massive discharges of icebergs into the North Atlantic ocean during the last glacial period. *Nature*, 360(6401), pp.245-249.
- Borejsza, A. and Frederick, C.D., 2010. Fluvial response to Holocene climate change in low-order streams of central Mexico. *Journal of Quaternary Science*, 25(5), pp.762-781.
- Bourgeon, L., Burke, A. and Higham, T., 2017. Earliest Human Presence in North America Dated to the Last Glacial Maximum: New Radiocarbon Dates from Bluefish Caves, Canada. *PLoS one*, 12(1), p.e0169486.
- Bowman, S., 1990. *Radiocarbon dating (Vol. 1)*. Univ of California Press.
- Boyd, R., Dalrymple, R.W. and Zaitlin, B.A., 2006. Estuarine and incised-valley facies models. *SPECIAL PUBLICATION-SEPM*, 84, p.171.
- Bradbury, J.P., 1971. Paleolimnology of Lake Texcoco, Mexico. Evidence from diatoms. *Limnology and Oceanography*, 16(2), pp.180-200.

- Bradbury, J.P., 1989. Late Quaternary lacustrine paleoenvironments in the Cuenca de Mexico. *Quaternary Science Reviews*, 8(1), pp.75-100.
- Bradbury, J.P., 1997. Sources of glacial moisture in Mesoamerica. *Quaternary International*, 43, pp.97-110.
- Braithwaite, C.J.R., 1989. Displacive calcite and grain breakage in sandstones. *Journal of Sedimentary Research*, 59(2).
- Brasier, A.T., 2011. Searching for travertines, calcretes and speleothems in deep time: processes, appearances, predictions and the impact of plants. *Earth-Science Reviews*, 104(4), pp.213-239.
- Bravo-Cuevas, V.M., Priego-Vargas, J., Cabral-Perdomo, M.Á. and Pineda Maldonado, M.A., 2016. First occurrence of *Panthera atrox* (Felidae, Pantherinae) in the Mexican state of Hidalgo and a review of the record of felids from the Pleistocene of Mexico. *Fossil Record*, 19(2), pp.131-141.
- Brennan, R. and Quade, J., 1997. Reliable Late-Pleistocene Stratigraphic Ages and Shorter Groundwater Travel Times from ¹⁴C in Fossil Snails from the Southern Great Basin. *Quaternary Research*, 47(3), pp.329-336.
- Brett, M.J., Baldini, J.U. and Gröcke, D.R., 2014. Environmental controls on stable isotope ratios in New Zealand Podocarpaceae: Implications for palaeoclimate reconstruction. *Global and Planetary Change*, 120, pp.38-45.
- Broecker, W.S., 2003. Does the trigger for abrupt climate change reside in the ocean or in the atmosphere?. *Science*, 300(5625), pp.1519-1522.
- Bronk Ramsey, C., 2008. Radiocarbon dating: revolutions in understanding. *Archaeometry*, 50(2), pp.249-275.
- Brook, G.A., Ellwood, B.B., Railsback, L.B. and Cowart, J.B., 2006. A 164 ka record of environmental change in the American Southwest from a Carlsbad Cavern speleothem. *Palaeogeography, Palaeoclimatology, Palaeoecology*, 237(2-4), pp.483-507.
- Brown, E.T., Werne, J.P., Lozano-García, S., Caballero, M., Ortega-Guerrero, B., Cabral-Cano, E., Valero-Garces, B.L., Schwalb, A. and Arciniega-Ceballos, A., 2012. Scientific drilling in the basin of Mexico to evaluate climate history, hydrological resources, and seismic and volcanic hazards. *Scientific Drilling*, 14, pp.72-75.
- Brunner, C.A., 1982. Paleooceanography of surface waters in the Gulf of Mexico during the late Quaternary. *Quaternary Research*, 17(1), pp.105-119.
- Bull, W.B., 1997. Discontinuous ephemeral streams. *Geomorphology*, 19(3-4), pp.227-276.
- Burjachs, F. and Julià, R., 1994. Abrupt climatic changes during the last glaciation based on pollen analysis of the Abric Romani, Catalonia, Spain. *Quaternary Research*, 42(3), pp.308-315.
- Caballero, M. and Guerrero, B.O., 1998. Lake levels since about 40,000 years ago at Lake Chalco, near Mexico City. *Quaternary Research*, 50(1), pp.69-79.
- Caballero, M. and Ortega, G.B., 1998. Lake levels since about 40,000 years ago at Lake Chalco, near Mexico City. *Quaternary Research*, 50(1), pp.69-79.
- Caballero, M., 1997. The last glacial maximum in the basin of Mexico: the diatom record between 34,000 and 15,000 years BP from Lake Chalco. *Quaternary International*, 43, pp.125-136.
- Caballero, M., Lozano, S., Ortega, B., Urrutia, J. and Macias, J.L., 1999. Environmental characteristics of Lake Tecocomulco, northern basin of Mexico, for the last 50,000 years. *Journal of Paleolimnology*, 22(4), pp.399-411.
- Caballero, M., Lozano-García, S., Vázquez-Selem, L. and Ortega, B., 2010. Evidencias de cambio climático y ambiental en registros glaciales y en cuencas lacustres del centro de México durante el último máximo glacial. *Boletín de la Sociedad Geológica Mexicana*, 62(3), pp.359-377.
- Caballero, M., Ortega, B., Valadez, F., Metcalfe, S., Macias, J.L. and Sugiura, Y., 2002. Sta. Cruz Atizapán: a 22-ka lake level record and climatic implications for the late Holocene human occupation in the Upper Lerma Basin, Central Mexico. *Palaeogeography, Palaeoclimatology, Palaeoecology*, 186(3), pp.217-235.
- Caballero, M.C., 1997. The last glacial maximum in the basin of Mexico: the diatom record between 34,000 and 15,000 years BP from Lake Chalco. *Quaternary International*, 43, pp.125-136.
- Cameron, N.G., 1995. The representation of diatom communities by fossil assemblages in a small acid lake. *Journal of Paleolimnology*, 14(2), pp.185-223.

- Campos - Enríquez, J., Sánchez - Zamora, O., 2000. Crustal structure across Southern Mexico, inferred from gravity data. *Journal of South America Earth Sciences*, 13: 479 - 489.
- Campos-Martínez, M.S. and Pérez-Roldán, G., WORKED HUMAN BONE FROM TEOTIHUACAN, MEXICO (1ST-6TH CENTURIES AD). *Close to the bone: current studies in bone technologies*, p.98.
- Camuera, J., Alonso-Zarza, A.M., Rodríguez-Berriguete, Á. and Meléndez, A., 2015. Variations of fluvial tufa sub-environments in a tectonically active basin, Pleistocene Teruel Basin, NE Spain. *Sedimentary Geology*, 330, pp.47-58.
- Candy, I., Abrook, A., Elliot, F., Lincoln, P., Matthews, I.P. and Palmer, A., 2016. Oxygen isotopic evidence for high?magnitude, abrupt climatic events during the Lateglacial Interstadial in north?west Europe: analysis of a lacustrine sequence from the site of Tirinie, Scottish Highlands. *Journal of Quaternary Science*, 31(6), pp.607-621.
- Candy, I., Adamson, K., Gallant, C.E., Whitfield, E. and Pope, R., 2012. Oxygen and carbon isotopic composition of Quaternary meteoric carbonates from western and southern Europe: their role in palaeoenvironmental reconstruction. *Palaeogeography, Palaeoclimatology, Palaeoecology*, 326, pp.1-11.
- Candy, I., Farry, A., Darvill, C.M., Palmer, A., Blockley, S.P.E., Matthews, I.P., MacLeod, A., Deepprose, L., Farley, N., Kearney, R. and Conneller, C., 2015. The evolution of Palaeolake Flixton and the environmental context of Star Carr: an oxygen and carbon isotopic record of environmental change for the early Holocene. *Proceedings of the Geologists' Association*, 126(1), pp.60-71.
- Cant, D.J. and Walker, R.G., 1976. Development of a braided-fluvial facies model for the Devonian Battery Point Sandstone, Quebec. *Canadian Journal of Earth Sciences*, 13(1), pp.102-119.
- Cantagrel, J.M. and Robin, C., 1979. K-Ar dating on eastern Mexican volcanic rocks-relations between the andesitic and the alkaline provinces. *Journal of volcanology and geothermal research*, 5(1-2), pp.99-114.
- Cantarero, S., 2013. Multiproxy paleoclimatic record from geochemical analyses of Lake Chalco sediments, a closed basin lake in central Mexico. University of Minnesota.
- Capezzuoli, E., Gandin, A. and Pedley, M., 2014. Decoding tufa and travertine (fresh water carbonates) in the sedimentary record: The state of the art. *Sedimentology*, 61(1), pp.1-21.
- Capra, L., Bernal, J.P., Carrasco-Núñez, G. and Roverato, M., 2013. Climatic fluctuations as a significant contributing factor for volcanic collapses. Evidence from Mexico during the Late Pleistocene. *Global and Planetary Change*, 100, pp.194-203.
- Capra, L., Mac?as, J.L., Scott, K.M., Abrams, M. and Garduño-Monroy, V.H., 2002. Debris avalanches and debris flows transformed from collapses in the Trans-Mexican Volcanic Belt, Mexico-behavior, and implications for hazard assessment. *Journal of Volcanology and Geothermal Research*, 113(1-2), pp.81-110.
- Carroll, A.R. and Bohacs, K.M., 1999. Stratigraphic classification of ancient lakes: Balancing tectonic and climatic controls. *Geology*, 27(2), pp.99-102.
- Caso, J.M.R., 2010. El bulldog y el arzobispo: una discusión evolutiva.
- Castro, C.L., McKee, T.B. and Pielke Sr, R.A., 2001. The relationship of the North American monsoon to tropical and North Pacific sea surface temperatures as revealed by observational analyses. *Journal of Climate*, 14(24), pp.4449-4473.
- Catuneanu, O., 2006. *Principles of sequence stratigraphy*. Elsevier.
- Catuneanu, O., Galloway, W.E., Kendall, C.G.S.C., Miall, A.D., Posamentier, H.W., Strasser, A. and Tucker, M.E., 2011. Sequence stratigraphy: methodology and nomenclature. *Newsletters on stratigraphy*, 44(3), pp.173-245.
- Cervantes - Mendel, A., Armienta, M, A., 2004. Influence of faulting on groundwater quality in the Valle del Mezquita, Mexico. *Geofísica Internacional* 43: 3 477 - 493
- Chafetz, H., Rush, P.F. and Utech, N.M., 1991. Microenvironmental controls on mineralogy and habit of CaCO₃ precipitates: an example from an active travertine system. *Sedimentology*, 38(1), pp.107-126.
- Chafetz, H.S. and Folk, R.L., 1984. Travertines: depositional morphology and the bacterially constructed constituents. *Journal of Sedimentary Research*, 54(1).

- Chafetz, H.S., Utech, N.M. and Fitzmaurice, S.P., 1991b. Differences in the ^{18}O and ^{13}C signatures of seasonal laminae comprising travertine stromatolites. *Journal of Sedimentary Research*, 61(6).
- Chang, C., 2007. Impacts, Adaptation and Vulnerability. Contribution of Working Group II to the Fourth Assessment Report of the Intergovernmental Panel on Climate Change/ML Parry, OF Canziani, JP Palutikof et al., eds.
- Chang, P., Ji, L. and Li, H., 1997. A decadal climate variation in the tropical Atlantic Ocean from thermodynamic air-sea interactions. *Nature*, 385(6616), p.516.
- Chen, Y., 2013. Early Holocene vegetation dynamics of lake Barrine basin northeast Queensland Australia.
- Cheng, H., Adkins, J., Edwards, R.L. and Boyle, E.A., 2000. U-Th dating of deep-sea corals. *Geochimica et Cosmochimica Acta*, 64(14), pp.2401-2416.
- Cheng, W., Bitz, C.M. and Chiang, J.C., 2007. Adjustment of the global climate to an abrupt slowdown of the Atlantic meridional overturning circulation. *Ocean Circulation: Mechanisms and Impacts-Past and Future Changes of Meridional Overturning*, pp.295-313.
- Chiang, J.C. and Bitz, C.M., 2005. Influence of high latitude ice cover on the marine Intertropical Convergence Zone. *Climate Dynamics*, 25(5), pp.477-496.
- Chiang, J.C., Biasutti, M. and Battisti, D.S., 2003. Sensitivity of the Atlantic intertropical convergence zone to last glacial maximum boundary conditions. *Paleoceanography*, 18(4).
- Chiang, J.C., Kushnir, Y. and Giannini, A., 2002. Deconstructing Atlantic Intertropical Convergence Zone variability: Influence of the local cross-equatorial sea surface temperature gradient and remote forcing from the eastern equatorial Pacific. *Journal of Geophysical Research: Atmospheres*, 107(D1).
- Chivas, A.R., De Deckker, P., Cali, J.A., Chapman, A., Kiss, E., Shelley, G. and Michael, J., 1993. Coupled Stable Isotope and Trace Element Measurements of Lacustrine Carbonates as Paleoclimatic Indicators. *Climate change in continental isotopic records*, pp.113-121.
- Cipriani, N., Malesani, P., Vannucci, S., 1977. I travertine dell'Italia Centrale. *Boll. Serv. Geol. Ital.* 98: 58 - 115.
- Clark, I.D. and Fritz, P., 1997. *Environmental isotopes in hydrogeology*. CRC press.
- Clark, P.U., Dyke, A.S., Shakun, J.D., Carlson, A.E., Clark, J., Wohlfarth, B., Mitrovica, J.X., Hostetler, S.W. and McCabe, A.M., 2009. The last glacial maximum. *science*, 325(5941), pp.710-714.
- Clausing, A. and Boy, J.A., 2000. Lamination and primary production in fossil lakes: relationship to palaeoclimate in the Carboniferous-Permian transition. *Geological Society, London, Special Publications*, 181(1), pp.5-16.
- Clemens, S.C., Prell, W.L., Sun, Y., Liu, Z. and Chen, G., 2008. Southern Hemisphere forcing of Pliocene ^{18}O and the evolution of Indo-Asian monsoons. *Paleoceanography*, 23(4).
- Clement, A.C. and Peterson, L.C., 2008. Mechanisms of abrupt climate change of the last glacial period. *Reviews of Geophysics*, 46(4).
- CNA, B., LSHTM and UB, 1998. Effects of Wastewater Reuse on Groundwater in the Mezquital Valley, Hidalgo State, Mexico. Final Report-November 1998. BGS Technical Report WC/98/42.
- Cochran, U.A., 2002. Detection of large Holocene earthquakes in the sedimentary record of Wellington, New Zealand, using diatom analysis.
- Colman, S.M., Kaufman, D.S., Bright, J., Heil, C., King, J.W., Dean, W.E., Rosenbaum, J.G., Forester, R.M., Bischoff, J.L., Perkins, M. and McGeehin, J.P., 2006. Age model for a continuous, ca 250-ka Quaternary lacustrine record from Bear Lake, Utah-Idaho. *Quaternary Science Reviews*, 25(17), pp.2271-2282.
- Corona-M, E., 2008. The origin of archaeozoology in México: An overview. *Quaternary International*, 185(1), pp.75-81.
- Corona-M, E., 2015. An Overview of Late Pleistocene Faunal Research and the Early Peopling of Mexico. *WORLD HERITAGE HEADS* 5, p.75.
- Correa-Metrio, A., Lozano-García, S., Xelhuantzi-López, S., Sosa-Nájera, S. and Metcalfe, S.E., 2012. Vegetation in western Central Mexico during the last 50 000 years: modern analogs and climate in the Zacapu Basin. *Journal of Quaternary Science*, 27(5), pp.509-518.

- Cortes, A. and Farvolden, R.N., 1989. Isotope studied of precipitation and groundwater in the sierra de las Cruces, Mexico. *Journal of Hydrology*, 107(1), pp.147-153.
- Cortés, A., Durazo, J. and Farvolden, R.N., 1997. Studies of isotopic hydrology of the basin of Mexico and vicinity: annotated bibliography and interpretation. *Journal of Hydrology*, 198(1-4), pp.346-376.
- Craig, H., 1961. Isotopic variations in meteoric waters. *Science*, 133(3465), pp.1702-1703.
- Cross, J.K., Roberge, J. and Jerram, D.A., 2012. Constraining the degassing processes of Popocatepetl Volcano, Mexico: A vesicle size distribution and glass geochemistry study. *Journal of Volcanology and Geothermal Research*, 225, pp.81-95.
- Dalrymple, R.W. and James, N.P. eds., 2010. *Facies models 4*. Geological Association of Canada
- Damuth, J.E. and Fairbridge, R.W., 1970. Equatorial Atlantic deep-sea arkosic sands and ice-age aridity in tropical South America. *Geological Society of America Bulletin*, 81(1), pp.189-206.
- Dansgaard, W., Johnsen, S.J., Clausen, H.B., Dahl-Jensen, D., Gundestrup, N.S., Hammer, C.U., Hvidberg, C.S., Steffensen, J.P., Sveinbjörnsdóttir, A.E., Jouzel, J. and Bond, G., 1993. Evidence for general instability of past climate from a 250-kyr ice-core record. *Nature*, 364(6434), pp.218-220.
- Davis, O.K., 1999. Pollen analysis of Tulare Lake, California: Great Basin-like vegetation in Central California during the full-glacial and early Holocene. *Review of Palaeobotany and Palynology*, 107(3), pp.249-257.
- De Cserna, Z. M., De la Fuente - Duch, M., Palacios Nieto, L., Triay, L., Mitres Saazar., Mota Palomino, R., 1988. Estructura geológica, gravimetría, sismicidad y relaciones neotectónicas regionales de la Cuenca de Mexico. *Boletín 104*. Mexico, Instituto de Geología UNAM, 71.
- De Filippis, L., Faccenna, C., Billi, A., Anzalone, E., Brillì, M., Özkul, M., Soligo, M., Tuccimei, P. and Villa, I.M., 2012. Growth of fissure ridge travertines from geothermal springs of Denizli Basin, western Turkey. *Geological Society of America Bulletin*, 124(9-10), pp.1629-1645.
- De Terra, H., Romero, J., Stewart, T.D. and Linton, R., 1949. Tepexpan man (No. 11-12). Viking Fund.
- Dean Jr, W.E., 1974. Determination of carbonate and organic matter in calcareous sediments and sedimentary rocks by loss on ignition: comparison with other methods. *Journal of Sedimentary Research*, 44(1).
- Delcourt, H.R. and Delcourt, P., 1991. *Quaternary ecology: a paleoecological perspective*. Springer Science & Business Media.
- Delworth, T.L., Clark, P.U., Holland, M., Johns, T., Kuhlbrodt, T., Lynch-Stieglitz, C., Morrill, C., Seager, R., Weaver, A. and Zhang, R., 2008. The potential for abrupt change in the Atlantic meridional overturning circulation. *Abrupt climate change. A report by the US climate change science program and the subcommittee on global change research*, pp.258-359.
- DFID (1998) *Better Water Services in Developing Countries: Public-Private Partnership-The Way Ahead*. London: Department for International Development
- Dhir, R.P., Tandon, S.K., Sareen, B.K., Ramesh, R., Rao, T.K.G., Kailath, A.J. and Sharma, N., 2004. Calcretes in the Thar desert: genesis, chronology and palaeoenvironment. *Journal of Earth System Science*, 113(3), pp.473-515.
- Dickinson, W.R. and Lawton, T.F., 2001. Carboniferous to Cretaceous assembly and fragmentation of Mexico. *Geological Society of America Bulletin*, 113(9), pp.1142-1160.
- Dimbleby, G.W., 1957. Pollen analysis of terrestrial soils. *New Phytologist*, 56(1), pp.12-28.
- Douglas, M.W., Maddox, R.A., Howard, K. and Reyes, S., 1993. The mexican monsoon. *Journal of Climate*, 6(8), pp.1665-1677.
- Drake, N.A., Blench, R.M., Armitage, S.J., Bristow, C.S. and White, K.H., 2011. Ancient watercourses and biogeography of the Sahara explain the peopling of the desert. *Proceedings of the National Academy of Sciences*, 108(2), pp.458-462.

- Droxler, A.W., Alley, R.B., Howard, W.R., Poore, R.Z. and Burckle, L.H., 2003. Unique and exceptionally long interglacial Marine Isotope Stage 11: window into Earth warm future climate. *Earth's Climate and Orbital Eccentricity: The Marine Isotope Stage 11 Question*, pp.1-14.
- Durand, N., Gunnell, Y., Curmi, P. and Ahmad, S.M., 2007. Pedogenic carbonates on Precambrian silicate rocks in South India: Origin and paleoclimatic significance. *Quaternary International*, 162, pp.35-49.
- Durazo, J. and Farvolden, R.N., 1989. The groundwater regime of the Valley of Mexico from historic evidence and field observations. *Journal of Hydrology*, 112(1-2), pp.171-190.
- Dutton, A.R., 1995. Groundwater isotopic evidence for paleorecharge in US High Plains aquifers. *Quaternary Research*, 43(2), pp.221-231.
- Edmunds, M., Carrillo-Rivera, J. J., Cardona, A., 2002. Geochemical evolution of groundwater beneath Mexico City. *Journal of Hydrology*, 258: 1 - 24.
- Edwards, R.L., Gallup, C.D., Ludwig, K.R., Simmons, K.R., Winograd, I.J., Szabo, B.J. and Riggs, A.C., 1993. Dating of the Devils Hole calcite vein. *Science*, 259(5101), pp.1626-1628.
- Ehlers, J., Ehlers, J., Gibbard, P.L. and Hughes, P.D. eds., 2011. *Quaternary glaciations-extent and chronology: a closer look*. Elsevier.
- Elliot, T., Andrews, J.N. and Edmunds, W.M., 1999. Hydrochemical trends, palaeorecharge and groundwater ages in the fissured Chalk aquifer of the London and Berkshire Basins, UK. *Applied Geochemistry*, 14(3), pp.333-363.
- Elliott, J. G., Gellis, A. C., Aby, J. C., 1999. Incised River Channels.
- Enzel, Y., Ely, L.L., Mishra, S., Ramesh, R., Amit, R., Lazar, B., Rajaguru, S.N., Baker, V.R. and Sandler, A., 1999. High-resolution Holocene environmental changes in the Thar Desert, northwestern India. *Science*, 284(5411), pp.125-128.
- Ersoy, O., Chinga, G., Aydar, E., Gourgaud, A., Cubukcu, H.E. and Ulusoy, I., 2006. Texture discrimination of volcanic ashes from different fragmentation mechanisms: A case study, Mount Nemrut stratovolcano, eastern Turkey. *Computers & geosciences*, 32(7), pp.936-946.
- Esteban, M. and Klappa, C.F., 1983. Subaerial exposure environment. *Carbonate Depositional Environments: American Association of Petroleum Geologists, Memoir*, 33, pp.1-54.
- Farrell, J.W. and Prell, W.L., 1989. Climatic change and CaCO₃ preservation: an 800,000 year bathymetric reconstruction from the central equatorial Pacific Ocean. *Paleoceanography*, 4(4), pp.447-466.
- Felstead, N.J., 2012. *Palaeoenvironmental Reconstruction and Geoarchaeology of the Cuatro Ciénegas Basin, NE Mexico, from the Late Pleistocene to the present (Doctoral dissertation, Ph. D. thesis) Liverpool John Moores University, UK*.
- Ferrari, L., 2009. Geological origins of the lacustrine basins of the Trans Mexican Volcanic Belt. Abstract taken from the Programme of Abstracts, International Palaeolimnology Symposium, IPA, Guadalajara, Mexico, December 2009., pres.com, unpublished.
- Ferrari, L., Conticelli, S., Vaggelli, G., Petrone, C.M. and Manetti, P., 2000. Late Miocene volcanism and intra-arc tectonics during the early development of the Trans-Mexican Volcanic Belt. *Tectonophysics*, 318(1), pp.161-185.
- Ferrari, L., Morán - Zenteno, D., González-Torres, E.A., 2007. *Actualización de la Carta Geológica de México, escala 1:4,000,000: Universidad Nacional Autónoma de México, Instituto de Geografía, Nuevo Atlas Nacional de México*
- Ferrari, L., Orozco-Esquivel, T., Manea, V. and Manea, M., 2012. The dynamic history of the Trans-Mexican Volcanic Belt and the Mexico subduction zone. *Tectonophysics*, 522, pp.122-149.
- Ferreira, M.G. and Absy, M.L., 2017. Pollen analysis of honeys of *Melipona (Melichmia) seminigra merrillae* and *Melipona (Melikerria) interrupta* (Hymenoptera: Apidae) bred in Central Amazon, Brazil. *Grana*, pp.1-14.
- Fielding, C.R., Allen, J.P., Alexander, J. and Gibling, M.R., 2009. Facies model for fluvial systems in the seasonal tropics and subtropics. *Geology*, 37(7), pp.623-626.
- Flenley, J.R., 1979. *A geological history of tropical rainforest*.

- Flores-Márquez, E.L., Jiménez-Suárez, G., Martínez-Serrano, R.G., Chávez, R.E. and Pérez, D.S., 2006. Study of geothermal water intrusion due to groundwater exploitation in the Puebla Valley aquifer system, Mexico. *Hydrogeology Journal*, 14(7), pp.1216-1230.
- Flügel, E., 2004. *Microfacies Data: Fabrics*. In *Microfacies of Carbonate Rocks* (pp. 177-242). Springer Berlin Heidelberg.
- Fogg, G.E., 1989, March. Emergence of geologic and stochastic approaches for characterization of heterogeneous aquifers. In *Proceedings of the Robert S. Kerr Research Laboratory of the USEPA Conference on: New Field Techniques for Quantifying the Physical and Chemical Properties of Heterogeneous Aquifers*, Dallas, TX.
- Forbes, E.B., 2010. Holocene paleoclimate variation from major and trace elements and stable isotopes in a Wisconsin tufa deposit.
- Ford, T. D., Pedley, H. M., 1996. A review of tufa and travertine deposits of the world. *Earth-Science Reviews*, 41: 117 - 175.
- Ford, T.D. and Pedley, H.M., 1992. Tufa deposits of the world. *Journal of the Speleological Society of Japan*, 17, pp.46-63.
- Fox, D.J., 1965. Man-water relationships in metropolitan Mexico. *Geographical review*, 55(4), pp.523-545.
- Frank, N., Turpin, L., Cabioch, G., Blamart, D., Tressens-Fedou, M., Colin, C. and Jean-Baptiste, P., 2006. Open system U-series ages of corals from a subsiding reef in New Caledonia: implications for sea level changes, and subsidence rate. *Earth and Planetary Science Letters*, 249(3), pp.274-289.
- Freytet, P. and Plaziat, J.C., 1982. Continental carbonate sedimentation and pedogenesis-Late Cretaceous and Early Tertiary of southern France.
- Freytet, P. and Verrecchia, E.P., 1998. Freshwater organisms that build stromatolites: a synopsis of biocrystallization by prokaryotic and eukaryotic algae. *Sedimentology*, 45(3), pp.535-563.
- Freytet, P. and Verrecchia, E.P., 2002. Lacustrine and palustrine carbonate petrography: an overview. *Journal of Paleolimnology*, 27(2), pp.221-237.
- Fronval, T., Bo Jensen, N. and Buchardt, B., 1995. Oxygen isotope disequilibrium precipitation of calcite in Lake Arresø, Denmark. *Geology*, 23(5), pp.463-466.
- G?slason, S. and Eugster, H.P., 1987. Meteoric water-basalt interactions. II: a field study in NE Iceland. *Geochim. Cosmochim. Acta*, 51, pp.2841-2855.
- Gandin, A. and Capezzuoli, E., 2008. Travertine versus calcareous tufa: distinctive petrologic features and stable isotopes signatures. *Italian Journal of Quaternary Sciences*, 21(1B).
- Gandin, A. and Capezzuoli, E., 2014. Travertine: Distinctive depositional fabrics of carbonates from thermal spring systems. *Sedimentology*, 61(1), pp.264-290.
- Gani, M.R. and Alam, M.M., 2004. Fluvial facies architecture in small-scale river systems in the Upper Dupi Tila Formation, northeast Bengal Basin, Bangladesh. *Journal of Asian Earth Sciences*, 24(2), pp.225-236.
- García-Palomo, A., Macías, J.L. and Garduño, V.H., 2000. Miocene to Recent structural evolution of the Nevado de Toluca volcano region, central Mexico. *Tectonophysics*, 318(1-4), pp.281-302.
- Garcés, B.L.V. and Aguilar, J.G., 1992. Shallow carbonate lacustrine facies models in the Permian of the Aragon-Bearn basin (Western Spanish-French Pyrenees). *Carbonates and Evaporites*, 7(2), p.94.
- Garcés, B.V., Moreno, A., Navas, A., Mata, P., Machín, J., Huertas, A.D., Sampériz, P.G., Schwalb, A., Morellón, M., Cheng, H. and Edwards, R.L., 2008. The Taravilla lake and tufa deposits (Central Iberian Range, Spain) as palaeohydrological and palaeoclimatic indicators. *Palaeogeography, Palaeoclimatology, Palaeoecology*, 259(2), pp.136-156.
- García-Castellanos, D., Vergés, J., Gaspar-Escribano, J. and Cloetingh, S., 2003. Interplay between tectonics, climate, and fluvial transport during the Cenozoic evolution of the Ebro Basin (NE Iberia). *Journal of Geophysical Research: Solid Earth*, 108(B7).

- García-Palomo, A., Macías, J.L., Arce, J.L., Capra, L., Garduño, V.H. and Espíndola, J.M., 2002. Geology of the Nevado de Toluca volcano and surrounding areas, Central Mexico.
- Gargaud, M., Amils, R. and Cleaves, H.J. eds., 2011. Encyclopedia of astrobiology (Vol. 1). Springer Science & Business Media.
- Garnett, E.R., Andrews, J.E., Preece, R.C. and Dennis, P.F., 2004. Climatic change recorded by stable isotopes and trace elements in a British Holocene tufa. *Journal of Quaternary Science*, 19(3), pp.251-262.
- Garnett, J., 2006. Analytic capacity and measure (Vol. 297). Springer.
- Garrison, J.M., Davidson, J.P., Hall, M. and Mothes, P., 2011. Geochemistry and petrology of the most recent deposits from Cotopaxi Volcano, Northern Volcanic Zone, Ecuador. *Journal of Petrology*, p.egr023.
- Garziona, C.N., Dettman, D.L., Quade, J., DeCelles, P.G. and Butler, R.F., 2000. High times on the Tibetan Plateau: Paleoelevation of the Thakkhola graben, Nepal. *Geology*, 28(4), pp.339-342.
- Gasse, F., 2000. Hydrological changes in the African tropics since the Last Glacial Maximum. *Quaternary Science Reviews*, 19(1), pp.189-211.
- Genise, J.F., Melchor, R.N., Belloso, E.S. and Verde, M., 2010. Invertebrate and vertebrate trace fossils from continental carbonates. *Developments in Sedimentology*, 61, pp.319-369.
- Ghannem, N., Tlili, F., Riahi, C. and Regaya, K., 2016. Sedimentologic study of palustrine continental carbonate deposits of the Tajerouine area, NW Tunisia. *CARNETS DE GEOLOGIE*, 16(4).
- Ghinassi, M. and Ielpi, A., 2015. Stratal architecture and morphodynamics of downstream-migrating fluvial point bars (Jurassic Scalby Formation, UK). *Journal of Sedimentary Research*, 85(9), pp.1123-1137.
- Ghosh, S. and Guchhait, S.K., 2014. Palaeoenvironmental significance of fluvial facies and archives of Late Quaternary deposits in the floodplain of Damodar River, India. *Arabian Journal of Geosciences*, 7(10), pp.4145-4161.
- Gierlowski-Kordesch, E. and Rust, B.R., 1994. The Jurassic East Berlin Formation, Hartford Basin, Newark Supergroup (Connecticut and Massachusetts): A Saline Lake Playa Alluvial Plain System.
- Gierlowski-Kordesch, E.H., 2010. Lacustrine carbonates. *Developments in Sedimentology*, 61, pp.1-101.
- Gile, L.H., Hawley, J.W. and Grossman, R.B., 1981. Soils and geomorphology in the Basin and Range area of southern New Mexico: Guidebook to the Desert Project (Vol. 39). New Mexico Bureau of Mines & Mineral Resources.
- Gillespie, R., 1997. Burnt and unburnt carbon: dating charcoal and burnt bone from the Willandra Lakes, Australia. *Radiocarbon*, 39(03), pp.239-250.
- Glenn, C.R. and Kelts, K., 1991. Sedimentary rhythms in lake deposits. *Cycles and events in stratigraphy*, pp.188-221.
- Glover, C. and Robertson, A.H., 2003. Origin of tufa (cool?water carbonate) and related terraces in the Antalya area, SW Turkey. *Geological journal*, 38(3?4), pp.329-358.
- Godwin, H., 1962. Half-life of radiocarbon. *Nature*, 195, p.984.
- Golubic, S., Violante, C., Ferreri, V., D'Argenio, B. and Barattolo, F., 1993. Algal control and early diagenesis in Quaternary travertine formation (Rocchetta a Volturno, Central Apennines). *Studies on fossil benthic algae. Boll Soc Paleont Ital, Spec*, 1, pp.231-247.
- Gómez-Tuena, A., Orozco-Esquivel, M.T. and Ferrari, L., 2007. Igneous petrogenesis of the Trans-Mexican volcanic belt. *Geological Society of America Special Papers*, 422, pp.129-181.
- Gonzalez, S. and Huddart, D., 2008. The late pleistocene human occupation of Mexico. In *Memoria de Simposio Internacional de FUMDHAM*.
- Gonzalez, S., Huddart, D., Israde-Alcántara, I., Domínguez-Vázquez, G., Bischoff, J. and Felstead, N., 2015. Paleoinian sites from the Basin of Mexico: Evidence from stratigraphy, tephrochronology and dating. *Quaternary International*, 363, pp.4-19.

- Gonzalez, S., Jimenez-Lopez, J. C., Hedges, R., Huddart, D., Ohman, J. C., Turner, A., Pompa y Padilla, J. A., 2003. Earliest Humans in the Americas, New Evidence from Mexico, *Journal of Human Evolution* 44: 379-387.
- Gonzalez, S., Pastrana, A., Siebe, C. and Duller, G., 2000. Timing of the prehistoric eruption of Xitle Volcano and the abandonment of Cuicuilco Pyramid, Southern Basin of Mexico. Geological Society, London, Special Publications, 171(1), pp.205-224.
- González-Quintero, L. and Fuentes Mata, M., 1980. El Holoceno de la porción central de la Cuenca de México. *Mem Inst N Antrop Hist III Coloquio sobre Paleobotanica y PalinologmHa* (Mexico City, 1977), 86, pp.133-158.
- Goodfriend, G.A. and Stipp, J.J., 1983. Limestone and the problem of radiocarbon dating of land-snail shell carbonate. *Geology*, 11(10), pp.575-577.
- Goudie, A., 1975. Petrographic Characteristics of Calcrete (caliches): Modern Analogues of Ancient Concretions.
- Goudie, A.S., 1996. Organic agency in calcrete development. *Journal of Arid Environments*, 32(2), pp.103-110.
- Gradziński, M., 2010. Factors controlling growth of modern tufa: results of a field experiment. Geological Society, London, Special Publications, 336(1), pp.143-191.
- Griffin, D.G., 2017. Ancient Artifact or New Age Totem: Analysis of a Carved Sacrum from the Oregon Coast. *Journal of Northwest Anthropology*, 51(1).
- Grimm, E.C., 1991. 2004. TILIA, TILIA.GRAPH, and TGView. Illinois State Museum, Research and Collections Center, Springfield, USA.
- Grove, A.T. and Goudie, A.S., 1971. Late quaternary lake levels in the rift valley of southern Ethiopia and elsewhere in tropical Africa. *Nature*, 234(5329), pp.403-405.
- Gruszka, B. and van Loon, A.T., 2007. Pleistocene glaciolacustrine breccias of seismic origin in an active graben (central Poland). *Sedimentary Geology*, 193(1), pp.93-104.
- Gruszka, B., 2007. The Pleistocene glaciolacustrine sediments in the Be?chatów mine (central Poland): Endogenic and exogenic controls. *Sedimentary Geology*, 193(1), pp.149-166.
- Guerreiro, P., Cunha, L. and Ribeiro, C., 2011. Geomorphological settings and tufa models in Algre flexure (Algarve, Portugal).
- Guerrero, B.O., Thompson, R. and Fucugauchi, J.U., 2000. Magnetic properties of lake sediments from Lake Chalco, central Mexico, and their palaeoenvironmental implications. *Journal of Quaternary Science*, 15(2), pp.127-140.
- Gulbranson, E.L., 2004, November. Calcretes and Plaustrine Carbonates as indicators of Climate Shift, Late Triassic and Early Cretaceous of the Southwestern. In 2004 Denver Annual Meeting.
- Guo, L. and Riding, R., 1992. Aragonite laminae in hot water travertine crusts, Rapolano Terme, Italy. *Sedimentology*, 39(6), pp.1067-1079.
- Guo, L. and Riding, R., 1998. Hot?spring travertine facies and sequences, Late Pleistocene, Rapolano Terme, Italy. *Sedimentology*, 45(1), pp.163-180.
- Guo, X. and Chafetz, H.S., 2012. Large tufa mounds, Searles Lake, California. *Sedimentology*, 59(5), pp.1509-1535.
- Harvey, A.M., Whitfield, E., Stokes, M. and Mather, A., 2014. The late Neogene to Quaternary drainage evolution of the uplifted neogene sedimentary basins of Almería, Betic chain. In *Landscapes and Landforms of Spain* (pp. 37-61). Springer, Dordrecht.
- Heath, R.C., 1989. Basic Ground-Water Hydrology. U.S. Geological Survey Water-Supply Paper 2220, 84p
- Hedges, J.I., 1992. Global biogeochemical cycles: progress and problems. *Marine chemistry*, 39(1-3), pp.67-93.
- Heiken, G. and Wohletz, K., 1985. Volcanic ash. University Presses of California, Chicago, Harvard & MIT.
- Heine, K. and Schönhals, E., 1973. Entstehung und Alter der" toba"-Sedimente in Mexiko. *Eiszeitalter und Gegenwart= E & G*, 23, pp.201-215.

- Heine, K., 1984. The classical Late Weichselian climatic fluctuations in Mexico. In *Climatic changes on a yearly to millennial basis* (pp. 95-115). Springer Netherlands.
- Heine, K., 2003. Paleopedological evidence of human-induced environmental change in the Puebla-Tlaxcala area (Mexico) during the last 3,500 years. *Revista Mexicana de Ciencias Geológicas*, 20(3), pp.235-244.
- Hemming, S.R., 2004. Heinrich events: Massive late Pleistocene detritus layers of the North Atlantic and their global climate imprint. *Reviews of Geophysics*, 42(1).
- Henchiri, M., 2014a. Quaternary paludal tufas from the Ben Younes spring system, Gafsa, southwestern Tunisia: Interactions between tectonics and climate. *Quaternary International*, 338, pp.71-87.
- Henchiri, M., 2014b. Sedimentology of Quaternary calcareous tufas from Gafsa, southwestern Tunisia. *Arabian Journal of Geosciences*, 7(5), pp.2081-2091.
- Hendy, I.L., Minckley, T.A. and Whitlock, C., 2016. Eastern tropical Pacific vegetation response to rapid climate change and sea level rise: A new pollen record from the Gulf of Tehuantepec, southern Mexico. *Quaternary Science Reviews*, 145, pp.152-160.
- Hernández-Cerda, M.E. and Carrasco-Anaya, G., 2007. Rasgos climáticos más importantes. *Biodiversidad de la Faja Volcánica Transmexicana*, Universidad Nacional Autónoma de México, pp.57-72.
- Hibbard, C.W., 1955. Pleistocene vertebrates from the Upper Becerra (Becerra Superior) formation, Valley of Tequiquiac, Mexico, with notes on other Pleistocene forms.
- Higgins, R.W., Mo, K.C. and Yao, Y., 1998. Interannual variability of the US summer precipitation regime with emphasis on the southwestern monsoon. *Journal of Climate*, 11(10), pp.2582-2606.
- Hjulstrom, F., 1939. Transportation of detritus by moving water: Part 1. Transportation.
- Hodell, D.A., Anselmetti, F.S., Ariztegui, D., Brenner, M., Curtis, J.H., Gilli, A., Grzesik, D.A., Guilderson, T.J., Müller, A.D., Bush, M.B. and Correa-Metrio, A., 2008. An 85-ka record of climate change in lowland Central America. *Quaternary Science Reviews*, 27(11), pp.1152-1165.
- Holz, M., Troccoli, E. and Vieira, M., 2014. Sequence Stratigraphy of Continental Rift Basins II: An Example from the Brazilian Cretaceous Recôncavo Basin. In *STRATI 2013* (pp. 15-18). Springer International Publishing.
- Horbury, A.D. and Adams, A.E., 1996. Microfacies associations in Asbian carbonates: an example from the Urswick Limestone Formation of the southern Lake District, northern England. *Geological Society, London, Special Publications*, 107(1), pp.221-237.
- HSÜ, K., 1979. Non-annual cycles of varve-like sedimentation in Walensee, Switzerland. *Sedimentology*, 26(3), pp.453-461.
- <https://www.usgs.gov/>
- Huang, Y. and Fairchild, I.J., 2001. Partitioning of Sr²⁺ and Mg²⁺ into calcite under karst-analogue experimental conditions. *Geochimica et Cosmochimica Acta*, 65(1), pp.47-62.
- Hughes, P.D., Gibbard, P.L. and Ehlers, J., 2013. Timing of glaciation during the last glacial cycle: evaluating the concept of a global 'Last Glacial Maximum'(LGM). *Earth-Science Reviews*, 125, pp.171-198.
- Ihlenfeld, C., Norman, M.D., Gagan, M.K., Drysdale, R.N., Maas, R. and Webb, J., 2003. Climatic significance of seasonal trace element and stable isotope variations in a modern freshwater tufa. *Geochimica et Cosmochimica Acta*, 67(13), pp.2341-2357.
- Imbrie, J., 1979. Imbrie.
- INEGI., 1997. Carta Topografica, 1: 50,000, Zumpango de Ocampo, E14A19, Mexico, Hidalgo.
- Irion, G. and Müller, G., 1968. Mineralogy, petrology and chemical composition of some calcareous tufa from the Schwäbische Alb, Germany. In *Recent developments in carbonate sedimentology in Central Europe* (pp. 157-171). Springer Berlin Heidelberg.
- Israde Alcántara, I., Garduño-Monroy, V.H. and Ortega Murillo, R., 2002. Paleambiente lacustre del Cuaternario tardío en el centro del lago de Cuitzeo. *Hidrobiológica*, 12(1), pp.61-78.

- Israde-Alcántara, I., Garduño-Monroy, V.H., Fisher, C.T., Pollard, H.P. and Rodríguez-Pascua, M.A., 2005. Lake level change, climate, and the impact of natural events: the role of seismic and volcanic events in the formation of the Lake Patzcuaro Basin, Michoacan, Mexico. *Quaternary International*, 135(1), pp.35-46.
- Israde-Alcántara, I., Miller, W.E., Garduño-Monroy, V.H., Barron, J. and Rodríguez-Pascua, M.A., 2010. Palaeoenvironmental significance of diatom and vertebrate fossils from Late Cenozoic tectonic basins in west-central México: A review. *Quaternary International*, 219(1-2), pp.79-94.
- Issar, A., Quijano, J.L., Gat, J.R. and Castro, M., 1984. The isotope hydrology of the groundwaters of central Mexico. *Journal of Hydrology*, 71(3), pp.201-224.
- Jacobson, G. and Arakel, A.V., 1986. Calcrete aquifers in the Australian arid zone. In *Proceedings of the International Conference on Groundwater Systems Under Stress*, Brisbane, Australian Water Resources Council (pp. 515-523).
- James, N.P. and Dalrymple, R.W., 2010. *Facies Models 4: St. John's, Newfoundland*, Geological Association of Canada.
- Jasso, R.H., 2017. Dinámica de la estructura de comunidades del Cenozoico tardío de Norteamérica: Episodios de Recambio Rápido de Fauna (RTE) dentro del concepto de Cronofauna. *Estudios Geológicos*, 73(1), p.063.
- Jiménez, B. and Asano, T., 2008. Water reclamation and reuse around the world. *Water Reuse: an international survey of current practice, issues and needs*, 20, p.3.
- Jiménez, B. and Chávez, A., 2004. Quality assessment of an aquifer recharged with wastewater for its potential use as drinking source: "El Mezquital Valley" case. *Water Science and Technology*, 50(2), pp.269-276.
- Jimenez, B., Asano, T., 2008. *Water Reuse an international survey of current practices, issues and needs*. Scientific and Technical report, 20. IWA. London.
- Johnson, C.A. and Harrison, C.G.A., 1990. Neotectonics in central Mexico. *Physics of the Earth and Planetary Interiors*, 64(2-4), pp.187-210.
- Jones, B. and Renaut, R.W., 2010. Calcareous spring deposits in continental settings. *Developments in Sedimentology*, 61, pp.177-224.
- Jones, V.J. and Birks, H.J.B., 2004. Lake-sediment records of recent environmental change on Svalbard: results of diatom analysis. *Journal of Paleolimnology*, 31(4), pp.445-466.
- Jourdan, F., Mark, D.F. and Verati, C. eds., 2014, April. *Advances in ⁴⁰Ar/³⁹Ar Dating: From Archaeology to Planetary Sciences*. Geological Society of London.
- Jutras, P., Utting, J. and McLeod, J., 2007. Link between long-lasting evaporitic basins and the development of thick and massive phreatic calcrete hardpans in the Mississippian Windsor and Percé groups of eastern Canada. *Sedimentary Geology*, 201(1), pp.75-92.
- Kabanov, P., Anadón, P. and Krumbein, W.E., 2008. Microcodium: an extensive review and a proposed non-rhizogenic biologically induced origin for its formation. *Sedimentary geology*, 205(3), pp.79-99.
- Kadir, S. and Akbulut, A., 2011. Palygorskite-dominated clayey sedimentary beds of the Çameli formation in the Neogene Sapaca lacustrine basin, Honaz, Denizli Province, SW Turkey. *Neues Jahrbuch für Mineralogie-Abhandlungen: Journal of Mineralogy and Geochemistry*, 188(2), pp.151-167.
- Kämpf, L., Plessen, B., Lauterbach, S., Nantke, C., Meyer, H., Chaplignin, B., Höllerer, H. and Brauer, A., 2016, April. Impact of flood events on lacustrine carbonate isotope records. In *EGU General Assembly Conference Abstracts* (Vol. 18, p. 7814).
- Kendall, A.C. and Broughton, P.L., 1978. Origin of fabrics in speleothems composed of columnar calcite crystals. *Journal of Sedimentary Research*, 48(2).
- Kendall, C. and Caldwell, E.A., 1998. *Fundamentals of isotope geochemistry. Isotope tracers in catchment hydrology*, pp.51-86.
- Kendall, C. and McDonnell, J.J. eds., 2012. *Isotope tracers in catchment hydrology*. Elsevier.

- Kendall, C., Burns, D.A., Silva, S.R., Chang, C.C.Y. and McMahon, P.B., 1995. Sources of variation in the oxygen and nitrogen isotopic composition of nitrate in soils. *AGU Trans*, 76, p.210.
- Kerr, R.A., 2001. The tropics return to the climate system.
- Khadkikar, A.S., Merh, S.S., Malik, J.N. and Chamyal, L.S., 1998. Calcretes in semi-arid alluvial systems: formative pathways and sinks. *Sedimentary Geology*, 116(3-4), pp.251-260.
- Khalaf, F.I. and Gaber, A.S., 2008. Occurrence of cyclic palustrine and calcrete deposits within the lower Pliocene Hagul formation, East Cairo district, Egypt. *Journal of African Earth Sciences*, 51(5), pp.298-312.
- Klappa, C.F., 1978. Biolithogenesis of *Microcodium*: elucidation. *Sedimentology*, 25(4), pp.489-522.
- Klappa, C.F., 1979. Lichen stromatolites: criterion for subaerial exposure and a mechanism for the formation of laminar calcretes (caliche). *Journal of Sedimentary Research*, 49(2).
- Klappa, C.F., 1980. Rhizoliths in terrestrial carbonates: classification, recognition, genesis and significance. *Sedimentology*, 27(6), pp.613-629.
- Klein, J., Lerman, J.C., Damon, P.E. and Ralph, E.K., 1982. Calibration of radiocarbon dates: tables based on the consensus data of the Workshop on Calibrating the Radiocarbon Time Scale. *Radiocarbon*, 24(02), pp.103-150.
- Knox, G.J., 1977. Caliche profile formation, Saldanha Bay (South Africa). *Sedimentology*, 24(5), pp.657-674.
- Knudsen, M.F., Seidenkrantz, M.S., Jacobsen, B.H. and Kuijpers, A., 2011. Tracking the Atlantic Multidecadal Oscillation through the last 8,000 years. *Nature communications*, 2, p.178.
- Koçun, E., 2012. Facies characteristics and depositional environments of Quaternary tufa deposits, Antalya, SW Turkey. *Carbonates and evaporites*, 27(3-4), pp.269-289.
- Košir, A., 2004. *Microcodium* revisited: root calcification products of terrestrial plants on carbonate-rich substrates. *Journal of Sedimentary Research*, 74(6), pp.845-857.
- Kowallis, B.J., Swisher, C.C., III, Carranza-Castañeda, O., Miller, W.E., and Tingey, D.G., 1998. Fission-track and single crystal $^{40}\text{Ar}/^{39}\text{Ar}$ laser-fusion ages from volcanic ash layers in fossil-bearing Pliocene sediments in central Mexico. *Revista Mexicana de Ciencias Geológicas*, 15: 157-160.
- Kraus, S., Kurbatov, A. and Yates, M., 2013. Geochemical signatures of tephras from Quaternary Antarctic Peninsula volcanoes. *Andean Geology*, 40(1), pp.1-40.
- Kutzbach, J.E. and Street-Perrott, F.A., 1985. Milankovitch forcing of fluctuations in the level of tropical lakes from 18 to 0 kyr BP. *Nature* 317, 130-34.
- Lamb, A.L., Gonzalez, S., Huddart, D., Metcalfe, S.E., Vane, C.H. and Pike, A.W., 2009. Tepexpan Palaeoindian site, Basin of Mexico: multi-proxy evidence for environmental change during the late Pleistocene-late Holocene. *Quaternary Science Reviews*, 28(19), pp.2000-2016.
- Larrasoaña, J.C., Roberts, A.P., Rohling, E.J., Winkhofer, M. and Wehausen, R., 2003. Three million years of monsoon variability over the northern Sahara. *Climate Dynamics*, 21(7-8), pp.689-698.
- Larsen, C.P.S., Pienitz, R., Smol, J.P., Moser, K.A., Cumming, B.F., Blais, J.M., MacDonald, G.M. and Hall, R.I., 1998. Relations between lake morphometry and the presence of laminated lake sediments: a re-examination of Larsen and MacDonald (1993). *Quaternary Science Reviews*, 17(8), pp.711-717.
- Ledesma-Guerrero, O., 1967. Resumen de la geología de la Hoja Parras, 13R-1 (6) escala 1: 100000: México, DF, Universidad Nacional Autónoma de México, Instituto de Geología. Carta Geológica de México Serie de, 1(100000), p.1.
- Ledru, M.P., Rousseau, D.D., Cruz, F.W., Riccomini, C., Karmann, I. and Martin, L., 2005. Paleoclimate changes during the last 100,000 yr from a record in the Brazilian Atlantic rainforest region and interhemispheric comparison. *Quaternary Research*, 64(3), pp.444-450.
- Lee, J.Y., Marti, K., Severinghaus, J.P., Kawamura, K., Yoo, H.S., Lee, J.B. and Kim, J.S., 2006. A redetermination of the isotopic abundances of atmospheric Ar. *Geochimica et Cosmochimica Acta*, 70(17), pp.4507-4512.

- Leite, Y.L., Costa, L.P., Loss, A.C., Rocha, R.G., Batalha-Filho, H., Bastos, A.C., Quaresma, V.S., Fagundes, V., Paresque, R., Passamani, M. and Pardini, R., 2016. Neotropical forest expansion during the last glacial period challenges refuge hypothesis. *Proceedings of the National Academy of Sciences*, 113(4), pp.1008-1013.
- Leng, M. J., Marshall, J. D., 2004. Palaeoclimate interpretation of stable isotope data from lake sediment archives, *Quaternary Science Reviews*, 23: 811-831.
- Leng, M.J. ed., 2006. *Isotopes in palaeoenvironmental research* (Vol. 10, p. 307). New York: Springer.
- Leng, M.J., Baneschi, I., Zanchetta, G., Jex, C.N., Wagner, H. and Vogel, H., 2010. Late Quaternary palaeoenvironmental reconstruction from Lakes Ohrid and Prespa (Macedonia/Albania border) using stable isotopes. *Biogeosciences discussion*.
- Leng, M.J., Lamb, A.L., Heaton, T.H., Marshall, J.D., Wolfe, B.B., Jones, M.D., Holmes, J.A. and Arrowsmith, C., 2006. *Isotopes in lake sediments* (pp. 147-184). Springer Netherlands.
- Leng, M.J., Roberts, N., Reed, J.M. and Sloane, H.J., 1999. Late Quaternary palaeohydrology of the Konya Basin, Turkey, based on isotope studies of modern hydrology and lacustrine carbonates. *Journal of Paleolimnology*, 22(2), pp.187-204.
- Levin, N.E., Quade, J., Simpson, S.W., Semaw, S. and Rogers, M., 2004. Isotopic evidence for Plio-Pleistocene environmental change at Gona, Ethiopia. *Earth and Planetary Science Letters*, 219(1), pp.93-110.
- Li, J., Pang, Z., Froehlich, K., Huang, T., Kong, Y., Song, W. and Yun, H., 2015. Paleo-environment from isotopes and hydrochemistry of groundwater in East Junggar Basin, Northwest China. *Journal of Hydrology*, 529, pp.650-661.
- Li, Z., Shi, X., Chen, M.T., Wang, H., Liu, S., Xu, J., Long, H., Troa, R.A., Zuraida, R. and Triarso, E., 2016. Late Quaternary fingerprints of precession and sea level variation over the past 35 kyr as revealed by sea surface temperature and upwelling records from the Indian Ocean near southernmost Sumatra. *Quaternary International*, 425, pp.282-291.
- Libby, W.F., Anderson, E.C. and Arnold, J.R., 1949. Age determination by radiocarbon content: world-wide assay of natural radiocarbon. *Science*, 109(2827), pp.227-228.
- Linares, R., Rosell, J., Roqué, C. and Gutiérrez, F., 2009. Origin and evolution of tufa mounds related to artesian karstic springs in Isona area (Pyrenees, NE Spain). *Geodinamica Acta*, 22(5-6/1-3), p.129.
- Lindqvist, J.K., 1994. Lacustrine stromatolites and oncoids: Manuherikia Group (Miocene), New Zealand. In *Phanerozoic stromatolites II* (pp. 227-254). Springer Netherlands.
- Liutkus, C.M., Wright, J.D., Ashley, G.M. and Sikes, N.E., 2005. Palaeoenvironmental interpretation of lake-margin deposits using $\delta^{13}\text{C}$ and $\delta^{18}\text{O}$ results from early Pleistocene carbonate rhizoliths, Olduvai Gorge, Tanzania. *Geology*, 33(5), pp.377-380.
- Lopez Pearce, J., 2010. Syntectonic deposition and paleohydrology of the spring-fed Hualapai Limestone and implications for 5-6 MA integration of the Colorado River system through Grand Canyon: evidence from sedimentology, geochemistry and detrital zircon analysis (Doctoral dissertation).
- Lopez-Hernandez, A. and Castillo-Hernandez, D., 1997. Exploratory drilling at Acoculco, Puebla, Mexico: a hydrothermal system with only nonthermal manifestations (No. CONF-971048-). Geothermal Resources Council, Davis, CA (United States).
- Lorenzo, J.L., 1969. *Piezas de arte mobiliario en la prehistoria de México* (Vol. 3). Instituto Poblano de Antropología e Historia.
- Lounejeva Baturina, E., Morales Puente, P., Cabadas Báez, H.V., Cienfuegos Alvarado, E., Sedov, S., Vallejo Gómez, E. and Solleiro Rebolledo, E., 2006. Late Pleistocene to Holocene environmental changes from $\delta^{13}\text{C}$ determinations in soils at Teotihuacan, Mexico. *Geofísica internacional*, 45(2), pp.85-98.
- Love, K.M. and Chafetz, H.S., 1988. Diagenesis of laminated travertine crusts, Arbuckle Mountains, Oklahoma. *Journal of Sedimentary Research*, 58(3).
- Lowe, J.J. and Walker, M.J., 2014. *Reconstructing quaternary environments*. Routledge.

- Lozano-García, M.S., Ortega-Guerrero, B., Caballero-Miranda, M. and Urrutia-Fucugauchi, J., 1993. Late Pleistocene and Holocene paleoenvironments of Chalco lake, central Mexico. *Quaternary Research*, 40(3), pp.332-342.
- Lozano-García, M. and Ortega-Guerrero, B., 1998. Late Quaternary environmental changes of the central part of the Basin of Mexico; correlation between Texcoco and Chalco basins. *Review of Palaeobotany and Palynology*, 99(2), pp.77-93.
- Lozano-García, S., 1996. La vegetación Cuaternaria en el Centro de México: Registros Palinológicos e Implicaciones Paleoclimáticas. *Boletín de la Sociedad Botánica de México* 57, 79-102.
- Lozano-García, S., Ortega, B., Roy, P.D., Beramendi-Orosco, L. and Caballero, M., 2015. Climatic variability in the northern sector of the American tropics since the latest MIS 3. *Quaternary Research*, 84(2), pp.262-271.
- Lozano-García, S., Sosa-Nájera, S., Sugiura, Y. and Caballero, M., 2005. 23,000 yr of vegetation history of the Upper Lerma, a tropical high-altitude basin in Central Mexico. *Quaternary Research*, 64(1), pp.70-82.
- Lozano-García, S., Torres-Rodríguez, E., Ortega, B., Vázquez, G. and Caballero, M., 2013. Ecosystem responses to climate and disturbances in western central Mexico during the late Pleistocene and Holocene. *Palaeogeography, Palaeoclimatology, Palaeoecology*, 370, pp.184-195.
- Machette, M.N., 1985. Calcic soils of the southwestern United States. *Geological Society of America Special Papers*, 203, pp.1-22.
- Macías, J.L., 2007. Geology and eruptive history of some active volcanoes of México. *Geological Society of America Special Papers*, 422, pp.183-232.
- Macías, J.L., Arce, J.L., García-Tenorio, F., Layer, P.W., Rueda, H., Reyes-Agustín, G., López-Pizaña, F. and Avellán, D., 2012. Geology and geochronology of Tlaloc, Telapón, Iztaccihuatl, and Popocatepetl volcanoes, Sierra Nevada, central Mexico. *Field Guides*, 25, pp.163-193.
- Macías, J.L., Capra, L., Arce, J.L., Espíndola, J.M., García-Palomo, A. and Sheridan, M.F., 2008. Hazard map of El Chichón volcano, Chiapas, México: Constraints posed by eruptive history and computer simulations. *Journal of Volcanology and Geothermal Research*, 175(4), pp.444-458.
- Macías, M.C. and Tagle, S.G., 1989. *El origen del hombre en América*. GV Editores.
- Mack, G.H., Cole, D.R. and Treviño, L., 2000. The distribution and discrimination of shallow, authigenic carbonate in the Pliocene-Pleistocene Palomas Basin, southern Rio Grande rift. *Geological Society of America Bulletin*, 112(5), pp.643-656.
- Macklin, M.G., Benito, G., Gregory, K.J., Johnstone, E., Lewin, J., Michczyńska, D.J., Soja, R., Starkel, L. and Thorndycraft, V.R., 2006. Past hydrological events reflected in the Holocene fluvial record of Europe. *Catena*, 66(1), pp.145-154.
- Magaña, V.O., Vázquez, J.L., Pérez, J.L. and Pérez, J.B., 2003. Impact of El Niño on precipitation in Mexico. *Geofísica internacional*, 42(3), pp.313-330.
- Magnani, G., Bartolomei, P., Cavulli, F., Esposito, M., Marino, E.C., Neri, M., Rizzo, A., Scaruffi, S. and Tosi, M., 2007. U-series and radiocarbon dates on mollusc shells from the uppermost layer of the archaeological site of KHB-1, Ra's al Khabbah, Oman. *Journal of Archaeological Science*, 34(5), pp.749-755.
- Maher, E. and Harvey, A.M., 2008. Fluvial system response to tectonically induced base-level change during the late-Quaternary: The Rio Alias southeast Spain. *Geomorphology*, 100(1-2), pp.180-192.
- Mahlknecht J, Schneider J, Merkel B, de Leon IN, Bernasconi S. 2004. Groundwater recharge in a sedimentary basin in semi-arid Mexico. *Hydrogeology Journal* 12: 511-530.
- "Mahlknecht, J., Garfias-Solis, J., Aravena, R., Tesch, R., 2006. Geochemical and isotopic investigations on groundwater residence time and flow in the Independence Basin, Mexico. *Journal of Hydrology* 324 (1-4), 283-300."
- Mahoney, J.B., 2005. Nd and Sr isotopic signatures of fine-grained clastic sediments: A case study of western Pacific marginal basins. *Sedimentary Geology*, 182(1), pp.183-199.

- Maldonado-Koerdell, M. and de Anda, L.A.A., 1949. Nota preliminar sobre dos artefactos del pleistoceno superior hallados en la región de Tequixquiak, México. na.
- Mann, A.W. and Horwitz, R.C., 1979. Groundwater calcrete deposits in Australia: some observations from Western Australia. *Journal of the Geological Society of Australia*, 26.
- Marín-Córdova, S., Aguayo, C.J.E. and Mandujano, V.J., 1986. Sistemas mayores de fallamiento en la Cuenca de México y su relación con la sismicidad.
- Marín-Córdova, S., Campos - Enríquez, O., Herrera - Moro - Castillo, M., 2004. Neotectonic related risk to dams in the Mexico Basin - Guadalupe dam. *Geofísica International* 43: 3. 435 - 443.
- Mark, D.F., Rice, C.M., Fallick, A.E., Trewin, N.H., Lee, M.R., Boyce, A. and Lee, J.K.W., 2011. 40 Ar/39 Ar dating of hydrothermal activity, biota and gold mineralization in the Rhynie hot-spring system, Aberdeenshire, Scotland. *Geochimica et Cosmochimica Acta*, 75(2), pp.555-569.
- Matsuoka, J., Kano, A., Oba, T., Watanabe, T., Sakai, S. and Seto, K., 2001. Seasonal variation of stable isotopic compositions recorded in a laminated tufa, SW Japan. *Earth and Planetary Science Letters*, 192(1), pp.31-44.
- Mattey, D., Lowry, D., Duffet, J., Fisher, R., Hodge, E. and Frisia, S., 2008. A 53 year seasonally resolved oxygen and carbon isotope record from a modern Gibraltar speleothem: reconstructed drip water and relationship to local precipitation. *Earth and Planetary Science Letters*, 269(1), pp.80-95.
- Mayte, G.B., García-Zepeda, M.L., López-García, R., Arroyo-Cabrales, J., Marín-Leyva, A.H., Meléndez-Herrera, E. and Fuentes-Farías, A.L., 2016. Diet and habitat of *Mammuthus columbi* (Falconer, 1857) from two Late Pleistocene localities in central western Mexico. *Quaternary International*, 406, pp.137-146.
- McDougall, I. and Harrison, T.M., 1999. *Geochronology and Thermochronology by the 40Ar/39Ar Method*. Oxford University Press on Demand.
- McGuire, W.J. ed., 2000. *The archaeology of geological catastrophes*. Geological Society.
- Metcalfe, S., Say, A., Black, S., McCulloch, R. and O'Hara, S., 2002. Wet conditions during the last glaciation in the Chihuahuan Desert, Alta Babicora Basin, Mexico. *Quaternary Research*, 57(1), pp.91-101.
- Metcalfe, S.E. and Nash, D.J. eds., 2012. *Quaternary environmental change in the tropics*. John Wiley & Sons.
- Metcalfe, S.E., 1997. Palaeolimnological records of climate change in México-Frustrating past, promising future?. *Quaternary International*, 43, pp.111-116.
- Metcalfe, S.E., 2006. Late Quaternary environments of the northern deserts and central transvolcanic belt of Mexico. *Annals of the Missouri Botanical Garden*, 93(2), pp.258-273.
- Metcalfe, S.E., Barron, J.A. and Davies, S.J., 2015. The Holocene history of the North American Monsoon: 'known knowns' and 'known unknowns' in understanding its spatial and temporal complexity. *Quaternary Science Reviews*, 120, pp.1-27.
- Metcalfe, S.E., Leng, M.J., Kirby, J.R., Huddart, D., Vane, C.H. and Gonzalez, S., 2016. Early-Mid Pleistocene environments in the Valsequillo Basin, Central Mexico: a reassessment. *Journal of Quaternary Science*.
- Metcalfe, S.E., O'Hara, S.L., Caballero, M. and Davies, S.J., 2000. Records of Late Pleistocene-Holocene climatic change in Mexico-a review. *Quaternary Science Reviews*, 19(7), pp.699-721.
- Metcalfe, S.E., Street-Perrott, F.A., Perrott, R.A. and Harkness, D.D., 1991. Palaeolimnology of the Upper Lerma Basin, Central Mexico: a record of climatic change and anthropogenic disturbance since 11 600 yr BP. *Journal of Paleolimnology*, 5(3), pp.197-218.
- Meurant, G., 1976. *Tectonics and Metamorphism: Indexes of (Vol. 1)*. Elsevier.
- Meyers, P.A. and Lallier-Vergès, E., 1999. Lacustrine sedimentary organic matter records of Late Quaternary paleoclimates. *Journal of Paleolimnology*, 21(3), pp.345-372.
- Miall, A., 2013. *The geology of fluvial deposits: sedimentary facies, basin analysis, and petroleum geology*. Springer.
- Miall, A.D., 1977. *Fluvial sedimentology: an historical review*.

- Miall, A.D., 1980. Cyclicity and the facies model concept in fluvial deposits. *Bulletin of Canadian Petroleum Geology*, 28(1), pp.59-80.
- Miall, A.D., 1985. Architectural-element analysis: a new method of facies analysis applied to fluvial deposits. *Earth-Science Reviews*, 22(4), pp.261-308.
- Miall, A.D., 1997. The Four Basic Types of Stratigraphic Cycle. In *The Geology of Stratigraphic Sequences* (pp. 49-56). Springer Berlin Heidelberg.
- Miall, A.D., 2016. Facies Models. In *Stratigraphy: A Modern Synthesis* (pp. 161-214). Springer International Publishing.
- Miller, W.E. and Carranza-Castañeda, O., 1984. Late Cenozoic mammals from central Mexico. *Journal of Vertebrate Paleontology*, 4(2), pp.216-236.
- Miranda, M.C., 1997. The last glacial maximum in the basin of Mexico: the diatom record between 34,000 and 15,000 years BP from Lake Chalco. *Quaternary International*, 43, pp.125-136.
- Mohtadi, M., Hebbeln, D., Nuñez Ricardo, S. and Lange, C.B., 2006. El Niño-like pattern in the Pacific during marine isotope stages (MIS) 13 and 11?. *Paleoceanography*, 21(1).
- Moore, P.D., Webb, J.A. and Collison, M.E., 1991. *Pollen analysis*. Blackwell scientific publications.
- Mooser F., 1975. *Historia geológica de la Cuenca de México: Memorias sobre las Obras del*
- Mooser, F., 1975. *Historia geológica de la Cuenca de México. Memoria de las obras del sistema de drenaje profundo del Distrito Federal: México, DF, Departamento del Distrito Federal*, 1, pp.7-38.
- Moreno, P.I., Denton, G.H., Moreno, H., Lowell, T.V., Putnam, A.E. and Kaplan, M.R., 2015. Radiocarbon chronology of the last glacial maximum and its termination in northwestern Patagonia. *Quaternary Science Reviews*, 122, pp.233-249.
- Morett, A.L., González, S., Arroyo-Cabrales, J., Polaco, Ó.J., Sherwood, G.J. and Turner, A., 2003. The late Pleistocene paleoenvironment of the Basin of Mexico. *Deinsea*, 9(1), pp.267-272.
- Moretti, M. and Sabato, L., 2007. Recognition of trigger mechanisms for soft-sediment deformation in the Pleistocene lacustrine deposits of the Sant'Arcangelo Basin (Southern Italy): seismic shock vs. overloading. *Sedimentary Geology*, 196(1), pp.31-45.
- Mueller, R.G., Joyce, A.A. and Borejsza, A., 2012. Alluvial archives of the Nochixtlan valley, Oaxaca, Mexico: age and significance for reconstructions of environmental change. *Palaeogeography, Palaeoclimatology, Palaeoecology*, 321, pp.121-136.
- Mukhopadhyay, A., Mazumdar, P. and Van Loon, A.T., 2016. A new 'superassemblage' model explaining proximal-to-distal and lateral facies changes in fluvial environments, based on the Proterozoic Sanjauli Formation (Lesser Himalaya, India). *Journal of Palaeogeography*, 5(4), pp.391-408.
- Mullineaux, D.R., 1996. *Pre-1980 tephra-fall deposits erupted from Mount St. Helens, Washington*. US Government Printing Office.
- Myrow, P.M., 1990. A new graph for understanding colors of mudrocks and shales. *Journal of Geological Education*, 38(1), pp.16-20.
- Nanson, G.C. and Huang, H.Q., 2008. Least action principle, equilibrium states, iterative adjustment and the stability of alluvial channels. *Earth Surface Processes and Landforms*, 33(6), pp.923-942.
- Nash, D.J. and Smith, R.F., 1998. Multiple calcrete profiles in the Tabernas Basin, southeast Spain: their origins and geomorphic implications. *Earth Surface Processes and Landforms*, 23(11), pp.1009-1029.
- Nash, D.J. and Smith, R.F., 2003. Properties and development of channel calcretes in a mountain catchment, Tabernas Basin, southeast Spain. *Geomorphology*, 50(1), pp.227-250.
- Nelson, D., 2002. *Natural variations in the composition of groundwater. Drinking Water Program*. Oregon Department of Human Services, Springfield, Oregon, 3.
- Netterberg, F., 1969. The interpretation of some basic calcrete types. *The South African Archaeological Bulletin*, 24(95/96), pp.117-122.

- Neu, T.R., 2000. Confocal laser scanning microscopy (CLSM) of biofilms. *Biofilms-Investigative Methods and Applications*. Flemming, H.-C., U. Szewzyk, and T. Griebel (Eds.). Technomic Publishing Co. Inc., PA, USA, pp.211-224.
- Newton, A.J. and Metcalfe, S.E., 1999. Tephrochronology of the Toluca basin, central Mexico. *Quaternary Science Reviews*, 18(8-9), pp.1039-1059.
- Nichols, G., 2009. *Sedimentology and stratigraphy*. Wiley - Blackwell, Oxford.
- Nickel, E., 1983. Environmental significance of freshwater oncoids, Eocene guarga formation, Southern Pyrenees, Spain. In *Coated Grains* (pp. 308-329). Springer Berlin Heidelberg.
- Nowak, M. and Weiss, C., 2013, April. Facies, facies architecture and formation processes of a calcareous, self-build tufa channel (Steinerne Rinne) from Engelthal, Southern Germany. In *EGU General Assembly Conference Abstracts* (Vol. 15, p. 3348).
- Oguchi, T., Hori, K. and Oguchi, C.T., 2008. Paleohydrological implications of late Quaternary fluvial deposits in and around archaeological sites in Syria. *Geomorphology*, 101(1), pp.33-43.
- O'Hara, S.L. and Metcalfe, S.E., 1997. The climate of Mexico since the Aztec period. *Quaternary International*, 43, pp.25-31.
- Oliver, R.D., Nieva, F., Flores, H.F., Verma, S.P., Santoyo, E. and Portugal, E., 1987. Evaluación hidrogeológica en la cuenca de México y parte del Alto Lerma (Proceedings). *Geos-Boletín de la Unión Geofísica Mexicana*, 1: 27.
- Olsen, P.E., 1990. Tectonic, climatic, and biotic modulation of lacustrine ecosystems-examples from Newark Supergroup of eastern North America. *Lacustrine basin exploration: Case studies and modern analogs: AAPG Memoir*, 50, pp.209-224.
- Ortega, A. and Farvolden, R.N., 1989. Computer analysis of regional groundwater flow and boundary conditions in the Basin of Mexico. *Journal of Hydrology*, 110(3-4), pp.271-294.
- Ortega, B., Caballero, C., Lozano, S., Israde, I. and Vilaclara, G., 2002. 52 000 years of environmental history in Zacapú basin, Michoacán, Mexico: the magnetic record. *Earth and Planetary Science Letters*, 202(3), pp.663-675.
- Ortega-Guerrero, B. and Newton, A.J., 1998. Geochemical characterization of Late Pleistocene and Holocene tephra layers from the Basin of Mexico, Central Mexico. *Quaternary Research*, 50(1), pp.90-106.
- Ortega-Guerrero, B., 1992. *Paleomagnetismo, magnetoestratigrafía y paleoecología del Cuaternario tardío en el Lago de Chalco, Cuenca de México* (Doctoral dissertation, Dissertation, National University of México).
- Ortiz, J.E., Gallego, J.L.R., Torres, T., Díaz-Bautista, A. and Sierra, C., 2010. Palaeoenvironmental reconstruction of Northern Spain during the last 8000calyr BP based on the biomarker content of the Roñanzas peat bog (Asturias). *Organic Geochemistry*, 41(5), pp.454-466.
- Ovando-Shelley, E., Ossa, A. and Romo, M.P., 2007. The sinking of Mexico City: Its effects on soil properties and seismic response. *Soil Dynamics and Earthquake Engineering*, 27(4), pp.333-343.
- Padmakumari, V.M. and Ahmad, S.M., 2004. Ash layer at? 8 Ma in ODP Site 758 from the Bay of Bengal: evidence from Sr, Nd isotopic compositions and rare earth elements. *CURRENT SCIENCE-BANGALORE*, 86(9), pp.1323-1325.
- Parsons, J.R., Gorenflo, L.J., Parsons, M.H. and Wilson, D.J., 2008. Prehispanic settlement patterns in the northwestern Valley of Mexico: the Zumpango region (Vol. 45). University of Michigan Museum.
- Pastouret, L., Chamley, H., Delibrias, G., Duplessy, J.C. and Thiede, J., 1978. Late Quaternary climatic changes in western tropical Africa deduced from deep-sea sedimentation off the Niger delta. *Oceanologica Acta*, 1(2), pp.217-232.
- Payne, B.R., 1976. The interaction of irrigation water with groundwater and River Tula in the Mezquital Valley. Int. At. Energy Agency--Sect. Agric. Recur. Hidraul. (I.A.E.A. -- S.A.R.H.) Rep.(unpublished).
- Pedley, H. M. 2009. Tufas and travertines of the Mediterranean region: a testing ground for freshwater carbonate concepts and developments. *Sedimentology*, 56: 221 - 246

- Pedley, H. M., 1990. Classification and environmental models of cool freshwater tufas. *Sedimentary Geology*, 68: 143-154.
- Pedley, H. M., 1992. Freshwater (phytoherm) reefs: the role of biofilms and their bearing on marine reef cementation. *Sediment geology*, 79: 255 - 274
- Pedley, H. M., Rogerson, M., Middleton, R. 2009. Freshwater calcite precipitates from in vitro mesocosm flume experiments: a case for biomediation of tufas. *Sedimentology*, 56: 511 - 257
- Pedley, H.M. and Rogerson, M. eds., 2010. Tufas and speleothems: unravelling the microbial and physical controls. Geological Society of London.
- Pedley, H.M. and Rogerson, M., 2010. In vitro investigations of the impact of different temperature and flow velocity conditions on tufa microfabric. Geological Society, London, Special Publications, 336(1), pp.193-210.
- Pedley, H.M., Hill, I., Denton, P. and Brasington, J., 2000. Three-dimensional modelling of a Holocene tufa system in the Lathkill Valley, north Derbyshire, using ground-penetrating radar. *Sedimentology*, 47(3), pp.721-738.
- Pedley, M. and Hill, I., 2003. The recognition of barrage and paludal tufa systems by GPR: case studies in the geometry and correlation of Quaternary freshwater carbonates. Geological Society, London, Special Publications, 211(1), pp.207-223.
- Pedley, M., 1992. Freshwater (phytoherm) reefs: the role of biofilms and their bearing on marine reef cementation. *Sedimentary Geology*, 79(1-4), pp.255-274.
- Pedley, M., Andrews, J., Ordonez, S., del Cura, M.A.G., Martin, J.A.G. and Taylor, D., 1996. Does climate control the morphological fabric of freshwater carbonates? A comparative study of Holocene barrage tufas from Spain and Britain. *Palaeogeography, Palaeoclimatology, Palaeoecology*, 121(3-4), pp.239-257.
- Pedley, M., Martin, J. A. G., Delgado, S. O., Garcia Del Cura, M., 2003. Sedimentology of Quaternary perched springline and paludal tufas: criteria for recognition, with examples from Guadalajara Province, Spain *Sedimentology*, 50: 23-44.
- Pedley, M., Rogerson, M. and Middleton, R., 2009. Freshwater calcite precipitates from in vitro mesocosm flume experiments: a case for biomediation of tufas. *Sedimentology*, 56(2), pp.511-527.
- Pellicer, X.M., Corella, J.P., Gutiérrez, F., Roqué, C., Linares, R., Carbonel, D., Zarroca, M., Guerrero, J. and Comas, X., 2016. Sedimentological and palaeohydrological characterization of Late Pleistocene and Holocene tufa mound palaeolakes using trenching methods in the Spanish Pyrenees. *Sedimentology*, 63(6), pp.1786-1819.
- Pentecost, A. and Viles, H., 1994. A review and reassessment of travertine classification. *Géographie physique et Quaternaire*, 48(3), pp.305-314.
- Pentecost, A., 1990. The formation of travertine shrubs: Mammoth Hot springs, Wyoming. *Geological Magazine*, 127(2), pp.159-168.
- Pentecost, A., 2005. *Travertine*. Springer Science & Business Media.
- Pentecost, A., Riding, R., 1986. Calcification in cyanobacterial. In: *Biom mineralization in Lower Plants and Animals* (Eds B.S.C. Leadbeater and R. Riding), 73 - 86. Clarendon Press, Open University Oxford.
- Pérez-Crespo, V.A., Arroyo-Cabrales, J., Alva-Valdivia, L.M., Morales-Puente, P., Cienfuegos-Alvarado, E. and Otero, F.J., 2016. Inferences of feeding habits of Late Pleistocene *Equus* sp. from eight Mexican localities. *Neues Jahrbuch für Geologie und Paläontologie-Abhandlungen*, 279(1), pp.107-121.
- Peterson, L.C., Haug, G.H., Hughen, K.A. and Röhl, U., 2000. Rapid changes in the hydrologic cycle of the tropical Atlantic during the last glacial. *Science*, 290(5498), pp.1947-1951.
- Pietras, J.T. and Carroll, A.R., 2006. High-resolution stratigraphy of an underfilled lake basin: Wilkins Peak member, Eocene Green River Formation, Wyoming, USA. *Journal of Sedimentary Research*, 76(11), pp.1197-1214.
- Pigati, J.S., Rech, J.A. and Nekola, J.C., 2010. Radiocarbon dating of small terrestrial gastropod shells in North America. *Quaternary Geochronology*, 5(5), pp.519-532.
- Pilcher, J.R., 1991. Radiocarbon dating for the Quaternary scientist. In *Quaternary Proceedings* (pp. 27-33).

- Pla-Pueyo, S., Viseras, C., Candy, I., Soria, J.M., García-García, F. and Schreve, D., 2015. Climatic control on palaeohydrology and cyclical sediment distribution in the Plio-Quaternary deposits of the Guadix Basin (Betic Cordillera, Spain). *Quaternary International*, 389, pp.56-69.
- Platt, N.H. and Wright, V.P., 1992. Palustrine carbonates and the Florida everglades: towards an exposure index for the fresh-water environment?. *Journal of Sedimentary Research*, 62(6).
- Platt, N.H. and Wright, V.P., 2009. Lacustrine carbonates: facies models, facies distributions and hydrocarbon aspects. *Lacustrine facies analysis*, pp.57-74.
- Platt, N.H., 1989. Lacustrine carbonates and pedogenesis: sedimentology and origin of palustrine deposits from the Early Cretaceous Rupelo Formation, W Cameros Basin, N Spain. *Sedimentology*, 36(4), pp.665-684.
- Poage, M.A. and Chamberlain, C.P., 2001. Empirical relationships between elevation and the stable isotope composition of precipitation and surface waters: Considerations for studies of paleoelevation change. *American Journal of Science*, 301(1), pp.1-15.
- Polyak, V.J. and Asmerom, Y., 2005. Orbital control of long-term moisture in the southwestern USA. *Geophysical research letters*, 32(19).
- Porter, R.J. and Gallois, R.W., 2008. Identifying fluvio-lacustrine intervals in thick playa-lake successions: An integrated sedimentology and ichnology of arenaceous members in the mid-late Triassic Mercia Mudstone Group of south-west England, UK. *Palaeogeography, Palaeoclimatology, Palaeoecology*, 270(3-4), pp.381-398.
- Posamentier, H.W. and Walker, R.G., 2006. Facies models revisited.
- Potter, P.E., 1959. Facies model conference. *Science*, 129(3358), pp.1292-1294.
- Potter, P.E., Maynard, J.B. and Depetris, P.J., 2005. *Mud and mudstones: Introduction and overview*. Springer Science & Business Media.
- Price, G.J., Webb, G.E., Zhao, J.X., Feng, Y.X., Murray, A.S., Cooke, B.N., Hocknull, S.A. and Sobbe, I.H., 2011. Dating megafaunal extinction on the Pleistocene Darling Downs, eastern Australia: the promise and pitfalls of dating as a test of extinction hypotheses. *Quaternary Science Reviews*, 30(7), pp.899-914.
- Price, G.J., Zhao, J.X., Feng, Y.X. and Hocknull, S.A., 2009. New records of Plio-Pleistocene koalas from Australia: palaeoecological and taxonomic implications. *Records of the Australian Museum*, 61(1), pp.39-48.
- Prokopenko, A.A., Hinnov, L.A., Williams, D.F. and Kuzmin, M.I., 2006. Orbital forcing of continental climate during the Pleistocene: a complete astronomically tuned climatic record from Lake Baikal, SE Siberia. *Quaternary Science Reviews*, 25(23-24), pp.3431-3457.
- Quade, J., Miffin, M.D., Pratt, W.L., McCoy, W. and Burckle, L., 1995. Fossil spring deposits in the southern Great Basin and their implications for changes in water-table levels near Yucca Mountain, Nevada, during Quaternary time. *Geological Society of America Bulletin*, 107(2), pp.213-230.
- Quijano, L., 1978. Comentario sobre el muestreo isotópico de las aguas subterráneas de la zona de Texcoco. Int. At. Energy Agency -- Secr. Agric. Recur. Hidraul. (I.A.E.A. -- S.A.R.H.) Rep. (unpublished).
- Quijano, L., 1980. Isotope analysis done by Earth Science Department, University of Waterloo, Canada. Chemical analysis done by Secr. Agric. Recur. Hidraul. (S.A.R.H.), Mexico (unpublished).
- Quintanar, L., Rodríguez-González, M., Campos-Enríquez, O., 2004. A shallow crustal earthquake doublet from the Trans-Mexican Volcanic Belt (Central Mexico). *Bulletin of the Seismological Society of America*, 94: 845 - 855.
- Ramírez-Cruz, G.A. and Montellano-Ballesteros, M., 2014. Two new glyptodont records (Mammalia: Cingulata) from the late Pleistocene of Tamaulipas and Tlaxcala, Mexico: Implications for the taxonomy of the genus *Glyptotherium*. *The Southwestern Naturalist*, 59(4), pp.522-530.
- Ramsey, B. C. 2008. Radiocarbon dating: Revolutions in understanding. *Archaeometry*, 50 (2): 249 - 275.
- Ramsey, B. C. 2008. Radiocarbon dating: Revolutions in understanding. *Archaeometry*, 50 (2): 249 - 275.
- Remy, R.R. and Ferrell, R.E., 1989. Distribution and origin of analcime in marginal lacustrine mudstones of the Green River Formation, south-central Uinta Basin, Utah. *Clays and Clay minerals*, 37(5), pp.419-432.

- Renne, P.R., Balco, G., Ludwig, K.R., Mundil, R. and Min, K., 2011. Response to the comment by WH Schwarz et al. on "Joint determination of 40 K decay constants and 40 Ar/40 K for the Fish Canyon sanidine standard, and improved accuracy for 40 Ar/39 Ar geochronology" by PR Renne et al.(2010). *Geochimica et Cosmochimica Acta*, 75(17), pp.5097-5100.
- Renne, P.R., Sharp, W.D., Deino, A.L., Orsi, G. and Civetta, L., 1997. 40Ar/39Ar dating into the historical realm: calibration against Pliny the Younger. *Science*, 277(5330), pp.1279-1280.
- Renne, Paul R., Greg Balco, Kenneth R. Ludwig, Roland Mundil, and Kyoungwon Min. "Response to the comment by WH Schwarz et al. on "Joint determination of 40K decay constants and 40Ar/40K for the Fish Canyon sanidine standard, and improved accuracy for 40Ar/39Ar geochronology" by PR Renne et al.(2010)." *Geochimica et Cosmochimica Acta* 75, no. 17 (2011): 5097-5100.
- Rich, J., 2013. A 250,000-year record of lunette dune accumulation on the Southern High Plains, USA and implications for past climates. *Quaternary Science Reviews*, 62, pp.1-20.
- Riding, R. ed., 2012. *Calcareous algae and stromatolites*. Springer Science & Business Media.
- Rivas, H., Bostelmann, E., Le Roux, J. and Ugalde, R., 2015. Fluvial facies and architecture of the late middle Miocene, Mayoan, deposits of Chilean Patagonia. In XIV Congreso Geológico Chileno, Actas (Vol. 1, pp. 812-815).
- Rodríguez-Pascua, M., Becker, A., Calvo, J.P., Davenport, C.A. and Gómez-Gras, D., 2003. Sedimentary record of seismic events, with examples from recent and fossil lakes. *Limnogeology in Spain: a tribute to Kerry Kelts*. Consejo Superior de Investigaciones Científicas, pp.253-280.
- Rosenbaum, J. and Sheppard, S.M.F., 1986. An isotopic study of siderites, dolomites and ankerites at high temperatures. *Geochimica et Cosmochimica Acta*, 50(6), pp.1147-1150.
- Rosenmeier, M.F., Hodell, D.A., Brenner, M., Curtis, J.H. and Guilderson, T.P., 2002. A 4000-year lacustrine record of environmental change in the southern Maya lowlands, Peten, Guatemala. *Quaternary Research*, 57(2), pp.183-190.
- Rosenmeier, M.F., Hodell, D.A., Brenner, M., Curtis, J.H., Martin, J.B., Anselmetti, F.S., Ariztegui, D. and Guilderson, T.P., 2002. Influence of vegetation change on watershed hydrology: implications for paleoclimatic interpretation of lacustrine $\delta^{18}\text{O}$ records. *Journal of Paleolimnology*, 27(1), pp.117-131.
- Rowley, D.B., Pierrehumbert, R.T. and Currie, B.S., 2001. A new approach to stable isotope-based paleoaltimetry: implications for paleoaltimetry and paleohypsometry of the High Himalaya since the Late Miocene. *Earth and Planetary Science Letters*, 188(1-2), pp.253-268.
- Roy, P.D., Arce, J.L., Lozano, R., Jonathan, M.P., Centeno, E. and Lozano, S., 2012. Geochemistry of late Quaternary tephra-sediment sequence from north-eastern Basin of Mexico (Mexico): implications to tephrochronology, chemical weathering and provenance. *Revista Mexicana de Ciencias Geológicas*, 29(1).
- Roy, P.D., Caballero, M., Lozano, R. and Smykatz-Kloss, W., 2008. Geochemistry of late quaternary sediments from Tecocomulco lake, central Mexico: Implication to chemical weathering and provenance. *Chemie der erde-geochemistry*, 68(4), pp.383-393.
- Roy, P.D., Caballero, M., Lozano, R., Ortega, B., Lozano, S., Pi, T., Israde, I. and Morton, O., 2010. Geochemical record of Late Quaternary paleoclimate from lacustrine sediments of paleo-lake San Felipe, western Sonora Desert, Mexico. *Journal of South American Earth Sciences*, 29(3), pp.586-596.
- Roy, P.D., Caballero, M., Lozano, R., Pi, T. and Morton, O., 2009. Late Pleistocene-Holocene geochemical history inferred from Lake Tecocomulco sediments, Basin of Mexico, Mexico. *Geochemical Journal*, 43(1), pp.49-64.
- Roy, P.D., Quiroz-Jiménez, J.D., Chávez-Lara, C.M., Sánchez-Zavala, J.L., Pérez-Cruz, L.L. and Sankar, G.M., 2014. Humid Pleistocene-Holocene transition and early Holocene in subtropical northern Mexico and possible Gulf of California forcing. *Boreas*, 43(3), pp.577-587.
- Rozanski, K., 1985. Deuterium and oxygen-18 in European groundwaters-links to atmospheric circulation in the past. *Chemical Geology: Isotope Geoscience section*, 52(3-4), pp.349-363.
- Rueda, H., Arce, J., Macías, J. and García-Palomo, A., 2006, December. A~ 31 ka Plinian-subplinian eruption at Tláloc volcano, Sierra Nevada, México. In AGU Fall Meeting Abstracts (Vol. 1, p. 0668).

- Rueda, H., Arce, J.L., Macías, J.L. and García-Palomo, A., 2007. Pyroclastic sequences at the N-NE slopes of Tlaloc volcano, Sierra Nevada, central Mexico, in a Commemorative Conference, El Chichón volcano: 25 years later,. San Cristóbal de las Casas. Chiapas, México, p.100.
- Rueda, H., Macías, J.L., Arce, J.L., Gardner, J.E. and Layer, P.W., 2013. The ~ 31 ka rhyolitic Plinian to sub-Plinian eruption of Tlaloc Volcano, Sierra Nevada, central Mexico. *Journal of Volcanology and Geothermal Research*, 252, pp.73-91.
- Rühlemann, C., Mulitza, S., Müller, P.J., Wefer, G. and Zahn, R., 1999. Warming of the tropical Atlantic Ocean and slowdown of thermohaline circulation during the last deglaciation. *Nature*, 402(6761), pp.511-514.
- Ryan, M.C., 1989. An investigation of nitrogen compounds in the groundwater in the Valley of Mexico. *Geof? s. Int.*, 28(2): 417-433.
- Salinas, M.S., Hidalgo, J. and Posadas, C., 2016. Mamíferos fósiles del Pleistoceno tardío (Rancholabreano) de San Mateo Huexoyucán, Tlaxcala, México. *Boletín de la Sociedad Geológica Mexicana*, p.497.
- Sato, Y., Matsuoka, H., Okamura, M. and Kashima, K., 2016. Late Holocene environmental changes of coastal lagoon inferred from a fossil diatom analysis of sediment core from Lake Hamana, central Japan. *Quaternary International*, 397, pp.317-329.
- Scherer, C.M., Goldberg, K. and Bardola, T., 2015. Facies architecture and sequence stratigraphy of an early post-rift fluvial succession, Aptian Barbalha Formation, Araripe Basin, northeastern Brazil. *Sedimentary Geology*, 322, pp.43-62.
- Schneider, J., Schröder, H.G. and Le Campion-Alsumard, T., 1983. Algal micro-reefs-coated grains from freshwater environments. In *Coated grains* (pp. 284-298). Springer Berlin Heidelberg.
- Schnellmann, M., Anselmetti, F.S., Giardini, D. and McKenzie, J.A., 2006. 15,000 Years of mass-movement history in Lake Lucerne: Implications for seismic and tsunami hazards. *Eclogae Geologicae Helveticae*, 99(3), pp.409-428.
- Schumm, S.A., 1977. *The Fluvial System* PDF.
- Schütt, B., 1998. Chemical and mineralogical characters of lacustrine sediments as paleoenvironmental indicators- An example from the Laguna Jabonera, Central Ebro Basin. *Terra Nostra*, 98(6), pp.115-120.
- Schütt, B., 2000. Holocene paleohydrology of playa lakes in northern and central Spain: a reconstruction based on the mineral composition of lacustrine sediments. *Quaternary International*, 73, pp.7-27.
- Schweger, C.E., 2013. Late Pleistocene vegetation of eastern Beringia: pollen analysis. *Paleoecology of Beringia*, p.95.
- Sedov, S., Lozano-García, S., Solleiro-Rebolledo, E., de Tapia, E.M., Ortega-Guerrero, B. and Sosa-Nájera, S., 2010. Tepexpan revisited: A multiple proxy of local environmental changes in relation to human occupation from a paleolake shore section in Central Mexico. *Geomorphology*, 122(3), pp.309-322.
- Sedov, S., Solleiro-Rebolledo, E., Gama-Castro, J.E., Vallejo-Gómez, E. and González-Velázquez, A., 2001. Buried palaeosols of the Nevado de Toluca: an alternative record of Late Quaternary environmental change in central Mexico. *Journal of Quaternary Science*, 16(4), pp.375-389.
- Sedov, S., Solleiro-Rebolledo, E., Terhorst, B., Solé, J., Flores-Delgadillo, M.D.L., Werner, G. and Poetsch, T., 2009. The Tlaxcala basin paleosol sequence: a multiscale proxy of middle to late Quaternary environmental change in central Mexico. *Revista Mexicana de Ciencias Geológicas*, 26(2), pp.448-465.
- Seegerstrom, K., 1962. *Geology of South-central Hidalgo and North-eastern México*, Mexico. US Government Printing Office.
- Seegerstrom, K., 1963. *Geology of South Central Hidalgo and Northeastern Mexico*, Mexico. Geological Survey Bulletin, pp.87-162.
- Seegerstrom, K., Williams, H., Wilcox, R.E., Foshag, W.P. and Gonzales, J.R., 1956. *Geologic investigations in the Parícutin area, Mexico* (No. 965). US Government Printing Office.
- Semeniuk, V. and Meagher, T.D., 1981. Calcrete in Quaternary coastal dunes in southwestern Australia: A capillary-rise phenomenon associated with plants. *Journal of Sedimentary Research*, 51(1).

- Sharp, Z., 2007. Principles of stable isotope geochemistry (p. 344). Upper Saddle River, NJ: Pearson education.
- Siebe, C., 2000. Age and archaeological implications of Xitle volcano, southwestern Basin of Mexico-City. *Journal of Volcanology and Geothermal Research*, 104(1), pp.45-64.
- Siebe, C., Salinas, S., Arana-Salinas, L., Macías, J.L., Gardner, J. and Bonasia, R., 2017. The ~ 23,500 y 14 C BP White Pumice Plinian eruption and associated debris avalanche and Tochimilco lava flow of Popocatepetl volcano, México. *Journal of Volcanology and Geothermal Research*, 333, pp.66-95.
- Siemens, J., Huschek, G., Siebe, C. and Kaupenjohann, M., 2008. Concentrations and mobility of human pharmaceuticals in the world's largest wastewater irrigation system, Mexico City-Mezquital Valley. *Water Research*, 42(8), pp.2124-2134.
- Sienkiewicz, E., 2013. Limnological record inferred from diatoms in sediments of Lake Skalska (north-eastern Poland). *Acta Palaeobotanica*, 53(1), pp.99-104.
- Sigleo, W.R. and Colhoun, E.A., 1982. Terrestrial dunes, man and the late Quaternary environment in southern Tasmania. *Palaeogeography, Palaeoclimatology, Palaeoecology*, 39(1-2), pp.87-121.
- Singh, A. and Bhardwaj, B.D., 1991. Fluvial facies model of the Ganga River sediments, India. *Sedimentary Geology*, 72(1-2), pp.135-146.
- Sinha, R., Smykatz-Kloss, W., Stüben, D., Harrison, S.P., Berner, Z. and Kramar, U., 2006. Late Quaternary palaeoclimatic reconstruction from the lacustrine sediments of the Sambhar playa core, Thar Desert margin, India. *Palaeogeography, Palaeoclimatology, Palaeoecology*, 233(3), pp.252-270.
- Smith, P., 2004. How long before a change in soil organic carbon can be detected?. *Global Change Biology*, 10(11), pp.1878-1883.
- Smol, J.P. and Stoermer, E.F. eds., 2010. The diatoms: applications for the environmental and earth sciences. Cambridge University Press.
- Smoot, J.P. and Olsen, P.E., 1988. Massive mudstones in basin analysis and paleoclimatic interpretation of the Newark Supergroup. In *Developments in Geotectonics* (Vol. 22, pp. 249-274). Elsevier.
- Soler-Arechalde, A.M. and Urrutia-Fucugauchi, J., 2000. Paleomagnetism of the Acambay Graben, central Trans-Mexican volcanic belt. *Tectonophysics*, 318(1), pp.235-248.
- Solleiro-Rebolledo, E., Sedov, S., de Tapia, E.M., Cabadas, H., Gama-Castro, J. and Vallejo-Gómez, E., 2006. Spatial variability of environment change in the Teotihuacan Valley during the Late Quaternary: Paleopedological inferences. *Quaternary International*, 156, pp.13-31.
- Solleiro-Rebolledo, E., Sedov, S., Gama-Castro, J., Roman, D.F. and Escamilla-Sarabia, G., 2003. Paleosol-sedimentary sequences of the Glacis de Buenavista, Central Mexico: interaction of Late Quaternary pedogenesis and volcanic sedimentation. *Quaternary International*, 106, pp.185-201.
- Steel, R.J., 1974. Cornstone (fossil caliche): its origin, stratigraphic, and sedimentological importance in the New Red Sandstone, Western Scotland. *The Journal of Geology*, 82(3), pp.351-369.
- Stevens, R.E., Metcalfe, S.E., Leng, M.J., Lamb, A.L., Sloane, H.J., Naranjo, E. and González, S., 2012. Reconstruction of late Pleistocene climate in the Valsequillo Basin (Central Mexico) through isotopic analysis of terrestrial and freshwater snails. *Palaeogeography, Palaeoclimatology, Palaeoecology*, 319, pp.16-27.
- Stinnesbeck, S.R., Frey, E., Stinnesbeck, W., Olguín, J.A., Zell, P., Mata, A.T., Sanvicente, M.B., González, A.G., Sandoval, C.R. and Nuñez, E.A., 2017. A new fossil peccary from the Pleistocene-Holocene boundary of the eastern Yucatán Peninsula, Mexico. *Journal of South American Earth Sciences*, 77, pp.341-349.
- Stojanowski, C.M. and Johnson, K.M., 2011. Labial canine talon cusp from the early Holocene site of Gobero, Central Sahara Desert, Niger. *International Journal of Osteoarchaeology*, 21(4), pp.391-406.
- Stow, D.A., 2005. *Sedimentary rocks in the field: a color guide*. Gulf Professional Publishing.
- Street, F.A. and Grove, A.T., 1976. Environmental and climatic implications of late Quaternary lake-level fluctuations in Africa. *Nature*, 261(5559), pp.385-390.
- Stuiver, M. and Polach, H.A., 1977. Discussion reporting of 14 C data. *Radiocarbon*, 19(03), pp.355-363.

Summerfield, M.A., 2014. *Global geomorphology*. Routledge.

Sun, Y., Chen, J., Clemens, S.C., Liu, Q., Ji, J. and Tada, R., 2006. East Asian monsoon variability over the last seven glacial cycles recorded by a loess sequence from the northwestern Chinese Loess Plateau. *Geochemistry, Geophysics, Geosystems*, 7(12).

Suter, M., Aguirre, G., Siebe, C., Quintero, O., Komorowski, J. C., 1991. Volcanism and active faulting in the central part of the Trans-Mexican volcanic belt, Mexico. In: Walawender, M.J., Hanan, B.B., eds., *Geological excursions in southern California and Mexico*: San Diego, California, Department of Geological Sciences, San Diego State University, Guidebook, 1991 Annual Meeting, Geological Society of America, San Diego, California, October 21-24, 1991, p. 224-243.

Suter, M., Carrillo-Martínez, M., Quintero-Legorreta, O., 1996. Macroseismic study of shallow earthquakes in the central and eastern parts of the Trans-Mexican volcanic belt, Mexico. *Seismological Society of America Bulletin*, 86: p. 1952 - 1963.

Suter, M., López-Martínez, M., Quintero-Legorreta, O., Carrillo-Martínez, M., 2001. Quaternary intra-arc extension in the central Trans-Mexican volcanic belt. *Geological Society of America Bulletin*, 113 (6): 693 - 703.

Sutton, R.T. and Hodson, D.L., 2005. Atlantic Ocean forcing of North American and European summer climate. *science*, 309(5731), pp.115-118.

Zsynkaruk, E., Graduño-Monroy, V.H. and Bocco, G., 2004. Active fault systems and tectono-topographic configuration of the central Trans-Mexican Volcanic Belt. *Geomorphology*, 61(1-2), pp.111-126.

Talbot, M.R., 1990. A review of the palaeohydrological interpretation of carbon and oxygen isotopic ratios in primary lacustrine carbonates. *Chemical Geology: Isotope Geoscience Section*, 80(4), pp.261-279.

Talbot, M.R., Holm, K. and Williams, M.A.J., 1994. Sedimentation in low-gradient desert margin systems: A comparison of the Late Triassic of northwest Somerset. *Paleoclimate and basin evolution of playa systems*, 289, p.97.

Talma, A.S. and Vogel, J.C., 1992. Late Quaternary paleotemperatures derived from a speleothem from Cango caves, Cape province, South Africa. *Quaternary Research*, 37(2), pp.203-213.

Talma, A.S. and Vogel, J.C., 1993. A simplified approach to calibrating 14 C dates. *Radiocarbon*, 35(02), pp.317-322.

Tandon, S.K. and Friend, P.F., 1989. Near-surface shrinkage and carbonate replacement processes, Arran Cornstone Formation, Scotland. *Sedimentology*, 36(6), pp.1113-1126.

Tandon, S.K. and Gibling, M.R., 1997. Calcretes at sequence boundaries in Upper Carboniferous cyclothems of the Sydney Basin, Atlantic Canada. *Sedimentary Geology*, 112(1-2), pp.43-67.

Tandon, S.K. and Narayan, D., 1981. Calcrete conglomerate, case-hardened conglomerate and cornstone—a comparative account of pedogenic and non-pedogenic carbonates from the continental Siwalik Group, Punjab, India. *Sedimentology*, 28(3), pp.353-367.

Tanner, L.H., 2000. Palustrine-lacustrine and alluvial facies of the (Norian) Owl Rock Formation (Chinle Group), Four Corners region, southwestern uSa: implications for Late Triassic paleoclimate. *Journal of Sedimentary Research*, 70(6).

Teller, J.T. and Last, W.M., 1990. Paleohydrological indicators in playas and salt lakes, with examples from Canada, Australia, and Africa. *Palaeogeography, Palaeoclimatology, Palaeoecology*, 76(3-4), pp.215-240.

Theriault, P. and Desrochers, A., 1993. Carboniferous calcretes in the Canadian Arctic. *Sedimentology*, 40(3), pp.449-465.

Timmermann, A., Okumura, Y., An, S.I., Clement, A., Dong, B., Guilyardi, E., Hu, A., Jungclaus, J.H., Renold, M., Stocker, T.F. and Stouffer, R.J., 2007. The influence of a weakening of the Atlantic meridional overturning circulation on ENSO. *Journal of climate*, 20(19), pp.4899-4919.

Tófaló, O.R. and Pazos, P.J., 2010. Paleoclimatic implications (Late Cretaceous-Paleogene) from micromorphology of calcretes, palustrine limestones and silcretes, southern Paraná Basin, Uruguay. *Journal of South American Earth Sciences*, 29(3), pp.665-675.

- Toker, M.E., 2016. Quaternary fluvial tufas of Sar?kavak area, southwestern Turkey: Facies and depositional systems. *Quaternary International*.
- Tooth, S., 2009. Arid geomorphology: emerging research themes and new frontiers. *Progress in Physical Geography*, 33(2), pp.251-287.
- TORRES?RODRÍGUEZ, E., LOZANO?GARCÍA, S., Roy, P., Ortega, B., BERAMENDI? OROSCO, L., CORREA? METRIO, A. and Caballero, M., 2015. Last Glacial droughts and fire regimes in the central Mexican highlands. *Journal of Quaternary Science*, 30(1), pp.88-99.
- Tovar, R.E., Sedov, S., Montellano-Ballesteros, M., Solleiro, E. and Benammi, M., 2014. Paleosols, bones, phytoliths, and? 13 C signatures of humus and teeth in the alluvial sequence of Axamilpa, Puebla: Inferences for landscape evolution and megafauna paleoecology during MIS 3-2 in Southern Mexico. *Catena*, 112, pp.25-37.
- Tovar, R.E., Sedov, S., Solís, B. and Solleiro, E., 2013. Dark humic alluvial paleosols in Central and Southern Mexico: micromorphological indicators of Late Pleistocene megafauna habitats. *J Soil Sci*, 3, pp.217-223.
- Tucker, G.E. and Slingerland, R., 1996. Predicting sediment flux from fold and thrust belts. *Basin Research*, 8(3), pp.329-349.
- Tucker, M.E. and Wright, V.P., 1990. Carbonate mineralogy and chemistry. *Carbonate Sedimentology*, pp.284-313.
- Tucker, M.E. and Wright, V.P., 1990. Dolomites and dolomitization models. *Carbonate sedimentology*, pp.365-400.
- Tucker, M.E., 2003. Mixed clastic-carbonate cycles and sequences: Quaternary of Egypt and Carboniferous of England. *Geologia Croatica*, 56(1), pp.19-37.
- Tzedakis, P.C., 2010. The MIS 11-MIS 1 analogy, southern European vegetation, atmospheric methane and the "early anthropogenic hypothesis". *Climate of the Past*, 6(2), pp.131-144.
- UCL, 2017. <https://www.ucl.ac.uk/earth-sciences/impact/geology/london/ucl/materials/clay>
- Universalis, E., 2017. Méso-Amérique: Les Grands Articles d'Universalis. *Encyclopaedia Universalis*.
- Unkel, I., Kadereit, A., Mächtle, B., Eitel, B., Kromer, B., Wagner, G. and Wacker, L., 2007. Dating methods and geomorphic evidence of palaeoenvironmental changes at the eastern margin of the South Peruvian coastal desert (14° 30' S) before and during the Little Ice Age. *Quaternary International*, 175(1), pp.3-28.
- Valero, L., Huerta, P., Garcés, M., Armenteros, I., Beamud, E. and Gómez?Paccard, M., 2015. Linking sedimentation rates and large?scale architecture for facies prediction in nonmarine basins (Paleogene, Almazán Basin, Spain). *Basin Research*.
- Van Devender, T.R. and Burgess, T.L., 1985. Late Pleistocene woodlands in the Bolson de Mapimi: A refugium for the Chihuahuan Desert Biota?. *Quaternary Research*, 24(3), pp.346-353.
- Vandenbergh, J. and Maddy, D., 2001. The response of river systems to climate change.
- Vandenschrck, G., Van Wesemael, B., Frot, E., Pulido-Bosch, A., Molina, L., Stievenard, M. and Souchez, R., 2002. Using stable isotope analysis (?D-? 18 O) to characterise the regional hydrology of the Sierra de Gador, south east Spain. *Journal of Hydrology*, 265(1), pp.43-55.
- Vázquez?Urbez, M.A.R.T.A., Arenas, C. and Pardo, G., 2012. A sedimentary facies model for stepped, fluvial tufa systems in the Iberian Range (Spain): the Quaternary Piedra and Mesa valleys. *Sedimentology*, 59(2), pp.502-526.
- Vázquez-Sánchez, E. and Jaimes-Palomera, R., 1989. Geología de la Cuenca de México. *Geofísica Internacional*, 28(2), pp.133-190.
- Vázquez-Selem, L. and Heine, K., 2004. Late quaternary glaciation of Mexico. *Developments in Quaternary Sciences*, 2, pp.233-242.
- Verati, C. and Jourdan, F., 2014. Modelling effect of sericitization of plagioclase on the 40K/40Ar and 40Ar/39Ar chronometers: implication for dating basaltic rocks and mineral deposits. *Geological Society, London, Special Publications*, 378(1), pp.155-174.

- Verrecchia, E.P., Dumont, J.L. and Verrecchia, K.E., 1993. Role of calcium oxalate biomineralization by fungi in the formation of calcretes: a case study from Nazareth, Israel. *Journal of Sedimentary Research*, 63(5).
- Verrecchia, E.P., Freytet, P., Verrecchia, K.E. and Dumont, J.L., 1995. Spherulites in calcrete laminar crusts: biogenic CaCO₃ precipitation as a major contributor to crust formation. *Journal of Sedimentary research*, 65(4).
- Verrecchia, E.P.V.K.E., 1994. Needle-fiber calcite: a critical review and a proposed classification. *Journal of Sedimentary Research*, 64(3).
- Viles, H. and Pentecost, A., 2007. Tufa and travertine. *Geochemical Sediments and Landscapes*, pp.173-199.
- Violante, C., Ferreri, V., D'Argenio, B. and Golubic, S., 1994. -Quaternary Travertines at Rocchetta a Volturno (Isernia, Central Italy). *Facies analysis and Sedimentary model of an Organogenic Carbonate System*.
- Walker, R.G. and James, N.P., 1992. *Facies models: Response to sea level change: St. John's, Newfoundland*, Geological Association of Canada.
- Walker, R.G., 1976. *Facies models 2. Turbidites and associated coarse clastic deposits*. *Geoscience Canada*, 3(1).
- Walker, R.G., 1990. *Facies modeling and sequence stratigraphy: perspective*. *Journal of Sedimentary Research*, 60(5).
- Walther, J., 1894. *Einleitung in die Geologie als historische Wissenschaft* Fischer Verlag. Léna, Allemagne (1893-1894)(3 vols.).
- Wang, L.C., Behling, H., Kao, S.J., Li, H.C., Selvaraj, K., Hsieh, M.L. and Chang, Y.P., 2015. Late Holocene environment of subalpine northeastern Taiwan from pollen and diatom analysis of lake sediments. *Journal of Asian Earth Sciences*, 114, pp.447-456.
- Wang, P., Tian, J., Cheng, X., Liu, C. and Xu, J., 2004. Major Pleistocene stages in a carbon perspective: The South China Sea record and its global comparison. *Paleoceanography*, 19(4).
- Waters, M. R., Haynes, C. V., 2001. Late Quaternary arroyo formation and climate change in the American Southwest. *Geology*, 29: 399 - 402.
- Waters, M.R., 2008. Alluvial chronologies and archaeology of the Gila River drainage basin, Arizona. *Geomorphology*, 101(1), pp.332-341.
- Watts, N.L., 1980. Quaternary pedogenic calcretes from the Kalahari (southern Africa): mineralogy, genesis and diagenesis. *Sedimentology*, 27(6), pp.661-686.
- Wayne Higgins, R., Douglas, A., Hahmann, A., Berbery, E.H., Gutzler, D., Shuttleworth, J., Stensrud, D., Amador, J., Carbone, R., Cortez, M. and Douglas, M., 2003. Progress in Pan American CLIVAR research: the North American monsoon system. *Atmósfera*, 16(1), pp.29-65.
- Webb, G.E., Price, G.J., Nothdurft, L.D., Deer, L. and Rintoul, L., 2007. Cryptic meteoric diagenesis in freshwater bivalves: implications for radiocarbon dating. *Geology*, 35(9), pp.803-806.
- Wei, K. and Gasse, F., 1999. Oxygen isotopes in lacustrine carbonates of West China revisited: implications for post glacial changes in summer monsoon circulation. *Quaternary Science Reviews*, 18(12), pp.1315-1334.
- Weissmann, G.S., Hartley, A.J., Nichols, G.J., Scuderi, L.A., Olson, M., Buehler, H. and Banteah, R., 2010. Fluvial form in modern continental sedimentary basins: Distributive fluvial systems. *Geology*, 38(1), pp.39-42.
- Wendt, K.A., Moseley, G.E., Dublyansky, Y.V., Spötl, C. and Edwards, R.L., 2016, April. 500,000 years of water table fluctuations recorded in Devils Hole 2 cave from southwestern Nevada, USA. In *EGU General Assembly Conference Abstracts* (Vol. 18, p. 11194).
- Weninger, B. and Jöris, O., 2008. A 14 C age calibration curve for the last 60 ka: the Greenland-Hulu U/Th timescale and its impact on understanding the Middle to Upper Paleolithic transition in Western Eurasia. *Journal of Human Evolution*, 55(5), pp.772-781.
- Westall, F., Steele, A., Toporski, J., Walsh, M., Allen, C., Guidry, S., McKay, D., Gibson, E. and Chafetz, H., 2000. Polymeric substances and biofilms as biomarkers in terrestrial materials: implications for extraterrestrial samples. *Journal of Geophysical Research: Planets*, 105(E10), pp.24511-24527.

- White, S.E., 1986. Quaternary glacial stratigraphy and chronology of Mexico. *Quaternary Science Reviews*, 5, pp.201-205.
- Wieder, M. and Yaalon, D.H., 1982. Micromorphological fabrics and developmental stages of carbonate nodular forms related to soil characteristics. *Geoderma*, 28(3-4), pp.203-220.
- Wilber, R.J. and Neumann, A.C., 1993. Effects of submarine cementation on microfibrils and physical properties of carbonate slope deposits, Northern Bahamas. In *Carbonate microfibrils* (pp. 79-94). Springer, New York, NY.
- Winograd, I., Coplen, T., Landwehr, J., Riggs, A., Ludwig, K., Szabo, B., Kolesar, P. and Revesz, K., 1992. Continuous 500, 000-year climate record from vein calcite in Devils Hole, Nevada. *Science*, 258(5080), pp.255-260.
- Woodbridge, J. and Roberts, N., 2011. Late Holocene climate of the Eastern Mediterranean inferred from diatom analysis of annually-laminated lake sediments. *Quaternary Science Reviews*, 30(23), pp.3381-3392.
- Wright, V., 1986. The role of fungal biomineralization in the formation of Early Carboniferous soil fabrics. *Sedimentology*, 33(6), pp.831-838.
- Wright, V.P. and Tucker, M.E. eds., 1991. *Calcretes*. Blackwell Scientific Publications.
- Wright, V.P., Beck, V.H. and Sanz-Montero, M.E., 1996. Spherulites in calcrete laminar crusts: Biogenic CaCO₃ precipitation as a major contributor to crust formation: discussion. *Journal of Sedimentary Research*, 66(5).
- Wright, V.P., Platt, N.H. and Wimbledon, W.A., 1988. Biogenic laminar calcretes: evidence of calcified root/mat horizons in paleosols. *Sedimentology*, 35(4), pp.603-620.
- www.es.wikipedia.org/tequiquiac
- Yang, X., Scuderi, L., Paillou, P., Liu, Z., Li, H. and Ren, X., 2011. Quaternary environmental changes in the drylands of China—a critical review. *Quaternary Science Reviews*, 30(23), pp.3219-3233.
- Yokoo, Y., Nakano, T., Nishikawa, M. and Quan, H., 2004. Mineralogical variation of Sr-Nd isotopic and elemental compositions in loess and desert sand from the central Loess Plateau in China as a provenance tracer of wet and dry deposition in the northwestern Pacific. *Chemical Geology*, 204(1), pp.45-62.
- Ypsilon., 2015. en.wikivoyage.org/wiki/Central_Mexico
- Yu, P.S. and Chen, M.T., 2011. A prolonged warm and humid interval during marine isotope stage 13-15 as revealed by hydrographic reconstructions from the South China Sea (IMAGES MD972142). *Journal of Asian Earth Sciences*, 40(6), pp.1230-1237.
- YUEN, S.G., 2014, October. PLEISTOCENE MAMMALS FROM EL TAJO QUARRY, STATE OF MEXICO, MEXICO. In 2014 GSA Annual Meeting in Vancouver, British Columbia.
- Zanchetta, G., Borghini, A., Fallick, A.E., Bonadonna, F.P. and Leone, G., 2007. Late Quaternary palaeohydrology of Lake Pergusa (Sicily, southern Italy) as inferred by stable isotopes of lacustrine carbonates. *Journal of Paleolimnology*, 38(2), pp.227-239.
- Zhang, R. and Delworth, T.L., 2006. Impact of Atlantic multidecadal oscillations on India/Sahel rainfall and Atlantic hurricanes. *Geophysical Research Letters*, 33(17).
- Zhang, S., Cui, K., Zhang, C. and Jin, M.Y., 2011. Controlling factors and distribution patterns of lithologic pools in the fluvial facies of the 3rd and 4th members of the Quantou Formation in the Songliao Basin. *Oil & gas geology*, 32(3), pp.411-419.